BIOFABRICATION AND BIOPOLYMERIC MATERIALS INNOVATION FOR MUSCULOSKELETAL TISSUE REGENERATION

EDITED BY: Farnaz Ghorbani, Chaozong Liu, Derek H. Rosenzweig and Megan Elin Cooke

PUBLISHED IN: Frontiers in Bioengineering and Biotechnology and Frontiers in Materials

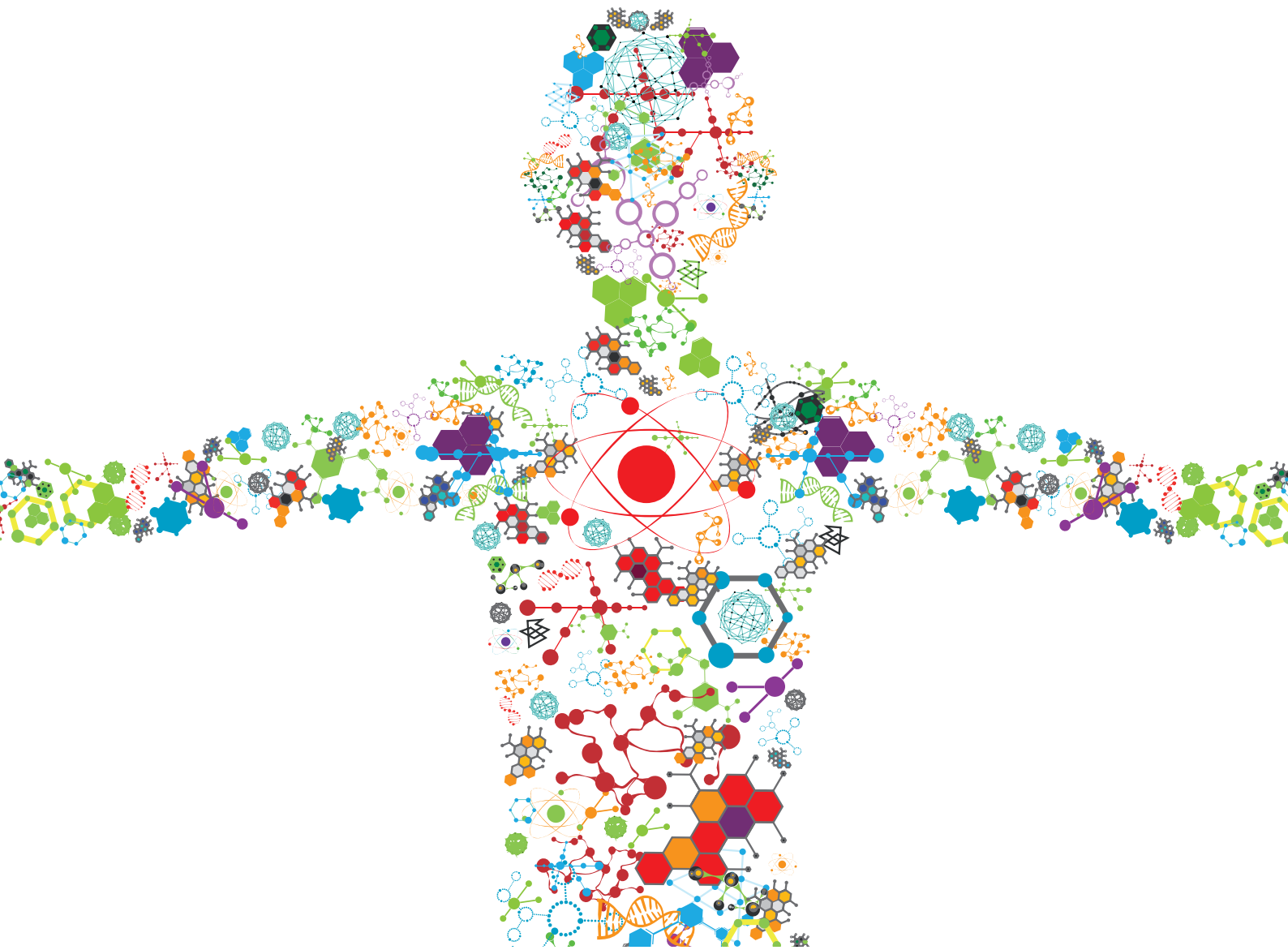

frontiers Research Topics

frontiers

ISSN 1664-8714
ISBN 978-2-88974-989-8
DOI 10.3389/978-2-88974-989-8

About Frontiers

Frontiers is more than just an open-access publisher of scholarly articles: it is a pioneering approach to the world of academia, radically improving the way scholarly research is managed. The grand vision of Frontiers is a world where all people have an equal opportunity to seek, share and generate knowledge. Frontiers provides immediate and permanent online open access to all its publications, but this alone is not enough to realize our grand goals.

Frontiers Journal Series

The Frontiers Journal Series is a multi-tier and interdisciplinary set of open-access, online journals, promising a paradigm shift from the current review, selection and dissemination processes in academic publishing. All Frontiers journals are driven by researchers for researchers; therefore, they constitute a service to the scholarly community. At the same time, the Frontiers Journal Series operates on a revolutionary invention, the tiered publishing system, initially addressing specific communities of scholars, and gradually climbing up to broader public understanding, thus serving the interests of the lay society, too.

Dedication to Quality

Each Frontiers article is a landmark of the highest quality, thanks to genuinely collaborative interactions between authors and review editors, who include some of the world's best academicians. Research must be certified by peers before entering a stream of knowledge that may eventually reach the public - and shape society; therefore, Frontiers only applies the most rigorous and unbiased reviews.
Frontiers revolutionizes research publishing by freely delivering the most outstanding research, evaluated with no bias from both the academic and social point of view. By applying the most advanced information technologies, Frontiers is catapulting scholarly publishing into a new generation.

What are Frontiers Research Topics?

Frontiers Research Topics are very popular trademarks of the Frontiers Journals Series: they are collections of at least ten articles, all centered on a particular subject. With their unique mix of varied contributions from Original Research to Review Articles, Frontiers Research Topics unify the most influential researchers, the latest key findings and historical advances in a hot research area! Find out more on how to host your own Frontiers Research Topic or contribute to one as an author by contacting the Frontiers Editorial Office: frontiersin.org/about/contact

BIOFABRICATION AND BIOPOLYMERIC MATERIALS INNOVATION FOR MUSCULOSKELETAL TISSUE REGENERATION

Topic Editors:
Farnaz Ghorbani, University of Erlangen Nuremberg, Germany
Chaozong Liu, University College London, United Kingdom
Derek H. Rosenzweig, McGill University, Canada
Megan Elin Cooke, McGill University, Canada

Citation: Ghorbani, F., Liu, C., Rosenzweig, D. H., Cooke, M. E., eds. (2022). Biofabrication and Biopolymeric Materials Innovation for Musculoskeletal Tissue Regeneration. Lausanne: Frontiers Media SA. doi: 10.3389/978-2-88974-989-8

Table of Contents

frontiers | Frontiers in Bioengineering and Biotechnology

EDITORIAL
published: 24 May 2022
doi: 10.3389/fbioe.2022.909577

Editorial: Biofabrication and Biopolymeric Materials Innovation for Musculoskeletal Tissue Regeneration

Megan E. Cooke[1]*, *Derek H. Rosenzweig*[2], *Chaozong Liu*[3] and *Farnaz Ghorbani*[4]

[1]BioFrontiers Institute, University of Colorado at Boulder, Boulder, CO, United States, [2]Department of Surgery, The Research Institute of McGill University Health Centre, McGill University, Montreal, QC, Canada, [3]Institute of Orthopaedic and Musculoskeletal Science, Royal National Orthopaedic Hospital, University College London, London, United Kingdom, [4]Institute of Biomaterials, University of Erlangen-Nuremberg, Erlangen, Germany

Keywords: bioprinting, biofabrication, biomaterials, biopolymers, tissue engineering, musculoskeletal

Editorial on the Research Topic

Biofabrication and Biopolymeric Materials Innovation for Musculoskeletal Tissue Regeneration

The human musculoskeletal system provides form, support, stability, and movement to the body. It is made up of the bones of the skeleton, muscles, cartilage, tendons, ligaments, joints, and other connective tissues. The primary functions of the musculoskeletal system include supporting the body, allowing motion, and protecting vital organs. The skeletal portion of the system serves as the main storage system for calcium and phosphorus and contains critical components of the hematopoietic system (Li and Niu, 2020). Musculoskeletal Disorders (MSDs) include injuries and diseases that primarily affect the movement of the human body. They are characterized by pain and limitations in mobility, dexterity, and overall level of functioning, reducing patients' ability to work and maintain a good quality of life. A recent analysis of Global Burden of Disease data showed that approximately 1.71 billion people globally have musculoskeletal conditions (Woolf and Pfleger, 2003). MSDs such as osteoarthritis, rheumatoid arthritis, psoriatic arthritis, gout, and ankylosing spondylitis affect joints (McInnes and Schett, 2011; Loeser et al., 2012; Litwic et al., 2013); osteoporosis, osteopenia and associated fragility fractures, as well as traumatic fractures, affect bones (Florencio-Silva et al., 2015); sarcopenia affects muscles, and back and neck pain affect the spine of the human body.

Tissue engineering is a concept whereby cells are taken from a patient, their number is then expanded before being seeded on a biomaterial scaffold. The appropriate stimuli (chemical, biological, mechanical and electrical) are applied, and new tissue is formed over time. This new tissue is then implanted to help restore function for the patient (Liu et al., 2007). To achieve the repair and regeneration of musculoskeletal tissues is still a challenge that requires the combined effort of biomaterials scientists, tissue biologists, and engineers. Material selection is critical to ensuring that cell-seeded tissue constructs have appropriate mechanical and biological environments.

Biopolymers are natural materials derived from plants and animals including polysaccharides such as alginate, chitosan, hyaluronic acid, and polypeptides such as gelatin, silk fibroin and elastin. Many biopolymers have properties such as cell adhesion and degradability and form highly swollen networks that provide physiologically relevant environments for cell culture (Muir and Burdick, 2021). Biopolymers can also be chemically functionalised to bring about control over their cell-binding and cross-linking capabilities (Muir and Burdick, 2021). In TE of soft MSK tissues, such as cartilage, ligaments and intervertebral discs biopolymer hydrogels have been extensively used as they provide a highly hydrated 3D matrix for these largely avascular tissues (Kesti et al., 2015). Bone is the hard tissue of the musculoskeletal system and is a commonly investigated tissue for regeneration. Tissue engineering approaches are usually combinatorial between hard and soft materials to produce

OPEN ACCESS

Edited and reviewed by:
Hasan Uludag,
University of Alberta, Canada

***Correspondence:**
Megan E. Cooke
megan.cooke.research@gmail.com

Specialty section:
This article was submitted to Biomaterials, a section of the journal Frontiers in Bioengineering and Biotechnology

Received: *31 March 2022*
Accepted: *15 April 2022*
Published: *24 May 2022*

Citation:
Cooke ME, Rosenzweig DH, Liu C and Ghorbani F (2022) Editorial: Biofabrication and Biopolymeric Materials Innovation for Musculoskeletal Tissue Regeneration. Front. Bioeng. Biotechnol. 10:909577. doi: 10.3389/fbioe.2022.909577

composite scaffolds for cell attachment with load-bearing capacity, and often osteogenic or osseointegrative cues.

A common material for spinal cages is PEEK (polyether-ether-ketone) but the lack of osseointegration is a concern. Li et al. produced a nanohydroxyapatite/polyamide 66 composite which showed better osseointegration, as demonstrated by push-out tests in a rabbit femoral condyle model. Higher forces required to push out the new composite indicate better bone-implant integration. Ghorbani et al. developed polydopamine microspheres with unique, pomegranate-like morphology. Using self-oxidative polymerization of dopamine hydrochloride and precise pH control, porous microspheres were produced from agglomerated nanospheres. Molecular calculations then demonstrated that this material could interact with BMP2, Decorin, and Matrilin-1, enabling the formation of a protein layer that could be utilised in bone and cartilage tissue engineering. Polyhydroxyalkanoates are biopolyesters produced by microbes under unbalanced culture conditions. Their biocompatibility and biodegradability *in vivo* make them attractive materials for tissue engineering. Li et al., review their synthesis, properties and applications in bone tissue engineering, including manufacturing through 3D printing.

Musculoskeletal tissues have mechanical functions, so introducing mechanical loading during culture is used to increase extracellular matrix production in tissue-engineered constructs. Hart et al. present a perspective on the challenges of regenerating these tissues that natively reside in unique biomechanical environments. A key takeaway is that anabolic cues are present in the growth and maturation of these tissues, so replicating the *in vivo* loading environment during the maturation of a tissue construct *in vitro* is likely to be beneficial. Loading regimes in cartilage TE were reviewed by Sardroud et al., in the context of undesirable fibrocartilage formation. Collagen type II is found in native cartilage, but there is usually a combination of collagen types I and II in tissue-engineered cartilage. This forms fibrocartilage, a mechanically inferior form of cartilage. Of particular interest is the literature on the mechanotransduction pathways that lead to this fibrocartilage formation. Ge et al. studied the effects of mechanical compression in driving chondrogenesis in agarose hydrogels. They found that dynamic mechanical loading of synovial MSC-agarose constructs on day 1 of culture resulted in unwanted markers, but when loaded on day 21 expression of chondrocyte-specific markers was increased and hypertrophy markers were decreased. The host body response of tissue-engineered cartilage was reviewed by Wei et al. Most implanted materials will activate a response from the innate and adaptive immune systems. This guides a remodelling process that when understood may be beneficial to promoting cartilage regeneration and better integration of implanted tissue constructs. The authors consider synthetic and natural biomaterials, including a strong rationale for the use of a decellularized extracellular matrix to remove immune components that would otherwise cause a negative implantation response. Biopolymers for tissue engineering of other connective tissues were also investigated in this Research Topic. Li et al. reviewed advances in materials for intervertebral disk regeneration. These include polymers such as chitosan and collagen that, in combination with growth factors and cell transplantation show promise for endogenous regeneration. Kang et al. investigated polydopamine as a coating to immobilise BMP-2 on PET scaffolds for ligament tissue engineering. Modified grafts significantly improved bone integration in a rabbit model compared to PET alone.

Bioprinting, defined as "*the use of computer-aided transfer processes for patterning and assembling living and non-living materials with a prescribed 2D or 3D organization in order to produce bioengineered structures serving in regenerative medicine, pharmacokinetic and basic cell biology studies*" (Guillemot et al., 2010) is a rapidly growing field of tissue engineering. Bioprinting gives exceptional control over the spatial deposition of materials, cells, and other factors to enable the production of both implantable materials as well as *in vitro* tissue models for personalized medicine and drug screening applications (Cooke and Rosenzweig, 2021). Importantly the use of an additive manufacturing process enables the production of patient-specific geometries without the use of traditional subtractive manufacturing processes. Biomaterial inks, used as materials in bioprinting, must meet specific rheological parameters to ensure extrudability as well as rapid shape recovery to produce high fidelity constructs. With the addition of cells and other biological materials, the term bioink is used to describe these materials (Groll et al., 2018). Through bioink and application developments, bioprinting has been applied to a range of tissue-like constructs including soft, hard, and interfacing musculoskeletal tissues (Moxon et al., 2017; Alcala-Orozco et al., 2020).

Several articles in this issue consider the use of bioprinting for connective musculoskeletal tissues. Aerosol jet printing was employed by Gibney and Ferraris to produce droplets of collagen types I and II with size ranges less than 5 um. These were then extruded through a nozzle to print dense scaffolds, 576 layers high that resulted in aligned scaffolds post-neutralization. These dense scaffolds strongly replicate the native dense ECM of connective tissues. In another connective tissue study by Li et al., a PCL template scaffold was printed before being injected with a meniscal extracellular matrix. The addition of kartogenin-loaded microspheres was shown to increase chondrogenesis of synovium-derived MSCs *in vitro*. Increased secretion of total collagen and aggrecan show that this is a promising scaffold for meniscal tissue engineering. Lan et al. produced a bioink of meniscal fibrochondrocytes in a TEMPO-oxidized alginate. Following rheological characterization to optimize the formulation, they were printed into discs and cultured in low oxygen conditions to mimic the avascular meniscus environment. Histologically and biochemical analyses showed that compared to collagen type I control constructs, the TEMPO-alginate scaffolds had significantly higher COL2A1 expression and more meniscal-like phenotypes. There was clear increased production of aggrecan histologically in the TEMPO scaffolds. A review of recent trends in biofabrication for skeletal muscle disease modelling investigated the other aspect of bioprinting technology, to investigate diseases in more physiologically relevant culture systems than common 2D monolayer cultures.

Cho and Jang discuss studies that encourage uniaxial cell alignment, as is observed in skeletal muscle, and how different biofabricated *in vitro* models have been used to replicate muscular dystrophies and inflammatory diseases.

There are still many challenges facing clinical translation of bioprinted tissues/organs such as bone, cartilage, muscle, or ligaments/tendons. Two main challenges include mechanical integrity and vascularization of generated tissues. Much progress is being made using gel-in-gel printing strategies to incorporate vasculature in bioprinted tissues. However, mechanical integrity is often overlooked. Current gold standard treatments of autografts and allografts (e.g., ligament and bone) consider mechanics and nutrient supply to the tissue. Prostheses for total joint replacement do not require vascularization but possess appropriate biomechanical properties. Therefore, the future of bioprinted tissues for MSK repair and regeneration will depend on the advancement of tissue maturation with increased mechanical strength, and improved methods for vascularization for nutrient supply upon implantation. Much progress has been made in scaffold design and compartmentalization but fully functional human anatomic biofabricated organs are still perhaps many years away from being realized. Perhaps the most practical current use of bioprinted human MSK-like constructs lies in screening novel therapeutics and better understanding the mechanisms of disease. Nonetheless, the emergence of bioprinting is an inspiring and exciting advance in the field of tissue engineering.

AUTHOR CONTRIBUTIONS

All authors listed have made a substantial, direct, and intellectual contribution to the work and approved it for publication.

REFERENCES

Alcala-Orozco, C. R., Mutreja, I., Cui, X., Kumar, D., Hooper, G. J., Lim, K. S., et al. (2020). Design and Characterisation of Multi-Functional Strontium-Gelatin Nanocomposite Bioinks with Improved Print Fidelity and Osteogenic Capacity. *Bioprinting* 18, e00073. doi:10.1016/j.bprint.2019.e00073

Cooke, M. E., and Rosenzweig, D. H. (2021). The Rheology of Direct and Suspended Extrusion Bioprinting. *Apl. Bioeng.* 5, 011502. doi:10.1063/5.0031475

Florencio-Silva, R., Sasso, G. R. d. S., Sasso-Cerri, E., Simões, M. J., and Cerri, P. S. (2015). Biology of Bone Tissue: Structure, Function, and Factors that Influence Bone Cells. *BioMed Res. Int.* 2015, 1–17. doi:10.1155/2015/421746

Groll, J., Burdick, J. A., Cho, D.-W., Derby, B., Gelinsky, M., Heilshorn, S. C., et al. (2018). A Definition of Bioinks and Their Distinction from Biomaterial Inks. *Biofabrication* 11, 013001. doi:10.1088/1758-5090/aaec52

Guillemot, F., Mironov, V., and Nakamura, M. (2010). Bioprinting Is Coming of Age: Report from the International Conference on Bioprinting and Biofabrication in Bordeaux (3B'09). *Biofabrication* 2, 010201. doi:10.1088/1758-5082/2/1/010201

Kesti, M., Eberhardt, C., Pagliccia, G., Kenkel, D., Grande, D., Boss, A., et al. (2015). Bioprinting Complex Cartilaginous Structures with Clinically Compliant Biomaterials. *Adv. Funct. Mat.* 25, 7406–7417. doi:10.1002/adfm.201503423

Li, G., and Niu, W. (2020). "Challenges toward Musculoskeletal Injuries and Diseases," in *Nanoeng. Musculoskelet. Regen.* (Academic Press), 1–41. doi:10.1016/b978-0-12-820262-3.00001-3

Litwic, A., Edwards, M. H., Dennison, E. M., and Cooper, C. (2013). Epidemiology and Burden of Osteoarthritis. *Br. Med. Bull.* 105, 185–199. doi:10.1093/bmb/lds038.Epidemiology

Liu, C., Xia, Z., and Czernuszka, J. T. (2007). Design and Development of Three-Dimensional Scaffolds for Tissue Engineering. *Chem. Eng. Res. Des.* 85, 1051–1064. doi:10.1205/cherd06196

Loeser, R. F., Goldring, S. R., Scanzello, C. R., and Goldring, M. B. (2012). Osteoarthritis: A Disease of the Joint as an Organ. *Arthritis & Rheumatism* 64, 1697–1707. doi:10.1002/art.34453

McInnes, I. B., and Schett, G. (2011). The Pathogenesis of Rheumatoid Arthritis. *N. Engl. J. Med.* 365, 2205–2219. doi:10.1056/NEJMRA1004965

Moxon, S. R., Cooke, M. E., Cox, S. C., Snow, M., Jeys, L., Jones, S. W., et al. (2017). Suspended Manufacture of Biological Structures. *Adv. Mat.* 29, 1605594–1605596. doi:10.1002/adma.201605594

Muir, V. G., and Burdick, J. A. (2021). Chemically Modified Biopolymers for the Formation of Biomedical Hydrogels. *Chem. Rev.* 121, 10908–10949. doi:10.1021/acs.chemrev.0c00923

Woolf, A. D., and Pfleger, B. (2003). Burden of Major Musculoskeletal Conditions. *Bull. World Health Organ.* 81, 646–656.

Conflict of Interest: The authors declare that the research was conducted in the absence of any commercial or financial relationships that could be construed as a potential conflict of interest.

frontiers in Bioengineering and Biotechnology

ORIGINAL RESEARCH
published: 30 April 2021
doi: 10.3389/fbioe.2021.662381

3D Printed Poly(ε-Caprolactone)/Meniscus Extracellular Matrix Composite Scaffold Functionalized With Kartogenin-Releasing PLGA Microspheres for Meniscus Tissue Engineering

*Hao Li[1,2†], Zhiyao Liao[1,2†], Zhen Yang[1,2], Cangjian Gao[1,2], Liwei Fu[1,2], Pinxue Li[1,2], Tianyuan Zhao[1,2], Fuyang Cao[1,3], Wei Chen[1,2], Zhiguo Yuan[4], Xiang Sui[1], Shuyun Liu[1] and Quanyi Guo[1,2]**

[1] Institute of Orthopedics, The First Medical Center, Chinese PLA General Hospital, Beijing Key Lab of Regenerative Medicine in Orthopedics, Key Laboratory of Musculoskeletal Trauma and War Injuries PLA, Beijing, China, [2] School of Medicine, Nankai University, Tianjin, China, [3] Department of Orthopedics, The First Affiliated Hospital of Zhengzhou University, Zhengzhou, China, [4] Department of Bone and Joint Surgery, Renji Hospital, School of Medicine, Shanghai Jiao Tong University, Shanghai, China

OPEN ACCESS

Edited by:
Farnaz Ghorbani,
Fudan University, China

Reviewed by:
Katayoun Nazemi,
Amirkabir University of Technology, Iran
Soodeh Abasloo,
Sahand University of Technology, Iran

***Correspondence:**
Quanyi Guo
doctorguo_301@163.com

[†] These authors have contributed equally to this work

Specialty section:
This article was submitted to Biomaterials, a section of the journal Frontiers in Bioengineering and Biotechnology

Received: 01 February 2021
Accepted: 22 March 2021
Published: 30 April 2021

Citation:
Li H, Liao Z, Yang Z, Gao C, Fu L, Li P, Zhao T, Cao F, Chen W, Yuan Z, Sui X, Liu S and Guo Q (2021) 3D Printed Poly(ε-Caprolactone)/Meniscus Extracellular Matrix Composite Scaffold Functionalized With Kartogenin-Releasing PLGA Microspheres for Meniscus Tissue Engineering. Front. Bioeng. Biotechnol. 9:662381. doi: 10.3389/fbioe.2021.662381

Meniscus tissue engineering (MTE) aims to fabricate ideal scaffolds to stimulate the microenvironment for recreating the damaged meniscal tissue. Indeed, favorable mechanical properties, suitable biocompatibility, and inherent chondrogenic capability are crucial in MTE. In this study, we present a composite scaffold by 3D printing a poly(ε-caprolactone) (PCL) scaffold as backbone, followed by injection with the meniscus extracellular matrix (MECM), and modification with kartogenin (KGN)-loaded poly(lactic-co-glycolic) acid (PLGA) microsphere (μS), which serves as a drug delivery system. Therefore, we propose a plan to improve meniscus regeneration via KGN released from the 3D porous PCL/MECM scaffold. The final results showed that the hydrophilicity and bioactivity of the resulting PCL/MECM scaffold were remarkably enhanced. *In vitro* synovium-derived mesenchymal stem cells (SMSCs) experiments suggested that introducing MECM components helped cell adhesion and proliferation and maintained promising ability to induce cell migration. Moreover, KGN-incorporating PLGA microspheres, which were loaded on scaffolds, showed a prolonged release profile and improved the chondrogenic differentiation of SMSCs during the 14-day culture. Particularly, the PCL/MECM-KGN μS seeded by SMSCs showed the highest secretion of total collagen and aggrecan. More importantly, the synergistic effect of the MECM and sustained release of KGN can endow the PCL/MECM-KGN μS scaffolds with not only excellent cell affinity and cell vitality preservation but also chondrogenic activity. Thus, the PCL/MECM-KGN μS scaffolds are expected to have good application prospects in the field of MTE.

Keywords: PCL, meniscus extracellular matrix, kartogenin, 3D printing, meniscus tissue engineering

INTRODUCTION

The meniscus plays a crucial role in protecting articular cartilage and maintaining joint congruence (Fox et al., 2012, 2015). However, the meniscus damage caused by sports injuries, trauma, and aging may eventually lead to articular cartilage loss and symptomatic osteoarthritis (OA) (Englund et al., 2012; Bilgen et al., 2018). Surgical treatments involving arthroscopic meniscectomy and meniscal allograft transplantation (MAT) are the primary approaches in clinical practice but still present drawbacks (Li H. et al., 2020). Recently, tissue-engineered scaffolding strategies have become one of the mainstream choices in meniscus therapeutic field (Kwon et al., 2019). To date, a wide range of biomaterials, such as synthetic polymers, natural polymers, and tissue-derived materials, have been utilized to fabricate tissue-engineered meniscal scaffold (Makris et al., 2011). Nevertheless, it is well known that meniscus is an anisotropic complex composed of zonal cell phenotypes and extracellular matrix (ECM), which make it hard to mimic microenvironment, hierarchical structure, and morphology of native meniscus (Lee et al., 2014; Zhang et al., 2019). Hence, the construction of a structurally and functionally optimized scaffold with biomimetic microenvironmental characteristics of native meniscus is of great significance for meniscus regeneration.

As a scaffold for MTE, the suitable porous structure is urgently important with regard to the necessity of cell infiltration and growth (Zhang et al., 2016). 3D printing is a promising technology that is capable of individually and accurately manufacturing complex structures (Zhu et al., 2020). Fuse deposition modeling (FDM) has been widely used among these technologies owing to its convenient operation and favorable accuracy (Ngo et al., 2018). Considering the suitable polymers for FDM, poly (ε-caprolactone) (PCL), a kind of biodegradable aliphatic polyester with excellent biocompatibility and mechanical properties, has been utilized as the choice in melt-based extrusion printing systems owing to its proper melting temperature (60°C) and rheological and viscoelastic properties (Visser et al., 2013; Malikmammadov et al., 2018). However, the limited resolution of 3D printed scaffold could not construct an ECM-mimicking porous structure alone. Furthermore, poor hydrophilicity and lack of biochemical cues, as well as avoiding abrasion of the articular cartilage, make the PCL scaffolds require the addition of complementary materials to enhance the biological functions and reduce the frictional force between the scaffold and cartilage to a certain extent. Therefore, the combination of additional materials to form macro–microstructure with improved biological functions has been utilized as an important strategy in tissue engineering (Giannitelli et al., 2015; Zhu et al., 2020).

According to the literature, decellularized extracellular matrix-combined scaffold exhibited more excellent cell adhesion and marked differentiation potential, which was due to its ability to recapitulate most features of natural ECM and regulate cell fate (Cunniffe et al., 2019; Hussey et al., 2018). In addition, decellularized extracellular matrix-only scaffolds possess dissatisfactory mechanical strength, which limits their application in MTE (Li H. et al., 2020). Thus, the construction of hybrid scaffolds with fiber-reinforced structure and biomimetic ECM is of great significance in the treatment of meniscus injuries. Our team has previously demonstrated the regenerative potential of the 3D printing PCL scaffolds infused with meniscus extracellular matrix (MECM) and alginate, from which the meniscal fibrochondrocyte-loaded hybrid scaffold presented promising meniscus regeneration in the rabbit meniscectomy model (Chen et al., 2019). Given that the PCL scaffolds are not adequate to recreate an instructive microenvironment for cell growth and tissue regeneration, incorporating MECM as a bioactive material into the PCL scaffold not only can achieve a macro-/microporous hierarchical structure but also conducive to cell migration and infiltration, and may subsequently be capable enough to promote the neo-meniscal tissue formation.

In addition to biocompatibility, mechanical strength, and porous structure, the potent activity to induce stem cells to differentiate into cartilaginous cells also is essential for MTE scaffolds (Liu et al., 2019). Kartogenin (KGN), a small heterocyclic compound, is known for its prochondrogenic activity on MSCs of humans, rabbits, and rats. The introduction of KGN into the defect area may ideally induce endogenous stem/progenitor cells (ESPCs) to differentiate into cartilage cells. However, the uncontrolled delivery of bioactive factors may limit reparative potentials and cause further unwanted side effects (Yang et al., 2020). In the present study, when therapeutic drugs were intra-articularly injected into the joint, retention of these bioactive factors is relatively short and ineffective, which is mainly owing to their small molecular size (Patel et al., 2019). Therefore, the management of meniscus damages would be significantly enhanced with localized and sustained delivery of bioactive factors (Li H. et al., 2020). Liu et al. (2019) reported that injection of KGN directly into the meniscal wound area could not maintain enough concentration of this drugs for wound healing; however, a platelet-rich plasma (PRP) gel acted as a good carrier for KGN delivery and achieved augmented reparative results *in vivo*. In the study present, the development of drug delivery approaches in MTE is relatively short of examples. Therefore, there is an urgent need to develop such novel drug delivery systems (DDSs) for the sustained release of bioactive factors for meniscus regeneration. It is well known that poly(lactic-co-glycolic) acid (PLGA) microparticles are excellent DDSs to improve drug pharmacokinetics and pharmacodynamics (Martins et al., 2018). Therefore, we aim to use PLGA microparticles to improve KGN-releasing characteristics and, consequently, facilitate chondrogenesis, and achieve desired therapeutic results on meniscus defects.

The main objective of this study is to fabricate biomimetic PCL/MECM scaffolds with a controlled drug delivery system to mimic an ideal microenvironment for chondrogenesis both *in vitro* and *in vivo*. We first proposed to fabricate a composite scaffold with a fibrous hierarchical structure by utilizing 3D printing PCL scaffold as a mechanical support and MECM as a natural microenvironment for cell migration and internal infiltration. Moreover, introducing MECM components can also be expected to benefit the proliferation and cartilage matrix formation. Then, bioactive KGN was chosen to further functionalize the PCL/MECM scaffold through a

PLGA microsphere (μS). The physicochemical properties of the as-prepared composite scaffolds including morphology, composition, hydrophilicity, mechanical properties, and the release profile of KGN were studied. Moreover, the biocompatibility, promigration property and chondrogenic activity of the scaffolds were also systematically evaluated. At last, we used PCL/MECM-KGN μS scaffolds to repair meniscus defects in a rabbit model, and the regenerated effects were presented and discussed. Based on such studies, it is believed that the KGN-functionalized PCL/MECM scaffolds with hierarchical structure, excellent biocompatibility, enhanced migration and chondrogenesis will be ideal substitutes for meniscus regeneration.

MATERIALS AND METHODS

Preparation of the Scaffolds

Preparation of KGN μS

Kartogenin-loaded PLGA μS were prepared using oil-in-water (O/W) emulsion-solvent evaporation method as previously described (Wang et al., 2019; Asgari et al., 2020). In detail, 120 mg of PLGA (Daigang Biomaterial, Jinan, China) was dissolved in 2 ml of dichloromethane and then added with 2 ml mixed solution of dimethyl sulfoxide (DMSO) and dichloromethane (v/v = 1:4) containing 4 mg of KGN (Sigma-Aldrich, United States). Then, the primary emulsion was generated via an ultrasonic homogenizer (Qsonica Q125, United States) operating at an amplitude of 60% (power of 75 W) for 30 s. After this, the resultant emulsion was immediately added to 40 ml 1% (w/v) PVA solution and magnetically stirred for 12 h at room temperature to volatilize dichloromethane. After these steps, KGN μS were washed five times with distilled water and freeze dried overnight for collection (**Figure 1**). The KGN-free μS were fabricated following the same procedure. To determine the encapsulation efficiency (EE) of the KGN μS, the final amount of KGN in supernatants was detected by monitoring the absorbance at 287.4 nm using calculated UV spectrophotometry (Beckman, Fullerton, CA, United States) based on a pre-established KGN standard curve (**Supplementary Figure 1**). Then, the amount of KGN in final PLGA μS was indirectly determined by measuring the amount of KGN that remained in the PVA solution; subsequently, the amount of KGN entrapped into the microspheres was calculated according to the following formulae:

$$EE = \frac{Total amount of\ KGN\ added - Amount\ of\ free\ KGN\ after\ entrapment}{Total\ amount\ of\ KGN\ added} \times 100\%$$

Fabrication of MECM

Decellularized MECM slurry was physicochemically prepared from swine menisci as described previously with some modifications (Yuan et al., 2016). Briefly, the menisci were harvested from a swine knee joint and washed with phosphate-buffered saline (PBS, Sigma, United States) and sterilizing with 3% hydrogen peroxide (H_2O_2, Sigma-Aldrich, United States). The minced menisci were treated with pepsin and acetic acid (Sigma Aldrich, United States) and homogenized at 4°C (Kinematica AG, Lucerne, Switzerland). These meniscal tissues were decellularized according to the differential centrifugation methods adopted at 2000 rpm for 10 min, 6000 rpm for 30 min, and 10,000 rpm for 30 min. These procedures were repeated five times to achieve decellularization, and the decellularized MECM slurry was stored at 4°C for later use (**Figure 1**).

Fabrication of PCL, PCL/MECM, and KGN μS Incorporated PCL/MECM Scaffolds

The pure PCL scaffolds were designed with CAD using Mimics 17.0 software to export in STL format and then fabricated using a 3D layer-by-layer fused deposition modeling (FDM) printer (FUNMAT, INTAMSYS TECHNOLOGY, China). In detail, PCL (Mw = 45,000, Sigma, United States) beads were put into the printing chamber and preheated at 90°C. The melt PCL were extruded through a heated metal nozzle (diameter, 0.25 mm) at a printing speed of 220 mm/min and finally deposited onto a receiving platform with a lay-down patten of 0°/90°/180° along the *z*-axis. Subsequently, the PCL scaffold with a fiber diameter of 250 μm and filament gap of 500 μm was produced. Then, freeze-dried KGN μS were incorporated into MECM gel with a ratio of 20 mg/ml to form KGN μS-containing MECM gels. Lastly, the PCL scaffolds were injected with liquid MECM slurry (2% w/v) with or without KGN μS and put into an ultrasonicator for another 2 h and subsequently lyophilized for collection. Finally, PCL/MECM and PCL/MECM-KGN μS scaffolds were crosslinked using carbodiimide solution [14 mM 1-ethyl-3-(3-dimethylaminopropyl) carbodiimide hydrochloride (EDAC) and 5.5 mM N-hydroxysuccinimide (NHS); Sigma] for 2 h and sterilized using ethylene oxide. All scaffolds for *in vivo* implantation were formed by crescent-shaped molds.

Analysis of Microparticles

We incorporated goat antimouse immunoglobulin G (IgG) Alexa Fluor 594 secondary antibody into PLGA microspheres to investigate the drug distribution in the microspheres, and these microspheres were observed under a fluorescence microscope with excitation wavelengths of 565 nm. The fluorescence images of the microparticles were captured. To observe the shape and surface morphology of KGN-containing PLGA microspheres, the freeze-dried KGN μS were uniformly coated on the surface of the conductive adhesive of the sample table and observed by a scanning electron microscope [S-4800 field emission scanning electron microscope (SEM); Hitachi, Tokyo, Japan]. In order to measure the average size of the microspheres, pictures of three independent microparticle samples were captured, and ImageJ (United States) was used to calculate and present the average particle size distribution.

Characterization of Scaffolds

Biochemical Analysis and Histological Staining

The prepared MECM was biochemically analyzed for total DNA, GAG, and collagen content, respectively. The DNA of MECM sample was extracted using the TIANamp Genomic DNA kit (TIANamp, Beijing, China) and then measured by the PicoGreen DNA assay kit (Invitrogen, Carlsbad, CA, United States). The content of GAG was estimated by using the Tissue GAG Total Content DMMB Colorimetry kit (Genmed

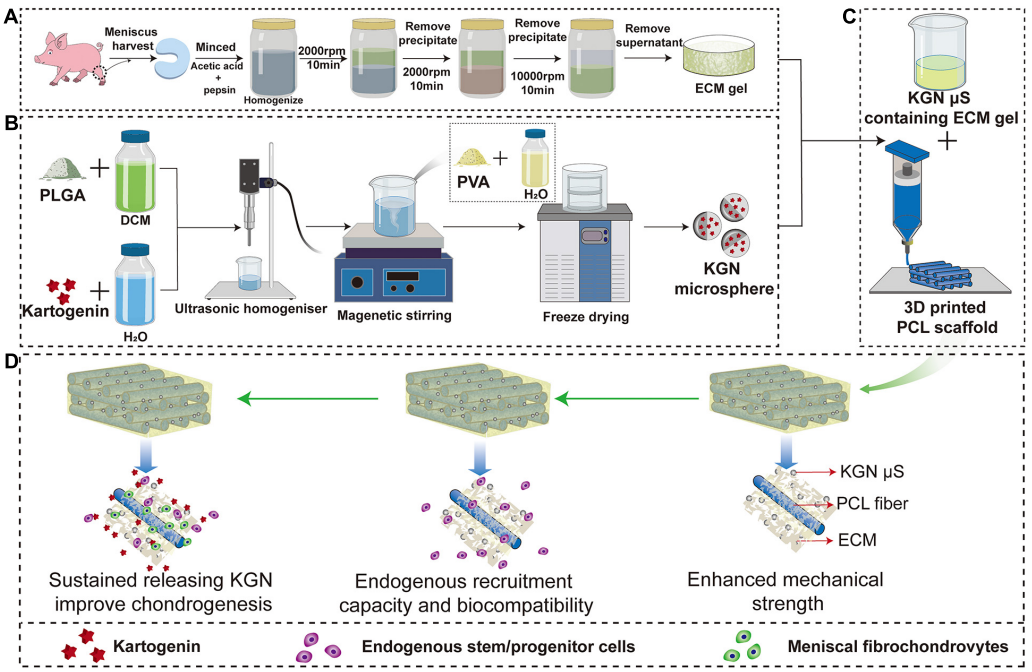

FIGURE 1 | Schematic representation of the preparation process of the scaffolds. Flow chart of the preparation of the **(A)** MECM gel, **(B)** KGN-containing PLGA microspheres and **(C)** PCL/MECM-KGN μS scaffold; **(D)** Possible mechanism of meniscus regeneration. Enhanced mechanical strength, endogenous stem cells and sustained releasing KGN contributed to meniscus regeneration in these experiments. Abbreviations: MECM, meniscus extracellular matrix; KGN, kartogenin; PLGA, poly(lactic-co-glycolic) acid; μS, microspheres.

Scientific Inc., Shanghai, China). The hydroxyproline assay kit (Nanjing Jiancheng, Jiangsu, China) was used to quantify collagen content. For histological assessment, 4′,6-diamidino-2-phenylindole (DAPI) and hematoxylin and eosin (H&E) staining were used to detect nucleic acids. Toluidine blue (TB) and Safranin O staining were used to determine the GAG content. The collagen distribution was identified by Sirius red staining.

Scanning Electron Microscopy

Scanning Electron Microscopy (S-4800 field emission scanning electron microscope; Hitachi, Tokyo, Japan) was performed to observe the morphological microstructure of KGN μS, PCL scaffolds, PCL/MECM scaffolds, and PCL/MECM-KGN μS scaffolds, respectively. Before this step, all samples were lyophilized for 24 h and then coated with Au.

Fourier Transform Infrared Spectroscopy

A Bruker Tensor 27 Fourier transform infrared (FTIR) spectrometer (Nicolet IS5, Germany) was used to identify the functional groups in PCL, MECM, and PCL-ECM scaffolds. Samples were cut to a size of 10 mm × 10 mm and used for conducting FTIR analysis in a reflection mode. All spectra were recorded between 4000 and 1000 cm^{-1} at a resolution of 1 cm^{-1}.

Pore Size Distribution and Porosity Measurement

A mercury porosimeter (Micromeritics AutoPore IV 9500, United States) was used to determine pore geometry and pore volume of PCL/MECM and PCL/MECM-KGN μS scaffolds, respectively. First, the samples were completely evacuated to remove air. Then, porosimetry experiments were conducted with an equilibration time of 10 s, and mercury was forced into the pores with increasing pressure from 0.10 to 30,000 psia; after that, the pressure was reduced incrementally back to atmospheric pressure. For each group, about 0.015 g of the samples was analyzed with a 3-ml penetrometer.

Mechanical Testing

Scaffold samples were prepared into different sizes for mechanical testing. The 5 × 5 × 3 mm samples were used for the compression tests, which were performed using a BOSE biomechanical testing machine (BOSE 5100; TE Instruments, New Castle, DE, United States). For tensile strength, 4 × 10 2 mm specimens were measured using a uniaxial materials testing machine (Model 5969; Instron, High Wycombe, United Kingdom). The compression and tensile moduli were calculated according to the slope of the linear fit to the strain–stress curves. All tests included three parallel replicates for each group.

Hydrophilic Characteristic

Dynamic contact angle measurement was conducted to assess the scaffolds' hydrophilic properties by using optical contact angle measuring and contour analysis systems (Dataphysics OCA20, Germany). Briefly, a droplet of deionized water was dropped on the sample surface, and the contact angle was captured and calculated at four time points (1, 5, 15, and 30 s) at room temperature, and five parallel sites of samples were used to analyze each group.

The Release of KGN From the Scaffolds

The lyophilized PCL/MECM-KGN μS scaffolds were soaked in 10 ml of PBS solution, which was shaken with 80 rpm for 28 days at 37°C. At each sampling time, 2 ml of PBS was removed by centrifugation and replaced by fresh PBS with the same amount. The supernatants were stored at −20°C until measured. The total amount of released KGN on the PCL/MECM-KGN μS scaffolds was checked by UV spectrophotometry (Beckman, Fullerton, CA, United States) at 278.4 nm based on a standard curve (**Supplementary Figure 1**).

In vitro Cytocompatibility Studies

In vitro SMSCs Culture

Synovium-derived mesenchymal stem cells were isolated and cultured as previously described with slight modification (Moriguchi et al., 2013; Li Z. et al., 2020). In brief, the synovial tissue was obtained from the rabbit joint and thoroughly washed three times with PBS containing 1% penicillin–streptomycin (Sigma, United States) and then meticulously minced and digested with 0.25% collagenase (Gibco, United States) in Dulbecco's modified Eagle's medium/F12 (Corning, United States) in the incubator for 2 h at 37°C. After neutralization with Dulbecco's modified Eagle's medium (DMEM)/F12 with 10% fetal bovine serum (Gibco, United States), the cells were centrifuged at 1500 rpm for 10 min for collection and finally resuspended in growth medium and subsequently cultured in 25-cm^2 flasks (Corning, United States). After 90% confluence was reached, the cells were progressed to passage after cell fusion, and passage 3 of SMSCs was used to conduct the following studies.

Cell Viability

The viability of SMSCs seeded onto the different scaffolds was assessed using a Live/Dead assay (Beyotime, China). Cell/scaffold composites were cultured for 4 days and then stained using a Live/Dead assay according to the manufacturer's instructions. Briefly, 400 μl staining solution containing 2 mM calcein AM and 4 mM ethidium homodimer-1 was added to the cell/scaffold composites and incubated for 30 min at 37°C in the dark. The samples were then washed twice in PBS buffer solution for 5 min. Cells that were alive (stained green) and dead (stained red) and their distribution were observed and captured using a confocal laser scanning microscope (Leica, Germany). Cell viability was measured according to the following formula: (live cells/total cells) × 100% (n = 5).

Cell Proliferation

For cell proliferation assays, SMSCs were seeded on the scaffolds (2×10^4 cells/sample) in wells of a 24-well plate and incubated for 4 h to allow for cell attachment; then, the cell/scaffold composites were transferred to another 24-well plate and cultured for 1, 3, and 7 days, respectively. In testing time point, the scaffold with cells were relocated to a new culture plate with 10% Cell Counting Kit-8 (CCK-8) work solution at 37°C and 5% CO_2 incubator for 1 h. Subsequently, the optical density (OD) of the sample solutions (n = 4 per group) at 450 nm were measured by a microplate reader (Beckman, Fullerton, CA, United States).

Cell Adhesion and Spreading

Cell adhesion and morphology of SMSCs grown on these three groups of scaffolds were assessed by SEM and phalloidin-rhodamine and DAPI staining. P3 SMSCs (2×10^5) were inoculated in different scaffolds and incubated at 37°C with 5% CO_2 for 3 days. The cell/scaffold composites were removed and fixed with 4% paraformaldehyde for 30 min, then permeabilized with 0.3% Triton X-100 for 10 min, followed with bovine serum albumin (BSA) blockage and PBS rinse; phalloidin-rhodamine was added to stain the cytoskeletal protein F-actin overnight at 4°C and finally counterstained with DAPI for 10 min. Cell morphology and spreading were observed by using a Leica TCS-SP8 confocal microscope (Leica, Germany) to collect images. The adhesion of SMSCs cultured *in vitro* on the scaffolds were also observed by SEM. Briefly, cell/scaffold composites were fixed in 2.5% (w/v) glutaraldehyde after 3 days culture and were observed using S-4800 field emission SEM (Hitachi, Tokyo, Japan).

Biochemical Assays for the Secretion of GAG and Collagen

After 7, 14, and 21 days of culture, the collagen and glycosaminoglycan secretion assays were carried out. The secreted collagen and GAG were all measured both in scaffold and medium. For collagen quantification, the content of hydroxyproline was measured by the hydroxyproline assay kit (Nanjing Jiancheng Bioengineering Institute, Nanjing, China) to indicate collagen contents. For GAG quantification, the Tissue GAG Total Content DMMB Colorimetry kit (Genmed Scientific Inc., Shanghai, China) was used to detect GAG contents according to the standard curve.

In vitro and *in vivo* Cell Migration

In vitro Cell Migration Assay

In order to determine the recruitment capacity of different scaffolds on SMSCs, we used a Transwell system (Corning, United States). Briefly, 100 μl of DMEM medium containing 2×10^4 SMSCs was added in the upper chamber, and 600 μl of DMEM and scaffolds (10 mm × 10 mm) were placed in the lower chamber. This Transwell system was cultured for 24 h and then the migrated cells were fixed with 4% paraformaldehyde for 20 min and stained with crystal violet (2%, w/v). Six replicates of each scaffold groups were imaged. The migrated cell numbers per view were calculated by ImageJ software.

Endogenous MSCs Recruitment Study *in vivo*

To investigate the ability of the various scaffolds on recruiting SMSCs *in vivo*, the PCL, PCL/MECM, and PCL/MECM-KGN μS scaffolds were implanted in the meniscus of the Sprague–Dawley rats. CD73 and CD105, which were defined as MSC markers and assessed by immunofluorescence staining to determine the endogenous MSC recruitment capacity of the three scaffolds. Briefly, after the samples were harvested, we used 4% paraformaldehyde to fix them at room temperature for 30 min, and then, the target antigens were retrieved by 2% sodium citrate for 20 min and blocked by 10% goat serum. Subsequently, the samples were incubated with primary antibodies against CD73 (1:150, Novus Biologicals)

and CD105 (1:150, Novus Biologicals) at 4°C overnight, followed by incubation with secondary antibodies, which were conjugated with Alexa Fluor488 and Fluor594 (1:100, Abcam, Cambridge, United Kingdom) for 1 h and DAPI (1:1000, Life Technologies) for 10 min. The samples were imaged by a TCS-SP8 confocal microscope (Leica, Germany) to determine the total cell numbers and CD29 and CD90 double-labeled cell numbers.

Cell Chondrogenic Differentiation

Pellet Culture

Chondrogenic differentiation was performed according to a previously published study (Fan et al., 2008). Approximately 5×10^5 SMMCs at passage 2 were centrifuged at 1500 rpm for 5 min in 15 ml Falcon tubes to form cell pellets. The pellets were maintained at 37°C with 5% CO_2 in basal media for 24 h, following which they were put in Transwell plates placed in 24-well plates. The 24-well plates contained either PCL scaffold, PCL/MECM scaffold, or PCL/MECM/KGN-μS scaffold. Each well of the 24-well plates containing scaffold was nourished with chondrogenic differentiation medium (MSCgo^{TM}, Biological Industries, Israel), and the medium was replenished every 3 days for 3 weeks. Chondrogenesis was evaluated through H&E, Alcian blue, Safranin O, and collagen II immunofluorescence staining after 21 days, respectively ($n = 4$).

In vitro Cartilage-Related Gene Expression Analysis

Cartilaginous gene expression levels of cells seeded into scaffolds after 7 and 14 days of culture were analyzed by quantitative real-time PCR (qRT-PCR). Briefly, total RNA was extracted by commercial TRIZol (Invitrogen, United States) reagent and reverse transcribed into complementary DNA (cDNA) by using the ReverTra Ace qPCR RT Kit (FSQ-201; TOYOBO) according to the manufacturer's protocol. Then, qRT-PCR was carried out using a StepOne TM Real-Time PCR system (Applied 1113 Biosystems) with SYBR Green PCR Mater Mix (Genestar, United States). The related gene primer sequences for *Col2al*, *Col1a1*, *Sox9, Acan*, and *GAPDH* are listed in **Table 1**. The relative amount of the messenger RNA (mRNA) expression was normalized to housekeeping gene (GAPDH), and gene expression was calculated using the $2^{-\Delta\Delta CT}$ method.

TABLE 1 | Primer sequences used for *in vivo* chondrogenic RT-qPCR.

Target gene		Sequence
SOX9	F: 5′-3′ R: 3′-5′	GCGGAGGAAGTCGGTGAAGAAT AAGATGGCGTTGGGCGAGAT
COL 2A1	F: 5′-3′ R: 3′-5′	CACGCTCAAGTCCCTCAACA TCTATCCAGTAGTCACCGCTCT
COL 1A1	F: 5′-3′ R: 3′-5′	GCCACCTGCCAGTCTTTACA CCATCATCACCATCTCTGCCT
ACAN	F: 5′-3′ R: 3′-5′	GGAGGAGCAGGAGTTTGTCAA TGTCCATCCGACCAGCGAAA
GAPDH	F: 5′-3′ R: 3′-5′	CAAGAAGGTGGTGAAGCAGG CACTGTTGAAGTCGCAG

In vivo Meniscus Repair Study

Animal Surgery

Animal experiments were approved by the Institutional Animal Care and Use Committee at PLA General Hospital. A total of 12 male New Zealand rabbits (8 months old, 2.5–3.0 kg) were randomly allocated into four groups: PCL group, PCL/MECM group, PCL/MECM/-KGN μS group, and positive control group (**Figure 7A**). The animals were first anesthetized by intramuscular injections of 160 mg ketamine and 12 mg xylazine. Major medial meniscectomy (only left with 5% of the external rim) was created and received with various groups of scaffolds implantation (**Figure 7B**). Those rabbits that underwent only meniscectomy were selected as positive control group. After the surgery, the animals were allowed to return to their cages and move freely. The rabbits were euthanized at 3 months and prepared for evaluations.

Macroscopic and Histological Evaluation

The repaired medial meniscus of the rabbit was collected for macroscopy and photographed at 3 months after implantation. Then, the regenerated menisci were fixed in 4% paraformaldehyde for 72 h. After fixation, the samples were embedded in paraffin and sectioned into 7-μm slices and stained with H&E and toluidine blue (TB), Safranin O, and Sirius Red according to standard protocols.

Semiquantitative Histological Scoring

To further evaluate the regenerated meniscal tissue, semiquantification of three assessment points including the reparative tissue with bonding, fibrochondrocytes existence, and Safranin O stainability were also evaluated blindly according to the Ishida score system by three independently trained researchers (Ishida et al., 2007).

Statistical Analysis

All statistical data are presented as mean ± standard deviations, using SPSS 17.0 statistical software, using t test (two groups) or one-way analysis of variance (multiple groups) to determine statistical significance. For all analyses, $P < 0.05$ means that the difference is significant.

RESULTS

Fabrication and Characterization of KGN μS

Fluorescent image (Arshady, 1991; **Figure 2A**) was captured, which shows successful encapsulation of goat antimouse IgG Alexa Fluor 594, and these proteins were well distributed in μS. While KGN-free μS did not exhibit obvious fluorescence in this wavelength. According to the SEM image, the μS had an average diameter of 12.55 ± 4.97 μm with a distribution ranging from 2.5 μm to roughly 30 μm (**Figure 2B**). The fabricated KGN μS presented a spherical morphology and also had a smooth surface (**Figure 2C**). A standard curve was formulated to detect KGN concentration. Analysis of KGN loading revealed that the encapsulation efficiency of KGN loading was approximately 70%.

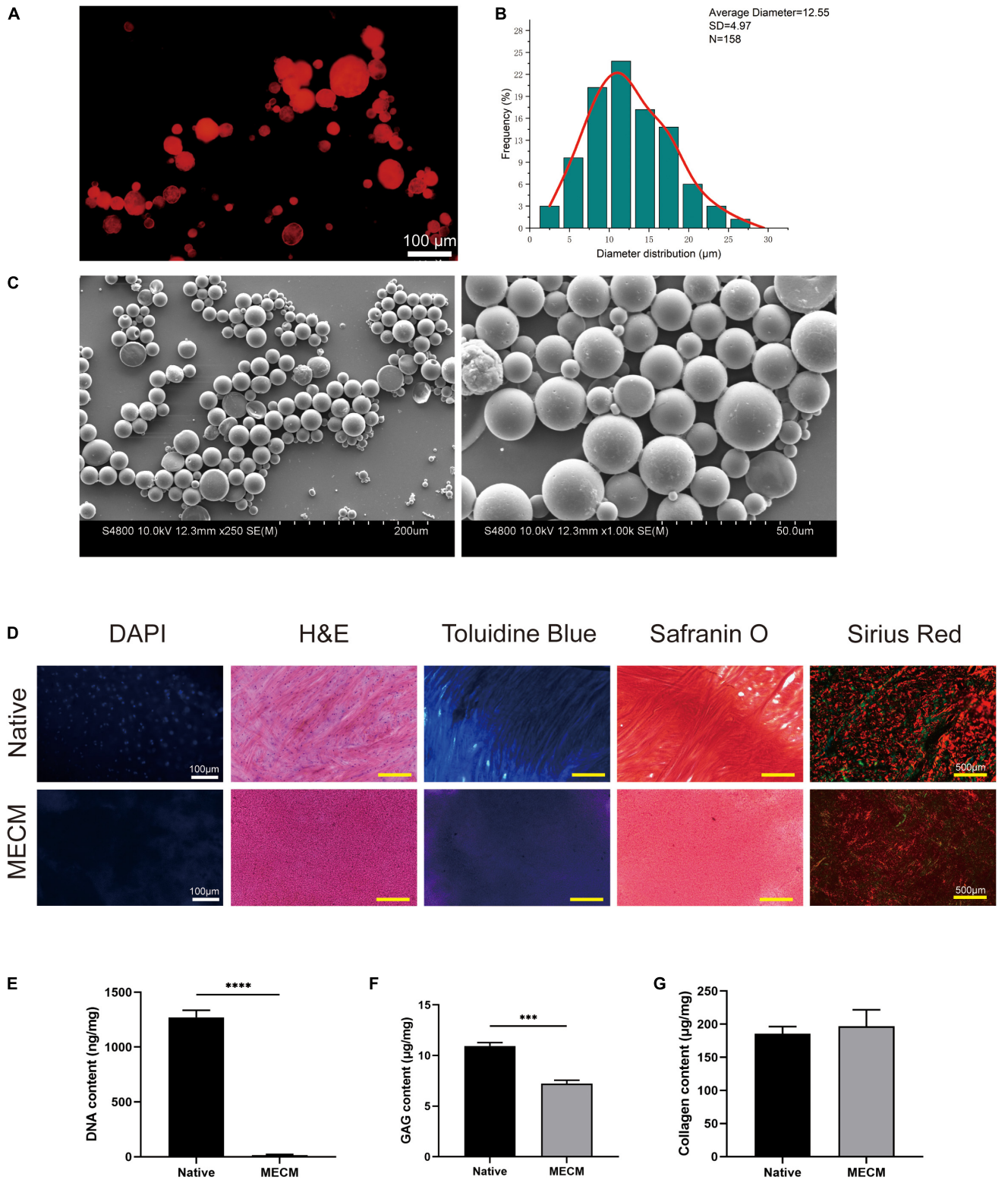

FIGURE 2 | (A) The protein distributions in poly(lactic-co-glycolic) acid (PLGA) microspheres; **(B)** the particle size distributions of kartogenin (KGN)-incorporated PLGA microspheres; **(C)** SEM images of KGN μS; **(D)** histological staining of meniscus extracellular matrix (MECM) and native meniscus; **(E)** residual DNA, **(F)** glycosaminoglycan (GAG), and **(G)** total collagen content of MECM and native meniscus. ***$p < 0.005$, ****$p < 0.001$.

Characterization of MECM

The histological staining and biochemical assays presented that the decellularization process achieves complete cell removal and maintenance of collagenous and GAG component (**Figures 2D–G**). DAPI and H&E staining both showed complete cell nuclei absence in the MECM. The effective removal of DNA was also demonstrated by DNA quantification, which showed that the DNA component was no more than 20 ng/mg (**Figures 2D,E**). Positive TB and Safranin O staining results indicated that GAG contents were partly reduced in the MECM after decellularized process, which was further confirmed by the quantitative GAG assay (**Figures 2D,F**). Sirius red staining confirmed that collagen fibers were well preserved in the MECM, which was stained as yellow or red (**Figure 2D**). No significant difference of collagen contents was presented by the quantitative collagen assay (**Figure 2G**).

Characterization of Hybrid Scaffolds

Scaffold Macro- and Microstructure

The macro- and microstructures of the scaffolds were characterized by a stereomicroscope (SMZ2, Nikon, Japan) and SEM, as shown in **Figure 3A**. Crescent-shaped PCL scaffolds were orthogonally printed with square holes as shown in **Figure 3A**. With the introduction of MECM, the whole PCL scaffold was filled with white porous MECM structure. Microscopic structures were further observed by SEM, from which we found numerous microporous structures on gaps between PCL fibers in PCL/MECM group and PCL/MECM/-KGN μS scaffold. In order to compare the porous structure of PCL/MECM and PCL/MECM/-KGN μS samples, intrusion porosimeter was used to calculate and present pore size distribution of these two scaffolds (**Figures 3C,D**). The diameter of the dominant pores in the PCL/MECM/-KGN μS group was about 18 μm (**Figure 3C**). In comparison, the pores in PCL/MECM scaffolds had a diameter of about 32 μm (**Figure 3D**). These findings suggested that both PCL/MECM and PCL/MECM/-KGN μS scaffolds had hierarchical pore microstructure, and the μS-containing scaffold seems to be slightly less porous than PCL/MECM scaffold, which was consistent with SEM images. The porosity of each scaffold was also measured: 78.96 ± 7.70% for the PCL scaffold, 71.75 ± 4.64% for the PCL/MECM scaffold, and 68.17 ± 4.23% for the PCL/MECM/KGN-μS scaffold (**Figure 3E**).

FTIR

The FTIR spectra of the PCL, MECM, and PCL/MECM are shown in **Figure 3B**. The results showed the different characteristic peaks for PCL scaffolds, MECM scaffold, and PCL/MECM scaffolds. In the spectrogram of PCL, there was a characteristic peak of the carbonyl group (C=O) at about 1750 cm^{-1} (black arrow in **Figure 3B**). Characteristic peaks at 1270 and 1185 cm^{-1} corresponded to the C–O bond in PCL. As for the FTIR spectrogram of MECM, the peak at 1580 cm^{-1} (blue arrow in **Figure 3B**) could be recognized as a characteristic peak of the amine group (N–H bend) in MECM. Meanwhile, the peak at 1580 cm^{-1} increased, demonstrating the successful introduction of MECM into PCL scaffold.

Mechanical Characterization

To calculate compression and tensile moduli (**Figures 3F,G**), the slope of the linear region was chosen to measure the stress-strain curve. The results showed that the compression modulus of the PCL scaffold was 3.98 ± 0.34 MPa. Hybrid PCL/MECM scaffold had similar moduli (4.14 ± 0.08 MPa) to the KGN-μS-containing scaffold, whereas PCL/MECM/KGN μS scaffolds also showed a much likely modulus of 4.59 ± 0.18 MPa (**Supplementary Figure 3**). The tensile modulus was 20.20 ± 1.54 MPa for the PCL scaffold and 27.15 ± 1.30 MPa and 27.46 ± 2.33 MPa for the PCL/MECM and PCL/MECM/-KGN μS scaffolds, respectively (**Supplementary Figure 3**). As reported by Chen et al. (2019) the compression and tensile moduli of the native rabbit meniscus is 3.76 ± 0.14 MPa and 45.58 ± 1.30 MPa, respectively. Although the mechanical strength of these scaffolds was inferior to the native meniscus in terms of tensile modulus, the hybrid scaffold is desirably strong enough to withstand biomechanical forces and maintain structural integrity (Makris et al., 2011).

Contact Angle

The wettability of PCL, PCL/MECM, and PCL/MECM/-KGN μS scaffolds was evaluated by measuring the contact angle of distilled water. The changes in the scaffold surface hydrophobicity along with prolonged time are shown in **Figure 3H** and **Supplementary Figure 4**. The pure PCL scaffold was hydrophobic, with a contact angle of 115.61° ± 5.85°. With the introduction of MECM, the hybrid scaffold surface became more hydrophilic. The contact angles for the PCL/MECM and PCL/MECM/-KGN μS scaffolds were 86.30° ± 7.77° and 92.70° ± 6.02°, respectively. The obtained result indicated that the hydrophilicity of 3D printed PCL scaffolds was greatly enhanced by the introduction of MECM components.

The Release Profile of KGN

From the release curves of the scaffolds shown in **Figure 3I**, an initial burst release of KGN was obvious, and the majority of the drug (nearly 60%) was released within 3 days, followed by a slower, more sustained released for all drug-loaded PCL/MECM-KGN μS, with a cumulative release rate of 78% at 28 days.

Cytocompatibility Analysis

Cell Viability, Proliferation, and Adhesion Assessment

The cytocompatibility of fabricated scaffolds was assessed by cell viability, cell proliferation, and cell adhesion assays. The live/dead staining showed that the SMSCs grew uniformly on both the PCL/MECM and PCL/MECM-KGN μS scaffolds; the MECM filling gaps between PCL fibers may provide excellent microenvironment for cell growth (**Figure 4A**). For PCL scaffold, the living cells were mainly arranged along the orthogonally printed fibers. A minority of the stained cells were fluorescent red (dead cells); the cell viability of various groups was also calculated by quantitative analysis, and the results exhibited that these scaffolds all have favorable viability more than 85%, indicating that all scaffolds were suitable for cell growth (**Figure 4B**).

Cell counting kit-8 assay was performed to quantitatively measure the proliferation of SMSCs in all types of scaffolds. As

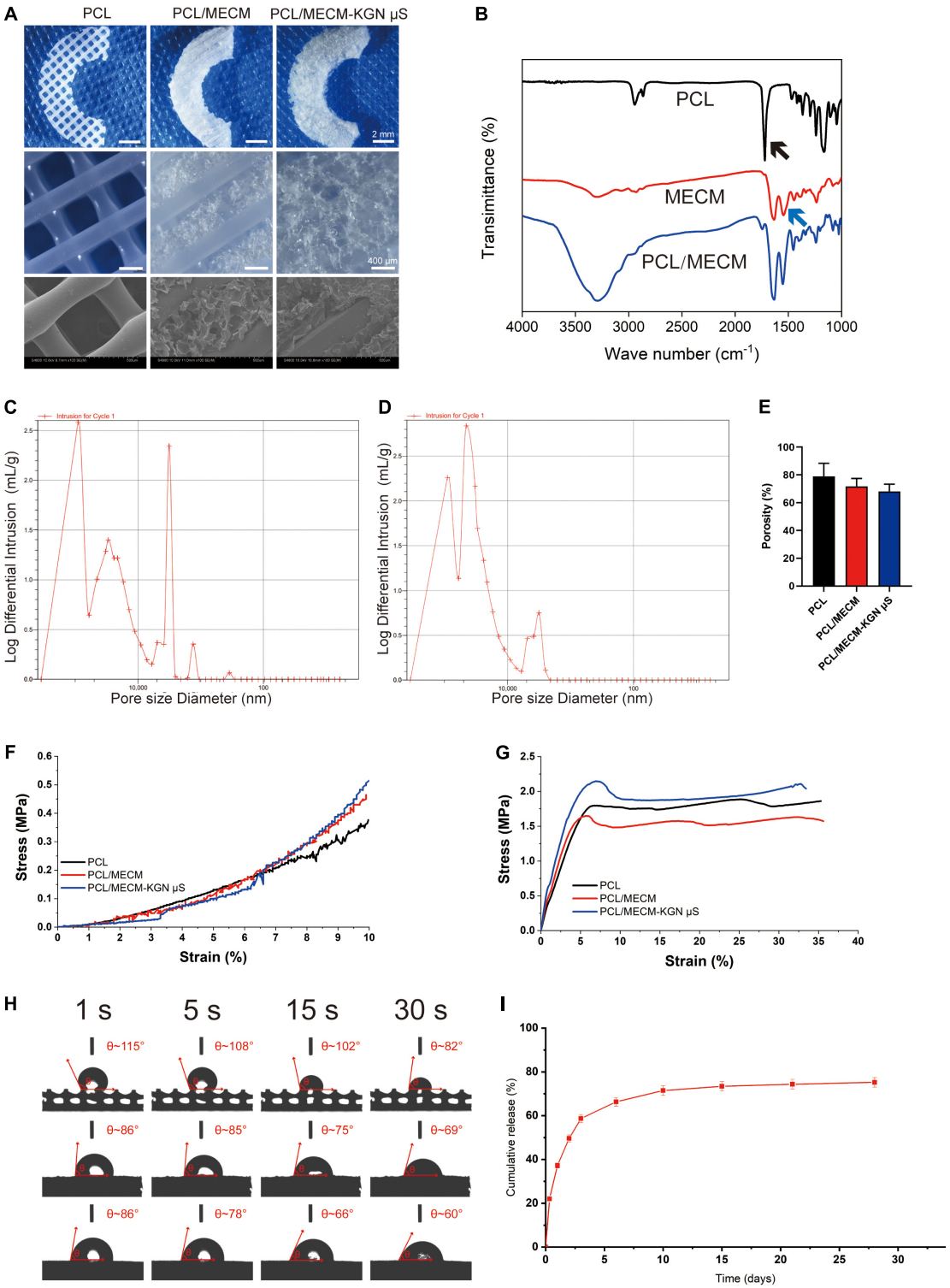

FIGURE 3 | (A) Macroscopic and SEM images of the poly(ε-caprolactone) (PCL), PCL/meniscus extracellular matrix (MECM), and PCL/MECM-KGN μS scaffolds. **(B)** Fourier-transform infrared spectroscopy (FTIR) spectra of PCL, MECM, and PCL/MECM. Pore sizes distribution of **(C)** PCL/MECM and **(D)** PCL/MECM-KGN μS scaffolds. **(E)** Mean porosity of PCL, PCL/MECM, and PCL/MECM-KGN μS scaffolds (n = 3). **(F)** Compression stress–strain curve. **(G)** Tensile stress–strain curve. **(H)** Contact angles of three groups of scaffolds. Four time points (1, 5, 15, and 30 s) were chosen to vary (n = 3). **(I)** KGN release kinetic of PCL/MECM-KGN μS scaffold (n = 3).

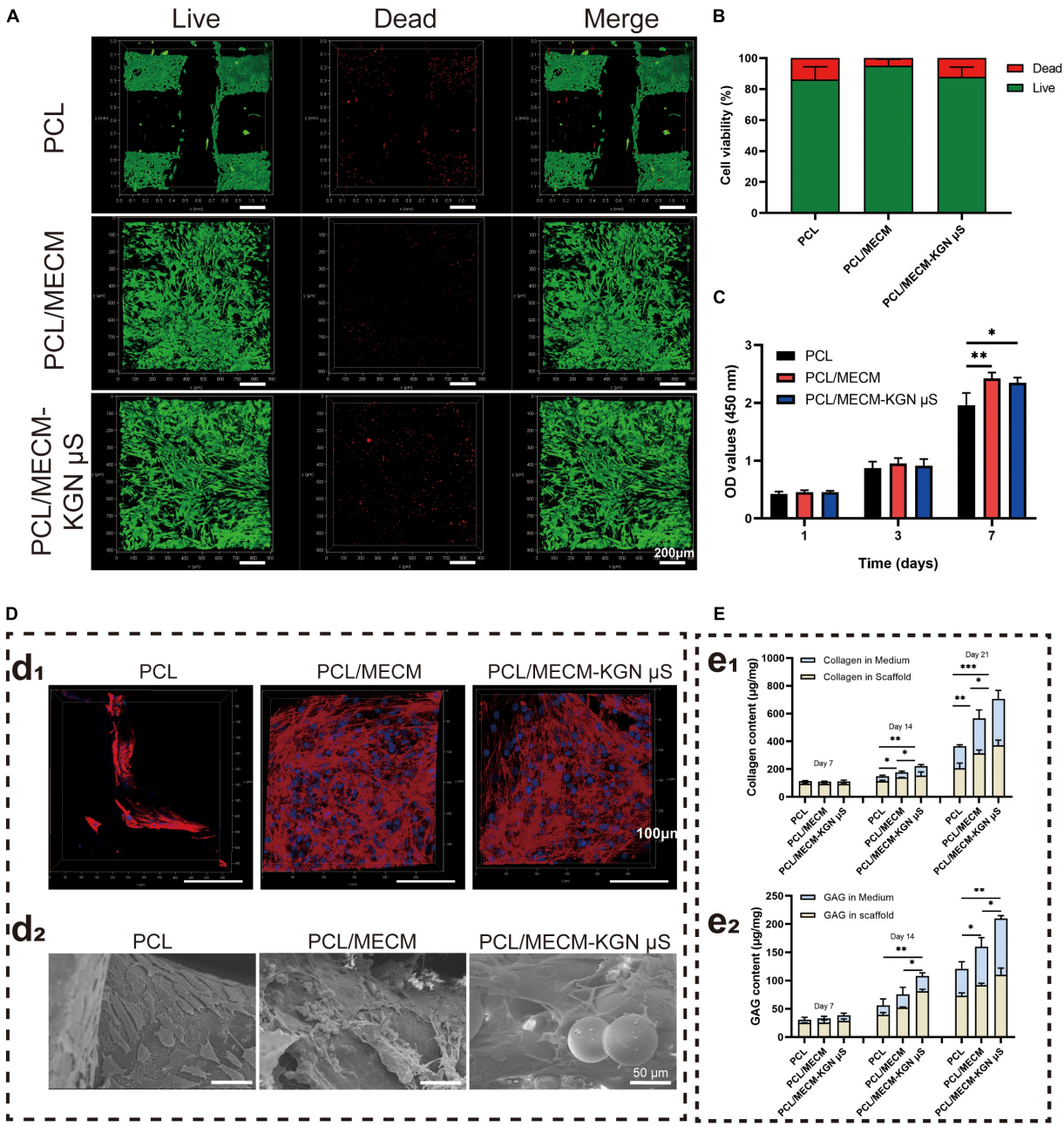

FIGURE 4 | (A) Live/dead staining (green, live cells; red, dead cells) of synovium-derived mesenchymal stem cells (SMSCs) on the poly(ε-caprolactone) (PCL), PCL/meniscus extracellular matrix (MECM), and PCL/MECM-KGN μS scaffolds. **(B)** Cell viability analysis. **(C)** CCK-8 assay ($n = 4$) of SMSCs after 1, 3, and 7 days of culture. **(D)** Confocal morphology (red, F-actin; blue, nucleus) and SEM of the scaffolds on which SMSCs were seeded for 4 days. **(E)** Total GAG and collagen of the cell/scaffold composites at different time points ($n = 3$). $^{*}p < 0.05$, $^{**}p < 0.01$, $^{***}p < 0.005$.

shown in **Figure 4C**, the OD value of cells cultured on all of the scaffolds increased with time in all the groups, and the absorbance values on the PCL/MECM and PCL/MECM/-KGN μS groups were obviously improved compared to the PCL group on day 7. These results suggested that the cell proliferation ability was greater on the MECM-containing scaffold.

A confocal laser scanning microscope was further used to evaluate the cell-spreading morphology and attachment after 72 h of seeding, and **Figure 4D** shows the cytoskeletal protein F-actin (red) and nucleus (blue) of cultured SMSCs on the scaffolds. Compared to the cells on the PCL scaffold, SMSCs on the MECM-containing scaffold was well distributed not only on the surfaces of PCL fibers but also in the pores of scaffolds and exhibited more fusiform morphology and pseudopods as well as a larger cell spreading area. According to SEM images of cell adhesion on the MECM-containing scaffold, the SMSCs with

rough morphology were contracted together to form a stretched cell sheet (**Figure 4D**). These results further validated that the MECM-containing scaffolds are beneficial for cell adhesion and proliferation.

Biochemical Analysis for GAG and Collagen Secretion

The effects of scaffolds on the cartilaginous ECM secretion of SMSCs were evaluated by GAG and collagen quantitatively assays (**Figure 4E**). Evident GAG and collagen content increased along with prolonged time in each of the three scaffolds. Indeed, the secretion of the GAG and hydroxyproline was considerably higher in the PCL/MECM/-KGN μS scaffold than in the other groups after 21 days of culture in chondrogenic medium, demonstrating that the addition of KGN could strongly enhance the production of GAG and collagen, which were the main components of the meniscus matrix. Similarly, the PCL/MECM scaffold can also promote the GAG and collagen deposition to a certain extent. By day 21, total collagen and GAG in the PCL/MECM scaffold were significantly higher than in the PCL scaffold. All data indicate that the PCL/MECM and PCL/MECM/-KGN μS scaffolds are capable to stimulate the secretion of collagen and GAG by SMSCs.

Cell Recruitment Assessment

A Transwell assay was performed to investigate stem cell migration toward different scaffolds *in vitro* (**Figure 5A**). Placing these three scaffolds in the lower chamber, the migrated cell numbers after 24 h were significantly higher in the PCL/MECM and PCL/MECM/-KGN μS scaffolds than that in the PCL group (**Figures 5A,B**). However, the recruitment capability of PCL/MECM and PCL/MECM/-KGN μS scaffolds was not significantly different. These results indicated that both the KGN-loaded scaffold and PCL/MECM scaffold could promote SMSCs migration.

The recruitment ability of scaffold *in vivo* was also verified. After 1 week of *in vivo* implantation, immunofluorescence results showed that the total cell number was higher in the PCL/MECM and PCL/MECM/-KGN μS scaffolds, with a more uniform and abundant cell distribution (**Figures 5C,D**). Furthermore, the more migrated ESPCs within the MECM-containing scaffold were validated by the significantly higher number of CD73 and CD105 double-positive cells (**Figures 5C,E**). These results collectively suggested that the MECM component can effectively enhance the capability of scaffolding system to recruit surrounding MSCs to the defect site.

Chondrogenic Differentiation Assays

In order to investigate the bioactivity of these scaffold, the 3D pellet system was performed, and histological and immunohistochemical staining was used to evaluate the chondrogenesis (**Figure 6B**). As shown in **Figure 6A**, H&E staining results revealed that the pellets were successfully cultured and generated. In addition, Safranin O and Alcian blue staining, which are related to proteoglycan synthesis, exhibited the predominant intensity of the pellet in the PCL/MECM-KGN μS scaffold. Furthermore, the type II collagen immunohistochemical staining results also proved that the released KGN markedly enhanced the type II collagen deposition. In terms of histological score, the Bern score evaluation showed that KGN-incorporated scaffold could prominently promote the chondrogenesis of SMSCs compared with the PCL and PCL/MECM scaffold (**Figure 6C**). Meanwhile, the MECM-containing scaffold also slightly enhanced the chondrogenesis of SMSCs, indicating that the instructive microenvironment was provided by MECM for SMSCs differentiation.

The expression of cartilage-associated genes of the scaffolds was also evaluated by qRT-PCR (**Figure 6D**). Compared with that in PCL scaffolds, the levels of *Col 2a1*, *Acan*, and *Sox9*, which are specific for cartilaginous tissues, were upregulated in the PCL/ECM groups at each time point and were also markedly enhanced after KGN incorporation in the PCL/ECM-KGN μS group. Meanwhile, the *COL1Al* expression was not significantly different within these scaffolds. Taken together, these results demonstrated that PCL/ECM-KGN μS could provide an ideal platform for chondrogenic differentiation of SMSCs.

In vivo Meniscus Repair Assessment

Histological Staining Analysis

The neo-menisci were harvested 3 months after the implantation and were further evaluated by gross observation and histological staining. Compared with the PCL group, the regenerated meniscus in the PCL/MECM and PCL/ECM-KGN μS groups exhibited more complete and uniform morphology. Additionally, the meniscus regenerated in the PCL/ECM-KGN μS group was the most similar to native meniscus. The histological features of neo-menisci of different groups were also presented, respectively (**Figure 7B**).

In the PCL group, the results of HE staining showed only a few round-like cells and cartilage lacuna structures in the inner area of the neo-meniscal tissue, and there were basically no round-like cells in the outer area, whereas the cells were mostly long spindle-shaped cells without lacuna structure. Toluidine blue staining showed that regenerated tissues were stained weak positive. Sirius red staining also showed disordered and loosely arranged collagen fibers in both inner and outer regions. In the PCL/MECM group, the inner area of the meniscal tissue had more round-like cells and cartilage lacuna structures than the PCL group, and the outer area also exhibited a small number of round-like cells, while others are long, fusiform cells. For TB staining, newly formed meniscal tissues were stained positive. The collagen arrangement, stained with Sirius red, was improved compared to that in the PCL group. In the PCL/MECM/-KGN μS group, a large number of round-like cells can be seen in the medial area of the regenerated meniscus tissue with many cartilage lacunas structures, and the outer area is mostly long spindle-shaped cells. The TB staining in both the medial area and the outer area is strongly positive but is inferior to the native

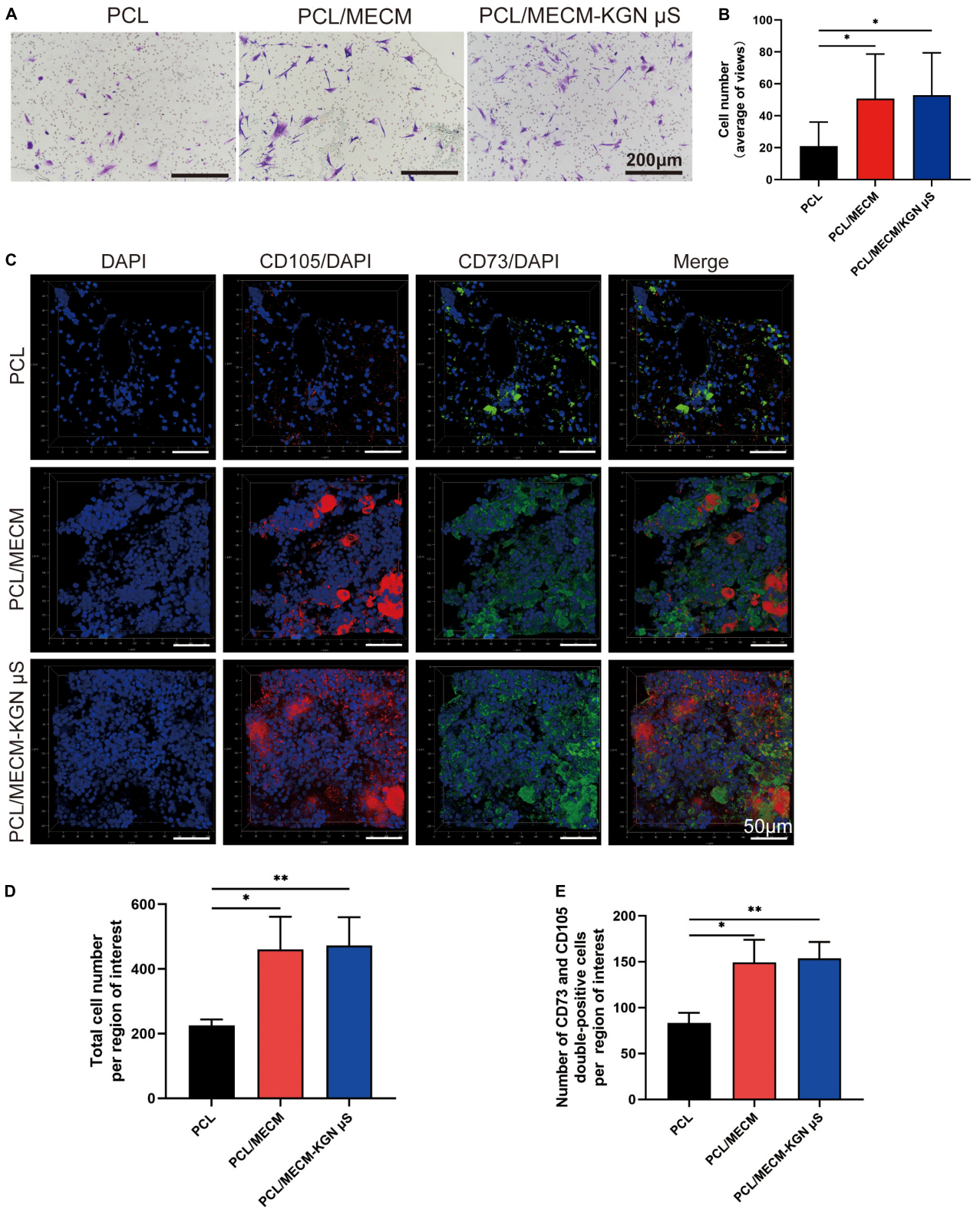

FIGURE 5 | Recruitment capacity of the scaffolds on synovium-derived mesenchymal stem cells (SMSCs) *in vitro* and *in vivo*. **(A)** Effects of different scaffolds on the migration of SMSCs. The migratory cells stained with crystal violet after cultured for 24 h ($n = 5$). **(B)** Statistical analysis of average migratory cell number per region of interest from different scaffolds. **(C)** Images of CD105+/CD73+ MSCs in various implanted scaffolds 4 weeks post-surgery. **(D)** Quantification of total cell number in the injury sites. **(E)** Quantification of MSCs recruited to the injury sites. $^{*}p < 0.05$, $^{**}p < 0.01$.

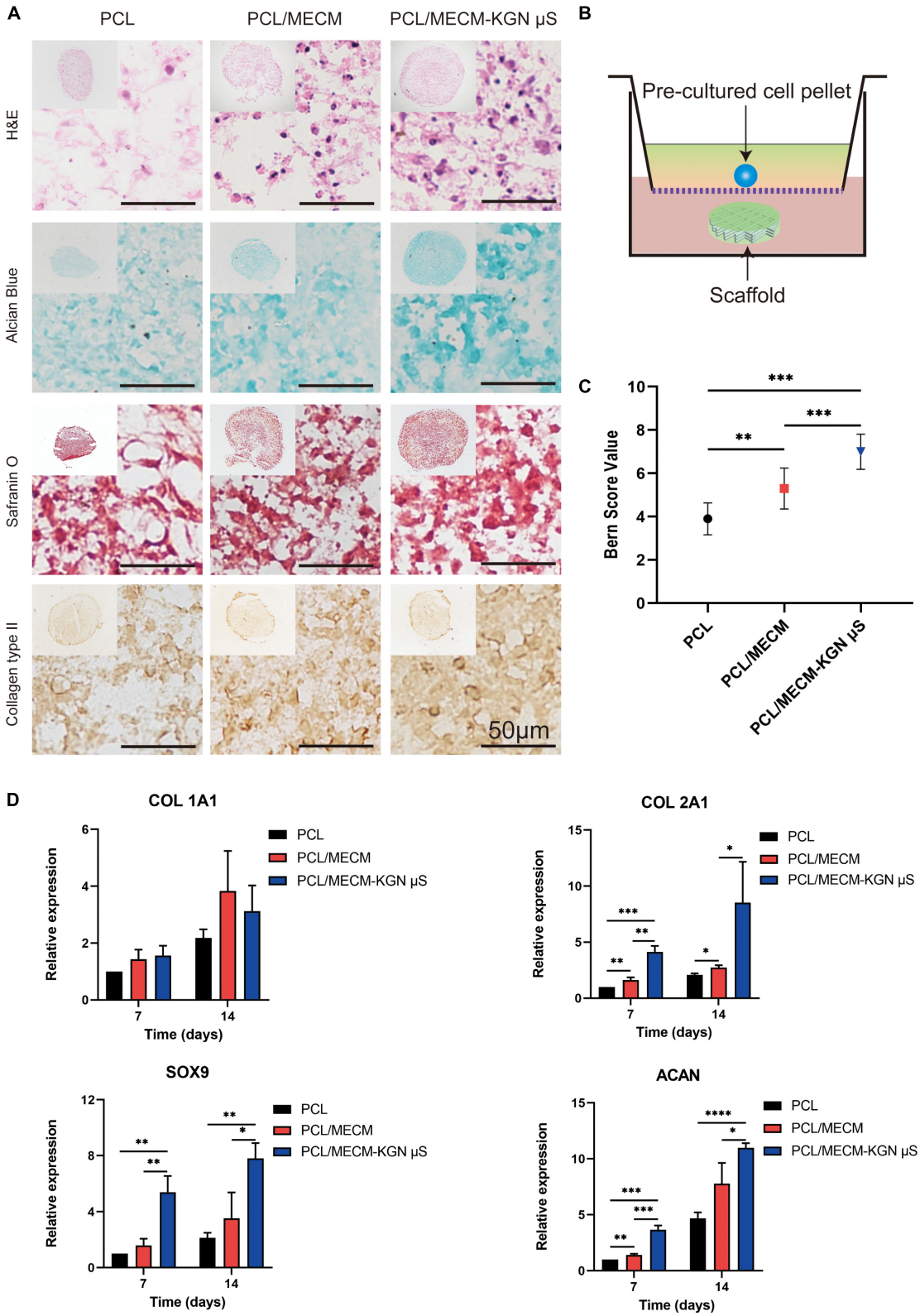

FIGURE 6 | (A) Histological and immunohistochemical analysis of the pellets that were cocultured in **(B)** Transwell for 21 days. **(C)** Bern score for chondrogenic pellets. **(D)** Expression of Col 1A1, Col 2A1, Sox 9, and ACAN of the synovium-derived mesenchymal stem cells (SMSCs) on three different scaffolds. $^{*}p < 0.05$, $^{**}p < 0.01$, $^{***}p < 0.005$, $^{****}p < 0.001$.

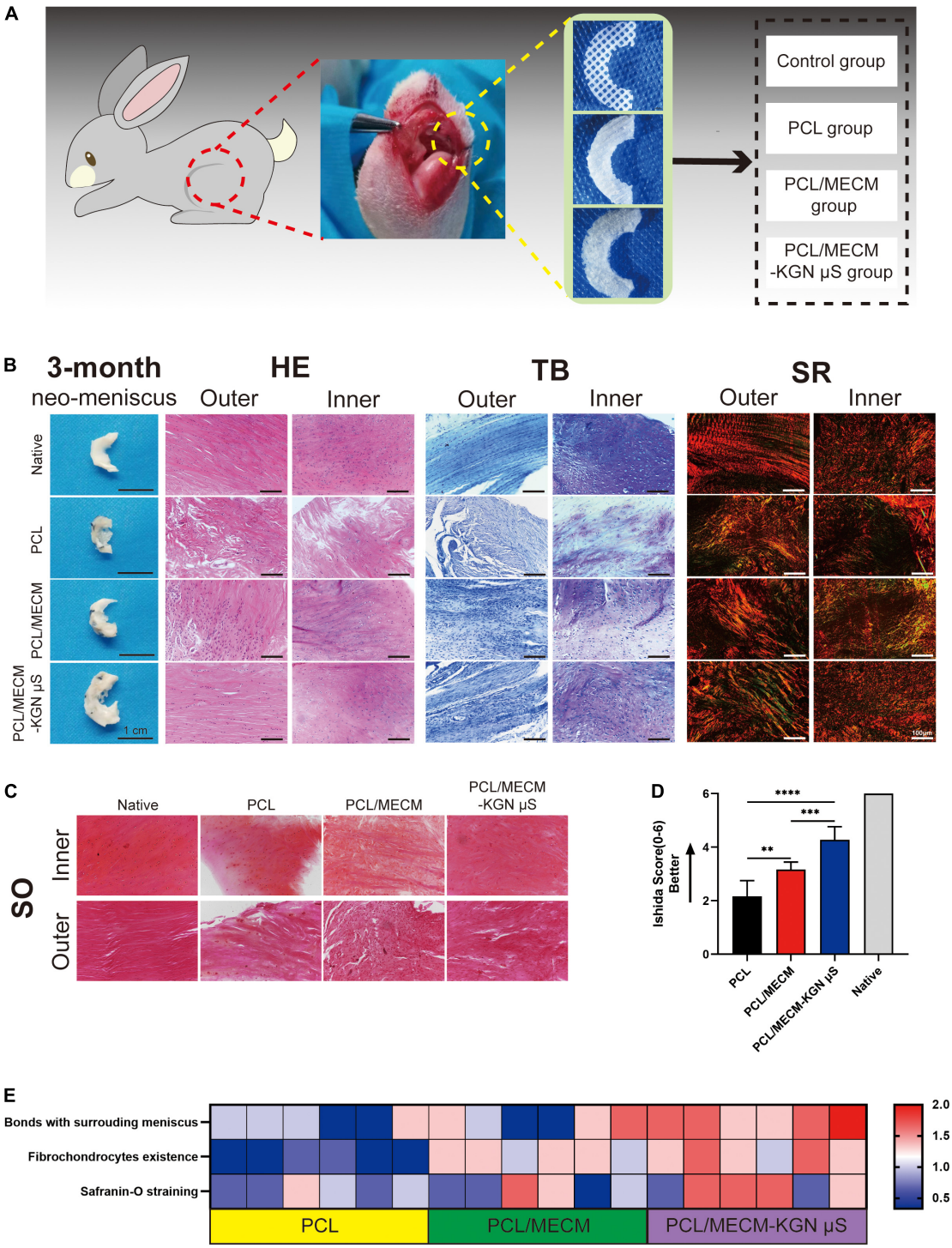

FIGURE 7 | (A) Schematic diagram of scaffold implantation and experiment groups. **(B)** Histological staining analyses of the regenerated menisci. **(C)** Safranin O staining of the regenerated meniscus. **(D)** Ishida histological score for regenerated meniscus. **(E)** Heat map of variables of the Ishida histological scoring.

meniscus tissue. Sirius red staining shows a large number of collagen fibers with strong refractive index, and the well-organized arrangement of collagen fibers is closer to that of the normal meniscus.

Semiquantitative Histological Scoring

In order to further analyze the regeneration quality of the neo-menisci, we used the Ishida score to conduct a histological semiquantitative analysis. The result

(**Figures 7C–E**) shows that the regenerated menisci in the PCL/MECM/-KGN μS group were significantly better than those in the PCL and PCL/MECM groups at the same time point.

DISCUSSION

The complex structure and function and limited blood supply of the native meniscus significantly hamper the successful reconstruction of this heterogeneous fibrocartilage (Li Y. et al., 2020). Tissue engineering approaches have made many advances in developing alternatives for meniscus regeneration. In a study, Liu et al. (2019) reported that KGN-loaded PRP gels successfully regenerated the wounded rabbit meniscus *in vivo* through the codelivery of stem cells and prochondrogenic factors. However, considering the drawbacks of cell-based strategies, *in situ* tissue engineering strategies that rely on leveraging the body's innate regeneration potential provide a new avenue for injured meniscus repair and regeneration (Chen et al., 2019). Therefore, we proposed a combinatorial approach of constructing a scaffold that is capable of recruiting ESPCs, as well as maintaining chondrogenic microenvironment to regenerate the reconstructed knee meniscus. In this study, we fabricated a kartogenin-loaded hybrid scaffold by 3D printing a PCL scaffold followed by injection with the μS-incorporated MECM. We found that MECM enhanced the adhesion, proliferation, and migration of SMSCs, and the sustained release of KGN from PLGA microspheres significantly enhanced the chondrogenesis of SMSCs. The orchestrated functional microenvironment provided by this drug delivery scaffolding system in our study led to the whole meniscus regeneration in rabbits.

During the meniscus regeneration process, the implanted scaffold should provide a structural framework with suitable biophysical and biochemical properties to help the adhesion and migration of host cells. In our previous study, we fabricated and studied an ingredient and structure-mimicking hybrid scaffold derived from demineralized cancellous bone and MECM, which could act as a temporal "home" for resident cells and facilitate meniscus regeneration (Yuan et al., 2016). However, the biomechanical properties of demineralized cancellous bone are also relatively insufficient. The synthetic polymer PCL with good 3D printability, favorable mechanical support, and prolonged duration can be tuned to facilitate neo-meniscus regeneration (Shao et al., 2015). Here, the PCL fiber bundles of our scaffold presented favorable mechanical properties close to the native meniscus reported by Chen et al. (2019), as shown in **Supplementary Figure 3**. Furthermore, when implanted *in vivo*, the PCL fibers of the scaffold fixed at the anterior and posteriors horns can ideally resist the downward pressure and tensile strength and subsequently avoid damage and dislocation of the newly formed meniscus (Li Z. et al., 2020).

Although the MECM is not able to provide much mechanical support for meniscal tissue formation, the porous structure and various functional cues of this decellularized materials are helpful to dictate cell fate and may further help improve the meniscus regeneration (Chen et al., 2019). The microarchitectures of tissue-engineered scaffold can significantly affect the cells' behaviors; therefore, the optimal scaffold architecture (e.g., average pore size) is a prerequisite for meniscus regeneration (Zhang et al., 2016). In our present study, MECM gel was infused into the PCL fibers and crosslinked and lyophilized to form macro–microporous structures. After the MECM infusion into the PCL scaffold, the composites had an average pore size near 30 μm and a porosity around 70%, which were believed to be helpful for cell ingrowth and proliferation (Rowland et al., 2016; **Figures 3C–E**). In addition, The KGN μS loaded into MECM exhibited a tendency to reduce the pore size and porosity but did not significantly change the microstructure of the whole scaffold in the present loading amount (**Figures 3D,E**). Another key prerequisite of the scaffold for tissue regeneration is cellular attachment and spreading onto the scaffold. The dynamic contact angle test suggested that the MECM significantly increases the hydrophilicity of composite scaffold (**Figure 3H**), while the loaded KGN μS did not influence the scaffold's aqueous environment. The decreased water contact angle of the PCL/MECM scaffold can provide a more favorable microenvironment for cell adhesion. On the other hand, the biochemical cues of MECM also contribute to modulating cell behavior and providing a more instructive microenvironment. Notably, the addition of MECM supplies the constructs with excellent biocompatibility, which was further demonstrated by the results of cell viability and CCK-8 assessment shown in **Figures 4A–C**. *In vitro* adhesion studies also showed that the hybrid scaffold with appropriate pore structure and adhesion proteins serves as a guide for SMSCs adhesion, distribution, and proliferation (**Figure 4D**). Collectively, the MECM-infused PCL scaffold may retain suitable pore size, porosity, hydrophilicity, and bioactivity and further provide biomimetic microenvironment for cell infiltration, proliferation, and nutrition diffusion.

To more leveraging of innate regenerative abilities, the engineered scaffold could incorporate with bioactive factors to direct ESPCs to injury sites and aid the healing of the damaged tissue. It has been shown that the migration and infiltration of SMSCs to the injury site play a vital role in the meniscus regeneration process (Li Z. et al., 2020). In the present study, the *in vitro* and *in vivo* cell migration assay revealed that the MECM components exert recruitment capacity on SMSCs (**Figures 5A–E**). Although we could not figure out which kind of biomolecules in MECM are inducive to cell mobilization, the present results first proved that the MECM components can induce ESPCs migration. Some evidence showed that KGN can induce bone-marrow-derived mesenchymal stem cells (BMSCs) migration *in vitro* (Yang et al., 2019), but the results of *in vitro* and *in vivo* recruitment tests did not show that the KGN released from the PLGA microsphere exerted positive effects on cell migration, which may due to the fact that different source of stem cells or the recruitment effects of KGN was much weaker than that in MECM (**Figures 5A–E**).

To effectively stimulate the migrated stem cells to differentiate into matured meniscal cells, a potent chondrogenic inducer is

needed. KGN has raised much attention in cartilaginous tissue engineering due to its favorable stability, cartilage protective effects, and strong chondrogenic ability (Johnson et al., 2012). However, to avoid the side effects and unwanted circulatory clearance, an ideal delivery platform that fully utilized the KGN to provide sustained chondrogenic induction is required (Zhao et al., 2020). PLGA μS were good drug carriers and capable of sustaining and localizing delivery of bioactive drugs to dictate surrounding cell behaviors (Asgari et al., 2020; Zhao et al., 2020). In the present study, the release profile of KGN-incorporated PCL/MECM hybrid scaffold exhibited an initial burst release in the early phase, followed by a slow constant release for over 28 days, which suggested that this drug delivery scaffold system can provide sustained chondrogenic environment for meniscus tissue regeneration (**Figure 3I**). In addition, concerning the unfavorable acidic by-product of PLGA microsphere, *in vitro* cytocompatibility assessments were also conducted. The results of live/dead assay and CCK-8 assay showed that the KGN-μS-loaded scaffold did not significantly affect the cell viability and proliferation, which proved the safety of this polymeric drug delivery system.

To validate the chondrogenic effects of the KGN-loaded composite scaffold, *in vitro* chondrogenic experiments were performed (**Figure 6**). After 21 days of pellet culture, we harvested and captured the pellet and histological performance and found that the PCL/MECM group promoted extracellular matrix production to some extent, but the PCL/MECM-KGN μS group exhibited more cartilaginous matrix staining than the scaffold without additional KGN (**Figures 6A–C**). Additionally, more chondrogenic-related gene expressions of SOX9, COL 2A1, and ACAN were also observed in the PCL/MECM-KGN μS group after 14 days of *in vitro* culture, while the PCL/MECM group can only upregulate COL 2A1 expression (**Figure 6D**). The cartilaginous matrix formation was also evaluated by GAG and collagen quantitative assays, and the results indicated that KGN strongly promoted ECM formation compared to the MECM only group (**Figure 4E**). These results further supported that KGN-loaded PCL/MECM scaffolds not only possess excellent biocompatibility but also capable of inducing chondrogenesis of stem cells. Importantly, although the optimized microstructure and hydrophilic environment of MECM are conducive to cell attachment and proliferation, a potent trophic factor that can activate and accelerate chondrogenesis of stem cells is needed and may further induce significant difference when applied *in vivo*.

In the *in vivo* studies, the better macroscopic performance of the neo-menisci in the PCL/MECM-KGN μS group is mainly owing to the superior ESPCs recruitment and differentiation ability. The poor macroscopic performance in the PCL group may be owing to the scarce biochemical cues of the PCL scaffold, which makes it hard to capture and dictate ESPCs. Compared to the PCL group, the PCL/MECM group exhibited facilitated meniscus repair to a certain extent, but the repair rate was not significantly faster, and the repaired tissue was more likely fibrous tissue. After 3 months, the regenerated meniscus of the PCL/MECM-KGN μS group were histologically more similar to the native meniscus in terms of H&E, Toluidine blue, Sirius red, and Safranin O staining. Semiquantitative histological score for the neo-menisci also showed that the PCL/MECM-KGN μS group presented better than those of the PCL and PCL/MECM groups. These findings collectively confirmed the capability of the PCL/MECM-KGN μS scaffold in facilitating meniscus regeneration. Based on our findings, we proposed a possible mechanism of meniscus regeneration induced by the present composite scaffold. First are the mobilization and migration of ESPCs to the defects. In this study, the MECM with optimized microstructure and biochemical factors successfully facilitate the enrichment of ESPCs. Second, ESPCs well proliferate and differentiate in the macro–microporous PCL/MECM, and KGN released from PLGA μS further provide potent facilitation effects on their chondrogenic differentiation. Additionally, the faster and improved cartilaginous tissue formation that was induced by KGN also further helped in achieving a positive regeneration feedback process. The accelerated meniscus-specific ECM formation may not only induce fast mechanical functions recovery but also promote the cells interaction with microenvironment and further resulting in more reparative factors releasing.

In summary, although MECM-based scaffold and PLGA microspheres have been widely used in MTE, the combination of these two components has not been seen. In our study, we first combined the KGN-loaded μS, PCL fibers, and MECM to form a hybrid scaffold, which not only provided mechanical support and excellent biocompatibility but also exerted cell recruitment ability and constantly released cartilage-inducing bioactive factors. This study also has some limitations. First, the chondroprotective effect needs to be further explored. Second, the *in vivo* results were accessed in 3 months; therefore, the scaffold should be examined in longer term similar to the natural healing process.

CONCLUSION

In this study, to explore the potential of *in situ* tissue engineering strategy in meniscus regeneration, we successfully fabricated a macro–microporous PCL/ MECM-KGN μS scaffold. The PCL scaffold was produced by using 3D printing technology and then injected with KGN-μS-loaded MECM to prepare a hybrid functional scaffold that aims to promote meniscus repair and regeneration. This scaffolding system with optimal microarchitecture and prochondrogenic capacity through a combination of MECM-enhancing cell migration, adhesion, and KGN facilitating chondrogenesis was evaluated both *in vitro* and *in vivo*. *In vitro* studies have demonstrated that the MECM-based scaffolds provide a favorable microenvironment to support the SMSCs migration, adhesion, and proliferation. The chondrogenic differentiation and cartilaginous matrix formation were further improved via the incorporated KGN. Moreover, *in vivo* analysis suggested that the PCL/MECM-KGN μS scaffold presented superior *in situ* meniscus regeneration. To conclude, the PCL/MECM-KGN μS scaffolding system may be a promising small molecule-based alternative, which hold great promise for MTE in the future.

DATA AVAILABILITY STATEMENT

The original contributions presented in the study are included in the article/**Supplementary Material**, further inquiries can be directed to the corresponding author/s.

ETHICS STATEMENT

The animal study was reviewed and approved by the Institutional Animal Care and Use Committee at PLA General Hospital.

AUTHOR CONTRIBUTIONS

HL and QG did the conceptualization. HL, ZL, and ZYa did the methodology. HL, ZL, ZYu, and CG did the investigation. ZYa, LF, PL, and ZYu did the resources. HL wrote. SL and QG edited. All authors contributed to the article and approved the submitted version.

FUNDING

This work was supported by the National Key R&D Program of China (2019YFA0110600) and the National Natural Science Foundation of China (81972070).

SUPPLEMENTARY MATERIAL

The Supplementary Material for this article can be found online at: https://www.frontiersin.org/articles/10.3389/fbioe.2021.662381/full#supplementary-material

REFERENCES

Arshady, R. (1991). Preparation of biodegradable microspheres and microcapsules: 2. Polyactides and related polyesters. *J. Control. Release* 17, 1–21. doi: 10.1016/0168-3659(91)90126-x

Asgari, N., Bagheri, F., Eslaminejad, M. B., Ghanian, M. H., Sayahpour, F. A., and Ghafari, A. M. (2020). Dual functional construct containing kartogenin releasing microtissues and curcumin for cartilage regeneration. *Stem Cell Res. Ther.*. 11, 1–15.

Bilgen, B., Jayasuriya, C. T., and Owens, B. D. (2018). Current concepts in meniscus tissue engineering and repair. *Adv. Healthcare Mater.* 7:1701407. doi: 10.1002/adhm.201701407

Chen, M., Feng, Z., Guo, W., Yang, D., Gao, S., Li, Y., et al. (2019). hydrogel hybrid scaffolds and meniscal Fibrochondrocytes promote whole meniscus regeneration in a rabbit Meniscectomy model. *ACS Appl. Mater. Interfaces* 11, 41626–41639. doi: 10.1021/acsami.9b13611

Cunniffe, G. M., Díaz-Payno, P. J., Sheehy, E. J., Critchley, S. E., Almeida, H. V., Pitacco, P., et al. (2019). Tissue-specific extracellular matrix scaffolds for the regeneration of spatially complex musculoskeletal tissues. *Biomaterials* 188, 63–73. doi: 10.1016/j.biomaterials.2018.09.044

Englund, M., Roemer, F. W., Hayashi, D., Crema, M. D., and Guermazi, A. (2012). Meniscus pathology, osteoarthritis and the treatment controversy. *Nat. Rev. Rheumatol.* 8:412. doi: 10.1038/nrrheum.2012.69

Fan, H., Zhang, C., Li, J., Bi, L., Qin, L., Wu, H., et al. (2008). Gelatin microspheres containing TGF-β3 enhance the chondrogenesis of mesenchymal stem cells in modified pellet culture. *Biomacromolecules* 9, 927–934. doi: 10.1021/bm7013203

Fox, A. J., Bedi, A., and Rodeo, S. A. (2012). The basic science of human knee menisci: structure, composition, and function. *Sports Health* 4, 340–351. doi: 10.1177/1941738111429419

Fox, A. J., Wanivenhaus, F., Burge, A. J., Warren, R. F., and Rodeo, S. A. (2015). The human meniscus: a review of anatomy, function, injury, and advances in treatment. *Clin. Anat.* 28, 269–287. doi: 10.1002/ca.22456

Giannitelli, S., Mozetic, P., Trombetta, M., and Rainer, A. (2015). Combined additive manufacturing approaches in tissue engineering. *Acta Biomater.* 24, 1–11. doi: 10.1016/j.actbio.2015.06.032

Hussey, G. S., Dziki, J. L., and Badylak, S. F. (2018). Extracellular matrix-based materials for regenerative medicine. *Nat. Rev. Mater.* 3, 159–173. doi: 10.1038/s41578-018-0023-x

Ishida, K., Kuroda, R., Miwa, M., Tabata, Y., Hokugo, A., Kawamoto, T., et al. (2007). The regenerative effects of platelet-rich plasma on meniscal cells in vitro and its in vivo application with biodegradable gelatin hydrogel. *Tissue Eng.* 13, 1103–1112. doi: 10.1089/ten.2006.0193

Johnson, K., Zhu, S., Tremblay, M. S., Payette, J. N., Wang, J., Bouchez, L. C., et al. (2012). A stem cell–based approach to cartilage repair. *Science* 336, 717–721.

Kwon, H., Brown, W. E., Lee, C. A., Wang, D., Paschos, N., Hu, J. C., et al. (2019). Surgical and tissue engineering strategies for articular cartilage and meniscus repair. *Nat. Rev. Rheumatol.* 15, 550–570. doi: 10.1038/s41584-019-0255-1

Lee, C. H., Rodeo, S. A., Fortier, L. A., Lu, C., Erisken, C., and Mao, J. J. (2014). Protein-releasing polymeric scaffolds induce fibrochondrocytic differentiation of endogenous cells for knee meniscus regeneration in sheep. *Sci. Transl. Med.* 6:266ra171. doi: 10.1126/scitranslmed.3009696

Li, H., Yang, Z., Fu, L., Yuan, Z., Gao, C., Sui, X., et al. (2020). Advanced polymer-based drug delivery strategies for meniscal regeneration. *Tissue Eng. B Rev.* doi: 10.1089/ten.TEB.2020.0156 [Epub ahead of print].

Li, Y., Chen, M., Zhou, W., Gao, S., Luo, X., Peng, L., et al. (2020). Cell-free 3D wet-electrospun PCL/silk fibroin/Sr2+ scaffold promotes successful total meniscus regeneration in a rabbit model. *Acta Biomater.* 113, 196–209. doi: 10.1016/j.actbio.2020.06.017

Li, Z., Wu, N., Cheng, J., Sun, M., Yang, P., Zhao, F., et al. (2020). Biomechanically, structurally and functionally meticulously tailored polycaprolactone/silk fibroin scaffold for meniscus regeneration. *Theranostics* 10:5090. doi: 10.7150/thno.44270

Liu, F., Xu, H., and Huang, H. (2019). A novel kartogenin-platelet-rich plasma gel enhances chondrogenesis of bone marrow mesenchymal stem cells in vitro and promotes wounded meniscus healing in vivo. *Stem Cell Res. Ther.* 10:201.

Makris, E. A., Hadidi, P., and Athanasiou, K. A. (2011). The knee meniscus: structure–function, pathophysiology, current repair techniques, and prospects for regeneration. *Biomaterials* 32, 7411–7431. doi: 10.1016/j.biomaterials.2011.06.037

Malikmammadov, E., Tanir, T. E., Kiziltay, A., Hasirci, V., and Hasirci, N. (2018). PCL and PCL-based materials in biomedical applications. *J. Biomater. Sci. Polym. Ed.* 29, 863–893. doi: 10.1080/09205063.2017.1394711

Martins, C., Sousa, F., Araujo, F., and Sarmento, B. (2018). Functionalizing PLGA and PLGA derivatives for drug delivery and tissue regeneration applications. *Adv. Healthcare Mater.* 7:1701035. doi: 10.1002/adhm.201701035

Moriguchi, Y., Tateishi, K., Ando, W., Shimomura, K., Yonetani, Y., Tanaka, Y., et al. (2013). Repair of meniscal lesions using a scaffold-free tissue-engineered construct derived from allogenic synovial MSCs in a miniature swine model. *Biomaterials* 34, 2185–2193. doi: 10.1016/j.biomaterials.2012.11.039

Ngo, T. D., Kashani, A., Imbalzano, G., Nguyen, K. T., and Hui, D. (2018). Additive manufacturing (3D printing): A review of materials, methods, applications and challenges. *Compos. B Eng.* 143, 172–196. doi: 10.1016/j.compositesb.2018.02.012

Patel, J. M., Saleh, K. S., Burdick, J. A., and Mauck, R. L. (2019). Bioactive factors for cartilage repair and regeneration: improving delivery, retention, and activity. *Acta Biomater.* 93, 222–238. doi: 10.1016/j.actbio.2019.01.061

Rowland, C. R., Colucci, L. A., and Guilak, F. (2016). Fabrication of anatomically-shaped cartilage constructs using decellularized cartilage-derived matrix scaffolds. *Biomaterials* 91, 57–72. doi: 10.1016/j.biomaterials.2016.03.012

Shao, Z., Zhang, X., Pi, Y., Yin, L., Li, L., Chen, H., et al. (2015). Surface modification on polycaprolactone electrospun mesh and human decalcified bone scaffold with synovium-derived mesenchymal stem cells-affinity peptide for tissue engineering. *J. Biomed. Mater. Res. A* 103, 318–329. doi: 10.1002/jbm.a.35177

Visser, J., Peters, B., Burger, T. J., Boomstra, J., Dhert, W. J., Melchels, F. P., et al. (2013). Biofabrication of multi-material anatomically shaped tissue constructs. *Biofabrication* 5:035007. doi: 10.1088/1758-5082/5/3/035007

Wang, J., Sun, X., Zhang, Z., Wang, Y., Huang, C., Yang, C., et al. (2019). Silk fibroin/collagen/hyaluronic acid scaffold incorporating pilose antler polypeptides microspheres for cartilage tissue engineering. *Mater. Sci. Eng. C* 94, 35–44. doi: 10.1016/j.msec.2018.09.017

Yang, W., Zhu, P., Huang, H., Zheng, Y., Liu, J., Feng, L., et al. (2019). Functionalization of novel theranostic hydrogels with kartogenin-grafted USPIO nanoparticles to enhance cartilage regeneration. *ACS Appl. Mater. Interfaces* 11, 34744–34754. doi: 10.1021/acsami.9b12288

Yang, Z., Li, H., Yuan, Z., Fu, L., Jiang, S., Gao, C., et al. (2020). Endogenous cell recruitment strategy for articular cartilage regeneration. *Acta Biomater.* 50, 198–208. doi: 10.1016/j.semarthrit.2019.11.001

Yuan, Z., Liu, S., Hao, C., Guo, W., Gao, S., Wang, M., et al. (2016). AMECM/DCB scaffold prompts successful total meniscus reconstruction in a rabbit total meniscectomy model. *Biomaterials* 111, 13–26. doi: 10.1016/j.biomaterials.2016.09.017

Zhang, Z.-Z., Chen, Y.-R., Wang, S.-J., Zhao, F., Wang, X.-G., Yang, F., et al. (2019). Orchestrated biomechanical, structural, and biochemical stimuli for engineering anisotropic meniscus. *Sci. Transl. Med.* 11:eaao0750. doi: 10.1126/scitranslmed.aao0750

Zhang, Z.-Z., Jiang, D., Ding, J.-X., Wang, S.-J., Zhang, L., Zhang, J.-Y., et al. (2016). Role of scaffold mean pore size in meniscus regeneration. *Acta Biomater.* 43, 314–326. doi: 10.1016/j.actbio.2016.07.050

Zhao, Y., Zhao, X., Zhang, R., Huang, Y., Li, Y., Shan, M., et al. (2020). Cartilage extracellular matrix scaffold with kartogenin-encapsulated PLGA microspheres for cartilage regeneration. *Front. Bioeng. Biotechnol.* 8:600103. doi: 10.3389/fbioe.2020.600103

Zhu, L., Chen, S., Liu, K., Wen, W., Lu, L., Ding, S., et al. (2020). 3D poly (L-lactide)/chitosan micro/nano fibrous scaffolds functionalized with quercetin-polydopamine for enhanced osteogenic and anti-inflammatory activities. *Chem. Eng. J.* 391:123524. doi: 10.1016/j.cej.2019.123524

Conflict of Interest: The authors declare that the research was conducted in the absence of any commercial or financial relationships that could be construed as a potential conflict of interest.

frontiers in Bioengineering and Biotechnology

REVIEW
published: 04 May 2021
doi: 10.3389/fbioe.2021.664592

Host Response to Biomaterials for Cartilage Tissue Engineering: Key to Remodeling

Fu Wei[1,2†], Shuyun Liu[1], Mingxue Chen[3], Guangzhao Tian[1,4], Kangkang Zha[1,4], Zhen Yang[1,4], Shuangpeng Jiang[5], Muzhe Li[2], Xiang Sui[1], Zhiwei Chen[2] and Quanyi Guo[1*]*

[1] Beijing Key Lab of Regenerative Medicine in Orthopedics, Key Laboratory of Musculoskeletal Trauma and War Injuries, PLA, Institute of Orthopedics, Chinese PLA General Hospital, Beijing, China, [2] Department of Orthopedics, The First Affiliated Hospital of University of South China, Hengyang, China, [3] Department of Orthopedic Surgery, Beijing Jishuitan Hospital, Fourth Clinical College of Peking University, Beijing, China, [4] School of Medicine, Nankai University, Tianjin, China, [5] The First Hospital of China Medical University, Shenyang, China

OPEN ACCESS

Edited by:
Farnaz Ghorbani,
Fudan University, China

Reviewed by:
Amir Seyedsalehi,
University of Connecticut, United States
Ebrahim Tavakoli,
Materials and Energy Research Center, Iran
Farnoosh Saeedinejad,
University of Connecticut, United States

***Correspondence:**
Quanyi Guo
doctorguo_301@163.com
Zhiwei Chen
czw9915@sina.com

[†] These authors share first authorship

Specialty section:
This article was submitted to Biomaterials, a section of the journal Frontiers in Bioengineering and Biotechnology

Received: 05 February 2021
Accepted: 14 April 2021
Published: 04 May 2021

Citation:
Wei F, Liu S, Chen M, Tian G, Zha K, Yang Z, Jiang S, Li M, Sui X, Chen Z and Guo Q (2021) Host Response to Biomaterials for Cartilage Tissue Engineering: Key to Remodeling. Front. Bioeng. Biotechnol. 9:664592. doi: 10.3389/fbioe.2021.664592

Biomaterials play a core role in cartilage repair and regeneration. The success or failure of an implanted biomaterial is largely dependent on host response following implantation. Host response has been considered to be influenced by numerous factors, such as immune components of materials, cytokines and inflammatory agents induced by implants. Both synthetic and native materials involve immune components, which are also termed as immunogenicity. Generally, the innate and adaptive immune system will be activated and various cytokines and inflammatory agents will be consequently released after biomaterials implantation, and further triggers host response to biomaterials. This will guide the constructive remolding process of damaged tissue. Therefore, biomaterial immunogenicity should be given more attention. Further understanding the specific biological mechanisms of host response to biomaterials and the effects of the host-biomaterial interaction may be beneficial to promote cartilage repair and regeneration. In this review, we summarized the characteristics of the host response to implants and the immunomodulatory properties of varied biomaterial. We hope this review will provide scientists with inspiration in cartilage regeneration by controlling immune components of biomaterials and modulating the immune system.

Keywords: biomaterials, immunomodulation, macrophage, tissue engineering, cartilage

INTRODUCTION

Articular cartilage lacks blood vessels, nerves and lymphatic vessels, has a smooth surface and is translucent. It is a form of hyaline cartilage, which is a highly organized connective tissue (Sophia-Fox et al., 2009). Articular cartilage bears mechanical loads and provides cushioning and lubrication, and its protective function is weakened after injury. Due to the lack of self-healing capacity of cartilage, joint injury and progressive degeneration, osteoarthritis (OA) eventually develops, and it becomes difficult to avoid joint arthroplasty (Widuchowski et al., 2007). Therefore, the early repair of damaged articular cartilage is necessary.

Non-operative treatment often involves oral glucosamine sulfate to nourish cartilage and intra-articular injections of Hyaluronic acid (HA) to lubricate the joint. Traditional surgical treatment includes abrasion, subchondral drilling, microfracture, osteochondral autograft transfer system (OATS) (also known as mosaicplasty), and autologous chondrocyte implantation (ACI) (Pestka et al., 2012; Albright and Daoud, 2017; Solheim et al., 2018). However, these methods have achieved limited success. HA offers little protection against early cartilage damage (Nathani et al., 2019). Microfracture is used to treat small articular cartilage lesions that form fibrocartilage and are therefore mechanically weak and prone to degeneration (Benthien and Behrens, 2013). Mosaicplasty is usually suitable for the damage involving subchondral bone, but donor area complications and dead spaces between cylindrical grafts may increase the chance of repair failure (Kock et al., 2008). ACI is a cell-engineering base surgical procedure, but the quality of restoration is severely compromised by the loss of therapeutic chondrocytes (McCarthy et al., 2016). There is an urgent clinical need for new strategies to induce cartilage regeneration. Tissue engineering has emerged in recent years as a promising approach to repair injured cartilage (Makris et al., 2015), aiming to exploit the inherent regenerative potential of human tissues and organs in the degraded state and restore or reconstruct the normal function of the body.

As an indispensable element of the tissue engineering triad, biomaterials not only provide mechanical support for cells, but also act as carriers for bioactive molecules (e.g., growth factors). The biomaterials used to fabricate scaffolds can be roughly divided into two main categories: synthetic polymers, including polycaprolactone (PCL), poly(lactic acid) (PLA), poly(glycolic acid) (PGA), poly(lactic-co-glycolic acid) (PLGA), and poly(L-lactic acid) (PLLA), among others. Alternatively, naturally derived biomaterials are for instance decellularized extracellular matrix (dECM) from diverse tissues and natural molecules such as collagen, gelatin, silk fibroin, HA, alginate, and chitosan, et al. These materials can be used to fabricate different geometric shapes by 3D printing, electrospinning, injection molding techniques and among others (Chen et al., 2018; Lukanina et al., 2018; Xia et al., 2018; Lu et al., 2019). The scaffolds fabricated using these two kinds of biomaterials have advantages and disadvantages (Londono and Badylak, 2015). Compared with synthetic polymers, naturally derived biomaterials have a composition closer to that of cartilage, good biocompatibility and low cytotoxicity, and they are beneficial for cell adhesion, proliferation and differentiation (Huang et al., 2019; Xiao et al., 2019). However, these materials are limited in terms of processability and manipulatable degradation time (Pati et al., 2014). In contrast, synthetic polymers have good mechanical strength, controllable degradation and high plasticity (Li et al., 2019b; Stefani et al., 2020). But they also have shortcomings, such as poor biocompatibility, acidic degradation products, low biological activity, hydrophobicity and limited interfacial integration with tissue (Stocco et al., 2014; Park et al., 2018; Lin et al., 2019).

The great potential of tissue engineering for cartilage repair has given rise to new hope. As mentioned above, a wide variety of biomaterials have been researched and developed to achieve better repair and regeneration outcomes. But up to now, when implanted into vivo, most of the biomaterials have not worked as expected, some even lead to acute or chronic inflammation (Cipriano et al., 2017; Vollkommer et al., 2019). An important link seems to have been ignored by us. Numerous researches on cartilage tissue engineering are focused on the effect of biomaterial's physical properties and physicochemical properties on repair outcome. However, limited studies have focused on how biomaterials affect host response, such as inflammation and immune modulation. Studies have suggested that implanted biomaterial induced adverse immune response is associated with a prolonged reaction time, delayed interface connection and integration, and reconstruction failure (Sirlin et al., 2001; Fraitzl et al., 2008). It has also been shown that the host immune response has a positive effect on the reparative effect of tissue engineering scaffolds to some extent (Sadtler et al., 2019). Direct use of acellular extracellular matrix (ECM) or native ECM components can elicit a favorable immune response prior to tissue remodeling outcome. This immunomodulation usually depends on the composition and structure of the scaffold. Tissue-derived ECM scaffolds induce a pro-regeneration immune environment through Th2 immune response, which drive macrophage polarization toward M2 phenotype via IL-4 (Cipriano et al., 2017). Besides, the regulatory role of pore size and porosity of scaffold in host response has also been confirmed (Orenstein et al., 2010; Junge et al., 2012). In scaffold strategy based on loading immunomodulatory function cells, mesenchymal stem cells (MSCs), as commonly used seed cells, can regulate local immune response by secreting anti-inflammatory and pro-inflammatory cytokines to promote repair (English, 2013; Nagubothu et al., 2020). Indeed, the interaction between implanted biomaterial and host immune system is crucial in determining the constructive and functional outcome. Host response is considered to be influenced by the immune components (also known as immunogenicity) of biomaterial, cytokines, or inflammatory agents induced by implants and injured tissue. As such the immunogenicity of implanted biomaterials should not be ignored. Additionally, cartilage is believed to be a tissue with "immune privilege," located in a relatively closed environment (Smith et al., 2015). Nevertheless, cartilage tissue injury is accompanied by the disruption of balanced environment, release of inflammatory cytokines and chemokines, and immune/inflammatory cells migration will further promote the response of the host immune system to the implanted biomaterial.

The host response to biomaterials plays a central role in tissue repair and regeneration, have both positive and negative implication for the healing process. An effective biomaterial-based immune modulation strategy is becoming an attractive approach in the field of regenerative medicine (Hachim et al., 2019; Shahbaz et al., 2020; Wu et al., 2020). This review summarizes the characteristics of the interaction between host immune system and implanted biomaterial, and the immunomodulatory properties of common biomaterials in the hope of providing inspiration for next generation of tissue engineering regeneration strategy.

HOST RESPONSE FOLLOWING BIOMATERIAL IMPLANTATION

Biomaterials implanted into damaged tissues come into contact with cells, surrounding tissues and blood and thus cannot avoid activating the immune system by triggering a foreign body reaction. In fact, the relationship between biomaterial-mediated tissue healing and immune response is very complex, with many cell types, plasma proteins, and extracellular fluid components being involved. The reaction of the biomaterial with the surrounding environment is actually an important factor in determining its biocompatibility. The host response (including immune, inflammatory and foreign body reactions, etc.) can be local or systemic, which is mainly influenced by immune components of the implant, type of biomaterial or injured tissue, and biomaterial surface chemistry and degradation characteristics, and so on. This will ultimately affect the lifespan of the implant and the outcome of the repair.

The Vroman Effect of Implanted Biomaterials

Biomaterial-mediated host reactions are primarily caused by host cell recognition of the biomaterial surface, which is based on the adsorption of adhesion proteins to the surface of the biomaterial. Adhesion proteins, such as fibrinogen, vitronectin, fibronectin, albumin, γ globulin, complement, and others, form a protein layer on the surface of the biomaterial to modulate host inflammatory cell interactions and adhesion (Pape et al., 2017; Tanaka et al., 2017; Horbett, 2018). The process of cell adsorption to and spreading on the biomaterial surface is mediated by adhesion proteins. The effect of a biomaterial on the cell or host reaction is actually achieved by influencing the adhesion behavior of proteins to the surface. The type, concentration and spatial conformation of the adhesion protein will directly activate the response of the host immune cell to the biomaterial (Wilson et al., 2005), i.e., resulting in an innate or adaptive immune response. In turn, the type, concentration and spatial conformation of these adsorbed proteins depend on the surface characteristics of the biomaterial, which determine the adsorption, survival and function of cells (especially monocytes and macrophages) in the protein layer (Anderson et al., 2008). Protein adhesion is a dynamic process, a high concentration of adhesion proteins first arrive and adsorb onto the surface of the implant, and these proteins will eventually be replaced by proteins with a high affinity for the surface of the biomaterial. The phenomenon of protein adsorption and desorption is known as the Vroman effect (**Figure 1**; Hirsh et al., 2013; Kim, 2017). After implantation, biomaterial is immediately covered by proteins in the blood and tissue fluid, which direct the subsequent cascade biological reactions. Studies have shown that the orientation and conformation of fibrinogen on the surface of biomaterials can modulate neutrophils adhesion (Milleret et al., 2015). There is a direct relationship between a stronger adhesion capacity on the surface of biomaterials and more desirable cell adhesion and growth (Shamloo and Sarmadi, 2016). It is well known that at similar surface roughness, hydrophilic surfaces preferentially adsorb proteins and promote cell adhesion and growth compared to hydrophobic surfaces (Chaudhary et al., 2012). By immobilizing proteins on the biomaterial surface, developing a biointerface that can enhance cell "homing" ability is one of the critical factors in biomaterial development (Chrzanowski et al., 2012). The biomaterial surface properties, protein adsorption and cellular responses are considered to be interrelated and ultimately determine the biocompatibility of the biomaterial (Allen et al., 2006). The relationship between these different but related phenomena remains to be elucidated.

The Main Actors in Host-Biomaterial Interaction

There is a class of integrin receptors on the cell surface that can specifically recognize certain peptides of adhesion proteins, thereby affecting cell adhesion, migration, activity, and other functions (Yang et al., 2013). The type and level of cell adhesion proteins change in a time-dependent manner (Xu and Siedlecki, 2007). The early stage of host response following tissue injury is characterized by a predominance of neutrophils, which are the first inflammatory cell type to arrive at the site of injury. Neutrophils are capable of phagocytosis and degradation of foreign substances, dead cells, and providing signaling molecules to recruit macrophages to injury site. Mast cells modulate the inflammatory response by releasing particles, such as histamine, IL-4, and IL-13 that can recruit macrophages and facilitate their fusion into foreign body giant cells (DeFife et al., 1997; Ang et al., 1998; McNally and Anderson, 2002). Macrophages begin to infiltrate approximately 12 h post-injury, but their response lasts longer than that of neutrophils, and subsequently become the dominant cell type within the site of injury. The role of macrophages in tissue repair and regeneration is very complex, could perform beneficial or detrimental functions. That is, deciding toward to a constructive and functional outcome or scar tissue formation. The T lymphocyte cell population plays an important regulatory role in tissue repair by the secretion of cytokines and chemokines, many of which are considered to influence macrophage polarization. Moreover, dendritic cells, natural killer (NK) cells, B lymphocytes, plasmocytes, and among others also participate in the immune response to varying degrees (**Figure 1**). The occurrence and outcome of a series of events will vary according to the surface chemistry, stiffness, and degradation properties of biomaterials, as well as other factors that have not been elucidated (Brodbeck et al., 2001).

With the advances in tissue engineering and regeneration medicine, it has now become clear that the immune system plays a critical role in tissue repair process (Julier et al., 2017). Repair strategy of immune system regulated through biomaterials is aim at activating desired components of inflammatory, proliferation, and remolding phase to promote a constructive and functional remolding outcome. Allowing specific biological response is beneficial to both the integration and performance, the current challenge is the development of biomaterials or delivery systems capable of modulating the immune system as a way of stimulating tissue repair and regeneration (Badylak et al., 2008). Therefore, a deeper understanding of immunological profile of biomaterials

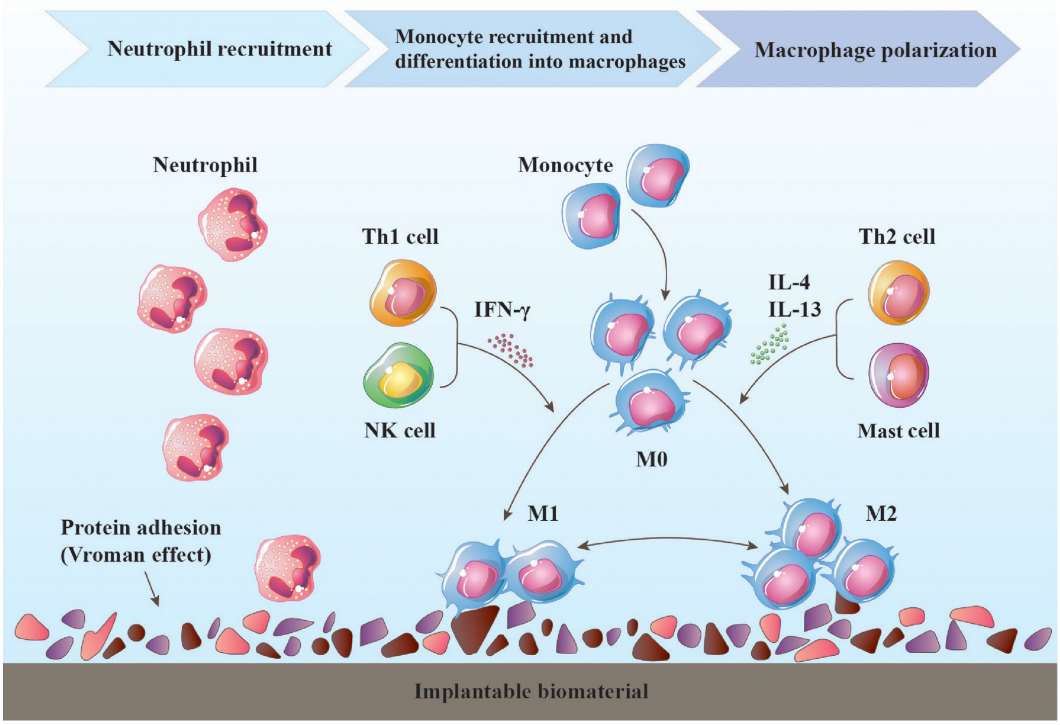

FIGURE 1 | Immune response to an implantable biomaterial. Various proteins adhere to the surface of the biomaterial. Neutrophils are first recruited, followed by monocyte-derived macrophages, which become the dominant cell type around the biomaterial. Macrophage differentiation is temporary, and the polarization state may change depending on the tissue milieu. The timely transition of the macrophage phenotype from proinflammatory M1 to anti-inflammatory and immunomodulatory M2 is critical for constructive tissue remodeling, and other immune cells (T helper cells, NK cells, mast cells, etc.) are also involved in this process.

and the interaction of immune system and biomaterials interaction is essential for the better repair outcomes.

IMMUNOLOGICAL CHARACTERIZATION OF BIOMATERIALS

Synthetic Polymers

In the body, articular cartilage is subjected to multiaxial loads, including those resulting from compression, tension, shear and fluid flow (Pattappa et al., 2019). Articular cartilage exhibits excellent biomechanics due to its unique hyaline-like cartilage composition and the ultrastructure of the ECM, especially the tight network of type II collagen (Col II) fibrils and abundant negatively charged proteoglycan chains. The controlled mechanical properties of synthetic polymers can meet the biomechanical requirements of the process of cartilage regeneration (Silva et al., 2020). Synthetic polymers have good plasticity, and their microstructure, morphology, and degradation rate can be predesigned and regulated according to the biology of specific tissue (Wang et al., 2020b). PCL (Venugopal et al., 2019), PLA (Baena et al., 2019), PGA (Lin et al., 2017), and PLGA (Kim et al., 2019) are the most representative and widely used synthetic polymers, and have been approved by the FDA for clinical human use. Scaffolds made from synthetic polymers temporarily provide mechanical support after implantation, as well as a microenvironment for cell growth, proliferation and differentiation, thereby regulating and inducing tissue differentiation and regeneration (Li S. et al., 2020; Salonius et al., 2020). The structure of the scaffold is very important for cartilage regeneration, and tissue engineering applications often require the use of porous three-dimensional (3D) scaffolds to facilitate cell migration and cell-cell interactions (Schipani et al., 2020). Secondly, during the process of regeneration, scaffold should also have sufficient strength to resist the physiological load, and the stress should be properly distributed to the surrounding tissue (Lohfeld et al., 2015). The good printing properties of synthetic polymers allow their combination with 3D printing techniques to effectively address this issue. The controllability, reproducibility and good mechanical properties of synthetic polymers show promising applications in cartilage tissue engineering. However, the lower bioactivity they exhibit is not favorable for incorporating with host tissues, as they may lead to increased local pH through acidic degradation products, immune response or toxicity, and inflammation associated with high molecular weight polymers.

Acidic Degradation Products of Synthetic Polymers

Synthetic polymers have one common feature: degradability. Degradation occurs progressively (by chemical hydrolysis or enzymatic degradation) over time after implantation. Acidic

degradation products reduce the pH of the surrounding environment, leading to inflammatory cell infiltration and aseptic inflammation (Lendlein and Langer, 2002). Clinical reports have shown that up to approximately 8% of patients treated with PGA had non-infectious inflammation (Peppas and Langer, 1994). The longer the biodegradation cycle of synthetic polymers, the greater the probability of inducing an adverse host response, this event is related to the acidic degradation products and immunogenicity of the polymer. Acidic products (e.g., lactic acid, glycolic acid) will trigger an autocatalytic reaction when reducing the pH, which can accelerate the formation of the products (Göpferich, 1996; Burkersroda et al., 2002; Eglin and Alini, 2008). When the accumulation of acidic products exceeds the metabolic capacity of the body, the gradually decreasing acidity of the environment in turn accelerates the degradation of the biomaterial. These acidic products are one of the factors involved in the host-biomaterial reaction (Rezwan et al., 2006). In addition, the surface chemistry, structure, type, purity, and crystallinity of the biomaterials also influence the occurrence, extent and outcome of the host-biomaterial interaction (Milleret et al., 2015; Jiang et al., 2016; Stratton et al., 2016).

Surface Chemistry: Hydrophobicity/Hydrophilicity, Chemical Groups, Charge Characteristics

As previously mentioned, the adsorption of proteins on biomaterial surface is essential for the cell-biomaterial interaction (Ekdahl et al., 2012). A factor that directly determines the type, amount and conformation of adhesion proteins is the biomaterial surface chemistry, such as its hydrophobicity/hydrophilicity, chemical moieties and charge characteristics. By changing the biomaterial surface chemistry to regulate the adsorption of proteins, it has been shown that hydrophilic and anionic chemistries are more likely to induce macrophage apoptosis than hydrophobic or cationic surfaces, which may result in no inflammatory outcome (Brodbeck et al., 2001). Macrophages play an important and complex role in the regulation of the immune microenvironment of implant, moreover, the adhesion and activation of lymphocytes also depend on macrophages. Macrophage plasticity allows their adaptation to different stimuli (Rostam et al., 2016). M1 macrophages can drive the inflammatory response, causing the scaffold to be wrapped in fibrous tissue, separating it from the surrounding tissue (Fujihara et al., 2020). In contrast, M2 macrophages have anti-inflammatory properties and promote repair (Ma et al., 2014; Hotchkiss et al., 2018; Deng et al., 2020).

The commonly used synthetic polymers are hydrophobic, with a surface that has a high affinity for many kinds of proteins. When protein molecules adsorb onto the surface of a hydrophobic biomaterial, their conformation changes through hydrophobic interactions, exposing the hydrophobic domain and facilitating close binding to the surface (Lu and Park, 1991; Hu et al., 2001; Collier and Anderson, 2002; Heuberger et al., 2005; Evans-Nguyen et al., 2006). There is a direct correlation between the hydrophobicity of biomaterials and activation of the host immune system (Hu et al., 2001; Moyano et al., 2012). The conformational change of adhesion proteins on the biomaterial surface may be one of the reasons for the occurrence of adverse response. For instance, the foreign body reaction, inflammation, and the exposure of hidden structures and sequences of adhesion proteins allows them to act as receptors for the binding of inflammatory or immune cells to the surface (Thevenot et al., 2008). Innate immune cells are able to recognize invaders and induce an immune response through pattern recognition receptors (PRPs) (Brubaker et al., 2015), based on the combination of PRPs and ligands [pathogen-associated molecular patterns (PAMPs) (Janeway, 1989); damage-associated molecular patterns (DAMPs) (Matzinger, 1994)]. Hydrophobicity is considered to be a DAMP, in other words, the hydrophobic property of a biomaterial is its inherent immunogenicity, which may initiates constructive remolding or scar tissue formation (Seong and Matzinger, 2004). It has been found that hydrophobic biomaterial surfaces selectively interact with CD8+ T lymphocytes, while hydrophilic/neutral surfaces tend to interact with CD4+ T lymphocytes (Chang et al., 2009). The hydrophilicity and hydrophobicity of a biomaterial can regulate the behavior of immune cells (Brodbeck et al., 2002; Jones et al., 2007), and the effects on tissue repair need to be further explored. To minimize adverse events triggered by the immunogenic of hydrophobic biomaterial surfaces, the hydrophilic molecules polyethylene oxide (PEO) and polyethylene glycol (PEG) are often used as biomaterial coatings to reduce surface protein adhesion and increase hydrophilicity (Tiller et al., 2001; Drury and Mooney, 2003). These coatings can also prevent implantation-related infection and biofilm formation (Busscher et al., 2012). It has also been reported that the hydrophilicity of biomaterial can be improved by adjusting the content of graphene oxide (GO), which improved in correspondence to an increase of GO (Aidun et al., 2019; Jabari et al., 2019).

Chemical groups are another important surface characteristic of biomaterials, with amino ($-NH_2$), carboxyl (-COOH), hydroxyl (-OH), and methyl ($-NH_3$) groups being commonly explored. These chemical moieties have a significant effect on the host response to biomaterials. Surfaces with hydrophilic $-NH_2$ or -OH groups (positively and neutrally charged, respectively) strongly stimulated inflammatory cell recruitment and the fibrotic response *in vivo* (Kamath et al., 2008). While surfaces with hydrophobic, neutral $-NH_3$ groups induced a more severe inflammatory response, and hydrophilic surfaces with -COOH groups (negatively charged) resulted in reduced cell infiltration and a milder inflammatory reaction (Barbosa et al., 2003, 2006; Barbosaa et al., 2004; Nair et al., 2008). These different results suggest that the $-NH_3$ surface can eliminate the adsorption of leukocytes and reduce the immune reaction (Sperlinga et al., 2005). It has also been shown that $-NH_2$ groups shift macrophage polarization toward an anti-inflammatory M2 phenotype and decrease the number of proinflammatory M1 macrophages, while -COOH groups yield the opposite result (Bartneck et al., 2010). This suggests that these findings cannot be explained by a single experimental model and may vary *in vivo* and *in vitro*. Based on the existing knowledge, studies have begun to use chemical groups to modify the surface of engineered scaffolds to facilitate repair and regeneration.

A scaffold surface was modified with either -NH_2 or -COOH, and it was found that both modified scaffolds could promote the adhesion and proliferation of adipose-derived stem cells (ADSCs). The difference was that scaffolds functionalized with -NH_2 moieties promoted the osteogenic differentiation of ADSCs, while those functionalized with -COOH moieties promoted chondrogenic differentiation (Griffin et al., 2017). In terms of the ability to induce cell differentiation, -OH groups showed the strongest ability to induce osteogenic differentiation, followed by -NH_2, -COOH, and -NH_3 groups. Among them, -NH_3 groups appeared to induce moderate myogenic differentiation (Keselowsky et al., 2004; Lan et al., 2005). Further studies revealed that -NH_2-modified surfaces activate the extracellular signal-related kinase (ERK1/2) signaling pathway by promoting the expression of bone marrow stromal cell (BMSC) integrins to induce osteogenic differentiation (Bai et al., 2013). Further expanding the understanding of biomaterial surface characteristics and how biomaterials interact with host immune system is needed to more effectively repair damaged tissues (Damanik et al., 2014). In fact, biomaterial-mediated tissue repair and regeneration is influenced by a variety of factors, such as immune components of implant, immune milieu. The properties of biomaterials need to be more comprehensively understood for improved application.

Natural Biomaterials

The other type of biomaterials is natural biomaterials, including decellularized tissues, natural polymers, and cell-derived matrix. Compared to synthetic polymers, they are derived from biological tissues and are more suitable for cell adhesion, proliferation, differentiation and so on. Secondly, there are no acidic products. Natural polymers include polysaccharides (such as HA, alginate, and chitosan) and proteins (gelatin, silk fibroin, and fibrin), are widely used in the production of scaffolds for cartilage regeneration. Due to their origins, These materials are characterized by high biocompatibility, bioactivity, and the degradation products are non-toxic; but, their low mechanical stability, rapid degradation, and poor stability greatly limits their applications (Wasyłeczko et al., 2020). For example, alginate based hydrogel scaffolds can support the growth and proliferation of enveloped chondrocytes and maintain their chondrocyte morphology, but they have poor stability and loss of mechanical strength in a short period of time (Bao et al., 2020). Secondly, alginate has low cell adhesion and cell interaction ability. Compared with other natural synthetic polymers, the main advantage of silk fibroin is its good strength and toughness, which is more suitable for the preparation of load bearing tissue engineering such as cartilage regeneration (Kundu et al., 2013). Gelatin was modified by methacrylate anhydride, and the prepared product methacrylamide enhanced the mechanical properties and degradation rate of gelatin, which makes it play an important role in the application of cartilage tissue engineering (Han et al., 2017). Unfortunately, these natural polymers are difficult to achieve hyaline cartilage regeneration, but rather non-valuable fibrocartilage. Natural biomaterials are favored by a wide range of researches, especially naturally derived ECM biomaterials. Decellularized ECM is considered to be the best choice because it can provide a microenvironment similar to natural ECM and further modulate the cellular behavior and function.

Rationale for Using Extracellular Matrix (ECM) as Biomaterial

The optimal scaffold biomaterial should be able to provide an environment like that in which tissue-resident cells survive, i.e., the ECM. It is a precise and orderly structural network composed of large molecules such as proteins and polysaccharides. The ECM provides physical structure, and the basic biochemical and biomechanical signals for regulating tissue morphology, differentiation and homeostasis (Wang et al., 2018; Nie et al., 2020). Tissue engineering technology is to mimic the structure and composition of the damaged tissue, providing an optimal environment for cell survival, cell-cell and cell-tissue interactions and signal transduction. The fabrication of functionalized scaffolds with biological activity made of natural biomaterials is undoubtedly a promising approach (Feng et al., 2020; Vainieri et al., 2020). Natural biomaterials such as dECM and natural polymers (collagen, silk fibroin, alginate, and chitosan) show repair potential in animal models of cartilage lesion (Dai et al., 2019; Pérez-Silos et al., 2019; Singh et al., 2019). Tissue (or organ) from various species after decellularization can be utilized for the repair of a damaged tissue (Sun et al., 2018; Lindberg et al., 2019). Such as there are studies have successfully used acellular human umbilical cord Wharton's jelly as a biomaterial to repair articular cartilage (Zhao et al., 2018).

Natural biomaterials are being explored and applied increasingly extensively. The mechanism of the natural biomaterial-driven tissue remolding remains to be elucidated, and adverse immune responses after implantation is a great challenge hindering application (Wu et al., 2019). Because of natural composition and structure, natural biomaterials elicit different host responses than others. There is a growing body of evidence suggesting that the host immune response to a biomaterial not only affects its function but must also be the primary factor determining the success of the repair. The issue of the host immune response induced by natural biomaterials, especially dECM, is reviewed below.

Remove Immune Components via Decellularization

In recent decades, the decellularization of tissues (or organs) has been developed and applied as an emerging technology in tissue engineering and regenerative medicine. The main purpose of the decellularization process is to remove immune components (such as cells and nuclear materials), while preserving the natural structure and biochemical components. Acellular ECM has good biocompatibility and biological activity. Similar to the natural matrix environment, acellular ECM can regulate the biological function of resident cells and multifunctional stem cells and promote the recovery of the structure and function of the damaged tissue (Agrawal et al., 2010; Li et al., 2018). In addition to its application in the repair of articular cartilage, acellular ECM has been applied in various tissues (or organs) such as bone (Huber et al., 2017), tendon (Zhang S. et al., 2018), nerve (Chen et al., 2019), blood vessels (Gong et al., 2016), cornea

(Chakraborty et al., 2019), and skin (Milan et al., 2019), and some success in achieving repair.

Evaluate the Decellularize Degree of ECM

The host immune response to natural biomaterial can be activated by cell surface markers, residual DNA, alpha-Gal epitopes, and major histocompatibility complexes (MHCs), among others (Sutherland et al., 2015). Few researchers have studied the immunogenicity of allogeneic or xenogeneic cartilage-derived biomaterials. Cartilage tissue is considered to be "immune privilege" and does not elicit an host immune response. Studies have shown that unsatisfying outcomes are still caused by cartilage-derived biomaterials *in vivo*. The decellularization of tissues (or organs) is typically achieved using one or a combination of the following approaches: chemical (Ventura et al., 2019), physical (Schneider et al., 2016), and enzymatic (Luo et al., 2015; Li et al., 2019c). Decellularization technology broadens the source of biomaterials by reducing immune components. Compared to other tissues, the cartilage ECM is dense and difficult to decellularize (Gong et al., 2011). Insufficient decellularization easily leads to excessive residual immunogenic components. While intense decellularization will result in damage to the ECM ultrastructure and the loss of composition (Gilpin and Yang, 2017; Shen et al., 2020). Both run counter to the purpose of decellularization. Although a large number of studies have claimed to be able to achieve effective decellularization, there are still residual cellular constituents (Elder et al., 2010; Luo et al., 2015; Roth et al., 2017; Ghassemi et al., 2019; Bordbar et al., 2020). Effectively balancing the removal of immune components with the destruction of the ECM ultrastructure (or the loss of ECM components), and determining the impact of residual substances on host-biomaterial interactions remain long-debated topics. There is still a large gap in the understanding of the innate and adaptive immune responses resulting from the application of dECM, as well as the role of macrophages and other immune cells in the remodeling of dECM.

Residual cellular material within the ECM may contribute to cytocompatibility problems, and some even led to acute or chronic inflammation (Brown et al., 2009; Nagata et al., 2010; Zhang et al., 2010). The probability of such adverse events can be reduced to some extent through decellularization. Currently, there are no uniform criteria for measuring the degree of decellularization. Most researchers have accepted the following minimum criteria to satisfy the intent of tissue decellularization: (1) the content of double-stranded DNA (dsDNA) should be $<$50 ng per mg ECM dry weight; (2) the length of DNA fragments should be $<$200 bp; and (3) staining with 4′,6-diamidino-2-phenylindole (DAPI) or H&E should indicate the lack of visible nuclear material in tissue sections (Crapo et al., 2011). Badylak et al. (2008) proposed these conditions based on the outcomes of research in which an *in vivo* constructive remodeling process was observed, while adverse events were avoided. Of course, these guidelines are not sacrosanct and can differ depending on tissue type, implantation site and host immune function. There is still a lack of a clear scientific basis to establish optimal criteria, and most studies based on decellularization have been evaluated according to the universal criteria described above. The success or failure of any implanted material is related to the host immune system, and host innate or adaptive immune cells will respond to the cellular content, DNA and other immune components of the ECM (Badylak and Gilbert, 2008; Keane and Badylak, 2015).

Residual immunogenic substances in biomaterials resulted from mildly or inadequately decellularized matrix may have proinflammatory effects, which are associated with poor tissue remodeling outcomes (Brown et al., 2009). The focus on nucleic acids in the criteria for decellularization is reasonable, as residual DNA is directly associated with adverse host reactions (Zheng et al., 2005; Nagata et al., 2010). Numerous commercial products composed of dECM are now available for clinical use, such as Restore®, GraftJacket®, TissueMend®, Oasis®, and Alloderm®. Although most commercial products still contain DNA, the effect of the clinical application of these products is positive to a large extent. The residual DNA content is below 50 ng/mg ECM dry weight, or even lower, which is not enough to cause adverse host reactions that interfere with tissue remodeling (Gilbert et al., 2009).

Residual DNA is usually present in small fragments, which reduces the likelihood that it will play any substantial role in an adverse tissue remodeling response. In the majority of biomaterials used in the clinic, residual DNA consists of fragments that are less than 300 bp in length, and seems to be too short to be of concern. In addition to the low content and short length of residual DNA, degradation of the DNA along with the ECM is another important reason that undesirable host reactions can be avoided *in vivo*, especially for some uncross-linked ECM materials that degrade rapidly. One of the important reasons why DNA fragments are required to be less than 200 bp as a minimal criterion of decellularization may be that the chromosomal DNA of apoptotic cells is autonomously degraded into 180 bp nucleosomal units by caspase-activated DNase (CAD). This DNA is then phagocytosed by macrophages and further degraded by deoxyribonuclease II (DNase II) in lysosomes (Kawane et al., 2003). The accumulation of undigested 180 bp fragmented DNA in macrophages causes them to produce proinflammatory cytokines, such as IFN-β and TNF-α (Yoshida et al., 2005; Kawane et al., 2006). TNF-α may be linked to the development of polyarthritis (Kawane et al., 2006). Additionally, residual DNA is recognized by macrophages as a DAMP through TLRs, especially TLR9 (Hemmi et al., 2000; Zhang et al., 2010; Ohto et al., 2015). Related studies have shown that macrophages can be activated by DNA fragments as small as 24 bp (Karayel et al., 2009; Aamodt and Grainger, 2016). Thus, the current threshold for residual DNA in decellularized tissues does not seem to be ideal, and it serves more as a benchmark established to aid research. As innate immune cells, macrophages participate in the host response to biomaterials in the early stage, and the phenotype of macrophage is significantly associated with tissue remodeling. As mentioned previously, DNA may be one cause of skewed polarization toward an M1 proinflammatory phenotype (Brown et al., 2009). Study found that more M1 proinflammatory macrophages adsorbed onto the dECM scaffold more residual content or longer DNA fragments, while the surroundings of the scaffold from which DNA was effectively eliminated were dominated by M2 anti-inflammatory and remodeling macrophages (Keane et al., 2012).

However, what is puzzling is the paucity of research on the interaction between macrophages and residual DNA in dECM. Obviously, there is a large gap in the understanding of the role of these molecules in the host response to dECM.

An in-depth investigation of macrophage-dECM interactions would be helpful in designing tissue engineering scaffolds more scientifically and rationally, thus enhancing the reparative effect and optimizing performance; further research is urgently needed.

ROLE OF MACROPHAGES IN ECM-MEDIATED TISSUE REGENERATION

Critical Regulator and Effector Cell in Host-Biomaterial Interaction

In tissue engineering, the host response to biomaterials is a key determinant of the success or failure of constructive tissue remodeling. The repair of damaged tissues using biomaterials is a complex process that involves the interaction of diverse immunological and biological systems. These activities do not occur randomly but as a series of finely regulated steps and events, which are correlated with the emergence of different cell types during distinct stages. The repair can be defined as wound healing, which is traditionally divided into many complex and overlapping stages, including coagulation and hemostasis, inflammation, proliferation and remodeling. Similarly, the host response to an implanted biomaterial involves the same steps observed in these stages. The ideal biomaterial should be able to modulate the different stages of the healing response by inducing a transition from inflammation and scar tissue formation to constructive remodeling and functional tissue recovery (Waters et al., 2017). ECM-derived tissue engineering biomaterials, unlike their synthetic counterparts, have been shown to prompt unique and constructive tissue remodeling (Sadtler et al., 2019). ECM has an immunomodulatory effect, particularly in terms of regulating macrophages–the key regulator and effector cells in the host response to biomaterials (Slivka et al., 2014; He et al., 2018). The phenotypical response of macrophages is a key factor in determining the outcome of downstream tissue remodeling (Brown et al., 2012b).

As previously described, macrophages begin to infiltrate in the early stage after implantation and become the primary immune cells in the host response to ECM-derived scaffolds after approximately 3–4 days (Brown et al., 2009). Recently, macrophages have gained extensive attention and been researched, and they are considered to be most relevant to tissue repair mediated by ECM-derived scaffolds. Previous studies have demonstrated the importance of macrophages in tissue reconstruction and regeneration, especially in applications involving tissue engineering biological scaffolds (Linares et al., 2016; Dai et al., 2018b, 2020; Zhang et al., 2020). Specifically, the process of ECM-mediated tissue remodeling depends on the activation of host macrophages toward the M2 phenotype, with anti-inflammatory and immunomodulatory functions (Dearth et al., 2016). At early points, a larger M2/M1 macrophage phenotype ratio predicts the later development of favorable organizational reconstruction (Brown et al., 2012a). Understanding the immunomodulatory effect of biological scaffolds provides potential guidance for the further development of ideal biomaterials to promote tissue repair and regeneration. Unfortunately, to date, the underlying mechanisms by which ECM-derived scaffolds modulate the macrophage phenotype shift from M1 to M2 are largely unknown.

Phenotypic, Function and Plasticity Features of Macrophages

Macrophages are a heterogeneous cell population with various functional phenotypes that participate in a variety of biological processes, including tissue homeostasis, inflammation, disease progression, and functional reconstruction. Human peripheral blood monocytes can be differentiated into macrophages (M0) and then polarized to different phenotypes. Macrophage phenotypes have been classified along a spectrum ranging from M1 (classically activated, proinflammatory) to M2 (alternatively activated, anti-inflammatory, immunomodulation, remodeling), with multiple subclasses (Martinez and Gordon, 2014; Alvarez et al., 2016). The nomenclature is similar to that used for Th1/Th2 lymphocytes (Mills et al., 2000). These diverse phenotypes can be distinguished by cell surface markers (CD molecules), secreted cytokines and effector molecules, and the metabolism of arginine (Anderson and Jones, 2007). M1 macrophages, the classical proinflammatory phenotype, are known to be activated by IFN-γ alone or in combination with LPS or GM-CSF (Tarique et al., 2015). These cells are able to secrete a series of proinflammatory factors, including TNF-α, IL-1β, IL-6, IL-12, and IL-23 (Lopa et al., 2015). Additionally, M1 macrophages can produce reactive oxygen species (ROS) and present antigens and are inducers and effectors of the Th1 inflammatory response (Mosser, 2003). M1 macrophages produce high levels of inducible nitric oxide synthase (iNOS), leading to the metabolism of arginine into nitric oxide (NO). In contrast, "alternatively activated" M2 macrophages are anti-inflammatory and promote constructive tissue remodeling. M0 macrophages are polarized to the M2 phenotype by exposure to a variety of signals, including the cytokines IL-4 (classical M2-polarizing factor) and IL-13, immune complexes, and matricryptic peptides released during the degradation of ECM-derived scaffolds (Sicari et al., 2014). M2 macrophages are characterized by the secretion of IL-10, chemokine (CCL)-1, CCL-18, and TGF-β (Fahy et al., 2014; Manferdini et al., 2017), the expression of high levels of scavenger, galactose and mannose receptors (e.g., CD206), and promotion of the Th2 response (Mills et al., 2000). Unlike the metabolism of arginine in M1 macrophages, in M2 macrophages, highly expressed arginase (Arg-1) metabolizes it to ornithine and polyamines instead of NO. According to its specific markers and functions, the M2 subphenotype can be further divided into four different subclasses (M2a, M2b, M2c, and M2d) (Ryszer, 2015; Yue et al., 2017), which are often overlooked and regarded as a single group. The functions of the M2 subtypes and others are shown in **Table 1**. **Table 1** summarizes information related to

TABLE 1 | Summary of macrophage subtypes and functions.

Macrophage phenotype	Inducers	Expressed markers	Secreted molecules	Functions	References
M1	IFN-γ, LPS, GM-CSF	CD80, CD86, CD68, CCR7	TNF-α, IL-1β, IL-6, IL-12, IL-23, iNOS, ROS, MMPs, VEGF	Proinflammatory, tissue damage, Th1-type reaction	Mosser, 2003; Verreck et al., 2004; Lopa et al., 2015; Tarique et al., 2015; Qiu et al., 2018
M2a	IL-4, IL-13	CD206, CD163	FIZZ1, Arg-1, TGF-β, CCL-18	Tissue repair and remodeling, anti-inflammatory	Spiller et al., 2014; Raimondo and Mooney, 2018; Wiktorowicz et al., 2019
M2b	ICs, LPS, IL-1β, TLR ligand	IL-10R, CD86, CD163	IL-10, IL-1β, IL-6, TNF-α	Immunoregulation, homeostasis	Gerber and Mosser, 2001; Yue et al., 2017; Yang et al., 2019
M2					
M2c	IL-10, TGF-β, glucocorticoid	CD163, CD206	TGF-β, Arg-1, CCL-16, CCL-18, MMPs	Pro-wound healing, matrix deposition, tissue remodeling	Zizzo et al., 2012; Spiller et al., 2014; Waters et al., 2017; Becker et al., 2018
M2d	TLR ligand, adenosine	VEGF, IL-12^{low}	IL-10, VEGF	Angiogenesis	Grinberg et al., 2009; Ferrante and Leibovich, 2012

IL, interleukin; IFN-γ, interferon-gamma; CD: cluster of differentiation; ICs: immune complexes; LPS, lipopolysaccharide; TLR, Toll-like receptor; TGF-β, transforming growth factor-beta; iNOS, inducible nitric oxide synthase; TNF-α, tumor necrosis factor-alpha; CCL, chemokine ligand; ROS, reactive oxygen species; GM-CSF: granulocyte-macrophage colony stimulating factor, Th1: type 1 helper; MMPs, matrix metalloproteinases; CCR, chemokine receptor; FIZZ1: Found in inflammatory zone 1; Arg-1, arginase-1; VEGF, vascular endothelial growth factor.

the M1 and M2 phenotypes, including the inducers, expressed markers, secreted molecules and functions.

Promote Tissue Regeneration by Modulate Macrophage Polarization

Significant effort has been made to regulate macrophage polarization using biomaterial and scaffold design strategies to promote tissue regeneration, which is known as immuno-informed techniques. It is hoped that the development of biomaterials that can stimulate the polarization of macrophages toward reparative functional phenotypes is becoming a research hotspot (Spiller et al., 2015). Designing a biomaterial with immunomodulatory function is a practical and efficient strategy. One study investigated the immunomodulatory properties of fabricated biomimetic with a bone-like staggered nanointerface during bone regeneration, and it was found that the hierarchical nanointerface possess the ability to facilitated M2 macrophage polarization to promote endogenous bone regeneration (Jin et al., 2019). Controlling the macrophage polarization by manipulating the nanomorphology of biomaterial surface may be an effective way to improve the performance of biomaterials (Ma et al., 2014). MSCs exosomes-mediated response in cartilage repair was also found to be associated with regenerative M2 macrophages (Zhang C.H. et al., 2018). In designing an immune-informed regenerative biomaterial, the most targeted approach to modulate macrophage polarization is to release factors (such as IL-4, IL-10) that direct polarization, and this can be achieved through a controlled release system (Sridharan et al., 2015; Li M. et al., 2020).

Extracellular matrix-based scaffolds exhibit such immunoregulation potential, and the resulting constructive remodeling response is associated with a timely transition of the macrophage phenotype from proinflammatory M1 to immunomodulatory and constructive M2 (Sicari et al., 2014; Wu et al., 2019). Both the classically and alternatively activated macrophage phenotypes are transient and difficult to define, which means that macrophages can polarize into diverse phenotypes based on changes in the microenvironment (Tarique et al., 2015). The microenvironment in which biomaterials are implanted *in vivo* is complex, and macrophages are exposed to a variety of stimuli, including various cytokines and effectors secreted by host immune cells (Kimura et al., 2016), immune components, biochemical cues (e.g., surface chemical and composition) (Palmer et al., 2014; Hotchkiss et al., 2018) and biophysical cues (e.g., topography, stiffness, and pore size) (Madden et al., 2010; Bartneck et al., 2012; Abaricia et al., 2020) of biomaterials or scaffolds, and degradation products (Sicari et al., 2014). The activation and phenotypical polarization of macrophages *in vivo* is modulated by multiple factors. These factors should be taken into account in the design of future tissue engineering bioscaffolds to regulate the host response in a direction that favors constructive tissue remodeling (e.g., polarization of macrophages toward an M2 phenotype) (Garg et al., 2013; Alvarez et al., 2016).

The implantation of a biomaterial can induce a host response, which determines the outcome of constructive remodeling of the damaged tissue. The mechanism of ECM derived scaffolds mediate immunomodulation (e.g., the macrophage phenotype shifts from M1 to M2) *in vivo* is still unclear (Mimura et al., 2016; Huleihel et al., 2017). Moreover, not all ECM

scaffolds derived from diverse source tissues can induce this phenomenon. The effect of ECM scaffolds derived from eight different source tissues (all porcine) on the polarization of macrophages was investigated. Macrophages exposed to ECM from the small intestinal submucosa, urinary bladder, brain, esophagus, and colon expressed a predominantly M2 phenotype. Conversely, macrophage exposure to dermal ECM resulted in a predominantly M1 phenotype, whereas liver ECM and skeletal muscle ECM did not significantly change the phenotype of the macrophages (Dziki et al., 2017). It is notable that some studies on regulation of the macrophage phenotype by ECM have conflicting results (Meng et al., 2015). Different decellularization protocols are applied to each tissue, which makes the analysis more complicated. In addition, unique ECM components from diverse source tissues make the seemingly contradictory results somewhat reasonable. Despite the marked differences and heterogeneity among various macrophage subtypes, their phenotype is highly plastic and dynamic (Hume, 2015). In fact, macrophage phenotypes exist in a range, with M1 and M2 as extreme values. Any given cell can express or co-express characteristics of the M1 or M2 phenotype, rather than exhibit a discrete functional state with a well-defined boundary (Mosser and Edwards, 2008). The description of macrophage activation and polarization is currently controversial and confusing, and the lack of a consensus diminishes the reference value of research and hinders progress to some extent. A guideline, published in 2014, will contribute to the better unification of experimental standards in future research (Murray et al., 2014). Although there is evidence that it is too simple to classify activated macrophages as M1 or M2, many studies in the literature have adopted these categories to illustrate specific findings. The simple classification of macrophages into M1 and M2 is inadequate, but it is useful for examining the inflammatory phenotype in response to biomaterials, especially when measuring the levels of inflammatory cytokines. The process of ECM-derived scaffolds facilitating tissue repair by regulating macrophage phenotypical transformation is complex. A clear and detailed report on distinguishing macrophage phenotypes will help analyze and understand this process. Modulating the components of the immune system to promote tissue regeneration. Once we have a clear understanding of host-biomaterial interactions, it will be possible to construct suitable immuno-informed decellularized tissue that can control tissue remodeling and initiate beneficial reprogramming *in vivo* (Taraballi et al., 2018).

ARTICULAR CARTILAGE ECM (AC-ECM)

Rich in Collagen

Articular cartilage ECM (AC-ECM) is a biomaterial widely studied in cartilage tissue engineering at present. It has good biocompatibility and is very similar to the natural cartilage matrix in terms of composition. AC-ECM scaffolds support cell adhesion and proliferation and are able to recruit autologous endogenous stem cells and induce their differentiation toward chondrocytes *in vivo*, allowing them to maintain the chondrocyte phenotype and thus achieving the *in situ* regeneration of cartilage (Xue et al., 2012; Almeida et al., 2016; Nasiri and Mashayekhan, 2017; Li et al., 2019a). The main components of AC-ECM are Col II and proteoglycans, and Col II accounts for over 80% of the dry weight of AC-ECM. The collagen network is essential in determining the mechanical properties of cartilage, and small amounts of other collagen types (I, III, V, VI, IX, X, and XI) also exist in AC-ECM (Gannon et al., 2015a,b; Campos et al., 2019; Wang et al., 2020a). Col II plays a vital role in the development and maturation of chondrocytes. It has an immunomodulatory effect, relieving the degeneration of cartilage matrix in OA by inhibiting the STAT1 signaling pathway of proinflammatory macrophages (Dai et al., 2018a). Macrophages express prochondrogenic cytokines, which stimulate chondrocytes to secrete matrix components while activating glycine receptors and reducing the intracellular calcium concentration to inhibit chondrocyte apoptosis and hypertrophy (Dai et al., 2018b). In short, both AC-ECM and Col II-based engineering scaffolds have great potential for the repair of damaged cartilage.

However, what is often overlooked and worrying is that Col II has immunogenicity and can induce arthritis by emulsification with an adjuvant, which is known as collagen-induced arthritis (CIA) (Trentham et al., 1977). The following discussion of this problem is mainly focused on the frequently studied AC-ECM scaffold.

Antigenic and Immunogenic Responses to Collagen

Before discussing the immunochemical property of any protein, it is important to draw a distinction between the potentially ambiguous terms "antigenicity" and "immunogenicity." Although it is difficult to make such a distinction due to the presence of a number of extrinsic factors, and for the purpose of the present discussion, the following simple distinction is adopted: antigenicity will be used to refer to the ability of a substance to interact with antibodies or cellular receptors, whereas immunogenicity will be used to refer to the ability to induce an immune response–a process that includes antibody synthesis and interaction. Therefore, we can think of any biomaterial that has immunogenicity to also have antigenicity.

Collagen is considered to be a safe and multifunctional biomaterial, but it has also raised concerns regarding its potential to elicit an immune response. Although the clinical incidence of adverse reactions to collagen implants is low, this do occur. Previously, it was widely accepted that collagen is an inert protein and does not have immunogenicity. Later studies have shown that it can interact with antibodies, but still regarded as a weak antigen. In tissue engineering, the interpretation of the immunogenicity of collagen-based scaffolds is often complicated by the presence of other non-collagen components, including cellular and nuclear contents, MHCs, and alpha-Gal epitopes, among others (Wong and Griffiths, 2014; Sutherland et al., 2015). Currently, few studies have targeted the immunological properties of collagen. Due to most collagen-based scaffolds were composed of type I collagen (and a small amount of type III collagen), which is generally not thought to evoke a potentially adverse host immune response (Bayrak

et al., 2013; Shetty et al., 2013; Yuan et al., 2014). However, as research progresses to address the issue of cartilage repair and regeneration, AC-ECM (enriched with Col II) and marine collagen (extracted from marine organisms) have shown good prospects for application and thus received increasing attention from researchers (Pustlauk et al., 2016; Tamaddon et al., 2017; Dai et al., 2018b). Allogeneic or xenogeneic Col II can induce arthritis (i.e., CIA) when emulsified with an adjuvant. Therefore, the immunological property of collagen has once again raised concern, which will be described in detail below.

Trentham et al. (1977) first discovered that emulsified Col II could induce arthritis and established an experimental arthritis model–a CIA model (Trentham et al., 1977). CIA is the most extensively studied model of rheumatoid arthritis (RA), mainly involving distal joints (especially the posterior ankle joint) (Wu et al., 2015). Its pathological features are similar to those of RA, including synovial hyperplasia, inflammatory cell infiltration, and cartilage destruction (Scarneo et al., 2019; De et al., 2020). Col II is the major protein in the cartilage of joints targeted by RA, and anti-Col II autoantibodies are present in the serum of RA patients, which indicates that Col II can induce an autoimmune response of an arthritic nature in the body (Manivel et al., 2015). There is some evidence that antibodies in RA patients target the same Col II molecular regions as in those in CIA (Burkhardt et al., 2002). In addition, the presence of T and B cell immunity has also been reported (Dimitrijević et al., 2020), but it is not clear whether this is a pathogenic factor or result of RA. Recent studies have also shown that the immune response may be involved in the development of OA. When inflammation occurs on the surface of articular cartilage for some reason, various components (mainly Col II) are exposed and thus stimulate B lymphocytes to produce anti-Col II antibodies, resulting in an immune response in OA. Therefore, as a biomaterial in cartilage tissue engineering, whether AC-ECM rich in Col II will cause an intraarticular immune reaction has become a concern. The mechanism of CIA is still unclear, but it is certainly inextricably linked to the structural characteristics of Col II.

A Col II molecule consists of three identical α_1 chains (a homotrimer), each containing 1487 amino acids with a molecular weight of approximately 130 kDa (Miller, 1971). Each of the three α_1 chains forms a left-handed helix by itself and then further intertwines to form a right-handed triple-superhelical structure, which is the main and unique structural region of the molecule, known as the "triple-helical domain." The greatest feature of the "triple-helical domain" is the periodically repeated arrangement of amino acids presenting $[Gly\text{-}X\text{-}Y]_n$, in which the positions of X and Y are usually occupied by proline (Pro) and hydroxyproline (Hyp), respectively (Canty and Kadler, 2005). Each chain has a short peptide extension at each end of the helix, the telopeptide (i.e., the amino (N)- and carboxyl (C)-telopeptides), which is a non-helical structure and does not contain Gly-X-Y repeats (Liu et al., 2015). The telopeptide region determines the intermolecular interactions that contribute to (and stabilize) normal fiber assembly. The amino acid sequences of telopeptides may vary from species to species, while certain cross-linked regions involved in fiber formation are highly conserved. Once secreted into the ECM, collagen molecules will be arranged head to tail in a quarter-stagger array and then covalently cross-linked into fibers through polymerization and disulfide bonds, forming the skeleton of the cartilage matrix. The structures of the Col II molecule and assembled fibrils are shown in **Figure 2A**.

The antigenic epitopes that determine the immunogenicity of Col II can be divided into three main categories: (1) those located the non-helical terminal regions (telopeptides), existing in both natural and denatured collagen; (2) those dependent on the amino acid sequence of the helical region of the molecule, exposed after this region is unwound and thus present in denatured collagen; and (3) those dependent on the triple-helical conformation, which only exist in natural collagen as the integrity of the triple helix must be maintained (**Figure 2B**). Sequence homology is highly conserved in the helical portion of Col II among different species, and the degree of change in the amino acid sequence is less than a few percent. Hidden epitopes (such as amino acid sequences in the helical region) interact with antibodies when the triple helix is unwound (Dodge and Poole, 1989). This fact may have implications for the host immune response to AC-ECM implants as they denature and degrade. The degree of telopeptide variation is much greater, which is considered to be the main determinant of Col II immunogenicity. Some studies have tried to reduce the immunogenicity by using proteolytic enzymes (e.g., pepsin) to remove the terminal telopeptides, resulting in what is known as Atelocollagen (Lin and Liu, 2006; Jeevithan et al., 2015; **Figure 2B**). However, there is still a lack of scientific evidence regarding the effect of this treatment on collagen immunogenicity. It should be made clear that pepsin treatment does not completely remove telopeptides. Furthermore, although this process cannot disrupt the triple-helical structure, the destruction of fiber networks will reduce the mechanical properties of collagenous implants (Shayegan et al., 2016). In the absence of a clear immunological benefit obtained by Atelocollagen, the other two types of antigenic epitopes of collagen molecules cannot be ignored.

It should be clarified that Col II-induced arthritis (CIA) develops slowly with the aid of an adjuvant, thus stimulating a high and persistent antibody response, which can be interpreted as an amplification effect. AC-ECM derived scaffolds usually undergo cross-linking, which delays the degradation of the scaffold and appears to have an effect similar to that of adjuvant. Col II is capable of inducing CIA in different species, but the sensitivity to Col II varies among species. Despite the fact that some implants containing Col II did not elicit adverse immune reactions in animal models (Nehrer et al., 1998; Mainil-Varlet et al., 2001), none of these studies were conducted in species previously shown to be susceptible to CIA. Although there is no evidence to support the theory that the implantation of biomaterials containing Col II could induce autoimmunity, there is also no direct evidence to disprove this theory.

Discussion of Potential Immune Response to AC-ECM

Articular cartilage ECM derived scaffolds are typically obtained in two ways: the granulation of cartilage by chopping or crushing,

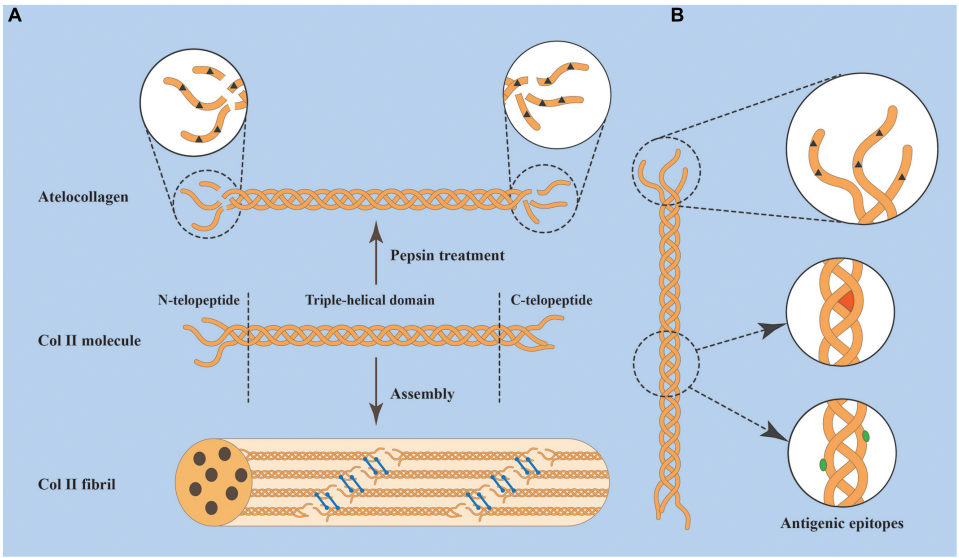

FIGURE 2 | (A) Three α_1 chains intertwine to form a type II collagen (Col II) molecule, which consists of three parts: a triple-helical domain and N- and C-telopeptides. Collagen molecules spontaneously assemble into fibrils head to tail in a quarter-stagger array and are stabilized by covalent bonds (blue bars). The molecule can be treated with pepsin to remove (not completely remove) telopeptides, yielding Atelocollagen. **(B)** Antigenic epitopes of Col II include those located within the telopeptides (dark brown triangles), those located in the helical region and dependent on the conformation (red sector), and those located in the helical region and dependent on the amino acid sequence (green ovals).

followed by decellularization and cross-linking to produce a highly porous customized scaffold structure, but at the expense of mechanical properties (Yang et al., 2008; Browe et al., 2019). Or the decellularization of intact cartilage explants without complete disruption of the collagen network, with relatively better mechanical properties but a very low porosity that limits the infiltration of cells (Schwarz et al., 2012; Li et al., 2019c). To some extent, these two kinds of scaffolds may alter the immune response induced by Col II. The purification of commercial collagen products is usually conducted at 4°C to prevent denaturation, a requirement apparently not met in the preparation of AC-ECM derived scaffolds. Whether Col II in AC-ECM derived scaffolds retains its natural structure, whether the decellularization process leads to the exposure of antigenic epitopes and whether cross-linking can hide antigenic epitopes remains unknown. In contrast to pure Col II-derived scaffolds, AC-ECM derived scaffolds contain other components such as GAGs that wrap around Col II, which may hide its antigenic determinants. These questions remain to be answered by follow-up research. An in-depth understanding of the immunological properties of Col II-containing scaffolds and their impact on cartilage will lay a foundation for the more scientific design of optimal scaffolds for use in cartilage tissue engineering.

CONCLUDING REMARKS AND FUTURE PERSPECTIVES

Nowadays, a wide variety of biomaterials are used for the repair of cartilage and other tissues in tissue engineering. However, most of biomaterials do not function as expected, or some even lead to the occurrence of adverse events. These unsatisfactory results are mainly due to the adverse interaction between the implanted biomaterials and the host's immune system. The host-biomaterial interaction is crucial to determining the outcome of downstream tissue reconstruction. It is influenced by numerous factors, such as immune components of material, cytokines and inflammatory agents induce by implants. Macrophages are the critical immune regulators, and can promote inflammatory or facilitate repair and regeneration attributing to their plasticity and versatility. The relationship between tissue healing and the immune system is very complex, since immune components of material or the cells involved could drastically change the repair outcome. Modulating the immune system through immunomodulatory biomaterials to promote repair is an effective strategy in future tissue engineering.

In recent years, Col II-containing scaffolds, especially AC-ECM-derived scaffolds, have become a hot research topic. It is worth noting that Col II has immunogenicity and could induce arthritis (i.e., CIA), an issue that is easily overlooked by the public and has attracted our attention. In this paper, the immunological characteristics of Col II are analyzed, and the potential immunogenicity of Col II-containing biomaterials is summarized.

An in-depth exploration of the host immune response to biomaterials not only is critical to understanding the repair mechanisms of these biomaterials but also paves the way for the development of ideal cartilage repair biomaterials in the future. All kinds of biomaterials have been explored for their potential in cartilage repair, and some have shown good results, which largely depend on the host response to the implanted

biomaterial. Biomaterials have been designed with a keen interest in the development of "passive biomaterials" to limit undesirable immune responses. Emphasis has been placed on promoting repair by preventing (or reducing) protein adhesion to the surface of the implanted biomaterial and the resulting inflammatory/immune cell activation and interaction. However, researchers have come to realize that the immune system plays a fundamental role in coordinating and defining the nature of the repair process. Allowing specific biological reactions is helpful for biomaterial-mediated remodeling. The link between the host response and tissue repair is complicated, and studies of host-biomaterial interactions have mainly focused on macrophages. The concept of the optimal biomaterial is shifting from reducing the host response to triggering the desired immune response, thereby facilitating constructive remodeling. With the continuous development of tissue engineering and regeneration medicine, regulating the interaction between biomaterials and the host must be a key part of the design and a focus of future work in this field. This future work will lead to developments that will hopefully promote the clinical translation of biomaterials.

AUTHOR CONTRIBUTIONS

All authors listed have made a substantial, direct and intellectual contribution to the work, and approved it for publication.

FUNDING

This work was supported by the National Key R&D Program of China (2018YFC1105900) and the Chinese PLA General Hospital Medical Youth Program (QNC19042).

REFERENCES

Aamodt, J. M., and Grainger, D. W. (2016). Extracellular matrix-based biomaterial scaffolds and the host response. *Biomaterials* 86, 68–82. doi: 10.1016/j.biomaterials.2016.02.003

Abaricia, J. O., Shah, A. H., Chaubal, M., Hotchkiss, K. M., and Olivares-Navarrete, R. (2020). Wnt signaling modulates macrophage polarization and is regulated by biomaterial surface properties. *Biomaterials* 243:119920. doi: 10.1016/j.biomaterials.2020.119920

Agrawal, V., Johnson, S. A., Reing, J., Zhang, L., Tottey, S., Wang, G., et al. (2010). Epimorphic regeneration approach to tissue replacement in adult mammals. *Proc. Natl. Acad. Sci. U S A.* 107, 3351–3355. doi: 10.1073/pnas.0905851106

Aidun, A., Firoozabady, A. S., Moharrami, M., Ahmadi, A., Haghighipour, N., Bonakdar, S., et al. (2019). Graphene oxide incorporated polycaprolactone/chitosan/collagen electrospun scaffold: enhanced osteogenic properties for bone tissue engineering. *Artif. Organs* 43, E264–E281.

Albright, J. C., and Daoud, A. K. (2017). Microfracture and microfracture plus. *Clin. Sports Med.* 36, 501–507. doi: 10.1016/j.csm.2017.02.012

Allen, L. T., Tosetto, M., Miller, I. S., O'Connor, D. P., Penney, S. C., Lynch, I., et al. (2006). Surface-induced changes in protein adsorption and implications for cellular phenotypic responses to surface interaction. *Biomaterials* 27, 3096–3108. doi: 10.1016/j.biomaterials.2006.01.019

Almeida, H. V., Eswaramoorthy, R., Cunniffe, G. M., Buckley, C. T., O'Brien, F. J., and Kelly, D. J. (2016). Fibrin hydrogels functionalized with cartilage extracellular matrix and incorporating freshly isolated stromal cells as an injectable for cartilage regeneration. *Acta Biomater.* 36, 55–62. doi: 10.1016/j.actbio.2016.03.008

Alvarez, M. M., Liu, J. C., Santiago, G. T.-D., Cha, B.-H., Vishwakarma, A., Ghaemmaghami, A., et al. (2016). Delivery strategies to control inflammatory response: modulating M1-M2 polarization in tissue engineering application. *J. Control. Release* 240, 349–363. doi: 10.1016/j.jconrel.2016.01.026

Anderson, J. M., and Jones, J. A. (2007). Phenotypic dichotomies in the foreign body reaction. *Biomaterials* 28, 5114–5120. doi: 10.1016/j.biomaterials.2007.07.010

Anderson, J. M., Rodriguez, A., and Chang, D. T. (2008). Foreign body reaction to biomaterials. *Semin. Immunol.* 20, 86–100. doi: 10.1016/j.smim.2007.11.004

Ang, L. T., Jennings, T. A., and Eaton, J. W. (1998). Mast cells mediate acute inflammatory responses to implanted biomaterials. *Proc. Natl. Acad. Sci. U S A.* 95, 8841–8846. doi: 10.1073/pnas.95.15.8841

Badylak, S. F., and Gilbert, T. W. (2008). Immune response to biologic scaffold materials. *Semin. Immunol.* 20, 109–116. doi: 10.1016/j.smim.2007.11.003

Badylak, S. F., Valentin, J. E., Ravindra, A. K., McCABE, G. P., and Stewart-Akers, A. M. (2008). Macrophage phenotype as a determinant of biologic scaffold remodeling. *Tissue Eng Part A* 14, 1835–1842. doi: 10.1089/ten.tea.2007.0264

Baena, J., Jiménez, G., López-Ruiz, E., Antich, C., Gri'án-Lisón, C., Perán, M., et al. (2019). Volume-by-volume bioprinting of chondrocytes-alginate bioinks in high temperature thermoplastic scaffolds for cartilage regeneration. *Exp. Biol. Med.* 244, 13–21. doi: 10.1177/1535370218821128

Bai, B., He, J., Li, Y.-S., Wang, X.-M., Ai, H.-J., and Cui, F.-Z. (2013). Activation of the ERK1/2 signaling pathway during the osteogenic differentiation of mesenchymal stem cells cultured on substrates modified with various chemical groups. *Biomed. Res. Int.* 2013:361906.

Bao, W., Li, M., Yang, Y., Wan, Y., and Wang, X. (2020). Advancements and frontiers in the high performance of natural hydrogels for cartilage tissue engineering. *Front. Chem.* 8:53. doi: 10.3389/fchem.2020.00053

Barbosa, J. N., Barbosa, M. R., and Aguas, A. P. A. (2003). Adhesion of human leukocytes to biomaterials: an in vitro study using alkanethiolate monolayers with different chemically functionalized surfaces. *J. Biomed. Mater. Res. A* 65, 429–434. doi: 10.1002/jbm.a.10488

Barbosa, J. N., Madureira, P., Barbosa, M. A., and Águas, A. P. (2006). The influence of functional groups of self-assembled monolayers on fibrous capsule formation and cell recruitment. *J. Biomed. Mater. Res. A* 76, 737–743. doi: 10.1002/jbm.a.30602

Barbosaa, J. N., Barbosa, M. A., and Aguas, A. P. (2004). Inflammatory responses and cell adhesion to self-assembled monolayers of alkanethiolates on gold. *Biomaterials* 25, 2557–2563. doi: 10.1016/j.biomaterials.2003.09.047

Bartneck, M., Heffels, K.-H., Pan, Y., Bovi, M., Zwadlo-Klarwasser, G., and Groll, J. (2012). Inducing healing-like human primary macrophage phenotypes by 3D hydrogel coated nanofibres. *Biomaterials* 33, 4136–4146. doi: 10.1016/j.biomaterials.2012.02.050

Bartneck, M., Keul, H. A., Singh, S., Czaja, K., Bornemann, J., Bockstaller, M., et al. (2010). Rapid uptake of gold nanorods by primary human blood phagocytes and immunomodulatory effects of surface chemistry. *ACS Nano* 4, 3073–3086. doi: 10.1021/nn100262h

Bayrak, A., Prüger, P., Stock, U. A., and Seifert, M. (2013). Absence of immune responses with xenogeneic collagen and elastin. *Tissue Eng. Part A* 19, 1592–1600. doi: 10.1089/ten.tea.2012.0394

Becker, M., Maring, J. A., Schneider, M., Martin, A. X. H., Seifert, M., Klein, O., et al. (2018). Towards a novel patch material for cardiac applications: tissue-specific extracellular matrix introduces essential key features to decellularized amniotic membrane. *Int. J. Mol. Sci.* 19:20.

Benthien, J. P., and Behrens, P. (2013). Reviewing subchondral cartilage surgery: considerations for standardised and outcome predictable cartilage remodelling. *Int. Orthop.* 37, 2139–2145. doi: 10.1007/s00264-013-2025-z

Bordbar, S., Bakhshaiesh, N. L., Khanmohammadi, M., Sayahpour, F. A., Alini, M., and Eslaminejad, M. B. (2020). Production and evaluation of decellularized extracellular matrix hydrogel for cartilage regeneration derived from knee cartilage. *J. Biomed. Mater. Res. A* 108, 938–946. doi: 10.1002/jbm.a.36871

Brodbeck, W. G., Patel, J., Voskerician, G., Christenson, E., Shive, M. S., Nakayama, Y., et al. (2002). Biomaterial adherent macrophage apoptosis is increased by hydrophilic and anionic substrates in vivo. *Proc. Natl. Acad. Sci. U S A.* 99, 10287–10292. doi: 10.1073/pnas.162124199

Brodbeck, W. G., Shive, M. S., Colton, E., Nakayama, Y., Matsuda, T., and Anderson, J. M. (2001). Influence of biomaterial surface chemistry on the apoptosis of adherent cells. *J. Biomed. Mater. Res.* 55, 661–668. doi: 10.1002/1097-4636(20010615)55:4<661::aid-jbm1061>3.0.co;2-f

Browe, D. C., Mahon, O. R., Díaz-Payno, P. J., Cassidy, N., Dudurych, I., Dunne, A., et al. (2019). Glyoxal cross-linking of solubilized extracellular matrix to produce highly porous, elastic, and chondro-permissive scaffolds for orthopedic tissue engineering. *J. Biomed. Mater. Res. A* 107, 2222–2234. doi: 10.1002/jbm.a.36731

Brown, B. N., Londono, R., Tottey, S., Zhang, L., Kukla, K. A., Wolf, M. T., et al. (2012a). Macrophage phenotype as a predictor of constructive remodeling following the implantation of biologically derived surgical mesh materials. *Acta Biomater.* 8, 978–987.

Brown, B. N., Ratner, B. D., Goodman, S. B., Amar, S., and Badylak, S. F. (2012b). Macrophage polarization: an opportunity for improved outcomes in biomaterials and regenerative medicine. *Biomaterials* 33, 3792–3802. doi: 10.1016/j.biomaterials.2012.02.034

Brown, B. N., Valentin, J. E., Stewart-Akers, A. M., McCabe, G. P., and Badylak, S. F. (2009). Macrophage phenotype and remodeling outcomes in response to biologic scaffolds with and without a cellular component. *Biomaterials* 30, 1482–1491. doi: 10.1016/j.biomaterials.2008.11.040

Brubaker, S. W., Bonham, K. S., Zanoni, I., and Kagan, J. C. (2015). Innate immune pattern recognition: a cell biological perspective. *Annu. Rev. Immunol.* 33, 257–290. doi: 10.1146/annurev-immunol-032414-112240

Burkersroda, F. V., Schedl, L., and Göpferich, A. (2002). Why degradable polymers undergo surface erosion or bulk erosion. *Biomaterials* 23, 4221–4231. doi: 10.1016/s0142-9612(02)00170-9

Burkhardt, H., Koller, T., Engström, Å, Nandakumar, K. S., Turnay, J., Kraetsch, H. G., et al. (2002). Epitope-specific recognition of type II collagen by rheumatoid arthritis antibodies is shared with recognition by antibodies that are arthritogenic in collagen-induced arthritis in the mouse. *Arthritis Rheum* 46, 2339–2348. doi: 10.1002/art.10472

Busscher, H. J., Mei, H. C. V. D., Subbiahdoss, G., Jutte, P. C., Dungen, J. J. A. M. V. D., Zaat, S. A. J., et al. (2012). Biomaterial-Associated infection: locating the finish line in the race for the surface. *Sci. Transl. Med.* 4:153rv10. doi: 10.1126/scitranslmed.3004528

Campos, Y., Almirall, A., Fuentes, G., Bloem, H. L., Kaijzel, E. L., and Cruz, L. J. (2019). Tissue engineering: an alternative to repair cartilage. *Tissue Eng. Part B Rev.* 25, 357–373. doi: 10.1089/ten.teb.2018.0330

Canty, E. G., and Kadler, K. E. (2005). Procollagen trafficking, processing and fibrillogenesis. *J. Cell Sci.* 118, 1341–1353. doi: 10.1242/jcs.01731

Chakraborty, J., Roy, S., Murab, S., Ravani, R., Kaur, K., Devi, S., et al. (2019). Modulation of macrophage phenotype, maturation and graft integration through chondroitin sulfate crosslinking to decellularized cornea. *ACS Biomater. Sci. Eng.* 5, 165–179. doi: 10.1021/acsbiomaterials.8b00251

Chang, D. T., Colton, E., Matsuda, T., and Anderson, J. M. (2009). Lymphocyte adhesion and interactions with biomaterial adherent macrophages and foreign body giant cells. *J. Biomed. Mater. Res. A* 91, 1210–1220. doi: 10.1002/jbm.a.32218

Chaudhary, P., Pesacreta, T. C., and Misra, R. D. K. (2012). Interplay between protein-modified surface and functional response of osteoblasts. *J. Biomed. Mater. Res. A* 100, 3157–3166. doi: 10.1002/jbm.a.34232

Chen, S., Du, Z., Zou, J., Qiu, S., Rao, Z., Liu, S., et al. (2019). Promoting neurite growth and schwann cell migration by the harnessing decellularized nerve matrix onto nanofibrous guidance. *ACS Appl. Mater. Interfaces* 11, 17167–17176. doi: 10.1021/acsami.9b01066

Chen, Y., Sui, J., Wang, Q., Yin, Y., Liu, J., Wang, Q., et al. (2018). Injectable self-crosslinking HA-SH/Col I blend hydrogels for in vitro construction of engineered cartilage. *Carbohydr. Polym.* 190, 57–66. doi: 10.1016/j.carbpol.2018.02.057

Chrzanowski, W., Kondyurin, A., Lee, J. H., Lord, M. S., Bilek, M. M. M., and Kim, H.-W. (2012). Biointerface: protein enhanced stem cells binding to implant surface. *J. Mater. Sci. Mater. Med.* 23, 2203–2215. doi: 10.1007/s10856-012-4687-2

Cipriano, A. F., Sallee, A., Tayoba, M., Alcaraz, M. C. C., Lin, A., Guan, R.-G., et al. (2017). Cytocompatibility and early inflammatory response of human endothelial cells in direct culture with Mg-Zn-Sr alloys. *Acta Biomater.* 48, 499–520. doi: 10.1016/j.actbio.2016.10.020

Collier, T. O., and Anderson, J. M. (2002). Protein and surface effects on monocyte and macrophage adhesion, maturation, and survival. *J. Biomed. Mater. Res.* 60, 487–496. doi: 10.1002/jbm.10043

Crapo, P. M., Gilbert, T. W., and Badylak, S. F. (2011). An overview of tissue and whole organ decellularization processes. *Biomaterials* 32, 3233–3243. doi: 10.1016/j.biomaterials.2011.01.057

Dai, L., He, Z., Jiang, Y., Zhang, X., Ren, S., Zhu, J., et al. (2019). One-step strategy for cartilage repair using acellular bone matrix scaffold based in situ tissue engineering technique in a preclinical minipig model. *Am. J. Transl. Res.* 11, 6650–6659.

Dai, M., Liu, X., Wang, N., and Sun, J. (2018a). Squid type II collagen as a novel biomaterial: isolation, characterization, immunogenicity and relieving effect on degenerative osteoarthritis via inhibiting STAT1 signaling in pro-inflammatory macrophages. *Mater. Sci. Eng. C Biomim. Supramol. Syst.* 89, 283–294. doi: 10.1016/j.msec.2018.04.021

Dai, M., Sui, B., Xue, Y., Liu, X., and Sun, J. (2018b). Cartilage repair in degenerative osteoarthritis mediated by squid type II collagen via immunomodulating activation of M2 macrophages, inhibiting apoptosis and hypertrophy of chondrocytes. *Biomaterials* 180, 91–103. doi: 10.1016/j.biomaterials.2018.07.011

Dai, M., Sui, B., Hua, Y., Zhang, Y., Bao, B., Lin, Q., et al. (2020). A well defect-suitable and high-strength biomimetic squid type II gelatin hydrogel promoted in situ costal cartilage regeneration via dynamic immunomodulation and direct induction manners. *Biomaterials* 240:119841. doi: 10.1016/j.biomaterials.2020.119841

Damanik, F. F. R., Rothuizen, T. C., Blitterswijk, C. V., Rotmans, J. I., and Moroni, L. (2014). Towards an in vitro model mimicking the foreign body response: tailoring the surface properties of biomaterials to modulate extracellular matrix. *Sci. Rep.* 4:6325.

De, S., Kundu, S., and Chatterjee, M. (2020). Generation of a robust model for inducing autoimmune arthritis in Sprague Dawley rats. *J. Pharmacol. Toxicol. Methods* 102:106659. doi: 10.1016/j.vascn.2019.106659

Dearth, C. L., Slivka, P. F., Stewart, S. A., Keane, T. J., Tay, J. K., Londono, R., et al. (2016). Inhibition of COX1/2 alters the host response and reduces ECM scaffold mediated constructive tissue remodeling in a rodent model of skeletal muscle injury. *Acta Biomater.* 31, 50–60. doi: 10.1016/j.actbio.2015.11.043

DeFife, K. M., Jenne, C. R., McNally, A. K., Colton, E., and Anderson, J. M. (1997). Interleukin-13 induces human monocyte/macrophage fusion and macrophage mannose receptor expression. *J. Immunol.* 158, 3385–3390.

Deng, M., Tan, J., Hu, C., Hou, T., Peng, W., Liu, J., et al. (2020). Modification of PLGA scaffold by MSC-Derived extracellular matrix combats macrophage inflammation to initiate bone regeneration via TGF-beta-Induced protein. *Adv. Healthc. Mater.* 9:e2000353.

Dimitrijević, M., NevenaArsenović-Ranin, Kosec, D., Bufan, B., Nacka-Aleksić, M., Pilipović, I., et al. (2020). Sex diferences in Tf cell help to B cells contribute to sexual dimorphism in severity of rat collagen-induced arthritis. *Sci. Rep.* 10:1214.

Dodge, G. R., and Poole, A. R. (1989). Immunohistochemical detection and immunochemical analysis of type II collagen degradation in human normal, rheumatoid, and osteoarthritic articular cartilages and in explants of bovine articular cartilage cultured with interleukin 1. *J. Clin. Invest.* 83, 647–661. doi: 10.1172/jci113929

Drury, J. L., and Mooney, D. J. (2003). Hydrogels for tissue engineering: scaffold design variables and applications. *Biomaterials* 24, 4337–4351. doi: 10.1016/s0142-9612(03)00340-5

Dziki, J. L., Wang, D. S., Pineda, C., Sicari, B. M., Rausch, T., and Badylak, S. F. (2017). Solubilized extracellular matrix bioscaffolds derived from diverse source tissues differentially influence macrophage phenotype. *J. Biomed. Mater. Res. A* 105, 138–147. doi: 10.1002/jbm.a.35894

Eglin, D., and Alini, M. (2008). Degradable polymeric materials for osteosynthesis: tutorial. *Eur. Cells Mater.* 16, 80–91. doi: 10.22203/ecm.v016a09

Ekdahl, K. N., Lambris, J. D., Elwing, H., Elwing, H., Nilsson, P. H., Teramura, Y., et al. (2012). Innate immunity activation on biomaterial surfaces: a mechanistic model and coping strategies. *Adv. Drug Deliv. Rev.* 63, 1042–1050. doi: 10.1016/j.addr.2011.06.012

Elder, B. D., Kim, D. H., and Athanasiou, K. A. (2010). Developing an articular cartilage decellularization process toward facet Joint cartilage replacement. *Neurosurgery* 66, 722–727. doi: 10.1227/01.neu.0000367616.49291.9f

English, K. (2013). Mechanisms of mesenchymal stromal cell immunomodulation. *Immunol. Cell Biol.* 91, 19–26. doi: 10.1038/icb.2012.56

Evans-Nguyen, K. M., Fuierer, R. R., Fitchett, B. D., Tolles, L. R., Conboy, J. C., and Schoenfisch, M. H. (2006). Changes in adsorbed fibrinogen upon conversion to fibrin. *Langmuir* 22, 5115–5121. doi: 10.1021/la053070y

Fahy, N., de-Vries-van-Melle, M. L., Lehmann, J., Wei, W., Grotenhuis, N., Farrell, E., et al. (2014). Human osteoarthritic synovium impacts chondrogenic differentiation of mesenchymal stem cells via macrophage polarisation state. *Osteoarthritis Cartilage* 22, 1167–1175. doi: 10.1016/j.joca.2014.05.021

Feng, X., Xu, P., Shen, T., Zhang, Y., Ye, J., and Gao, C. (2020). Influence of pore architectures of silk fibroin/collagen composite scaffolds on the regeneration of osteochondral defects in vivo. *J. Mater. Chem. B* 8, 391–405. doi: 10.1039/c9tb01558b

Ferrante, C. J., and Leibovich, S. J. (2012). Regulation of macrophage polarization and wound healing. *Adv. Wound Care* 1, 10–16. doi: 10.1089/wound.2011.0307

Fraitzl, C. R., Egli, R. J., Wingenfeld, C., Ganz, R., Hofstetter, W., and Leunig, M. (2008). Time course of biological activity in fresh murine osteochondral allografts paralleled to the recipient's immune response. *J. Invest. Surg.* 21, 109–117. doi: 10.1080/08941930802043540

Fujihara, Y., Abe, T., and Hoshi, K. (2020). Controlling the phenotype of macrophages promotes maturation of tissue-engineered cartilage. *Tissue Eng. Part A* 26, 1005–1013. doi: 10.1089/ten.tea.2019.0190

Gannon, A. R., Nagel, T., Bell, A. P., Avery, N. C., and Kelly, D. J. (2015a). Postnatal changes to the mechanical properties of articular cartilage are driven by the evolution of its collagen network. *Eur. Cells Mater.* 29, 105–123.

Gannon, A. R., Nagel, T., Bell, A. P., Avery, N. C., and Kelly, D. J. (2015b). The changing role of the superficial region in determining the dynamic compressive properties of articular cartilage during postnatal development. *Osteoarthritis Cartilage* 23, 975–984. doi: 10.1016/j.joca.2015.02.003

Garg, K., Pullen, N. A., Oskeritzian, C. A., Ryan, J. J., and Bowlin, G. L. (2013). Macrophage functional polarization (M1/M2) in response to varying fiber and pore dimensions of electrospun scaffolds. *Biomaterials* 34, 4439–4451. doi: 10.1016/j.biomaterials.2013.02.065

Gerber, J. S., and Mosser, D. M. (2001). Reversing lipopolysaccharide toxicity by ligating the macrophage Fc gamma receptors. *J. Immunol.* 166, 6861–6868. doi: 10.4049/jimmunol.166.11.6861

Ghassemi, T., Saghatoleslami, N., Mahdavi-Shahri, N., Matin, M. M., Gheshlaghi, R., and Moradi, A. (2019). A comparison study of different decellularization treatments on bovine articular cartilage. *J. Tissue Eng. Regen. Med.* 13, 1861–1871. doi: 10.1002/term.2936

Gilbert, T. W., Freund, J. M., and Badylak, S. F. (2009). Quantification of DNA in biologic scaffold materials. *J. Surg. Res.* 152, 135–139. doi: 10.1016/j.jss.2008.02.013

Gilpin, A., and Yang, Y. (2017). Decellularization strategies for regenerative medicine: from processing techniques to applications. *Biomed Res. Int.* 2017:9831534.

Gong, W., Lei, D., Li, S., Huang, P., Qi, Q., Sun, Y., et al. (2016). Hybrid small-diameter vascular grafts: anti-expansion effect of electrospun poly ε-caprolactone on heparin-coated decellularized matrices. *Biomaterials* 76, 359–370. doi: 10.1016/j.biomaterials.2015.10.066

Gong, Y. Y., Xue, J. X., Zhang, W. J., Zhou, G. D., Liu, W., and Cao, Y. (2011). A sandwich model for engineering cartilage with acellular cartilage sheets and chondrocytes. *Biomaterials* 32, 2265–2273. doi: 10.1016/j.biomaterials.2010.11.078

Göpferich, A. (1996). Mechanisms of polymer degradation and erosion. *Biomaterials* 17, 103–114. doi: 10.1016/0142-9612(96)85755-3

Griffin, M., Ibrahim, A., Seifalian, A., Butler, P., Kalaskar, D., and Ferretti, P. (2017). Chemical group-dependent plasma polymerisation preferentially directs adipose stem cell differentiation towards osteogenic or chondrogenic lineages. *Acta Biomater.* 50, 450–461. doi: 10.1016/j.actbio.2016.12.016

Grinberg, S., Hasko, G., Wu, D., and Leibovich, S. J. (2009). Suppression of PLCb2 by endotoxin plays a role in the adenosine A2A receptor-mediated switch of macrophages from an inflammatory to an angiogenic phenotype. *Am. J. Pathol.* 175, 2439–2453. doi: 10.2353/ajpath.2009.090290

Hachim, D., Iftikhar, A., LoPresti, S. T., Nolfi, A. L., Ravichandar, S., Skillen, C. D., et al. (2019). Distinct release strategies are required to modulate macrophage phenotype in young versus aged animals. *J. Control. Release* 305, 65–74. doi: 10.1016/j.jconrel.2019.05.020

Han, L., Xu, J., Lu, X., Gan, D., Wang, H., Wang, K., et al. (2017). Biohybrid methacrylated gelatin/polyacrylamide hydrogels for cartilage repair. *J. Mater. Chem. B* 5, 731–741. doi: 10.1039/c6tb02348g

He, C., Yang, Z., Jin, Y., Qi, X., Chu, J., and Deng, X. (2018). ADM scaffolds generate a pro-regenerative microenvironment during full-thickness cutaneous wound healing through M2 macrophage polarization via Lamtor1. *Front. Physiol.* 9:657. doi: 10.3389/fphys.2018.00657

Hemmi, H., Takeuchi, O., Kawai, T., Kaisho, T., Sato, S., Sanjo, H., et al. (2000). A toll-like receptor recognizes bacterial DNA. *Nature* 408, 740–745. doi: 10.1038/35047123

Heuberger, M., Drobek, T., and Spencer, N. D. (2005). Interaction forces and morphology of a protein-resistant poly(ethylene glycol) layer. *Biophys. J.* 88, 495–504. doi: 10.1529/biophysj.104.045443

Hirsh, S. L., McKenzie, D. R., Nosworthy, N. J., Denman, J. A., Sezerman, O. U., and Bilek, M. M. M. (2013). The Vroman effect: competitive protein exchange with dynamic multilayer protein aggregates. *Colloids Surf B Biointerfaces* 103, 395–404. doi: 10.1016/j.colsurfb.2012.10.039

Horbett, T. A. (2018). Fibrinogen adsorption to biomaterials. *J. Biomed. Mater. Res. A* 106, 2777–2788. doi: 10.1002/jbm.a.36460

Hotchkiss, K. M., Clark, N. M., and Olivares-Navarrete, R. (2018). Macrophage response to hydrophilic biomaterials regulates MSC recruitment and thelper cell populations. *Biomaterials* 182, 202–215. doi: 10.1016/j.biomaterials.2018.08.029

Hu, W. J., Eaton, J. W., and Tang, L. (2001). Molecular basis of biomaterial-mediated foreign body reactions. *Blood* 98, 1231–1238. doi: 10.1182/blood.v98.4.1231

Huang, Y., Seitz, D., König, F., Müller, P. E., Jansson, V., and Klar, R. M. (2019). Induction of articular chondrogenesis by chitosan/hyaluronic-acid-based biomimetic matrices using human adipose-derived stem cells. *Int. J. Mol. Sci.* 20:4487. doi: 10.3390/ijms20184487

Huber, E., Pobloth, A.-M., Bormann, N., Kolarczik, N., Schmidt-Bleek, K., Schell, H., et al. (2017). DBM as a carrier for BMP-2: burst release combined with long term binding and osteoinductive activity evaluated in vitro and in vivo. *Tissue Eng. Part A*. 23, 1321–1330. doi: 10.1089/ten.tea.2017.0005

Huleihel, L., Dziki, J. L., Bartolacci, J. G., Rausch, T., Scarritt, M. E., Cramera, M. C., et al. (2017). Macrophage phenotype in response to ECM bioscaffolds. *Semin. Immunol.* 29, 2–13. doi: 10.1016/j.smim.2017.04.004

Hume, D. A. (2015). The many alternative faces of macrophage activation. *Front. Immunol.* 6:370. doi: 10.3389/fimmu.2015.00370

Jabari, F., Hesaraki, S., and Houshmand, B. (2019). The physical, mechanical, and biological properties of silk fibroin/chitosan/reduced graphene oxide composite membranes for guided bone regeneration. *J. Biomater. Sci. Polym. Ed.* 30, 1779–1802. doi: 10.1080/09205063.2019.1666235

Janeway, C. A. (1989). Approaching the asymptote? evolution and revolution in immunology. *Cold Spring Harb. Symp. Quant. Biol.* 54, 1–13. doi: 10.1101/sqb.1989.054.01.003

Jeevithan, E., Jingyi, Z., Wang, N., He, L., Bao, B., and Wu, W. (2015). Physico-chemical, antioxidant and intestinal absorption properties of whale shark type-II collagen based on its solubility with acid and pepsin. *Process Biochem.* 50, 463–472. doi: 10.1016/j.procbio.2014.11.015

Jiang, J., Li, Z., Wang, H., Wang, Y., Carlson, M. A., Teusink, M. J., et al. (2016). Expanded 3D nanofiber scaffolds: cell penetration, neovascularization, and host response. *Adv. Healthc. Mater.* 5, 2993–3003. doi: 10.1002/adhm.201600808

Jin, S.-S., He, D.-Q., Luo, D., Wang, Y., Yu, M., Guan, B., et al. (2019). A biomimetic hierarchical nanointerface orchestrates macrophage polarization and mesenchymal stem cell recruitment to promote endogenous bone regeneration. *ACS Nano* 13, 6581–6595. doi: 10.1021/acsnano.9b00489

Jones, J. A., Chang, D. T., Meyerson, H., Colton, E., Kwon, I. K., Matsuda, T., et al. (2007). Proteomic analysis and quantification of cytokines and chemokines from biomaterial surface-adherent macrophages and foreign body giant cells. *J. Biomed. Mater. Res. A* 83, 585–596. doi: 10.1002/jbm.a.31221

Julier, Z., Park, A. J., Briquez, P. S., and Martino, M. M. (2017). Promoting tissue regeneration by modulating the immune system. *Acta Biomater.* 53, 13–28. doi: 10.1016/j.actbio.2017.01.056

Junge, K., Binnebösel, M., Trotha, K. T. V., Rosch, R., Klinge, U., Neumann, U. P., et al. (2012). Mesh biocompatibility: effects of cellular inflammation and tissue remodelling. *Langenbecks Arch. Surg.* 397, 255–270. doi: 10.1007/s00423-011-0780-0

Kamath, S., Bhattacharyya, D., Padukudru, C., Timmons, R. B., and Tang, L. (2008). Surface chemistry influences implant-mediated host tissue responses. *J. Biomed. Mater. Res. A* 86, 617–626. doi: 10.1002/jbm.a.31649

Karayel, E., Bürckstümmer, T., Bilban, M., Dürnberger, G., Weitzer, S., Martinez, J., et al. (2009). The TLR-independent DNA recognition pathway in murine

macrophages: ligand features and molecular signature. *Eur. J. Immunol.* 39, 1929–1936. doi: 10.1002/eji.200939344

Kawane, K., Fukuyama, H., Yoshida, H., Nagase, H., Ohsawa, Y., Uchiyama, Y., et al. (2003). Impaired thymic development in mouse embryos deficient in apoptotic DNA degradation. *Nat. Immunol.* 4, 138–144. doi: 10.1038/ni881

Kawane, K., Ohtani, M., Miwa, K., Kizawa, T., Kanbara, Y., Yoshioka, Y., et al. (2006). Chronic polyarthritis caused by mammalian DNA that escapes from degradation in macrophages. *Nature* 443, 998–1002. doi: 10.1038/nature05245

Keane, A. N. J., Londono, R., Turner, N. J., and Badylak, S. F. (2012). Consequences of ineffective decellularization of biologic scaffolds on the host response. *Biomaterials* 33, 1771–1781. doi: 10.1016/j.biomaterials.2011.10.054

Keane, T. J., and Badylak, S. F. (2015). The host response to allogeneic and xenogeneic biological scaffold materials. *J. Tissue Eng. Regen. Med.* 9, 504–511. doi: 10.1002/term.1874

Keselowsky, B. G., Collard, D. M., and Garcńıa, A. J. (2004). Surface chemistry modulates focal adhesion composition and signaling through changes in integrin binding. *Biomaterials* 25, 5947–5954. doi: 10.1016/j.biomaterials.2004.01.062

Kim, H. J., Han, M. A., Shin, J. Y., Jeon, J. H., Lee, S. J., Yoon, M. Y., et al. (2019). Intra-articular delivery of synovium-resident mesenchymal stem cells via BMP-7-loaded fibrous PLGA scaffolds for cartilage repair. *J. Control. Release* 302, 169–180. doi: 10.1016/j.jconrel.2019.04.002

Kim, J. (2017). Mathematical modeling approaches to describe the dynamics of protein adsorption at solid interfaces. *Colloids Surf B Biointerfaces* 162, 370–379. doi: 10.1016/j.colsurfb.2017.12.006

Kimura, T., Nada, S., Takegahara, N., Okuno, T., Nojima, S., Kang, S., et al. (2016). Polarization of M2 macrophages requires Lamtor1 that integrates cytokine and amino-acid signals. *Nat. Commun.* 7:13130.

Kock, N. B., Smolders, J. M. H., Susante, J. L. C. V., Buma, P., Kampen, A. V., and Verdonschot, N. (2008). A cadaveric analysis of contact stress restoration after osteochondral transplantation of a cylindrical cartilage defect. *Knee. Surg. Sports Traumatol. Arthrosc.* 16, 461–468. doi: 10.1007/s00167-008-0494-1

Kundu, B., Rajkhowa, R., Kundu, S. C., and Wang, X. (2013). Silk fibroin biomaterials for tissue regenerations. *Adv. Drug Deliv. Rev.* 65, 457–470. doi: 10.1016/j.addr.2012.09.043

Lan, M. A., Gersbach, C. A., Michael, K. E., Keselowsky, B. G., and García, A. J. (2005). Myoblast proliferation and differentiation on fibronectin-coated self assembled monolayers presenting different surface chemistries. *Biomaterials* 26, 4523–4531. doi: 10.1016/j.biomaterials.2004.11.028

Lendlein, A., and Langer, R. (2002). Biomedical applications biodegradable. elastic shape-memory polymers for potential. *Science* 296, 1673–1676. doi: 10.1126/science.1066102

Li, A., Wei, Y., Hung, C., and Vunjak-Novakovic, G. (2018). Chondrogenic properties of collagen type XI, a component of cartilage extracellular matrix. *Biomaterials* 173, 47–57. doi: 10.1016/j.biomaterials.2018.05.004

Li, M., Wei, F., Yin, X., Xiao, L., Yang, L., Su, J., et al. (2020). Synergistic regulation of osteoimmune microenvironment by IL-4 and RGD to accelerate osteogenesis. *Mater. Sci. Eng. C Mater. Biol. Appl.* 109:110508. doi: 10.1016/j.msec.2019.110508

Li, S., Tallia, F., Mohammed, A. A., Stevens, M. M., and Jones, J. R. (2020). Scaffold channel size influences stem cell differentiation pathway in 3-D printed silica hybrid scaffolds for cartilage regeneration. *Biomater. Sci.* 8, 4458–4466. doi: 10.1039/c9bm01829h

Li, X., Guo, W., Zha, K., Jing, X., Wang, M., Zhang, Y., et al. (2019a). Enrichment of CD146+ Adipose-Derived stem cells in combination with articular cartilage extracellular matrix scaffold promotes cartilage regeneration. *Theranostics* 9, 5105–5121. doi: 10.7150/thno.33904

Li, Y., Liu, Y., Xun, X., Zhang, W., Xu, Y., and Gu, D. (2019b). Three-dimensional porous scaffolds with biomimetic microarchitecture and bioactivity for cartilage tissue engineering. *ACS Appl. Mater. Interfaces* 11, 36359–36370. doi: 10.1021/acsami.9b12206

Li, Y., Xu, Y., Liu, Y., Wang, Z., Chen, W., Duan, L., et al. (2019c). Decellularized cartilage matrix scaffolds with laser-machined micropores for cartilage regeneration and articular cartilage repair. *Mater. Sci. Eng. C Biomim. Supramol. Syst.* 105:110139. doi: 10.1016/j.msec.2019.110139

Lin, T.-H., Wang, H.-C., Cheng, W.-H., Hsu, H.-C., and Yeh, M.-L. (2019). Osteochondral tissue regeneration using a tyramine-modified bilayered PLGA scaffold combined with articular chondrocytes in a porcine model. *Int. J. Mol. Sci.* 20:326. doi: 10.3390/ijms20020326

Lin, X., Wang, W., Zhang, W., Zhang, Z., Zhou, G., Cao, Y., et al. (2017). Hyaluronic acid coating enhances biocompatibility of nonwoven PGA scaffold and cartilage formation. *Tissue Eng. Part C Methods* 23, 86–97. doi: 10.1089/ten.tec.2016.0373

Lin, Y. K., and Liu, D. C. (2006). Effects of pepsin digestion at different temperatures and times on properties of telopeptide-poor collagen from bird feet. *Food Chem.* 94, 621–625. doi: 10.1016/j.foodchem.2004.12.007

Linares, J., Fernández, A. B., Feito, M. J., Matesanz, M. C., Sánchez-Salcedo, S., Arcos, D., et al. (2016). Effects of nanocrystalline hydroxyapatites on macrophage polarization. *J. Mater. Chem. B* 4, 1951–1959. doi: 10.1039/c6tb00014b

Lindberg, G., Longoni, A., Lim, K., Rosenberg, A., Hooper, G., Gawlitta, D., et al. (2019). Intact vitreous humor as a potential extracellular matrix hydrogel for cartilage tissue engineering applications. *Acta Biomater.* 85, 117–130. doi: 10.1016/j.actbio.2018.12.022

Liu, D., Nikoo, M., Boran, G., Zhou, P., and Regenstein, J. M. (2015). Collagen and gelatin. *Annu. Rev. Food Sci. Technol.* 6, 527–557.

Lohfeld, S., Cahill, S., Doyle, H., and McHugh, P. E. (2015). Improving the finite element model accuracy of tissue engineering scaffolds produced by selective laser sintering. *J. Mater. Sci. Mater. Med.* 26, 1–12.

Londono, R., and Badylak, S. F. (2015). Biologic scaffolds for regenerative medicine: mechanisms of in vivo remodeling. *Ann. Biomed. Eng.* 43, 577–592. doi: 10.1007/s10439-014-1103-8

Lopa, S., Leijs, M. J. C., Moretti, M., Lubberts, E., van Osch, G. J., and Bastiaansen-Jenniskens, Y. M. (2015). Arthritic and non-arthritic synovial fluids modulate IL10 and IL1RA gene expression in differentially activated primary human monocytes. *Osteoarthritis Cartilage* 23, 1853–1857. doi: 10.1016/j.joca.2015.06.003

Lu, D. R., and Park, K. (1991). Effect of surface hydrophobicity on the conformational changes of adsorbed fibrinogen. *J. Colloid Interface Sci.* 144, 271–281. doi: 10.1016/0021-9797(91)90258-a

Lu, Z., Liu, S., Le, Y., Qin, Z., He, M., Xu, F., et al. (2019). An injectable collagen-genipin-carbon dot hydrogel combined with photodynamic therapy to enhance chondrogenesis. *Biomaterials* 2018:119190. doi: 10.1016/j.biomaterials.2019.05.001

Lukanina, K. I., Grigoriev, T. E., Krasheninnikov, S. V., Mamagulashvilli, V. G., Kamyshinsky, R. A., and Chvalun, S. N. (2018). Multi-hierarchical tissue-engineering ECM-like scaffolds based on cellulose acetate with collagen and chitosan fillers. *Carbohydr. Polym.* 191, 119–126. doi: 10.1016/j.carbpol.2018.02.061

Luo, L., Eswaramoorthy, R., Mulhall, K. J., and Kelly, D. J. (2015). Decellularization of porcine articular cartilage explants and their subsequent repopulation with human chondroprogenitor cells. *J. Mech. Behav. Biomed. Mater.* 55, 21–31. doi: 10.1016/j.jmbbm.2015.10.002

Ma, Q.-L., Zhao, L.-Z., Liu, R.-R., Jin, B.-Q., Song, W., Wang, Y., et al. (2014). Improved implant osseointegration of a nanostructured titanium surface via mediation of macrophage polarization. *Biomaterials* 35, 9853–9867. doi: 10.1016/j.biomaterials.2014.08.025

Madden, L. R., Mortisen, D. J., Sussman, E. M., Dupras, S. K., Fugate, J. A., Cuy, J. L., et al. (2010). Proangiogenic scaffolds as functional templates for cardiac tissue engineering. *Proc. Natl. Acad. Sci. U S A.* 107, 15211–15216. doi: 10.1073/pnas.1006442107

Mainil-Varlet, P., Rieser, F., Grogan, S., Mueller, W., Saager, C., and Jakob, R. P. (2001). Articular cartilage repair using a tissue-engineered cartilage-like implant: an animal study. *Osteoarthritis Cartilage* 9(Suppl. A), S6–S15.

Makris, E. A., Gomoll, A. H., Malizos, K. N., Hu, J. C., and Athanasiou, K. A. (2015). Repair and tissue engineering techniques for articular cartilage. *Nat. Rev. Rheumatol.* 11, 21–34. doi: 10.1038/nrrheum.2014.157

Manferdini, C., Paolella, F., Gabusi, E., Gambari, L., Piacentini, A., Filardo, G., et al. (2017). Adipose stromal cells mediated switching of the pro-inflammatory profile of M1-like macrophages is facilitated by PGE2: in vitro evaluation. *Osteoarthritis Cartilage* 25, 1161–1171. doi: 10.1016/j.joca.2017.01.011

Manivel, V. A., Sohrabian, A., Wick, M. C., Mullazehi, M., Håkansson, L. D., and Rönnelid, J. (2015). Anti-type II collagen immune complex-induced granulocyte reactivity is associated with joint erosions in RA patients with anti-collagen antibodies. *Arthritis Res. Ther.* 17:8. doi: 10.1186/s13075-015-0523-7

Martinez, F. O., and Gordon, S. (2014). The M1 and M2 paradigm of macrophage activation: time for reassessment. *F1000Prime Rep.* 6:13.

Matzinger, P. (1994). Tolerance, danger, and the extended family. *Annu. Rev. Immunol.* 12, 991–1045. doi: 10.1146/annurev.iy.12.040194.005015

McCarthy, H. S., Richardson, J. B., Parker, J. C. E., and Roberts, S. (2016). Evaluating joint morbidity after chondral harvest for Autologous Chondrocyte Implantation (ACI): a study of ACI-Treated ankles and hips with a knee chondral harvest. *Cartilage* 7, 7–15. doi: 10.1177/1947603515607963

McNally, A. K., and Anderson, J. M. (2002). β1 and β2 integrins mediate adhesion during macrophage fusion and multinucleated foreign body giant cell formation. *Am. J. Pathol.* 160, 621–630. doi: 10.1016/s0002-9440(10)64882-1

Meng, F. W., Slivka, P. F., Dearth, C. L., and Badylak, S. F. (2015). Solubilized extracellular matrix from brain and urinary bladder elicits distinct functional and phenotypic responses in macrophages. *Biomaterials* 46, 131–140. doi: 10.1016/j.biomaterials.2014.12.044

Milan, P. B., Pazouki, A., Joghataei, M. T., Mozafari, M., Amini, N., Kargozar, S., et al. (2019). Decellularization and preservation of human skin: a platform for tissue engineering and reconstructive surgery. *Methods* 171, 62–67. doi: 10.1016/j.ymeth.2019.07.005

Miller, E. J. (1971). Isolation and characterization of a collagen from chick cartilage containing three identical alpha chains. *Biochemistry* 10, 1652–1659. doi: 10.1021/bi00785a024

Milleret, V., Buzzi, S., Gehrig, P., Ziogas, A., Grossmann, J., Schilcher, K., et al. (2015). Protein adsorption steers blood contact activation on engineered cobalt chromium alloy oxide layers. *Acta Biomater.* 24, 343–351. doi: 10.1016/j.actbio.2015.06.020

Mills, C. D., Kincaid, K., Alt, J. M., Heilman, M. J., and Hill, A. M. (2000). M-1/M-2 macrophages and the Th1/Th2 Paradigm. *J. Immunol.* 164, 6166–6173. doi: 10.4049/jimmunol.164.12.6166

Mimura, K. K. O., Moraes, A. R., Miranda, A. C., Greco, R., Ansari, T., Sibbons, P., et al. (2016). Mechanisms underlying heterologous skin scaffold-mediated tissue remodeling. *Sci. Rep.* 6:35074.

Mosser, D. M. (2003). The many faces of macrophage activation. *J. Leukoc. Biol.* 73, 209–212. doi: 10.1189/jlb.0602325

Mosser, D. M., and Edwards, J. P. (2008). Exploring the full spectrum of macrophage activation. *Nat. Rev. Immunol.* 8, 958–969. doi: 10.1038/nri2448

Moyano, D. F., Goldsmith, M., Solfiell, D. J., Landesman-Milo, D., Miranda, O. R., Peer, D., et al. (2012). Nanoparticle hydrophobicity dictates immune response. *J. Am. Chem. Soc.* 134, 3965–3967. doi: 10.1021/ja2108905

Murray, P. J., Allen, J. E., Biswas, S. K., Fisher, E. A., Gilroy, D. W., Goerdt, S., et al. (2014). Macrophage activation and polarization: nomenclature and experimental guidelines. *Immunity* 41, 14–20. doi: 10.1016/j.immuni.2014.06.008

Nagata, S., Hanayama, R., and Kawane, K. (2010). Autoimmunity and the clearance of dead cells. *Cell* 140, 619–630. doi: 10.1016/j.cell.2010.02.014

Nagubothu, S. R., Sugars, R. V., Tudzarovski, N., Andrén, A. T., Bottai, M., Davies, L. C., et al. (2020). Mesenchymal stromal cells modulate tissue repair responses within the injured vocal fold. *Laryngoscope* 130, E21–E29.

Nair, A., Zou, L., Bhattacharyya, D., Timmons, R. B., and Tang, L. (2008). Species and density of implant surface chemistry affect the extent of foreign body reactions. *Langmuir* 24, 2015–2024. doi: 10.1021/la7025973

Nasiri, B., and Mashayekhan, S. (2017). Fabrication of porous scaffolds with decellularized cartilage matrix for tissue engineering application. *Biologicals* 48, 39–46. doi: 10.1016/j.biologicals.2017.05.008

Nathani, A., Gold, G. E., Monu, U., Hargreaves, B., Finlay, A. K., Rubin, E. B., et al. (2019). Does injection of hyaluronic acid protect against early cartilage injury seen after marathon running? a randomized controlled trial utilizing high-field magnetic resonance imaging. *Am. J. Sports Med.* 47, 3414–3422. doi: 10.1177/0363546519879138

Nehrer, S., Breinan, H. A., Ramappa, A., Hsu, H.-P., Minas, T., Shortkrof, S., et al. (1998). Chondrocyteseeded collagen matrices implanted in a chondral defect in a canine model. *Biomaterials* 19, 2313–2328. doi: 10.1016/s0142-9612(98)00143-4

Nie, X., Chuah, Y. J., Zhu, W., He, P., Peck, Y., and Wang, D.-A. (2020). Decellularized tissue engineered hyaline cartilage graft for articular artilage repair. *Biomaterials* 235:119821. doi: 10.1016/j.biomaterials.2020.119821

Ohto, U., Shibata, T., Tanji, H., Ishida, H., Krayukhina, E., Uchiyama, S., et al. (2015). Structural basis of CpG and inhibitory DNA recognition by Toll-like receptor 9. *Nature* 520, 702–705. doi: 10.1038/nature14138

Orenstein, S. B., Saberski, E. R., Klueh, U., Kreutzer, D. L., and Novitsky, Y. W. (2010). Effects of mast cell modulation on early host response to implanted synthetic meshes. *Hernia* 14, 511–516. doi: 10.1007/s10029-010-0680-1

Palmer, J. A., Abberton, K. M., Mitchell, G. M., and Mitchell, G. M. (2014). Macrophage phenotype in response to implanted synthetic scaffolds: an immunohistochemical study in the rat. *Cells Tissues Organs* 199, 169–183. doi: 10.1159/000363693

Pape, A. C. H., Ippel, B. D., and Dankers, P. Y. W. (2017). Cell and protein fouling properties of polymeric mixtures containing supramolecular poly(ethylene glycol) additives. *Langmuir* 33, 4076–4082. doi: 10.1021/acs.langmuir.7b00467

Park, K.-S., Kim, B.-J., Lih, E., Park, W., Lee, S.-H., Joung, Y. K., et al. (2018). Versatile effects of magnesium hydroxide nanoparticles in PLGA scaffold–mediated chondrogenesis. *Acta Biomater.* 73, 204–216. doi: 10.1016/j.actbio.2018.04.022

Pati, F., Jang, J., Ha, D.-H., Kim, S. W., Rhie, J.-W., Shim, J.-H., et al. (2014). Printing three-dimensional tissue analogues with decellularized extracellular matrix bioink. *Nat. Commun.* 5:3935.

Pattappa, G., Zellner, J., Johnstone, B., Docheva, D., and Angele, P. (2019). Cells under pressure - the relationship between hydrostatic pressure and mesenchymal stem cell chondrogenesis. *Eur. Cells Mater.* 37, 360–381. doi: 10.22203/ecm.v037a22

Peppas, N. A., and Langer, R. (1994). New challenges in biomaterials. *Science* 263, 1715–1720. doi: 10.1126/science.8134835

Pérez-Silos, V., Moncada-Saucedo, N. K., Peña-Martínez, V., Lara-Arias, J., Marino-Martínez, I. A., and Camacho, A. (2019). A cellularized biphasic implant based on a bioactive silk fibroin promotes integration and tissue organization during osteochondral defect repair in a porcine model. *Int. J. Mol. Sci.* 20:5145. doi: 10.3390/ijms20205145

Pestka, J. M., Bode, G., Salzmann, G., Südkamp, N. P., and Niemeyer, P. (2012). Clinical outcome of autologous chondrocyte implantation for failed microfracture treatment of full-thickness cartilage defects of the knee joint. *Am. J. Sports Med.* 40, 325–331. doi: 10.1177/0363546511425651

Pustlauk, W., Paul, B., Gelinsky, M., and Bernhardt, A. (2016). Jellyfish collagen and alginate: combined marine materials for superior chondrogenesis of hMSC. *Mater. Sci. Eng. C Biomim. Supramol. Syst.* 64, 190–198. doi: 10.1016/j.msec.2016.03.081

Qiu, X., Liu, S., Zhang, H., Zhu, B., Su, Y., Zheng, C., et al. (2018). Mesenchymal stem cells and extracellular matrix scaffold promote muscle regeneration by synergistically regulating macrophage polarization toward the M2 phenotype. *Stem Cell Res. Ther.* 9:88.

Raimondo, T. M., and Mooney, D. J. (2018). Functional muscle recovery with nanoparticle-directed M2 macrophage polarization in mice. *Proc. Natl. Acad. Sci. U S A.* 115, 10648–10653. doi: 10.1073/pnas.1806908115

Rezwan, K., Chen, Q. Z., Blaker, J. J., and Boccaccini, A. R. (2006). Biodegradable and bioactive porous polymer/inorganic composite scaffolds for bone tissue engineering. *Biomaterials* 27, 3413–3431. doi: 10.1016/j.biomaterials.2006.01.039

Rostam, H. M., Singh, S., Salazar, F., Magennis, P., Hook, A., Singh, T., et al. (2016). The impact of surface chemistry modification on macrophage polarisation. *Semin. Immunol.* 221, 1237–1246. doi: 10.1016/j.imbio.2016.06.010

Roth, S. P., Glauche, S. M., Plenge, A., Erbe, I., Heller, S., and Burk, J. (2017). Automated freeze-thaw cycles for decellularization of tendon tissue - a pilot study. *BMC Biotechnol.* 17:13. doi: 10.1186/s12896-017-0329-6

Ryszer, T. (2015). Understanding the mysterious M2 macrophage through activation markers and effector mechanisms. *Med. Inflamm.* 2015:816460.

Sadtler, K., Wolf, M. T., Ganguly, S., Moad, C. A., Chung, L., Majumdar, S., et al. (2019). Divergent immune responses to synthetic and biological scaffolds. *Biomaterials* 192, 405–415. doi: 10.1016/j.biomaterials.2018.11.002

Salonius, E., Kontturi, L., Laitinen, A., Haaparanta, A. M., Korhonen, M., Nystedt, J., et al. (2020). Chondrogenic differentiation of human bone marrow-derived mesenchymal stromal cells in a three-dimensional environment. *J. Cell. Physiol.* 235, 3497–3507. doi: 10.1002/jcp.29238

Scarneo, S. A., Eibschutz, L. S., Bendele, P. J., Yang, K. W., Totzke, J., Hughes, P., et al. (2019). Pharmacological inhibition of TAK1, with the selective inhibitor takinib, alleviates clinical manifestation of arthritis in CIA mice. *Arthritis Res. Ther.* 21:292.

Schipani, R., Nolan, D. R., Lally, C., and Kelly, D. J. (2020). Integrating finite element modelling and 3D printing to engineer biomimetic polymeric scaffolds for tissue engineering. *Connect. Tissue Res.* 61, 174–189. doi: 10.1080/03008207.2019.1656720

Schneider, C., Lehmann, J., van-Osch, G. J. V. M., Hildner, F., Teuschl, A., Monforte, X., et al. (2016). Systematic comparison of protocols for the preparation of human articular cartilage for use as scaffold material in cartilage tissue engineering. *Tissue Eng. Part C Methods* 22, 1095–1107. doi: 10.1089/ten.tec.2016.0380

Schwarz, S., Koerber, L., Elsaesser, A. F., Goldberg-Bockhorn, E., Seitz, A. M., Dürselen, L., et al. (2012). Decellularized cartilage matrix as a novel biomatrix for cartilage tissue-engineering applications. *Tissue Eng. Part A* 18, 2195–2209. doi: 10.1089/ten.tea.2011.0705

Seong, S.-Y., and Matzinger, P. (2004). Hydrophobicity: an ancient damageassociated molecular pattern that initiates innate immune responses. *Nat. Rev. Immunol.* 4, 469–478. doi: 10.1038/nri1372

Shahbaz, S. K., Foroughi, F., Soltaninezhad, E., Jamialahmadi, T., Penson, P. E., and Sahebkar, A. (2020). Application of PLGA nano/microparticle delivery systems for immunomodulation and prevention of allotransplant rejection. *Expert Opin. Drug Delivery* 17, 767–780. doi: 10.1080/17425247.2020.1748006

Shamloo, A., and Sarmadi, M. (2016). Investigation of the adhesive characteristics of polymer-protein systems through molecular dynamics simulation and their relation to cell adhesion and proliferation. *Integr. Biol. (Camb)* 8, 1276–1295. doi: 10.1039/c6ib00159a

Shayegan, M., Altindal, T., Kiefl, E., and Forde, N. R. (2016). Intact telopeptides enhance interactions between collagens. *Biophys. J.* 111, 2404–2416. doi: 10.1016/j.bpj.2016.10.039

Shen, W., Berning, K., Tang, S. W., and Lam, Y. W. (2020). Rapid and detergent-free decellularization of cartilage. *Tissue Eng. Part C Methods* 26, 201–206. doi: 10.1089/ten.tec.2020.0008

Shetty, A. A., Kim, S. J., Bilagi, P., and Stelzeneder, D. (2013). Autologous collagen-induced chondrogenesis: single-stage arthroscopic cartilage repair technique. *Orthopedics* 36, e648–e652.

Sicari, B. M., Dziki, J. L., Siu, B. F., Medberry, C. J., Dearth, C. L., and Badylak, S. F. (2014). The promotion of a constructive macrophage phenotype by solubilized extracellular matrix. *Biomaterials* 35, 8605–8612. doi: 10.1016/j.biomaterials.2014.06.060

Silva, J. C., Udangawa, R. N., Chen, J., Mancinelli, C. D., Garrudo, F. F. F., Mikael, P. E., et al. (2020). Kartogenin-loaded coaxial PGS/PCL aligned nanofibers for cartilage tissue engineering. *Mater. Sci. Eng. C Biomim. Supramol. Syst.* 107:110291. doi: 10.1016/j.msec.2019.110291

Singh, Y. P., Bandyopadhyay, A., and Mandal, B. B. (2019). 3D bioprinting using cross-linker free silkgelatin bioink for cartilage tissue engineering. *ACS Appl. Mater. Interfaces* 11, 33684–33696. doi: 10.1021/acsami.9b11644

Sirlin, C. B., Brossmann, J., Boutin, R. D., Pathria, M. N., Convery, F. R., Bugbee, W., et al. (2001). Shell osteochondral allografts of the knee: comparison of MR imaging findings and immunologic responses. *Radiology* 219, 35–43. doi: 10.1148/radiology.219.1.r01ap0435

Slivka, P. F., Dearth, C. L., Keane, T. J., Meng, F. W., Medberry, C. J., Riggio, R. T., et al. (2014). Fractionation of an ECM hydrogel into structural and soluble components reveals distinctive roles in regulating macrophage behavior. *Biomater. Sci.* 2, 1521–1534. doi: 10.1039/c4bm00189c

Smith, B., Sigal, I. R., and Grande, D. A. (2015). Immunology and cartilage regeneration. *Immunome Res.* 63, 181–186. doi: 10.1007/s12026-015-8720-7

Solheim, E., Hegna, J., Strand, T., Harlem, T., and Inderhaug, E. (2018). Randomized study of long-term(15-17 Years)outcome after microfracture versus mosaicplasty in knee articular cartilage defects. *Am. J. Sports Med.* 46, 826–831. doi: 10.1177/0363546517745281

Sophia-Fox, A. J., Bedi, A., and Rodeo, S. A. (2009). The basic science of articular cartilage: structure, composition, and function. *Sports Health* 1, 461–468. doi: 10.1177/1941738109350438

Sperlinga, C., Schweissa, R. B., Strellera, U., and Werner, C. (2005). In vitro hemocompatibility of self-assembled monolayers displaying various functional groups. *Biomaterials* 26, 6547–6557. doi: 10.1016/j.biomaterials.2005.04.042

Spiller, K. L., Anfang, R. R., Spiller, K. J., Ng, J., Nakazawa, K. R., Daulton, J. W., et al. (2014). The role of macrophage phenotype in vascularization of tissue engineering scaffolds. *Biomaterials* 35, 4477–4488. doi: 10.1016/j.biomaterials.2014.02.012

Spiller, K. L., Nassiri, S., Witherel, C. E., Anfang, R. R., Ng, J., Nakazawa, K. R., et al. (2015). Vunjak-Novakovic, G., Sequential delivery of immunomodulatory cytokines to facilitate the M1-to-M2 transition of macrophages and enhance vascularization of bone scaffolds. *Biomaterials* 37, 194–207. doi: 10.1016/j.biomaterials.2014.10.017

Sridharan, R., Cameron, A. R., Kelly, D. J., Kearney, C. J., and O'Brien, F. J. (2015). Biomaterial based modulation of macrophage polarization: a review and suggested design principles. *Mater. Today* 18, 313–325. doi: 10.1016/j.mattod.2015.01.019

Stefani, R. M., Lee, A. J., Tan, A. R., Halder, S. S., Hu, Y., Guo, X. E., et al. (2020). Sustained Low-dose dexamethasone delivery via a PLGA microsphere-embedded agarose implant for enhanced osteochondral repair. *Acta Biomater.* 102, 326–340. doi: 10.1016/j.actbio.2019.11.052

Stocco, E., Barbon, S., Dalzoppo, D., Lora, S., Sartore, L., Folin, M., et al. (2014). Tailored PVA/ECM scaffolds for cartilage regeneration. *Biomed Res. Int.* 2014:762189.

Stratton, S., Shelke, N. B., Hoshino, K., Rudraiah, S., and Rudraiah, S. (2016). Bioactive polymeric scaffolds for tissue engineering. *Bioact Mater.* 1, 93–108. doi: 10.1016/j.bioactmat.2016.11.001

Sun, X., Yin, H., Wang, Y., Lu, J., Shen, X., Lu, C., et al. (2018). In situ articular cartilage regeneration through endogenous reparative cell homing using a functional bone marrow-specific scaffolding system. *ACS Appl. Mater. Interfaces* 10, 38715–38728. doi: 10.1021/acsami.8b11687

Sutherland, A. J., Converse, G. L., Hopkins, R. A., and Detamore, M. S. (2015). The bioactivity of cartilage extracellular matrix in articular cartilage regeneration. *Adv. Healthc. Mater.* 4, 29–39. doi: 10.1002/adhm.201400165

Tamaddon, M., Burrows, M., Ferreira, S. A., Dazzi, F., Apperley, J. F., Bradshaw, A., et al. (2017). Monomeric, porous type II collagen scaffolds promote chondrogenic differentiation of human bone marrow mesenchymal stem cells in vitro. *Sci. Rep.* 7:43519.

Tanaka, M., Kawai, S., and Iwasaki, Y. (2017). Well-defined protein immobilization on photo-responsive phosphorylcholine polymer surfaces. *J. Biomater. Sci. Polym. Ed.* 28, 2021–2033. doi: 10.1080/09205063.2017.1366251

Taraballi, F., Sushnitha, M., Tsao, C., Guillermo, B., Liverani, C., Shi, A., et al. (2018). Biomimetic tissue engineering: tuning the immune and inflammatory response to implantable biomaterials. *Adv. Healthc. Mater.* 7:1800490. doi: 10.1002/adhm.201800490

Tarique, A. A., Logan, J., Thomas, E., Holt, P. G., Sly, P. D., and Fantino, E. (2015). Phenotypic, functional and plasticity features of classical and alternatively activated human macrophages. *Am. J. Respir. Cell Mol. Biol.* 53, 676–688. doi: 10.1165/rcmb.2015-0012oc

Thevenot, P., Hu, W., and Tang, L. (2008). Surface chemistry influences implant biocompatibility. *Curr. Top. Med. Chem.* 8, 270–280. doi: 10.2174/156802608783790901

Tiller, J. C., Bonner, G., Pan, L.-C., and Klibanov, A. M. (2001). Improving biomaterial properties of collagen films by chemical modification. *Biotechnol. Bioeng.* 73, 246–252. doi: 10.1002/bit.1057

Trentham, D. E., Townes, A. S., and Kang, A. H. (1977). Autoimmunity to type II collagen: an experimental model of arthritis. *J. Exp. Med.* 146, 857–868. doi: 10.1084/jem.146.3.857

Vainieri, M. L., Lolli, A., Kops, N., D'Atri, D., Eglin, D., Yayon, A., et al. (2020). Evaluation of biomimetic hyaluronic-based hydrogels with enhanced endogenous cell recruitment and cartilage matrix formation. *Acta Biomater.* 101, 293–303. doi: 10.1016/j.actbio.2019.11.015

Ventura, R. D., Padalhin, A. R., Park, C. M., and Lee, B. T. (2019). Enhanced decellularization technique of porcine dermal ECM for tissue engineering applications. *Mater. Sci. Eng. C Biomim. Supramol. Syst.* 104:109841. doi: 10.1016/j.msec.2019.109841

Venugopal, E., Sahanand, K. S., Orthopedic, M., Bhattacharyya, A., and Rajendran, S. (2019). Electrospun PCL nanofibers blended with Wattakaka volubilis active phytochemicals for bone and cartilage tissue engineering. *Nanomedicine* 21:102044. doi: 10.1016/j.nano.2019.102044

Verreck, F. A. W., Boer, T. D., Langenberg, D. M. L., Hoeve, M. A., Kramer, M., Vaisberg, E., et al. (2004). Human IL-23-producing type 1 macrophages promote but IL-10-producing type 2 macrophages subvert immunity to (myco)bacteria. *Proc. Natl. Acad. Sci. U S A.* 101, 4560–4565. doi: 10.1073/pnas.0400983101

Vollkommer, T., Henningsen, A., Friedrich, R. E., Felthaus, O. H., Eder, F., Morsczeck, C., et al. (2019). Extent of inflammation and foreign body reaction to porous polyethylene in vitro and in vivo. *In Vivo* 33, 337–347. doi: 10.21873/invivo.11479

Wang, C., Brisson, B. K., Terajima, M., Li, Q., Hoxha, K. H., Han, B., et al. (2020a). Type III collagen is a key regulator of the collagen fibrillar structure and biomechanics of articular cartilage and meniscus. *Matrix Biol.* 8, 47–67. doi: 10.1016/j.matbio.2019.10.001

Wang, C., Yue, H., Huang, W., Lin, X., Xie, X., He, Z., et al. (2020b). Cryogenic 3D printing of heterogeneous scaffolds with gradient mechanical strengths and spatial delivery of osteogenic peptide/TGF-β1 for osteochondral tissue regeneration. *Biofabrication* 12:025030. doi: 10.1088/1758-5090/ab7ab5

Wang, Z., Li, Z., Li, Z., Wu, B., Liu, Y., and Wu, W. (2018). Cartilaginous extracellular matrix derived from decellularized chondrocyte sheets for the reconstruction of osteochondral defects in rabbits. *Acta Biomater.* 81, 129–145. doi: 10.1016/j.actbio.2018.10.005

Wasyłeczko, M., Sikorska, W., and Chwojnowski, A. (2020). Review of synthetic and hybrid scaffolds in cartilage tissue engineering. *Membranes (Basel)* 10, 1–28.

Waters, M., VandeVord, P., and Dyke, M. V. (2017). Keratin biomaterials augment anti-inflammatory macrophage phenotype in vitro. *Acta Biomater.* 66, 213–223. doi: 10.1016/j.actbio.2017.10.042

Widuchowski, W., Widuchowski, J., and Trzaska, T. (2007). Articular cartilage defects: study of 25,124 knee arthroscopies. *Knee* 14, 177–182. doi: 10.1016/j.knee.2007.02.001

Wiktorowicz, J. E., Chowdhury, I. H., Stafford, S., Choudhuri, S., Dey, N., and Garg, N. J. (2019). Integrated functional analysis of the nuclear proteome of classically and alternatively activated macrophages. *Mediators Inflamm.* 2019:3481430.

Wilson, C. J., Clegg, R. E., Leavesley, D. I., and Pearcy, M. J. (2005). Mediation of biomaterial–cell interactions by adsorbed proteins: a review. *Tissue Eng.* 11, 1–18. doi: 10.1089/ten.2005.11.1

Wong, M. L., and Griffiths, L. G. (2014). Immunogenicity in xenogeneic scaffold generation: antigen removal vs. decellularization. *Acta Biomater.* 10, 1806–1816. doi: 10.1016/j.actbio.2014.01.028

Wu, Q. Y., Xiong, X. T., Zhang, X. L., Lu, J. Q., Zhang, X. M., Chen, W., et al. (2015). Secondary osteoporosis in collagen-induced arthritis rats. *J. Bone Miner. Metab.* 34, 500–516. doi: 10.1007/s00774-015-0700-4

Wu, R.-X., He, X.-T., Zhu, J.-H., Yin, Y., Li, X., Liu, X., et al. (2019). Modulating macrophage responses to promote tissue regeneration by changing the formulation of bone extracellular matrix from filler particles to gel bioscaffolds. *Mater. Sci. Eng. C Biomim. Supramol. Syst.* 101, 330–340. doi: 10.1016/j.msec.2019.03.107

Wu, R.-X., Ma, C., Liang, Y., Chen, F.-M., and Liu, X. (2020). ECM-mimicking nanofibrous matrix coaxes macrophages toward an anti-inflammatory phenotype: cellular behaviors and transcriptome analysis. *Appl. Mater. Today* 18:100508. doi: 10.1016/j.apmt.2019.100508

Xia, H., Zhao, D., Zhu, H., Hua, Y., Xiao, K., Xu, Y., et al. (2018). Lyophilized scaffolds fabricated from 3D-printed photocurable natural hydrogel for cartilage regeneration. *ACS Appl. Mater. Interfaces* 10, 31704–31715. doi: 10.1021/acsami.8b10926

Xiao, H., Huang, W., Xiong, K., Ruan, S., Yuan, C., Mo, G., et al. (2019). Osteochondral repair using scaffolds with gradient pore sizes constructed with silk fibroin, chitosan, and nano-hydroxyapatite. *Int. J. Nanomed.* 14, 2011–2027. doi: 10.2147/ijn.s191627

Xu, L. C., and Siedlecki, C. A. (2007). Effects of surface wettability and contact time on protein adhesion to biomaterial surfaces. *Biomaterials* 28, 3273–3283. doi: 10.1016/j.biomaterials.2007.03.032

Xue, J. X., Gong, Y. Y., Zhou, G. D., Liu, W., Cao, Y. L., and Zhang, W. J. (2012). Chondrogenic differentiation of bone marrow-derived mesenchymal stem cells induced by acellular cartilage sheets. *Biomaterials* 33, 5832–5840. doi: 10.1016/j.biomaterials.2012.04.054

Yang, D., Lü, X., Hong, Y., Xi, T., and Zhang, D. (2013). The molecular mechanism of mediation of adsorbed serum proteins to endothelial cells adhesion and growth on biomaterials. *Biomaterials* 34, 5747–5758. doi: 10.1016/j.biomaterials.2013.04.028

Yang, Q., Peng, J., Guo, Q., Huang, J., Zhang, L., Yao, J., et al. (2008). A cartilage ECM-derived 3-D porous acellular matrix scaffold for in vivo cartilage tissue engineering with PKH26-labeled chondrogenic bone marrow-derived mesenchymal stem cells. *Biomaterials* 29, 2378–2387. doi: 10.1016/j.biomaterials.2008.01.037

Yang, R., Liao, Y., Wang, L., He, P., Hu, Y., Yuan, D., et al. (2019). Exosomes derived from M2b macrophages attenuate DSS-induced colitis. *Front. Immunol.* 10:2346. doi: 10.3389/fimmu.2019.02346

Yoshida, H., Okabe, Y., Kawane, K., Fukuyama, H., and Nagata, S. (2005). Lethal anemia caused by interferon-b produced in mouse embryos carrying undigested DNA. *Nat. Immunol.* 6, 49–56. doi: 10.1038/ni1146

Yuan, T., Zhang, L., Li, K., Fan, H., Fan, Y., Liang, J., et al. (2014). Collagen hydrogel as an immunomodulatory scaffold in cartilage tissue engineering. *J. Biomed. Mater. Res. Part B Appl. Biomater.* 102, 337–344. doi: 10.1002/jbm.b.33011

Yue, Y., Yang, X., Feng, K., Wang, L., Hou, J., Mei, B., et al. (2017). M2b macrophages reduce early reperfusion injury after myocardial ischemia in mice: a predominant role of inhibiting apoptosis via A20. *Int. J. Cardiol.* 245, 228–235. doi: 10.1016/j.ijcard.2017.07.085

Zhang, C.-H., Jiang, Y.-L., Ning, L.-J., Li, Q., Fu, W.-L., Zhang, Y.-J., et al. (2018). Evaluation of decellularized bovine tendon sheets for achilles tendon defect reconstruction in a rabbit model. *Am. J. Sports Med.* 46, 2687–2699. doi: 10.1177/0363546518787515

Zhang, J., Xie, B., Xi, Z., Zhao, L., Cen, L., and Yang, Y. (2020). A comparable study of polyglycolic acid's degradation on macrophages' activation. *Mater. Sci. Eng. C Biomim. Supramol. Syst.* 109:110574. doi: 10.1016/j.msec.2019.110574

Zhang, Q., Raoof, M., Chen, Y., Sumi, Y., Sursal, T., Junger, W., et al. (2010). Circulating mitochondrial DAMPs cause inflammatory responses to injury. *Nature* 464, 104–107.

Zhang, S., Chuah, S. J., Lai, R. C., Hui, J. H. P., Lim, S. K., and Toh, W. S. (2018). MSC exosomes mediate cartilage repair by enhancing proliferation, attenuating apoptosis and modulating immune reactivity. *Biomaterials* 156, 16–27. doi: 10.1016/j.biomaterials.2017.11.028

Zhao, P., Liu, S., Bai, Y., Lu, S., Peng, J., Zhang, L., et al. (2018). hWJECM-Derived oriented scaffolds with autologous chondrocytes for rabbit cartilage defect repairing. *Tissue Eng. Part A* 24, 905–914. doi: 10.1089/ten.tea.2017.0223

Zheng, M. H., Chen, J., Kirilak, Y., Willers, C., Xu, J., and Wood, D. (2005). Porcine small intestine submucosa (SIS) is not an acellular collagenous matrix and contains porcine DNA: possible implications in human implantation. *J. Biomed. Mater. Res. Part B Appl. Biomater.* 73, 61–67. doi: 10.1002/jbm.b.30170

Zizzo, G., Hilliard, B. A., Monestier, M., and Cohen, P. L. (2012). Efficient clearance of early apoptotic cells by human macrophages requires M2c polarization and MerTK induction. *J. Immunol.* 189, 3508–3520. doi: 10.4049/jimmunol.1200662

Conflict of Interest: The authors declare that the research was conducted in the absence of any commercial or financial relationships that could be construed as a potential conflict of interest.

frontiers in Materials

ORIGINAL RESEARCH
published: 04 June 2021
doi: 10.3389/fmats.2021.678550

Insight Into Osseointegration of Nanohydroxyapatite/Polyamide 66 Based on the Radiolucent Gap: Comparison With Polyether-Ether-Ketone

*Jianxiao Li[1], Haitao Peng[2], Zhiyu Chen[1], Chenbo Hu[1], Tao He[1], Hong Li[2] and Zhengxue Quan[1]**

[1]Department of Orthopedics, The First Affiliated Hospital of Chongqing Medical University, Chongqing, China, [2]College of Physics, Sichuan University, Chengdu, China

Spinal fusion cages have been used in spinal fusion surgery for over 20 years. Polyether-ether-ketone (PEEK) cages are one of the most widely used materials. However, an increasing number of clinical and preclinical studies have shown that as a bioinert material the PEEK cage causes implant failure owing to limited osseointegration. The most common complication is a radiolucent zone at the bone-implant interface. Nanohydroxyapatite/polyamide 66 (n-HA/PA66) is a bioactive composite with sufficient load-bearing properties and good osseointegration abilities. However, in the early stage after surgery, a radiolucent gap can also be observed at the margin of the bone-implant interface. To better assess osseointegration performance as a fusion cage and compare the radiolucent gaps between the two materials, PEEK and n-HA/PA66, implants were prepared and implanted into the femoral condyles of adult New Zealand white rabbits to create a line-to-line bone-implant interface model. The interfaces were systematically investigated using X-ray radiography, histological analysis, scanning electron microscopy (SEM), elemental mapping analysis, micro-computed tomography evaluation, and push-out tests at 4, 8, 12, 24, and 52 weeks. Analysis of X-ray films and histological sections indicated a radiolucent gap around the margin of n-HA/PA66 in the early weeks after implantation (4–8 weeks). The gap narrowed and decreased gradually at 24–52 weeks. Histological analysis and SEM suggested that the formed bone could integrate and adhere in some regions of the implant surface. In addition, a better bone-like apatite layer was formed between the bone and the n-HA/PA66 implant interface than with the PEEK implant. Push-out tests conducted at 24 and 52 weeks to evaluate integrated strength showed that the n-HA/PA66 implants have better bonding strength and sufficient stability, whereas PEEK implants possess poor integrated strength. Therefore, the n-HA/PA66 composite exhibits good osseointegration properties and an improved integrated bone-implant interface.

Keywords: osseointegration, bioactive material, bone-implant interface, spinal fusion, hydroxyapatite/polyamide 66, polyetheretherketone

OPEN ACCESS

Edited by:
Derek H Rosenzweig, McGill University, Canada

Reviewed by:
Rahul Gawri, McGill University, Canada
Luciano Vidal, Ecole Centrale de Nantes, France

****Correspondence:***
Zhengxue Quan
quanzx18@126.com

Specialty section:
This article was submitted to Biomaterials, a section of the journal Frontiers in Materials

Received: *09 March 2021*
Accepted: *12 May 2021*
Published: *04 June 2021*

Citation:
Li J, Peng H, Chen Z, Hu C, He T, Li H and Quan Z (2021) Insight Into Osseointegration of Nanohydroxyapatite/Polyamide 66 Based on the Radiolucent Gap: Comparison With Polyether-Ether-Ketone. Front. Mater. 8:678550. doi: 10.3389/fmats.2021.678550

INTRODUCTION

Interbody spinal fusion using interbody fusion cages has many advantages for the treatment of spinal disorders. Fusion cages have been clinically used routinely for more than 20 years with a variety of implant materials and different designs (Albrektsson and Jacobsson, 1987; Bagby, 1988; Cloward, 2007). Most currently used fusion cages are constructed from polyether-ether-ketone (PEEK)

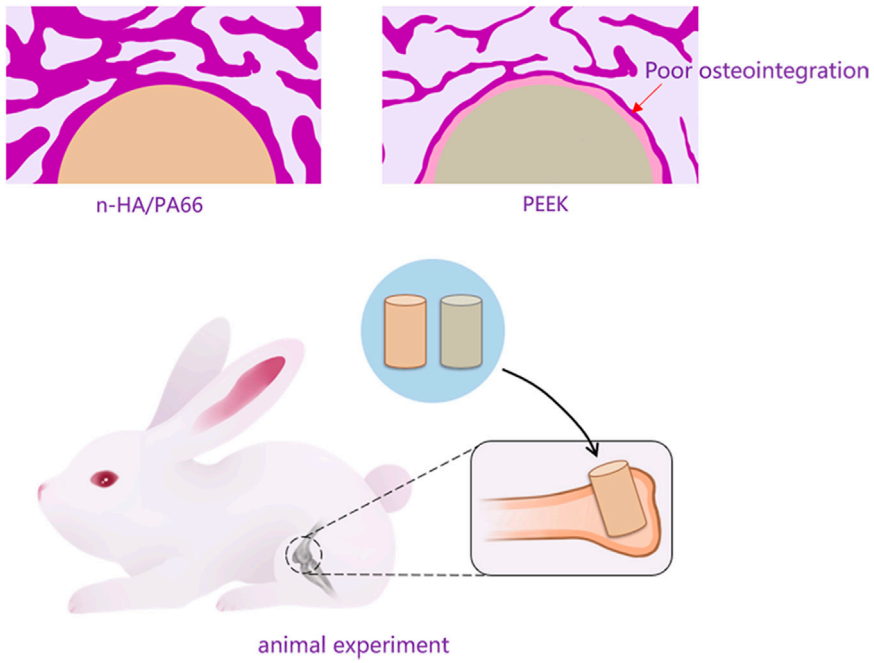

GRAPHICAL ABSTRACT | schematic diagram.

materials. Owing to its good biocompatibility, a cortical bone with a similar elastic modulus and mechanical characteristics has now been widely used in spinal fusion or non-fusion, trauma, and neurosurgical and cranio-maxillofacial surgeries for more than 15 years (Toth et al., 2006; Kurtz and Devine, 2007). However, bone does not bond to PEEK, a potential complication of PEEK is that its limited osseointegration with the surrounding bone results in a "PEEK-halo" effect (Phan et al., 2016). This "PEEK-halo" denotes a "radiolucent zone" that can be clearly seen on X-ray radiographs at the bone-implant interface, which may inhibit a successful fusion in the spinal interbody space. Radiolucent zones around the implant may be an indication of weak osseointegration, and fibrous encapsulation may be formed at the PEEK-bone interface, potentially leading to clinical failure with long-term implantation in the body (Noiset et al., 1999; Wu et al., 2013; Walsh et al., 2015).

Weak osteointegration affects the long-term stability of the interbody cages (Yuan et al., 2018). Much work has been conducted to improve the osteointegration property of interbody cages. Several interbody cages now have additional surface coating to enhance the bone-cage interface. Achieving long-term clinical success of interbody cage implants remains a significant and multifaceted challenge (Torstrick et al., 2018). Understanding the osseointegration of the cage materials will help the selecting and designing of new interbody cages materials in the future. The nanohydroxyapatite/polyamide 66 (n-HA/PA66) and PEEK are two materials currently utilized in interbody cages. The n-HA/PA66 composite is a bioactive material with the ability to promote new bone formation and osteogenesis. However, in our previous studies, we discovered the presence of a "radiolucent gap" between the implant and the adjacent endplate bone in the radiographic images with this material also (Zhang et al., 2016). We evaluated: 1) whether the "radiolucent gap" is the same as the "Peek-halo" and 2) if n-HA/P66 exhibits an improved bone-implant interface compared to that of PEEK.

In the present study, to better identify the bone-implant interface and assess the long-term osseointegration effects between the n-HA/P66 and PEEK, we used bone defects in rabbits to create a line-to-line fit bone-implant interface model previously reported by the literature (Bertollo et al., 2011). X-ray radiography and histology were used to observe the bone-implant interface. Micro-computed tomography (micro-CT) was used to evaluate new bone formation around the implant. Additionally, to evaluate the microstructure and dynamic change in chemical elements at the bone-implant interface, scanning electron microscopy (SEM) and energy dispersive X-ray spectroscopy (EDX) were performed at 4, 8, 12, 24, and 52 weeks. Finally, to evaluate the integrated strength of implants and bone, the push-out test was applied at 24 and 52 weeks.

MATERIALS AND METHODS

Sample Preparation

The n-HA/P66 rods (φ = 6 mm, L = 10 mm) were provided by Sichuan Guona Technology Co., Ltd. (Chengdu, China) and had an HA content of approximately 40%. The PEEK composite was provided by Shandong WEGO Orthopedic Device Co., Ltd.

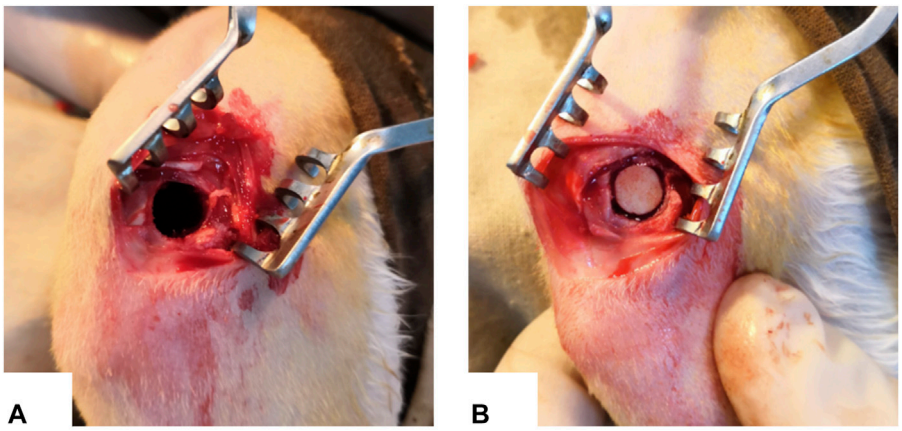

FIGURE 1 | (A) A line-to-line bone-implant interface model was constructed in the femoral condyle of New Zealand white rabbits using a 6 mm diameter defect. **(B)** An implant 6 mm in diameter was implanted into the defect region.

(Weihai, China). Commercially available PEEK rods (φ = 6 mm, L = 10 mm) were used in this study. Prior to surgical implantation, the samples were sterilized by γ-ray irradiation at a dose of 25 kGy.

Animal Model and Implantation Surgery

The animal experiments were approved by the Ethical Committee of The First Affiliated Hospital of Chongqing Medical University. Thirty male New Zealand white rabbits (12 weeks old, body weight 2.8–3.0 kg) were randomly divided into two groups. All animal experiments were performed following the "Guidance Suggestions for the Care and Use of Laboratory Animals" of the National Science and Technology Committee of the People's Republic of China, outlined in order No. 2, 2006. Surgeries were performed under general anesthesia by intravenous injection (1.0 ml/kg) with a 3% pentobarbital sodium solution (Sigma-Aldrich Co.) under sterile conditions. After proper preparation, a defect (φ = 6 mm, L = 10 mm) was drilled through the femoral condyle using 4 mm diameter and 6 mm diameter sterile drills (**Figure 1A**). An n-HA/PA66 implant was implanted into the condyle of one femur, and a PEEK implant was implanted into the contralateral femoral condyle as the control (**Figure 1B**). The wounds were sutured in layers. Postoperatively, gentamicin (5 mg/kg) and penicillin (50 kU/kg) were administered intramuscularly for 3 days. After the operation, all animals were allowed to bear full weight and received a normal diet. At 4, 8, 12, 24, and 52 weeks after surgery, the animals were sacrificed *via* celiac injection of an excessive amount of pentobarbital sodium. Implants were harvested from the surrounding tissues and fixed in 4% formaldehyde at 4°C for 1 week.

X-Ray Radiography and Micro-CT

X-ray radiographs were taken at 4, 8, 12, 24, and 52 weeks after implantation to investigate the interface between the material and bone tissue. The retrieved specimens at each time point (4, 8, 12, 24, and 52 weeks, n = 3) were examined using micro-CT (VivaCT80, Scanco Medical AG, Bassersdorf, Switzerland; pixel size: 30 μm, scan voltage: 70 kV, scan current: 200 μA, integral time: 300 ms).

A global threshold was utilized to segment the newly formed bone from each implant. After thresholding, the specific area within 1 mm from the implant surface was reconstructed and defined as the volume of interest (VOI) (Xu et al., 2018), the percentage of bone volume (BV) to the total tissue volume (TV; BV/TV%) within the VOI was calculated, trabecular thickness (TbTh; mm), trabecular number (TbN; 1/mm), and trabecular spacing (TbSp; mm) were calculated by using its auxiliary software (SCANCO VivaCT80, Switzerland) (Chai et al., 2012; Ji et al., 2020).

Histological Observations

After micro-CT analysis, the harvested samples (n = 3) at each time point and groups were dehydrated through a series of increasing ethanol concentrations (70~100%) and subsequently embedded in methyl methacrylate. The embedded samples were then longitudinally cut into 20 μm sections using a diamond saw (Leica SP-1600, Germany) and stained with 1% methylene blue (Sigma) and 0.3% basic fuchsin (Sigma) solutions for qualitative and quantitative histological observations.

To obtain the histological overview of each bone-implant interface and perform histomorphometry, the histological slides were scanned (Dimage Scan Elite 5400II, Konica Minolta Photo Imaging Inc., Tokyo, Japan). Subsequently, the acquired images were subject to the quantitative analysis for new bone using Adobe Photoshop CS5 software regarding the bone-implant contact (BIC) and bone area (BA). The bone-implant gap was defined as the interface area. The new bone growth at the interface were analyzed. The bone-implant contact defined as the percentage of the implant perimeter in direct contact with the mineralized bone tissue. The bone area was calculated as the area percentage of new bone in the interface area. Besides, the newly formed bone at the bone-implant interface was observed by observing the slides at a light

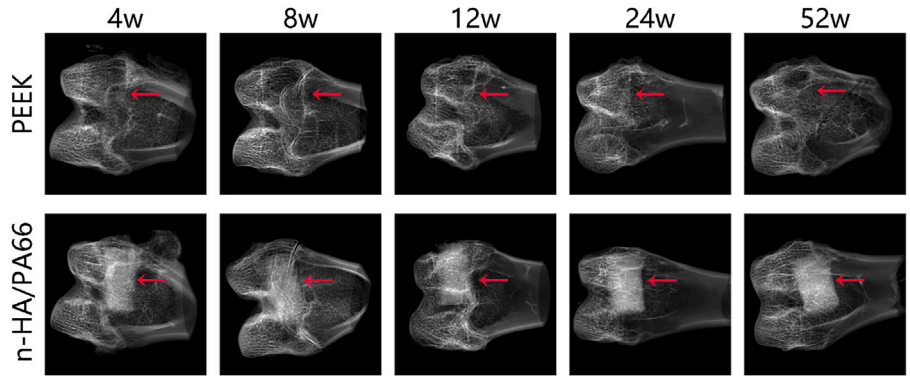

FIGURE 2 | X-ray radiographs of the bone-implant interface with polyether-ether-ketone (PEEK) and nanohydroxyapatite/polyamide 66 (n-HA/PA66) implants at 4, 8, 12, 24, and 52 weeks. (red arrow: interface).

microscope under high magnification (Nikon Eclipse E200, Tokyo, Japan) (Peng et al., 2020).

SEM and EDX Analysis

The newly retrieved specimens (n = 3) were cut longitudinally into 1 mm thick sections using a microtome (Leica SP-1600). The sections were then coated with a thin layer of gold, and the microstructure of the bone-implant interfaces was observed *via* SEM (ThermoFisher, Apreo S, 15 kV), and elemental analyses were subsequently conducted using EDX (ThermoFisher, Aztec X-Max80) and elemental mapping to determine the interface composition at each time point (n = 3).

Push-Out Tests

To investigate the integrated strength of the bone-implant interface, push-out tests were performed using an electric universal testing apparatus (SHIMADZU, AGS-X-10 KN) at 24 and 52 weeks. The newly harvested bone specimens from each group were stored at −80°C, and were measured within 24 h after sacrificing the animals (n = 3). Peri-implant soft tissue was carefully removed and exposure the outside of the implant. The specimens were fixed into the self-curing resin for 30 min for making the long axis of the implant consistent with the direction of the applied force. The tests were performed at a loading rate of 5 mm/min until the bone and implant interface was destroyed (**Figures 6A,B**). The load-displacement curve was obtained and the pressure at the point of a sudden drop in the push-out stress of the specimen was recorded (Xiu et al., 2016; Wang et al., 2019).

STATISTICS

Data are presented as mean ± standard deviation (SD). Statistical analyses were performed using SPSS16.0 software, and analyzed using analysis of variance (ANOVA) followed by Fisher's multiple comparison tests. $p < 0.05$ was considered statistically significant.

RESULTS

X-ray Observations

According to the X-ray radiographs (**Figure 2**), the n-HA/PA66 implant was conducive to observation and evaluation at the bone-implant interface because of its high density. The appearance of the defect after implantation could be clearly seen in the PEEK group because of the radiolucent nature of PEEK. After implantation for 4 weeks, no lucency or gap could be identified between the bone and implant at either of the interfaces. However, after implantation for 8 weeks, we found that PEEK implants began to exhibit a peek-halo effect, and a similar radiolucent gap formed around the n-HA/PA66 implant. In the PEEK group, the peek-halo effect continued to be identified around PEEK implants and did not seem to change during the healing process at 12, 24, and 52 weeks. In the n-HA/PA66 group, we discovered that the radiolucent gap was considerable at 8 weeks but began to narrow and decrease gradually from weeks 24 to 52, which is consistent with the healing process.

Micro-CT Analysis

New bone formation around the implants was evaluated at 4, 8, 12, 24, and 52 weeks postoperatively using micro-CT. The cross-sectional and 3D images of all implants are shown in **Figures 3A,B**. The implants (yellow) and newly formed bone tissue (red) in identically sized ROIs were reconstructed using 3D reconstructed images. Further quantitative analysis of the newly formed bone around the implants is shown in **Figure 3C–F**. At 4, 8, and 12 weeks after implantation, sparse new bone tissue growth at the interface (or gap) could be clearly observed. More newly formed bone was observed around the n-HA/PA66 than PEEK implants. With the prolongation of the implanting time, as part of the healing process, the new bone tissue gradually transformed into a more mature trabecular bone or woven bone at the later stage (24 and 52 weeks).

According to the quantitative analysis, at 4, 8, 12, and 52 weeks after implantation, n-HA/PA66 implants had higher

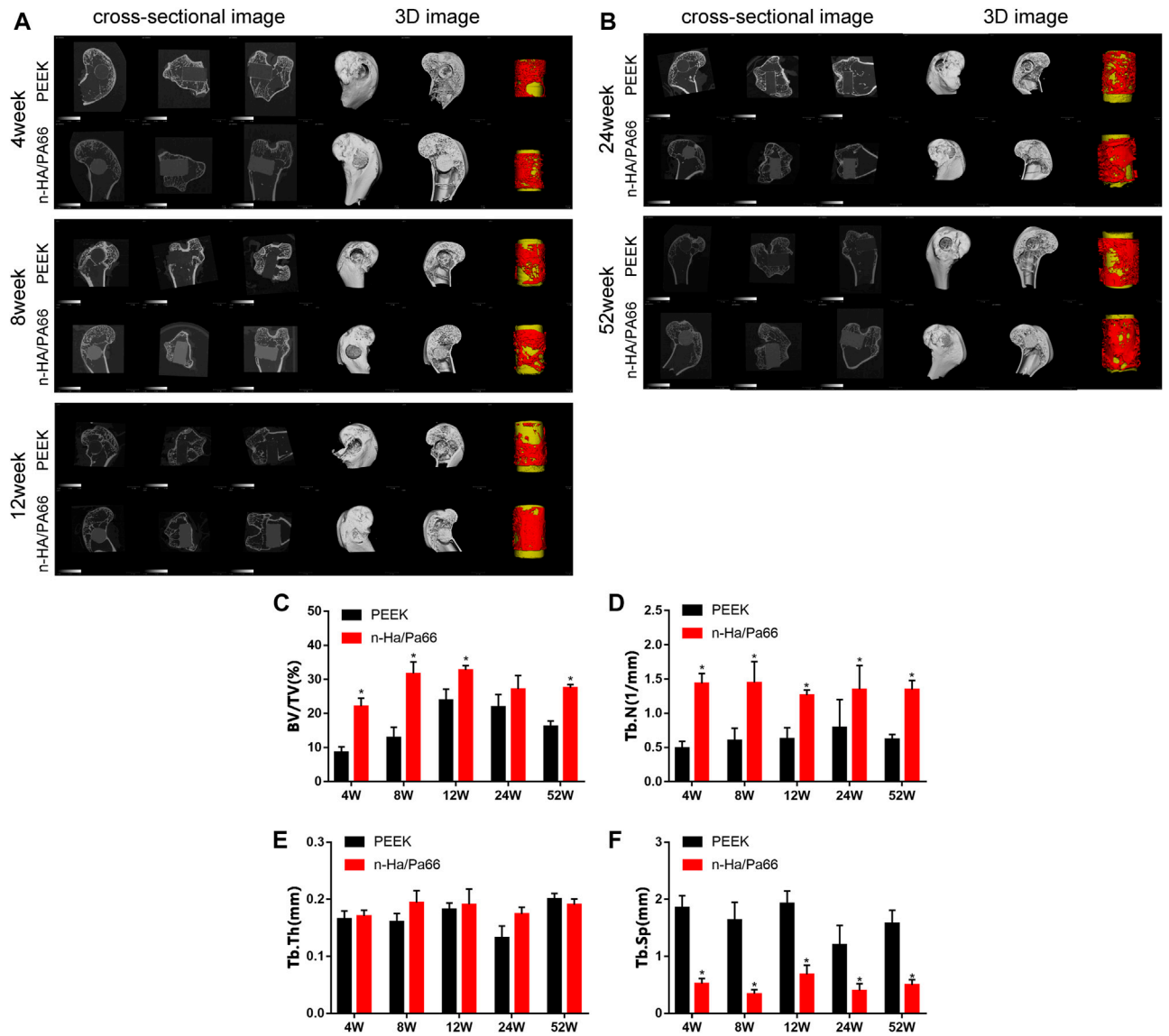

FIGURE 3 | (A) 2D cross-sectional images and 3D constructive images using micro-computed tomography (CT) at 4, 8, and 12 weeks. **(B)** 2D cross-sectional images and 3D constructive images using micro-computed tomography (CT) at 24 and 52 weeks. Quantitative analysis of micro-CT data: **(C)** bone volume/total volume (BV/TV), **(D)** trabecular number (Tb.N), **(E)** trabecular thickness (Tb.Th), **(F)** trabecular spacing (Tb.Sp). [* represents $p < 0.05$, when comparing polyether-ether-ketone (PEEK) and nanohydroxyapatite/polyamide 66 (n-HA/PA66)].

BV/TV and TbN indices than the PEEK implants indicating greater new bone formation ($p < 0.05$, $n = 3$). At all time points after implantation, PEEK implants had significantly higher TbSp values ($p < 0.05$, $n = 3$). This indicates that the trabecular bone around the PEEK was sparse. These results proved that the quality of bone tissue around n-HA/PA66 was better than that of PEEK.

Histological Observations

After micro-CT analysis, all the gross specimens showed direct contact with the surrounding bones. Fuchsin and methylene blue staining shows the tissue response to the PEEK and n-HA/P66 implants after 4, 8, 12, 24, and 52 weeks (**Figures 4A,B**). Further quantitative analysis of the new bone area rate (BA%) and bone-implant contact ratio (BIC) are shown in **Figures 4C,D**. No special inflammatory reaction was observed in any region of the implant during the entire implantation period.

For the n-HA/PA66 implants, in the early weeks after implantation from 4 to 12 weeks, the results showed there was a "interface" between the bone and implant. Many immature woven bones filled the interface around the implant and gradually grew on the surface of the n-HA/PA66. Moreover, with the prolongation of the implantation

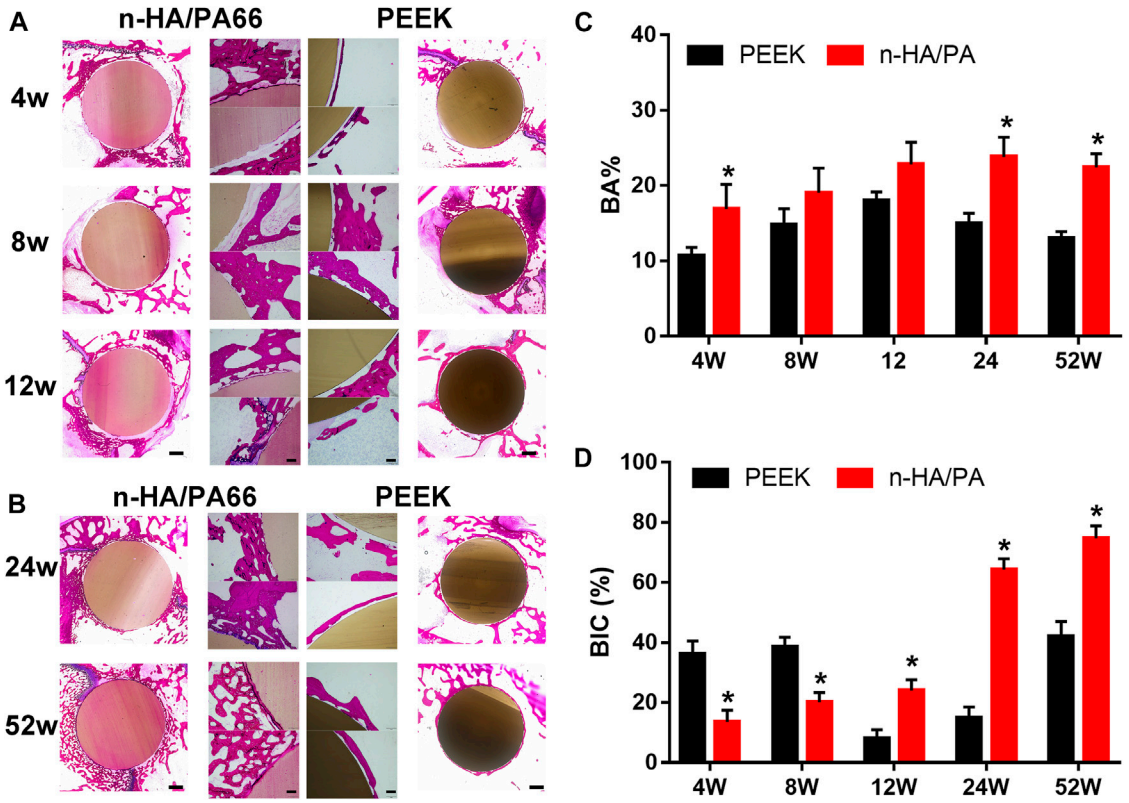

FIGURE 4 | (A) Histological overviews of polyether-ether-ketone (PEEK; left) and nanohydroxyapatite/polyamide 66 (n-HA/PA66; right) bone-implant interfaces at 4, 8, and 12 weeks (scale = 2 mm); Middle: detailed light microscopic images of the selected region in the histological overviews (scale = 250 mm); methylene blue and basic fuchsin staining. **(B)** Histological overviews of PEEK- and n-HA/PA66 bone-implant interfaces at 24 and 52 weeks (scale = 2 mm). **(C)** The new bone area rate (BA %) and **(D)** bone-implant contact ratio (BIC) were analyzed from the images shown in A and B. (* $p < 0.05$).

time, the immature woven bone gradually disappeared, accompanied by growth of new trabecular bone around the implant surface. At 24 and 52 weeks after implantation, the formed trabecular bone on the n-HA/PA66 implants was continuous and bonded tightly to the implant surface, and excellent osseointegration could be confirmed by the images at the interface area (**Figure 4B**). In the PEEK group, we could easily identify the poor osseointegrated interface (or gap) on histological sections at all time points, which could possibly be missed on the X-ray. With time, the layer of fibrous encapsulation became thinner than before; however, it persisted. Furthermore, almost no visible bone tissue formation was observed, and only a small number of new bones were sparsely distributed around the PEEK implants.

SEM and Surface Element Analysis

Typical SEM images of the bone-implant sections and their elemental analyses are shown in **Figures 5A,B**. The new bones bonded to the n-HA/PA66 surface directly, and the gap between the new bone and the implant narrowed as the implantation time increased. In the PEEK group, the gap between the bone and implant could still be observed at each time point. At 24 and 52 weeks after implantation, excellent osteointegration between the host bone and the implant could be confirmed by the local magnified images at the interface area, and a continuity zone of n-HA/PA66 adhered to the bone without intervening space could be seen clearly (**Figure 5B**).

Electron microscopy of the bone-implant interface revealed interesting ultrastructural information, but it is difficult to identify the type of tissue around the implant. The EDX analysis of newly formed bone at the bone-implant interface revealed that the n-HA/PA66-bone interface contained Ca and P at a Ca/P ratio of approximately 1.59. The PEEK-bone interface showed less calcification and a lower Ca/P ratio (**Table 1**).

Biomechanical Push-Out Test

Push-out tests were conducted on the specimens after implantation for 24 and 52 weeks (**Figure 6A**). The typical load-displacement curves, along with the average maximum push-out force (Fmax) of the specimens are shown in **Figure 6B**. For all the specimens, the loading force increased gradually with increasing displacement until the bone-implant interface was destroyed, indicating the Fmax. PEEK had a low bonding strength with the surrounding bone; the Fmax were 272.6 ± 5.5 at 24 weeks and 320.3 ± 13.7 N at 52 weeks. However, the Fmax of n-HA/PA66 were 518.6 ± 9.4 and 530.4 ± 8.8 N at 24 and 52 weeks, respectively. Accordingly, the maximum failure load of n-HA/PA66 implants was greater than that of PEEK implants at 24 (18.3 ± 0.11 vs. 9.6 ± 0.10 MPa; $p <$

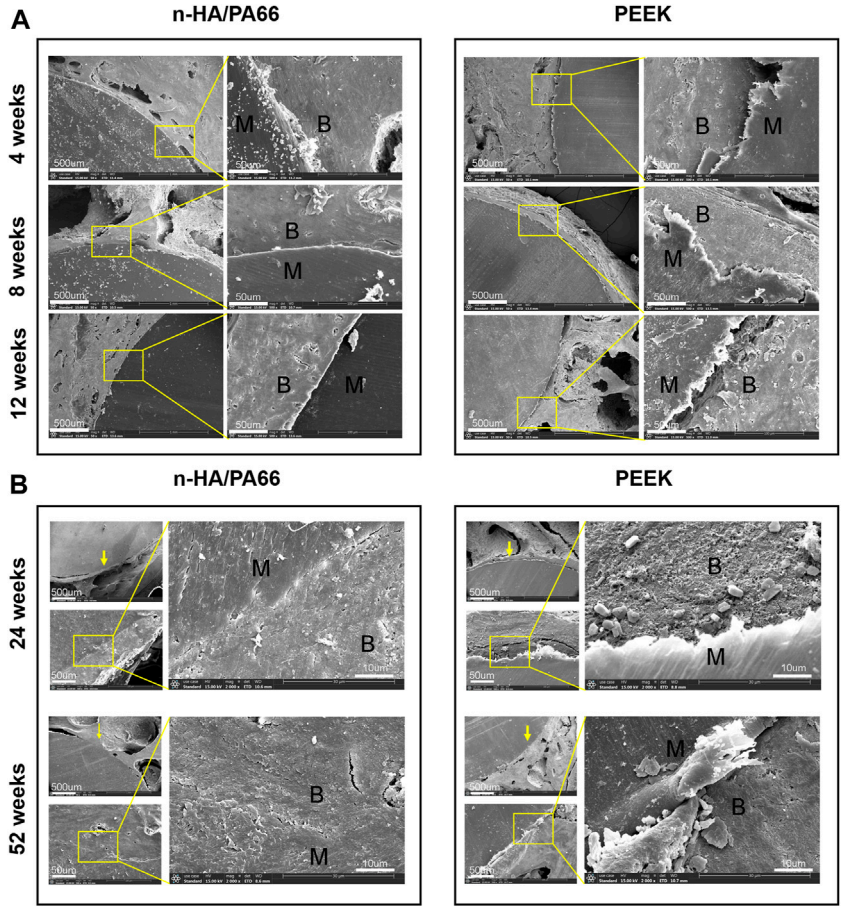

FIGURE 5 | (A) Scanning electron microscopy (SEM) image of the bone-implant interface 4, 8, and 12 weeks after implantation. **(B)** SEM image of the bone-implant interface 24 and 52 weeks after implantation.

TABLE 1 | EDS results of the calcium and phosphorus ratio at the bone-implant interface of n-HA/PA66 and PEEK.

Sample	4 weeks	8 weeks	12 weeks	24 weeks	52 weeks
n-HA/PA66	1.47 ± 0.03	1.53 ± 0.06	1.52 ± 0.11	1.57 ± 0.04[a]	1.59 ± 0.05[a]
PEEK	1.52 ± 0.04	1.48 ± 0.06	1.50 ± 0.05	1.37 ± 0.15	1.30 ± 0.04

[a]$p < 0.05$, *versus PEEK.*

0.05) and 52 weeks (18.6 ± 0.18 vs. 11.7 ± 0.09 MPa; $p < 0.05$). Thus, the integrated strength of n-HA/PA66 was significantly higher than that of PEEK (**Figures 6C, D**).

DISCUSSION

Although radiolucent zones around the implant may be an indication that the implant is encapsulated by fibrous tissue, the lack of such zones does not indicate osseointegration (Albrektsson and Jacobsson, 1987). The poor osseointegration of PEEK is often attributed to its relatively bio-inert and hydrophobic properties. In contrast, n-HA/PA66 is a bioactive composite made by infiltrating nano-HA into PA66; it mimics natural bone in that the apatite is distributed within a collagen matrix (Xu et al., 2018). Thus, the composite possesses both the bioactive effects of HA and the mechanical strength of PA66. We hypothesized that the bioactive n-HA/PA66 would enhance the *in vivo* osseointegration effects at the bone-implant interface. We explored whether the "radiolucent gap" and "Peek-halo" were similar and if an improved bone-implant interface was exhibited with n-HA/PA66 in comparison to that with PEEK. To determine the difference between the radiolucent gaps of the two implants between the bone and the implant we assessed the differences in

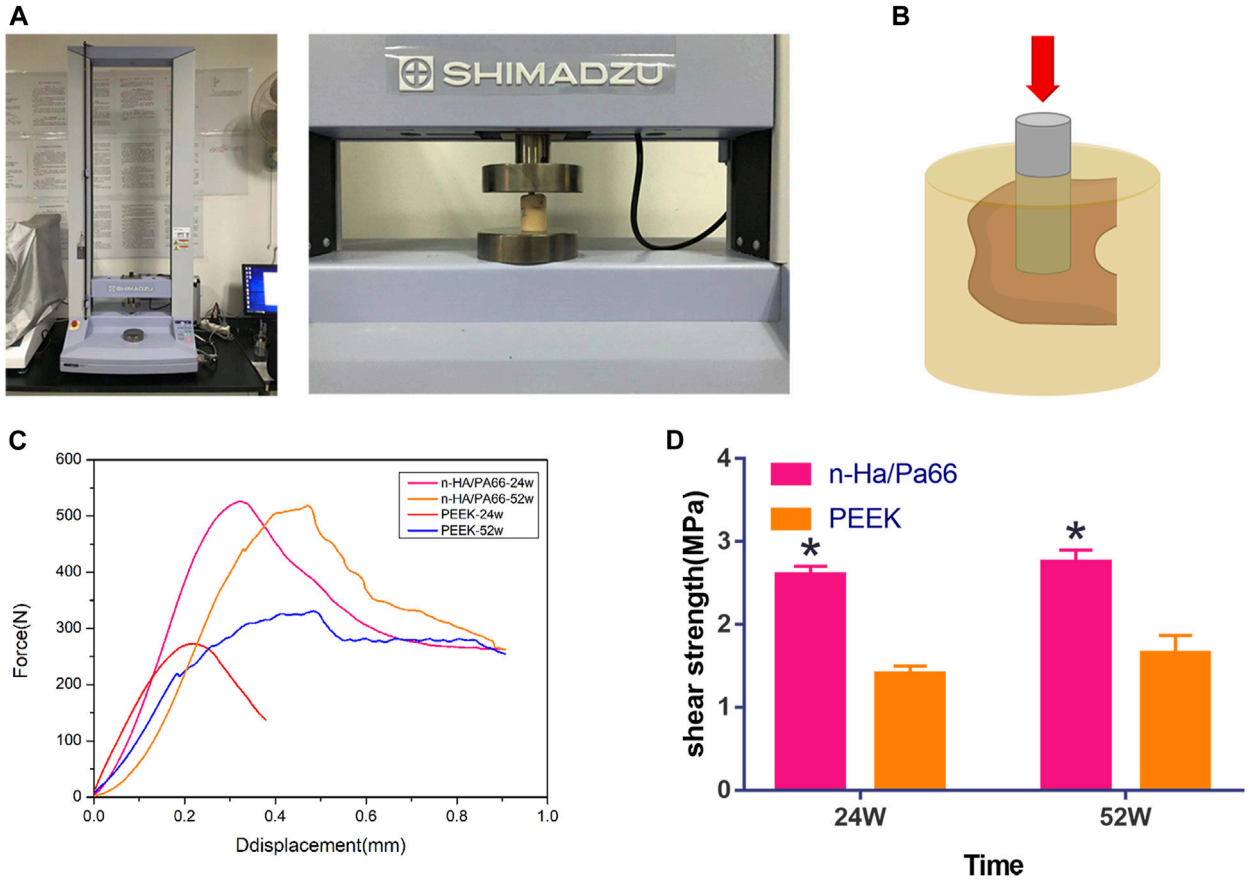

FIGURE 6 | (A,B): Schematic image shows the design of the pushing-out test. **(C)** Typical push-out force displacement curve of the polyether-ether-ketone (PEEK) and nanohydroxyapatite/polyamide 66 (n-HA/PA66) bone-implant interface. **(D)** Average shear strength of the two implants at 24 and 52 weeks. (*$p < 0.05$).

osseointegration effects of the two implants after implantation for 4, 8, 12, 24, and 52 weeks. These results demonstrate that the n-HA/PA66 implant exhibited a better osseointegrated bone-implant interface than PEEK. We found a radiolucent line around n-HA/PA66 in the early weeks after implantation, and the zone decreased and disappeared gradually. The PEEK implant showed a fibrous inert interface and less bone formation. The PEEK-halo line could be seen clearly during long-term observation. In addition, the push-out tests also demonstrated that the interface of n-HA/PA66 had a higher integrated strength than the PEEK implant.

Osseointegration has been used to describe the successful healing of an implant within the host bone for a long time (Kuzyk and Schemitsch, 2011; Shah et al., 2019). Knowledge of this bone-implant interface is useful for interpreting the reasoning behind orthopedic implant design strategies and their long-term success, and it is imperative for surgeons to have a basic understanding of the bone-implant interface healing process (Shah et al., 2019). In the present study, we discovered a radiolucent gap at the margin of the n-HA/PA66 implant by X-ray radiography and histological sections in the early weeks after implantation (4–8 weeks). Subsequently, the gap decreased and disappeared gradually at 24 weeks and becoming more narrow at 52 weeks, which is consistent with the healing process. Through histological analysis, we could clearly observe the space between the bone and implant in the early weeks after implantation (4–12 weeks). The space was gradually filled with new bone, which suggested that n-HA/PA66 had good osseointegration properties with the surrounding bones. At 24 and 52 weeks, we found that n-HA/PA66 could integrate and be connected with host bone in some regions where new bone grew into the n-HA/PA66 implant after implantation. In contrast, in the PEEK group, a radiolucent halo line could be identified by X-ray film at 4 and 8 weeks, and the fibrous gap could be clearly observed by histological assessment. Furthermore, there was no change in the fibrous interface during the healing process after 12, 24, and 52 weeks. This indicates that the PEEK-bone interface becomes inert, and the surrounding tissue has formed a stable bioinert structure. The same results were reported by Walsh and etc. who tried to incorporate HA into PEEK and plasma spraying of titanium to PEEK in order to improve osseointegration (Pelletier et al., 2016; Walsh et al., 2018).

Clinically, the success or failure of an implanted device is often measured by X-ray radiography and CT examination. The "PEEK-halo" and "radiolucent gap" effects in many clinical studies reflect the inadequacy of clinical methods for evaluating osseointegration. These tests are indirect methods, that indicate, but do not verify osseointegration. The classical description of osseointegration is a direct contact between the implant surface and bone at the light microscopic level (Shah et al., 2019), which is mainly distinguished from fibrous integration. However, this definition ignores the presence of other interposed components of the tissue along the interface. The interface should include bone-implant areas and the peri-implant bone. Micro-CT is frequently used to evaluate bone formation around the implant, but the bone-implant interface is often obscured and cannot be clearly determined (Palmquist et al., 2017). In the present study, the results of micro-CT and histological analysis showed that the n-HA/PA66 implant had higher BV/TV values and bone volumes than PEEK at 4, 8, and 12 weeks, which remained stable from 24 to 52 weeks. This demonstrated that the n-HA/PA66 surface may favor new bone formation. To assert that an implant achieved good osseointegration and solid fusion must imply that most of it is anchored with bone tissue. We therefore investigated the ultrastructure of the bone-implant interface using SEM and EDX mapping. Electron microscopy of the tissue interface is capable of producing interesting information, but it is difficult to identify the precise components of tissue around the entire implant. The results demonstrated that the n-HA/PA66 implant has a thin interface gap and a continuous mineralized interface zone, and the EDX analysis showed that a fiber medial layer was found between the PEEK implant and bone, whereas the n-HA/PA66 implant exhibited an improved mineralized implant-bone interface.

The aim of determining an optimized spinal fusion device is to achieve good osseointegration and promote long-term success (Shah et al., 2019). Through push-out tests, we could see that n-HA/PA66 implants can possess stronger bonding strength with the surrounding bone tissue and could obtain sufficient stability at 24 and 52 weeks, whereas the PEEK implant could be pushed out easily, which indicates that the surrounding bone tissue cannot adhere to PEEK. Therefore, our hypothesis that n-HA/PA66 would have better osseointegration properties and higher bonding strength than PEEK was confirmed. Several efforts have been made to improve the bioactivity and osteointegration properties of PEEK to prolong its long-term stability (Johansson et al., 2015; Torstrick et al., 2017; Liu et al., 2018); for example, plasma-sprayed titanium or HA coatings on PEEK and the incorporation of HA into PEEK (Walsh et al., 2016; Torstrick et al., 2017). However, these studies only showed good improvements in bone formation by histological analysis and micro-CT evaluation. Bone formation begins at the implant surface in response to the surface physicochemical properties of the implant surface (Liu et al., 2018). Remodeling of the bone in contact with the implant surface continues throughout the lifetime of the implant. This remodeling may allow for increased contact between the implant and the bone over time and likely continues for longer than six months. Our previous studies have shown that a bone-like apatite layer can be formed on the surface of n-HA/PA66 in simulated body fluid (Wang et al., 2002), and the n-HA/PA66 composite could promote the growth and osteogenic differentiation of mesenchymal stem cells (Xu et al., 2018). The EDX mapping results revealed that Ca and phosphonium were successfully incorporated on the surface of n-HA/PA66 and were homogeneously distributed. Thus, the n-HA particles on the surface provide a good osteoconductive surface, which has a positive effect on bone apposition and mineralization.

In summary, we found that the n-HA/PA66 implant has good osseointegration properties and exhibits an improved bone-implant interface. Thus, this composite is appropriate for bone formation and bonding with the surrounding bone and provides better biomechanical stability than PEEK. Consequently, the n-HA/PA66 composite exhibited good osseointegration properties for clinical applications. Additional clinical and experimental studies are required to elucidate the precise bonding mechanisms underlying the bone-implant interface.

DATA AVAILABILITY STATEMENT

The raw data supporting the conclusions of this article will be made available by the authors, without undue reservation.

ETHICS STATEMENT

The animal study was reviewed and approved by The Ethical Committee of The First Affiliated Hospital of Chongqing Medical University.

AUTHOR CONTRIBUTIONS

JL and HP performed the experiments, analyzed and interpreted the results. HP, CH, ZC, and TH performed the animal experiments. JL, HL, and ZQ acquired the research operating funding, advised on the conception and conduction of the experiments and data analysis.

FUNDING

The authors thank Science and Health Project of Chongqing Health Commission(2021MSXM143) and Research and Innovation Project of Graduate students in Chongqing (CYB19142) for providing funding for this research.

REFERENCES

Albrektsson, T., and Jacobsson, M. (1987). Bone-metal Interface in Osseointegration. *The J. Prosthetic Dentistry* 57 (5), 597–607. doi:10.1016/0022-3913(87)90344-1

Bagby, G. W. (1988). Arthrodesis by the Distraction-Compression Method Using a Stainless Steel Implant. *Orthopedics* 11 (6), 931–934. doi:10.3928/0147-7447-19880601-13

Bertollo, N., Matsubara, M., Shinoda, T., Chen, D., Kumar, M., and Walsh, W. R. (2011). Effect of Surgical Fit on Integration of Cancellous Bone and Implant Cortical Bone Shear Strength for a Porous Titanium. *The J. Arthroplasty* 26 (7), 1000–1007. doi:10.1016/j.arth.2010.12.007

Chai, Y. C., Kerckhofs, G., Roberts, S. J., Van Bael, S., Schepers, E., Vleugels, J., et al. (2012). Ectopic Bone Formation by 3D Porous Calcium Phosphate-Ti6Al4V Hybrids Produced by Perfusion Electrodeposition. *Biomaterials* 33 (16), 4044–4058. doi:10.1016/j.biomaterials.2012.02.026

Cloward, R. B. (2007). The Anterior Approach for Removal of Ruptured Cervical Disks. *J. Neurosurg. Spine.* 6 (5), 496–511. doi:10.3171/spi.2007.6.5.496

Ji, M., Chen, H., Yan, Y., Ding, Z., Ren, H., and Zhong, Y. (2020). Effects of Tricalcium Silicate/sodium Alginate/calcium Sulfate Hemihydrate Composite Cements on Osteogenic Performances *In Vitro* and *In Vivo*. *J. Biomater. Appl.* 34 (10), 1422–1436. doi:10.1177/0885328220907784

Johansson, P., Jimbo, R., Kozai, Y., Sakurai, T., Kjellin, P., Currie, F., et al. (2015). Nanosized Hydroxyapatite Coating on PEEK Implants Enhances Early Bone Formation: A Histological and Three-Dimensional Investigation in Rabbit Bone. *Materials* 8 (7), 3815–3830. doi:10.3390/ma8073815

Kurtz, S. M., and Devine, J. N. (2007). PEEK Biomaterials in Trauma, Orthopedic, and Spinal Implants. *Biomaterials* 28 (32), 4845–4869. doi:10.1016/j.biomaterials.2007.07.013

Kuzyk, P., and Schemitsch, E. (2011). The Basic Science of Peri-Implant Bone Healing. *Indian J. Orthop.* 45 (2), 108–115. doi:10.4103/0019-5413.77129

Liu, W., Li, J., Cheng, M., Wang, Q., Yeung, K. W. K., Chu, P. K., et al. (2018). Zinc-Modified Sulfonated Polyetheretherketone Surface with Immunomodulatory Function for Guiding Cell Fate and Bone Regeneration. *Adv. Sci.* 5 (10), 1800749. doi:10.1002/advs.201800749

Noiset, O., Schneider, Y.-J., and Marchand-Brynaert, J. (1999). Fibronectin Adsorption Or/and Covalent Grafting on Chemically Modified PEEK Film Surfaces. *J. Biomater. Sci. Polym. Edition* 10 (6), 657–677. doi:10.1163/156856299x00865

Palmquist, A., Shah, F. A., Emanuelsson, L., Omar, O., and Suska, F. (2017). A Technique for Evaluating Bone Ingrowth into 3D Printed, Porous Ti6Al4V Implants Accurately Using X-ray Micro-computed Tomography and Histomorphometry. *Micron* 94, 1–8. doi:10.1016/j.micron.2016.11.009

Pelletier, M. H., Cordaro, N., Punjabi, V. M., Waites, M., Lau, A., and Walsh, W. R. (2016). PEEK versus Ti Interbody Fusion Devices. *Clin. Spine Surg.* 29 (4), E208–E214. doi:10.1097/BSD.0b013e31826851a4

Peng, H., Li, J., Xu, Y., and Lv, G. (2020). Icaritin Enhancing Bone Formation Initiated by Sub-microstructured Calcium Phosphate Ceramic for Critical Size Defect Repair. *Front. Mater.* 7, 598057. doi:10.3389/fmats.2020.598057

Phan, K., Hogan, J. A., Assem, Y., and Mobbs, R. J. (2016). PEEK-halo Effect in Interbody Fusion. *J. Clin. Neurosci.* 24, 138–140. doi:10.1016/j.jocn.2015.07.017

Shah, F. A., Thomsen, P., and Palmquist, A. (2019). Osseointegration and Current Interpretations of the Bone-Implant Interface. *Acta Biomater.* 84, 1–15. doi:10.1016/j.actbio.2018.11.018

Torstrick, F. B., Lin, A. S. P., Potter, D., Safranski, D. L., Sulchek, T. A., Gall, K., et al. (2018). Porous PEEK Improves the Bone-Implant Interface Compared to Plasma-Sprayed Titanium Coating on PEEK. *Biomaterials* 185, 106–116. doi:10.1016/j.biomaterials.2018.09.009

Torstrick, F. B., Safranski, D. L., Burkus, J. K., Chappuis, J. L., Lee, C. S. D., Guldberg, R. E., et al. (2017). Getting PEEK to Stick to Bone: The Development of Porous PEEK for Interbody Fusion Devices. *Tech. Orthop.* 32 (3), 158–166. doi:10.1097/bto.0000000000000242

Toth, J. M., Wang, M., Estes, B. T., Scifert, J. L., Seim, H. B., 3rd, and Turner, A. S. (2006). Polyetheretherketone as a Biomaterial for Spinal Applications. *Biomaterials* 27 (3), 324–334. doi:10.1016/j.biomaterials.2005.07.011

Walsh, W. R., Bertollo, N., Christou, C., Schaffner, D., and Mobbs, R. J. (2015). Plasma-sprayed Titanium Coating to Polyetheretherketone Improves the Bone-Implant Interface. *Spine J.* 15 (5), 1041–1049. doi:10.1016/j.spinee.2014.12.018

Walsh, W. R., Pelletier, M. H., Bertollo, N., Christou, C., and Tan, C. (2016). Does PEEK/HA Enhance Bone Formation Compared with PEEK in a Sheep Cervical Fusion Model? *Clin. Orthop. Relat. Res.* 474 (11), 2364–2372. doi:10.1007/s11999-016-4994-x

Walsh, W. R., Pelletier, M. H., Christou, C., He, J., Vizesi, F., and Boden, S. D. (2018). The *In Vivo* Response to a Novel Ti Coating Compared with Polyether Ether Ketone: Evaluation of the Periphery and Inner Surfaces of an Implant. *Spine J.* 18 (7), 1231–1240. doi:10.1016/j.spinee.2018.02.017

Wang, H., Su, K., Su, L., Liang, P., Ji, P., and Wang, C. (2019). Comparison of 3D-Printed Porous Tantalum and Titanium Scaffolds on Osteointegration and Osteogenesis. *Mater. Sci. Eng. C* 104, 109908. doi:10.1016/j.msec.2019.109908

Wang, X., Li, Y., Wei, J., and de Groot, K. (2002). Development of Biomimetic Nano-Hydroxyapatite/poly(hexamethylene Adipamide) Composites. *Biomaterials* 23 (24), 4787–4791. doi:10.1016/s0142-9612(02)00229-6

Wu, S.-H., Li, Y., Zhang, Y.-Q., Li, X.-K., Yuan, C.-F., Hao, Y.-L., et al. (2013). Porous Titanium-6 Aluminum-4 Vanadium Cage Has Better Osseointegration and Less Micromotion Than a Poly-Ether-Ether-Ketone Cage in Sheep Vertebral Fusion. *Artif. Organs* 37 (12), E191–E201. doi:10.1111/aor.12153

Xiu, P., Jia, Z., Lv, J., Yin, C., Cheng, Y., Zhang, K., et al. (2016). Tailored Surface Treatment of 3D Printed Porous Ti6Al4V by Microarc Oxidation for Enhanced Osseointegration *via* Optimized Bone In-Growth Patterns and Interlocked Bone/Implant Interface. *ACS Appl. Mater. Inter.* 8 (28), 17964–17975. doi:10.1021/acsami.6b05893

Xu, Y., Li, H., Wu, J., Yang, Q., Jiang, D., and Qiao, B. (2018). Polydopamine-induced Hydroxyapatite Coating Facilitates Hydroxyapatite/polyamide 66 Implant Osteogenesis: an *In Vitro* and *In Vivo* Evaluation. *Int. J. Nanomedicine.* Vol. 13, 8179–8193. doi:10.2147/ijn.S181137

Yuan, B., Cheng, Q., Zhao, R., Zhu, X., Yang, X., Yang, X., et al. (2018). Comparison of Osteointegration Property between PEKK and PEEK: Effects of Surface Structure and Chemistry. *Biomaterials* 170, 116–126. doi:10.1016/j.biomaterials.2018.04.014

Zhang, Y., Deng, X., Jiang, D., Luo, X., Tang, K., Zhao, Z., et al. (2016). Long-term Results of Anterior Cervical Corpectomy and Fusion with Nano-Hydroxyapatite/polyamide 66 Strut for Cervical Spondylotic Myelopathy. *Sci. Rep.* 6, 26751. doi:10.1038/srep26751

Conflict of Interest: The authors declare that the research was conducted in the absence of any commercial or financial relationships that could be construed as a potential conflict of interest.

frontiers in Bioengineering and Biotechnology

ORIGINAL RESEARCH
published: 19 July 2021
doi: 10.3389/fbioe.2021.697281

Effects of Mechanical Compression on Chondrogenesis of Human Synovium-Derived Mesenchymal Stem Cells in Agarose Hydrogel

Yuxiang Ge[1,2], Yixuan Li[1,2], Zixu Wang[1,2], Lan Li[1,3], Huajian Teng[2]* and Qing Jiang[1,2]**

[1] State Key Laboratory of Pharmaceutical Biotechnology, Department of Sports Medicine and Adult Reconstructive Surgery, Nanjing Drum Tower Hospital, The Affiliated Hospital of Nanjing University Medical School, Nanjing, China, [2] Laboratory for Bone and Joint Disease, Model Animal Research Center, Nanjing University, Nanjing, China, [3] Jiangsu Engineering Research Center for 3D Bioprinting, Nanjing, China

OPEN ACCESS

Edited by:
Farnaz Ghorbani, Friedrich–Alexander University Erlangen–Nürnberg, Germany

Reviewed by:
Andrea Cochis, University of Eastern Piedmont "Amedeo Avogadro", Italy
Viviana Salvatore, University of Bologna, Italy
Dinesh Parate, National University of Singapore, Singapore

***Correspondence:**
Qing Jiang
qingj@nju.edu.cn
Huajian Teng
tenghj@nicemice.cn
Lan Li
lanl17@163.com

Specialty section:
This article was submitted to Biomaterials, a section of the journal Frontiers in Bioengineering and Biotechnology

Received: *19 April 2021*
Accepted: *22 June 2021*
Published: *19 July 2021*

Citation:
Ge Y, Li Y, Wang Z, Li L, Teng H and Jiang Q (2021) Effects of Mechanical Compression on Chondrogenesis of Human Synovium-Derived Mesenchymal Stem Cells in Agarose Hydrogel. Front. Bioeng. Biotechnol. 9:697281. doi: 10.3389/fbioe.2021.697281

Mechanical compression is a double-edged sword for cartilage remodeling, and the effect of mechanical compression on chondrogenic differentiation still remains elusive to date. Herein, we investigate the effect of mechanical dynamic compression on the chondrogenic differentiation of human synovium-derived mesenchymal stem cells (SMSCs). To this aim, SMSCs encapsulated in agarose hydrogels were cultured in chondrogenic-induced medium with or without dynamic compression. Dynamic compression was applied at either early time-point (day 1) or late time-point (day 21) during chondrogenic induction period. We found that dynamic compression initiated at early time-point downregulated the expression level of chondrocyte-specific markers as well as hypertrophy-specific markers compared with unloaded control. On the contrary, dynamic compression applied at late time-point not only enhanced the levels of cartilage matrix gene expression, but also suppressed the hypertrophic development of SMSCs compared with unloaded controls. Taken together, our findings suggest that dynamic mechanical compression loading not only promotes chondrogenic differentiation of SMSCs, but also plays a vital role in the maintenance of cartilage phenotype, and our findings also provide an experimental guide for stem cell-based cartilage repair and regeneration.

Keywords: chondrocytes, mechanical compression, chondrogenesis, cartilage repair, SMSCs

INTRODUCTION

Cartilage damage caused by osteoarthritis (OA) or traumatic injury has become a major clinical problem, affecting a large number of people worldwide. Damaged articular cartilage generally leads to the gradual degradation of hyaline cartilage, which hardly repairs spontaneously due to the lack of vascularity and cellularity (Muir, 1995; Williams et al., 2003). As the articular tissue has a limited capacity to regenerate, current treatment is inefficient and not able to restore the function and mobility of damaged cartilage (Smith et al., 2005). Surgical treatments such as microfracture and autograft cartilage transplantation have shown great improvement but still result in fibrillation of

cartilage, lacking in function and mobility of native cartilage. In this manner, there is great demand for the advanced techniques for the regeneration of cartilage (Bedi et al., 2010).

Cell-based tissue engineering has been widely studied and considered as an encouraging treatment of damaged cartilage. However, autologous chondrocyte implantation (ACI) has its disadvantage as isolated chondrocytes have a limited ability to proliferate (Wakitani et al., 2002). Mesenchymal stem cells (MSCs) are widely recognized as a multipotent cell source as they are easy to isolate and have a high capacity of self-renewing and chondrogenic differentiation (Tuan et al., 2003). Among these, synovium-derived mesenchymal stem cells (SMSCs) are considered as an ideal cell resource for cartilage tissue engineering due to their higher chondrogenic potential compared with other kinds of tissue-derived MSCs such as bone marrow-derived mesenchymal stem cells (BMSCs) (Sakaguchi et al., 2005; Pei et al., 2008).

Cartilage tissue engineering involves seeding MSCs into scaffolds such as different kinds of hydrogels, which are able to promote the production of extracellular matrix (ECM) components in three-dimensional (3D) culture (Bedi et al., 2010). There are various kinds of hydrogels for cartilage tissue engineering, including sodium alginate and agarose. Agarose has been specifically effective in cultivating engineered cartilage constructs with analogous mechanical and biochemical properties compared with native articular cartilage (O'Connell et al., 2017). Cell-based scaffolds are implanted after preculture *in vitro* for a short time or cultured for a long period to form a tissue, which has more proteoglycan and collagen contents. Despite the promising future of MSCs in cartilage regeneration, the ability of MSCs to regenerate hyaline-like cartilage is limited in that MSCs are more likely to differentiate into hypertrophic phenotypes followed by mineralization, and are eventually replaced with bone, which is known as endochondral ossification (Pelttari et al., 2006; Mueller and Tuan, 2008). Meanwhile, it has been demonstrated that the mechanical properties of cell-based scaffolds are much lower compared with those of native chondrocytes, implying that further optimization is needed (Mauck et al., 2006).

Many biochemical approaches have been applied to improve the chondrogenic potential of MSCs, such as members of transforming growth factor-β (TGF-β) family. TGF-β has been proved to act as a vital role in chondrogenesis, which is most commonly used in chondrogenic differentiation and induction (Toh et al., 2005). On the other hand, it has been demonstrated that biophysical cues such as compressive strain play a central role in chondrogenic differentiation (Mouw et al., 2007; Li et al., 2012; O'Conor et al., 2013; McKee et al., 2017). Chondrocytes in articular cartilage are surrounded by ECM, mainly composed of collagen 2 and aggrecan. During the daily activity, articular cartilage is exposed to great compressive strain, transmitting physical signals through the articular cartilage tissue into chemical cues, including changes in cell morphology and local osmolarity (Schiavi et al., 2018).

Accumulating evidence has suggested that mechanical cues significantly influence ECM synthesis of chondrocytes and play an important role in the differentiation of MSCs (Haugh et al., 2011; Fahy et al., 2018; Chen et al., 2021). Although great efforts have been made to optimize loading parameters to maximize the mechanical regulation on chondrogenic differentiation, especially in frequency and magnitude, rare studies have focused on how and when the mechanical stimulation should be applied (Zuscik et al., 2008; Kisiday et al., 2009; Li et al., 2010). In most studies, mechanical stimulation was applied at the initiation or relative early stage of chondrogenic differentiation period. Huang et al. (2010) reported that dynamic compression for 7 days from the initiation of chondrogenic differentiation displayed higher levels of chondrogenic markers. However, it was reported that preculture for 16 days increased the expression of chondrogenic markers compared with preculture for only 8 days during the chondrogenic differentiation (Mouw et al., 2007). Haugh et al. (2011) also reported that dynamic compression applied at 3 weeks was found to promote cartilage-specific ECM gene expression. These studies suggest that the mechanosensitivity of stem cells may vary during the process of chondrogenic differentiation (Mouw et al., 2007; Yang et al., 2009). Moreover, it has been shown that allowing ECM accumulation by delaying the application of mechanical compression enhanced mechanical properties of cartilage constructs or sulfated glycosaminoglycan (sGAG) synthesis (Demarteau et al., 2003; Lima et al., 2007). Moreover, Aisenbrey et al. reported that mechanical loading inhibited hypertrophy in chondrogenic differentiation of MSCs (Aisenbrey and Bryant, 2016). In this study, SMSCs were allowed to undergo chondrogenic differentiation in the presence of TGF-β3 for 4 weeks and dynamic compression was applied at either early time-points (day 1) or late time-points (day 21) of chondrogenic induction. The objective of the study is to investigate the influence of dynamic compression loading on the chondrogenic differentiation and hypertrophy of SMSCs.

MATERIALS AND METHODS

Cell Isolation

The study was approved by the Ethical Committee of Nanjing Drum Tower Hospital, The Affiliated Hospital of Nanjing University Medical School, and informed consent was obtained from all the subjects. Synovium tissues were harvested from 13 donors (nine women and four men; mean age, 66.5 years; age range, 51–75 years) when they underwent total knee arthroplasty. The procedures for the isolation of SMSCs have been established as described previously (Shi et al., 2016). Briefly, synovium was minced, digested with type I collagenase (3 mg/mL; Gibco, United States), and passed through 70-μm nylon filter to yield single-cell suspension. The released cells were washed in PBS; resuspended in expansion medium (DMEM/F12; Gibco) containing 10% fetal bovine serum (FBS), 100 U/mL penicillin, and 100 mg/mL streptomycin (Invitrogen, United States); and plated at 5×10^4 cells/cm in 100-cm^2 culture dishes. Cells were allowed to attach for 3 days, and non-adherent cells were removed by changing the culture medium every 3 days. At day 7–10, cells were treated with trypsin–EDTA (0.25% trypsin, 1 mM EDTA; Hyclone, United States) and mixed together as passage 0

(P0). Cells were re-plated at a 1:2 dilution for subculture when cells reached confluence. Cells at passage 3 (P3) were used for all experiments.

Fluorescence-Activated Cell Sorting Analysis

Human SMSCs at passage 3 were incubated with 1 μg of fluorescein isothiocyanate (PE)-conjugated antibodies against CD11b, CD34, CD45, CD90, and CD105 (MACS, Miltenyi Biotec, Germany). After incubation in the dark for 10 min, the cells were washed with PBS and centrifuged at 400 *g* for 10 min. Then, the stained cells were resuspended with 500 μl of ice-cold PBS and subjected to fluorescence-activated cell sorting analysis (Becton Dickinson).

Preparation of SMSC–Agarose Constructs and Chondrogenic Induction

Cells at passage 3 were encapsulated in 2% low-melting-temperature agarose (Invitrogen, Chicago, IL, United States) at a concentration of 10×10^6 cells/mL, as previously described (Mouw et al., 2007). Cell–agarose constructs were cultured in chondrogenic medium, which was high-glucose DMEM (Gibco, United States) containing 10^{-7} M dexamethasone (Sigma, United States), 50 μg/ml ascorbic acid phosphate (Sigma, United States), 100 μg/ml sodium pyruvate (Sigma, United States), 40 μg/ml proline (Sigma, United States), 1% ITS (Gibco, United States), and 10 ng/ml TGF-β3 (243-B3, R&D Systems, United States).

Mechanical Compression System

Before loading, the SMSC–agarose constructs were placed within the 13-mm-diameter foam ring of Biopress^{TM} compression plate wells (Flexcell, United States), and 4 mL chondrogenic medium was added to each well. Dynamic compression was applied by a computer-controlled FX-5000^{TM} Compression System as described in the manufacturer's manual. The constructs were exposed to sinusoidal dynamic compression at 10 kPa with a frequency of 0.25 Hz, and the daily regime was applied at 1 h per day. The loading scheme is shown in **Figures 1A,B**. The compression experiments were initiated from day 1 or day 21 in the chondrogenic differentiation period and performed for daily until day 28, which lasted for 28 days or 7 days, respectively. Cell viability was assessed by a CCK-8 kit (Dojindo, Japan) at day 28 after the final compression procedure. The CCK-8 solution was added to the culture medium of each group at the ratio of 1:10. The absorbance values were measured at 450 nm after incubation for 2 h following the manufacturer's instruction. Unloaded groups were placed in wells but not exposed to dynamic compression.

RNA Isolation and Real-Time Reverse Transcriptase-Polymerase Chain Reaction (q-PCR)

Cell–agarose constructs were dissolved in Qiagen lysis buffer (Qiagen, Chatsworth, CA, United States) supplemented with β-mercaptoethanol as described previously (Bougault et al., 2009). Then RNeasy Total RNA Kit was used according to the manufacturer's protocols followed by reverse transcription using PrimeScript RT Reagent Kit (TaKaRa, Japan). Q-PCR was performed as described previously. Primer names and sequences are listed in **Table 1**. SYBR Green PCR Mix (Thermo Fisher Scientific, United States) was mixed with primers and cDNA, and Q-PCR was performed in ABI Step One Instruments (Applied Biosystems). The expression level of genes was calculated by the $2^{-\Delta\Delta Ct}$ method, and data were normalized to human β-actin gene.

Western Blot

Cells were recovered from the constructs at the indicated time and dissolved in lysis buffer (Thermo Fisher Scientific, United States), supplemented with inhibitors of phosphatases and proteases (Millipore, United States) as described previously (Bougault et al., 2009; Ge et al., 2019). BCA Protein Assay Kit (Pierce, United States) was used to determine the concentration of protein. Equal amount of protein was electrophoresed on a 10% Bis–Tris gel (Bio-Rad, United States) before transferring onto a nitrocellulose membrane. The membranes were then incubated with the following antibodies: SOX9 (Millipore, United States), RUNX2 (Cell signaling, United States), and GAPDH (Cell signaling, United States). All primary antibodies were applied at 1:1,000 dilution. Blots were then incubated with horseradish peroxidase (HRP)-conjugated secondary antibodies (Cell signaling, United States). The immune complexes were detected using a chemiluminescence kit (Thermo Fisher Scientific, United States) and visualized *via* the Odyssey Infrared Imaging System.

Immunofluorescent Analysis

Immunofluorescent staining was performed to detect the accumulation of SOX9 and COL2 within the constructs. The constructs were harvested at day 28, washed with PBS, fixed in 4% paraformaldehyde at room temperature for 4 h, and rinsed with PBS. Then, the constructs were transferred to 30% sucrose overnight, frozen in OCT, and cryostat-sectioned. Sections were treated with 0.1% peroxide followed by 1% bovine serum albumin (Sigma) in PBS for blocking at room temperature. The sections were then incubated with primary antibodies at 4°C overnight. Subsequently, the sections were washed and incubated with secondary antibodies (Cell signaling, United States). The following antibodies were used: anti-SOX9 (Cell signaling, United States) and anti-COL2 (Boster, China). Then, the sections were scanned using a Leica SP5 laser confocal microscope.

Statistical Analysis

All the data were expressed as the mean ± SD. One-way ANOVA was applied for multiple comparisons between independent groups. *P*-values less than 0.05 were considered statistically significant. SPSS 11.5 statistical software was used for statistical analysis.

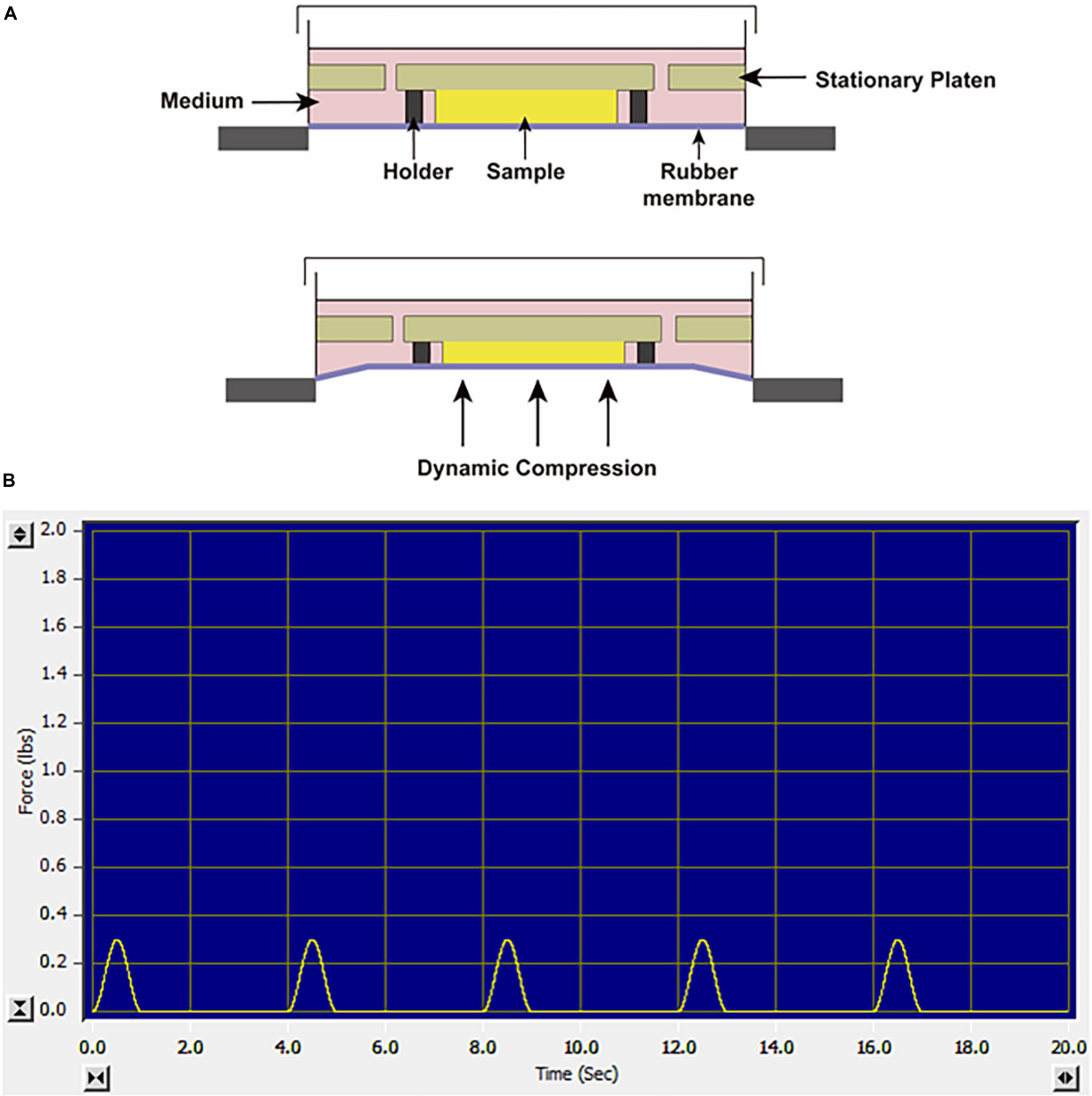

FIGURE 1 | (A) Schematic diagram of the FX-5000^{TM} Compression System. **(B)** The screenshot of the monitor system when the constructs were exposed to sinusoidal dynamic compression at 10 kPa, 0.25 Hz.

RESULTS

Profiles of SMSCs in Chondrogenic Induction

Flow cytometric analysis revealed that the majority of isolated cells expressed CD90 and CD105 (CD90: 98.2% and CD105: 98.9% in hSMSCs) and were negative for CD11b, CD34, and CD45 (**Figure 2A**). Our results showed that adherent cells exhibited a fibroblast-like morphology (**Figure 2B**).

As shown in **Figure 2C**, SMSC-agarose constructs were prepared. Transcription of ECM genes was done to analyze the profiles for chondrogenic differentiation applied in the system. The results showed that the gene expression level of collagen type II (COL2α1) and aggrecan sharply increased after being treated with TGF-β3 for 14 days, but attenuated the increase after 21 days (**Figure 2D**). Expression level of SRY-box transcription factor 9 (SOX9) began to spurt after 7 days but got slowly increased after 7 days (**Figures 2D–F**).

Hypertrophy-related genes collagen type I (COL1α1), collagen type X (COL10α1), matrix metalloproteinases 13 (MMP13), and alkaline phosphatase (ALP) exhibited a gradually increasing trend during the 28-day induction (**Figure 2D**). However, the mRNA and protein level of RUNX family transcription

TABLE 1 | Primers names and sequences.

Primer	Forward (5′-3′)	Reverse (3′-5′)
Col2α1	TGGACGATCAGGCGAAACC	GCTGCGGATGCTCTCAATCT
Aggrecan	CCCCTGCTATTTCATCGACCC	GACACACGGCTCCACTTGAT
SOX9	AGCGAACGCACATCAAGAC	CTGTAGGCGATCTGTTGGGG
RUNX2	TGGTTACTGTCATGGCGGGTA	TCTCAGATCGTTGAACCTTGCTA
MMP13	ACTGAGAGGCTCCGAGAAATG	GAACCCCGCATCTTGGCTT
Col10α1	CATAAAAGGCCCACTACCCAAC	ACCTTGCTCTCCTCTTACTGC
Col1α1	AAAGATGGACTCAACGGTCTC	CATCGTGAGCCTTCTCTTGAG
ALP	TACACGGTCCTCCTATACGGAA	CTCTCGCTCTCGGTAACATC
β-actin	CATGTACGTTGCTATCCAGGC	CTCCTTAATGTCACGCACGAT

factor 2 (RUNX2) greatly increased after chondrogenic induction for 21 days (**Figures 2D–F**).

Chondrogenic and Hypertrophic Gene Expression Stimulated by Dynamic Compression Without Preculture

The SMSCs constructs were subjected to dynamic compression from the first day of chondrogenic induction (**Figure 3A**). The cell viability was assessed by CCK-8 after the final compression period. As shown in **Supplementary Figure 1A**, the viability of SMSCs was not altered after subjected to mechanical compression. Of note, significant difference was found in the expression levels of all chondrogenic genes between compression groups and unloaded controls at each time period, with the unloaded controls having the highest production of aggrecan, COL2α1, and SOX9 genes (**Figures 3B–D**). The chondrogenic master protein SOX9 and ECM-related collage type II (COL2) were also evaluated by immunofluorescence. The results showed that the expression of COL2 and SOX9 decreased after being exposed to mechanical compression for 28 days (**Figure 4**).

The effect of dynamic compression without preculture on hypertrophic development of the differentiated SMSCs was analyzed. Dynamic compression led to a significant decrease in the expression level of hypertrophic markers COL1α1, COL10α1, MMP13, and ALP (**Figure 3D**). For RUNX2, the expression level of groups under mechanical compression in every time-point was significantly downregulated compared with unloaded controls (**Figures 3B–D**).

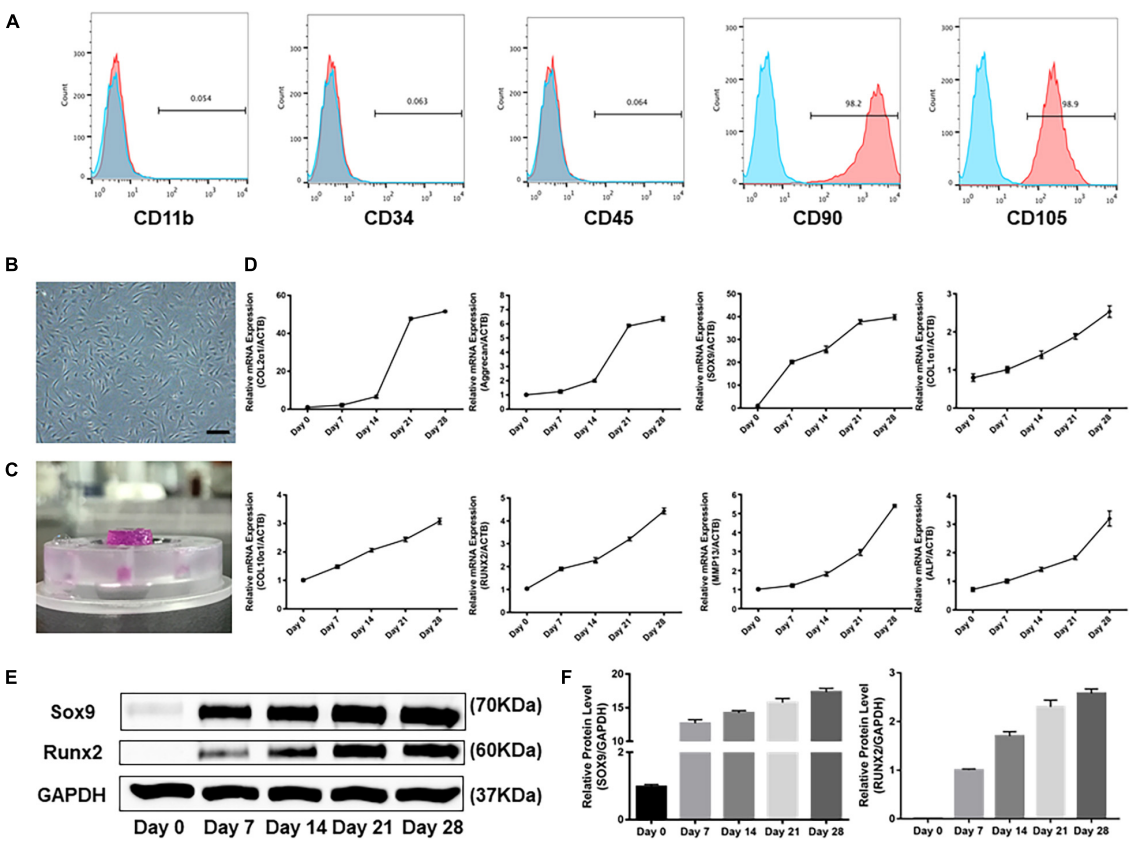

FIGURE 2 | Profiles of human SMSCs in this experiment. **(A)** Flow cytometric analysis of human SMSCs at passage 3. SMSCs were positive for CD90 and CD105, while negative for CD11b, CD34, and CD45. **(B)** SMSCs at passage 3. **(C)** Patterns of SMSC constructs. **(D)** Gene expression of chondrogenesis and hypertrophy development was examined at days 0, 7, 14, 21, and 28. **(E)** Western blot analysis of expression level of SOX9 and RUNX2. **(F)** Expression level of SOX9 and RUNX2 was shown in the histograms normalized with GAPDH. COL2α1, collagen type II; SOX9, SRY-box transcription factor 9; COL1α1, collagen type I; COL10α1, collagen type X; RUNX2, RUNX family transcription factor 2; MMP13, metalloproteinases 13; ALP, alkaline phosphatase.

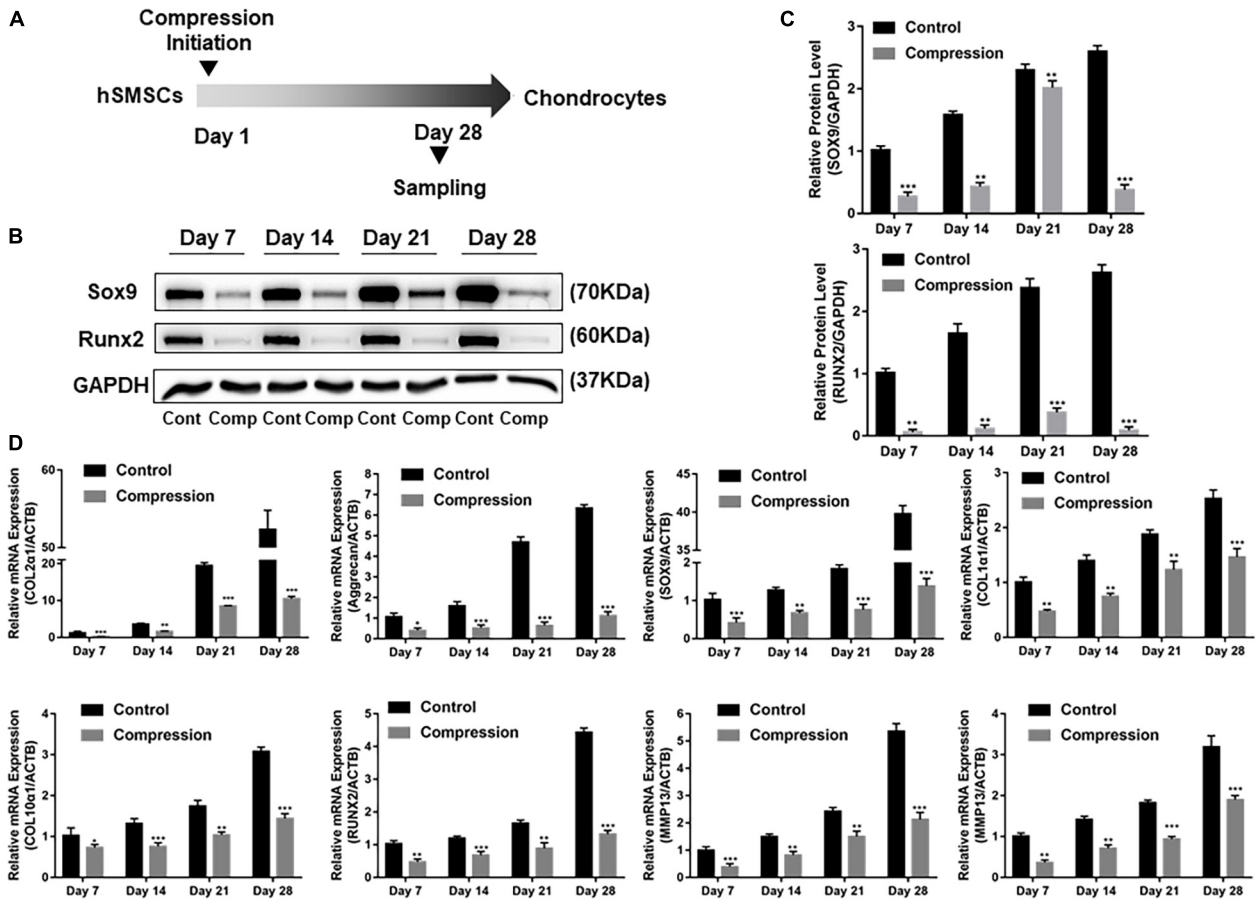

FIGURE 3 | Dynamic compression without preculture inhibited both chondrogenesis and hypertrophy of SMSCs. **(A)** Schematic of the experimental protocol. **(B)** Western blot analysis of expression level of SOX9 and RUNX2 at days 7, 14, 21, and 28. **(C)** Expression level of SOX9 and RUNX2 was shown in the histograms normalized with GAPDH. **(D)** Gene expression of chondrogenesis and hypertrophy development. Results are presented as the mean ± S.D. $^{*}P < 0.05$, $^{**}P < 0.01$, $^{***}p < 0.001$. COL2α1, collagen type II; SOX9, SRY-box transcription factor 9; COL1α1, collagen type I; COL10α1, collagen type X; RUNX2, RUNX family transcription factor 2; MMP13, metalloproteinases 13; ALP, alkaline phosphatase.

Chondrogenic and Hypertrophic Gene Expression Stimulated by Delayed Dynamic Compression

After 3-week chondrogenic preculture, dynamic compressive stress was applied to the MSC-laden constructs and samples were harvested after 7 days of compression (**Figure 5**). Likewise, the application of mechanical compression did not inhibit the viability of SMSC construct (**Supplementary Figure 1B**). Subsequently, two trends were observed in the delayed compressive loading experiments. First, delayed dynamic compression promoted the chondrocyte marker gene expression. Expression level of SOX9 was found to increase following mechanical compression (**Figures 5B,C**). Correspondingly, the mRNA level of aggrecan in loaded specimens was higher compared with their unloaded counterparts. Similarly, delayed mechanical compression resulted in higher COL2α1 expression in mRNA levels (**Figure 5D**). COL2 immunostaining demonstrated that dynamic compression for 7 succession days led to an increase in the accumulation of COL2 matrix around the SMSCs (**Figure 6**). Second, delayed dynamic compression was found to significantly suppress the expression of hypertrophic marker during chondrogenic differentiation. The mRNA levels of COL1α1, COL10α1, MMP13, RUNX2, and ALP in unloaded groups increased steadily from day 1 to day 28 (**Figures 2D–F**). Comparatively, under delayed dynamic compression conditions, the expression of COL1α1, COL10α1, MMP13, and ALP was significantly suppressed compared with unloaded counterparts in day 28 (**Figure 5D**). Similarly, the expression level of RUNX2 significantly downregulated in response to delayed dynamic compression (**Figures 5B–D**).

DISCUSSION

Numerous diseases may lead to cartilage damage or OA, which is a worldwide clinical problem (Muir, 1995). Although efforts have been made for cartilage repair and approaches such as ACI and microfracture show great prospects in clinical therapy, these treatments stills do not lead to the full regeneration of cartilage in its native form (Bedi et al., 2010). MSCs have become an ideal selection for the regeneration of cartilage, and several studies have

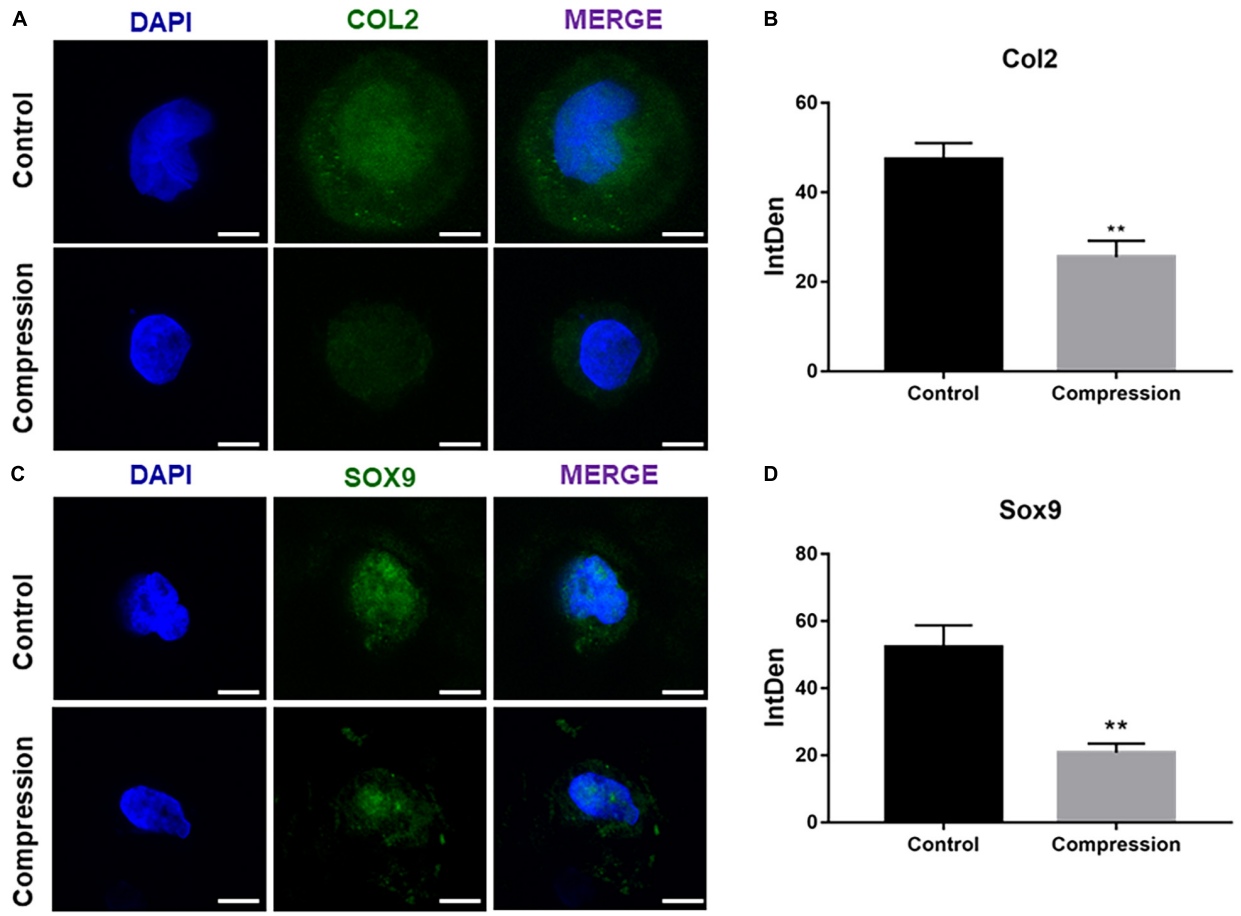

FIGURE 4 | (A,C) Immunofluorescence staining of COL2 and SOX9 after dynamic compression without preculture at day 28. Scale bars = 10 μm. **(B,D)** Integrated density of COL2 and SOX9 by ImageJ. Results are presented as the mean ± S.D. $^{**}P < 0.01$. COL2, collagen type II; SOX9, SRY-box transcription factor 9.

been performed with different kinds of MSCs such as BMSCs. Although BMSCs show great potentials in bone regeneration, the ability of BMSCs for cartilage regeneration remains limited considering the fact that BMSCs display a much great tendency for osteogenesis during chondrogenic differentiation (Djouad et al., 2005; Pelttari et al., 2006; De Bari et al., 2008). SMSCs is a promising cell source for cartilage tissue engineering given their strong potential to undergo chondrogenic differentiation (Pei et al., 2008). The superiority of SMSCs for cartilage repair is as follows. First, the gene expression profile of chondrocytes resembles SMSCs as it showed that they all express COL2α1, and both chondrocytes and SMSCs share the same pool of precursor cells. The gene profile of SMSCs matches the chondrocytes more closely than that of BMSCs (Horie et al., 2009). Second, SMSCs possess a more prominent colony-forming potential than BMSCs (Jo et al., 2007). Third, the acquisition of SMSCs in clinical fields is appealing in that synovium in the joint can be obtained with fewer complications and minimal invasiveness compared with the isolation of other types of MSCs such as BMSCs or adipose-derived stem cells (ASCs) (Sakaguchi et al., 2005). Considering all these advantages and great potentials of SMSCs in cartilage repair, we applied the SMSCs for further studies.

It was reported that chondrogenic differentiation of MSCs toward hypertrophy that it was inevitable *in vitro* (Pelttari et al., 2006; Yang et al., 2012). Several lines of evidence showed that SMSCs displayed a much lighter potential for chondrogenic hypertrophy in pellet culture (Pei et al., 2008). However, in accordance with previous reports, our results showed that SMSC constructs in unloaded conditions were not maintained *in vitro* culture for 4 weeks, even in the presence of TGF-β, which indicated that further optimizations may be required to generate SMSC-seeded constructs akin to that of articular neo-cartilage. Cartilage in our body is exposed to a large range of mechanical stresses (Holmvall et al., 1995; Gemmiti and Guldberg, 2006; Verteramo and Seedhom, 2007). Mechanical stimulation has been reported to show great application prospect in regulating MSC chondrogenic differentiation (Huang et al., 2010; Zhang et al., 2015). The present study was aimed to determine the feasibility of mechanical compression to promote chondrogenic differentiation of SMSCs and maintain the chondrocyte phenotype.

First, we applied dynamic mechanical compression daily to SMSC constructs from the first day of chondrogenic induction. The results showed that dynamic compression without preculture

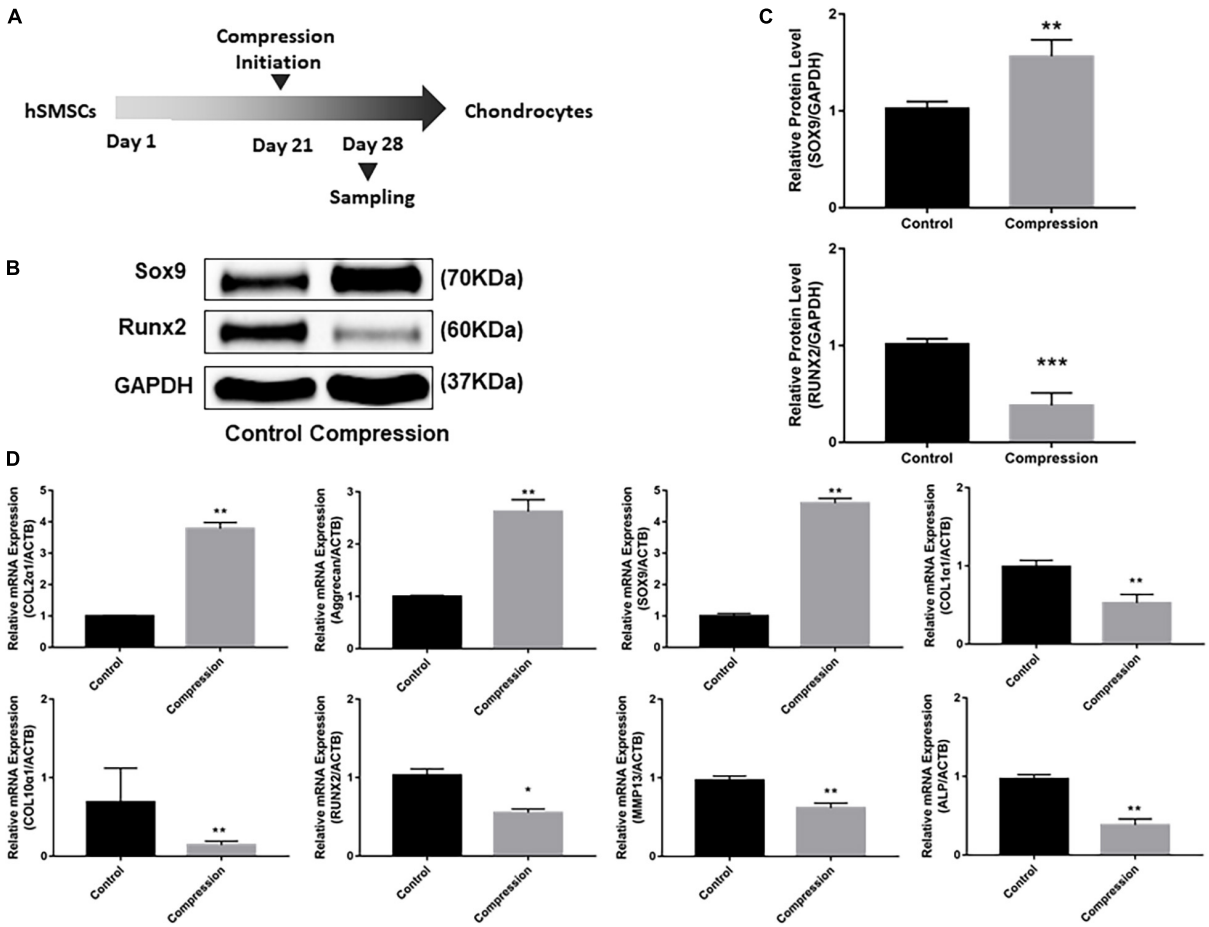

FIGURE 5 | Dynamic compression applied after 3-week chondrogenic induction led to the promotion of chondrogenesis as well as the suppression of hypertrophy development of SMSCs. **(A)** Schematic of the experimental protocol. **(B)** Western blot analysis of expression levels of SOX9 and RUNX2 at day 28. **(C)** Expression levels of SOX9 and RUNX2 were shown in the histograms normalized with GAPDH. **(D)** Gene expression of chondrogenesis and hypertrophy development. Results are presented as the mean ± S.D. $^{*}P < 0.05$, $^{**}P < 0.01$, $^{***}p < 0.001$. COL2α1, collagen type II; SOX9, SRY-box transcription factor 9; COL1α1, collagen type I; COL10α1, collagen type X; RUNX2, RUNX family transcription factor 2; MMP13, metalloproteinases 13; ALP, alkaline phosphatase.

inhibited chondrogenic differentiation of SMSCs. This is in line with numerous studies showing the detrimental effect of mechanical compression on chondrogenic differentiation of MSCs without preculture (Thorpe et al., 2008, 2010; Huang et al., 2010). Huang et al. (2010) reported that continuous loading which initiated immediately following the construct creation resulted in a negative effect of sGAG and collagen content. Another study showed that loading without preculture led to a decrease in sGAG content (Thorpe et al., 2010). A number of factors may explain the results observed. Although mechanical compression promoted cartilage-related gene expression and protein synthesis in chondrocyte constructs, SMSCs may not respond to mechanical stimulation at the early stage of the differentiation process in a similar manner. Mouw et al. (2007) observed that mechanical stress applied to MSCs after 16 days increased COL2α1 and aggrecan gene expression or protein synthesis, while loading in the early time-points did not alter all these measurements. Huang et al. (2010) reported that preculture for a relatively long time (21 days) led to a significant increase in COL2α1 and aggrecan expression compared with those constructs that precultured for a relatively short time. Likewise, chondrocytes in agarose gels under mechanical stress may synthesize more cartilage matrix at later time-points than early, indicating that a mature and developed matrix was required for transduction from mechanical compression to biochemical signals (Buschmann et al., 1995). Also, the mechanical compression was applied from day 7 or day 14 daily until day 28, the final day of chondrogenic differentiation during our observation period. Likewise, as displayed in **Supplementary Figures 2, 3**, our results showed that mechanical compression from either day 7 or day 14 exerted an inhibitory effect of chondrogenesis. However, despite the unwanted inhibition in chondrogenesis, mechanical compression dramatically resulted in a significant decrease in the expression of hypertrophic genes such as COL1α1, COL10α1, RUNX2, MMP13, and ALP, implying that mechanical stress may inhibit hypertrophy of chondrocytes during chondrogenic induction.

To find out the appropriate initial time for dynamic compression, we examined the profile of SMSCs under chondrogenic induction by analyzing chondrocyte-specific

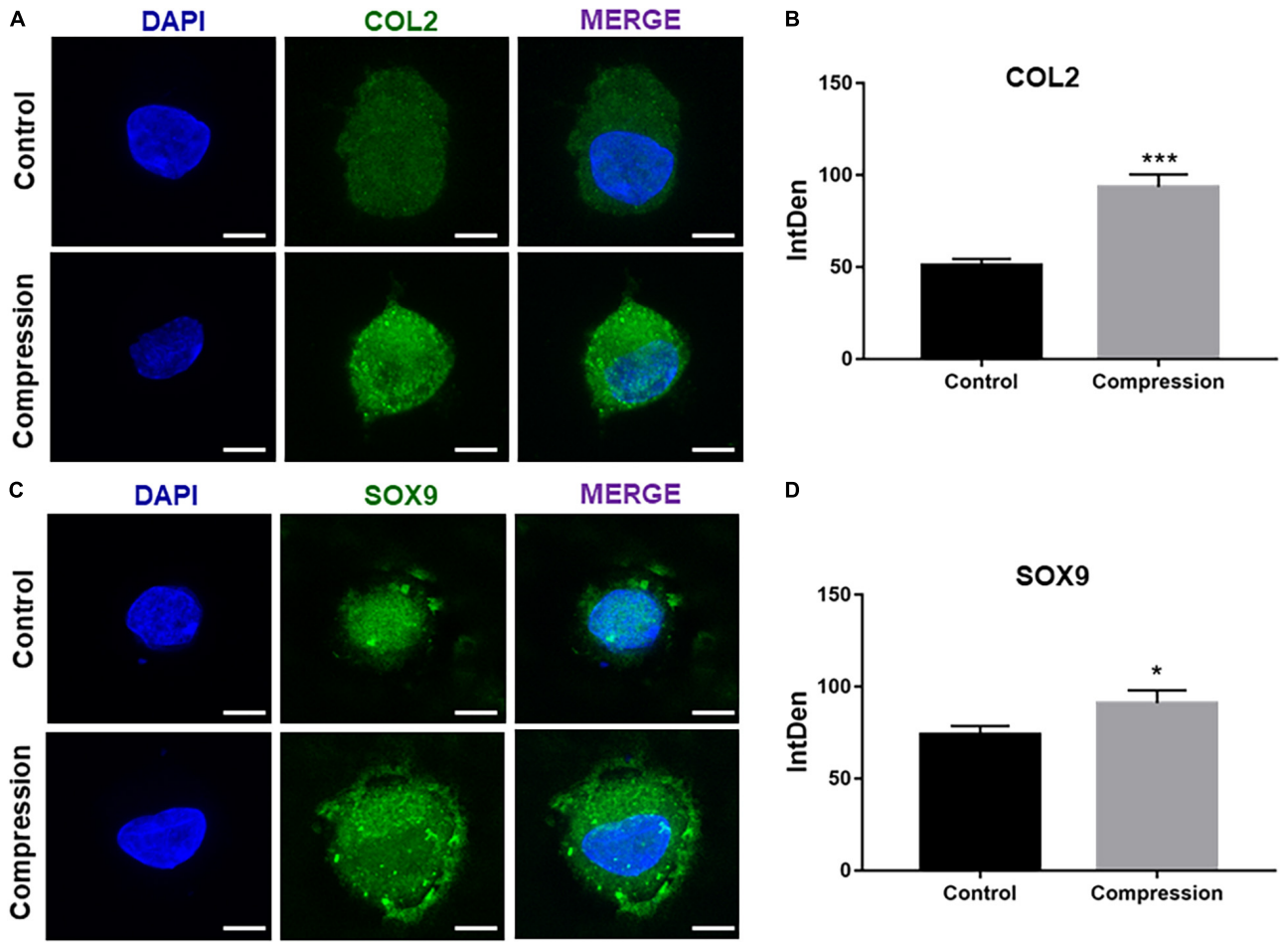

FIGURE 6 | (A,C) Immunofluorescence staining of COL2 and SOX9 after dynamic compression applied with preculture at day 28. Scale bars = 10 μm. **(B,D)** Integrated density of COL2 and SOX9 by ImageJ. Results are presented as the mean ± S.D. *$P < 0.05$, ***$p < 0.001$. COL2, collagen type II; SOX9, SRY-box transcription factor 9.

markers. Our results revealed that ECM gene transcription increased quickly after 2-week chondrogenic differentiation but slowed down after 3 weeks. Although the expression level of ECM genes seemed to reach a plateau, a relative slight but constant increase was also observed from day 21 to day 28. Meanwhile, hypertrophy-related gene transcription increased gradually during 3-week chondrogenic induction but began to spurt after 3 weeks. Therefore, in the following study, we delayed the application of dynamic compression for 3 weeks, and the application of compression was initiated from day 21, hoping for a further promotion in chondrogenesis as well as a suppression in hypertrophy.

Another major concern of long-term MSC culture is the hypertrophic differentiation and ossification during chondrogenic induction (Pelttari et al., 2006; Bian et al., 2012). Our results showed that delayed dynamic compression promoted the gene expression of aggrecan and COL2α1 as well as the expression level of chondrogenic master gene SOX9, which is in line with various studies showing the favorable effect of delayed dynamic compression on the differentiation of MSCs, when the parameters were up to 4 h per day within 0.1–1 Hz of frequency of dynamic stimulation (Huang et al., 2010; Li et al., 2012; Zhang et al., 2015). In our study, we showed that under our stimulation parameters, the increase in ECM gene expression with delayed dynamic compression was accompanied by a suppression of hypertrophy during chondrogenic differentiation. Contrasting results on hypertrophic differentiation under the stimulation of mechanical compression have been reported. Huang et al. (2010) reported that long-term dynamic compressive stress led to an increase in the expression of hypertrophic genes. Li et al. (2012) reported that higher expression of COL10α1 was noticed under the stimulation of axial compressive stress in the low dose of TGF-β. In these studies, dynamic compression was applied in the absence or low dose of TGF-β. On the other hand, other studies reported that dynamic compression contributed to the suppression of hypertrophy after chondrogenic induction in the presence of high dose of TGF-β, which is similar to our study (Zhang et al., 2015). These outcomes above indicated that the reaction of MSCs to dynamic compression depended on the parameters of the loading regime, including dose of growth factors, frequency, duration, and intensity, as well as types of scaffolds and differentiation stage of MSCs.

In our experiments, the exogenous cytokine TGF-β3 was added in the induction medium during the full period of experiment. Although previous studies reported that dynamic compression may exert a pro-chondrogenic effect and increase the accumulation of sGAG, TGF-β3 alone led to far greater accumulation of sGAG as well as collagen content compared with stimulation with mechanical compression alone (Kisiday et al., 2009). Moreover, the chondrogenic effect induced by mechanical compression in the absence of exogenous cytokine appeared to be transient and the expression level of COL2α1 and aggrecan returned to the baseline shortly after the removal of the exogenous cytokine TGF-β3 (Huang et al., 2010). Of note, we also tried to replace TGF-β3 by mechanical compression in our preliminary experiments considering the cost of this kind of expensive cytokine. The SMSC constructs were allowed to undergo chondrogenic differentiation until day 21. Subsequently, TGF-β3 was withdrawn in half numbers of the constructs, and the constructs subjected to compression or control were further divided into TGF-β3-continued group and TGF-β3-discontinued group. Dramatically, in accordance with the previous report, the expression of chondrogenic marker as COL2α1, aggrecan, and SOX9 sharply decreased after the removal of exogenous cytokine TGF-β3. Although mechanical compression alone did induce an increase in the expression level of pro-chondrogenic genes, the TGF-β3 led to a far greater increase in pro-chondrogenic genes. Moreover, in the presence of mechanical compression, TGF-β3 led to an increase in the expression level of pro-chondrogenic genes. Besides, considering the hypertrophic markers, mechanical compression exerted an anti-hypertrophy effect regardless of the presence or absence of TGF-β3 (**Supplementary Figure 3**).

Our study has several limitations. First, it was reported that several signaling pathways have been involved in the regulation of chondrogenesis under the stimulation of mechanical compression, including mitogen-activated protein kinase (MAPK), insulin-like factor-1 (IGF-1), and TGF-β signaling pathways (Li et al., 2012). Among them, TGF-β/SMAD plays a dominant role in the development of cartilage and maintenance of cartilage phenotype (Wang et al., 2014). The downstream target of TGF-β/SMAD includes SMAD2/3 and SMAD1/5/8. SMAD2/3 mainly participates in the chondrogenesis, while SMAD1/5/8 is involved in the chondrogenic hypertrophy. Previous report had demonstrated that mechanical compression promoted the phosphorylation of SMAD2/3, while it suppressed the phosphorylation of SMAD1/5/8 (Hellingman et al., 2011). Our results showed that mechanical compression promoted the chondrogenesis in a time-dependent manner and compression initiated before preculture with TGF-β3 for 3 weeks led to the inhibitory effect of chondrogenic differentiation, which may imply that the effect of mechanical stress on phosphorylation of SMAD2/3 is also dependent on the period of chondrogenesis. In future studies, a robust research about the regulation of mechanical compression on the phosphorylation of SMAD2/3 would be conducted. Second, the SMSCs in our study were isolated from the synovium tissues of patients with OA who underwent total knee arthroplasty. It was reported that the ability to differentiate into chondrocytes and proliferate varied from different donors, and MSCs from patients with OA may be surrounded by different kinds of inflammatory factors such as interleukin-1β or tumor necrosis factor-α, which may interfere with the chondrogenesis of SMSCs (García-Álvarez et al., 2011). Synovium obtained from patients who undergo meniscectomy or anterior cruciate ligament (ACL) reconstruction arthroscopically may be better source for the isolation of SMSCs.

Taken together, our results suggest that the applications of mechanical compression have a significant influence on both the chondrogenic and hypertrophic differentiation of SMSCs, and that allowing for a period of chondrogenic induction produced a tissue which reacted more positively to mechanical compression. To our knowledge, this is the first study to demonstrate the beneficial effect of dynamic compression to promote the stabilization of chondrocyte phenotype in SMSCs. Our findings also give new insight into the important implications of mechanical compression to postoperative rehabilitation management following clinical cell-based treatment for cartilage replacement and regeneration. Future studies are required to further elucidate the specific underlying mechanism involving the role mechanical stimulation plays in the regulation of chondrogenic differentiation of MSCs.

DATA AVAILABILITY STATEMENT

The raw data supporting the conclusions of this article will be made available by the authors upon reasonable request, without undue reservation.

ETHICS STATEMENT

The studies involving human participants were reviewed and approved by the Ethics Committee of Nanjing Drum Tower Hospital, The Affiliated Hospital of Nanjing University Medical School. The patients/participants provided their written informed consent to participate in this study.

AUTHOR CONTRIBUTIONS

YG and YL wrote the manuscript. YL and ZW collected and analyzed the data. LL revised the manuscript. LL, HT, and QJ designed and supervised the study. All authors read and approved the final manuscript.

FUNDING

The current work was funded by the National Natural Science Foundation of China (NSFC 81991514 and 81730067), the National Key Research and Development Project (2018YFF0301100), and the Natural Science Foundation of Jiangsu Province (BK20200121).

SUPPLEMENTARY MATERIAL

The Supplementary Material for this article can be found online at: https://www.frontiersin.org/articles/10.3389/fbioe.2021.697281/full#supplementary-material

Supplementary Figure 1 | (A) Relative cell viability of SMSC construct after subjected to dynamic compression from day 1. **(B)** Relative cell viability of SMSC construct after subjected to dynamic compression applied after 3-week chondrogenic induction.

Supplementary Figure 2 | Dynamic compression applied after 1-week chondrogenic induction inhibited both chondrogenesis and hypertrophy development of SMSCs. Gene expression of chondrogenesis and hypertrophy development. Results are presented as the mean ± S.D. $^{*}P < 0.05$, $^{**}P < 0.01$, $^{***}p < 0.001$. COL2α1, collagen type II; SOX9, SRY-box transcription factor 9; COL1α1, collagen type I; COL10α1, collagen type X; RUNX2, RUNX family transcription factor 2; MMP13, metalloproteinases 13; ALP, alkaline phosphatase.

Supplementary Figure 3 | Dynamic compression applied after 2-week chondrogenic induction inhibited both chondrogenesis and hypertrophy development of SMSCs. Gene expression of chondrogenesis and hypertrophy development. Results are presented as the mean ± S.D. $^{*}P < 0.05$, $^{**}P < 0.01$, $^{***}p < 0.001$. COL2α1, collagen type II; SOX9, SRY-box transcription factor 9; COL1α1, collagen type I; COL10α1, collagen type X; RUNX2, RUNX family transcription factor 2; MMP13, metalloproteinases 13; ALP, alkaline phosphatase.

Supplementary Figure 4 | Gene expression of chondrogenesis and hypertrophy development after retraction of TGF-β3. The SMSC constructs were allowed to undergo chondrogenic differentiation until day 21. Subsequently, TGF-β3 was withdrawn in half of the constructs, and the constructs subjected to compression or control were further divided into TGF-β3-continued group and TGF-β3-discontinued group. Results are presented as the mean ± S.D. $^{*}P < 0.05$, $^{**}P < 0.01$, $^{***}p < 0.001$. COL2α1, collagen type II; SOX9, SRY-box transcription factor 9; COL10α1, collagen type X; RUNX2, RUNX family transcription factor 2; MMP13, metalloproteinases 13.

REFERENCES

Aisenbrey, E., and Bryant, S. (2016). Mechanical loading inhibits hypertrophy in chondrogenically differentiating hMSCs within a biomimetic hydrogel. *J. Mater. Chem. B* 4, 3562–3574.

Bedi, A., Feeley, B. T., and Williams, R. J. III (2010). Management of articular cartilage defects of the knee. *J. Bone Joint Surg. Am.* 92, 994–1009. doi: 10.2106/JBJS.I.00895

Bian, L., Zhai, D. Y., Zhang, E. C., Mauck, R. L., and Burdick, J. A. (2012). Dynamic compressive loading enhances cartilage matrix synthesis and distribution and suppresses hypertrophy in hMSC-laden hyaluronic acid hydrogels. *Tissue Eng. Part A* 18, 715–724. doi: 10.1089/ten.TEA.2011.0455

Bougault, C., Paumier, A., Aubert-Foucher, E., and Mallein-Gerin, F. (2009). Investigating conversion of mechanical force into biochemical signaling in three-dimensional chondrocyte cultures. *Nat. Protoc.* 4, 928–938. doi: 10.1038/nprot.2009.63

Buschmann, M. D., Gluzband, Y. A., Grodzinsky, A. J., and Hunziker, E. B. (1995). Mechanical compression modulates matrix biosynthesis in chondrocyte/agarose culture. *J. Cell Sci.* 108(Pt. 4), 1497–1508.

Chen, J., Chen, L., Hua, J., and Song, W. (2021). Long-term dynamic compression enhancement TGF-beta3-induced chondrogenesis in bovine stem cells: a gene expression analysis. *BMC Genom. Data* 22:13. doi: 10.1186/s12863-021-00967-2

De Bari, C., Dell'Accio, F., Karystinou, A., Guillot, P. V., Fisk, N. M., Jones, E. A., et al. (2008). A biomarker-based mathematical model to predict bone-forming potency of human synovial and periosteal mesenchymal stem cells. *Arthritis Rheum.* 58, 240–250. doi: 10.1002/art.23143

Demarteau, O., Wendt, D., Braccini, A., Jakob, M., Schäfer, D., Heberer, M., et al. (2003). Dynamic compression of cartilage constructs engineered from expanded human articular chondrocytes. *Biochem. Biophys. Res. Commun.* 310, 580–588. doi: 10.1016/j.bbrc.2003.09.099

Djouad, F., Bony, C., Häupl, T., Uzé, G., Lahlou, N., Louis-Plence, P., et al. (2005). Transcriptional profiles discriminate bone marrow-derived and synovium-derived mesenchymal stem cells. *Arthritis Res. Ther.* 7, R1304–R1315. doi: 10.1186/ar1827

Fahy, N., Alini, M., and Stoddart, M. J. (2018). Mechanical stimulation of mesenchymal stem cells: implications for cartilage tissue engineering. *J. Orthop. Res.* 36, 52–63. doi: 10.1002/jor.23670

García-Álvarez, F., Alegre-Aguarón, E., Desportes, P., Royo-Cañas, M., Castiella, T., Larrad, L., et al. (2011). Chondrogenic differentiation in femoral bone marrow-derived mesenchymal cells (MSC) from elderly patients suffering osteoarthritis or femoral fracture. *Arch. Gerontol. Geriatr.* 52, 239–242.

Ge, Y., Zhou, S., Li, Y., Wang, Z., Chen, S., Xia, T., et al. (2019). Estrogen prevents articular cartilage destruction in a mouse model of AMPK deficiency via ERK-mTOR pathway. *Ann. Transl. Med.* 7:336.

Gemmiti, C. V., and Guldberg, R. E. (2006). Fluid flow increases type II collagen deposition and tensile mechanical properties in bioreactor-grown tissue-engineered cartilage. *Tissue Eng.* 12, 469–479. doi: 10.1089/ten.2006.12.469

Haugh, M. G., Meyer, E. G., Thorpe, S. D., Vinardell, T., Duffy, G. P., Kelly, D. J., et al. (2011). Temporal and spatial changes in cartilage-matrix-specific gene expression in mesenchymal stem cells in response to dynamic compression. *Tissue Eng. Part A* 17, 3085–3093. doi: 10.1089/ten.tea.2011.0198

Hellingman, C. A., Davidson, E. N., Koevoet, W., Vitters, E. L., van den Berg, W. B., van Osch, G. J., et al. (2011). Smad signaling determines chondrogenic differentiation of bone-marrow-derived mesenchymal stem cells: inhibition of Smad1/5/8P prevents terminal differentiation and calcification. *Tissue Eng. Part A* 17, 1157–1167. doi: 10.1089/ten.TEA.2010.0043

Holmvall, K., Camper, L., Johansson, S., Kimura, J. H., and Lundgren-Akerlund, E. (1995). Chondrocyte and chondrosarcoma cell integrins with affinity for collagen type II and their response to mechanical stress. *Exp. Cell Res.* 221, 496–503. doi: 10.1006/excr.1995.1401

Horie, M., Sekiya, I., Muneta, T., Ichinose, S., Matsumoto, K., Saito, H., et al. (2009). Intra-articular injected synovial stem cells differentiate into meniscal cells directly and promote meniscal regeneration without mobilization to distant organs in rat massive meniscal defect. *Stem Cells* 27, 878–887. doi: 10.1634/stemcells.2008-0616

Huang, A. H., Farrell, M. J., Kim, M., and Mauck, R. L. (2010). Long-term dynamic loading improves the mechanical properties of chondrogenic mesenchymal stem cell-laden hydrogel. *Eur. Cells Mater.* 19, 72–85. doi: 10.22203/eCM.v019a08

Jo, C. H., Ahn, H. J., Kim, H. J., Seong, S. C., and Lee, M. C. (2007). Surface characterization and chondrogenic differentiation of mesenchymal stromal cells derived from synovium. *Cytotherapy* 9, 316–327. doi: 10.1080/14653240701291620

Kisiday, J. D., Frisbie, D. D., McIlwraith, C. W., and Grodzinsky, A. J. (2009). Dynamic compression stimulates proteoglycan synthesis by mesenchymal stem cells in the absence of chondrogenic cytokines. *Tissue Eng. Part A* 15, 2817–2824. doi: 10.1089/ten.TEA.2008.0357

Li, J., Wang, J., Zou, Y., Zhang, Y., Long, D., Lei, L., et al. (2012). The influence of delayed compressive stress on TGF-beta1-induced chondrogenic differentiation of rat BMSCs through smad-dependent and smad-independent pathways. *Biomaterials* 33, 8395–8405. doi: 10.1016/j.biomaterials.2012.08.019

Li, Z., Yao, S. J., Alini, M., and Stoddart, M. J. (2010). Chondrogenesis of human bone marrow mesenchymal stem cells in fibrin-polyurethane composites is modulated by frequency and amplitude of dynamic compression and shear stress. *Tissue Eng. Part A* 16, 575–584. doi: 10.1089/ten.TEA.2009.0262

Lima, E. G., Bian, L., Ng, K. W., Mauck, R. L., Byers, B. A., Tuan, R. S., et al. (2007). The beneficial effect of delayed compressive loading on tissue-engineered cartilage constructs cultured with TGF-beta3. *Osteoarthr. Cartil.* 15, 1025–1033. doi: 10.1016/j.joca.2007.03.008

Mauck, R. L., Yuan, X., and Tuan, R. S. (2006). Chondrogenic differentiation and functional maturation of bovine mesenchymal stem cells in long-term agarose culture. *Osteoarthr. Cartil.* 14, 179–189. doi: 10.1016/j.joca.2005.09.002

McKee, C., Hong, Y., Yao, D., and Chaudhry, G. R. (2017). Compression induced chondrogenic differentiation of embryonic stem cells in three-dimensional polydimethylsiloxane scaffolds. *Tissue Eng. Part A* 23, 426–435. doi: 10.1089/ten.TEA.2016.0376

Mouw, J. K., Connelly, J. T., Wilson, C. G., Michael, K. E., and Levenston, M. E. (2007). Dynamic compression regulates the expression and synthesis of chondrocyte-specific matrix molecules in bone marrow stromal cells. *Stem Cells* 25, 655–663. doi: 10.1634/stemcells.2006-0435

Mueller, M. B., and Tuan, R. S. (2008). Functional characterization of hypertrophy in chondrogenesis of human mesenchymal stem cells. *Arthritis Rheum.* 58, 1377–1388. doi: 10.1002/art.23370

Muir, H. (1995). The chondrocyte, architect of cartilage. biomechanics, structure, function and molecular biology of cartilage matrix macromolecules. *Bioessays* 17, 1039–1048. doi: 10.1002/bies.950171208

O'Connell, G., Garcia, J., and Amir, J. (2017). 3D Bioprinting: new directions in articular cartilage tissue engineering. *ACS Biomater. Sci. Eng.* 3, 2657–2668. doi: 10.1021/acsbiomaterials.6b00587

O'Conor, C. J., Case, N., and Guilak, F. (2013). Mechanical regulation of chondrogenesis. *Stem Cell. Res. Ther.* 4:61. doi: 10.1186/scrt211

Pei, M., He, F., and Vunjak-Novakovic, G. (2008). Synovium-derived stem cell-based chondrogenesis. *Differentiation* 76, 1044–1056. doi: 10.1111/j.1432-0436.2008.00299.x

Pelttari, K., Winter, A., Steck, E., Goetzke, K., Hennig, T., Ochs, B. G., et al. (2006). Premature induction of hypertrophy during in vitro chondrogenesis of human mesenchymal stem cells correlates with calcification and vascular invasion after ectopic transplantation in SCID mice. *Arthritis Rheum.* 54, 3254–3266. doi: 10.1002/art.22136

Sakaguchi, Y., Sekiya, I., Yagishita, K., and Muneta, T. (2005). Comparison of human stem cells derived from various mesenchymal tissues: superiority of synovium as a cell source. *Arthritis Rheum.* 52, 2521–2529. doi: 10.1002/art.21212

Schiavi, J., Reppel, L., Charif, N., de Isla, N., Mainard, D., Benkirane-Jessel, N., et al. (2018). Mechanical stimulations on human bone marrow mesenchymal stem cells enhance cells differentiation in a three-dimensional layered scaffold. *J. Tissue Eng. Regen. Med.* 12, 360–369. doi: 10.1002/term.2461

Shi, D., Xu, X., Ye, Y., Song, K., Cheng, Y., Di, J., et al. (2016). Photo-cross-linked scaffold with kartogenin-encapsulated nanoparticles for cartilage regeneration. *ACS Nano* 10, 1292–1299. doi: 10.1021/acsnano.5b06663

Smith, G. D., Knutsen, G., and Richardson, J. B. (2005). A clinical review of cartilage repair techniques. *J. Bone Joint Surg. Br.* 87, 445–449. doi: 10.1302/0301-620X.87B4.15971

Thorpe, S. D., Buckley, C. T., Vinardell, T., O'Brien, F. J., Campbell, V. A., Kelly, D. J., et al. (2008). Dynamic compression can inhibit chondrogenesis of mesenchymal stem cells. *Biochem. Biophys. Res. Commun.* 377, 458–462. doi: 10.1016/j.bbrc.2008.09.154

Thorpe, S. D., Buckley, C. T., Vinardell, T., O'Brien, F. J., Campbell, V. A., Kelly, D. J., et al. (2010). The response of bone marrow-derived mesenchymal stem cells to dynamic compression following TGF-beta3 induced chondrogenic differentiation. *Ann. Biomed. Eng.* 38, 2896–2909. doi: 10.1007/s10439-010-0059-6

Toh, W. S., Liu, H., Heng, B. C., Rufaihah, A. J., Ye, C. P., Cao, T., et al. (2005). Combined effects of TGFbeta1 and BMP2 in serum-free chondrogenic differentiation of mesenchymal stem cells induced hyaline-like cartilage formation. *Growth Factors* 23, 313–321. doi: 10.1080/08977190500252763

Tuan, R. S., Boland, G., and Tuli, R. (2003). Adult mesenchymal stem cells and cell-based tissue engineering. *Arthritis Res. Ther.* 5, 32–45. doi: 10.1186/ar614

Verteramo, A., and Seedhom, B. B. (2007). Effect of a single impact loading on the structure and mechanical properties of articular cartilage. *J. Biomech.* 40, 3580–3589. doi: 10.1016/j.jbiomech.2007.06.002

Wakitani, S., Imoto, K., Yamamoto, T., Saito, M., Murata, N., Yoneda, M., et al. (2002). Human autologous culture expanded bone marrow mesenchymal cell transplantation for repair of cartilage defects in osteoarthritic knees. *Osteoarthr. Cartil.* 10, 199–206. doi: 10.1053/joca.2001.0504

Wang, W., Rigueur, D., and Lyons, K. M. (2014). TGFbeta signaling in cartilage development and maintenance. *Birth Defects Res. C Embryo Today* 102, 37–51. doi: 10.1002/bdrc.21058

Williams, C. G., Kim, T. K., Taboas, A., Malik, A., Manson, P., Elisseeff, J., et al. (2003). In vitro chondrogenesis of bone marrow-derived mesenchymal stem cells in a photopolymerizing hydrogel. *Tissue Eng.* 9, 679–688. doi: 10.1089/107632703768247377

Yang, Z., Sui, L., Toh, W. S., Lee, E. H., and Cao, T. (2009). Stage-dependent effect of TGF-beta1 on chondrogenic differentiation of human embryonic stem cells. *Stem Cells Dev.* 18, 929–940. doi: 10.1089/scd.2008.0219

Yang, Z., Zou, Y., Guo, X. M., Tan, H. S., Denslin, V., Yeow, C. H., et al. (2012). Temporal activation of beta-catenin signaling in the chondrogenic process of mesenchymal stem cells affects the phenotype of the cartilage generated. *Stem Cells Dev.* 21, 1966–1976. doi: 10.1089/scd.2011.0376

Zhang, T., Wen, F., Wu, Y., Goh, G. S., Ge, Z., Tan, L. P., et al. (2015). Cross-talk between TGF-beta/SMAD and integrin signaling pathways in regulating hypertrophy of mesenchymal stem cell chondrogenesis under deferral dynamic compression. *Biomaterials* 38, 72–85. doi: 10.1016/j.biomaterials.2014.10.010

Zuscik, M. J., Hilton, M. J., Zhang, X., Chen, D., and O'Keefe, R. J. (2008). Regulation of chondrogenesis and chondrocyte differentiation by stress. *J. Clin. Invest.* 118, 429–438. doi: 10.1172/JCI34174

Conflict of Interest: The authors declare that the research was conducted in the absence of any commercial or financial relationships that could be construed as a potential conflict of interest.

frontiers in Bioengineering and Biotechnology

REVIEW
published: 28 September 2021
doi: 10.3389/fbioe.2021.760273

Perspective: Challenges Presented for Regeneration of Heterogeneous Musculoskeletal Tissues that Normally Develop in Unique Biomechanical Environments

David A. Hart[1,2,3]*, *Norimasa Nakamura*[4] *and Nigel G. Shrive*[3,5]

[1]Department of Surgery, Faculty of Kinesiology, University of Calgary, Calgary, AB, Canada, [2]Bone and Joint Health Strategic Clinical Network, Alberta Health Services, Edmonton, AB, Canada, [3]McCaig Institute for Bone & Joint Health, University of Calgary, Calgary, AB, Canada, [4]Institute for Medical Science in Sport, Osaka Health Science University, Osaka, Japan, [5]Biomedical Engineering Graduate Program, Department of Civil Engineering, University of Calgary, Calgary, AB, Canada

OPEN ACCESS

Edited by:
Farnaz Ghorbani, University of Erlangen Nuremberg, Germany

Reviewed by:
Maliheh Gharibshahian, Shahroud University of Medical Sciences, Iran
Mozhgan Keshavarz, Tarbiat Modares University, Iran
Mahshid Monavari, University of Erlangen Nuremberg, Germany

***Correspondence:**
David A. Hart
hartd@ucalgary.ca

Specialty section:
This article was submitted to Biomaterials, a section of the journal Frontiers in Bioengineering and Biotechnology

Received: *17 August 2021*
Accepted: *13 September 2021*
Published: *28 September 2021*

Citation:
Hart DA, Nakamura N and Shrive NG (2021) Perspective: Challenges Presented for Regeneration of Heterogeneous Musculoskeletal Tissues that Normally Develop in Unique Biomechanical Environments. Front. Bioeng. Biotechnol. 9:760273. doi: 10.3389/fbioe.2021.760273

Perspective: Musculoskeletal (MSK) tissues such as articular cartilage, menisci, tendons, and ligaments are often injured throughout life as a consequence of accidents. Joints can also become compromised due to the presence of inflammatory diseases such as rheumatoid arthritis. Thus, there is a need to develop regenerative approaches to address such injuries to heterogeneous tissues and ones that occur in heterogeneous environments. Such injuries can compromise both the biomechanical integrity and functional capability of these tissues. Thus, there are several challenges to overcome in order to enhance success of efforts to repair and regenerate damaged MSK tissues.

Challenges: 1. MSK tissues arise during development in very different biological and biomechanical environments. These early tissues serve as a template to address the biomechanical requirements evolving during growth and maturation towards skeletal maturity. Many of these tissues are heterogeneous and have transition points in their matrix. The heterogeneity of environments thus presents a challenge to replicate with regard to both the cells and the ECM. 2. Growth and maturation of musculoskeletal tissues occurs in the presence of anabolic mediators such as growth hormone and the IGF-1 family of proteins which decline with age and are low when there is a greater need for the repair and regeneration of injured or damaged tissues with advancing age. Thus, there is the challenge of re-creating an anabolic environment to enhance incorporation of implanted constructs. 3. The environments associated with injury or chronic degeneration of tissues are often catabolic or inflammatory. Thus, there is the challenge of creating a more favorable in vivo environment to facilitate the successful implantation of in vitro engineered constructs to regenerate damaged tissues.

Conclusions: The goal of regenerating MSK tissues has to be to meet not only the biological requirements (components and structure) but also the heterogeneity of function (biomechanics) in vivo. Furthermore, for many of these tissues, the regenerative approach has to overcome the site of injury being influenced by catabolism/inflammation. Attempts

to date using both endogenous cells, exogenous cells and scaffolds of various types have been limited in achieving long term outcomes, but progress is being made.

Keywords: musculoskeletal regeneration, tissue Engineering, biomechanics, tissue heterogeneity, complex tissue organization

INTRODUCTION

The repair or reconstitution of injured or damaged musculoskeletal (MSK) connective tissues has long been a goal of orthopedic surgeons, plastic surgeons, other health care providers and researchers. Many acutely injured MSK tissues heal naturally with formation of scar tissue which in many cases is severely compromised with regard to function, or they heal poorly due to very limited vascularity or innervation. Alternatively, surgeons have explored the use of transplanting allogeneic normal tissues in place of the injured or damaged ones. Such approaches to reconstitute torn anterior cruciate ligaments (ACL), damaged menisci of the knee, or articular cartilage has met with some success over the relatively short term, but even replacement of the ACL with an autologous piece of a tendon [e.g., middle third of the patellar tendon] leads to the stretching out (irreversible creep) of the tendon over time with loss of function.

Thus, there remains the challenge of developing new approaches to tissue engineer replacement connective tissues using autologous somatic cells + scaffolds of defined structure and content, autologous or allogeneic mesenchymal stem cells ± defined scaffolds, or other variations of cells± scaffolds or relevant extracellular matrix components. While such approaches have led to some successes, the field is still evolving and success, depending on the definition, is variable. In part, this variable success relates to whether one aspires to restoration of biological and/or mechanical long-term function. Of course, the ideal would be regeneration of the tissues injured via accidents or disease, but this challenge still persists, in part due to incomplete appreciation of the complexities of these tissues in different environments, and some confusion as to how to recapitulate development and maturation in a skeletally mature adult who may be normal or abnormal due to chronic disease. Finally, progress in the repair and regeneration of injured or damaged human connective tissues may be compromised by the dependence on small preclinical models that rely more on biological outcomes than ability to assess the integrity of the biomechanical function of the engineered replacement tissues.

Connective Tissue Heterogeneity

Connective tissues of the mammalian MSK system have evolved to allow for functioning in the one gravity (1 g) environment of Earth in a coordinated and integrated manner. Humans further adapted to walk upright with an accompanying ability to be highly mobile.

While the initial biological mechanisms that allowed individual cells to adapt to the 1 g environment of Earth evolved billions of years ago, they have been incorporated into increasingly complex organisms via multicellular organisms, various sea creatures, dinosaurs, birds, early mammals, primates and various iterations of humans. Thus, in humans, tissues of the MSK system range from hard tissue such as bone, to soft tissues such as muscles, tendons, ligaments, intervertebral discs, articular cartilage, and menisci. Not only do some of these tissues exhibit heterogeneity within a specific tissue functioning in its unique environment, but for the tissues of a joint such as the knee, the individual tissues must also work together for optimal functioning (i.e., the Joint as an Organ System; Radin et al., 1991; Frank et al., 2004; Loesser et al., 2012).

For tissues such as tendon, which connect muscles to bones, the tissues consist of a myotendinous junction, a mid-substance, and an insertion into bone. With multiple transition points, there is heterogeneity in the content of the tissue and its organization, heterogeneity that can change with age (Fallon et al., 2002; Kostrominova and Brooks, 2013; Thornton et al., 2015; Huisman et al., 2014). Furthermore, tendons operating in different mechanical environments, such as the Achilles tendon and the Supraspinatus (SS) tendon, appear to exhibit different properties (Thornton et al., 2010; Fallon et al., 2002). Other tendons that traverse around a boney prominence have a different structure at the site of such compression (Vogel and Koob, 1989; Vogel 2003, 2004; Vogel and Peters, 2005). That is, at sites of compression, the extracellular matrix becomes more cartilage-like with expression of type II collagen and an organization appropriate for addressing compressive rather than tensile loading. In addition, if the tissue is taken off the boney prominence, it undergoes a reversible transformation of its matrix. Interestingly, injuries to the SS tendon occur mainly at the transition of the tendon into bone, or the enthesis, which is a very unique transition tissue (Sevick et al., 2018, 2021).

Tendons are not unique with regard to this heterogeneity and variation in functioning in different environments. Certainly bone can adapt to its mechanical environment (discussed in Frost, 1996, 2004), muscles differ in their fibre types and metabolism via mitochondria content, and skin can vary depending on its location and use. Thus, connective tissues which may look fairly homogenous are in fact quite heterogeneous at multiple levels, Furthermore, many of these tissues also vary in response to transitions such as puberty, pregnancy, and menopause and are thus influenced by sex hormones (discussed in Rollick et al., 2018).

The ligaments of the knee are also heterogeneous. The medial collateral ligament (MCL) is a passive, extra-articular structure which stabilizes the knee and typically operates in the toe region of its load displacement curve [discussed in Bray et al., 2005]. In contrast, the anterior cruciate ligament (ACL) operates in the intra-articular space and experiences higher load levels than the MCL (discussed in Wan et al., 2014; Mallett and Arruda, 2017). Loading also depends on the angle of the knee. Similar variation

TABLE 1 | Challenges for tissue engineering success for repair/regeneration of musculoskeletal tissues.

Challenge	Potential solutions
1. Tissue Heterogeneitya Biologic	a) General template that allows for adaptation to *in vivo* biologic and mechanical cues b) Use of decellularized natural matrix + Progenitor cells capable of differentiation c) Facilitate integration to residual normal tissue-fibronectin/RGD sequences? d) Derivatize matrix with developmentally regulated anabolic mediators (i.e., IGF-1 family + IGF-1 binding proteins)
Biomechanical Environment	a) Apply relevant loading *in vitro* during development that corresponds to *in vivo* requirements b) Progressive *in vitro* loading increases to ensure survival post-implantation and enhance cellular response pattern
2. Complexity of ECM-Cell Organizationb	a) Use of decellularized natural matrix (ECM) +/- synthetic matrix elements that can be reconstituted with Progenitor or Normal cells b) 3D printing of natural ECM mimetic with immune privileged Progenitor cells c) Supplementation with a stable supply of developmentally regulated anabolic signals (i.e., slow release from a matrix store)
3. Control an Adverse *in vivo* Environment (i.e., Inflammation)	a) Exposure of *in vivo* environment to appropriate drugs to control the inflammatory environment (i.e., glucocorticoids) at the time of implantation b) Derivatize the matrix with slow release immunomodulatory cytokines and/or drugs to sustain an *in vivo* anti-inflammatory environment c) Inject autologous Platelet-rich Plasma at the time of implantation and as needed to both exert an immunomodulatory effect as well as provide anabolic signals d) Expose the implantation site to immunomodulatory exosomes from Progenitor Cells to suppress a catabolic environment and provide anabolic signals

[a]*Such as a tendon with a bony enthesis, mid-substance and myotendinous junction to muscle; or a meniscus of the knee with a cartilaginous inner section and an outer more ligamentous section.*

[b]*Such as a knee meniscus with a complex array of tie fibers and associated fibers (Andrews et al., 2014; Andrews et al., 2017) and colonized with cells in different configurations (Hellio Le Graverand et al., 2001).*

in normal loading occurs in tendons in different environments as well. For both ligaments and tendons, their normal loading can range from kPa to mPa, while those for articular cartilage is in the MPa range. Certainly, the complex structure of the ACL, a ligament which is often injured, is also difficult to replicate.

Another example of a heterogeneous tissue is a meniscus of the knee (Andrews et al., 2014; Andrews et al., 2017; Brzezinski et al., 2017; Arnoczky et al., 2010; Murphy et al., 2019, Rattner et al., 2011). In addition, age-related changes in menisci may further complicate the healing potential and may also influence the potential for success when tissue engineering approaches are attempted (Di Giancamillo et al., 2017).

Thus, a first challenge for those interested in regeneration of injured connective tissues is related to the tissue heterogeneity and the need to understand the relationships between that heterogeneity and function. For example, no two ligaments are exactly the same–they are each structured to do their specific job in unique biomechanical environments. Thus, such heterogeneity is likely tissue-specific, which could pose unique issues regarding the approaches taken to develop replacement tissues and regain function in different environments (**Table 1**).

Origin of Connective Tissue Heterogeneity and Organization During Development and Maturation

During fetal development the cellularity and organizational template for the connective tissues of the MSK system are laid down. For humans, after the articulating joints have developed and movement of the joints is achieved, the loading of the joint tissues (i.e., of the knee-ligaments, menisci, capsule, cartilage, bone, etc) in the absence of ground reaction forces still leads to further maturation in utero. At birth, there is considerable variation in the level of maturation of the tissues of different mammals (e.g., humans do not learn to walk for months while a young zebra or wildebeest is up and running in minutes).

When a rabbit is born, tissues such as the medial collateral ligament (MCL) are "cell rich and matrix poor" and during maturation *via* loading and growth, the MCL rapidly becomes "cell limited and matrix rich" (Meller et al., 2009; Ionescu et al., 2011). Interestingly, the DNA content of the MCL shortly after birth is very similar to that of the MCL of the skeletally mature adult so the tissue grows in a patterned manner coordinated with its loading environment: matrix is laid down between cells building on the original template. As the cells grow apart due to ECM deposition, they retain a cellular network via gap junctions (Lo et al., 2002): thus even if they look well separated on an H&E section of the tissue, they can still be in communication. Depriving the MCL of loading during growth and maturation leads to a cessation of growth (reviewed in Hart et al., 2002), so loading is necessary for a tissue to respond to whatever anabolic signals are present to enhance growth.

In menisci, cells also add to the complex template of matrix after birth, but the distribution of vascularization and innervation is also altered. At birth, the complete meniscus is innervated and vascularized, but as growth continues with loading, the inner aspect of the menisci gradually become avascular and aneural (discussed in Di Giancamillo et al., 2014). This inner aspect of the tissue is subjected to high compressive stresses between the femoral and tibial articular cartilage and low tensile circumferential stress, while the outer aspects are subjected to high circumferential tensile loading ("hoop stresses"). Thus, the tissue structure needs to "transition" in form between the inner and outer aspects to carry the different dominant stresses in those regions. The connectivity

between cells is also different in these different areas of the menisci (Hellio Le Graverand et al., 2001). The loss of vascularity in the inner aspect of the menisci is believed to contribute to their lack of healing when injured as an adult (Di Giancamillio et al., 2017).

Other connective tissues of the MSK system also appear to follow a similar pattern for growth and maturation. The consequence is tissues with unique ECM content and cellularity dependent on the unique loading environments in which they are expected to function, and within the "physiologic window" of loading that is associated with homeostasis in that particular environment. For all connective tissues, except for articular cartilage which is aneural and avascular, the cells in the tissues can be endogenous "fibroblast-types", microvascular endothelial cells, pericytes that can be either called mesenchymal stem cells or medicinal signaling cells (Caplan, 2017, 2019), all working together to allow for functioning in the 1 g environment of Earth.

After skeletal maturation, some connective tissues can continue to adapt and change over time. This may relate to epigenetic changes based on experiences of specific tissues (Peffers et al., 2016; Naue et al., 2018), or in the case of some tendons, loss of expression of the lubricant PRG4 can affect the gliding of fascicles (Kohrs et al., 2011; Hayashi et al., 2013). However, not all tissues are affected the same by aging (Lemmex et al., 2016; Thornton et al., 2015).

Thus, a second challenge for those interested in the regeneration of injured connective tissues is to understand the complexity of the organization and biochemical composition of the tissue that relates to function (**Table 1**). The composition and organization of the ECM is laid down by a biological response that is coordinated with mechanical stimuli during growth and maturation. An example of this process was shown by experiments depriving knee ligaments of loading in young rabbits which led to a cessation of growth (discussed in Hart et al., 2002; Walsh et al., 1992, 1992). This point has also been reported in other model systems where the Wnt signaling pathway has been implicated in the biological response to mechanical loading (Brunt et al., 2017). In the early post-natal period of humans, mechanical loading of joint tissues, as well as muscles and tendons would lead to tensile loading of muscles, tendons and ligaments, and compression and shear loading of cartilage and menisci via movement, crawling and ultimately walking. However, in the skeletally mature or aged adult there is likely the absence of some of the early anabolic stimuli when an implant may be required, as well as an established biomechanical set point for the integrated tissue of a joint. Likely, some of the anabolic mediators present during growth to maturation which then decline with age include those related to growth hormone and its downstream mediators of the IGF-1 family (Rosenfeld and Hwa, 2009; Yoshida and Delafontaine, 2020; Dixit et al., 2021). Furthermore, during early post-natal life, an individual could also be exposed to growth mediators present in human milk that would be available until lactation ceased (Suwaydi et al., 2021).

The Involvement of Acute and Chronic Inflammation Following Injury, Surgery and Disease in Connective Tissues

Following an injury to a connective tissue such as the anterior cruciate ligament (ACL), the menisci, or rupture of a tendon, the initial damage to the tissue results in an acute inflammatory response and its consequences. While such an inflammatory response may be limited in duration, it can set off a series of events leading to tissue fibrosis and loss of function. In other circumstances, such as rupture of the ACL, the torn ends of the ligament are separated, and if a reconstruction is not attempted, the ends of the ACL can be resorbed.

Interestingly, if one does reconstruct the ACL with a piece of autologous tendon, or an allograft, or even a tissue-engineered ligament, the surgery itself is an inflammatory stimulus that can impact the success of the operation. Of note, in the circumstance of an ACL reconstruction with a piece of autologous tendon that was initially mechanically stronger than the original ACL, over time the graft begins to exhibit creep, stretch out and lose function. This is likely facilitated by the presence of a more chronic inflammation that leads to the conversion of the tendon graft to scar tissue (discussed in Frank et al., 2004; 2004a).

In other conditions, such as osteoarthritis, the degeneration of the tissues of the joint is accompanied by a chronic inflammation in the intraarticular space (discussed in Woodell-May and Sommerfeld, 2020). Similarly, but more intense, is the intra-articular inflammation associated with rheumatoid arthritis (discussed in Hart et al., 2004). Thus, the environment of a joint exposed to chronic inflammation is very abnormal. Attempts to regenerate damaged or injured tissues in such environments may compromise even the most ideal tissue-engineered replacements unless the environment is altered (discussed in Hart et al., 2004).

Recently, it has been found in preclinical models that treating animals immediately after surgery or an insult to a joint with an anti-inflammatory such as a corticosteroid can diminish the consequences of the inflammation over the longer term (Heard et al., 2015; Heard et al., 2016; Heard et al., 2019; Heard et al., 2021; Barton et al., 2018; Sieker et al., 2016). The efficacy of such interventions has been demonstrated in both porcine models (Sieker et al., 2016) and rabbit models (Heard et al., 2015; Heard et al., 2016; Heard et al., 2019; Heard et al., 2021; Barton et al., 2018). The types of injuries to a joint range from ACL rupture and idealized autologous ACL repair, to a surgical injury mimicked by injection of blood into the joint. Thus, controlling inflammation and creating an environment more conducive to repair is possible and likely is necessary to enhance success.

While the treatments discussed above are likely not optimal as yet, the concept that one can suppress acute inflammation and prevent it from becoming chronic and/or inducing other sequelae such as osteoarthritis-like changes in a joint has been validated and could be translated to patient populations. However, if corticosteroids are used to control inflammation, care must be taken in the dosages used as too high a dose of corticosteroids can have detrimental effects on mesenchymal stem cells (Yasui et al., 2018).

Thus, a third challenge faced by those striving to regenerate injured or damaged connective tissues is to create an environment that will allow an *in vitro* generated tissue-engineered construct to optimally be integrated into the *in vivo* environment and restore function over the long term.

(Hart et al., 2004). Not only must a catabolic environment be neutralized, as most need for tissue engineered replacement tissues is in adults one may also have to generate an anabolic environment to enhance the success of the constructs. In other words, the surgery to implant the construct is perceived as an injury by the body, so one has to counteract both the associated inflammation and the consequential infiltration of the graft by scar-like fibrotic tissue and the remodelling that follows (**Table 1**).

The Way Forward

When faced with the challenges for success outlined above regarding whether *in vitro* generated tissue-engineered constructs via cells, complex scaffolds and 3D printed composites, as well as other composites containing anabolic molecules such as growth factors are up to the task of regenerating injured or damaged tissues, one needs to perhaps step back and re-evaluate the expectations associated with the term "regeneration". That is, one needs to define the objective: is there a need for exact biological regeneration (consistent with early mature tissue or tissue at the stage of the remainder of the host?), regeneration of biomechanical integrity, or long-term functional regeneration? With regard to functional regeneration, if an orthopedic surgeon sews the torn ends of a ruptured Achilles tendon back together with formation of scar tissue, the tendon may function quite well for >40 years if the goal is for the patient to be able to return to daily living rather than return to playing soccer or basketball at an elite level. Similarly, an ACL reconstructed with a tissue-engineered construct may be functionally adequate for daily living assuming the inflammation in the joint is controlled early, but the ACL is not fully regenerated. The same can be said perhaps for meniscal replacements. However, for those with osteoarthritis, the goal for regeneration of cartilage and the functionality of the joint as an organ system (Radin et al., 1991, Frank et al., 2004, 2004a; Loesser et al., 2012) may require a tissue engineered construct that is in fact very close to a regenerated cartilage after incorporation. However, if the other tissues of a joint have been influenced by the individual's life-experiences and epigenetically modified, one may ask if the relationship of the tissue-engineered regenerated tissue to other tissues in the joint will be appropriate (discussed in Frank et al., 2004; 2004a).

Recent studies with regard to regenerating articular cartilage not only provide insights into the boundary conditions associated with regeneration of such cartilage in defects in both preclinical models and more recently, in patients (Shimomura et al., 2018b, 2021), but also opportunities for success. Generation of Tissue-Engineered Constructs (TEC) with mesenchymal stem cells derived from autologous synovium were developed following culture *in vitro* to yield a composite of undifferentiated cells and a matrix generated by the cells themselves without an exogenous scaffold. When implanted into cartilage defects of adult patients (Shimomura et al., 2018b, 2021) or adult or adolescent pigs (Ando et al., 2007; Shimomura et al., 2010), the allogeneic MSC [i.e., male cells into female recipients] in the implanted TEC did not survive in the implant when assessed at 6 months [unpublished observations] but apparently were able to facilitate the migration of endogenous cells into the implanted TEC and their re-establishment of the cellular organization and conversion of the matrix to something more hyaline cartilage-like with a superficial zone, middle zone and deep zone (Fujie et al., 2015). However, after 1 year in the pigs, the resultant cartilage was not perfect in that the lamina splendens did not reform on the surface of the new cartilage (Ando et al., 2012). Thus, even in the adult environment, appropriate biological and mechanical cues are sufficient to evolve a histologically similar and biomechanically capable tissue compared to normal hyaline cartilage. Nevertheless, there is still room for improvement. Of note, the finding that MSC in implanted TEC did not survive is consistent with the literature (de Windt et al., 2017).

It should be noted that use of allogeneic MSC in the preparation of porcine TEC have also been used successfully to repair cartilage defects (Shimomura et al., 2010). Thus, in this circumstance, the MSC do not appear to be immunologically rejected by the host. Because of this apparent immunological privilege, the use of human MSC such as those derived from Wharton's jelly and other sources have been investigated (for example: Jiang et al., 2021).

In addition, while the TEC approach discussed above has been successful in the treatment of smaller cartilage defects, in many instances, a more extensive injury to meniscus, cartilage or a ligament or tendon may require a different approach, that of using scaffolds to augment implantation into the defects. Thus, incorporation of MSC into scaffolds have been investigated using scaffolds such as decellularized cartilage (Jiang et al., 2021), collagen (Sadlik et al., 2017), silk proteins (Barlian et al., 2020), or scaffolds made of chemical polymers (Liu et al., 2018). Such scaffolds may be biodegradable *in vivo*, but should have mechanical properties that allow for a sufficient time for the seeded cells to respond to the *in vivo* environment.

From some perspectives, articular cartilage may be a relatively simple test case for regeneration as it is avascular and aneural, and while it may be somewhat heterogeneous, it does not have overt transitions in tissue composition and function. Similarly a tendon transitions seamlessly between its enthesis, mid-substance, and myotendinous junction, as well as the innervation and a microvasculature that is restricted to the more surface layers of the tendon (i.e., paratenon or epitenon layers). The organization of a meniscus is more complex than the corresponding articular cartilage with its inner aneural/avascular aspect which sees high compressive loading, a transition zone, and then an innervated/vascular outer zone subjected to large hoop stresses and with two insertion sites into bone (discussed in Andrews et al., 2014; Andrews et al., 2017; Murphy et al., 2019; Markes et al., 2020). The complexity of the matrix with its three-dimensional mosaic array of tie fibres and other collagen and proteoglycan molecules intercalated with cells will be difficult to reproduce *in vitro*. While some of these challenges may be difficult to overcome *in vitro* even with 3D printing of tissue-specific decellularized ECM and cells, it may be that only an approximate replica of the original natural tissue is required. Subsequent further *in vivo* adaptations will occur following implantation as was observed with the TEC for cartilage repair discussed above. In spite of the complexity of

the menisci, some successes have been achieved (discussed in Shimomura et al., 2018, 2018a; Mauck and Burdick, 2015).

To achieve the best approximate tissue engineered construct for specific applications will likely require the involvement of a relevant biomechanical stimulus during its preparation. Certainly, applying tensile loading to a tissue engineered ligament construct as it is being developed enhances the mechanical integrity of the resultant tissue (Hart et al., 2005; Goulet et al., 2011, 2014), and potentially, its improved *in vivo* functioning. Depending on the application, the approach of exposing the constructs to mechanical loading may initially require a deformable scaffold or matrix that eventually becomes a composite of molecules secreted by the cells intercalated with the original scaffold as the construct matures (discussed in Hess et al., 2010). Thus, to make sure the cells in a construct are not stress shielded when exposed to a loading protocol *in vitro*, care should be given to the rigidity of any scaffold materials. Supplying biomechanical stimuli to developing tissue-engineered constructs may not only stimulate anabolic responses by the cells, but also inhibit potential catabolic molecules expressed by cells in the absence of mechanical loading (Natsu-ume et al., 2005). Recent developments using the MyoRobot system will allow assessment of the response of tissues such as muscles and cell-biomaterial constructs to defined mechanical loading (Haug et al., 2018; Friedrich et al., 2019). Such approaches will aid in assessing the integration of biology and biomechanics in such constructs.

While the human studies detailing repair of cartilage defects with TEC did not specifically attempt to regulate any post-surgery inflammation, attention perhaps should be directed to ensuring the existence of the best post-surgical environment so that this potential threat to successful regeneration is controlled, as has been shown in the preclinical studies discussed earlier (Heard et al., 2015; Heard et al., 2016; Heard et al., 2019; Heard et al., 2021; Barton et al., 2018; Sieker et al., 2016). Thus, preparing an approximate tissue *in vitro* followed by implantation into the most conducive environment for subsequent success will further enhance the improvement of tissue-engineered constructs, moving the field from tissue repair closer to tissue regeneration and hopefully, long term function. However, it should be noted that attempts to control any inflammation following implantation of TEC in the humans studies (Shimomura et al., 2015; 2018b, 2021) were not implemented so it may depend on the local environment and whether the inflammation is acute or chronic (Hart et al., 2004). This will require further research.

Finally, while not a challenge per se, choosing an appropriate preclinical model is also of critical importance going forward to optimize tissue engineering approaches for regeneration of connective tissues of the MSK system, particularly those of joints such as the knee where the engineered construct would function in a complex mechanical and biological environment. This would be facilitated by having a preclinical model where biology (histology and molecular biology) and biomechanics can be assessed, as well as imaging for longitudinal studies (Hart et al., 2021). Thus, models such as pigs (Ando et al., 2007; Shimomura et al., 2010; Sieker et al., 2016) or sheep (Hart et al., 2021; Brzezinski et al., 2017) should be considered rather than smaller models that are more constrained regarding assessment potential.

CONCLUSION

The return of a damaged or injured musculoskeletal tissue to long term function depends on the unique biological requirements of the tissue, the mechanical environment in which it has to function, and the expectations for the use of the tissue. Thus, depending on the circumstances, this may require assessment of where on the continuum of repair to regeneration the situation lies. The goal of regeneration of a tissue that cannot be adequately repaired will require tissue-engineering approaches that have both *in vitro* and *in vivo* challenges to overcome. These include regeneration of a tissue *in vivo* in an environment having some biological and mechanical cues, but lacking many of the anabolic cues present during growth and maturation. Thus, replicating the *in vivo* loading environment during the preparation of a tissue-engineered construct to condition the cells and the construct will likely be beneficial. Finally, there is also a need to control the *in vivo* environment to eliminate adverse conditions such as a catabolically oriented inflammatory state which could interfere with successful implantation of an *in vitro*-optimized construct. Thus, for successful regeneration, one needs to think about what should be introduced to the body to achieve what is needed after incorporation through scar creation and infiltration followed by tissue remodelling. In addition, there needs to be recognition that what is needed may not be a recapitulation of the original as other tissues in the joint will have moved to a new "set point" and may not go back to the original. Achievement of what is needed therefore involves both mechanical and biological compatibility with the other tissues in the joint in their evolved state for sustained functioning thereafter. While some of these challenges may be daunting, they likely can be overcome using innovative approaches. Some of these are summarized in **Table 1**.

AUTHOR CONTRIBUTIONS

DH wrote the first drafts of the manuscript and NS and NN contributed to further revisions and the final version.

ACKNOWLEDGMENTS

The author thanks Cy Frank (deceased), Kazu Shimomura, Wataru Ando, and Arin Sen for many interesting discussions and interactions on the topics addressed in this mini-review. The author also acknowledges the support of the Strategic Clinical Network Program of Alberta Health Services during the preparation of the manuscript.

REFERENCES

Achari, Y., Frank, C. B., Shrive, N. G., Hart, D. A., Rattner, J. B., and Hart, D. A. (2005). Normal Ligament Structure, Physiology and Function. *Sports Med. Arthrosc. Rev.* 13, 127–135. doi:10.1177/0363546518765098

Ando, W., Fujie, H., Fujie, H., Moriguchi, Y., Shimomura, K., Nansai, R., et al. (2012). Detection of Abnormalities in the Superficial Zone of Cartilage Repaired Using a Tissue Engineered Construct Derived from Synovial Stem Cells. *eCM* 24, 292–307. doi:10.22203/ecm.v024a21

Ando, W., Tateishi, K., Hart, D. A., Katakai, D., Tanaka, Y., Nakata, K., et al. (2007). Cartilage Repair Using an *In Vitro* Generated Scaffold-free Tissue-Engineered Construct Derived from Porcine Synovial Mesenchymal Stem Cells. *Biomaterials* 28, 5462–5470. doi:10.1016/j.biomaterials.2007.08.030

Andrews, S. H. J., Adesida, A. B., Abusara, Z., and Shrive, N. G. (2017). Current Concepts on Structure-Function Relationships in the Menisci. *Connect. Tissue Res.* 58, 271–281. doi:10.1080/03008207.2017.1303489

Andrews, S. H. J., Rattner, J. B., Abusara, Z., Adesida, A., Shrive, N. G., and Ronsky, J. L. (2014). Tie-fibre Structure and Organization in the Knee Menisci. *J. Anat.* 224, 531–537. doi:10.1111/joa.12170

Arnoczky, S. P., Cook, J. L., Carter, T., and Turner, A. S. (2010). Translational Models for Studying Meniscal Repair and Replacement: what They Can and Cannot Tell Us. *Tissue Eng. B: Rev.* 16, 31–39. doi:10.1089/ten.teb.2009.0428

Barlian, A., Judawisastra, H., Ridwan, A., Wahyuni, A. R., and Lingga, M. E. (2020). Chondrogenic Differentiation of Wharton's Jelly Mesenchymal Stem Cells on Silk Spidroin-Fibroin Mix Scaffold Supplemented with L-Ascorbic Acid and Platelet Rich Plasma. *Sci. Rep.* 10, 19449. doi:10.1038/s41598-020-76466-8

Barton, K. I., Heard, B. J., Sevick, J. L., Martin, C. R., Shekarforoush, S. M. M., Chung, M., et al. (2018). Posttraumatic Osteoarthritis Development and Progression in an Ovine Model of Partial Anterior Cruciate Ligament Transection and Effect of Repeated Intra-articular Methylprednisolone Acetate Injections on Early Disease. *Am. J. Sports Med.* 46, 1596–1605.

Brunt, L. H., Begg, K., Kague, E., Cross, S., and Hammond, C. L. (2017). Wnt Signalling Controls the Response to Mechanical Loading during Zebrafish Joint Development. *Development* 144, 2798–2809. doi:10.1242/dev.153528

Brzezinski, A., Ghodbane, S. A., Patel, J. M., Perry, B. A., Gatt, C. J., and Dunn, M. G. (2017). The Ovine Model for Meniscus Tissue Engineering: Considerations of Anatomy, Function, Implantation, and Evaluation. *Tissue Eng. C: Methods* 23, 829–841. doi:10.1089/ten.tec.2017.0192

Caplan, A. I. (2019). Medicinal Signalling Cells: They Work, So Use Them. *Nature* 566 (7742), 39. doi:10.1038/d41586-019-00490-6

Caplan, A. I. (2017). Mesenchymal Stem Cells: Time to Change the Name!. *STEM CELLS Translational Med.* 6, 1445–1451. doi:10.1002/sctm.17-0051

de Windt, T. S., Vonk, L. A., Slaper-Cortenbach, I. C. M., Nizak, R., van Rijen, M. H. P., and Saris, D. B. F. (2017). Allogeneic MSCs and Recycled Autologous Chondrons Mixed in a One-Stage Cartilage Cell Transplantion: A First-In-Man Trial in 35 Patients. *Stem Cells* 35, 1984–1993. doi:10.1002/stem.2657

Di Giancamillo, A., Deponti, D., Addis, A., Domeneghini, C., and Peretti, G. M. (2014). Meniscus Maturation in the Swine Model: Changes Occurring along with Anterior to Posterior and Medial to Lateral Aspect during Growth. *J. Cel. Mol. Med.* 18, 1964–1974. doi:10.1111/jcmm.12367

Di Giancamillo, A., Deponti, D., Modina, S., Tessaro, I., Domeneghini, C., and Peretti, G. M. (2017). Age-related Modulation of Angiogenesis-Regulating Factors in the Swine Meniscus. *J. Cel. Mol. Med.* 21, 3066–3075. doi:10.1111/jcmm.13218

Dixit, M., Poudel, S. B., and Yakar, S. (2021). Effects of GH/IGF axis on Bone and Cartilage. *Mol. Cell Endocrinol.* 519, 111052. doi:10.1016/j.mce.2020.111052

Fallon, J., Blevins, F. T., Vogel, K., and Trotter, J. (2002). Functional Morphology of the Supraspinatus Tendon. *J. Orthop. Res.* 20, 920–926. doi:10.1016/s0736-0266(02)00032-2

Frank, C. B., and Hart, D. A. (2004a). "Clinical Application of Tissue Engineered Tendon and Ligament," in *Tissue Engineering in Musculoskeletal Clinical Practice*. Editors L. J. Sandell, A. J. Grodzinsky, and R. AAOS (IL, USA), 241–256.

Frank, C. B., Shrive, N. G., Boorman, R. S., Lo, I. K. Y., and Hart, D. A. (2004). New Perspectives on Bioengineering of Joint Tissues: Joint Adaptation Creates a Moving Target for Engineering Replacement Tissues. *Ann. Biomed. Eng.* 32, 458–465. doi:10.1023/b:abme.0000017548.85451.b7

Friedrich, O., Haug, M., Reischl, B., Prölß, G., Kiriaev, L., Head, S. I., et al. (2019). Single Muscle Fibre Biomechanics and Biomechatronics - the Challenges, the Pitfalls and the Future. *Int. J. Biochem. Cel Biol.* 114, 105563. doi:10.1016/j.biocel.2019.105563

Frost, H. M. (2004). A 2003 Update of Bone Physiology and Wolff's Law for Clinicians. *Angle Orthod.* 74, 3–15. doi:10.1043/0003-3219(2004)074<0003:AUOBPA>2.0.CO;2

Frost, H. M. (1996). Perspectives: A Proposed General Model of the "mechanostat" (Suggestions from a New Skeletal-Biologic Paradigm). *Anat. Rec.* 244, 139–147. doi:10.1002/(sici)1097-0185(199602)244:2<139:aid-ar1>3.0.co;2-x

Fujie, H., Nansai, R., Ando, W., Shimomura, K., Moriguchi, Y., Hart, D. A., et al. (2015). Zone-specific Integrated Cartilage Repair Using a Scaffold-free Tissue Engineered Construct Derived from Allogenic Synovial Mesenchymal Stem Cells: Biomechanical and Histological Assessments. *J. Biomech.* 48, 4101–4108. doi:10.1016/j.jbiomech.2015.10.015

Goulet, F., Auger, F. A., Cloutier, R., Lamontagne, J., Simon, F., Chabaud, S., et al. (2014). "Tendons and Ligament Tissue Engineering," in *Principles of Tissue Engineering*. Editors R. Manza, R. Lauger, and J. Vacanti. 4th Edition (Elsevier), 1275–1287. doi:10.1016/b978-0-12-398358-9.00059-8

Goulet, F., Chabaud, S., Simon, F., Napa, I. D., Moulin, V., and Hart, D. A. (2011). "Potential of Tissue-Engineered Ligament Substitutes for ACL Replacement," in *Regenerative Medicine and Tissue Engineering: Cells and Biomaterials*. Editor D. Eberli. (InTec). ISBN 978-953-307-688-1.

Hart, D. A., Kydd, A. S., Frank, C. B., and Hildebrand, K. A. (2004). Tissue Repair in Rheumatoid Arthritis: Challenges and Opportunities in the Face of a Systemic Inflammatory Disease. *Best Pract. Res. Clin. Rheumatol.* 18, 187–202. doi:10.1016/j.berh.2004.02.007

Hart, D. A., Martin, C. R., Scott, M., and Shrive, N. G. (2021). The Instrumented Sheep Knee to Elucidate Insights into Osteoarthritis Development and Progression: a Sensitive and Reproducible Platform for Integrated Research Efforts. *Clin. Biomech.* 87, 105404. doi:10.1016/j.clinbiomech.2021.105404

Hart, D. A., Natsu-ume, T., Sciore, P., Tasveski, V., Frank, C. B., and Shrive, N. G. (2002). Mechanobiology: Similarities and Differences between *In Vivo* and *In Vitro* Analysis at the Functional and Molecular Levels. *Recent Res. Devel., Biophys. Biochem.* 2, 153–177.

Hart, D. A., Shrive, N. G., and Goulet, F. (2005). Tissue Engineering of ACL Replacements. *Sports Med. Arthroscop. Rev.* 13, 170–176. doi:10.1097/01.jsa.0000173242.15191.70

Haug, M., Reischl, B., Prölß, G., Pollman, C., Pollmann, C., Buckert, T., et al. (2018). The MyoRobot: A Novel Automated Biomechatronics System to Assess voltage/Ca2+ Biosensors and Active/passive Biomechanics in Muscle and Biomaterials. *Biosens. Bioelectron.* 102, 589–599. doi:10.1016/j.bios.2017.12.003

Hayashi, M., Zhao, C., Thoreson, A. R., Chikenji, T., Jay, G. D., An, K.-N., et al. (2013). The Effect of Lubricin on the Gliding Resistance of Mouse Intrasynovial Tendon. *PLoS One* 8, e83836. doi:10.1371/journal.pone.0083836

Heard, B. J., Barton, K. I., Abubacker, S., Chung, M., Martin, C. R., Schmidt, T. A., et al. (2021). Synovial and Cartilage Responsiveness to Peri-operative Hyaluronic Acid ± Dexamethasone Administration Following a Limited Injury to the Rabbit Stifle Joint. *J. Orthop. Res.*. Online ahead of print. doi:10.1002/jor.25108

Heard, B. J., Barton, K. I., Agbojo, O. M., Chung, M., Sevick, J. L., Bader, T. J., et al. (2019). Molecular Response of Rabbit Menisci to Surgically Induced Hemarthrosis and a Single Intra-Articular Dexamethasone Treatment. *J. Orthop. Res.* 37, 2043–2052. doi:10.1002/jor.24346

Heard, B. J., Barton, K. I., Chung, M., Achari, Y., Shrive, N. G., Frank, C. B., et al. (2015). Single Intra-articular Dexamethasone Injection Immediately post-surgery in a Rabbit Model Mitigates Early Inflammatory Responses and post-traumatic Osteoarthritis-like Alterations. *J. Orthop. Res.* 33, 1826–1834. doi:10.1002/jor.22972

Heard, B. J., Solbak, N. M., Chung, M., Achari, Y., Shrive, N. G., Frank, C. B., et al. (2016). The Infrapatellar Fat Pad Is Affected by Injury Induced Inflammation in the Rabbit Knee: Use of Dexamethasone to Mitigate Damage. *Inflamm. Res.* 65, 459–470. doi:10.1007/s00011-016-0928-z

Hellio Le Graverand, M.-P., Ou, Y., Schield-yee, T., Barclay, L., Hart, D., Natsume, T., et al. (2001). The Cells of the Rabbit Meniscus: Their Arrangement, Interrelationship, Morphological Variations and Cytoarchitecture. *J. Anat.* 198, 525–535. doi:10.1046/j.1469-7580.2000.19850525.x

Hess, R., Douglas, T., Myers, K. A., Rentsch, B., Rentsch, C., Worch, H., et al. (2010). Hydrostatic Pressure Stimulation of Human Mesenchymal Stem Cells Seeded on Collagen-Based Artificial Extracellular Matrices. *J. Biomech. Eng.* 132, 021001. doi:10.1115/1.4000194

Huisman, E. S., Andersson, G., Scott, A., Reno, C. R., Hart, D. A., and Thornton, G. M. (2014). Regional Molecular and Cellular Differences in the Female Rabbit Achilles Tendon Complex: Potential Implications for Understanding Responses to Loading. *J. Anat.* 224, 538–547. doi:10.1111/joa.12169

Ionescu, L. C., Lee, G. C., Garcia, G. H., Zachry, T. L., Shah, R. P., Sennett, B. J., et al. (2011). Maturation State-dependent Alterations in Meniscus Integration: Implications for Scaffold Design and Tissue Engineering. *Tissue Eng. A* 17, 193–204. doi:10.1089/ten.tea.2010.0272

Jiang, S., Tian, G., Yang, Z., Gao, X., Wang, F., Li, J., et al. (2021). Enhancement of Acellular Cartilage Matrix Scaffold by Wharton's Jelly Mesenchymal Stem Cell-Derived Exosomes to Promote Osteochondral Regeneration. *Bioactive Mater.* 6, 2711–2728. doi:10.1016/j.bioactmat.2021.01.031

Kohrs, R. T., Zhao, C., Sun, Y.-L., Jay, G. D., Zhang, L., Warman, M. L., et al. (2011). Tendon Fascicle Gliding in Wild Type, Heterozygous, and Lubricin Knockout Mice. *J. Orthop. Res.* 29, 384–389. doi:10.1002/jor.21247

Kostrominova, T. Y., and Brooks, S. V. (2013). Age-related Changes in Structure and Extracellular Matrix Protein Expression Levels in Rat Tendons. *Age* 35, 2203–2214. doi:10.1007/s11357-013-9514-2

Lemmex, D. B., Ono, Y., Reno, C. R., Hart, D. A., Lo, I. K. Y., and Thornton, G. M. (2016). Increased Lubricin/proteoglycan 4 Gene Expression and Decreased Modulus in Medial Collateral Ligaments Following Ovariohysterectomy in the Adult Rabbit: Evidence Consistent with Aging. *J. Biomech.* 49, 382–387. doi:10.1016/j.jbiomech.2015.12.026

Liu, X., Laurent, C., Du, Q., Targa, L., Cauchois, G., Chen, Y., et al. (2018). Mesenchymal Stem Cell Interacted with PLCL Braided Scaffold Coated with Poly-L -lysine/hyaluronic Acid for Ligament Tissue Engineering. *J. Biomed. Mater. Res.* 106, 3042–3052. doi:10.1002/jbm.a.36494

Lo, I. K. Y., Ou, Y., Rattner, J.-P., Hart, D. A., Marchuk, L. L., Frank, C. B., et al. (2002). The Cellular Networks of normal Ovine Medial Collateral and Anterior Cruciate Ligaments Are Not Accurately Recapitulated in Scar Tissue. *J. Anat.* 200, 283–296. doi:10.1046/j.1469-7580.2002.00024.x

Loeser, R. F., Goldring, S. R., Scanzello, C. R., and Goldring, M. B. (2012). Osteoarthritis: a Disease of the Joint as an Organ. *Arthritis Rheum.* 64, 1697–1707. doi:10.1002/art.34453

Mallett, K. F., and Arruda, E. M. (2017). Digital Image Correlation-Aided Mechanical Characterization of the Anteromedial and Posterolateral Bundles of the Anterior Cruciate Ligament. *Acta Biomater.* 56, 44–57. doi:10.1016/j.actbio.2017.03.045

Markes, A. R., Hodax, J. D., and Ma, C. B. (2020). Meniscus Form and Function. *Clin. Sports Med.* 39, 1–12. doi:10.1016/j.csm.2019.08.007

Mauck, R. L., and Burdick, J. A. (2015). From Repair to Regeneration: Biomaterials to Reprogram the Meniscus Wound Microenvironment. *Ann. Biomed. Eng.* 43, 529–542. doi:10.1007/s10439-015-1249-z

Meller, R., Schiborra, F., Brandes, G., Knobloch, K., Tschernig, T., Hankemeier, S., et al. (2009). Postnatal Maturation of Tendon, Cruciate Ligament, Meniscus and Articular Cartilage: a Histological Study in Sheep. *Ann. Anat. - Anatomischer Anzeiger* 191, 575–585. doi:10.1016/j.aanat.2009.08.005

Murphy, C. A., Garg, A. K., Silva-Correia, J., Reis, R. L., Oliveira, J. M., and Collins, M. N. (2019). The Meniscus in Normal and Osteoarthritic Tissues: Facing the Structure Property Challenges and Current Treatment Trends. *Annu. Rev. Biomed. Eng.* 21, 495–521. doi:10.1146/annurev-bioeng-060418-052547

Natsu-ume, T., Majima, T., Reno, C., Shrive, N. G., Frank, C. B., and Hart, D. A. (2005). Menisci of the Rabbit Knee Require Mechanical Loading to Maintain Homeostasis: Cyclic Hydrostatic Compression *In Vitro* Prevents Derepression of Catabolic Genes. *J. Orthopaedic Sci.* 10, 396–405. doi:10.1007/s00776-005-0912-x

Naue, J., Sänger, T., Hoefsloot, H. C. J., Lutz-Bonengel, S., Kloosterman, A. D., and Verschure, P. J. (2018). Proof of Concept Study of Age-dependent DNA Methylation Markers across Different Tissues by Massive Parallel Sequencing. *Forensic Sci. Int. Genet.* 36, 152–159. doi:10.1016/j.fsigen.2018.07.007

Peffers, M. J., Goljanek-Whysall, K., Collins, J., Fang, Y., Rushton, M., Loughlin, J., et al. (2016). Decoding the Regulatory Landscape of Ageing in Musculoskeletal Engineered Tissues Using Genome-wide DNA Methylation and RNASeq. *PLoS One* 11, e0160517. doi:10.1371/journal.pone.0160517

Radin, E. L., Burr, D. B., Caterson, B., Fyhrie, D., Brown, T. D., and Boyd, R. D. (1991). Mechanical Determinants of Osteoarthrosis. *Semin. Arthritis Rheum.* 21 (Suppl. 2), 12–21. doi:10.1016/0049-0172(91)90036-y

Rattner, J. B., Matyas, J. R., Barclay, L., Holowaychuk, S., Sciore, P., Lo, I. K. Y., et al. (2011). New Understanding of the Complex Structure of Knee Menisci: Implications for Injury Risk and Repair Potential for Athletes. *Scand. J. Sci. Med. Sport* 21, 543–553. doi:10.1111/j.1600-0838.2009.01073.x

Rollick, N., Lemmex, D., Ono, Y., Reno, C., Hart, D. A., Lo, I., et al. (2018). Gene-expression Changes in Knee-Joint Tissues with Aging and Menopause: Implications for the Joint as an Organ. *Cia* Vol. 13, 365–375. doi:10.2147/cia.s151453

Rosenfeld, R. G., and Hwa, V. (2009). The Growth Hormone cascade and its Role in Mammalian Growth. *Horm. Res.* 71 Suppl 2 (Suppl. 2), 36–40. doi:10.1159/000192434

Sadlik, B., Jaroslawski, G., Gladysz, D., Puszkarz, M., Markowska, M., Pawelec, K., et al. (2017). Knee Cartilage Regeneration with Umbilical Cord Mesenchymal Stem Cells Embedded in Collagen Scaffold Using Dry Arthroscopy Technique. *Adv. Exp. Med. Biol.* 1020, 113–122. doi:10.1007/5584_2017_9

Sevick, J. L., Abusara, Z., Andrews, S. H., Xu, M., Khurshid, S., Chatha, J., et al. (2018). Fibril Deformation under Load of the Rabbit Achilles Tendon and Medial Collateral Ligament Femoral Entheses. *J. Orthop. Res.* 36, 2506–2515. doi:10.1002/jor.23912

Sevick, J. L., Hart, D. A., and Shrive, N. G. (2021). "The Firbrocartilaginous Ligament Enthesis," in *From Biomaterials towards Medical Devices* (World Scientific Publishing Company), Vol. 3. chapter 5. doi:10.1142/978981120463-_0005

Shimomura, K., Ando, W., Moriguchi, Y., Sugita, N., Yasui, Y., Koizumi, K., et al. (2015). Next Generation Mesenchymal Stem Cell (MSC)-based Cartilage Repair Using Scaffold-free Tissue Engineered Constructs Generated with Synovial Mesenchymal Stem Cells. *Cartilage* 6 (2 Suppl. l), 13S–29S. doi:10.1177/1947603515571002

Shimomura, K., Rothrauff, B. B., Hart, D. A., Hamamoto, S., Kobayashi, M., Yoshikawa, H., et al. (2018a). Enhanced Repair of Meniscal Hoop Structure Injuries Using an Aligned Electrospun Nanofibrous Scaffold Combined with a Mesenchymal Stem Cell-Derived Tissue Engineered Construct. *Biomaterials* 192, 346–354. doi:10.1016/j.biomaterials.2018.11.009

Shimomura, K., Ando, W., Tateishi, K., Nansai, R., Fujie, H., Hart, D. A., et al. (2010). The Influence of Skeletal Maturity on Allogenic Synovial Mesenchymal Stem Cell-Based Repair of Cartilage in a Large Animal Model. *Biomaterials* 31, 8004–8011. doi:10.1016/j.biomaterials.2010.07.017

Shimomura, K., Hamada, H., Hart, D. A., Ando, W., Nishii, T., Trattnig, S., et al. (2021). Histological Analysis of Cartilage Defects Repaired with an Autologous Human Stem Cell Construct 48 Weeks Postimplantation Reveals Structural Details Not Detected by T2-Mapping MRI. *Cartilage* 1947603521989423, 194760352198942, 2021 . Online ahead of print. doi:10.1177/1947603521989423

Shimomura, K., Hamamoto, S., Hart, D. A., Yoshikawa, H., and Nakamura, N. (2018). Meniscal Repair and Regeneration: Current Strategies and Future Perspectives. *J. Clin. Orthopaedics Trauma* 9, 247–253. doi:10.1016/j.jcot.2018.07.008

Shimomura, K., Yasui, Y., Koizumi, K., Chijimatsu, R., Hart, D. A., Yonetani, Y., et al. (2018b). First-in-Human Pilot Study of Implantation of a Scaffold-free Tissue-Engineered Construct Generated from Autologous Synovial Mesenchymal Stem Cells for Repair of Knee Chondral Lesions. *Am. J. Sports Med.* 46, 2384–2393. doi:10.1177/0363546518781825

Sieker, J. T., Ayturk, U. M., Proffen, B. L., Weissenberger, M. H., Kiapour, A. M., and Murray, M. M. (2016). Immediate Administration of Intraarticular Triamcinolone Acetonide after Joint Injury Modulates Molecular Outcomes Associated with Early Synovitis. *Arthritis Rheumatol.* 68, 1637–1647. doi:10.1002/art.39631

Suwaydi, M. A., Gridneva, Z., Perrella, S. L., Wlodek, M. E., Lai, C. T., and Geddes, D. T. (2021). Human Milk Metabolic Hormones: Analytical Methods and Current Understanding. *Ijms* 22, 8708. doi:10.3390/ijms22168708

Thornton, G. M., Lemmex, D. B., Ono, Y., Beach, C. J., Reno, C. R., Hart, D. A., et al. (2015). Aging Affects Mechanical Properties and lubricin/PRG4 Gene Expression in normal Ligaments. *J. Biomech.* 48, 3306–3311. doi:10.1016/j.jbiomech.2015.06.005

Thornton, G. M., Shao, X., Chung, M., Sciore, P., Boorman, R. S., Hart, D. A., et al. (2010). Changes in Mechanical Loading lead to Tendonspecific Alterations in MMP and TIMP Expression: Influence of Stress Deprivation and Intermittent

Cyclic Hydrostatic Compression on Rat Supraspinatus and Achilles Tendons. *Br. J. Sports Med.* 44, 698–703. doi:10.1136/bjsm.2008.050575

Vogel, K. G., and Peters, J. A. (2005). Histochemistry Defines a Proteoglycan-Rich Layer in Bovine Flexor Tendon Subjected to Bending. *J. Musculoskelet. Neuronal Interact* 5, 64–69.

Vogel, K. G. (2003). Tendon Structure and Response to Changing Mechanical Load. *J. Musculoskelet. Neuronal Interact* 3, 323–324.

Vogel, K. G. (2004). What Happens when Tendons bend and Twist? Proteoglycans. *J. Musculoskelet. Neuronal Interact* 4, 202–203.

Vogel, K. G., and Koob, T. J. (1989). Structural Specialization in Tendons under Compression. *Int. Rev. Cytol.* 115, 267–293. doi:10.1016/s0074-7696(08)60632-4

Walsh, S., Frank, C., and Hart, D. (1992). Immobilization Alters Cell Metabolism in an Immature Ligament. *Clin. Orthopaedics Relat. Res.* &NA;, 277–288. doi:10.1097/00003086-199204000-00034

Walsh, S., Frank, C., Shrive, N., and Hart, D. (1993). Knee Immobilization Inhibits Biomechanical Maturation of the Rabbit Medial Collateral Ligament. *Clin. Orthopaedics Relat. Res.* &NA;, 253–261. doi:10.1097/00003086-199312000-00042

Wan, C., Hao, Z., and Wen, S. (2014). The Effect of the Variation in ACL Constitutive Model on Joint Kinematics and Biomechanics under Different Loads: a Finite Element Study. *J. Biomech. Eng.* 135, 041002. doi:10.1115/1.4023696

Woodell-May, J. E., and Sommerfeld, S. D. (2020). Role of Inflammation and the Immune System in the Progression of Osteoarthritis. *J. Orthop. Res.* 38, 253–257. doi:10.1002/jor.24457

Yasui, Y., Hart, D. A., Sugita, N., Chijimatsu, R., Koizumi, K., Koizumi, K., et al. (2018). Time-Dependent Recovery of Human Synovial Membrane Mesenchymal Stem Cell Function after High-Dose Steroid Therapy: Case Report and Laboratory Study. *Am. J. Sports Med.* 46, 695–701. doi:10.1177/0363546517741307

Yoshida, T., and Delafontaine, P. (2020). Mechanisms of IGF-1-Mediated Regulation of Skeletal Muscle Hypertrophy and Atrophy. *Cells* 9, 1970. doi:10.3390/cells9091970

Conflict of Interest: The authors declare that the research was conducted in the absence of any commercial or financial relationships that could be construed as a potential conflict of interest.

frontiers in Bioengineering and Biotechnology

REVIEW
published: 22 October 2021
doi: 10.3389/fbioe.2021.766087

Advances and Prospects in Biomaterials for Intervertebral Disk Regeneration

Chunxu Li[1†], Qiushi Bai[1†], Yuxiao Lai[2], Jingjing Tian[3], Jiahao Li[1], Xiaodan Sun[4] and Yu Zhao[1*]*

[1]Department of Orthopaedics, Peking Union Medical College Hospital, Peking Union Medical College and Chinese Academy of Medical Sciences, Beijing, China, [2]Centre for Translational Medicine Research and Development, Shenzhen Institute of Advanced Technology, Chinese Academy of Sciences, Shenzhen, China, [3]Medical Science Research Center, Peking Union Medical College Hospital, Peking Union Medical College and Chinese Academy of Medical Sciences, Beijing, China, [4]State Key Laboratory of New Ceramics and Fine Processing, School of Materials Science and Engineering, Tsinghua University, Beijing, China

OPEN ACCESS

Edited by:
Farnaz Ghorbani, University of Erlangen Nuremberg, Germany

Reviewed by:
Melika Sahranavard, Materials and Energy Research Center, Iran
Chaozong Liu, University College London, United Kingdom

***Correspondence:**
Yu Zhao
zhaoyupumch@163.com
Xiaodan Sun
sunxiaodan@tsinghua.edu.cn

[†]These authors have contributed equally to this work and share first authorship

Specialty section:
This article was submitted to Biomaterials, a section of the journal Frontiers in Bioengineering and Biotechnology

Received: *28 August 2021*
Accepted: *08 October 2021*
Published: *22 October 2021*

Citation:
Li C, Bai Q, Lai Y, Tian J, Li J, Sun X and Zhao Y (2021) Advances and Prospects in Biomaterials for Intervertebral Disk Regeneration. Front. Bioeng. Biotechnol. 9:766087. doi: 10.3389/fbioe.2021.766087

Low-back and neck-shoulder pains caused by intervertebral disk degeneration are highly prevalent among middle-aged and elderly people globally. The main therapy method for intervertebral disk degeneration is surgical intervention, including interbody fusion, disk replacement, and diskectomy. However, the stress changes caused by traditional fusion surgery are prone to degeneration of adjacent segments, while non-fusion surgery has problems, such as ossification of artificial intervertebral disks. To overcome these drawbacks, biomaterials that could endogenously regenerate the intervertebral disk and restore the biomechanical function of the intervertebral disk is imperative. Intervertebral disk is a fibrocartilaginous tissue, primarily comprising nucleus pulposus and annulus fibrosus. Nucleus pulposus (NP) contains high water and proteoglycan, and its main function is absorbing compressive forces and dispersing loads from physical activities to other body parts. Annulus fibrosus (AF) is a multilamellar structure that encloses the NP, comprises water and collagen, and supports compressive and shear stress during complex motion. Therefore, different biomaterials and tissue engineering strategies are required for the functional recovery of NP and AF based on their structures and function. Recently, great progress has been achieved on biomaterials for NP and AF made of functional polymers, such as chitosan, collagen, polylactic acid, and polycaprolactone. However, scaffolds regenerating intervertebral disk remain unexplored. Hence, several tissue engineering strategies based on cell transplantation and growth factors have been extensively researched. In this review, we summarized the functional polymers and tissue engineering strategies of NP and AF to endogenously regenerate degenerative intervertebral disk. The perspective and challenges of tissue engineering strategies using functional polymers, cell transplantation, and growth factor for generating degenerative intervertebral disks were also discussed.

Keywords: biomaterial, intervertebral disc, degeneration, nucleus pulposus, anulus fibrosus, cartilage endplate

INTRODUCTION

According to research statistics, 80% of people worldwide have experienced low-back pain in their lifetime (DALYs and Collaborators, 2017). This kind of pain, in severe cases, can radiate to the whole lower limbs, seriously affecting people's quality of life and work ability while causing a huge medical burden; this disease has become a global social and economic problem (March et al., 2014), and the main cause of this problem is intervertebral disk degeneration (Hoy et al., 2015). For this disease, the current mainstream treatment can be divided into nonsurgical and surgical treatments. Among them, non-surgical treatment methods mainly include drug and physical therapies. The prevailing view is that the causes of low-back pain caused by disk degeneration include an acidic environment caused by local inflammation, nerve root compression due to nucleus pulposus (NP) herniation or disk collapse, and ectopic sensory nerve fibers and blood vessels growing into the annulus and NP (Bailey et al., 2013; Binch et al., 2015; Lama et al., 2018). However, the most important reason is the local inflammatory environment, which is why low-back pain can be effectively ameliorated in the early stage of intervertebral disk degeneration using only NSaids, although there is still no NP herniation. Physical therapy is also thought to be effective in improving low-back pain caused by disk degeneration, and some animal studies have elucidated some of the mechanisms involved. Gawri et al. found that moderate exercise can boost the synthesis of intervertebral disk cells, but excessive exercise can break them down and promote inflammation (Gawri et al., 2014). Gullbrand et al. found that circulating compression and stretching of intervertebral disks can improve the viability of intervertebral disk cells by increasing nutrient transport, thus achieving the effect of physical therapy (Gullbrand et al., 2015). Although some studies have proven the effectiveness of drug and physical therapies, it is difficult for these nonsurgical treatments to achieve significant effects in some patients with severe degeneration because of the obvious inflammatory environment and irreversible cell senescence. At present, for patients with severe degeneration, surgical treatment is still the first choice. The mainstream surgical methods are minimally invasive lumbar discectomy and lumbar open surgery. Although surgery can relieve the symptoms of low back pain, there are problems of long recovery time, high treatment cost, and the possibility of complications such as adjacent segment degeneration and pain recurrence (Ghiselli et al., 2004; Eliasberg et al., 2016; Li et al., 2021). In general, the current mainstream treatment is aimed at the symptoms of treatment but cannot effectively restore the function of the intervertebral disk; therefore, how to restore the original biological and physical function of the intervertebral disk is the focus of scientists' efforts. Currently, several methods to promote disk regeneration have been reported, including total disk replacement (Takeoka et al., 2020), cell therapy (Hu et al., 2018; Peredo et al., 2020), and gene therapy (Feng et al., 2015; Feng et al., 2020). These new treatments, designed to fully restore or mimic original disk function, show great potential for development. Unlike most reviews, this study first reviews intervertebral disk anatomy and the pathophysiological process of intervertebral disk degeneration, and based on this process, introduces the body's requirements for regenerative materials. Then, we discussed how the hot materials for regeneration of NP, AF, and cartilage endplates discovered by researchers in recent years are working towards this demand. At the same time, we also analyzed the gap between the current research status and the ideal goal, and proposed that the intervertebral disk should be regarded as an integral movement unit to study its materials in the future, and also briefly introduces the research progress of the overall intervertebral disk regeneration strategy. At present, most review publications of the intervertebral disk regeneration choose to focus on one of the nucleus pulposus or the AF. In comparison, this study can better help researchers to comprehensively understand the materials' hotspots and provide help for exploring the overall regeneration strategy of intervertebral disk.

INTERVERTEBRAL DISK STRUCTURE AND FUNCTION

The spinal column is one of the most important bone structures in the human body. It protects the spinal cord, supports body weight, slows impact, and allows flexible movement of the trunk. The spine comprises vertebral bones and intervertebral disks (**Figure 1**). Intervertebral disks, joints between vertebral bones, ligaments, and muscles around them, constitute the most basic motion units of the spine, and intervertebral disks play the most important role in this process. Although many studies have explored intervertebral disk regeneration, its various structure are discussed separately. However, since a unified movement of any part of the overall structure and function of the anomalies is likely to induce the occurrence of low-back pain, we need to understand the various parts of physiology, anatomy, and pathophysiology characteristics, look for differences and commonness among components. It will be convenient to formulate a perfect regeneration plan for the whole structure.

The disk comprises a gelatinous NP, a fibrosus ring surrounding the NP, and a cartilaginous endplate next to the bones of the upper and lower vertebrae, which together bear the complex load caused by compression, extension, bending, and rotation of the spine (Roberts et al., 2006). Although these structures cooperate to accomplish the same task, their functions, compositions, and properties quite differ, and even the components of the inner and outer annulus fibrosus (AF) differ.

NP is located at the disk center; its composition slightly changes with age, and it mainly comprises water, type collagen II and elastic protein fiber, protein, polysaccharide, and notochord cells. As aging progresses, notochord cells completely degrade and are replaced by a sample of cartilage cells; concurrently, the collagen fibers begin to pair together; thus, NP by liquid becomes cartilage. However, water still occupies about 85% of the volume, making it viscoelastic and having compressive deformation resistance. NP plays an anisotropic uniformity in absorbing and diffusing stress, and diffuses the pressure to the AF through deformation, thus alleviating the

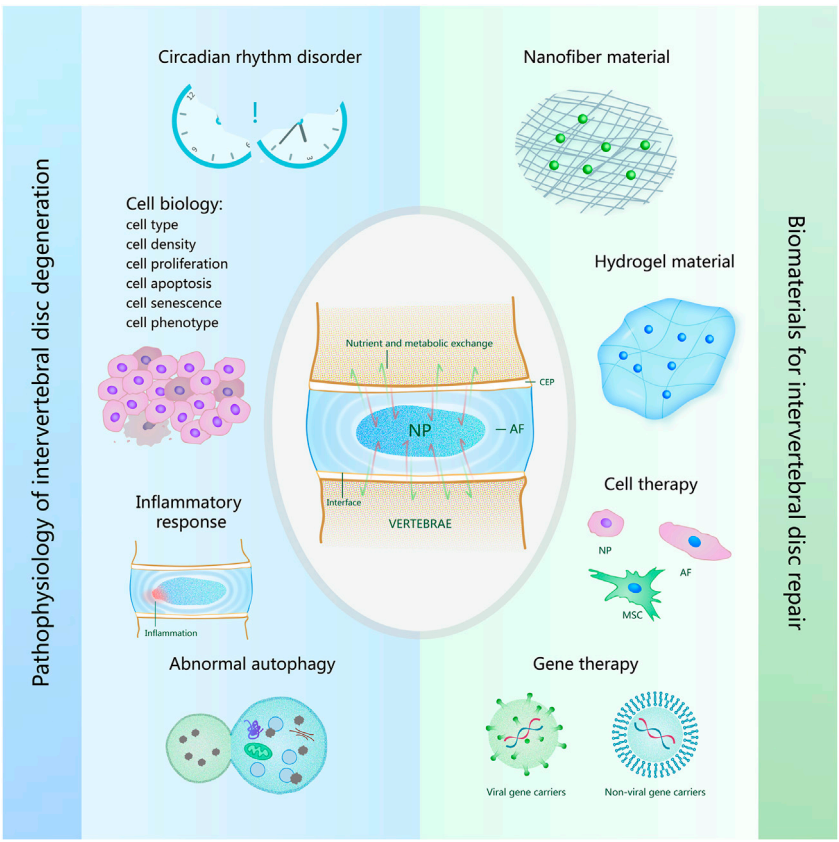

FIGURE 1 | Overview of pathophysiology of intervertebral disk degeneration and biomaterials for intervertebral disk repair. The pathophysiological causes of intervertebral disk degeneration shown on the left of the figure include circadian rhythm disorder, cell biology, inflammatory response, abnormal autophagy. The biomaterials for intervertebral disk repair shown on the right of the figure include nanofiber material, hydrogel material, biomaterials for cell therapy and gene therapy.

impact on the lower vertebral body (Iatridis et al., 1997). Chondroid cells are metabolically active cells in NP and can synthesize extracellular matrix (ECM) components, such as collagen and proteoglycan. It plays a role in maintaining the balance of the internal environment and is the main element in preventing intervertebral disk degeneration (Akkiraju and Nohe, 2015). Elastin fibers and proteoglycan synergize to maintain collagen activity and restore disk size and shape (Mouw et al., 2014).

AF is a kind of acellular and vascularless structure, mainly including fibrochondrocytes and chondrocytes, which are like fibroblasts in morphology. Its ECM components transition smoothly from inside to outside. The outer layer comprises mainly type I collagen, while the inner layer primarily comprises type II collagen (Guerin and Elliott, 2007). Type II collagen is hypoxic, hydrophilic, and proteoglycan rich, which is consistent with the physics of the hard outer layer and soft inner layer of the AF, which act as the outer layer to bind the NP during bending and twisting. The inner layer binds the NP during axial compression (Eyre and Muir, 1976). From a morphological viewpoint, the AF comprises 15–25 concentric annular lamella, constituting mainly neatly arranged bundles of collagen fibers. The direction of these collagen fibers is 30° to the horizontal plane (Humzah and Soames, 1988). These layers are filled with an interlaminar matrix comprising elastic fibers, cells, water, lipids, and proteoglycans. Proteoglycans including aggrecan, lubricating oil, GAGs, biglycan, decorin, perlecan, versican, etc., are responsible for lubrication and hydration. The cell morphology in the interlaminar matrix varies, from round to spindle and from center to periphery, which are related to the direction and density of elastic fibers, and the direction and magnitude of the load on the adjacent layers. The interlaminar stroma between the different layers is interconnected, connected by dividing boundaries, and comprises a dense elastic fibrosus structure consistent with the AF role in resisting NP expansion.

The cartilaginous endplate is a thin hyaline layer of cartilage, approximately 0.6–1.2 mm thick, with the thinnest and most porous central region (Zehra et al., 2015; Berg-Johansen et al., 2018). Regarding composition, the area adjacent to the cartilage endplate and AF has higher collagen, lower proteoglycan, and lower water contents than the NP (Roberts et al., 1989). Although the AF and the NP and cartilage endplate are anatomically distinct, their fine structures cross each other. The collagen fibers in the AF close to the NP are continuous with the collagen fibers in the cartilage endplate, which helps to reduce excessive concentrations of stress, such as disk stretching,

compression, and shearing, and prevent irreversible disk damage (Berg-Johansen et al., 2018). The cartilaginous endplate also acts as a medium for transferring forces in multiple directions between the disk and vertebral body. The cartilage endplate distributes the hydrostatic pressure generated by the NP evenly on the surface of the vertebral body to prevent the NP from expanding locally into the vertebral body. In addition, since the intervertebral disk is the largest vascularless structure in the human body, the blood vessels in the vertebral body are its main source of nutrition, and the capillary network formed by the aorta through all branches forms a capillary loop at the junction of the cartilage endplate and the intervertebral disk (Ashinsky et al., 2021). Therefore, the cartilage endplate is considered the main way for nutrition and waste to be transported to the vertebral body (**Figure 1**). With aging and degeneration, the cartilage endplate will undergo some composition changes, which will reduce permeability and limit the transportation of nutrients, and is considered one of the reasons for intervertebral disk degeneration (Schroeder et al., 2017).

PATHOPHYSIOLOGY OF INTERVERTEBRAL DISK DEGENERATION

The height and internal osmotic pressure of intervertebral disks will change under load bearing and resting states (Menon et al., 2021), which is mainly caused by day and night activities and the rest of human body. Interstitial fluid also flows in response to this differential pressure change, resulting in nutrient and metabolic exchanges to maintain intervertebral disk homeostasis (van der Veen et al., 2007). Disruption of circadian rhythms, however, may increase the risk of disk degeneration (**Figure 1**) (Dudek et al., 2017). Most intervertebral disk cells are nourished by capillaries from the vertebral body. With the deterioration of the intervertebral disk, bone marrow cavity occlusion leads to loss of contact between capillaries and cartilage endplate, and calcification of cartilage endplate increases (Benneker et al., 2005; Hristova et al., 2011).

Intervertebral disk degeneration can induce various cell biological changes, including cell type changes, cell density changes, cell apoptosis, cell proliferation, cell senescence, and cell phenotype changes (**Figure 1**) (Zhao et al., 2007). Notochord cells are a kind of cell existing in the early stage of human development. As humans grow, notochord cells are replaced by NP cells, suggesting that the onset of intervertebral disk degeneration may be related to the disappearance of notochord cells (McCann et al., 2012). Induction of pluripotent stem cells into notochord cells by injection has also been shown to reduce intervertebral disk degeneration in pig models (Sheyn et al., 2019). The density of NP cells in degenerated disks decreased compared to normal disk tissue (Liu C. et al., 2020). Since excessive mechanical load can induce apoptosis of NP-derived stem cells, some people try to delay intervertebral disk degeneration by anti-apoptosis (He et al., 2021), and promoting NP cell proliferation has also been proven to inhibit intervertebral disk degeneration (Cui et al., 2020). In recent years, with the deepening of research, the phenotypic characteristics of NP cells and the relationship between cell senescence and intervertebral disk degeneration have gradually been considered (Choi et al., 2015; Zhang Y. et al., 2020).

As aging increases, the occurrence of intervertebral disk degeneration is more and more likely (Cheung et al., 2009), and the most common clinically related symptom is low-back pain. According to existing studies, the cause of pain is most likely to be inflammation (**Figure 1**) (Lyu et al., 2021). Tessier et al. found significant pro-inflammatory pathway changes and age-related disk degeneration in a mouse that was deficient in a protein associated with embryonic disk development (Tessier et al., 2020). Chen et al. found that melatonin can delay the progression of disk degeneration and relieve associated low-back pain by studying its anti-inflammatory effect *in vivo* (Chen et al., 2020).

Recent studies have suggested that intervertebral disk degeneration is also associated with autophagy inhibition (**Figure 1**) (Lan et al., 2021). Autophagy plays a role in maintaining the homeostasis of the internal environment (Mizushima, 2007). It can meet metabolic requirements through lysosomal degradation and recovery of cell products, and protect cells by removing damaged organelles and misfolded proteins. Autophagy is also associated with other factors that may affect intervertebral disk degeneration. Circadian rhythms may maintain appropriate autophagy to prevent disk degeneration, while abnormal circadian rhythms may induce excessive autophagy and autophagy dysfunction to cause disk degeneration (Zhang T.-W. et al., 2020). Chen et al. found that by triggering autophagy, cell senescence and apoptosis could also be decreased, ultimately improving intervertebral disk degeneration (Chen et al., 2018). In subsequent studies, many people have reduced cell senescence and apoptosis by upregulating autophagy, thus maintaining intervertebral disk repair and delaying degeneration (He et al., 2021; Hu et al., 2021).

BIOMATERIALS FOR NUCLEUS PULPOSUS REPAIR

Nanofiber Material

The disk function depends on NP flexibility and AF toughness. Nanofiber material is a new type of biological material manufactured by stretching method, template synthesis, self-assembly, microphase separation, electrostatic spinning and other methods on the basis of various artificial polymers. Among them, the electrospinning method is widely used in the preparation of medical materials due to its advantages of simple operation, wide application range, and relatively high production efficiency. Because of its highly adjustable shape and structure, it often has excellent mechanical properties. Therefore, how to improve the biological stability of such materials is the focus of attention of researchers. Polyurethane (PU) series of biomaterials can adjust elasticity by changing the composition of monomer units and the block size of different monomers in the polymer chain. Among them, polycarbonate (PC) PU shows better biological stability and can be used as a good material to replace the NP and repair intervertebral disk. A

dual-phase PU stent comprising a core material with rapid swelling properties and a flexible electrospinning shell has been prepared and implanted into bovine intervertebral disks, restoring the mechanical properties of enucleated disks and showing the potential to delay further degeneration of natural disk tissue (Li et al., 2016). As cell behavior is affected by ECM characteristics, biomaterials that mimic ECM characteristics are generally beneficial to cell growth (Nesti et al., 2008; Kaur and Roy, 2021), and nanofiber scaffolds have unique physical characteristics that provide favorable cell-matrix cues to enhance cell activities (**Figure 1**) (Li et al., 2006). Zhang et al. developed a new type of nanofiber sponge microspheres (NF-SMS) with interconnected pore structure, which mimics the ECM protein fiber (Zhang et al., 2015), and has been proven to help mesenchymal stem cell adhesion, proliferation, and np-like differentiation, and the interconnected pores can effectively accommodate cells, promote transmitter transmission, and new ECM formation (Feng et al., 2020).

Hydrogel Material

Hydrogels can be prepared by physical crosslinking (through hydrophobic interaction, hydrogen bonding, electrostatic force, etc.) or chemical crosslinking (through covalent bonding). According to the source of hydrogels, it can be divided into three categories: natural, synthetic and composite hydrogels. Among them, natural materials include fibrin, alginate, chitosan, etc., which have great advantages in biocompatibility and low cytotoxicity, and thus are widely used in nucleus pulposus regeneration and repair. (**Figure 1**). However, its mismatched mechanical properties lead to the failure of the implant in the late stage of disk degeneration due to structural damage caused by long-term compression. Therefore, how to improve the mechanical properties of hydrogels is the focus of researchers. Gan et al. developed an interpenetrating network (IPN) reinforced and toughened hydrogel for NP regeneration, which has advantages such as NP-like mechanical properties and high toughness. The encapsulation of NP cells into the hydrogel clearly showed enhanced cell proliferation, natural cartilage formation phenotype, and ECM secretion. *In vivo* studies have also verified that IPN hydrogels can support cell retention and survival for a long time, thus promoting the rehydration and regeneration of degraded NP (Gan et al., 2017). Although the stiffness and toughness of the double network hydrogels were significantly improved, the long preparation time or continuous preparation made *in situ* curing difficult. The use of composite hydrogel is an alternative method, which has higher stiffness and strength, but also retains the characteristics of one-step hydrogel preparation, shortens the curing time, and is suitable for *in-situ* insertion. Schmocker et al. developed a composite hydrogel with functional properties like those of natural bovine NP. Disk height was restored from 65.6 to 99.0% in an *in vitro* study and remained the same after 500,000 loading cycles. Fifteen days after implantation, a continuous, undisturbed tissue/implant interface was observed histologically. This kind of composite hydrogel with excellent mechanical properties has great potential for clinical application (Schmocker et al., 2016).

The degeneration of the nucleus pith is characterized by loss of hydration and tissue sclerosis. Histologically, decreased cell density, loss of sulfated glycosaminoglycans (sGAGs) and type II collagen, and an increase in type I collagen can be observed. In response to this, Chiara Borrelli et al. proposed that the production of sGAG could be increased by adding chondroitin sulfate to the hydrogel, and found that its presence is critical to the synthesis of type II collagen.(**Figure 2**) The phenotype of the notochord-like NP cell population changes to a more fibroblast-like state (Chen et al., 2009; Risbud et al., 2015). Previous studies have shown that laminin 111 functionalized soft polyethylene glycol (PEG) substrate can re-express the juvenile phenotype of degenerative nucleus pulpocytes, suggesting that soft substrate plays a role in phenotypic recovery of degenerative nucleus pulpocytes (Gilchrist et al., 2011; Francisco et al., 2014; Fearing et al., 2019). However, in the study of NP-derived stem cells (NP-SCs), Navaro et al. found that cell proliferation and differentiation were independent of matrix hardness in the study of NP-SCs but emphasized the influence of matrix modulus on the fate of NP-SCs (Navaro et al., 2015). In a recent study, Barcellona et al. confirmed this point. We developed a dipeptide-functionalized hydrogel scaffold with adjustable mechanical properties and adherent ligand presentation to control NP cell morphology and phenotype. In experiments, it was demonstrated that strict control of peptide selection and peptide presentation induces younger NP cell phenotypes regardless of substrate hardness, so it could be adhesion ligand presentation that really affects the phenotypes of nucleus pulpocytes (Barcellona et al., 2020).

Loss of nutrients from the stent limits its effectiveness in promoting disk regeneration. Studies have shown that NP cells need oxygen and other nutrients to synthesize matrix molecules, and different oxygen concentrations also affect the composition ratio of ECM (Mwale et al., 2011). Sun et al. used perfluorotributylamine (PFTBA) to regulate oxygen without affecting alginate. The survival and proliferation of human NP cells cultured in PFTBA-rich alginate scaffolds were enhanced, and the ECM was modulated in intervertebral disk tissue. Disk height and ECM were restored in a mouse model of intervertebral disk degeneration, showing beneficial effects in alleviating intervertebral disk degeneration (Sun et al., 2016).

Gene Delivery Biomaterials

After NP degeneration, phenotypic changes of NP cells resulted in an imbalance of ECM anabolism and catabolism. Current treatment methods, such as symptomatic treatment or surgical treatment, can relieve symptoms in the short term but cannot solve the fundamental problem. Genetic modification of intervertebral disk cells through controlled and specific delivery of genetic material (DNA or RNA) is a promising therapeutic approach (**Figure 1**) (Roh et al., 2021). Many researchers have successfully transferred genes into intervertebral disk tissues through viral gene delivery systems (**Figure 1**) (Leckie et al., 2012; Han et al., 2021), but the obvious side effects limit further clinical application. The problem with retrovirus vectors is the risk of insertion mutation, while the problem with adenovirus vectors is the

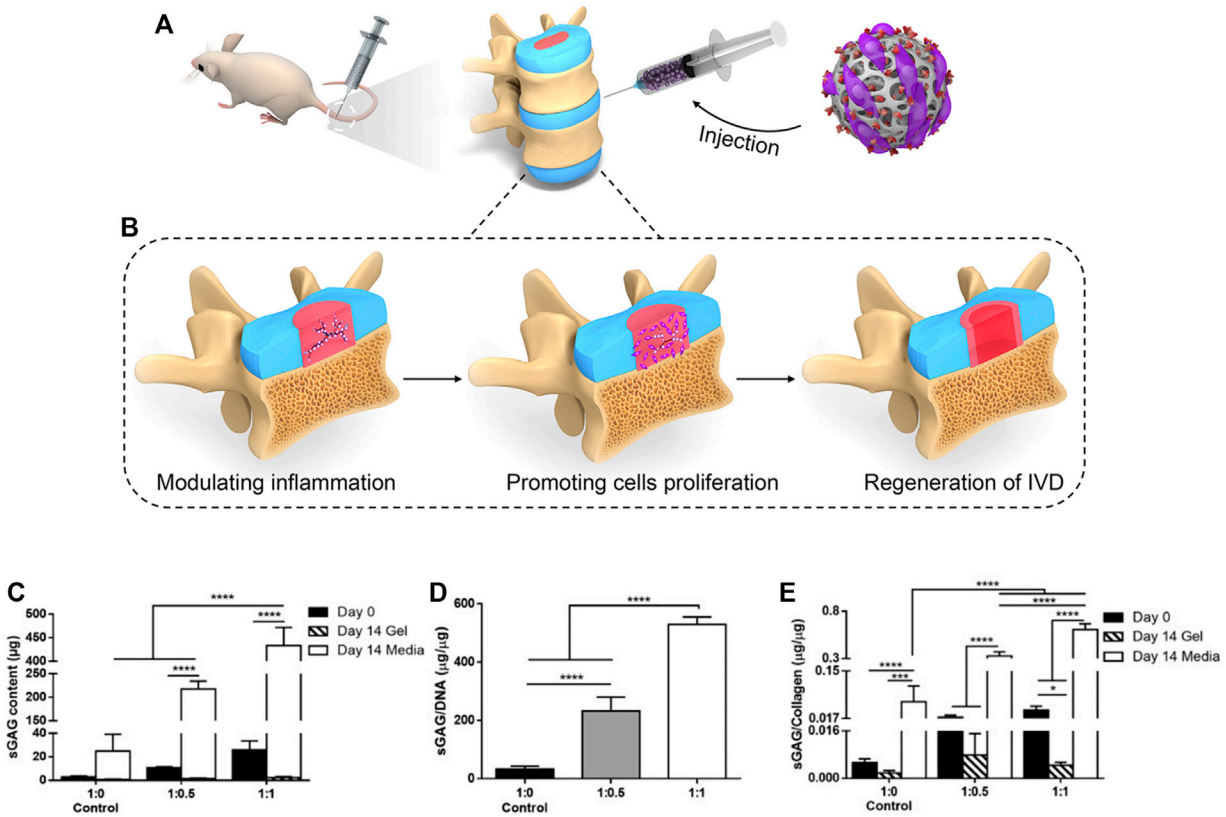

FIGURE 2 | (A) The injection of Hydrogels in the rat model of IVD degeneration (**(A)** Adapted from Borrelli and Buckley (2020)) **(B)** The function provided by hydrogel in the regeneration of IVD degeneration, including modulating local inflammation, romoting nucleus pulposus cells proliferation, and regeneration of the intervertebral disk (IVD) **(C,D)** Synthesis of sGAG was found to be dependent on the initial gel composition, with significantly more sGAG being deposited by cells in gels containing higher initial sGAG. **(E)** The sGAG/collagen ratio was found to increase linearly with increasing CS present in the initial gel composition. ((**B–E**) Adapted from Bian et al. (2021)).

immunogenicity of transduced cells (Tripathy et al., 1996; Wallach et al., 2006), and several patients have even died after viral vector administration in clinical trials (Evans et al., 2008). From a safety viewpoint, nonviral vectors and poly micelles are better choices for intervertebral disk gene therapy (**Figure 1**). Zhang et al. developed a new type of hyperbranched polymer (HP) carrier to deliver anti-miR-199a (AMO), combined with biodegradable poly (lactic acid-co-glycolic acid) (PLGA) nanospheres (NS) to sustainably release AMO, and by blocking miR-199a, can upregulate hypoxia inducible factor (HIF)-1α. NF-SMS as a mesenchymal stem cell (MSC)-carrying scaffold can finally promote MSC NP differentiation and inhibit its osteogenic differentiation while enhancing NP tissue regeneration (Feng et al., 2020). Feng et al. also synthesized a mixed composite micelle (MPM) for the delivery of therapeutic plasmid DNA (pDNA), which was verified by *in vitro* and *in vivo* evaluations to improve the transfection efficiency of NP cells. After binding to heme oxygenase-1 (HO-1) pDNA, it can weaken the inflammatory response and increase the production of NP ECM, thereby slowing intervertebral disk degeneration (Feng et al., 2015).

BIOMATERIALS FOR ANNULUS FIBROSUS REPAIR

In the process of low-back pain caused by intervertebral disk degeneration, NP degeneration certainly plays a leading role, but the incomplete AF structure is also one of the reasons for the occurrence and recurrence of low-back pain. According to research, most intervertebral disk degeneration is accompanied by AF damage, mostly after the NP herniation (Tavakoli et al., 2020). At this time, many of the curative effects currently targeted only at NP regeneration will be greatly reduced, such as cell therapy and bioactive factor therapy. Most of these therapies deliver drugs by local injection. After the AF is damaged, it will cause leakage of the injected material, which makes the injected material unable to stay in place for a long time and cannot exert its original effect. The structural integrity of the AF is the basis for the NP to maintain hydrostatic pressure. So, even if the NP is perfectly regenerated with AF unrepaired, it will cause the NP to herniate again under the action of axial pressure.

Therefore, scientists have long recognized the importance of AF regeneration. At the earliest, scientists used customized and personalized sutures to suture AF fractures or used polymer

meshes and anchored them on the adjacent vertebral bones (Bailey et al., 2013; Vukas et al., 2015; Bowles and Setton, 2017). However, these two types have not been widely used due to the long operation time and high operation cost, and some studies believe that this treatment can only reduce the pain and the rate of re-herniation of the NP for a certain period but cannot restore the original structure and function of the AF and accelerate the degeneration risks of the intervertebral disk (Trummer et al., 2013; Choy et al., 2018).

Hydrogel Material

Aiming at the idea of local repair, the biological patch applied to AF has been extensively studied. At present, several natural polymers or synthetic biological materials have been proven to effectively reconstruct the damaged structure of AF and prevent NP from hemiation again. For example, a hydrogel, a natural polymer, can be used for both NP and AF regenerations. Peng et al. developed an injectable genipin cross-linked acellular AF hydrogel (g-DAF-G) and proved that it has better biocompatibility, biological activity, and higher mechanical strength than a non-crosslinked acellular AF hydrogel, providing a simple and quick treatment alternative for repairing AF damage or tear (**Figure 3**) (Peng et al., 2020a). Another study found that, by adjusting the concentration of cross-linked genipin and changing the cross-linking conditions, its physical and chemical properties can be controlled to meet the different requirements for restoring the AF and NP tissue (Wang et al., 2020). There has also been a study on the optimal injection time of the hydrogel (Liu Z. et al., 2020). The study selected rhesus monkeys to construct a model of intervertebral disk degeneration, used MR to evaluate degeneration degree, and proved that the moderate degenerative stage (T1ρ value from 95 to 80 ms) may be the best time for hydrogel injection for regenerative intervention. Fibrin gel is also considered one of the most commonly used natural polymers in AF regeneration. Because AF tissue is rich in collagen, it has a lower immune rejection response. Cruz et al. studied the mechanical properties of genipin-cross-linked fibrin gels formed at different genipin concentrations (Cruz et al., 2017). The results showed that, as the genipin concentration increased, the compressive strength and shear modulus of the gel increased, surpassing the natural AF tissue. However, the improvement of the mechanical properties of fibrin gel will bring certain side effects, resulting in a decrease in the survival rate of local cells, because the gel is too hard and will hinder the supply of nutrients. Studies have found that 6% genipin can maintain a good cell survival rate and achieve sufficient mechanical strength. Another study found that high-density collagen gel (HDC) cross-linked with riboflavin can also be used for AF repair (Moriguchi et al., 2018). The study compared the disk height index (DHI), the size and the hydration of the NP of the untreated group, the cross-linked HDC group, and the cross-linked HDC group injected with AF cells after 5 weeks, and found that the average DHI of the two HDC gel groups exceeded that of the control group at 5 weeks. Compared with the cell-free HDC gel, the HDC gel loaded with AF cells had an acceleration repair the role of sealing. It has been proven that HDC gel loaded with AF cells has a better ability to repair ring defects after acupuncture than cell-free gel. Borem et al. proved that the addition of Interlamellar matrix (ILM) GAG can also effectively improve the ability of the patch to resist impact loads and can prevent natural IVD tissues from herniating during the application of super-physiological load (5.28 ± 1.24 MPa), which is a repair strategy that can be used for the AF of focal ring defects (Borem et al., 2019). In addition, many biosynthetic materials also show certain advantages in AF repair, such as D, l-acryloyl ester and trimethyl carbonate can have morphological memory function, poly (trimethylene carbonate) (PTMC) combined with elastic PU film can prevent bovine NP from protruding again within 14 days under dynamic load, and PCL triol malate can be degraded, so that the mechanical properties of the fiber ring can be adjusted (Pirvu et al., 2015).

In recent years, the research on hydrogels for the repair of fibrous annulus has become more and more in-depth. Peng et al. used bovine fibrous annulus acellular tissue matrix to make a hydrogel, and the integrin-mediated RhoA/LATS/YAP1 signaling pathway can promote the specific differentiation of stem cells into AF for AF repair (Peng et al., 2021). In addition, Liu et al. used the bionic structure to prepare the anisotropic wood cellulose hydrogel, which is mainly responsible for stress buffering and energy absorption (at least ~60% energy dissipation) just like the AF tissue (Liu et al., 2021). However, due to poor adhesion or low failure strength between hydrogels and wet tissue surface, DiStefano et al. developed a double-modified glycosaminoglycan to covalently bond hydrogels to AF tissue, thus optimizing the sealing method of AF defect (DiStefano et al., 2020).

Nanofiber Material

Some studies believe that both biological patches and suture technology only strengthen the AF but do not treat the inflammation that occurs in the AF (Wang et al., 2021). In this study, a PLGA/polycaprolactone (PCL) Zdextran (DEX) composite film loaded with testicular plastid extract (PTE) was prepared by electrospinning through an *in vitro* inflammation model. The cytocompatibility and anti-inflammatory effect of the material were verified, and we found that P10P8D2 (PLGA 10 g, PCL 8 g, DEX 2 g) composite nanofiber membranes exhibited the most uniform diameter distribution, best mechanical properties, moderate degradation rate, and best cell compatibility characteristics. It can simultaneously exhibit anti-inflammatory and cell proliferation promoting effects. Another studies have found that fibrosus poly (ether carbonate carbamide) urea (PECUU) scaffolds can regulate the differentiation of amniotic fluid-derived stem cells (AFSCs) attached to scaffolds by adjusting the changes in fiber size and elasticity of scaffolds (Zhu et al., 2016; Chu et al., 2021). On a scaffold with large fibers and strong elasticity, the expression of phenotypic marker genes in the outer annulus is upregulated; on a scaffold with small fibers and low elasticity, the expression of phenotypic marker genes in the inner annulus is enhanced. It has been proven that this is controlled by activating the CAV1-YAP mechanical transduction axis. Another study reached a similar conclusion. They proved that YAP-related proteins play a key role in

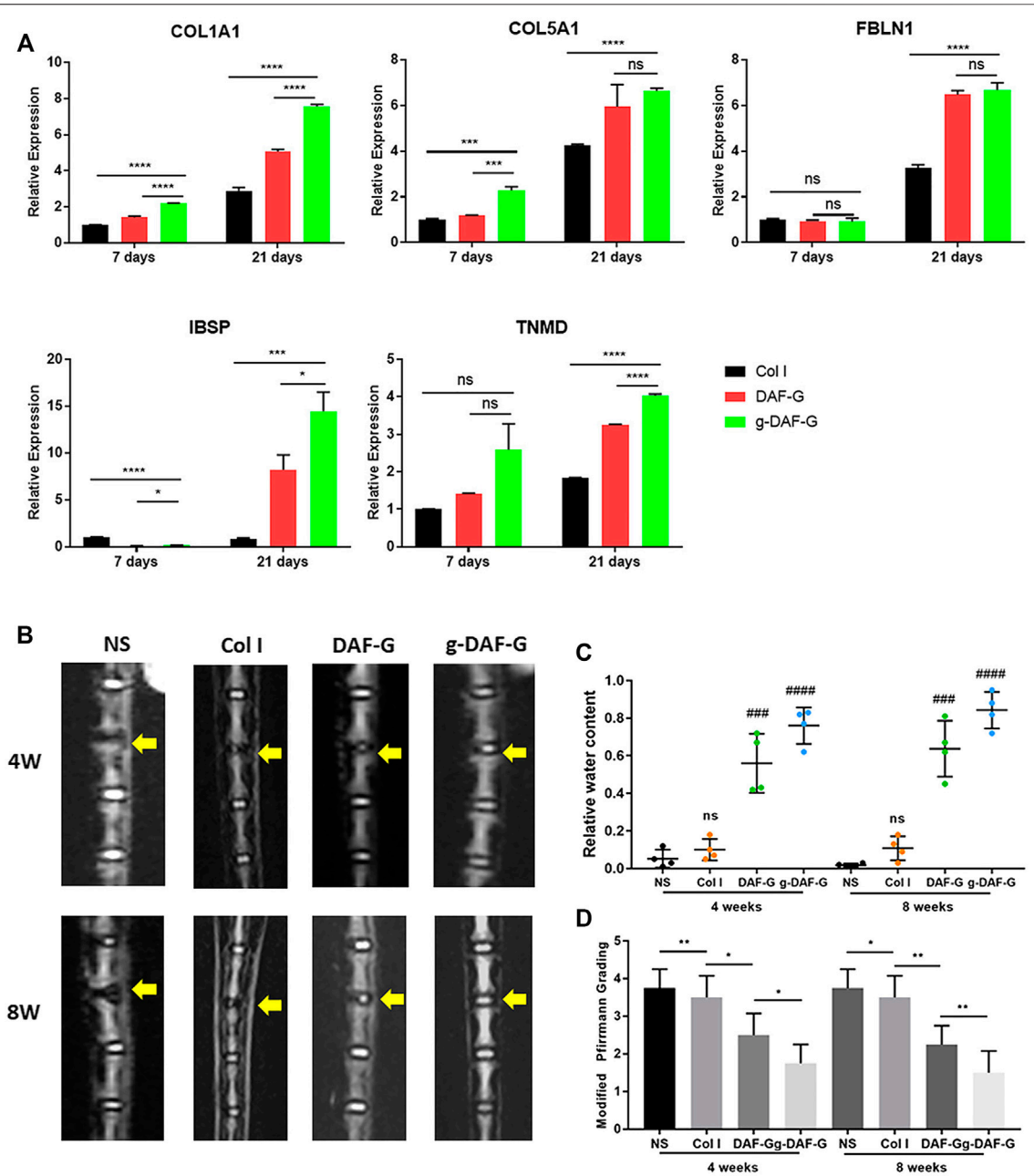

FIGURE 3 | (A) The level of expression of AF-specific genes (collagen-1A1(COL1A1), collagen-5A1(COL5A1), fibulin-1 (FBLN1), integrin-binding sialoprotein (IBSP), and tenomodulin (TNMD)) was significantly higher in the DAF-G and g-DAF-G groups than Col I group on Day 21, which indicated the potential induction of directing specific differentiation of hBMSCs towards AF cells on DAF-G and g-DAF-G hydrogels. **(B)**The T2-weighted images showed that intervertebral space became narrower and the signal intensity of the NP region sharply declined in normal saline (NS) group as compared with the adjacent and intact disks. **(C)** Quantitative analysis showed that relative water content of DAF-G and g-DAF-G groups were larger than the Col I gel and the NS groups, indicating a potential regenerative function of AF-derived hydrogels on AF tissue defect. **(C,D)** The restorative effect analyzed by quantitative analysis and modified Pfirrmann grading was better in g-DAF-G than DAF-G group, revealing that the mechanical strength improved by genipin might be a vital factor in AF repair. **((A–D)** Adapted from Peng et al. (2020a)).

influencing the differentiation direction of AFSCs (Chu et al., 2019). Liu et al. also contributed to the directional differentiation of AFSCs (**Figure 4**) (Liu et al., 2015). They proved that, compared with random stents, aligned fiber PU scaffolds can make AFSCs elongated and better aligned and increase the expression of collagen I and the proteoglycan matrix, providing a favorable microenvironment for the cells of the outer layer of AF cells. In summary, such a scaffold can effectively induce changes in cell shape, adhesion, and expression of ECM by adjusting fiber size so that engineered AF tissue has a hierarchical structure close to that of natural AF tissue (Zhou et al., 2021). Chen Liu et al. further improved the

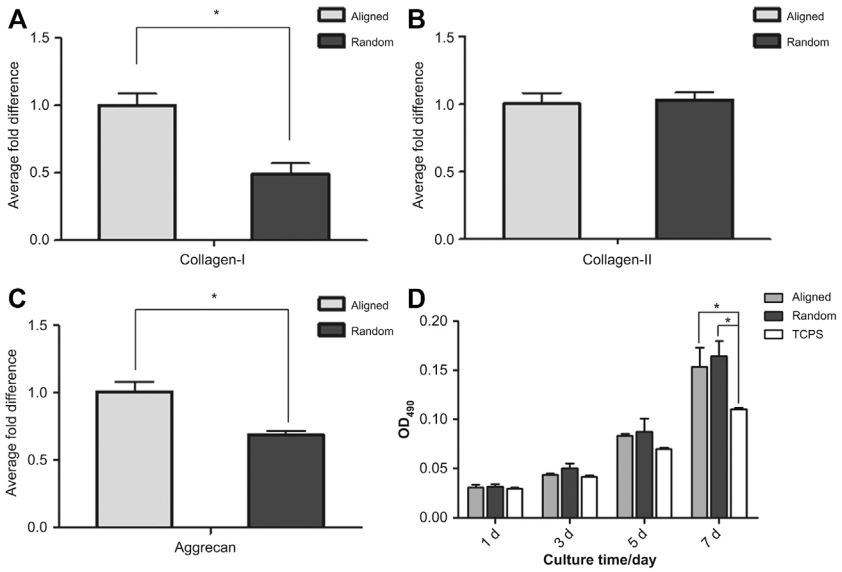

FIGURE 4 | (A) Real-time quantitative PCR was performed to compare the expression of collagen-I, collagen-II and aggrecan genes in AFSCs cultured on aligned and random scaffolds. After 7 days of culture, the expression level of collagen-I in AFSCs cultured on aligned scaffolds was almost twice that of cells grown on random scaffolds. **(B)** The expression of collagen-II was similar in both AFSCs cultured on aligned and random scaffolds. **(C)** The expression pattern of aggrecan was similar to that of collagen-I; cells cultured on aligned scaffolds had approximately 0.4 times higher aggrecan gene expression than those grown on random scaffolds. **(D)** There was no apparent difference in cell proliferation between AFSCs cultured on aligned scaffolds and those on random scaffolds. (**(A–D)** Adapted from Liu et al. (2015)).

PECUU nanofiber scaffold (Liu Y. et al., 2020). They found that PECUU is compatible with the mechanical properties of the natural AF ECM but lacks the biological activity of the natural ECM. The decellularized AF matrix (DAFM) has good biocompatibility and biodegradability and has been proven to promote the secretion of AF-related ECM. It uses coaxial electrospinning technology to manufacture a DAFM/PECUU hybrid electrospinning stand. It was also proved that the gene expression and ECM secretion of type I and II collagens and proteoglycan of the annulus-derived stem cells cultured on the DAFM/PECUU electrospun scaffold exceeded that of the PECUU fiber scaffold. In another study, a new type of scaffold made of PCL was manufactured by 3D printing technology (Christiani et al., 2019). This new type of scaffold can also effectively simulate the structure and biomechanical properties of natural tissues. Annulus fibroblasts can attach and diffuse on it, and type I collagen, aggrecan, and aponeurotic protein, a protein marker specific to AF, can be effectively expressed. Cell sheet rolling system (CSRS) has also been used in manufacturing AF. Shamsah et al., 2019 used CSRS technology to make an electrospun fiber scaffold comprising a synthetic biopolymer mixture of PCL and poly (L-lactic acid) acid (PLLA), which realizes the anatomical structure of the AF with a complete 3D circular structure for the first time, and proved that bovine annulus cells can maintain vitality on it (Shamsah et al., 2019).

Biomaterials for Cell Therapy

A major advantage of biomaterials is that they can be used to deliver cells. Cell therapy is a promising therapy that can be divided into endogenous and exogenous cell therapies (**Figure 1**). Endogenous cell therapy refers to local injection of cells to produce biologically active factors or direct injection of biologically active factors to stimulate *in situ* cell regeneration, while exogenous cell therapy regenerates AF by directly injecting annulus fibroblasts or stem cells that can be induced to differentiate into annulus fibroblasts. Because AF is a cell-deficient structure, coupled with the local inflammation caused by intervertebral disk degeneration, the number of AF cells *in situ* is further reduced. When stimulated by biologically active factors, it is not enough to proliferate and differentiate to compensate for the local inflammation of AF. This is the most severe challenge of endogenous cell therapy. The most important limitation of exogenous cell therapy is the poor retention of cells at the injection site. This is caused by the loss of anchorage, called anoikis, which can cause cell death (Discher et al., 2009).

Mesenchymal stem cell therapy is currently the most studied type of exogenous cell therapy (Sakai and Andersson, 2015). Some studies have reported that the injection of mesenchymal stem cells aggravates the degree of intervertebral disk degeneration (Vadala et al., 2012). This is because the cells injected in this study leaked. In most studies that did not leak, bone marrow mesenchymal stem cells (BMSCs) can effectively differentiate into intervertebral disk cells, promote the synthesis of intervertebral disk ECM (Chiang et al., 2019), and improve the clinical outcome of patients with intervertebral disk degeneration (Sun et al., 2019). Therefore, many scholars have recognized the idea that mesenchymal stem cells can regenerate intervertebral disks. At present, many researchers have focused on how to improve the delivery method of cells, how to induce the directional differentiation of mesenchymal stem cells, and how the delivered cells can maintain their biological activity for a longer time (Tibiletti et al., 2014). After years of exploration,

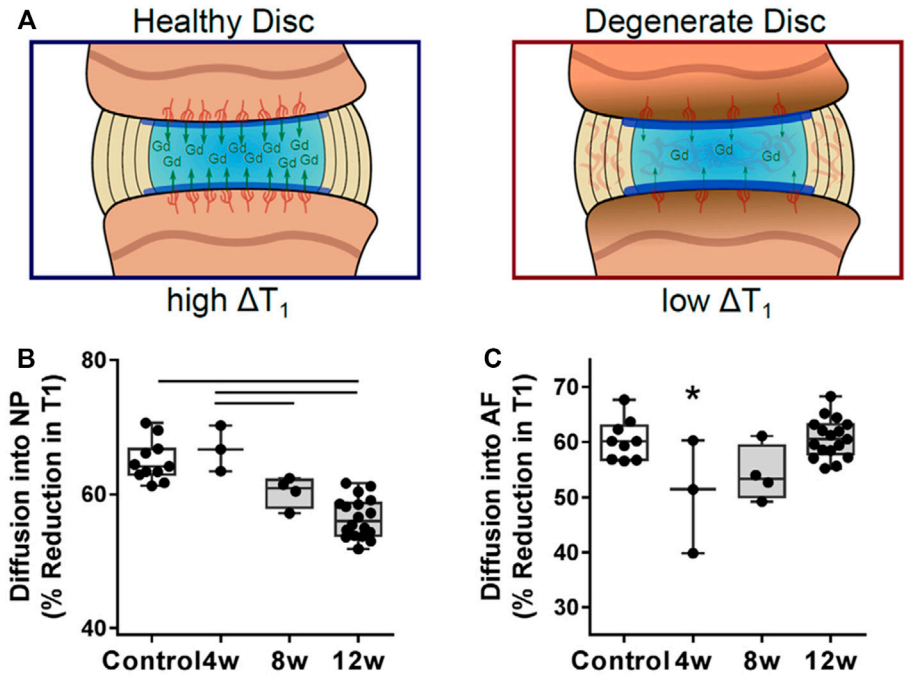

FIGURE 5 | (A) The change in T1 relaxation time within the intervertebral disk after administration of the contrast agent gadodiamide **(B)** Within the NP, gadodiamide diffusion into the disk progressively decreased and was significantly lower at 12 weeks compared with healthy controls. **(C)** Diffusion into the AF was significantly reduced at 4 weeks post-puncture, followed by a return to control levels. (**(A–C)** Adapted from Ashinsky et al. (2020)).

researchers have discovered that biomaterials are effective carriers for cell therapy (From the American Association of Neurological Surgeons et al., 2018). More and more engineering materials, including natural polymers, synthetic polymers, and their combinations, have been applied to intervertebral disk repair (Peng et al., 2020b). This is because biological materials can isolate these cells used for intervertebral disk regeneration from the inflammatory environment or other factors that cause the harsh biological environment of the intervertebral disk and can keep these cells at the injection site (Bertram et al., 2005). Therefore, how different materials affect stem cells is the focus of current research. Compared with cell therapy for NP regeneration, there are relatively few researchers on cell regeneration therapy for the AF. This is also related to the high complexity of the AF structure and the higher requirements for balancing mechanical and biological properties. Bhunia et al. created a multi-layer disk-shaped stratum corneum structure based on silk protein that comprises concentric lamellar layers, which mimics the native hierarchical structure of AF, and can effectively support cells' proliferation, differentiation, and deposition of ECM, which can promote AF regeneration (Bhunia et al., 2018). Adding to the structure of the material, the biologically active factors added to the material also play an important role in the efficacy of cell therapy. Blanquer et al. found that adding transforming growth factor (TGF)-β3 to an AF scaffold constructed with PTMC by stereolithography can support the differentiation of human adipose stem cells into AF (Blanquer et al., 2017). Fibrin gel inoculation can better the distribution and proliferation of adipose stem cells and the production of AF-like matrix. Not only is the production of sulfated sGAG and collagen significantly upregulated but the formed collagen is also oriented and arranged into bundles in the designed pores. Although natural polymers generally have better biocompatibility and better similarity to natural microstructures and ingredients, their mechanical properties are often limited. Therefore, a synthetic matrix with a good composition and controllable biodegradability is studied. Pirvu et al. developed a PTMC scaffold covered with a PU membrane and planted with human BMSCs, which can withstand dynamic loads, restore the fractured bovine AF tissue of the height of the intervertebral disk, prevent NP protrusion, and differentiate *in situ* (Pirvu et al., 2015).

Although exogenous cell therapy has achieved good results in AF regeneration, these cell carriers made of natural polymers or synthetic polymers remain foreign bodies compared to the human body, which can cause more or less immune rejection. Concurrently, the process of delivering these materials to the degenerated intervertebral disk of the human body is an invasive operation that will cause secondary damage to the AF and NP. Therefore, endogenous cell therapy based on the concept of inducing *in situ* cell regeneration and proliferation should be the main direction of future researchers' efforts. At present, researchers have found that using the homing effect of stem cells can effectively overcome the deficiencies of endogenous cell therapy (From the American Association of Neurological Surgeons et al., 2018). BMSCs homing is the process of recruiting cells from the initial biological environment to damaged or pathological tissues. When stem cells are

stimulated by a certain biologically active factor, they are mobilized into the peripheral bloodstream and migrate to damaged tissues or organs (Fong et al., 2011). However, the current understanding of the exact process and mechanism of how BMSCs are mobilized and guided to the position of the effector remains incomplete. However, researchers believe that BMSCs are jointly guided by multiple cell signaling molecules, and the damaged tissue itself expresses unique receptors or ligands to promote the penetration of BMSCs into the affected area (Sordi, 2009). At present, it has been proven that there are various growth factors and chemokines that can induce the migration of mesenchymal stem cells, such as tumor necrosis factor-α, interleukin-1β (IL-1β) (Ponte et al., 2007), insulin-like growth factor-1 (IGF-1), and platelet-derived growth factor-AB (PDGF-AB), etc., but these have an inducing-migration effect on various stem cells, and researchers have found that the chemokine that has the greatest impact on BMSCs is RANTES (also known as CCL5), Macrophage-derived chemokine (MDC), and stromal cell-derived factor-1 (SDF-1), and these are all elevated in degenerative disk tissues (Pattappa et al., 2014). However, it is frustrating that studies by Tam et al. and Cunha et al. found that the ability of stem cells to enter the body through intravenous injection is relatively limited (Tam et al., 2014; Cunha et al., 2017). This may be related to the lack of blood vessels in the intervertebral disk, but, in human degenerated intervertebral disks, there are many new blood vessels that grow in, which may not be simulated by animal experiments, and these new blood vessels may potentially promote BMSCs, reaching the damaged area and promoting regeneration.

BIOMATERIALS FOR CARTILAGE ENDPLATE REPAIR

Endplate is the main way for metabolites to enter and exit intervertebral disk (Malandrino et al., 2014), and an insufficient supply of essential nutrients and waste accumulation are often considered important factors inducing intervertebral disk degeneration (**Figure 5**) (Ashinsky et al., 2020). Calcification of endplate cartilage and occluded nutrient canals increase with age (Bernick and Cailliet, 1982). If the endplate is hardened or thickened, biomaterials implanted for disk repair may not have the desired effect. Therefore, biomaterials that restore the structure and function of the disk may not be sufficient, and the patency of the endplate requires consideration. In earlier studies, disk repair materials generally focused only on maintaining the structural and mechanical properties of the endplate. Ishiguro et al. developed a scaffold-free tissue-engineered construct (TEC), a 3D matrix comprising high density undifferentiated MSC. Intervertebral disk height, endplate, and AF were maintained 6 months after implantation in a rat model of disk degeneration, and age-related biomechanical impairment was reduced (Ishiguro et al., 2019). With the development of research, the importance of interface integration with cartilage endplates during disk repair has been greatly considered. Hamilton et al., *in vitro*, formed a three-phase construct comprising NP, CEP, and a calcium polyphosphate (CPP) matrix (as a bone substitute). After 8 weeks of culture, a continuous layer of NP tissue was formed and fused with the underlying cartilage tissue, which, in turn, was integrated with porous CPP to improve the interface properties of bone replacement and IVD tissue (Hamilton et al., 2006). In a recent study, Chong et al. attempted to construct a model of AF-cartilage interface *in vitro*, using contact co-culture from outer AF cells inoculated with an angular layer, multilayer PC PU scaffold, and articular chondral cells. After a few weeks, the OAF tissue was integrated with the cartilage and like the natural interface. The apparent tensile strength of the *in vitro* interface was also significantly increased, and it is expected to achieve clinical overall disk replacement by adding cartilage endplate repair (Chong et al., 2020). Currently, there are few studies on the repair and regeneration of cartilage endplates among intervertebral disk repair materials, but the importance of cartilage endplates in intervertebral disk repair has been discovered by more and more researchers. It is believed that there will be more studies on cartilage endplate repair in the future.

BIOMATERIALS FOR INTERVERTEBRAL DISK REPAIR USING COMBINATION STRATEGIES

Intervertebral disk degeneration is a process in which the cartilage endplate, NP, AF, or biological environment co-occur with pathophysiological changes. The upper and lower facet joints and surrounding muscles can even undergo degeneration. Therefore, study on intervertebral disk regeneration should not only consider repairing one of them but should be extensively repaired to completely eradicate the low-back pain symptom. The above-mentioned cell therapy and tissue engineering methods have only discussed the impact on a single structure in various studies, but, in fact, their impact on the intervertebral disk is all-round—it is just that the impact on other structures is not significant or has no clinical significance for the time being. Therefore, it is imperative to find a way to regenerate the intervertebral disk in an all-round way or to organically integrate the above-mentioned structural regeneration methods.

Eliminating the inflammatory environment and restoring the original ECM state are considered effective methods to improve the intervertebral disk in an all-round way (Hofmann et al., 2018). To achieve this goal, the degenerated intervertebral disk must be transformed into a physiological state. Potential strategies include eliminating pro-inflammatory cytokines and proteases in the ECM; reversing the gene expression of pro-inflammatory cytokines and proteases in the resident intervertebral disk cells; and stimulating the resident intervertebral disk cells to produce new ECM. Based on this strategy, Guo found that various growth factors can regulate ECM synthesis, including the inhibition of inflammation and downregulation of degrading enzymes (Guo et al., 2021). However, growth factors, including TGF-β, fibroblast growth factor (FGF), and IGF-1 may induce unwanted blood vessel growth, thereby accelerating the process of intervertebral disk degeneration. Only GDF-5 can effectively

TABLE 1 | Summary of various biomaterials for nucleus pulposus repair and their functions.

Material type	Material composition	Target cell/gene	*In vivo* experimental model	Repair effect	References
Nanofiber	PC-PU	Bovine NPCs and human MSCs	Bovine whole IVD organ culture model	Restore the mechanical properties of enucleated disks and delay further degradation of natural disk tissue	Li et al. (2016)
	PLLA NF-SMS	Rabbit MSCs	Rabbit lumbar degeneration model	Help mesenchymal stem cell adhesion, proliferation and np-like differentiation, promote transmitter transmission and new ECM formation	Feng et al. (2020)
Hydrogel	Dextran, gelatin and poly (ethylene glycol)	Porcine and rat NPCs	Rat tail IVD and porcine disk degeneration model	Support long-term cell retention and survival in the rat IVDs, and facilitate rehydration and regeneration of porcine degenerative NPs	Gan et al. (2017)
	Poly (ethylene glycol) dimethacrylate	NA	Bovine disk model	Has good mechanical properties and tissue integration ability, and maintain the height of the disk	Schmocker et al. (2016)
	Adducts of fibrinogen and poloxameric block copolymers called Tetronic 1307	Porcine NP–SCs	NA	Cell proliferation and differentiation have nothing to do with matrix hardness, but matrix modulus can affect the fate of NP-SCs	Navaro et al., 2015
	Poly (ethylene glycol), IKVAV and AG73 peptides	Human NP cells	NA	Close control of peptide selection and peptide presentation can lead to a more juvenile NP cell phenotype regardless of substrate stiffness	Barcellona et al. (2020)
	PFTBA and alginate	Human NP cells	Mouse disk degeneration model	Promote NP cell survival and proliferation, restore the disk height and the ECM, indicate its beneficial effect on alleviating disk degeneration	Sun et al. (2016)
Gene therapy	Hyperbranched polymer and AMO	Rabbit MSCs/ MiR-199a	Rabbit lumbar degeneration model	Promote MSC nucleus pulposus differentiation and inhibit its osteogenic differentiation, and enhance nucleus pulposus tissue regeneration	Feng et al. (2020)
	MPM and HO-1 pDNA	Rabbit NP cells/ HO-1 pDNA	Rat tail disks	Weaken the inflammatory response and increase the production of NP ECM, slow the degeneration of the intervertebral disk	Feng et al. (2015)

alleviate intervertebral disk degeneration without inducing the ingrowth of blood vessels. Saberi et al. found that mitochondrial dysfunction is also one of the factors in intervertebral disk degeneration (Saberi et al., 2021). This is because mitochondria are the main source of cellular energy supply and the main source of reactive oxygen species, which is the main cause of the inflammatory environment of the intervertebral disk. First, it has been proven that MitoQ, MitoTEMPO, SkQs, XJB-5-131, and other regulating mitochondrial functions can effectively play the role of intervertebral disk regeneration. Bai et al. also reached a similar conclusion. They found that hydrogel scaffold-carrying rapamycin can effectively eliminate the active oxygen components in the microenvironment of the intervertebral disk, thereby playing a role in intervertebral disk regeneration (Bai et al., 2020). Another study found that acid-sensitive ion channels (ASICs), as key receptors for extracellular protons of central and peripheral neurons, are related to intervertebral disk degeneration and a decrease in microenvironmental pH. By downregulating the expression of ASIC2 and ASIC4 in human IVD, it can slow down the senescence of intervertebral disk cells. Several other studies found that CCL25 (Stich et al., 2018), colony-stimulating factor (Abdel Fattah and Nasr El-Din, 2021), anti-inflammatory drug etanercept (Li et al., 2020), chitosan/poly-γ-glutamate nanocomplex (Cunha et al., 2020), HIF (Kim et al., 2021), stromal cell-derived factor-1α (Zhang et al., 2018) and containing platelet plasma (Chang et al., 2020; Fiani et al., 2021) can play the role of intervertebral disk regeneration by inhibiting the local inflammatory environment. As mentioned earlier, some cells can also stimulate the proliferation of endogenous stem cells or progenitor cells by secreting a broad spectrum of biologically active factors to produce new ECM. Sun et al. found that connective tissue growth factor (CTGF) and TGF-β3 can effectively induce the corresponding BMSCs to differentiate into NP-like cells and fibroblast-like cells and rebuild the ECM (Sun et al., 2021). In addition, more and more experimental results show that stem cell-derived exosomes have potential regenerative capabilities by promoting cell proliferation, enhancing angiogenesis, promoting the restoration of ECM homeostasis, inhibiting inflammation and other unknown effects (Hingert et al., 2020; Hu et al., 2020). Some of these beneficial mechanisms can also be implemented in repairing intervertebral disk degeneration.

In addition, replacing the entire intervertebral disk is considered one of the potential methods for regenerating the entire intervertebral disk. In fact, a long time ago, researchers have studied the clinical effect of artificially synthesized intervertebral disks directly replacing severely degenerated intervertebral disks, but the results obtained are negative because this synthetic intervertebral disk only considers the mechanical properties of the intervertebral disk without considering the biocompatibility—this product is slowly being phased out. However, in recent years, a heterogeneous decellularized scaffold has attracted the attention of researchers (Hensley et al., 2018). Since this type of scaffold is derived from the body of cattle, worrying about the shortage of donors is needless. Due to the acellular treatment, it lacks immunogenicity and has achieved good results in many

TABLE 2 | Summary of various biomaterials for AF repair and their functions.

Material type	Material composition	Target cell/gene	*In vivo* experimental model	Repair effect	References
Surgical suture	Anulex Technologies, Minnetonka, MN	NA	Patients with lumbar disc herniation	Reduce the need for subsequent reherniation surgery while retaining the benefits of discectomy with no increased risk for patients	Bailey et al. (2013)
	an anular closure device	NA	Patients with lumbar disc herniation	Provide very low rates of disk reherniation and exhibit excellent disk height maintenance and sustain disability, leg pain, and back pain improvement within a 24 months postoperative study period	Vukas et al. (2015)
Hydrogel	g-DAF-G	Human BMSCs	Rat tail acupuncture degenerative model	Exhibit well biocompatibility, great bioactivity, and much higher mechanical strength	Peng et al. (2020a)
	Genipin cross-linked fibrin gel (FibGen) adding PDLGA	NA	NA	FibGen is highly modifiable with tunable mechanical properties that can be formulated to be compatible with human AF compressive and shear properties and gelation kinetics and injection techniques compatible with clinical discectomy procedures	Cruz et al. (2017)
	HDC cross-linked with riboflavin	AF cell	Needle puncture-induced degeneration rat model	AF cell-laden HDC gels have the ability of better repairing annular defects than acellular gels after needle puncture	Moriguchi et al. (2018)
	ILM-GAG	NA	NA	Adding ILM glycosaminoglycan (GAG) can enable the annulus repair patch (AFRP) to withstand stronger impact strength and prevent the nucleus pulposus from herniating again when over physiological load	Borem et al. (2019)
	AF decellularized tissue matrix	Human BMSCs	AF defect rat model	AF specific differentiation of stem cells and AF tissue regeneration	Peng et al. (2021)
	Anisotropic wood cellulose hydrogel	Mouse BMSCs	NA	Possesses imitation and construction of the natural structure, favorable mechanical matching and good biocompatibility and unique mechanical buckling buffer characteristics	Liu et al. (2021)
	Double-modified glycosaminoglycan	NA	*Ex vivo* bovine model of discectomy	Covalently bond hydrogels to AF tissue to seal AF defect	DiStefano et al. (2020)
Nanofiber	PLGA/PCL DEX	AF cells	*in vitro* inflammation model induced by interleukin (IL)-1β	The nanofiber membrane composed of P10P8D2 and PTE has anti-inflammatory and pro-proliferation effects on AF cells	Wang et al. (2021)
	PECUU	AF-derived stem cells	NA	YAP-related proteins play a key role in influencing the differentiation direction of AFSC. The scaffold can effectively induce changes in cell shape, adhesion and expression of ECM by adjusting the fiber size, so that the engineered AF tissue has a layered structure close to that of natural AF tissue	Chu et al. (2019)
	DAFM/PECUU-blended electrospun scaffolds	AF-derived stem cells	NA	Gene expression and ECM secretion of collagen type I and II and aggrecan from AF-derived stem cells cultured on DAFM/PECUU electrospun scaffolds were higher than from those on PECUU fibrous scaffolds	Liu et al. (2020)
	PCL	Bovine AF cell	NA	Bovine AF cells can be attached and diffused on it, and type I collagen, aggrecan, and AF specific protein markers can be effectively expressed	Christiani et al. (2019)
	PCL and PLLA	Bovine AF cell	NA	For the first time, a custom-built Cell Sheet Rolling System (CSRS) was utilized to create a 3D circular lamellae construct that mimics the complex AF tissue and which overcomes this translational limitation	Shamsah et al., 2019
Cell therapy	Silk protein-based multilayered, disc-like angle-ply construct	Porcine AF cells and hMSCs	NA	The constructs supported cell proliferation, differentiation, and ECM deposition resulting in AF-like tissue features based on ECM deposition and morphology	Bhunia et al. (2018)
	PTMC and TGF-β3	HASCs	NA	Production of sGAG and collagen was significantly upregulated, but the formed collagen was also oriented and aligned into bundles within the designed pore channels. The differentiated hASCs seeded with fibrin gel were also found to have a comparable sGAG:collagen ratio and gene expression profile as native AF cells	Blanquer et al. (2017)
	PTMC and PU	Human BMSCs	AF rupture repair in a bovine organ culture annulotomy model	It can withstand dynamic loads, restore the height of the intervertebral disc, prevent the protrusion of the nucleus pulposus, and has the ability to differentiate *in situ*	Pirvu et al. (2015)

TABLE 3 | Summary of various biomaterials for cartilage endplate repair and their functions.

Material type	Material composition	Target cell/gene	*In vivo* experimental model	Repair effect	References
ADSC-TEC		Rat ADSCs	Rat disc degeneration model	Disc height, endplate, and annulus fibrinoid structure were maintained, and age-related biomechanical impairments were reduced	Ishiguro et al. (2019)
NP, CEP, and CPP substrate		Bovine articular chondrocytes and NP cells	NA	A continuous layer of NP tissue was formed and fused with the underlying cartilagenous tissue, which in turn was integrated with the porous CPP to improve the interface between the bone substitute and THE IVD tissue	Hamilton et al. (2006)
Outer AF cells inoculated with angular layer, multilayer PC PU scaffold and articular chondral cells		Bovine outer AF cells and articular chondral cells	NA	The outer AF tissue was integrated with the cartilage and similar to the natural interface. The apparent tensile strength of the *in vitro* interface was also significantly increased	Chong et al. (2020)

animal experiments (Fiordalisi et al., 2020; Norbertczak et al., 2020). However, the mammals used in these experiments are all four-legged, and the spinal column is parallel to the ground, so the load on their disks is not comparable to that in humans. So far, no corresponding clinical studies have proven that the acellular scaffold can effectively replace the function of the natural disk in humans.

Although most of the above regeneration strategies have achieved positive results, most of the treatment methods can only be applied to the early stages of intervertebral disk degeneration because most studies have proven that, whether it is stem cell therapy or growth factor therapy, for late degeneration, the harsh local environment of the intervertebral disk will cause the rapid loss of the biological activity of the injected substance, and then will cause these effective treatments to fail to achieve their intended effects. Therefore, the concept of intervertebral disk degeneration should be considered. It should be regarded as a disease like diabetes and hypertension. Tertiary prevention should be initiated, starting with primary prevention, such as the cause of the disease, and strengthening publicity and education to inform people of the seriousness of the disease and start early prevention. However, now, because the early degeneration of the intervertebral disk is symptomless and difficult to find, the current basic research requires an imperative development to find the biomarkers of early intervertebral disk degeneration and to intervene in time while avoiding the widespread occurrence of low-back pain in the world.

Although we advocate early intervention, the early symptoms are mild, and most of the current methods of administration are local injections. This is an invasive operation that will damage the surrounding muscles and joint capsule. If you want to inject the NP, it will definitely damage the AF. The damage to these tissues all has the risk of aggravating intervertebral disk degeneration, and whether the therapeutic effect brought by local injection of drugs can offset the risk of this damage remains unexplored. Therefore, finding a better drug delivery method with less trauma is imperative.

PRECLINICAL STUDY OF BIOMATERIALS FOR INTERVERTEBRAL DISK REPAIR

In preclinical studies of intervertebral disk repair, rats are the most common animal model. Barcellona et al. prepared a peptide functionalized hydrogel for the study of intervertebral disk repair (Barcellona et al., 2021). The gel has a stiffness similar to that of the degenerated nucleus pulposus (~10 kPa), which is conducive to simulating the cell living environment and playing a certain mechanical support role. After functionalization with laminin-mimetic peptides IKVAV and AG73, it can provide the delivered cells with biomimetic cues in order to promote phenotypic expression and increase biosynthetic activity. In the rat intervertebral disk degeneration model, it was also confirmed that after the gel was combined with primary NP cells, the cell retention rate and survival time were improved, and the degeneration was significantly improved. In the process of intervertebral disk repair, excessive local inflammatory reaction will greatly hinder the regeneration of intervertebral disk tissue. Therefore, in order to make the repair of the intervertebral disk proceed smoothly, many researchers have also tried *in vivo* experiments to suppress the inflammatory reaction that occurs during the degeneration. Bian et al. developed a hydrogel microsphere with an elastic modulus of 25.23 ± 2.58 kPa, which is sufficiently rigid to protect the cells from shear force during injection and avoid other mechanical stresses during application. Subsequently, the hydrogel microspheres loaded with NP cells and pro-inflammatory factor expression inhibitors were injected into the degenerated intervertebral disks of rats. It was observed that the reduction of inflammatory factors and the increase in the proliferation activity of NP-loaded cells and the increase in ECM deposition were all helpful to the regeneration of the intervertebral disk (Bian et al., 2021). While the degeneration of the intervertebral disk produces inflammation, the most urgent problem to be solved is pain. Mohd Isa et al. developed a new rat model of pain caused by intervertebral disk injury and proved that hyaluronic acid hydrogel can reduce inflammation while reducing pain, providing a method for the treatment of back pain caused by intervertebral disk degeneration (Mohd Isa et al., 2018).

The current research of biomaterials is still mainly based on *in vivo* experiments in small animals. The reason is that it is difficult

for materials to achieve sufficient mechanical strength while ensuring biological activity, while *in vivo* researches on large animals are mainly conducted on artificial intervertebral discs, which pay more attention to their long-term mechanical properties and durability. Shikinami et al. developed a flexible artificial intervertebral disc system. Compared with the traditional rigid system composed of a solid plate and a core material, it has been verified in baboons for its long-term durability and biocompatibility. At the same time, it simulates the movement of human intervertebral discs. The mechanical test also proved that the durability can reach a normal person for more than 50 years (Shikinami et al., 2010). The current clinical research on the alternative treatment of intervertebral disc degeneration is mainly total disc replacement, and different artificial disc materials have a certain impact on the clinical efficacy (Coban et al., 2021). At the same time, the high recurrence rate and unclear risk factors for secondary surgery also limit the development of surgery (Perfetti et al., 2021). The clinical transformation of artificial intervertebral discs still needs more in-depth and long-term research.

CONCLUDING REMARKS AND FUTURE PERSPECTIVES

We review the current approaches to biomaterial-based repair of degenerative intervertebral disks, including disk replacement, cell therapy, and gene therapy. **Tables 1–3** summarizes the biomaterials used in various intervertebral disk repair methods and their repair functions. Early studies focused on the restoration of the intervertebral disk structure and ignored the interaction between cells, so the success rate of intervertebral disk repair was not high. In a later study, many researchers began to pay close attention to the use of cell therapy to weaken and repair intervertebral disk degeneration, mainly because most of the cells are mesenchymal stem cells or between intervertebral disk cells. Through biomimetic ECM or form to ECM formation environment, promote cell proliferation and differentiation, thus to achieve the effect of repair of intervertebral disk. Although gene therapy uses viral vectors to treat degenerative disk disease and has achieved certain effects, the main problems of this method include carcinogenesis and immune response. Therefore, non-viral gene vectors are the preferred delivery system, although the transfection efficiency is lower than that of viral vectors. Intervertebral disk degeneration restorative materials mainly include water gel, nanofiber, etc., through the combination can be simulated natural intervertebral disk tissue regeneration of NP in the study, usually has a similar to natural NP material performance elastomer, and in the AF regeneration repair, is more concerned with the toughness of the material, the purpose is to form good sealing effect and prevent NP herniation again. Concurrently, many studies have been conducted to repair the cartilaginous endplate. Because the endplate affects the nutritional and metabolic exchange of the intervertebral disk after the material is implanted, the interface integration of the endplate with the NP and the AF is also important. The specific method is to form the cartilage layer through the chondrogenic differentiation ability of the material, and then fuse with the NP or AF to achieve interface contact. Otherwise, the accumulation of metabolic waste and nutrient deficiency will induce the failure of the repair process. In fact, disk degeneration is not a single degeneration, but the biological environment of the NP, AF or cartilaginous endplate has changed. Therefore, the repair method should be multi-faceted to eradicate the symptoms completely. Currently, biomaterials for repairing intervertebral disks have begun to have multifaceted repair functions, and this combined repair strategy is expected to achieve the overall repair of intervertebral disks. However, notably, research on intervertebral disk regeneration materials still faces many challenges. Requirements for materials with mechanical properties parallel natural intervertebral disk tissue, and after reaching long-term exercise load, they can still maintain a high standard of their structure and function. Concurrently, the materials also need to have the ability to integrate cartilage endplates to achieve the smooth exchange of nutrition and metabolism. In addition, pathophysiologically, circadian rhythm disorders, intervertebral disk cell apoptosis and senescence. Problems such as abnormal autophagy of the inflammatory response also provide great challenges for disk repair with biomaterial. Therefore, to achieve true disk regeneration and repair, both the improvement and development of biomaterial alongside a deeper understanding and study of the pathophysiology of disk degeneration are needed.

AUTHOR CONTRIBUTIONS

All authors listed have made a substantial, direct and intellectual contribution to the work, and approved it for publication.

FUNDING

This work was supported by Tsinghua University-Peking Union Medical College Hospital Initiative Scientific Research Program (20191080871).

REFERENCES

Abdel Fattah, I. O., and Nasr El-Din, W. A. (2021). Granulocyte-Colony Stimulating Factor Improves Intervertebral Disc Degeneration in Experimental Adult Male Rats: A Microscopic and Radiological Study. *Anat. Rec.* 304 (4), 787–802. doi:10.1002/ar.24519

Akkiraju, H., and Nohe, A. (2015). Role of Chondrocytes in Cartilage Formation, Progression of Osteoarthritis and Cartilage Regeneration. *J. Dev. Biol.* 3 (4), 177–192. doi:10.3390/jdb3040177

Ashinsky, B. G., Bonnevie, E. D., Mandalapu, S. A., Pickup, S., Wang, C., Han, L., et al. (2020). Intervertebral Disc Degeneration Is Associated With Aberrant Endplate Remodeling and Reduced Small Molecule Transport. *J. Bone Miner Res.* 35 (8), 1572–1581. doi:10.1002/jbmr.4009

Ashinsky, B., Smith, H. E., Smith, H., Mauck, R., and Gullbrand, S. (2021). Intervertebral Disc Degeneration and Regeneration: a Motion Segment Perspective. *Eur. Cell Mater.* 41, 370–387. doi:10.22203/eCM.v041a24

Bai, J., Zhang, Y., Fan, Q., Xu, J., Shan, H., Gao, X., et al. (2020). Reactive Oxygen Species-Scavenging Scaffold with Rapamycin for Treatment of Intervertebral Disk Degeneration. *Adv. Healthc. Mater.* 9 (3), 1901186. doi:10.1002/adhm.201901186

Bailey, A., Araghi, A., Blumenthal, S., Huffmon, G. V., and Anular Repair Clinical Study, G. (2013). Prospective, Multicenter, Randomized, Controlled Study of Anular Repair in Lumbar Discectomy. *Spine.* 38 (14), 1161–1169. doi:10.1097/BRS.0b013e31828b2e2f

Barcellona, M. N., Speer, J. E., Fearing, B. V., Jing, L., Pathak, A., Gupta, M. C., et al. (2020). Control of Adhesive Ligand Density for Modulation of Nucleus Pulposus Cell Phenotype. *Biomaterials.* 250, 120057. doi:10.1016/j.biomaterials.2020.120057

Barcellona, M. N., Speer, J. E., Jing, L., Patil, D. S., Gupta, M. C., Buchowski, J. M., et al. (2021). Bioactive *In Situ* Crosslinkable Polymer-Peptide Hydrogel for Cell Delivery to the Intervertebral Disc in a Rat Model. *Acta Biomater.* 131, 117–127. doi:10.1016/j.actbio.2021.06.045

Benneker, L. M., Heini, P. F., Alini, M., Anderson, S. E., and Ito, K. (2005). 2004 Young Investigator Award Winner: Vertebral Endplate Marrow Contact Channel Occlusions and Intervertebral Disc Degeneration. *Spine.* 30 (2), 167–173. doi:10.1097/01.brs.0000150833.93248.09

Berg-Johansen, B., Fields, A. J., Liebenberg, E. C., Li, A., and Lotz, J. C. (2018). Structure-function Relationships at the Human Spinal Disc-Vertebra Interface. *J. Orthop. Res.* 36 (1), 192–201. doi:10.1002/jor.23627

Bernick, S., and Cailliet, R. (1982). Vertebral End-Plate Changes With Aging of Human Vertebrae. *Spine.* 7 (2), 97–102. doi:10.1097/00007632-198203000-00002

Bertram, H., Kroeber, M., Wang, H., Unglaub, F., Guehring, T., Carstens, C., et al. (2005). Matrix-Assisted Cell Transfer for Intervertebral Disc Cell Therapy. *Biochem. Biophysical Res. Commun.* 331 (4), 1185–1192. doi:10.1016/j.bbrc.2005.04.034

Bhunia, B. K., Kaplan, D. L., and Mandal, B. B. (2018). Silk-Based Multilayered Angle-Ply Annulus Fibrosus Construct to Recapitulate Form and Function of the Intervertebral Disc. *Proc. Natl. Acad. Sci. USA.* 115 (3), 477–482. doi:10.1073/pnas.1715912115

Bian, J., Cai, F., Chen, H., Tang, Z., Xi, K., Tang, J., et al. (2021). Modulation of Local Overactive Inflammation via Injectable Hydrogel Microspheres. *Nano Lett.* 21 (6), 2690–2698. doi:10.1021/acs.nanolett.0c04713

Binch, A. L. A., Cole, A. A., Breakwell, L. M., Michael, A. L. R., Chiverton, N., Creemers, L. B., et al. (2015). Nerves Are More Abundant Than Blood Vessels in the Degenerate Human Intervertebral Disc. *Arthritis Res. Ther.* 17, 370. doi:10.1186/s13075-015-0889-6

Blanquer, S. B. G., Gebraad, A. W. H., Miettinen, S., Poot, A. A., Grijpma, D. W., and Haimi, S. P. (2017). Differentiation of Adipose Stem Cells Seeded Towards Annulus Fibrosus Cells on a Designed Poly(Trimethylene Carbonate) Scaffold Prepared by Stereolithography. *J. Tissue Eng. Regen. Med.* 11 (10), 2752–2762. doi:10.1002/term.2170

Borem, R., Madeline, A., Vela, R., Jr., Gill, S., and Mercuri, J. (2019). Multi-Laminate Annulus Fibrosus Repair Scaffold With an Interlamellar Matrix Enhances Impact Resistance, Prevents Herniation and Assists in Restoring Spinal Kinematics. *J. Mech. Behav. Biomed. Mater.* 95, 41–52. doi:10.1016/j.jmbbm.2019.03.030

Borrelli, C., and Buckley, C. T. (2020). Injectable Disc-Derived ECM Hydrogel Functionalised with Chondroitin Sulfate for Intervertebral Disc Regeneration. *Acta Biomater.* 117, 142–155. doi:10.1016/j.actbio.2020.10.002

Bowles, R. D., and Setton, L. A. (2017). Biomaterials for Intervertebral Disc Regeneration and Repair. *Biomaterials.* 129, 54–67. doi:10.1016/j.biomaterials.2017.03.013

Chang, Y., Yang, M., Ke, S., Zhang, Y., Xu, G., and Li, Z. (2020). Effect of Platelet-Rich Plasma on Intervertebral Disc Degeneration *In Vivo* and *In Vitro*: A Critical Review. *Oxidative Med. Cell Longevity.* 2020, 1–10. doi:10.1155/2020/8893819

Chen, F., Jiang, G., Liu, H., Li, Z., Pei, Y., Wang, H., et al. (2020). Melatonin Alleviates Intervertebral Disc Degeneration by Disrupting the IL-1β/NF-κB-NLRP3 Inflammasome Positive Feedback Loop. *Bone Res.* 8, 10. doi:10.1038/s41413-020-0087-2

Chen, J., Jing, L., Gilchrist, C. L., Richardson, W. J., Fitch, R. D., and Setton, L. A. (2009). Expression of Laminin Isoforms, Receptors, and Binding Proteins Unique to Nucleus Pulposus Cells of Immature Intervertebral Disc. *Connect. Tissue Res.* 50 (5), 294–306. doi:10.1080/03008200802714925

Chen, J., Xie, J.-J., Jin, M.-Y., Gu, Y.-T., Wu, C.-C., Guo, W.-J., et al. (2018). Sirt6 Overexpression Suppresses Senescence and Apoptosis of Nucleus Pulposus Cells by Inducing Autophagy in a Model of Intervertebral Disc Degeneration. *Cell Death Dis.* 9 (2), 56. doi:10.1038/s41419-017-0085-5

Cheung, K. M. C., Karppinen, J., Chan, D., Ho, D. W. H., Song, Y.-Q., Sham, P., et al. (2009). Prevalence and Pattern of Lumbar Magnetic Resonance Imaging Changes in a Population Study of One Thousand Forty-Three Individuals. *Spine.* 34 (9), 934–940. doi:10.1097/BRS.0b013e3181a01b3f

Chiang, E. R., Ma, H. L., Wang, J. P., Chang, M. C., Liu, C. L., Chen, T. H., et al. (2019). Use of Allogeneic Hypoxic Mesenchymal Stem Cells for Treating Disc Degeneration in Rabbits. *J. Orthop. Res.* 37 (6), 1440–1450. doi:10.1002/jor.24342

Choi, H., Johnson, Z., and Risbud, M. (2015). Understanding Nucleus Pulposus Cell Phenotype: a Prerequisite for Stem Cell Based Therapies to Treat Intervertebral Disc Degeneration. *Curr. Stem Cell Res Ther.* 10 (4), 307–316. doi:10.2174/1574888x10666150113112149

Chong, J. E., Santerre, J. P., and Kandel, R. A. (2020). Generation of an *In Vitro* Model of the Outer Annulus Fibrosus-cartilage Interface. *JOR Spine.* 3 (2), e1089. doi:10.1002/jsp2.1089

Choy, W. J., Phan, K., Diwan, A. D., Ong, C. S., and Mobbs, R. J. (2018). Annular Closure Device for Disc Herniation: Meta-Analysis of Clinical Outcome and Complications. *BMC Musculoskelet. Disord.* 19 (1), 290. doi:10.1186/s12891-018-2213-5

Christiani, T. R., Baroncini, E., Stanzione, J., and Vernengo, A. J. (2019). *In Vitro* Evaluation of 3D Printed Polycaprolactone Scaffolds With Angle-Ply Architecture for Annulus Fibrosus Tissue Engineering. *Regen. Biomater.* 6 (3), 175–184. doi:10.1093/rb/rbz011

Chu, G., Yuan, Z., Zhu, C., Zhou, P., Wang, H., Zhang, W., et al. (2019). Substrate Stiffness- and Topography-Dependent Differentiation of Annulus Fibrosus-Derived Stem Cells Is Regulated by Yes-Associated Protein. *Acta Biomater.* 92, 254–264. doi:10.1016/j.actbio.2019.05.013

Chu, G., Zhang, W., Zhou, P., Yuan, Z., Zhu, C., Wang, H., et al. (2021). Substrate Topography Regulates Differentiation of Annulus Fibrosus-Derived Stem Cells via CAV1-YAP-Mediated Mechanotransduction. *ACS Biomater. Sci. Eng.* 7 (3), 862–871. doi:10.1021/acsbiomaterials.9b01823

Coban, D., Pompliano, M., Changoor, S., Dunn, C., Sinha, K., Hwang, K. S., et al. (2021). Metal-on-Metal versus Metal-On-Plastic Artificial Discs in Two-Level Anterior Cervical Disc Replacement: a Meta-Analysis With Follow-Up of 5 Years or More. *Spine J.* S1529-9430(21)00215-1. doi:10.1016/j.spinee.2021.04.018

Cruz, M. A., McAnany, S., Gupta, N., Long, R. G., Nasser, P., Eglin, D., et al. (2017). Structural and Chemical Modification to Improve Adhesive and Material Properties of Fibrin-Genipin for Repair of Annulus Fibrosus Defects in Intervertebral Disks. *J. Biomech. Eng.* 139 (8), 0845011–7. doi:10.1115/1.4036623

Cui, Z. Y., Shen, L., Gao, X. S., Dong, X. B., and Fu, H. Y. (2020). S-Phase Kinase-Associated Protein-2 (Skp2) Promotes Nucleus Pulposus Cell Proliferation by Inhibition of P27 in Attenuating Intervertebral Disc Degeneration. *Eur. Rev. Med. Pharmacol. Sci.* 24 (6), 2802–2810. doi:10.26355/eurrev_202003_20641

Cunha, C., Almeida, C. R., Almeida, M. I., Silva, A. M., Molinos, M., Lamas, S., et al. (2017). Systemic Delivery of Bone Marrow Mesenchymal Stem Cells for *In Situ* Intervertebral Disc Regeneration. *Stem Cells Translational Med.* 6 (3), 1029–1039. doi:10.5966/sctm.2016-0033

Cunha, C., Teixeira, C., Pereira, C., Ferreira, J. R., Molinos, M., Santos, S., et al. (2020). Modulation of the *In Vivo* Inflammatory Response by Pro- Versus Anti-Inflammatory Intervertebral Disc Treatments. *Int. J. Mol. Sci.* 21 (5), 1730. doi:10.3390/ijms21051730

DALYs, G. B. D., and Collaborators, H. (2017). Global, Regional, and National Disability-Adjusted Life-Years (DALYs) for 333 Diseases and Injuries and Healthy Life Expectancy (HALE) for 195 Countries and Territories, 1990-2016: a Systematic Analysis for the Global Burden of Disease Study 2016. *Lancet.* 390 (10100), 1260–1344. doi:10.1016/S0140-6736(17)32130-X

Discher, D. E., Mooney, D. J., and Zandstra, P. W. (2009). Growth Factors, Matrices, and Forces Combine and Control Stem Cells. *Science.* 324 (5935), 1673–1677. doi:10.1126/science.1171643

DiStefano, T. J., Shmukler, J. O., Danias, G., Di Pauli von Treuheim, T., Hom, W. W., Goldberg, D. A., et al. (2020). Development of a Two-Part Biomaterial Adhesive Strategy for Annulus Fibrosus Repair and *Ex Vivo* Evaluation of Implant Herniation Risk. *Biomaterials.* 258, 120309. doi:10.1016/j.biomaterials.2020.120309

Dudek, M., Yang, N., Ruckshanthi, J. P., Williams, J., Borysiewicz, E., Wang, P., et al. (2017). The Intervertebral Disc Contains Intrinsic Circadian Clocks that

Are Regulated by Age and Cytokines and Linked to Degeneration. *Ann. Rheum. Dis.* 76 (3), 576–584. doi:10.1136/annrheumdis-2016-209428

Eliasberg, C. D., Kelly, M. P., Ajiboye, R. M., and SooHoo, N. F. (2016). Complications and Rates of Subsequent Lumbar Surgery Following Lumbar Total Disc Arthroplasty and Lumbar Fusion. *Spine.* 41 (2), 173–181. doi:10.1097/BRS.0000000000001180

Evans, C. H., Ghivizzani, S. C., and Robbins, P. D. (2008). Arthritis Gene Therapy's First Death. *Arthritis Res. Ther.* 10 (3), 110. doi:10.1186/ar2411

Eyre, D. R., and Muir, H. (1976). Types I and II Collagens in Intervertebral Disc. Interchanging Radial Distributions in Annulus Fibrosus. *Biochem. J.* 157 (1), 267–270. doi:10.1042/bj1570267

Fearing, B. V., Jing, L., Barcellona, M. N., Witte, S. E., Buchowski, J. M., Zebala, L. P., et al. (2019). Mechanosensitive Transcriptional Coactivators MRTF-A and YAP/TAZ Regulate Nucleus Pulposus Cell Phenotype Through Cell Shape. *FASEB j.* 33 (12), 14022–14035. doi:10.1096/fj.201802725RRR

Feng, G., Chen, H., Li, J., Huang, Q., Gupte, M. J., Liu, H., et al. (2015). Gene Therapy for Nucleus Pulposus Regeneration by Heme Oxygenase-1 Plasmid DNA Carried by Mixed Polyplex Micelles With Thermo-Responsive Heterogeneous Coronas. *Biomaterials.* 52, 1–13. doi:10.1016/j.biomaterials.2015.02.024

Feng, G., Zhang, Z., Dang, M., Rambhia, K. J., and Ma, P. X. (2020). Nanofibrous Spongy Microspheres to Deliver Rabbit Mesenchymal Stem Cells and Anti-miR-199a to Regenerate Nucleus Pulposus and Prevent Calcification. *Biomaterials.* 256, 120213. doi:10.1016/j.biomaterials.2020.120213

Fiani, B., Dahan, A., El-Farra, M. H., Kortz, M. W., Runnels, J. M., Suliman, Y., et al. (2021). Cellular Transplantation and Platelet-Rich Plasma Injections for Discogenic Pain: a Contemporary Review. *Regenerative Med.* 16 (2), 161–174. doi:10.2217/rme-2020-0146

Fiordalisi, M., Silva, A. J., Barbosa, M., Gonçalves, R., and Caldeira, J. (2020). Decellularized Scaffolds for Intervertebral Disc Regeneration. *Trends Biotechnol.* 38 (9), 947–951. doi:10.1016/j.tibtech.2020.05.002

Fong, E. L. S., Chan, C. K., and Goodman, S. B. (2011). Stem Cell Homing in Musculoskeletal Injury. *Biomaterials.* 32 (2), 395–409. doi:10.1016/j.biomaterials.2010.08.101

Francisco, A. T., Hwang, P. Y., Jeong, C. G., Jing, L., Chen, J., and Setton, L. A. (2014). Photocrosslinkable Laminin-Functionalized Polyethylene Glycol Hydrogel for Intervertebral Disc Regeneration. *Acta Biomater.* 10 (3), 1102–1111. doi:10.1016/j.actbio.2013.11.013

From the American Association of Neurological Surgeons; A.S.o.N.C.; Interventional Radiology Society of Europe, C.I.R.A.C.o.N.S.E.S.o.M.I.N.T.E.S.o.N.E.S.O.S.f.; C.A.Baxter, B., Campbell, B. C. V., Carpenter, J. S., Cognard, C., Dippel, D., Eesa, M., et al. (2018). Multisociety Consensus Quality Improvement Revised Consensus Statement for Endovascular Therapy of Acute Ischemic Stroke. *J. Neuroradiology.* 39 (6), E61–E76. doi:10.3174/ajnr.a5638

Gan, Y., Li, P., Wang, L., Mo, X., Song, L., Xu, Y., et al. (2017). An Interpenetrating Network-Strengthened and Toughened Hydrogel that Supports Cell-Based Nucleus Pulposus Regeneration. *Biomaterials.* 136, 12–28. doi:10.1016/j.biomaterials.2017.05.017

Gawri, R., Moir, J., Ouellet, J., Beckman, L., Steffen, T., Roughley, P., et al. (2014). Physiological Loading Can Restore the Proteoglycan Content in a Model of Early IVD Degeneration. *PLoS One.* 9 (7), e101233. doi:10.1371/journal.pone.0101233

Ghiselli, G., Wang, J. C., Bhatia, N. N., Hsu, W. K., and Dawson, E. G. (2004). Adjacent Segment Degeneration in the Lumbar Spine. *The J. Bone Jt. Surgery-American.* 86 (7), 1497–1503. doi:10.2106/00004623-200407000-00020

Gilchrist, C. L., Darling, E. M., Chen, J., and Setton, L. A. (2011). Extracellular Matrix Ligand and Stiffness Modulate Immature Nucleus Pulposus Cell-Cell Interactions. *PLoS One.* 6 (11), e27170. doi:10.1371/journal.pone.0027170

Guerin, H. L., and Elliott, D. M. (2007). Quantifying the Contributions of Structure to Annulus Fibrosus Mechanical Function Using a Nonlinear, Anisotropic, Hyperelastic Model. *J. Orthop. Res.* 25 (4), 508–516. doi:10.1002/jor.20324

Gullbrand, S. E., Peterson, J., Mastropolo, R., Roberts, T. T., Lawrence, J. P., Glennon, J. C., et al. (2015). Low Rate Loading-Induced Convection Enhances Net Transport into the Intervertebral Disc *In Vivo*. *Spine J.* 15 (5), 1028–1033. doi:10.1016/j.spinee.2014.12.003

Guo, S., Cui, L., Xiao, C., Wang, C., Zhu, B., Liu, X., et al. (2021). The Mechanisms and Functions of GDF -5 in Intervertebral Disc Degeneration. *Orthop. Surg.* 13 (3), 734–741. doi:10.1111/os.12942

Hamilton, D. J., Séguin, C. A., Wang, J., Pilliar, R. M., and Kandel, R. A. (2006). BioEngineering of Skeletal Tissues, T.Formation of a Nucleus Pulposus-Cartilage Endplate Construct *In Vitro*. *Biomaterials.* 27 (3), 397–405. doi:10.1016/j.biomaterials.2005.07.007

Han, Y., Ouyang, Z., Wawrose, R. A., Chen, S. R., Hallbaum, M., Dong, Q., et al. (2021). ISSLS Prize in Basic Science 2021: a Novel Inducible System to Regulate Transgene Expression of TIMP1. *Eur. Spine J.* 30 (5), 1098–1107. doi:10.1007/s00586-021-06728-0

He, R., Wang, Z., Cui, M., Liu, S., Wu, W., Chen, M., et al. (2021). HIF1A Alleviates Compression-Induced Apoptosis of Nucleus Pulposus Derived Stem Cells via Upregulating Autophagy. *Autophagy*, 1–23. doi:10.1080/15548627.2021.1872227

Hensley, A., Rames, J., Casler, V., Rood, C., Walters, J., Fernandez, C., et al. (2018). Decellularization and Characterization of a Whole Intervertebral Disk Xenograft Scaffold. *J. Biomed. Mater. Res.* 106 (9), 2412–2423. doi:10.1002/jbm.a.36434

Hingert, D., Ekström, K., Aldridge, J., Crescitelli, R., and Brisby, H. (2020). Extracellular Vesicles from Human Mesenchymal Stem Cells Expedite Chondrogenesis in 3D Human Degenerative Disc Cell Cultures. *Stem Cell Res Ther.* 11 (1), 323. doi:10.1186/s13287-020-01832-2

Hofmann, U. K., Steidle, J., Danalache, M., Bonnaire, F., Walter, C., and Rolauffs, B. (2018). Chondrocyte Death after Mechanically Overloading Degenerated Human Intervertebral Disk Explants Is Associated With a Structurally Impaired Pericellular Matrix. *J. Tissue Eng. Regen. Med.* 12 (9), 2000–2010. doi:10.1002/term.2735

Hoy, D. G., Smith, E., Cross, M., Sanchez-Riera, L., Blyth, F. M., Buchbinder, R., et al. (2015). Reflecting on the Global Burden of Musculoskeletal Conditions: Lessons Learnt From the Global Burden of Disease 2010 Study and the Next Steps Forward. *Ann. Rheum. Dis.* 74 (1), 4–7. doi:10.1136/annrheumdis-2014-205393

Hristova, G. I., Jarzem, P., Ouellet, J. A., Roughley, P. J., Epure, L. M., Antoniou, J., et al. (2011). Calcification in Human Intervertebral Disc Degeneration and Scoliosis. *J. Orthop. Res.* 29 (12), 1888–1895. doi:10.1002/jor.21456

Hu, B., He, R., Ma, K., Wang, Z., Cui, M., Hu, H., et al. (2018). Intervertebral Disc-Derived Stem/Progenitor Cells as a Promising Cell Source for Intervertebral Disc Regeneration. *Stem Cell Int.* 2018, 1–11. doi:10.1155/2018/7412304

Hu, S., Chen, L., Al Mamun, A., Ni, L., Gao, W., Lin, Y., et al. (2021). The Therapeutic Effect of TBK1 in Intervertebral Disc Degeneration via Coordinating Selective Autophagy and Autophagic Functions. *J. Adv. Res.* 30, 1–13. doi:10.1016/j.jare.2020.08.011

Hu, Z.-L., Li, H.-Y., Chang, X., Li, Y.-Y., Liu, C.-H., Gao, X.-X., et al. (2020). Exosomes Derived from Stem Cells as an Emerging Therapeutic Strategy for Intervertebral Disc Degeneration. *World J. Stem. Cells.* 12 (8), 803–813. doi:10.4252/wjsc.v12.i8.803

Humzah, M. D., and Soames, R. W. (1988). Human Intervertebral Disc: Structure and Function. *Anat. Rec.* 220 (4), 337–356. doi:10.1002/ar.1092200402

Iatridis, J. C., Setton, L. A., Weidenbaum, M., and Mow, V. C. (1997). Alterations in the Mechanical Behavior of the Human Lumbar Nucleus Pulposus With Degeneration and Aging. *J. Orthop. Res.* 15 (2), 318–322. doi:10.1002/jor.1100150224

Ishiguro, H., Kaito, T., Yarimitsu, S., Hashimoto, K., Okada, R., Kushioka, J., et al. (2019). Intervertebral Disc Regeneration With an Adipose Mesenchymal Stem Cell-Derived Tissue-Engineered Construct in a Rat Nucleotomy Model. *Acta Biomater.* 87, 118–129. doi:10.1016/j.actbio.2019.01.050

Kaur, H., and Roy, S. (2021). Designing Aromatic N-Cadherin Mimetic Short-Peptide-Based Bioactive Scaffolds for Controlling Cellular Behaviour. *J. Mater. Chem. B.* 9 (29), 5898–5913. doi:10.1039/d1tb00598g

Kim, J.-W., Jeon, N., Shin, D.-E., Lee, S.-Y., Kim, M., Han, D. H., et al. (2021). Regeneration in Spinal Disease: Therapeutic Role of Hypoxia-Inducible Factor-1 Alpha in Regeneration of Degenerative Intervertebral Disc. *Int. J. Mol. Sci.* 22 (10), 5281. doi:10.3390/ijms22105281

Lama, P., Le Maitre, C. L., Harding, I. J., Dolan, P., and Adams, M. A. (2018). Nerves and Blood Vessels in Degenerated Intervertebral Discs Are Confined to Physically Disrupted Tissue. *J. Anat.* 233 (1), 86–97. doi:10.1111/joa.12817

Lan, T., Shiyu-Hu, H., Shen, Z., Yan, B., and Chen, J. (2021). New Insights Into the Interplay between miRNAs and Autophagy in the Aging of Intervertebral Discs. *Ageing Res. Rev.* 65, 101227. doi:10.1016/j.arr.2020.101227

Leckie, S. K., Bechara, B. P., Hartman, R. A., Sowa, G. A., Woods, B. I., Coelho, J. P., et al. (2012). Injection of AAV2-BMP2 and AAV2-TIMP1 Into the Nucleus

Pulposus Slows the Course of Intervertebral Disc Degeneration in an *In Vivo* Rabbit Model. *Spine J.* 12 (1), 7–20. doi:10.1016/j.spinee.2011.09.011

Li, F., Zhan, X., Xi, X., Zeng, Z., Ma, B., Xie, N., et al. (2021). Do the Positioning Variables of the Cage Contribute to Adjacent Facet Joint Degeneration? Radiological and Clinical Analysis Following Intervertebral Fusion. *Ann. Transl Med.* 9 (9), 776. doi:10.21037/atm-20-7718

Li, W.-J., Jiang, Y. J., and Tuan, R. S. (2006). Chondrocyte Phenotype in Engineered Fibrous Matrix Is Regulated by Fiber Size. *Tissue Eng.* 12 (7), 1775–1785. doi:10.1089/ten.2006.12.1775

Li, Z., Gehlen, Y., Heizmann, F., Grad, S., Alini, M., Richards, R. G., et al. (2020). Preclinical *Ex-Vivo* Testing of Anti-Inflammatory Drugs in a Bovine Intervertebral Degenerative Disc Model. *Front. Bioeng. Biotechnol.* 8, 583. doi:10.3389/fbioe.2020.00583

Li, Z., Lang, G., Chen, X., Sacks, H., Mantzur, C., Tropp, U., et al. (2016). Polyurethane Scaffold with *In Situ* Swelling Capacity for Nucleus Pulposus Replacement. *Biomaterials.* 84, 196–209. doi:10.1016/j.biomaterials.2016.01.040

Liu, C., Zhu, C., Li, J., Zhou, P., Chen, M., Yang, H., et al. (2015). The Effect of the Fibre Orientation of Electrospun Scaffolds on the Matrix Production of Rabbit Annulus Fibrosus-Derived Stem Cells. *Bone Res.* 3, 15012. doi:10.1038/boneres.2015.12

Liu, J., Wang, D., Li, Y., Zhou, Z., Zhang, D., Li, J., et al. (2021). Overall Structure Construction of an Intervertebral Disk Based on Highly Anisotropic Wood Hydrogel Composite Materials With Mechanical Matching and Buckling Buffering. *ACS Appl. Mater. Inter.* 13 (13), 15709–15719. doi:10.1021/acsami.1c02487

Liu, C., Xiao, L., Zhang, Y., Zhao, Q., and Xu, H. (2020a). Regeneration of Annulus Fibrosus Tissue Using a DAFM/PECUU-Blended Electrospun Scaffold. *J. Biomater. Sci. Polym. Edition.* 31 (18), 2347–2361. doi:10.1080/09205063.2020.1812038

Liu, Y., Wang, H.-C., Xiang, H.-F., Jin, C.-H., and Chen, B.-H. (2020b). Expression of HSPA8 in Nucleus Pulposus of Lumbar Intervertebral Disc and Its Effect on Degree of Degeneration. *Adv. Ther.* 37 (1), 390–401. doi:10.1007/s12325-019-01136-9

Liu, Z., Li, J., Hu, M., Wang, X., Chen, N., Cui, S., et al. (2020c). The Optimal Timing of Hydrogel Injection for Treatment of Intervertebral Disc Degeneration. *Spine (Phila Pa 1976).* 45 (22), E1451–E1459. doi:10.1097/BRS.0000000000003667

Lyu, F.-J., Cui, H., Pan, H., Mc Cheung, K., Cao, X., Iatridis, J. C., et al. (2021). Painful Intervertebral Disc Degeneration and Inflammation: From Laboratory Evidence to Clinical Interventions. *Bone Res.* 9 (1), 7. doi:10.1038/s41413-020-00125-x

Malandrino, A., Lacroix, D., Hellmich, C., Ito, K., Ferguson, S. J., and Noailly, J. (2014). The Role of End Plate Poromechanical Properties on the Nutrient Availability in the Intervertebral Disc. *Osteoarthritis and Cartilage.* 22 (7), 1053–1060. doi:10.1016/j.joca.2014.05.005

March, L., Smith, E. U. R., Hoy, D. G., Cross, M. J., Sanchez-Riera, L., Blyth, F., et al. (2014). Burden of Disability Due to Musculoskeletal (MSK) Disorders. *Best Pract. Res. Clin. Rheumatol.* 28 (3), 353–366. doi:10.1016/j.berh.2014.08.002

McCann, M. R., Tamplin, O. J., Rossant, J., and Séguin, C. A. (2012). Tracing Notochord-Derived Cells Using a Noto-Cre Mouse: Implications for Intervertebral Disc Development. *Dis. Model. Mech.* 5 (1), 73–82. doi:10.1242/dmm.008128

Menon, R. G., Zibetti, M. V. W., Pendola, M., and Regatte, R. R. (2021). Measurement of Three-Dimensional Internal Dynamic Strains in the Intervertebral Disc of the Lumbar Spine With Mechanical Loading and Golden-Angle Radial Sparse Parallel-Magnetic Resonance Imaging. *J. Magn. Reson. Imaging.* 54 (2), 486–496. doi:10.1002/jmri.27591

Mizushima, N. (2007). Autophagy: Process and Function. *Genes Development.* 21 (22), 2861–2873. doi:10.1101/gad.1599207

Mohd Isa, I. L., Abbah, S. A., Kilcoyne, M., Sakai, D., Dockery, P., Finn, D. P., et al. (2018). Implantation of Hyaluronic Acid Hydrogel Prevents the Pain Phenotype in a Rat Model of Intervertebral Disc Injury. *Sci. Adv.* 4 (4), eaaq0597. doi:10.1126/sciadv.aaq0597

Moriguchi, Y., Borde, B., Berlin, C., Wipplinger, C., Sloan, S. R., Kirnaz, S., et al. (2018). *In Vivo* annular Repair Using High-Density Collagen Gel Seeded With Annulus Fibrosus Cells. *Acta Biomater.* 79, 230–238. doi:10.1016/j.actbio.2018.07.008

Mouw, J. K., Ou, G., and Weaver, V. M. (2014). Extracellular Matrix Assembly: a Multiscale Deconstruction. *Nat. Rev. Mol. Cell Biol.* 15 (12), 771–785. doi:10.1038/nrm3902

Mwale, F., Ciobanu, I., Giannitsios, D., Roughley, P., Steffen, T., and Antoniou, J. (2011). Effect of Oxygen Levels on Proteoglycan Synthesis by Intervertebral Disc Cells. *Spine.* 36 (2), E131–E138. doi:10.1097/BRS.0b013e3181d52b9e

Navaro, Y., Bleich-Kimelman, N., Hazanov, L., Mironi-Harpaz, I., Shachaf, Y., Garty, S., et al. (2015). Matrix Stiffness Determines the Fate of Nucleus Pulposus-Derived Stem Cells. *Biomaterials.* 49, 68–76. doi:10.1016/j.biomaterials.2015.01.021

Nesti, L. J., Li, W.-J., Shanti, R. M., Jiang, Y. J., Jackson, W., Freedman, B. A., et al. (2008). Intervertebral Disc Tissue Engineering Using a Novel Hyaluronic Acid-Nanofibrous Scaffold (HANFS) Amalgam. *Tissue Eng. A.* 14 (9), 1527–1537. doi:10.1089/ten.tea.2008.0215

Norbertczak, H. T., Ingham, E., Fermor, H. L., and Wilcox, R. K. (2020). Decellularized Intervertebral Discs: A Potential Replacement for Degenerate Human Discs. *Tissue Eng. C: Methods.* 26 (11), 565–576. doi:10.1089/ten.TEC.2020.0104

Pattappa, G., Peroglio, M., Peroglio, M., Sakai, D., Mochida, J., Benneker, L., et al. (2014). CCL5/RANTES Is a Key Chemoattractant Released by Degenerative Intervertebral Discs in Organ Culture. *Eur Cell Mater.* 27, 124–136. discussion 136. doi:10.22203/ecm.v027a10

Peng, Y., Huang, D., Li, J., Liu, S., Qing, X., and Shao, Z. (2020a). Genipin-Crosslinked Decellularized Annulus Fibrosus Hydrogels Induces Tissue-Specific Differentiation of Bone Mesenchymal Stem Cells and Intervertebral Disc Regeneration. *J. Tissue Eng. Regen. Med.* 14 (3), 497–509. doi:10.1002/term.3014

Peng, Y., Huang, D., Liu, S., Li, J., Qing, X., and Shao, Z. (2020b). Biomaterials-Induced Stem Cells Specific Differentiation Into Intervertebral Disc Lineage Cells. *Front. Bioeng. Biotechnol.* 8, 56. doi:10.3389/fbioe.2020.00056

Peng, Y., Qing, X., Lin, H., Huang, D., Li, J., Tian, S., et al. (2021). Decellularized Disc Hydrogels for hBMSCs Tissue-Specific Differentiation and Tissue Regeneration. *Bioactive Mater.* 6 (10), 3541–3556. doi:10.1016/j.bioactmat.2021.03.014

Peredo, A. P., Gullbrand, S. E., Smith, H. E., and Mauck, R. L. (2021). Putting the Pieces in Place: Mobilizing Cellular Players to Improve Annulus Fibrosus Repair. *Tissue Eng. B: Rev.* 27, 295–312. doi:10.1089/ten.TEB.2020.0196

Perfetti, D. C., Galina, J. M., Derman, P. B., Guyer, R. D., Ohnmeiss, D. D., and Satin, A. M. (2021). Risk Factors for Reoperation After Lumbar Total Disc Replacement at Short-, Mid-, and Long-Term Follow-Up. *Spine J.* 21 (7), 1110–1117. doi:10.1016/j.spinee.2021.02.020

Pirvu, T., Blanquer, S. B. G., Benneker, L. M., Grijpma, D. W., Richards, R. G., Alini, M., et al. (2015). A Combined Biomaterial and Cellular Approach for Annulus Fibrosus Rupture Repair. *Biomaterials.* 42, 11–19. doi:10.1016/j.biomaterials.2014.11.049

Ponte, A. L., Marais, E., Gallay, N., Langonné, A., Delorme, B., Hérault, O., et al. (2007). The *In Vitro* Migration Capacity of Human Bone Marrow Mesenchymal Stem Cells: Comparison of Chemokine and Growth Factor Chemotactic Activities. *Stem Cells.* 25 (7), 1737–1745. doi:10.1634/stemcells.2007-0054

Risbud, M. V., Schoepflin, Z. R., Mwale, F., Kandel, R. A., Grad, S., Iatridis, J. C., et al. (2015). Defining the Phenotype of Young Healthy Nucleus Pulposus Cells: Recommendations of the Spine Research Interest Group at the 2014 Annual ORS Meeting. *J. Orthop. Res.* 33 (3), 283–293. doi:10.1002/jor.22789

Roberts, S., Evans, H., Trivedi, J., and Menage, J. (2006). Histology and Pathology of the Human Intervertebral Disc. *J. Bone Jt. Surg Am.* 88 (Suppl. 2), 10–14. doi:10.2106/JBJS.F.00019

Roberts, S., Menage, J., and Urban, J. P. G. (1989). Biochemical and Structural Properties of the Cartilage End-Plate and its Relation to the Intervertebral Disc. *Spine.* 14 (2), 166–174. doi:10.1097/00007632-198902000-00005

Roh, E., Darai, A., Kyung, J., Choi, H., Kwon, S., Bhujel, B., et al. (2021). Genetic Therapy for Intervertebral Disc Degeneration. *Int. J. Mol. Sci.* 22 (4), 1579. doi:10.3390/ijms22041579

Saberi, M., Zhang, X., and Mobasheri, A. (2021). Targeting Mitochondrial Dysfunction With Small Molecules in Intervertebral Disc Aging and Degeneration. *Geroscience.* 43 (2), 517–537. doi:10.1007/s11357-021-00341-1

Sakai, D., and Andersson, G. B. J. (2015). Stem Cell Therapy for Intervertebral Disc Regeneration: Obstacles and Solutions. *Nat. Rev. Rheumatol.* 11 (4), 243–256. doi:10.1038/nrrheum.2015.13

Schmocker, A., Khoushabi, A., Frauchiger, D. A., Gantenbein, B., Schizas, C., Moser, C., et al. (2016). A Photopolymerized Composite Hydrogel and Surgical Implanting Tool for a Nucleus Pulposus Replacement. *Biomaterials.* 88, 110–119. doi:10.1016/j.biomaterials.2016.02.015

Schroeder, G. D., Markova, D. Z., Koerner, J. D., Rihn, J. A., Hilibrand, A. S., Vaccaro, A. R., et al. (2017). Are Modic Changes Associated With Intervertebral Disc Cytokine Profiles? *Spine J.* 17 (1), 129–134. doi:10.1016/j.spinee.2016.08.006

Shamsah, A. H., Cartmell, S. H., Richardson, S. M., and Bosworth, L. A. (2019). Tissue Engineering the Annulus Fibrosus Using 3D Rings of Electrospun PCL: PLLA Angle-Ply Nanofiber Sheets. *Front. Bioeng. Biotechnol.* 7, 437. doi:10.3389/fbioe.2019.00437

Sheyn, D., Ben-David, S., Tawackoli, W., Zhou, Z., Salehi, K., Bez, M., et al. (2019). Human iPSCs Can Be Differentiated into Notochordal Cells that Reduce Intervertebral Disc Degeneration in a Porcine Model. *Theranostics.* 9 (25), 7506–7524. doi:10.7150/thno.34898

Shikinami, Y., Kawabe, Y., Yasukawa, K., Tsuta, K., Kotani, Y., and Abumi, K. (2010). A Biomimetic Artificial Intervertebral Disc System Composed of a Cubic Three-Dimensional Fabric. *Spine J.* 10 (2), 141–152. doi:10.1016/j.spinee.2009.10.008

Sordi, V. (2009). Mesenchymal Stem Cell Homing Capacity. *Transplantation.* 87 (9 Suppl. l), S42–S45. doi:10.1097/TP.0b013e3181a28533

Stich, S., Möller, A., Cabraja, M., Krüger, J., Hondke, S., Endres, M., et al. (2018). Chemokine CCL25 Induces Migration and Extracellular Matrix Production of Anulus Fibrosus-Derived Cells. *Int. J. Mol. Sci.* 19 (8), 2207. doi:10.3390/ijms19082207

Sun, B., Lian, M., Han, Y., Mo, X., Jiang, W., Qiao, Z., et al. (2021). A 3D-Bioprinted Dual Growth Factor-Releasing Intervertebral Disc Scaffold Induces Nucleus Pulposus and Annulus Fibrosus Reconstruction. *Bioactive Mater.* 6 (1), 179–190. doi:10.1016/j.bioactmat.2020.06.022

Sun, Y., Leung, V. Y., and Cheung, K. M. (2019). Clinical Trials of Intervertebral Disc Regeneration: Current Status and Future Developments. *Int. Orthopaedics (Sicot).* 43 (4), 1003–1010. doi:10.1007/s00264-018-4245-8

Sun, Z., Luo, B., Liu, Z., Huang, L., Liu, B., Ma, T., et al. (2016). Effect of Perfluorotributylamine-Enriched Alginate on Nucleus Pulposus Cell: Implications for Intervertebral Disc Regeneration. *Biomaterials.* 82, 34–47. doi:10.1016/j.biomaterials.2015.12.013

Takeoka, Y., Yurube, T., Morimoto, K., Kunii, S., Kanda, Y., Tsujimoto, R., et al. (2020). Reduced Nucleotomy-Induced Intervertebral Disc Disruption Through Spontaneous Spheroid Formation by the Low Adhesive Scaffold Collagen (LASCol). *Biomaterials.* 235, 119781. doi:10.1016/j.biomaterials.2020.119781

Tam, V., Rogers, I., Chan, D., Leung, V. Y. L., and Cheung, K. M. C. (2014). A Comparison of Intravenous and Intradiscal Delivery of Multipotential Stem Cells on the Healing of Injured Intervertebral Disk. *J. Orthop. Res.* 32 (6), 819–825. doi:10.1002/jor.22605

Tavakoli, J., Diwan, A. D., and Tipper, J. L. (2020). Advanced Strategies for the Regeneration of Lumbar Disc Annulus Fibrosus. *Int. J. Mol. Sci.* 21 (14), 4889. doi:10.3390/ijms21144889

Tessier, S., Tran, V. A., Ottone, O. K., Novais, E. J., Doolittle, A., DiMuzio, M. J., et al. (2020). TonEBP-Deficiency Accelerates Intervertebral Disc Degeneration Underscored by Matrix Remodeling, Cytoskeletal Rearrangements, and Changes in Proinflammatory Gene Expression. *Matrix Biol.* 87, 94–111. doi:10.1016/j.matbio.2019.10.007

Tibiletti, M., Kregar Velikonja, N., Urban, J. P. G., and Fairbank, J. C. T. (2014). Disc Cell Therapies: Critical Issues. *Eur. Spine J.* 23 (Suppl. 3), 375–384. doi:10.1007/s00586-014-3177-2

Tripathy, S. K., Black, H. B., Goldwasser, E., and Leiden, J. M. (1996). Immune Responses to Transgene-Encoded Proteins Limit the Stability of Gene Expression after Injection of Replication-Defective Adenovirus Vectors. *Nat. Med.* 2 (5), 545–550. doi:10.1038/nm0596-545

Trummer, M., Eustacchio, S., Barth, M., Klassen, P. D., and Stein, S. (2013). Protecting Facet Joints Post-Lumbar Discectomy: Barricaid Annular Closure Device Reduces Risk of Facet Degeneration. *Clin. Neurol. Neurosurg.* 115 (8), 1440–1445. doi:10.1016/j.clineuro.2013.01.007

Vadalà, G., Sowa, G., Hubert, M., Gilbertson, L. G., Denaro, V., and Kang, J. D. (2012). Mesenchymal Stem Cells Injection in Degenerated Intervertebral Disc: Cell Leakage May Induce Osteophyte Formation. *J. Tissue Eng. Regen. Med.* 6 (5), 348–355. doi:10.1002/term.433

van der Veen, A. J., van Dieën, J. H., Nadort, A., Stam, B., and Smit, T. H. (2007). Intervertebral Disc Recovery after Dynamic or Static Loading *In Vitro*: Is There a Role for the Endplate? *J. Biomech.* 40 (10), 2230–2235. doi:10.1016/j.jbiomech.2006.10.018

Vukas, D., Grahovac, G., Barth, M., Bouma, G., Vilendecic, M., and Ledic, D. (2015). Effect of Anular Closure on Disk Height Maintenance and Reoperated Recurrent Herniation Following Lumbar Diskectomy: Two-Year Data. *J. Neurol. Surg. A. Cent. Eur. Neurosurg.* 76 (3), 211–218. doi:10.1055/s-0034-1393930

Wallach, C. J., Kim, J. S., Sobajima, S., Lattermann, C., Oxner, W. M., McFadden, K., et al. (2006). Safety Assessment of Intradiscal Gene Transfer: a Pilot Study. *Spine J.* 6 (2), 107–112. doi:10.1016/j.spinee.2005.05.002

Wang, X.-S., Yang, J.-M., Ding, R.-J., Liu, X.-Z., Jiang, X.-B., Yang, Z.-J., et al. (2021). Fabrication of a Polylactide-Glycolide/Poly-ε-Caprolactone/Dextran/Plastrum Testudinis Extract Composite Anti-Inflammation Nanofiber Membrane via Electrospinning for Annulus Fibrosus Regeneration. *J. Biomed. Nanotechnol.* 17 (5), 873–888. doi:10.1166/jbn.2021.3070

Wang, Z., Liu, H., Luo, W., Cai, T., Li, Z., Liu, Y., et al. (2020). Regeneration of Skeletal System With Genipin Crosslinked Biomaterials. *J. Tissue Eng.* 11, 204173142097486. doi:10.1177/2041731420974861

Zehra, U., Robson-Brown, K., Adams, M. A., and Dolan, P. (2015). Porosity and Thickness of the Vertebral Endplate Depend on Local Mechanical Loading. *Spine.* 40 (15), 1173–1180. doi:10.1097/BRS.0000000000000925

Zhang, H., Yu, S., Zhao, X., Mao, Z., and Gao, C. (2018). Stromal Cell-Derived Factor-1α-Encapsulated Albumin/heparin Nanoparticles for Induced Stem Cell Migration and Intervertebral Disc Regeneration *In Vivo*. *Acta Biomater.* 72, 217–227. doi:10.1016/j.actbio.2018.03.032

Zhang, T.-W., Li, Z.-F., Dong, J., and Jiang, L.-B. (2020a). The Circadian Rhythm in Intervertebral Disc Degeneration: an Autophagy Connection. *Exp. Mol. Med.* 52 (1), 31–40. doi:10.1038/s12276-019-0372-6

Zhang, Y., Yang, B., Wang, J., Cheng, F., Shi, K., Ying, L., et al. (2020b). Cell Senescence: A Nonnegligible Cell State Under Survival Stress in Pathology of Intervertebral Disc Degeneration. *Oxidative Med. Cell Longevity.* 2020, 1–12. doi:10.1155/2020/9503562

Zhang, Z., Marson, R. L., Ge, Z., Glotzer, S. C., and Ma, P. X. (2015). Simultaneous Nano- and Microscale Control of Nanofibrous Microspheres Self-Assembled From Star-Shaped Polymers. *Adv. Mater.* 27 (26), 3947–3952. doi:10.1002/adma.201501329

Zhao, C.-Q., Wang, L.-M., Jiang, L.-S., and Dai, L.-Y. (2007). The Cell Biology of Intervertebral Disc Aging and Degeneration. *Ageing Res. Rev.* 6 (3), 247–261. doi:10.1016/j.arr.2007.08.001

Zhou, P., Wei, B., Guan, J., Chen, Y., Zhu, Y., Ye, Y., et al. (2021). Mechanical Stimulation and Diameter of Fiber Scaffolds Affect the Differentiation of Rabbit Annulus Fibrous Stem Cells. *Tissue Eng. Regen. Med.* 18 (1), 49–60. doi:10.1007/s13770-020-00305-0

Zhu, C., Li, J., Liu, C., Zhou, P., Yang, H., and Li, B. (2016). Modulation of the Gene Expression of Annulus Fibrosus-Derived Stem Cells Using Poly(ether Carbonate Urethane)Urea Scaffolds of Tunable Elasticity. *Acta Biomater.* 29, 228–238. doi:10.1016/j.actbio.2015.09.039

Conflict of Interest: The authors declare that the research was conducted in the absence of any commercial or financial relationships that could be construed as a potential conflict of interest.

Publisher's Note: All claims expressed in this article are solely those of the authors and do not necessarily represent those of their affiliated organizations, or those of the publisher, the editors and the reviewers. Any product that may be evaluated in this article, or claim that may be made by its manufacturer, is not guaranteed or endorsed by the publisher.

GLOSSARY

AF Annulus fibrous
ECM Extracellular matrix
PU Polyurethane
PC Polycarbonate
NF-SMS Nanofiber sponge microspheres
NP Nuclear pulposus
IPN Interpenetrating network
sGAGs Sulfated glycosaminoglycans
PEG Polyethylene glycol
NP-SCs Nucleus pulposus-derived stem cells
PFTBA Perfluorotributylamine
HP Hyperbranched polymer
AMO Anti-miR-199a
PLGA Poly (lactic acid-co-glycolic acid)
NS Nanospheres
HIF Hypoxia inducible factor
MSC Mesenchymal stem cell
MPM Mixed composite micelle
pDNA Plasmid DNA
HO-1 Heme oxygenase-1
PCL Polycaprolactone
DEX Dextran
PTE Plastid extract
PECUU Poly (ether carbonate carbamide) urea
AFSCs Amniotic fluid-derived stem-cell
DAFM Decellularized AF matrix
CSRS Cell sheet rolling system
PLLA Poly(L-lactic acid) acid
g-DAF-G Genipin cross-linked acellular AF hydrogel
HDC High-density collagen gel
DHI Disk height index
ILM Interlamellar matrix
PTMC Poly (trimethylene carbonate)
TGF Transforming growth factor
BMSCs Bone marrow mesenchymal stem cells
IGF-1 Insulin-like growth factor-1
PDGF-AB Platelet-derived growth factor-AB
MDC Macrophage-derived chemokine
SDF-1 Stromal cell-derived factor-1
TEC Tissue engineered construct
CPP Calcium polyphosphate
FGF Fibroblast growth factor
ASICs Acid-sensitive ion channels
CTGF Connective tissue growth factor

frontiers in Bioengineering and Biotechnology

REVIEW
published: 27 October 2021
doi: 10.3389/fbioe.2021.782333

Recent Trends in Biofabrication Technologies for Studying Skeletal Muscle Tissue-Related Diseases

Seungyeun Cho[1] *and Jinah Jang*[1,2,3,4]*

[1]Department of Convergence IT Engineering, Pohang University of Science and Technology, Pohang, South Korea, [2]School of Interdisciplinary Bioscience and Bioengineering, Pohang University of Science and Technology, Pohang, South Korea, [3]Department of Mechanical Engineering, Pohang University of Science and Technology, Pohang, South Korea, [4]Institute for Convergence Research and Education in Advanced Technology, Yonsei University, Seoul, South Korea

In native skeletal muscle, densely packed myofibers exist in close contact with surrounding motor neurons and blood vessels, which are embedded in the fibrous connective tissue. In comparison to conventional two-dimensional (2D) cultures, the three-dimensional (3D) engineered skeletal muscle models allow structural and mechanical resemblance with native skeletal muscle tissue by providing geometric confinement and physiological matrix stiffness to the cells. In addition, various external stimuli applied to these models enhance muscle maturation along with cell–cell and cell–extracellular matrix interaction. Therefore, 3D *in vitro* muscle models can adequately recapitulate the pathophysiologic events occurring in tissue–tissue interfaces inside the native skeletal muscle such as neuromuscular junction. Moreover, 3D muscle models can induce pathological phenotype of human muscle dystrophies such as Duchenne muscular dystrophy by incorporating patient-derived induced pluripotent stem cells and human primary cells. In this review, we discuss the current biofabrication technologies for modeling various skeletal muscle tissue-related diseases (i.e., muscle diseases) including muscular dystrophies and inflammatory muscle diseases. In particular, these approaches would enable the discovery of novel phenotypic markers and the mechanism study of human muscle diseases with genetic mutations.

Keywords: disease modelling, hiPSC, extrusion printing, volumetric muscle loss, muscular dystrophy, self-repair

OPEN ACCESS

Edited by:
Farnaz Ghorbani,
University of Erlangen Nuremberg, Germany

Reviewed by:
Wanling Xuan,
Augusta University, United States
Francesco Chemello,
University of Texas Southwestern Medical Center, United States

***Correspondence:**
Jinah Jang
jinahjang@postech.ac.kr

Specialty section:
This article was submitted to Biomaterials, a section of the journal Frontiers in Bioengineering and Biotechnology

Received: *24 September 2021*
Accepted: *18 October 2021*
Published: *27 October 2021*

Citation:
Cho S and Jang J (2021) Recent Trends in Biofabrication Technologies for Studying Skeletal Muscle Tissue-Related Diseases. Front. Bioeng. Biotechnol. 9:782333. doi: 10.3389/fbioe.2021.782333

INTRODUCTION

Skeletal muscles constitute 35–40% of the human body weight and are essential for maintaining the posture, locomotion, and respiration of the human body. The tissue microenvironment comprises uniaxially aligned multinucleated muscle cells (myofibers) that are arranged in a three-dimensional (3D) extracellular matrix (ECM) scaffold. Owing to the presence of muscle-resident stem cells, also referred as satellite cells (SCs), the healthy skeletal muscles exhibit an inherent capacity for regeneration in response to small-scale injuries. However, the muscular self-repair mechanism is hindered by traumatic or surgical injuries, genetic mutations in ECM and sarcolemmal proteins, neurodegenerative diseases, aging-induced alterations in ECM compositions, regulatory cell behaviors, and signaling pathways that result in a wide range of diseases (Relaix et al., 2021).

In context, Duchenne muscular dystrophy (DMD) is a notable progressive muscle-wasting disease that results from failed production of dystrophin—a protein that stabilizes the myofibers. Although several antisense oligonucleotide-mediated exon-skipping therapies including eteplirsen,

golodirsen, and viltolarsen treatment were granted conditional approval by the United States Food and Drug Administration (FDA), no current cure exists for the DMD (Bursac et al., 2015; Alfano et al., 2019; Clemens et al., 2020; Frank et al., 2020). Charcot–Marie–Tooth disease (CMT) is the most commonly inherited neuromuscular disorder that causes distal muscle atrophy and results in a high-arched foot, impaired gait, and frequent falls. Although PXT3003—a drug that downregulates PMP22 mRNA expression—entered phase III of clinical trials in 2021, no clinically approved therapies currently exist for CMT (Vallat et al., 2013).

Genetically engineered mice lacking dystrophin and/or utrophin (a homolog of dystrophin) have been utilized to study the mechanism of DMD. Dystrophin-deficient mdx mice recapitulate mild dystrophic phenotypes. Compared with dog models and affected humans, mdx mice cannot model more severe disease phenotypes such as limb muscle fibrosis (McGreevy et al., 2015). However, dystrophin–utrophin double knockout (dko) mice (i.e., dko model) have been suggested as a more useful model to study the disease, as utrophin can compensate for the absence of dystrophin (Grady et al., 1997). Notably, a wide spectrum of degenerative musculoskeletal abnormalities has been reported using dko model (Isaac et al., 2012). However, this additional mutation in another gene, excluding dystrophin, does not correlate with the case in affected humans (McGreevy et al., 2015).

This genetic discrepancy has adversely affected the correct prediction of drug responses, as exemplified by the market withdrawal of cerivastatin, which caused fatal myopathies in human but was well-tolerated in mice (Furberg and Pitt et al., 2001). Although Idebenone apparently reduced the cardiac inflammation and fibrosis in a preclinical study with mdx mice, the phase III of the clinical trials assessing its capacity on delaying the respiratory decline in DMD patients was ceased in October 2020 after failing an interim analysis (Buyse et al., 2009). Thus, a preclinical human muscle tissue-related disease model is required to be developed to accurately mimic human pathophenotypes and disease progressions.

In context, complex biomimetic skeletal muscle structures have been developed using numerous biofabrication technologies that support the growth and maturation of cells in a 3D arrangement. Lithography-based methods and microfluidic devices have been utilized on micropattern surfaces with aligned topographical features (e.g., grooves) onto which seeded cells were directed to uniaxially align and differentiate into myofiber-like structures. Recent advancements in biofabrication methods such as 3D printing technology and electrospinning have yielded 3D tissue-engineered muscle models with multiscale structural cues resembling the hierarchical tissue geometry.

Physiologically relevant skeletal muscle phenotypes were obtained by placing endothelial, stromal, and neural cells in contact with myofibers, which could more precisely mimic the paracrine interactions occurring in the native tissue. In addition, the cell–matrix interaction that influences force transmission in native myofibers were also modeled. By contrast, conventional 2D models such as monoculture cellular assays are limited in recapitulating complex tissue architectures such as hierarchical arrangement. In addition, 2D models have limited capacity for muscle maturation, as contracting myofibers detach from the substrate, whereas 3D models support spontaneous cell fusion and myofiber enlargement (which resembles muscle hypertrophy) throughout several weeks of culture. Based on these advantages of the 3D models, a wide range of human muscle diseases have been recapitulated "in a dish." In addition, the incorporation of human-induced pluripotent stem cells (hiPSCs) enables the recapitulation of patient-specific disease phenotypes in these models.

In this review, we discuss the biomaterials widely utilized as 3D scaffold materials for muscle cells, followed by a review of multiple biofabrication technologies that yield aligned myofibers within the aforementioned biomaterials, such as shear/tensile force, aligned geometrical cues, and 3D bioprinting skills that allow deposition of cell-laden hydrogels in a desired geometry. Subsequently, we address the recent examples of vascularization, innervation, and electrical/mechanical stimuli that allowed additional maturation of 3D-engineered muscle. Ultimately, we highlight the application of these techniques for human muscle tissue-related disease modeling (i.e., muscular dystrophies and inflammatory muscle diseases).

BIOMATERIALS UTILIZED IN 3D TISSUE-ENGINEERED MUSCLE

In conventional 2D cultures, the mechanical properties of the rigid tissue culture substrates do not correspond to those of the native skeletal muscle tissue, which results in developmentally immature myotube structures such as poor striations and premyofibril myosin organization (Engler et al., 2004). Instead, several natural polymers have been proposed as a scaffold material to culture muscle cells in a 3D environment. In this section, we reviewed multiple biomaterials that are frequently used in fabricating 3D-engineered muscle, such as collagen, fibrin, and decellularized extracellular matrix (dECM) (**Table 1**). In addition, Matrigel, which is a basement membrane extract originating from Engelbreth–Holm–Swarm (EHS) sarcoma and is rich in ECM proteins such as laminin and collagen IV, has been used in combination with collagen and fibrin.

Collagen is an abundant component of the ECM in native muscle tissue that was utilized in the earliest cases of 3D-engineered muscle (Powell et al., 2002). Powell et al. (2002) observed that human primary muscle cells embedded in collagen/Matrigel mixture formed parallel arrays of differentiated myofibers under passive tension. However, the absence of collagen I-specific integrin in myotubes resulted in lesser contractility than that of the other types of integrin-binding ECM proteins such as fibrin and laminin (Mayer, 2003). Therefore, increasing the concentration of collagen could adversely affect the force generation (Hinds et al., 2011). In another research, Dixon et al. (2018) prepared a collagen/Matrigel/silk hydrogel that successfully induced myogenic differentiation, maintained its mechanical integrity during the

TABLE 1 | Different types of biomaterials used in skeletal muscle tissue engineering.

Biomaterials	Pros/Cons	Achievement	Relevant bioactivities	References
Collagen	Structural cues/low remodeling capacity	Uniaxial cell alignment Long-term construct stability	Fibril bundle formation Cell attachment Large pore size	Kim and Kim et al. (2019) Morimoto et al. (2020)
Fibrin	High contractile force/batch-to-batch variability	Human fetus-relevant force production High myofiber and vascular density after implantation	Native tissue stiffness Pro-angiogenic effect	Hinds et al. (2011) Gilbert-Honick et al. (2018)
Laminin	Cell attachment/degradation	Dose-dependent increase in cell proliferation	α7β1 integrin expression	Marcinczyk et al. (2017)
dECM	Biochemical and structural cues/low structural stability	*In vitro* AChR cluster formation	Presence of agrin	Choi et al. (2016)

compacting around silk cantilevers, and formed a 3D-engineered muscle (Dixon et al., 2018).

Fibrin is the fundamental component of a blood clot that is formed in the initial steps of the wound-healing process, and subsequently, replaced by the cell-produced ECM. Upon using in skeletal muscle tissue engineering, fibrin can exert a passive stiffness that is several orders of magnitude lower than that of collagen and comparable to that of native skeletal muscle. Madden et al. (2015) demonstrated tetanus force production that corresponded to that of the fetal human skeletal muscle in a fibrin-based 3D-engineered muscle. In addition, fibrin often prevents tissue deformation under tissue remodeling owing to its capacity to be degraded and replaced by endogenous ECM. Christensen et al. (2020) fabricated a contractile muscle tissue with fibrin/Matrigel, which was anchored to two cantilevers and maintained the tissue confined during cell-mediated compaction. Thus, the fibrin can support the spontaneous formation of contractile myotubes (Madden et al., 2015; Christensen et al., 2020).

Lastly, dECM has emerged as a potential candidate for inducing the elongation and fusion of muscle cells owing to its tissue-specific cell-binding moieties, ECM topography, and physical ultrastructures. Furthermore, studies have demonstrated that dECM could induce tissue-specific cell differentiation (Flynn, 2010; Uygun et al., 2010). Choi et al. (2016) developed the preparation process of skeletal muscle decellularized extracellular matrix (mdECM). Notably, agrin—an ECM protein that enhances the clustering of acetylcholine receptors—was conserved in the mdECM (Choi et al., 2016). In addition, dECM can be chemically processed or blended with other polymers before electrospinning or extrusion printing to fabricate a 3D scaffold integrated with tissue-specific biochemical cues and versatile structural cues (Baiguera et al., 2014; Kim et al., 2020; Kim et al., 2021). Baiguera et al. (2014) blended rat brain-derived dECM with gelatin prior to electrospinning and obtained a highly porous 3D scaffold that supported mesenchymal stem cell adhesion and growth. In another study, Kim et al. (2020) developed a chemically modified dECM using a methacrylate process for the extrusion of cell-laden skeletal muscle constructs that offer structural stability.

3D BIOFABRICATION TECHNOLOGIES IN SKELETAL MUSCLE ENGINEERING

The recent biofabrication technologies that enabled recapitulation of the skeletal muscle physiology in terms of uniaxial cell orientation and bundle-like fiber organization are discussed in this section with a focus on the benefits of 3D bioprinting technology. In particular, 3D bioprinting technology facilitates the layer-by-layer deposition of cell-laden bioinks in desired dimension under the optimized ink composition and post-printing crosslinking steps, which endows the engineered constructs with more physiologically relevant dimensions. In addition, cells or larger units such as cell aggregates, cell sheets, and cell-laden modules can be placed and assembled using the 3D bioprinting technology in a native organ-resembling spatial arrangement to maximize the cell–cell interaction.

Mimicking Uniaxial Cell Alignment

In general, uniaxial cell alignment is a representative morphological feature of the skeletal muscles that can be induced by applying shear (Mozetic et al., 2017; Kim and Kim et al., 2019; Kim et al., 2019) and tensile force (Choi et al., 2016; Agrawal et al., 2017; Cvetkovic et al., 2017; Das et al., 2019; Kong et al., 2021). The shear flow inside a cylindrical nozzle induces shear-thinning of the polymer solution. The wall shear forces exerted on the shear-thinning polymer induce the alignment of inherent polymer molecules (Compton and Lewis, 2014; Schwab et al., 2020). In particular, elongational forces are produced in the stretching region of the extruded polymer that can further accelerate the alignment and Kim et al. (2019) studied the shear-induced cell-laden collagen alignment and demonstrated that a fibrillating buffer solution (KCl and L-glycine) incorporated in the bioink induces the formation of collagen fibril bundle, closely mimicking its native structure (Kim and Kim et al., 2019). Based on their previous research, Kim et al. (2019) included gold nanowire as a nanofiller that was stably aligned during the extrusion process and strongly aligned upon electric field stimulation (**Figure 1A**). In addition, the orientation of the distribution of nanowires were manipulated under varying volume flow rates and nozzle speeds (Kim et al., 2019).

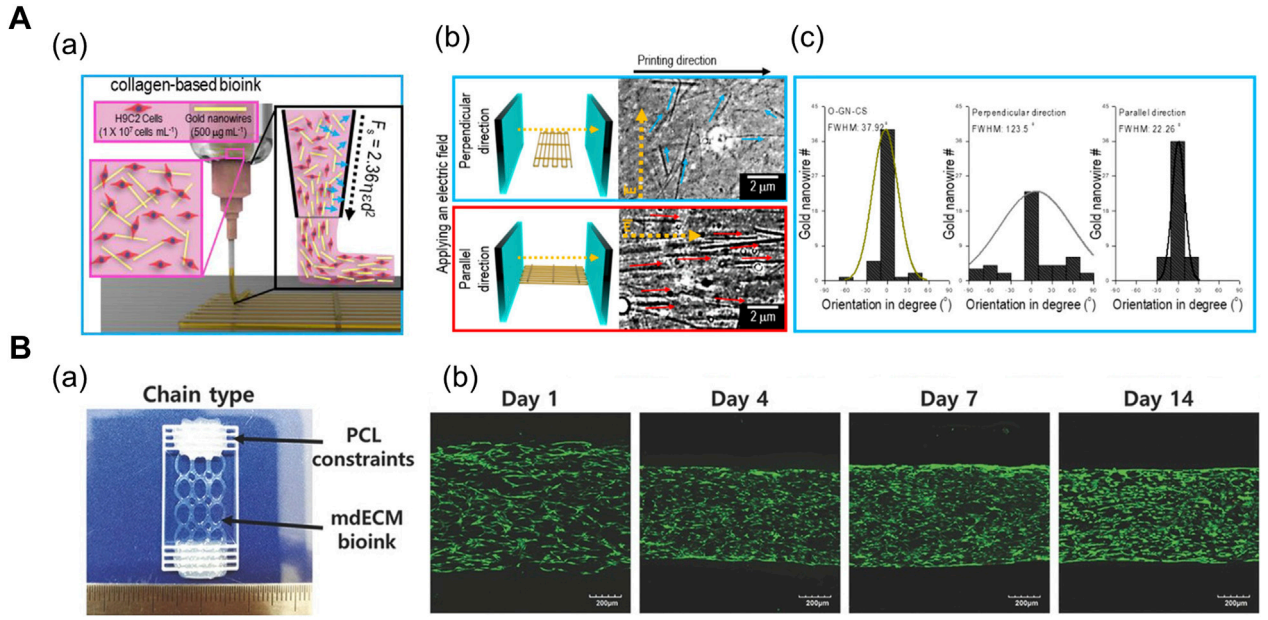

FIGURE 1 | (A) Shear force-mediated cell alignment method. (a) Schematic of cell alignment during the extrusion printing process with gold nanowires aligned along the printing direction. (b) Electric field applied to promote the alignment of muscle cells through the alignment of gold nanowires. The optical images display the spatial distribution of gold nanowires under the electric field in directions perpendicular and parallel to the printing direction. (c) Distribution of orientation of gold nanowires under three conditions: no applied electric field (left), electric field applied in directions perpendicular (middle) and parallel (right) to the printing direction. Reprinted with permission from (Kim et al., 2019). **(B)** 3D-printed anchor structure for applying tensile force. (a) 3D-printed muscle construct comprising geometric constraints and muscle cell-laden mdECM bioink in chain shape. (b) Live/dead staining of printed muscle constructs at Days 1, 4, 7, and 14 of culture, revealing high cell viability (>90%) with minimal cell death. Construct compaction is accompanied by the longitudinal alignment of cells. Reprinted with permission from (Choi et al., 2016).

In order to apply tensile force, the muscle cell-laden hydrogels are confined around the two micropillars or posts. Upon tissue maturation and cell-mediated gel compaction, the hydrogel remain anchored to the posts and the cells align along the longest axis of the system. Choi et al. (2016) induced uniaxial muscle cell alignment by depositing polycaprolactone (PCL) anchors as a geometric constraint at both ends of the muscle construct (**Figure 1B**). The PCL and cell-containing mdECM bioink were 3D printed using an integrated composite tissue/organ building system (Choi et al., 2016). Alternatively, Agrawal et al. (2017) fabricated a hydrogel pillar using a photopatterning method. After injecting the hydrogel precursor solution into an inlet of the microfluidic device, a prefabricated photomask was positioned on the bottom of the device, followed by exposure to ultraviolet (UV) radiation, which resulted in the formation of two circular pillars. Thereafter, the muscle cell-laden gelatin methacrylate solution was injected into the device for photopolymerization, which created patterns between the cells and around the pillars (Agrawal et al., 2017).

Mimicking Muscle Bundle Structure

In native skeletal muscle, a single fascicle comprises multiple muscle fibers arranged in a bundled form. Several biofabrication techniques have attempted to mimic the muscle bundle-like structures for recapitulating the hierarchical arrangement ranging from a single muscle fiber to a fascicle. This physiological aspect can be achieved as follows: fabrication of bundle-shaped 3D scaffold (Kim et al., 2018a; Kim et al., 2020), 3D bioprinting cell-laden construct with built-in channels (Miller et al., 2012; Kang et al., 2016; Kolesky et al., 2016; Kim et al., 2018b), and 3D embedded printing (Bertassoni et al., 2014; Choi et al., 2019; Skylar-Scott et al., 2019; Gao et al., 2021).

A 3D scaffold comprising multiple polymeric struts or fibers adjacent to each other has been fabricated to mimic the bundle structure. Kim et al. (2018a) demonstrated shear-induced poly (vinyl alcohol) (PVA) alignment during the printing of PVA/PCL mixture (**Figure 2A**). Subsequent leaching of PVA yielded aligned micropatterns on the surface of the PCL scaffold, which was seeded with muscle cell-laden collagen solution (Kim et al., 2018a). Alternatively, Jin et al. (2021) fabricated the thermally drawn PCL fiber-based microchannel scaffolds (**Figure 2B**). After the scaffolds were soaked in the skeletal muscle dECM/muscle cell mixture and gelated at 37°C, the nuclear elongation was observed along the orientation of fibers, indicating the cell-guiding effect of the aligned fiber structures. In addition, the highly porous scaffold surface obtained from the salt-leaching method allowed the absorption of the dECM pre-gel solution into the scaffolds, which was evident from the presence of collagen mesh-like structures on the inner and outer sides of the fiber (Jin et al., 2021).

Microchannel-guided formation of aligned units has been utilized in a broad range of target tissues, including bone, nervous tissues, and vasculatures (Daly et al., 2018; Huang et al., 2018; Lee et al., 2020; Hwangbo et al., 2021). Sacrificial

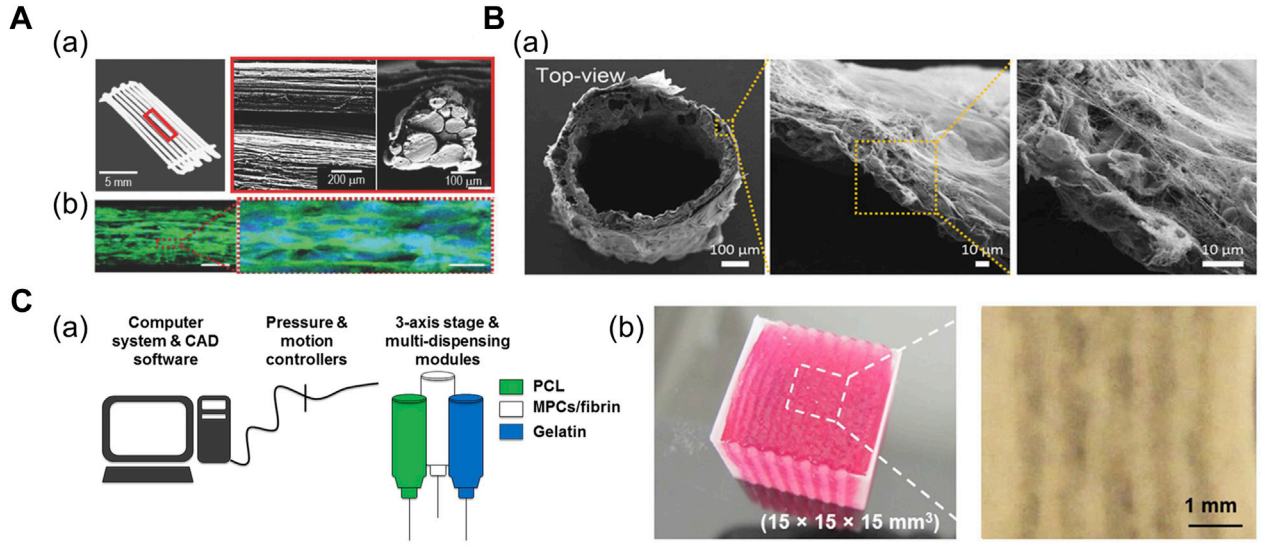

FIGURE 2 | (A) Fabrication of PCL strut-based 3D scaffold. (a) Optical and scanning electron microscopy (SEM) images of micropatterned PCL scaffold. (b) Confocal images of cells at Day 14 immunostained for myosin heavy chain (green) and nuclei (blue), indicating the myogenic differentiation induced on the micropatterned PCL scaffold. Reprinted with permission from (Kim et al., 2018a). **(B)** Fabrication of thermally drawn PCL-fiber based 3D scaffold. (a) SEM images of PCL fiber-based scaffold after dECM absorption on scaffold surface. Reprinted with permission from (Jin et al., 2021). **(C)** 3D bioprinted cell-laden construct with built-in channels. (a) Schematic of integrated tissue-organ printing system. (b) 3D bioprinted multilayered muscle construct at scale: 15 × 15 × 15 cm. Microchannels are formed inside the construct after removal of gelatin patterns. Reprinted with permission from (Kim et al., 2018b).

hydrogels—deposited as a temporary structure for structural support or generation of certain structures—are often removed by variations in temperature once the crosslinking of the engineered construct is complete; therefore, they have been widely adopted in 3D bioprinting for establishing built-in channels. In addition, thermoresponsive sacrificial polymers (i.e., gelatin and Pluronic F-127 (PF-127)) are printed as a temporary structure that dissolve in response to temperature variations after the bulk hydrogel has been crosslinked. Kang et al. (2016) printed supporting PCL pillars and sacrificial hydrogel patterns between cell-laden hydrogel patterns to yield a muscle bundle-like structure. Moreover, stretching and aligning muscle cells were observed inside these bundle structures 3 days after printing structure (Kang et al., 2016). Subsequently, Kim et al. (2018b) developed a larger construct (mm^3–cm^3) with multilayered muscle bundles to utilize cells from human biopsies and assess if the construct was applicable for severe muscle defect replacement (**Figure 2C**; Kim et al., 2018b).

Furthermore, 3D embedded printing utilizes a recently developed printing method named freeform reversible embedding of suspended hydrogel (FRESH). The major limitation of soft biomaterials such as ECM hydrogels is attributed to their poor shape-retention during the printing process that renders the desired resolution and 3D geometries unachievable (Hinton et al., 2015). The thermoreversible support bath prevents the collapse of the printed hydrogels and is subsequently melted away after the printing process. Moreover, complex structures such as branched tubular networks and trileaflet heart valves have been fabricated using the FRESH method (Bhattacharjee et al., 2015; Lee et al., 2019). Based on this method, Choi et al. (2019) directly printed a bundle-like structure in a granule-based support bath. Initially, they prepared the support bath by blending an 8% (w/v) gelatin solution to generate gelatin granules. Thereafter, mdECM struts were directly printed into the support bath with horizontal and vertical distances of 200 μm from each other. Subsequently, PVA was added into the gelatin granule to induce rapid polymerization of mdECM bioink during its extrusion (Choi et al., 2019).

MATURATION OF 3D TISSUE-ENGINEERED MUSCLE

The development of 3D-engineered muscles results in physiologically mimetic tissues that can reflect the phenotypes that remain undiscovered or neglected in conventional systems. In this section, we discuss the recent biofabrication technologies for vascularization and innervation. Skeletal muscle vasculature participates in specific interactions with myofibers, which aid in muscle maturation and homeostasis. In particular, vascular endothelial growth factor (VEGF) stimulates the Akt pathway of muscle cells and induces myofiber hypertrophy in an autocrine manner (Yin et al., 2013). Long-term denervation or depletion of motor neuron innervation prohibits satellite cells from entering the mitotic cell cycle and leads to progressive myofiber atrophy (Kuschel et al., 1999). In addition, we review the studies that utilized electrical and mechanical stimuli for the maturation of 3D-engineered muscles.

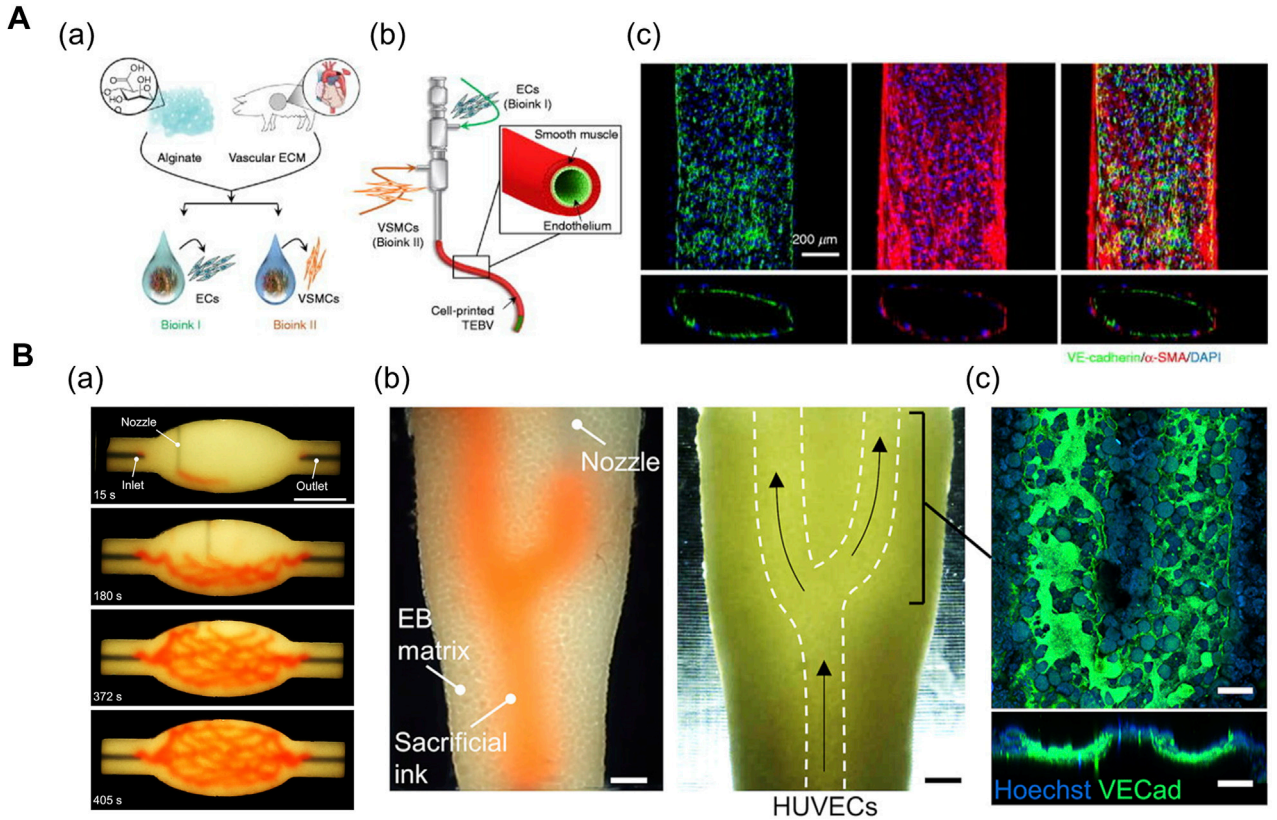

FIGURE 3 | (A) Coaxial printing method. (a) Formulation of vascular tissue-derived bioinks for promoting vascular maturation. (b) Schematic of triple-coaxial cell printing method yielding compartmentalized vascular structure. (c) Confocal image of printed vascular structure with combined expression of endothelial and muscular markers. Reprinted with permission from (Gao et al., 2019). **(B)** Direct ink-writing method. (a) Sequence of branched and hierarchical vascular network fabricated with direct ink-writing method. (b) Perfusion of ECs into evacuated channel (white-dashed lines). (c) Expression of VE-cadherin after 20 h of perfusion displays formation of endothelium monolayer. Reprinted with permission from (Skylar-Scott et al., 2019).

Vascularization

To date, several vascularization strategies have been developed to recapitulate the native vascular function (i.e., nutrient and oxygen supply to the highly oxygen-consuming organ) in the 3D-engineered muscle. The coaxial printing method and direct ink-writing method have been studied for the vascularization of engineered muscle as well as engineered tissues of other types.

Among the conventional vascularization methods, the hydrogel mold-casting method can generate hollow channel structures that are subsequently seeded with endothelial cells (ECs), forming endothelialized lumen structures (Bersini et al., 2018; Osaki et al., 2018; Redd et al., 2019). Osaki et al. (2018) observed emergent angiogenic sprouting from the surface of the endothelialized channels towards the muscle bundle between two channels, which mimicked myokine-regulated muscle angiogenesis. However, this method requires sequential stereolithography-based steps for obtaining the micropatterned mold. The multiple channel structures should be individually obtained to allow active diffusion of nutrients, thereby adding complexity to the mold-preparation step.

In general, 3D printing enables the iterative one-step fabrication of composite structures. For instance, the coaxial printing method enables direct fabrication of two- (Zhang et al., 2016; Gao et al., 2017; Choi et al., 2019) or three- (Gao et al., 2019; Gao et al., 2021) layered 3D conduits of varying geometries and dimensions (**Figure 3A**). Zhang et al. (2016) bioprinted a 3D microfibrous scaffold structure using a composite bioink comprising alginate (GelMA) and photoinitiator. The alginate in the core part of the nozzle was exposed to a chemical crosslinking agent (Ca^{2+}) provided from the shell part of the nozzle during the printing process. The printed scaffold manifested mechanical stability after the UV crosslinking of GelMA. Ultimately, the cardiomyocytes were seeded onto the stiffened microfibrous scaffold after the bioprinted ECs self-assembled into a layer of confluent endothelium, thereby resembling the structure of native myocardium (Zhang et al., 2016). In another research, Choi et al. (2019) fabricated a compartmentalized core–shell structure in which a layer of ECs surrounded the muscle fiber-like struts, thereby closely mimicking the hierarchical architecture of vascularized muscle. Within a coaxial nozzle, the syringe containing the muscle cell-laden mdECM bioink and the syringe containing the EC-laden vascular dECM bioink were attached to the core and shell parts, respectively.

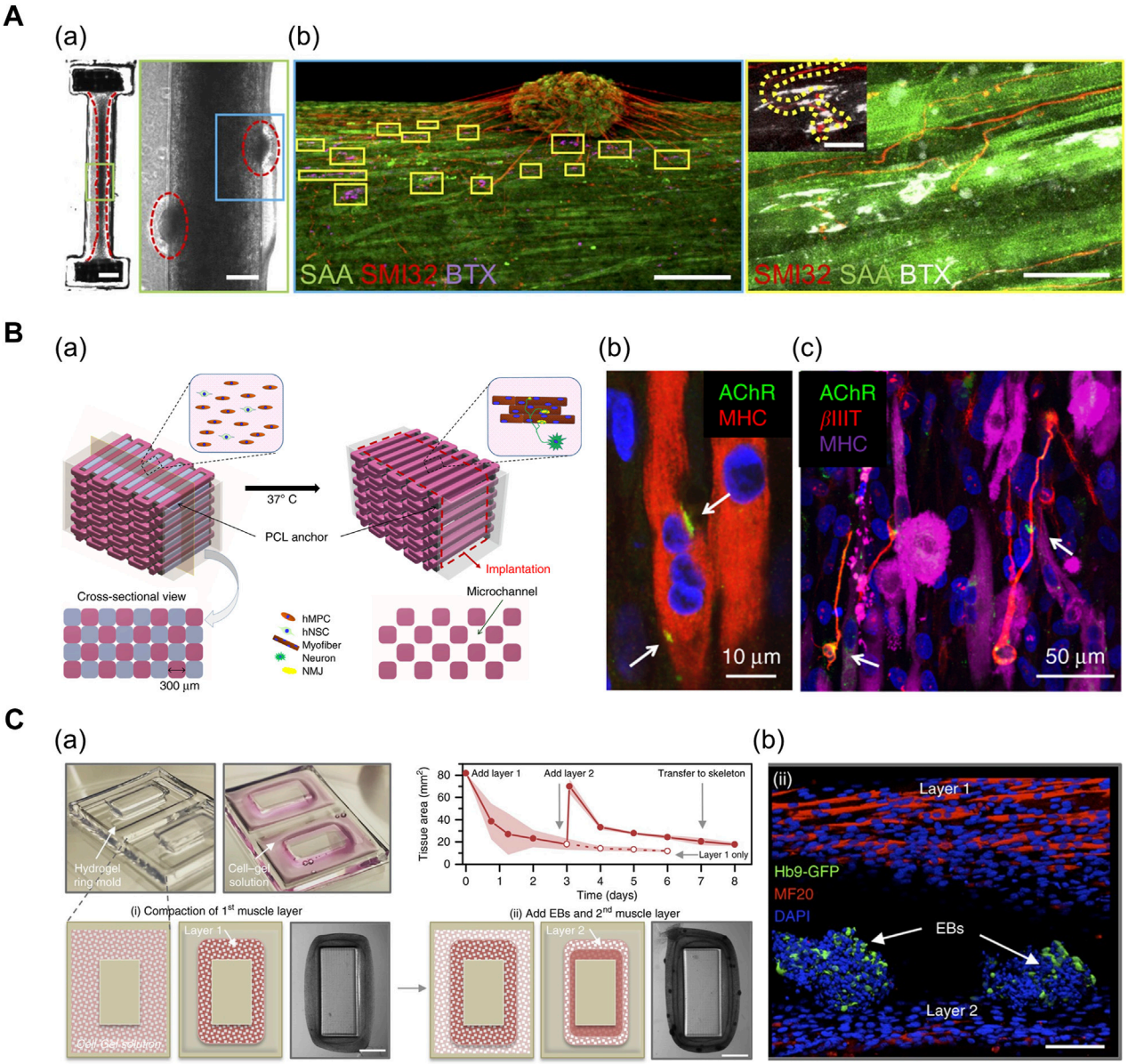

FIGURE 4 | (A) 3D muscle–motor neuron co-culture. (a) phase contrast image portraying differentiated myofiber co-cultured with motor neuron spheroid for 2 weeks. (b) Confocal image displaying co-localization of neurite terminals (red) and acetylcholine clusters (magenta/white) on a striated myofiber (green). SAA: sarcomeric α-actinin, SMI32: anti-200 kD neurofilament heavy antibody, BTX: α-bungarotoxin. Reprinted with permission from (Bakooshli et al., 2019). **(B)** 3D bioprinted innervated muscle construct. (a) 3D CAD modeling of bioprinted construct. Hollow microchannels formed after removing sacrificial patterns. (b) Confocal image of acetylcholine receptors (green) prepatterned on myofibers (red). (c) Confocal image of neurites (red) contacting acetylcholine receptor clusters (green). βIIIT: beta-III tubulin. Reprinted with permission from (Kim et al., 2020). **(C)** Modular muscle–motor neuron co-culture system. (a) Schematic of fabrication of multilayered tissue ring. The cross-sectional tissue area decreased over time as cell–gel solution compacted around the mold. (b) Confocal image indicating differentiated myofibers (red) and motor neuron EBs (green). Hb9: post-mitotic MN-specific Hb9 promoter. MF20: anti-myosin heavy-chain antibody. Reprinted with permission from (Cvetkovic et al., 2017).

In comparison to the muscle-only construct, the higher twitch and tetanic peak forces of the vascularized muscle confirmed its enhanced maturity (Choi et al., 2019).

The direct ink writing method proposed by Skylar-Scott et al. (2019) enables the fabrication of complex vasculature in a cell-filled support bath via 3D embedded printing (**Figure 3B**). This method is novel owing to the high cellular density of the support bath (up to 10^8 cells/ml) (i.e., living tissue matrix) which is the prerequisite for physiologically relevant tissue models. The living tissue matrix exhibited a self-healing, viscoplastic behavior that allowed the printing of sacrificial ink in the desired network structure without crevasses formation on the printing path. Subsequently, the temperature-mediated melting of sacrificial gelatin ink and the simultaneous stiffening of the matrix

yielded hollow vasculature networks, followed by the perfusion of EC suspension (Skylar-Scott et al., 2019). Based on a similar approach, Neufeld et al. (2021) fabricated a 3D glioblastoma model with a perfusable vasculature. Initially, the PF-127-based vascular bioink was deposited on the surface of cancer cell-laden fibrin bioink, followed by casting another layer of fibrin bioink onto the vasculature. Once the fibrin bioink achieved the desired physiological stiffness, the PF-127 was washed out with cold PBS, and a mixture of ECs and pericytes were injected into the vascular channels (Neufeld et al., 2021). Overall, the direct ink-writing method allows freeform fabrication of tissue-specific vascular structures. However, the mechanical properties of the support bath inks and vascular inks should be carefully manipulated in combination to achieve the desired geometry of vasculatures.

Innervation

Motor neuron innervates the skeletal muscle via neuron–myofiber contacts or neuromuscular junctions (NMJs), which mediate the conversion of neuronal signal into muscle contraction. Functional NMJs have been engineered by multiple biofabrication methods including 3D co-culture (Morimoto et al., 2013; Bakooshli et al., 2019) of neuron and myofibers, and 3D bioprinting of structures with a spatial organization that induces spontaneous neurite formation (Cvetkovic et al., 2017; Kim et al., 2020; Kong et al., 2021).

In particular, the neurons can self-organize to form NMJs in the 3D co-culture of motor neurons (MNs) and muscle cells. Multiple biofabrication skills, including the usage of patterned stamps and molds, facilitate the integration of MN spheroids with differentiated myofibers. Morimoto et al. (2013) used polydimethylsiloxane (PDMS) stamps for patterning Matrigel to form aligned muscle bundle, and subsequently, added mouse neural stem cell-derived spheroids (mNSCs) onto the muscle bundle. The mNSCs were successfully differentiated into motor neurons, and acetylcholine receptors were formed at the muscle bundle-spheroid contacts. Moreover, the muscle bundle contracted unidirectionally in response to glutamic acid activation of neurons, indicating the formation of functional NMJs (Morimoto et al., 2013). Based on a similar approach, Bakooshli et al. (2019) prepared a dumbbell-shaped PDMS mold that was seeded with a mixture of human pluripotent cell-derived MN spheroids and human muscle progenitor cells suspended in fibrin-based hydrogel (**Figure 4A**; Bakooshli et al., 2019). The expression of NMJ-localized protein, such as synaptic MuSK protein, confirmed the recapitulation of early NMJ synaptogenesis in this model.

In addition, 3D bioprinting technology facilitates the precise positioning of multiple cell types in a desired organization and array. Kim et al. (2020a) generated a functional NMJ inside a 3D-printed multilayered bundle-shaped construct containing a hollow microchannel structure (**Figure 4B**). Fibrinogen/gelatin/hyaluronic acid/glycerol bioink containing human muscle progenitor cells and human neural stem cells (hNSCs), acellular sacrificial bioink, and a supporting PCL pillar were deposited using multidispensing modules. Consequently, βIIIT^{+} neurites contacting the acetylcholine receptor clusters were formed on the myofibers, which confirm the formation of NMJs (Kim et al., 2020). In an alternative approach, Cvetkovic et al. (2017) used a stereolithography-based 3D-printing technique to fabricate a modular co-culture system (**Figure 4C**). A 3D tissue ring, previously formed by integrating two layers comprising differentiated myofibers and motor neuron embryoid bodies (EBs) in a 3D-printed ring mold, was transferred to the hydrogel skeleton to mimic the physiological muscle–tendon–bone arrangement. This co-culture arrangement exhibited the extension of the neurite toward the differentiated muscle and the formation of the acetylcholine receptor cluster (Cvetkovic et al., 2017).

Contractility

Contractility is one of the most widely accepted muscle functional readouts for distinguishing between normal and diseased muscle phenotypes (Sharples et al., 2012; Juhas et al., 2018). In context, the early detachment of spontaneously contracting myofibers allowed only partial contractility analysis in 2D cultures, which were confined to the variations in related gene expressions (Nikolić et al., 2012; Tarum et al., 2017). Various external stimuli have been applied to improve the contractility of the 3D-engineered muscle. These stimuli aim to mimic the native stimuli the developing skeletal muscle receives (Westerga and Gramsbergen, 1994; Eken et al., 2008), which induce muscle hypertrophy. In general, electrical stimulation and mechanical loading are frequently utilized in combination.

First, electrical stimulation is applied as a surrogate of neural input that are delivered to individual myofibers to induce muscular contraction. In addition, the regenerating muscles in the self-repair process require electrical signals from motor neurons, implying that the electrical stimulation can enhance the function of the engineered muscle (Kim et al., 2019). Upon applying the electrical stimulation, the pulse energy and width should be optimized to minimize the tissue damage (Khodabukus and Baar, 2012). Grosberg et al. (2011) applied an electrical field stimulation for cantilever-type thin muscular films and measured the transmembrane potential of cardiomyocytes. This revealed an action potential morphology, indicating the contractility achieved in the tissue (Grosberg et al., 2011). Additionally, Khodabukus et al. (2019) demonstrated that a 3D-engineered muscle electrically stimulated with 1 and 10 Hz of frequency for 1 week resulted in an increased contractile force (nonstimulated: 9.1 ± 0.38 mN mm^{-2}, 1 Hz: 19.3 ± 0.63 mN mm^{-2}, 10 Hz: 18.9 ± 0.69 mN mm^{-2}). More importantly, the stimulation of 1 Hz enabled the highest specific force generation among the outputs of engineered human muscle reported to date (Khodabukus et al., 2019).

On the other hand, mechanical loading mimics the consistent passive stretch exerted upon the embryonic muscle. Kim et al. (2019) reported that combined electrical and mechanical stimulation induced the remodelling of ECM network structures in engineered muscle tissue, such that the force transmission was facilitated without impeding muscle contraction. In particular, 20 min of alternating electrical and mechanical stimulations resulted in 31% higher contractile force (Kim et al., 2019). Moreover, Aguilar-Agon et al. (2019) studied the influences of mechanical loading on anabolic shift based on

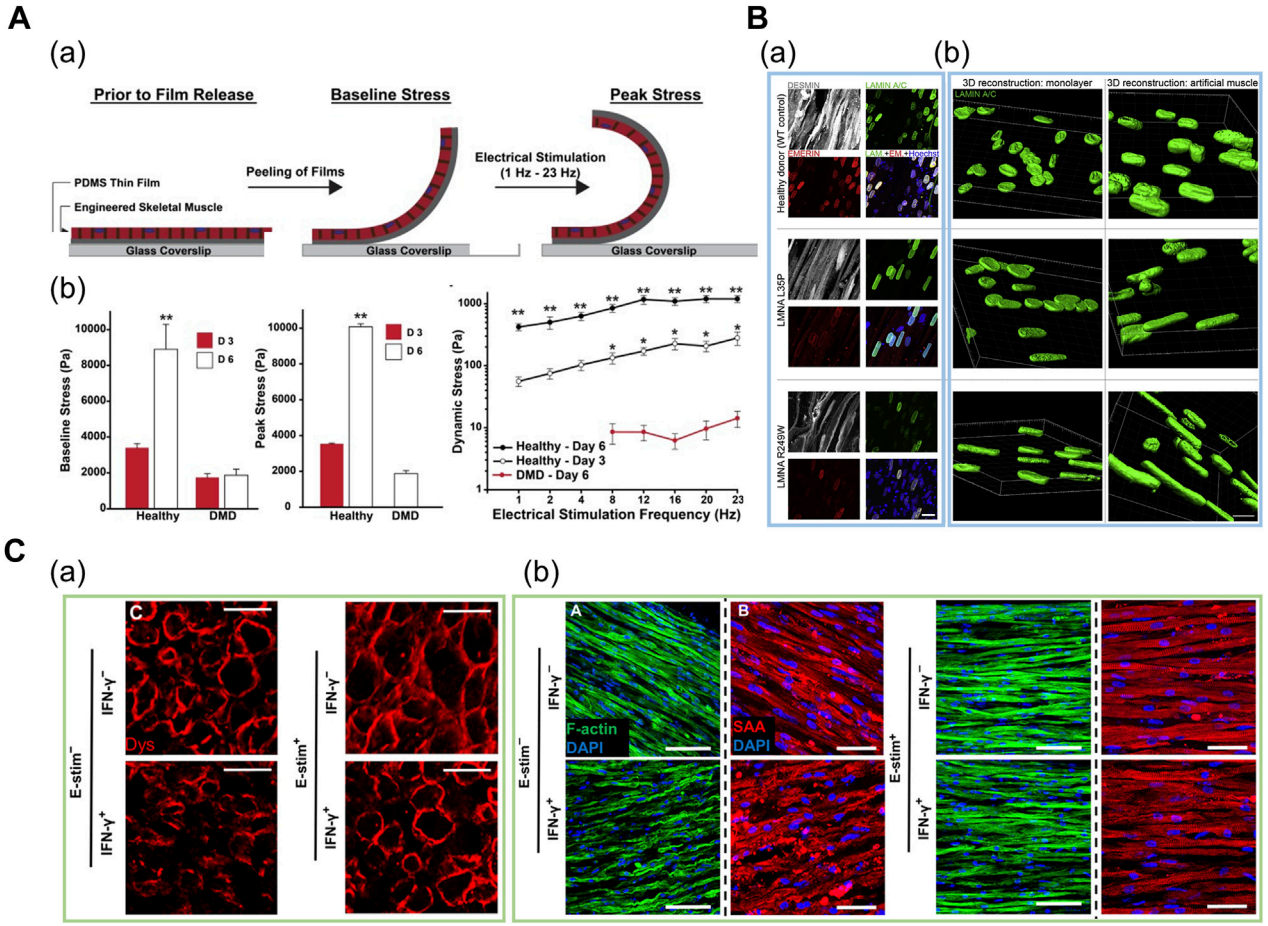

FIGURE 5 | (A) Engineered human DMD model in cantilevered design. (a) Schematic of tissues undergoing baseline and peak stress. (b) Baseline, peak, and dynamic stress in healthy tissues at day 3 and day 6, and in DMD tissues at day 6. Reprinted with permission from (Nesmith et al., 2016). **(B)** Patient-derived iPSC-based engineered LMNA model. (a) Whole-mount confocal images of myotubes (gray) and nuclear lamina (green for LAMIN A/C and red for emerin) on iPSC-based engineered muscles derived from healthy and two LMNA mutants. (b) 3D nuclear reconstructions of patient-derived iPSCs differentiated in 3D-engineered muscles highlight more prominent nuclear deformities and elongation as compared to monolayer cultures. Reprinted with permission from (Maffioletti et al., 2018). **(C)** Engineered human cardiac muscle for modeling exercise-mediated attenuation of IFN-γ-induced muscle wasting. (a) Cross-sections of engineered muscle immunostained for dystrophin indicates attenuated muscle atrophy under exercise–mimetic electrical stimulation. (b) Longitudinal sections of engineered muscle immunostained for F-actin (green) and sarcomeric α-actinin (red). Electrical stimulation prevented IFN-γ-induced decrease of sarcomere organization. Reprinted with permission from (Chen et al., 2021).

the results of *in vivo* resistance exercise regimens. Insulin-like growth factor-1, which is associated in skeletal muscle growth, was upregulated 21 h after the cessation of mechanical load (15% elongation of engineered construct); after 45 h from cessation, the atrophic gene MAFbx underwent significant downregulation. In addition, maximal isometric force exhibited an increase of 140% (21 h) and 265% (45 h) as compared to nonloaded constructs (Aguilar-Agon et al., 2019). Collectively, the electrical stimulation and mechanical loading could result in significant muscle hypertrophy and increase in force generation, which can potentially enable the maturation of engineered muscle to a similar extent as that in human adult muscle.

RECAPITULATION OF SKELETAL MUSCLE TISSUE-RELATED DISEASES

The representation of a more human-like pathology for preclinical studies relies on the maturity and complexity of the model. In context, several muscle-disease phenotypes have been achieved in 3D-engineered skeletal muscles, which were not earlier displayed in 2D cultures or animal models. The recent studies conducted using a 3D-engineered muscle model that recapitulated the major disease phenotypes of severe muscular dystrophies (MDs) and inflammatory muscle diseases are discussed and reviewed herein.

Muscular Dystrophies and Muscle Weakness

Muscular dystrophies arise from mutations in genes encoding various proteins such as muscle ECM, cytoplasmic and plasma membrane proteins that result in progressive muscle weakness or wasting (Tedesco and Cossu, 2012). The most common and severe type of dystrophy, DMD, is an X-linked recessive disorder that occurs almost exclusively in males. The underlying mechanism of DMD is attributed to the mutation in the gene encoding dystrophin, a membrane-bound cytoskeletal protein that links the intracellular actin cytoskeleton to extracellular matrix. Therefore, the absence of dystrophin destabilizes the membranes and causes consistent muscle fiber damage during contraction, which results in consistent fiber degeneration (Nowak and Davies, 2004; Allen and Whitehead, 2010).

Thus, patient-derived cells are cultured under uniaxial tension or micropatterned substrates to form a 3D myofiber for modeling DMD. During and after the culture, the cells are screened for degenerative morphologies such as less sarcomeric α-actinin organization and decreased contractile force. Nesmith et al. (2016) fabricated a thin, contractile muscular film composed of DMD patient-derived cells in a cantilevered design by printing an array of thin bands using a microcontact printing method (**Figure 5A**). Under electrical stimulation with increasing frequencies ranging from 1 to 4 Hz, the dynamic stress on the healthy tissues on day 6 was at least one order of magnitude higher in comparison to the diseased tissues, as evaluated based on the variations in the radius of film curvature. The results implied that the impaired force transmission caused by the absence of dystrophin was recapitulated in this system (Nesmith et al., 2016). Subsequently, Khodabukus et al. (2019) used fibrin-based 3D "myobundles" confined to rectangular Teflon frames to demonstrate the correct membrane-bound localization of dystrophin. Moreover, the electrical stimulation increased the dystrophin, myosin heavy chain, and sarcomeric α-actinin content (Khodabukus et al., 2019). Overall, the 3D-engineered muscle models can represent more adult-like phenotypes as compared to the developmentally less matured cytoplasmic localization of dystrophin in conventional 2D culture (Serena et al., 2016).

Maffioletti et al. (2018) applied a tensile force to fibrin-based 3D engineered tissue and generated a multilineage patient-specific model using a patient-derived iPSC of laminopathy (LMNA), which is one of the MD types (**Figure 5B**). LMNA results from the mutation of the LAMIN A/C gene encoding a protein that composes the nuclear lamina. Under uniaxial tension, hiPSCs were successfully differentiated into myofiber-resembling structures. Notably, the genotype–phenotype correlation was achieved as hiPSCs displayed significant nuclear abnormalities such as nuclear elongation, which was absent in normal muscles and other dystrophic hiPSC lines (Maffioletti et al., 2018). Moreover, Bersini et al. (2018) demonstrated a multicellular DMD model composed of cells from human biopsy to mimic the aberrant fibrosis. They fabricated a spatially organized mesoscale system where differentiated myofibers were surrounded by 3D microvascular network and a fibroblast layer. In particular, collagen and fibronectin secretion levels were significantly higher in patient-derived fibroblasts as compared to normal and TGF-β1 treated fibroblasts. This trend was not displayed in 2D triculture system, indicating that the 3D mesoscale system supported more physiologically relevant fibrosis progression such as muscle-specific fibroblast recruitment. Furthermore, the α-smooth muscle actin, which is expressed in the fibroblasts residing in the dystrophic muscle, was expressed in high levels in the DMD fibroblasts, thereby indicating an accurate representation of the DMD-affected tissue microenvironment (Bersini et al., 2018).

Inflammatory Muscle Disease and Skeletal Muscle Self-Repair

Skeletal muscle self-repair in response to mild injuries is modulated by the interaction between the muscle-resident satellite cells and the immune system via the process of satellite cell activation, proliferation, and differentiation. However, excessive and unregulated inflammatory responses are associated with muscle loss and weakness, which has been reported in several types of diseases including sarcopenia, cachexia, chronic obstructive pulmonary disease and rheumatoid arthritis. In particular, several clinical studies have reported that elevated IFN-γ levels in autoimmune diseases and chronic inflammation contribute toward muscle wasting.

Based on a 3D fibrin-based engineered cardiac muscle tissue composed of human primary cells, Chen et al. (2021) assessed the influence of exercise on IFN-γ-induced muscle wasting (**Figure 5C**). In this model, muscle atrophy was characterized by weaker and slower muscle contraction and reduced calcium-handling protein expression. Notably, the exercise-mimetic electrical stimulation with IFN-γ treatment rescued the sarcomeric protein organization and elongated the myotube, thereby implying an attenuated muscle atrophy condition. In particular, inhibited expression of IFN-γ-induced JAK (Janus kinase)/STAT (signal transducer and activator of transcription) pathway downstream proteins suggested the previously unknown, exercise-mediated cell autonomous anti-inflammatory response that occurs in the muscle tissue, besides the paracrine signalling which has been traditionally suggested as the fundamental mechanism. Furthermore, prevention of muscle atrophy after treatment of FDA-approved small-molecule inhibitors of JAK/STAT pathway confirmed the utility of this platform for preclinical drug screening (Chen et al., 2021).

Juhas et al. (2018) established a 3D co-culture system based on previously referred 3D engineered muscle to assess the role of macrophages in skeletal muscle regeneration process. An inhibited endogenous self-repair process was successfully mimicked as progressive myofiber degeneration was induced after cardiotoxic injury, which resembled a severe muscle

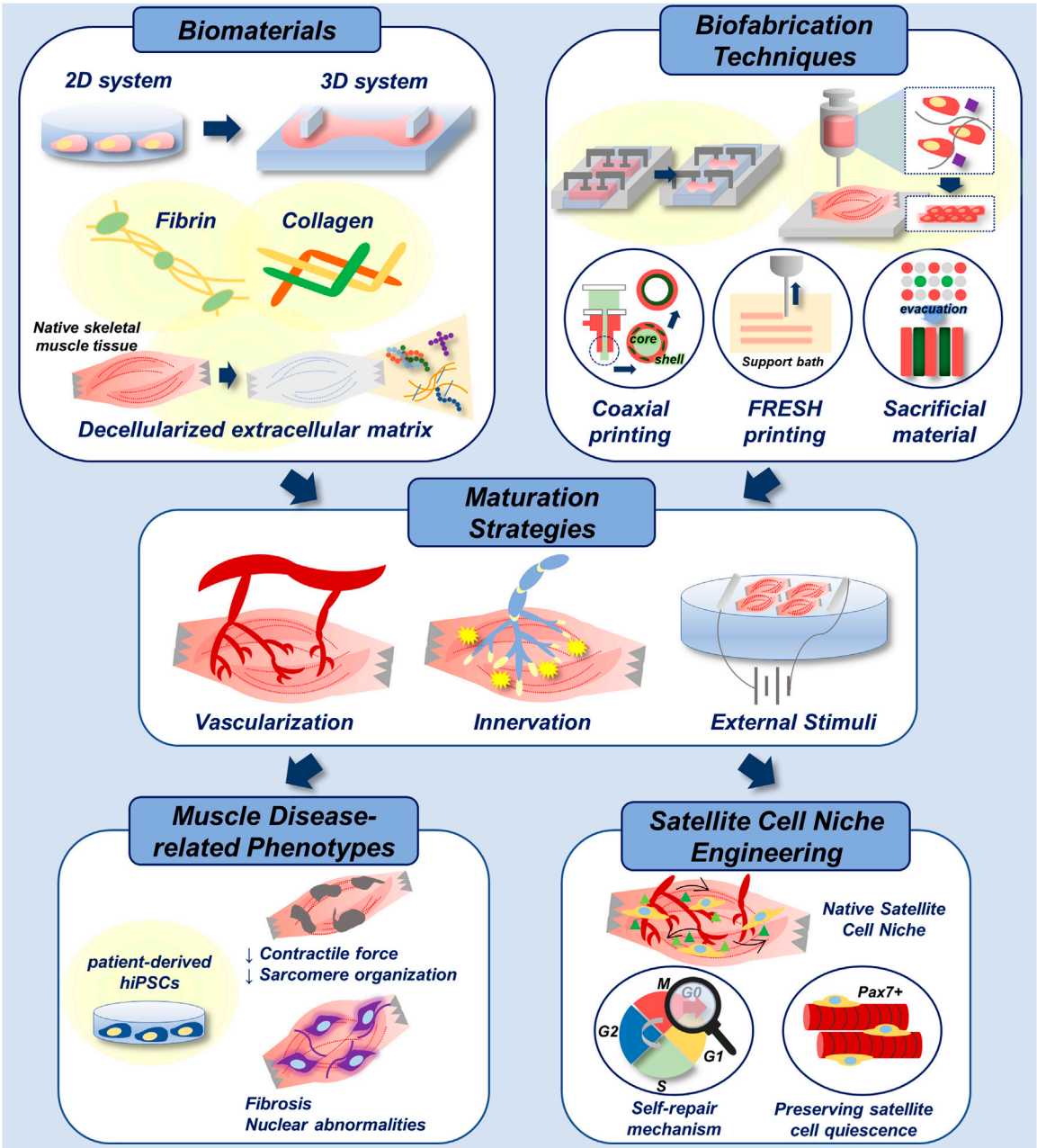

FIGURE 6 | Biofabrication of skeletal muscle disease models. Multiple biomaterials and biofabrication techniques can be utilized to develop 3D-engineered muscle with native tissue-like stiffness and topography (top). Functional maturation of 3D-engineered tissue is achieved by vascularization, innervation and electrical/mechanical stimuli (middle). With the incorporation of patient-derived hiPSCs, addressed biofabrication techniques can be applied in recapitulation of muscle disease-related phenotypes *in vitro*. In addition, they could be applied in engineering of native satellite cell niche for the study of muscle self-repair mechanism, and for the preservation of satellite cell quiescence *in vitro*, which enhances the therapeutic efficacy of cells (bottom).

injury. Then a robust regenerative response was induced upon incorporating bone-marrow derived macrophages with lower levels of activated caspase 3, which indicated that the anti-apoptotic paracrine signalling between the muscle and macrophages were mimicked in this model. Furthermore, the implantation of macrophage-incorporated engineered muscles in a mouse dorsal window-chamber model resulted in robust blood vessel ingrowth and functional muscle regeneration. As such, the *in vitro* incorporation of macrophages can be considered as an effective approach for preconditioning an implantable construct in a pro-regenerative milieu before implantation (Juhas et al., 2018).

FUTURE APPLICATIONS

To date, the incorporation of patient-derived cells and induction of chemical injuries in 3D-engineered muscle models have successfully modeled multiple types of muscle diseases. Although several muscle diseases exhibit combined features of muscle and connective tissue pathology (e.g., limb-girdle muscular dystrophy) (Csapo et al., 2020), only certain models have utilized the aspect of the diseased ECM. Aberrant fibrosis accounts for one of the most prominent features of DMD (Bersini et al., 2018), as it causes the accumulation of collagen I and fibronectin. In particular, the combination of mechanical stimuli and diseased ECM could accurately model the progression of multiple type of unveiled muscular dystrophies. Moreover, 3D muscle-like architecture in engineered muscles might aid in the accurate recapitulation of the cell–matrix interaction.

In addition, engineering a native satellite cell niche-mimicking microenvironment is an emerging topic. In an attempt to preserve satellite cell quiescence *in vitro*, Quarta et al. (2016) fabricated a 3D-engineered muscle composed of muscle satellite cells using a micropost platform. They screened for the micropost stiffness that was known to affect the stem cell behaviour. Moreover, they defined the factors that could assist satellite cell quiescence *in vitro* and applied it in the culture of the engineered muscle (Quarta et al., 2016). Alternatively, Lee et al. (2020) utilized a 3D microfluidic platform to establish vascular architecture of the satellite cell niche *in vitro*, where the intercirculation of niche factors between young and old satellite cells were demonstrated (Lee et al., 2020). These models are potentially useful for modelling the satellite cell activation, quiescence, self-renewal and differentiation (Ishii et al., 2018; Csapo et al., 2020) which all aid in skeletal muscle self-repair mechanism (**Figure 6**).

The preservation of satellite cell quiescence impacts the therapeutic efficacy of the cells as well. Ishii et al. (2018) identified a laminin-type component of basement membrane that encapsulates satellite cells. Thereafter, they prepared a recombinant protein that partially contained the C-terminal of the original basement membrane component, which was mixed with Matrigel. Under the *in vitro* culture of using the substrate, the satellite cell quiescence was preserved, and the enhanced muscle regeneration capacity was confirmed *in vivo* (Ishii et al., 2018). Overall, these approaches would endow isolated primary cells with enhanced engraftment potential and muscle regeneration capacities, which could facilitate the improvement of current regenerative therapies for volumetric muscle loss.

Endogenous muscle self-repair is supported by interactions between muscle satellite cells and multiple types of muscle-resident cells, including macrophages, $CD3^+$ T cells, endothelial cells, and fibro-adipogenic progenitors that collectively form a complex inflammatory milieu (Fu et al., 2015; Quarta et al., 2017; Judson et al., 2020). However, current *in vitro* models of muscle self-repair partially recapitulate the microenvironment of the regenerating muscle, as satellite cells are co-cultured with either macrophages or endothelial cells (Juhas et al., 2018; Lee et al., 2020). Therefore, the incorporation of multiple cell types is required for an in-depth understanding of the mechanism of satellite cell quiescence in regenerating muscles. Moreover, the sorting and expansion of the desired cell population among a larger pool of cells remain challenges for obtaining a sufficient number of cells and in applying these models in preclinical settings.

AUTHOR CONTRIBUTIONS

SC and JJ contributed with the draft design and conception. SC wrote the original draft and organized the figures, and JJ revised the draft and supervised the work. All authors agree on the final submission of the manuscript.

FUNDING

This work was supported by the National Research Foundation of Korea (NRF) grant funded by the Korea government (MSIT) (NRF-2020M3H4A1A02084827). This work was also supported by Korean Fund for Regenerative Medicine funded by Ministry of Science and ICT, and Ministry of Health and Welfare (NRF-2021M3E5E5096524, Republic of Korea).

REFERENCES

Afshar Bakooshli, M., Lippmann, E. S., Mulcahy, B., Iyer, N., Nguyen, C. T., Tung, K., et al. (2019). A 3d Culture Model of Innervated Human Skeletal Muscle Enables Studies of the Adult Neuromuscular junction. *eLife* 8, 1–29. doi:10.7554/eLife.44530

Agrawal, G., Aung, A., and Varghese, S. (2017). Skeletal Muscle-On-A-Chip: An *In Vitro* Model to Evaluate Tissue Formation and Injury. *Lab. Chip* 17, 3447–3461. doi:10.1039/c7lc00512a

Aguilar-Agon, K. W., Capel, A. J., Martin, N. R. W., Player, D. J., and Lewis, M. P. (2019). Mechanical Loading Stimulates Hypertrophy in Tissue-Engineered Skeletal Muscle: Molecular and Phenotypic Responses. *J. Cel. Physiol* 234, 23547–23558. doi:10.1002/jcp.28923

Alfano, L. N., Charleston, J. S., Connolly, A. M., Cripe, L., Donoghue, C., Dracker, R., et al. (2019). Long-term Treatment with Eteplirsen in Nonambulatory Patients with Duchenne Muscular Dystrophy. *Medicine* 98, e15858. doi:10.1097/MD.0000000000015858

Allen, D. G., and Whitehead, N. P. (2010). Duchenne Muscular Dystrophy-Wwhat Causes the Increased Membrane Permeability in Skeletal Muscle. *Int. J. Biochem. Cel Biol.* 43, 290–294. doi:10.1016/j.biocel.2010.11.005

Baiguera, S., Del Gaudio, C., Lucatelli, E., Kuevda, E., Boieri, M., Mazzanti, B., et al. (2014). Electrospun Gelatin Scaffolds Incorporating Rat Decellularized Brain Extracellular Matrix for Neural Tissue Engineering. *Biomaterials* 35, 1205–1214. doi:10.1016/j.biomaterials.2013.10.060

Bersini, S., Gilardi, M., Ugolini, G. S., Sansoni, V., Talò, G., Perego, S., et al. (2018). Engineering an Environment for the Study of Fibrosis: A 3D Human Muscle Model with Endothelium Specificity and Endomysium. *Cel Rep.* 25, 3858–3868. doi:10.1016/j.celrep.2018.11.092

Bertassoni, L. E., Cecconi, M., Manoharan, V., Nikkhah, M., Hjortnaes, J., Cristino, A. L., et al. (2014). Hydrogel Bioprinted Microchannel Networks for Vascularization of Tissue Engineering Constructs. *Lab. Chip* 14, 2202–2211. doi:10.1039/c4lc00030g

Bhattacharjee, T., Zehnder, S. M., Rowe, K. G., Jain, S., Nixon, R. M., Sawyer, W. G., et al. (2015). Writing in the Granular Gel Medium. *Sci. Adv.* 25, e1500655. doi:10.1126/sciadv.1500655

Bursac, N., Juhas, M., and Rando, T. A. (2015). Synergizing Engineering and Biology to Treat and Model Skeletal Muscle Injury and Disease. *Annu. Rev. Biomed. Eng.* 17, 217–242. doi:10.1146/annurev-bioeng-071114-040640

Buyse, G. M., Van Der Mieren, G., Erb, M., D'hooge, J., Herijgers, P., Verbeken, E., et al. (2009). Long-term Blinded Placebo-Controlled Study of SNT-MC17/idebenone in the Dystrophin Deficient Mdx Mouse: Cardiac protection and Improved Exercise Performance. *Eur. Heart J.* 30, 116–124. doi:10.1093/eurheartj/ehn406

Chen, Z., Li, B., Zhan, R. Z., Rao, L., and Bursac, N. (2021). Exercise Mimetics and JAK Inhibition Attenuate IFN-γ-Induced Wasting in Engineered Human Skeletal Muscle. *Sci. Adv.* 7, 4. doi:10.1126/sciadv.abd9502

Choi, Y.-J., Jun, Y.-J., Kim, D. Y., Yi, H.-G., Chae, S.-H., Kang, J., et al. (2019). A 3D Cell Printed Muscle Construct with Tissue-Derived Bioink for the Treatment of Volumetric Muscle Loss. *Biomaterials* 206, 160–169. doi:10.1016/j.biomaterials.2019.03.036

Choi, Y.-J., Kim, T. G., Jeong, J., Yi, H.-G., Park, J. W., Hwang, W., et al. (2016). 3D Cell Printing of Functional Skeletal Muscle Constructs Using Skeletal Muscle-Derived Bioink. *Adv. Healthc. Mater.* 5, 2636–2645. doi:10.1002/adhm.201600483

Christensen, R. K., Von Halling Laier, C., Kiziltay, A., Wilson, S., and Larsen, N. B. (2020). 3D Printed Hydrogel Multiassay Platforms for Robust Generation of Engineered Contractile Tissues. *Biomacromolecules* 21, 356–365. doi:10.1021/acs.biomac.9b01274

Clemens, P. R., Rao, V. K., Connolly, A. M., Harper, A. D., Mah, J. K., Smith, E. C., et al. (2020). Safety, Tolerability, and Efficacy of Viltolarsen in Boys with Duchenne Muscular Dystrophy Amenable to Exon 53 Skipping. *JAMA Neurol.* 77, 982–991. doi:10.1001/jamaneurol.2020.1264

Compton, B. G., and Lewis, J. A. (2014). 3D-Printing of Lightweight Cellular Composites. *Adv. Mater.* 26, 5930–5935. doi:10.1002/adma.201401804

Csapo, R., Gumpenberger, M., and Wessner, B. (2020). Skeletal Muscle Extracellular Matrix - what Do We Know about its Composition, Regulation, and Physiological Roles? A Narrative Review. *Front. Physiol.* 11, 253. doi:10.3389/fphys.2020.00253

Cvetkovic, C., Rich, M. H., Raman, R., Kong, H., and Bashir, R. (2017). A 3D-Printed Platform for Modular Neuromuscular Motor Units. *Microsyst. Nanoeng* 3, 17015–17019. doi:10.1038/micronano.2017.15

Daly, A. C., Pitacco, P., Nulty, J., Cunniffe, G. M., and Kelly, D. J. (2018). 3D Printed Microchannel Networks to Direct Vascularisation during Endochondral Bone Repair. *Biomaterials* 162, 34–46. doi:10.1016/j.biomaterials.2018.01.057

Das, S., Kim, S.-W., Choi, Y.-J., Lee, S., Lee, S.-H., Kong, J.-S., et al. (2019). Decellularized Extracellular Matrix Bioinks and the External Stimuli to Enhance Cardiac Tissue Development *In Vitro*. *Acta Biomater.* 95, 188–200. doi:10.1016/j.actbio.2019.04.026

Dixon, T. A., Cohen, E., Cairns, D. M., Rodriguez, M., Mathews, J., Jose, R. R., et al. (2018). Bioinspired Three-Dimensional Human Neuromuscular Junction Development in Suspended Hydrogel Arrays. *Tissue Eng. C: Methods* 24, 346–359. doi:10.1089/ten.tec.2018.0062

Eken, T., Elder, G. C. B., and Lømo, T. (2008). Development of Tonic Firing Behavior in Rat Soleus Muscle. *J. Neurophysiol.* 99, 1899–1905. doi:10.1152/jn.00834.2007

Engler, A. J., Griffin, M. A., Sen, S., Bönnemann, C. G., Sweeney, H. L., Discher, D. E., et al. (2004). Myotubes Differentiate Optimally on Substrates with Tissue-like Stiffness. *J. Cel. Biol.* 166, 877–887. doi:10.1083/jcb.200405004

Flynn, L. E. (2010). The Use of Decellularized Adipose Tissue to Provide an Inductive Microenvironment for the Adipogenic Differentiation of Human Adipose-Derived Stem Cells. *Biomaterials* 31, 4715–4724. doi:10.1016/j.biomaterials.2010.02.046

Frank, D. E., Schnell, F. J., Akana, C., El-Husayni, S. H., Desjardins, C. A., Morgan, J., et al. (2020). Increased Dystrophin Production with Golodirsen in Patients with Duchenne Muscular Dystrophy. *Neurology* 94, e2270–e2282. doi:10.1212/WNL.0000000000009233

Fu, X., Xiao, J., Wei, Y., Li, S., Liu, Y., Yin, J., et al. (2015). Combination of Inflammation-Related Cytokines Promotes Long-Term Muscle Stem Cell Expansion. *Cell Res.* 25, 655–673. doi:10.1038/cr.2015.58

Furberg, C. D., and Pitt, B. (2001). Withdrawal of Cerivastatin from the World Market. *Curr. Control. Trials Cardiovasc. Med.* 2, 205. doi:10.1186/cvm-2-5-205

Gao, G., Kim, H., Kim, B. S., Kong, J. S., Lee, J. Y., Park, B. W., et al. (2019). Tissue-engineering of Vascular Grafts Containing Endothelium and Smooth-Muscle Using Triple-Coaxial Cell Printing. *Appl. Phys. Rev.* 6, 041402. doi:10.1063/1.5099306

Gao, G., Lee, J. H., Jang, J., Lee, D. H., Kong, J. S., Kim, B. S., et al. (2017). Tissue Engineered Bio-Blood-Vessels Constructed Using a Tissue-specific Bioink and 3D Coaxial Cell Printing Technique: A Novel Therapy for Ischemic Disease. *Adv. Funct. Mater.* 27, 1–12. doi:10.1002/adfm.201700798

Gao, G., Park, W., Kim, B. S., Ahn, M., Chae, S., Cho, W. W., et al. (2021). Construction of a Novel *In Vitro* Atherosclerotic Model from Geometry-Tunable Artery Equivalents Engineered via in-Bath Coaxial Cell Printing. *Adv. Funct. Mater.* 31, 1–15. doi:10.1002/adfm.202008878

Gilbert-Honick, J., Iyer, S. R., Somers, S. M., Lovering, R. M., Wagner, K., Mao, H.-Q., et al. (2018). Engineering Functional and Histological Regeneration of Vascularized Skeletal Muscle. *Biomaterials* 164, 70–79. doi:10.1016/j.biomaterials.2018.02.006

Grady, R. M., Teng, H., Nichol, M. C., Cunningham, J. C., Wilkinson, R. S.., Sanes, J. R., et al. (1997). Skeletal and Cardiac Myopathies in Mice Lacking Utrophin and Dystrophin: A Model for Duchenne Muscular Dystrophy. *Cell* 90, 729–238. doi:10.1016/S0092-8674(00)80533-4

Grosberg, A., Alford, P. W., McCain, M. L., and Parker, K. K. (2011). Ensembles of Engineered Cardiac Tissues for Physiological and Pharmacological Study: Heart on a Chip. *Lab. Chip* 11, 4165–4173. doi:10.1039/C1LC20557A

Hinds, S., Bian, W., Dennis, R. G., and Bursac, N. (2011). The Role of Extracellular Matrix Composition in Structure and Function of Bioengineered Skeletal Muscle. *Biomaterials* 32, 3575–3583. doi:10.1016/j.biomaterials.2011.01.062

Hinton, T. J., Jallerat, Q., Palchesko, R. N., Park, J. H., Grodzicki, M. S., Shue, H. J., et al. (2015). Three-dimensional Printing of Complex Biological Structures by Freeform Reversible Embedding of Suspended Hydrogels. *Sci. Adv.* 1, e1500758. doi:10.1126/sciadv.1500758

Huang, L., Zhu, L., Shi, X., Xia, B., Liu, Z., Zhu, S., et al. (2018). A Compound Scaffold with Uniform Longitudinally Oriented Guidance Cues and a Porous Sheath Promotes Peripheral Nerve Regeneration *In Vivo*. *Acta Biomater.* 68, 223–236. doi:10.1016/j.actbio.2017.12.010

Hwangbo, H., Lee, H., Roh, E. J., Kim, W. J., Joshi, H. P., Kwon, S. Y., et al. (2021). Bone Tissue Engineering via Application of a Collagen/hydroxyapatite 4D-Printed Biomimetic Scaffold for Spinal Fusion. *Appl. Phys. Rev.* 8, 021403. doi:10.1063/5.0035601

Isaac, C., Wright, A., Usas, A., Li, H., Tang, Y., Mu, X., et al. (2012). Dystrophin and Utrophin "Double Knockout" Dystrophic Mice Exhibit a Spectrum of Degenerative Musculoskeletal Abnormalities. *J. Orthop. Res.* 31, 343–349. doi:10.1002/jor.22236

Ishii, K., Sakurai, H., Suzuki, N., Mabuchi, Y., Sekiya, I., Sekiguchi, K., et al. (2018). Recapitulation of Extracellular LAMININ Environment Maintains Stemness of Satellite Cells *In Vitro*. *Stem Cel Rep.* 10, 568–582. doi:10.1016/j.stemcr.2017.12.013

Jin, Y., Shahriari, D., Jeon, E. J., Park, S., Choi, Y. S., Back, J., et al. (2021). Functional Skeletal Muscle Regeneration with Thermally Drawn Porous Fibers and Reprogrammed Muscle Progenitors for Volumetric Muscle Injury. *Adv. Mater.* 33, 1–11. doi:10.1002/adma.202007946

Judson, R. N., and Rossi, F. M. V. (2020). Towards Stem Cell Therapies for Skeletal Muscle Repair. *NPJ Regen. Med.* 5, 10. doi:10.1038/s41536-020-0094-3

Juhas, M., Abutaleb, N., Wang, J. T., Ye, J., Shaikh, Z., Sriworarat, C., et al. (2018). Incorporation of Macrophages into Engineered Skeletal Muscle Enables Enhanced Muscle Regeneration. *Nat. Biomed. Eng.* 2, 942–954. doi:10.1038/s41551-018-0290-2

Kang, H.-W., Lee, S. J., Ko, I. K., Kengla, C., Yoo, J. J., Atala, A., et al. (2016). A 3D Bioprinting System to Produce Human-Scale Tissue Constructs with Structural Integrity. *Nat. Biotechnol.* 34, 312–319. doi:10.1038/nbt.3413

Khodabukus, A., and Baar, K. (2012). Defined Electrical Stimulation Emphasizing Excitability for the Development and Testing of Engineered Skeletal Muscle. *Tissue Eng. Part C: Methods* 18, 349–357. doi:10.1089/ten.tec.2011.0364

Khodabukus, A., Madden, L., Prabhu, N. K., Koves, T. R., Jackman, C. P., Muoio, D. M., et al. (2019). Electrical Stimulation Increases Hypertrophy and Metabolic Flux in Tissue-Engineered Human Skeletal Muscle. *Biomaterials* 198, 259–269. doi:10.1016/j.biomaterials.2018.08.058

Kim, H., Kang, B., Cui, X., Lee, S. H., Lee, K., Cho, D. W., et al. (2021). Light-Activated Decellularized Extracellular Matrix-Based Bioinks for Volumetric

Tissue Analogs at the Centimeter Scale. *Adv. Funct. Mater.* 31, 2011252. doi:10.1002/adfm.202011252

Kim, H., Kim, M.-C., and Asada, H. H. (2019). Extracellular Matrix Remodelling Induced by Alternating Electrical and Mechanical Stimulations Increases the Contraction of Engineered Skeletal Muscle Tissues. *Sci. Rep.* 9, 2732. doi:10.1038/s41598-019-39522-6

Kim, J. H., Kim, I., Seol, Y. J., Ko, I. K., Yoo, J. J., Atala, A., et al. (2020). Neural Cell Integration into 3D Bioprinted Skeletal Muscle Constructs Accelerates Restoration of Muscle Function. *Nat. Commun.* 11, 1025. doi:10.1038/s41467-020-14930-9

Kim, W., Kim, M., and Kim, G. H. (2018a). 3D-Printed Biomimetic Scaffold Simulating Microfibril Muscle Structure. *Adv. Funct. Mater.* 28, 1800405. doi:10.1002/adfm.201800405

Kim, J. H., Seol, Y. J., Ko, I. K., Kang, H. W., Lee, Y. K., Yoo, J. J., et al. (2018b). 3D Bioprinted Human Skeletal Muscle Constructs for Muscle Function Restoration. *Sci. Rep.* 8, 12307–12315. doi:10.1038/s41598-018-29968-5

Kim, W., Jang, C. H., and Kim, G. H. (2019). A Myoblast-Laden Collagen Bioink with Fully Aligned Au Nanowires for Muscle-Tissue Regeneration. *Nano Lett.* 19, 8612–8620. doi:10.1021/acs.nanolett.9b03182

Kim, W., and Kim, G. (2019). A Functional Bioink and its Application in Myoblast Alignment and Differentiation. *Chem. Eng. J.* 366, 150–162. doi:10.1016/j.cej.2019.02.071

Kim, W., Lee, H., Lee, J., Atala, A., Yoo, J. J., Lee, S. J., et al. (2020). Efficient Myotube Formation in 3D Bioprinted Tissue Construct by Biochemical and Topographical Cues. *Biomaterials* 230, 119632. doi:10.1016/j.biomaterials.2019.119632

Kolesky, D. B., Homan, K. A., Skylar-Scott, M. A., and Lewis, J. A. (2016). Three-dimensional Bioprinting of Thick Vascularized Tissues. *Proc. Natl. Acad. Sci. U.S.A* 113, 3179–3184. doi:10.1073/pnas.1521342113

Kong, J. S., Huang, X., Choi, Y. J., Yi, H. G., Kang, J., Kim, S., et al. (2021). Promoting Long-Term Cultivation of Motor Neurons for 3D Neuromuscular Junction Formation of 3D *In Vitro* Using Central-Nervous-Tissue-Derived Bioink. *Adv. Healthc. Mater.* 10, 2100581. doi:10.1002/adhm.202100581

Kuschel, R., Yablonka-Reuveni, Z., and Bornemann, A. (1999). Satellite Cells on Isolated Myofibers from normal and Denervated Adult Rat Muscle. *J. Histochem. Cytochem.* 47, 1375–1383. doi:10.1177/002215549904701104

Lee, A., Hudson, A. R., Shiwarski, D. J., Tashman, J. W., Hinton, T. J., Yerneni, S., et al. (2019). 3D Bioprinting of Collagen to Rebuild Components of the Human Heart. *Science* 365, 482–487. doi:10.1126/science.aav9051

Lee, J. B., Kim, D.-H., Yoon, J.-K., Park, D. B., Kim, H.-S., Shin, Y. M., et al. (2020). Microchannel Network Hydrogel Induced Ischemic Blood Perfusion Connection. *Nat. Commun.* 11, 615. doi:10.1038/s41467-020-14480-0

Lee, Y., Choi, J. J., Ahn, S. I., Lee, N. H., Han, W. M., Mohiuddin, M., et al. (2020). Engineered Heterochronic Parabiosis in 3D Microphysiological System for Identification of Muscle Rejuvenating Factors. *Adv. Funct. Mater.* 30, 2002924. doi:10.1002/adfm.202002924

Madden, L., Juhas, M., Kraus, W. E., Truskey, G. A., and Bursac, N. (2015). Bioengineered Human Myobundles Mimic Clinical Responses of Skeletal Muscle to Drugs. *ELife* 4, e04885. doi:10.7554/eLife.04885

Maffioletti, S. M., Sarcar, S., Henderson, A. B. H., Mannhardt, I., Pinton, L., Moyle, L. A., et al. (2018). Three-Dimensional Human iPSC-Derived Artificial Skeletal Muscles Model Muscular Dystrophies and Enable Multilineage Tissue Engineering. *Cel Rep.* 23, 899–908. doi:10.1016/j.celrep.2018.03.091

Marcinczyk, M., Elmashhady, H., Talovic, M., Dunn, A., Bugis, F., Garg, K., et al. (2017). Laminin-111 Enriched Fibrin Hydrogels for Skeletal Muscle Regeneration. *Biomaterials* 141, 233–242. doi:10.1016/j.biomaterials.2017.07.003

Mayer, U. (2003). Integrins: Redundant or Important Players in Skeletal Muscle. *J. Biol. Chem.* 278, 14587–14590. doi:10.1074/jbc.R200022200

McGreevy, J. W., Hakim, C. H., McIntosh, M. A., and Duan, D. (2015). Animal Models of Duchenne Muscular Dystrophy: From Basic Mechanisms to Gene Therapy. *Dis. Model. Mech.* 8, 195–213. doi:10.1242/dmm.018424

Miller, J. S., Stevens, K. R., Yang, M. T., Baker, B. M., Nguyen, D.-H. T., Cohen, D. M., et al. (2012). Rapid Casting of Patterned Vascular Networks for Perfusable Engineered Three-Dimensional Tissues. *Nat. Mater* 11, 768–774. doi:10.1038/nmat3357

Morimoto, Y., Kato-Negishi, M., Onoe, H., and Takeuchi, S. (2013). Three-dimensional Neuron-Muscle Constructs with Neuromuscular Junctions. *Biomaterials* 34, 9413–9419. doi:10.1016/j.biomaterials.2013.08.062

Morimoto, Y., Onoe, H., and Takeuchi, S. (2020). Biohybrid Robot with Skeletal Muscle Tissue Covered with a Collagen Structure for Moving in Air. *APL Bioeng.* 4, 026101. doi:10.1063/1.5127204

Mozetic, P., Giannitelli, S. M., Gori, M., Trombetta, M., and Rainer, A. (2017). Engineering Muscle Cell Alignment through 3D Bioprinting. *J. Biomed. Mater. Res.* 105, 2582–2588. doi:10.1002/jbm.a.36117

Nesmith, A. P., Wagner, M. A., Pasqualini, F. S., O'Connor, B. B., Pincus, M. J., August, P. R., et al. (2016). A Human *In Vitro* Model of Duchenne Muscular Dystrophy Muscle Formation and Contractility. *J. Cel Biol.* 215, 47–56. doi:10.1083/jcb.201603111

Neufeld, L., Yeini, E., Reisman, N., Shtilerman, Y., Ben-Shushan, D., Pozzi, S., et al. (2021). Microengineered Perfusable 3D-Bioprinted Glioblastoma Model for *In Vivo* Mimicry of Tumor Microenvironment. *Sci. Adv.* 7, 1–20. doi:10.1126/sciadv.abi9119

Nikolić, N., Skaret Bakke, S., Tranheim Kase, E., Rudberg, I., Flo Halle, I., Rustan, A. C., et al. (2012). Electrical Pulse Stimulation of Cultured Human Skeletal Muscle Cells as an *In Vitro* Model of Exercise. *PLoS ONE* 7, 1–10. doi:10.1371/journal.pone.0033203

Nowak, K. J., and Davies, K. E. (2004). Duchenne Muscular Dystrophy and Dystrophin: Pathogenesis and Opportunities for Treatment. *EMBO Rep.* 5, 872–876. doi:10.1038/sj.embor.7400221

Osaki, T., Sivathanu, V., and Kamm, R. D. (2018). Crosstalk between Developing Vasculature and Optogenetically Engineered Skeletal Muscle Improves Muscle Contraction and Angiogenesis. *Biomaterials* 156, 65–76. doi:10.1016/j.biomaterials.2017.11.041

Powell, C. A., Smiley, B. L., Mills, J., and Vandenburgh, H. H. (2002). Mechanical Stimulation Improves Tissue-Engineered Human Skeletal Muscle. *Am. J. Physiology-Cell Physiol.* 283, C1557–C1565. doi:10.1152/ajpcell.00595.2001

Quarta, M., Brett, J. O., DiMarco, R., De Morree, A., Boutet, S. C., Chacon, R., et al. (2016). An Artificial Niche Preserves the Quiescence of Muscle Stem Cells and Enhances Their Therapeutic Efficacy. *Nat. Biotechnol.* 34, 752–759. doi:10.1038/nbt.3576

Quarta, M., Cromie, M., Chacon, R., Blonigan, J., Garcia, V., Akimenko, I., et al. (2017). Bioengineered Constructs Combined with Exercise Enhance Stem Cell-Mediated Treatment of Volumetric Muscle Loss. *Nat. Commun.* 8, 15613. doi:10.1038/ncomms15613

Redd, M. A., Zeinstra, N., Qin, W., Wei, W., Martinson, A., Wang, Y., et al. (2019). Patterned Human Microvascular Grafts Enable Rapid Vascularization and Increase Perfusion in Infarcted Rat Hearts. *Nat. Commun.* 10, 584. doi:10.1038/s41467-019-08388-7

Relaix, F., Bencze, M., Borok, M. J., Der Vartanian, A., Gattazzo, F., Mademtzoglou, D., et al. (2021). Perspectives on Skeletal Muscle Stem Cells. *Nat. Commun.* 12, 1–11. doi:10.1038/s41467-020-20760-6

Schwab, A., Levato, R., D'Este, M., Piluso, S., Eglin, D., and Malda, J. (2020). Printability and Shape Fidelity of Bioinks in 3D Bioprinting. *Chem. Rev.* 120, 11028–11055. doi:10.1021/acs.chemrev.0c00084

Serena, E., Zatti, S., Zoso, A., Lo Verso, F., Tedesco, F. S., Cossu, G., et al. (2016). Skeletal Muscle Differentiation on a Chip Shows Human Donor Mesoangioblasts' Efficiency in Restoring Dystrophin in a Duchenne Muscular Dystrophy Model. *Med.* 5, 1676–1683. doi:10.5966/sctm.2015-0053

Sharples, A. P., Player, D. J., Martin, N. R. W., Mudera, V., Stewart, C. E., and Lewis, M. P. (2012). Modellingin Vivoskeletal Muscle Ageingin Vitrousing Three-Dimensional Bioengineered Constructs. *Aging Cell.* 11, 986–995. doi:10.1111/j.1474-9726.2012.00869.x

Skylar-Scott, M. A., Uzel, S. G. M., Nam, L. L., Ahrens, J. H., Truby, R. L., Damaraju, S., et al. (2019). Biomanufacturing of Organ-specific Tissues with High Cellular Density and Embedded Vascular Channels. *Sci. Adv.* 5, eaaw2459. doi:10.1126/sciadv.aaw2459

Tarum, J., Folkesson, M., Atherton, P. J., and Kadi, F. (2017). Electrical Pulse Stimulation: Anin Vitroexercise Model for the Induction of Human Skeletal Muscle Cell Hypertrophy. A Proof-Of-Concept Study. *Exp. Physiol.* 102, 1405–1413. doi:10.1113/EP086581

Tedesco, F. S., and Cossu, G. (2012). Stem Cell Therapies for Muscle Disorders. *Curr. Opin. Neurol.* 25, 597–603. doi:10.1097/WCO.0b013e328357f288

Uygun, B. E., Soto-Gutierrez, A., Yagi, H., Izamis, M.-L., Guzzardi, M. A., Shulman, C., et al. (2010). Organ Reengineering through Development of a Transplantable Recellularized Liver Graft Using Decellularized Liver Matrix. *Nat. Med.* 16, 814–820. doi:10.1038/nm.2170

Vallat, J.-M., Mathis, S., and Funalot, B. (2013). The Various Charcot-Marie-Tooth Diseases. *Curr. Opin. Neurol.* 26, 473–480. doi:10.1097/WCO.0b013e328364c04b

Westerga, J., and Gramsbergen, A. (1994). Development of the EMG of the Soleus Muscle in the Rat. *Develop. Brain Res.* 80, 233–243. doi:10.1016/0165-3806(94)90108-2

Yin, H., Price, F., and Rudnicki, M. A. (2013). Satellite Cells and the Muscle Stem Cell Niche. *Physiol. Rev.* 93, 23–67. doi:10.1152/physrev.00043.2011

Zhang, Y. S., Arneri, A., Bersini, S., Shin, S.-R., Zhu, K., Goli-Malekabadi, Z., et al. (2016). Bioprinting 3D Microfibrous Scaffolds for Engineering Endothelialized Myocardium and Heart-On-A-Chip. *Biomaterials* 110, 45–59. doi:10.1016/j.biomaterials.2016.09.003

Conflict of Interest: The authors declare that the research was conducted in the absence of any commercial or financial relationships that could be construed as a potential conflict of interest.

frontiers in Bioengineering and Biotechnology

ORIGINAL RESEARCH
published: 05 November 2021
doi: 10.3389/fbioe.2021.786945

Bioprinting of Collagen Type I and II *via* Aerosol Jet Printing for the Replication of Dense Collagenous Tissues

Rory Gibney[1,2]* *and Eleonora Ferraris*[1]*

[1]*Department of Mechanical Engineering, KU Leuven Campus De Nayer, Leuven, Belgium,* [2]*Department of Materials Engineering, KU Leuven, Leuven, Belgium*

Collagen has grown increasingly present in bioprinting, however collagen bioprinting has mostly been limited to the extrusion printing of collagen type I to form weak collagen hydrogels. While these weak collagen hydrogels have their applications, synthetic polymers are often required to reinforce gel-laden constructs that aim to replicate dense collagenous tissues found *in vivo*. In this study, aerosol jet printing (AJP) was used to print and process collagen type I and II into dense constructs with a greater capacity to replicate the dense collagenous ECM found in connective tissues. Collagen type I and II was isolated from animal tissues to form solutions for printing. Collagen type I and II constructs were printed with 576 layers and measured to have average effective elastic moduli of 241.3 ± 94.3 and 196.6 ± 86.0 kPa (±SD), respectively, without any chemical modification. Collagen type II solutions were measured to be less viscous than type I and both collagen type I and II exhibited a drop in viscosity due to AJP. Circular dichroism and SDS-PAGE showed collagen type I to be more vulnerable to structural changes due to the stresses of the aerosol formation step of aerosol jet printing while the collagen type II triple helix was largely unaffected. SEM illustrated that distinct layers remained in the aerosol jet print constructs. The results show that aerosol jet printing should be considered an effective way to process collagen type I and II into stiff dense constructs with suitable mechanical properties for the replication of dense collagenous connective tissues.

Keywords: bioprinting, 3D printing, biomaterials, connective tissue, collagen type II, collagen type I, viscosity, nanoindentation

OPEN ACCESS

Edited by:
Farnaz Ghorbani,
University of Erlangen Nuremberg, Germany

Reviewed by:
Behrouz Zandieh Doulabi,
Vrije Universiteit Amsterdam, Netherlands
Wei Long Ng,
Nanyang Technological University, Singapore

***Correspondence:**
Rory Gibney
rory.gibney2@mail.dcu.ie
Eleonora Ferraris
eleonora.ferraris@kuleuven.be

Specialty section:
This article was submitted to Biomaterials, a section of the journal Frontiers in Bioengineering and Biotechnology

Received: *30 September 2021*
Accepted: *19 October 2021*
Published: *05 November 2021*

Citation:
Gibney R and Ferraris E (2021) Bioprinting of Collagen Type I and II via Aerosol Jet Printing for the Replication of Dense Collagenous Tissues. Front. Bioeng. Biotechnol. 9:786945. doi: 10.3389/fbioe.2021.786945

INTRODUCTION

Collagens are a family of extracellular matrix proteins found in all metazoan ECM from sponges to humans. The first member of the collagen family (a collagen type IV variant) is thought to have evolved over 700 million years ago in the last common ancestor between metazoa, choanoflagellates and filasterean, and is regarded by some as having facilitated multicellularity (Fidler et al., 2018). From this first member of the collagen family the other members are thought to have evolved, which currently rests at 28 different collagens in mammals (Karsdal, 2016). All collagens possess a characteristic right-handed triple helix structure which is assembled by three polypeptide chains, called α-chains, with left-handed polyproline II helices (Adzhubei et al., 2013). The α-chains may be identical, like homotrimeric collagen type II, or a mix of two or more genetically distinct α chains, like heterotrimeric collagen type I. Collagens type I and type II are members of a collagen sub-family

called the fibrillar collagens which are the most common collagens in mammals and are responsible for most of the stereotypical collagen properties, such as, the ability to self-assemble into fibrils with D-banding. They are also used to make collagen hydrogels which are a very attractive tool for tissue engineering given their ability to mimic native ECM for a wide range of tissues (Sander and Barocas, 2008). The formation of collagen hydrogels is based on the self-assembly of fibrils *in vitro*, which is mainly controlled by pH, ionic strength, and temperature (Gobeaux et al., 2008; Li et al., 2009). Native type fibrils with characteristic D-banding begin to form *in vitro* within the pH range of 5.0–8.5, ionic strength between 0.1 and 0.8, and temperatures from 4 to 37°C (Li et al., 2009; Xie et al., 2017). There is a close relationship between time and temperature in respect to fibril formation, with lower incubation temperatures requiring much longer incubation times; around 15 h at 4°C compared to around 30 min or more at 37°C (Xie et al., 2017). When casting collagen gels this incubation period does not pose much of a problem since multiple samples can be cast simultaneously, meaning the main limitation on production is the number of available casts. However, when considering the layer-by-layer building process of additive manufacturing, this incubation step makes collagen less attractive if it must be implemented between layers.

Bioprinting has been facilitated by a number of additive manufacturing technologies. These are typically either extrusion-based, droplet based, or light based. Extrusion based methods usually extrude a hydrogel or hydrogel precursor through a nozzle *via* pneumatic or mechanical means (Ozbolat and Hospodiuk, 2016). Droplet, or jet-based methods, similar to conventional inkjet printing, generally use less viscous inks and eject droplets of the ink from a reservoir through a nozzle onto a substrate, facilitated by a stimulus in the printhead such as heat or piezoelectric actuation (Saunders and Derby, 2014; Gudapati and Ozbolat, 2020). The most common light based additive manufacturing methods used in bioprinting are vat polymerization methods which contain the ink in a transparent vat and use light to polymerize monomers within the ink *via* a photoinitiator (Ng et al., 2020). All these technologies execute code which contains the geometry of a virtual 3-dimensional object in 2-dimensional slices, or layers, which are executed consecutively to build the physical 3D object. Naturally, this relies on some form of phase transition from a fluid to some form of a solid, often a hydrogel. This phase transition can be an inherent feature of the material, like the self-assembly of collagen molecules into fibrils, or it can be the result of chemical modification of the material, such as the photocrosslinking of collagen methacrylamide (Drzewiecki et al., 2017). Most examples of collagen printing are extrusion methods that rely on collagen fibrillogenesis. However, the slow solution-to-gel transition of collagen fibrillogenesis allows time for a deposited print line to flow and spread away from its deposited position, which results in poor print resolution, and can make multiple layers difficult to achieve (Murphy et al., 2013). Innovative methods have managed to circumvent these limitations such as microvalve printing multiple thin layers of collagen with a nebulized alkaline solution providing a coating between layers to raise the pH and allow fibrillogenesis (Lee et al., 2009). For extrusion printing, it was found that at a high enough concentration and suitable pH the viscosity of a collagen solution can make it feasible to print multiple over-lying layers at room temperature with an incubation step at 37°C post-print rather than between layers (Diamantides et al., 2017). This understanding of the ideal rheology of a collagen solution for printing has been complemented by new extrusion printing techniques. Printing methods, such as the FRESH method, have further improved the accuracy and resolution of collagen printing (Park et al., 2014; Yoon et al., 2016; Lee et al., 2019a, 2021). However, the mechanical properties of printed collagen constructs remains limited when compared to the dense collagenous tissues from which the collagen is typically sourced and the replication of which is a often attempted. This can be attributed to the low range of collagen concentrations that are suitable for most printing techniques, generally <2% w/v (Diamantides et al., 2017). Whereas, collagen concentration in native dense collagenous tissues is often much higher ranging from >10% in cartilage, to >14% in the cornea (Leonard and Meek, 1997; Fox et al., 2009). At higher concentrations collagen becomes too viscous for extrusion or droplet methods, and likely too turbid for light based methods. Some chemical crosslinking techniques can greatly improve the mechanical properties of a printed scaffold, but this can also result in cytotoxicity, and/or the consumption of motifs that are involved in integrin-mediated cell binding (van Luyn et al., 1992; Bax et al., 2019).

Collagen printing thus far has focused almost exclusively on collagen type I, likely due to its commercial availability, particularly with the arrival of commecial collagen type I inks for extrusion bioprinting. However other fibrillar collagens such as collagen type II could prove useful particularly in cartilage tissue engineering. Collagen type II doesn't have the same commercial availability as collagen type I, and collagen type II is also associated with the induction of arthritis in rats, however this association is related to the intravenous administration of soluble (monomeric) collagen type II, and can be treated prophylactically (Morgan et al., 1980; Nagler-Anderson et al., 1986; Mikulowska et al., 1997). Collagen type II has been shown to improve attachment of mesenchymal stem cells (MSCs), and induce and maintain MSC chondrogenesis when used in TE scaffolds (Bosnakovski et al., 2006; Ragetly et al., 2010). Collagen type II has also been shown to perform similar to type I in comparative chondrogenic studies (Freyria et al., 2009; Rutgers et al., 2013). While commercial collagen type II might be less common, the extraction of collagen type II is very similar to that of collagen type I with the only major difference being the starting tissue, which is typically articular cartilage in place of the tendon, bone or skin that is typically used for the extraction of collagen type I. Therefore by investigating the bioprinting of collagen type II some of the advantages of collagen type I as a substrate for cell culture could be exploited with a different set of material properties for more bioprinting options.

Aerosol jet® printing (AJP) is a printing method that forms an aerosol from an ink and carrier gas, and forces the aerosol to coalesce on a substrate *via* impaction. It was developed as a way to

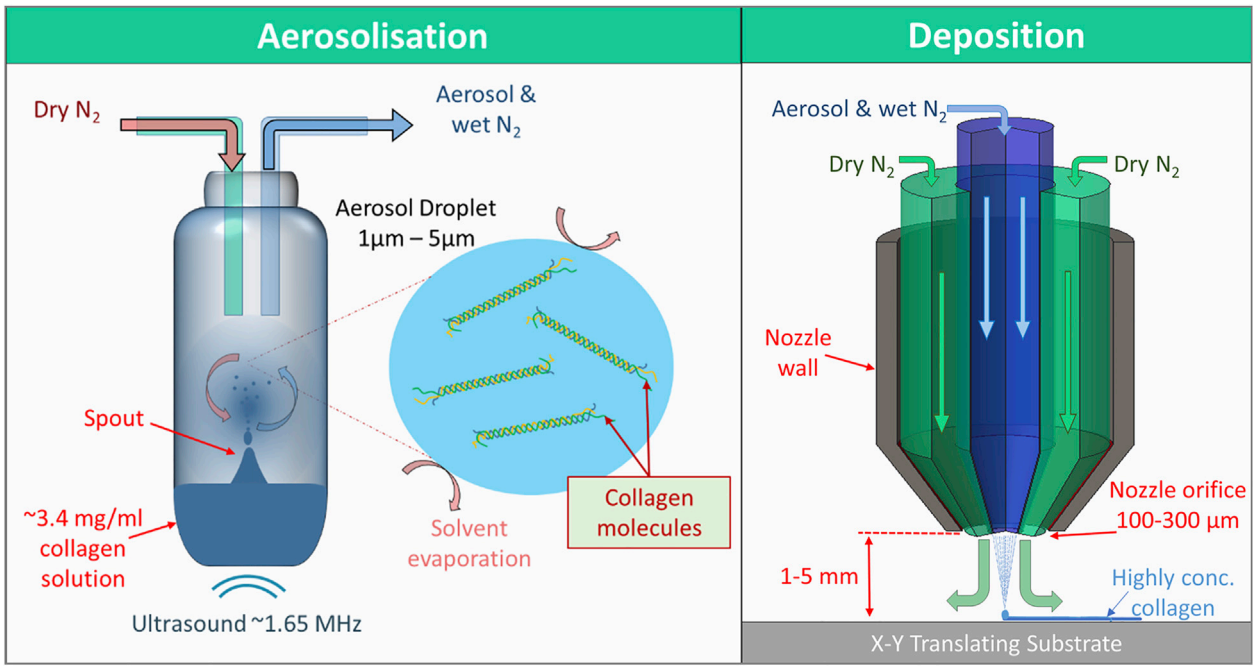

FIGURE 1 | The two major steps of aerosol jet printing. Firstly, aerosolization, where 1.65 MHz ultrasound generates a standing wave within the ink reservoir resulting in the formation of a spout, the surface of which resonates and disperses aerosol-sized (<5 μm diameter) droplets of ink. The droplets then mix and become entrained with a flow of nitrogen gas through the reservoir towards the deposition head. Secondly, in the deposition head, the aerosol-laden nitrogen is collimated by a secondary annular flow of nitrogen, separating the aerosol flow from the walls of the nozzle. The aerosol droplets then coalesce on an x-y translating print substrate. The collimation of the aerosol continues for up 5 mm after the nozzle. The high surface area to volume ratio of the aerosol and flow of dry nitrogen gas allows the ink to dry very quickly in transit and on the substrate resulting in highly concentrated printed collagen.

print electronic components on to virtually any surface topography, which has made some impact in bio-electrical applications (Sarreal and Bhatti, 2020; Seiti et al., 2020). AJP has also been investigated for the deposition of DNA, enzymes, and silk fibroin with moderate success (De Silva et al., 2006; Grunwald et al., 2010; Williams et al., 2019; Xiao et al., 2020). AJP could be considered a droplet or jet-based method similar to inkjet, yet it is very different. By forming an aerosol from the ink, AJP exploits some of the unique properties of aerosol droplets during their brief transit from the ink reservoir to the substrate. Aerosol (liquid) droplets have a very high surface area to volume ratios which can facilitate a high rate of solvent evaporation/diffusion from the droplet, as seen in **Figure 1** (Bzdek et al., 2020). Aerosol droplets can also reach solute concentrations that are much higher than the saturation concentration of bulk solutions (Yan et al., 2016; Bzdek et al., 2020). Hence a dilute collagen solution can be deposited as highly concentrated collagen *via* AJP. This is advantageous since viscosity is a limiting factor for AJP inks with inks typically in the range of 1–10 mPa s in viscosity (for ultrasonic atomization). As the ink aerosol approaches the nozzle it is confined and collimated into a dense stream of aerosol droplets by a coaxial annular flow of gas (sheath gas). The velocity and subsequent inertia of the droplets in this collimated stream, or aerosol jet, allows for the nozzle of the printer to be up to 5 mm away from the substrate, which facilitates the printing onto many different surfaces. As a result of the sheath gas the nozzle diameter does not equate to the print resolution. Printed lines or features can be printed that are 90% smaller [as low as 10 μm (Cai et al., 2016)] than the nozzle orifice diameter, which ranges from 100 to 300 μm in multiples of 50 μm. This helps prevent nozzle clogging and removes some of the complications regarding fabrication, handling and cleaning of a much smaller nozzle.

For the aerosol jet printer used in this work, the Optomec AJ300, the ink reservoir must be constantly radiated with ultrasound from a 1.65 MHz piezoelectric diaphragm during printing. The thermal stresses that arise from the ultrasound are somewhat mitigated by cooling of the atomizer, however there is no mitigating factor for the physical stress of the ultrasound and atomization. Sound and ultrasound has been shown to cause degradation of collagen type I into shorter triple helical fragments with the length of the triple helical fragments decreasing with increasing exposure (Nishihara and Doty, 1958; Giraud-Guille et al., 1994). The effects of sonic-induced heating must be mitigated to preserve the triple helix, however the thermal stability of the triple helix also decreases as it becomes more fragmented (Giraud-Guille et al., 1994). Nevertheless, this sonic fragmentation of collagen type I has been exploited to enhance the formation of dense tissue-like liquid crystalline collagen assemblies (Giraud-Guille, 1989; Mosser et al., 2006). This enhancement is suggested to be the result of the ultrasonic fragmentation causing a drop in viscosity of the collagen solution, and allowing a distribution of shorter collagen molecules to provide less obstruction to the alignment of the collagen molecules forming liquid crystalline assemblies quicker

than non-sonically fragmented solutions (Giraud-Guille, 1989). Therefore, despite the potential of this printing technique to degrade collagen, it could provide a way to print liquid crystalline assemblies of collagen, or at least print very dense collagen constructs with the potential to replicate highly collagenous tissues.

MATERIALS AND METHODS

Collagen Extraction

Collagen extractions were performed using protocols with some modifications (Zeugolis et al., 2008; Delgado et al., 2017; Sorushanova et al., 2021). Briefly, frozen bovine Achilles tendons were defrosted, fascia were trimmed, and the tendons cut into 1 cm cubes. The tendons were frozen and cryo-milled. The milled tendons were washed in 1XPBS at 4°C three times, after each wash the suspension was centrifuged and the supernatant discarded. The milled tendon was then re-suspended in 0.5 M acetic acid at 4°C using an overhead mixer over 48 h. Pepsin was then added to the suspension at a rate of 1 g per 100 g of wet tendon and left for another 72 h. The suspension was then filtered through a 100 µm sieve. Salt was then added to reach a 0.9 M NaCl solution and the collagen precipitated. Collagen fibrils were collected with a sieve and centrifuged to remove any remaining solution. The collagen fibrils were re-suspended in 1 M acetic acid at 4°C, then centrifuged, and any precipitated material was discarded. The purified collagen solution was put into dialysis tubing and dialyzed against 1 mM acetic acid, with the dialysate changed 5 times. The purity of the dialysed collagen solution was assessed by SDS-PAGE with silver staining, then frozen and lyophilized.

This process was repeated using porcine articular cartilage for the extraction of collagen type II. In brief, slices of cartilage were peeled from the femoral condyles and femoral head of porcine femurs using a scalpel. Resected cartilage pieces were immediately placed in 1XPBS on ice. The cartilage was then frozen and cryo-milled. All steps thereafter were identical to the collagen type I extraction. Collagen inks were made by adding the lyophilised collagen type I or type II to a suitable amount of cold 0.01 M hydrochloric acid and stirring at 4°C for at least 48 h.

Aerosol Jet Printing of Collagen Type I and II

All printing was performed using an Optomec® AJ300 aerosol jet printer. Six sets of samples were printed from 3 different inks, 3 mg/ml collagen type I, and 3 mg/ml & 6 mg/ml collagen type II, and 2 different print programs (A and B). Collagen type II solutions were clearly less viscous that type I solutions, hence the use of 6 mg/ml collagen type II while no higher concentrations of collagen type I could be printed in preliminary experiments. Both print program A and B consisted 576 layers of rectilinear rasters (or serpentine infill) of a circle, where each even-numbered layer was rotated 90° relative to the pattern of the previous layer, and each odd-numbered layer was rotated by 15° relative to the last odd-numbered layer. This regime was previously developed to avoid overlap of peaks and troughs and produce relatively flat samples. The programs were inherently different and were executed with different parameters, summarized in **Table 1**. Program A was for a 4 mm sample and the spacing between parallel print lines was 60 µm. Program A was executed with a 100 µm nozzle, 50 ml/min atomizer flow, 50 ml/min sheath flow, and a print speed of around 12.5 mm/s which typically resulted in print lines of 60–65 µm in width leading to continuous films as layers. Program B was for a 5 mm sample and the spacing between parallel print lines was 90 µm. Program B was executed with a 150 µm nozzle, 50 ml/min atomizer flow, 100 ml/min sheath flow, and a print speed of around 17.5 mm/s, which typically resulted in print lines of 60–70 µm, leading to more of a lattice structure. All samples were printed onto glass cover slips that had been washed for 12 h in 20% v/v nitric acid. In all cases print parameters were varied slightly during printing to account for changes in aerosol production, and the volume of ink in the vial was replenished with every hour of printing. This particular regime was selected as the print time and aerosol flow were similar for both samples despite the discrepancy in size. It was also desired to increase the sample surface area improve the likely outcome of cell-seeding and maximise the possible cell number. Hence, program B was developed to compare to program A, which had typically been typically employed for printing collagen. Once printed, the samples were stored in a well plate at 4°C to await processing.

TABLE 1 | Print parameters of samples printed with program A and program B.

Parameter	Program A	Program B
Sample diameter	4.5 mm	5.25 mm
Track spacing	60 µm	90 µm
Atomizer flow	50 ml/min	50 ml/min
Sheath flow	50 ml/min	100 ml/min
Print velocity	12.5 mm/s	17.5 mm/s
Exp. Print line width	60–65 µm	60–70 µm
Exp. print pressure	0.4–0.6 bar	0.1–0.2 bar

Post Print Processing of Aerosol Jet Printed Collagen Type I and II

Since all samples were printed from an acidic collagen solution, the samples possessed an inherent acidity and upon incubation in aqueous media residual solvent in the printed material would leach out leading to a low pH and re-solubilization of the material. Hence a neutralizing buffer was used which employed ethanol to slow the hydration of the printed material to allow time for any leachate to be neutralized, thereby preventing re-solubilization of the printed material. The neutralizing buffer consisted of 3 parts ethanol and 2 parts 1XPBS. Prior to mixing of the two parts of the neutralizing buffer, the pH of the PBS was adjusted to pH 8-9 with 1 M NaOH. Thereafter the ethanol was slowly added to the PBS while stirring, and left stirring for approximately 1 h. The pH was checked again at this point and adjusted as necessary to pH 8-9 with 1 M NaOH. The buffer was then stored at 4°C for around 1 h. Once cold, 1 ml of the neutralizing buffer was pipetted onto the samples in a well plate on ice, and incubated for at least 12 h at 4°C. The neutralizing buffer was then removed, and the samples were washed in PBS 3 times for 15 min and stored in PBS at 4°C

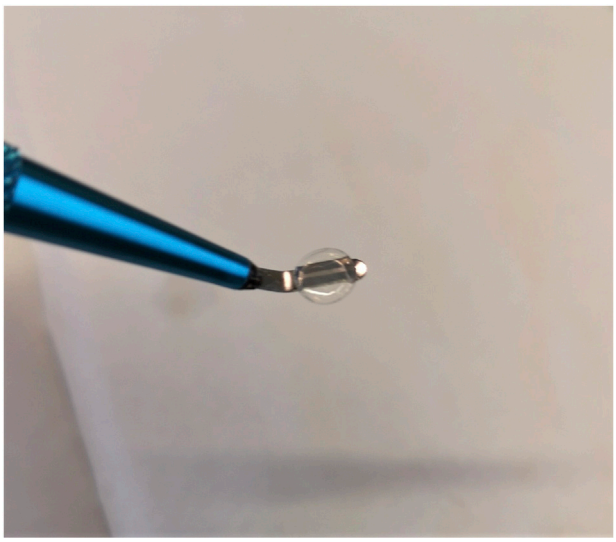

FIGURE 2 | A 6 mg/ml collagen type II 5.25 mm diameter sample after being removed from its print substrate post neutralization.

thereafter. At this point the samples could be removed from their print substrate as a dense swollen hydrogel, as seen in **Figure 2**.

Viscosity

Freshly made solutions of 3 mg/ml collagen type I, 3 mg/ml of collagen type II, and 6 mg/ml collagen type II in 10 mM hydrochloric acid were made by stirring at a low speed at 4°C for at least 48 h. Sonicated samples were treated by pipetting 850 µl of a solution into the vial and sonicating for 5 min, since this the volume normally used for printing. This was repeated 4 times so that there was 3–4 ml of sonicated solution for viscosity measurements. Both the untreated solutions and sonication solutions were tested on an Anton-Paar Lovis 2000 M rolling ball viscosity meter and density meter. In each measurement the solutions, at close to room temperature, were loaded into the 1.8 mm capillary tube already containing a gold ball, using a syringe. The capillary was checked for bubbles then sealed and loaded into the viscosity meter. Of the remaining material in the syringe around 1 ml was inserted into the density meter; a density measurement was required for an accurate viscosity measurement. All measurements were performed at 20°C. A measuring angle of 70° was used for the viscosity measurement.

Circular Dichroism

CD spectroscopy is particularly effective at detecting changes in collagen structure given the unique spectra resulting from the collagen triple helix with a minimum peak around 198 nm and maximum peak around 221 nm. The presence of randomly coiled denatured collagen should lead attenuation and broadening of the peak around 198 nm, and attenuation or removal of the peak around 221 nm (Greenfield, 2007; Wallace, 2019). Hence, CD was used to characterize any unravelling of the collagen triple helix due to exposure to ultrasonic atomization, or ultrasound alone. For the samples that were exposed to ultrasonic atomization, the set up was similar to a print but with a closed vial to prevent evaporation. Samples that were exposed to ultrasound alone were in a similar set up but with a much smaller starting volume, 150 µl, in the vial which was insufficient to generate the spout needed for atomization. In each case samples were taken at 20, 60, and 120 min. Samples were diluted to 0.15 mg/ml with 0.01 M HCl for the CD measurements. Sample CD spectra were collected between 260 and 185 nm using a Jasco J-1500 CD spectrophotometer with samples in quartz cuvettes with a 1 mm path length. The spectra of the samples were accumulations of 3 measurments between 260 and 185 nm with a scan speed of 20, and 1 nm bandwidth. The spectra of 0.01 M hydrochloric acid was automatically substracted from the spectra by the CD software as background. The ratio of positive to negative (Rpn) peak was calculated to represent any drop in the intensities of characterisitic collagen positive peak at 221 nm, and negative peak at 198 nm, relative to the control. This ratio, Rpn, has often been used as a numerical representation of the changes in collagen CD spectra in response to a denaturing reagent or force (Feng et al., 1996; Feng et al., 1997; Freudenberg et al., 2007).

Sodium Dodecyl-Sulphate Polyacrylamide Gel Electrophoresis

SDS-PAGE was employed to characterize any degradation of collagen type I or II from ultrasonic aerosolization. Collagen type I and II solutions at 3 mg/ml in 0.01 M hydrochloric acid were treated with 20, 60, or 120 min of ultrasonic aerosolization. These samples and their respective untreated controls of either collagen solution were diluted to 0.3 mg/ml in order to run the SDS-PAGE. The gels were subsequently stained using ProteoSilver stain kit from Sigma Aldrich.

Nanoindentation

The mechanical properties of the AJP samples were characterized using a Chiaro nanoindenter (Optics11). This ferrule-top nanoindenter and its sister system, the Piuma, have emerged in recent years as useful tools tools for measuring the mechanical properties of hydrogels, and for mechanobiology (Xie et al., 2018; Dobre et al., 2021; Emig et al., 2021). Both systems employ a spherical indenter on a cantilever of known stiffness, which is mounted on a ferrule-topped optical fiber (Chavan et al., 2012). A piezoelectric actuator displaces this assembly, or probe, by a user-defined distance and speed leading to the indenter making contact with the sample and deflection of the cantilever to which it is attached. Interferometry is used to measure the deflection of the cantilever. The deflection is then used to calculate the load, and the stiffness thereafter using a Hertzian (for visco-/elastic material) or Oliver-Pharr (for elastoplastic material) contact model (Mattei and Breel, 2017). While these systems are mostly used to measure local variations in stiffness, they are also used to measure the bulk modulus of hydrogels (Giobbe et al., 2019; Yue et al., 2019; Mattei et al., 2020). This form of micro/nano-indentation has provided results consistent with tensile and compressive test results (Ye et al., 2019). For these measurements a probe with a cantilever stiffness of 0.57 N/m and a 52.5 µm radius spherical indenter was selected. 25

indentations were performed on each sample in a 5 × 5 matrix with 200 µm spacing between indentations in both directions. The indentation profile went to a maximum of 10 µm at an indentation rate of 1.4 µm/s. This indentation included a 4 µm offset from the sample surface to ensure that the probe was not in contact with the material before beginning the indentation.

Swelling Ratio

Samples were swollen overnight in 1XPBS then blotted on filter paper before weighing for the wet weight. For dry weight measurements, samples were dehydrated in increasing concentrations of ethanol (30, 50, 70, 90% and twice in 100% v/v in ddH_2O) for 10 min each, and left on aluminium foil to dry overnight.

Scanning Electron Microscopy

SEM was employed to characterize the layered structure that resulted from the use of AJP. Samples were prepared using a protocol reported by Raub et al. with some modifications (Raub et al., 2007). Briefly, samples were fixed in 4% glutaraldehyde in 1X PBS for 1 h at room temperature, then washed 3 times in PBS for 7 min, and 2 times in ddH_2O for 7 min. Samples were then dehydrated in increasing concentrations of ethanol in ddH_2O (30, 50, 70, 90, and 100% v/v) for 10 min each and twice in 100% ethanol. The samples were further dehydrated in increasing concentrations of HMDS in ethanol (33, 50, 66, and 100% v/v) for 15 min each, and twice in 100%. Samples were then torn apart with tweezers and left to dry on aluminium foil under a fume hood overnight. The dried samples were mounted on SEM stubs using carbon tape, and sputter-coated with platinum to a thickness of 5 nm. The samples were imaged at 5 kV.

Statistical Analysis

Statistical analysis was performed on the nanoindentation and swelling ratio result to discern statistically significant differences between sample groups. In both cases a three-way (collagen type, concentration, and print program) ANOVA was performed with two levels. The values were considered significant if their p values were <0.05.

RESULTS

Aerosol Jet Printing of Collagen Type I and II

In observing samples printed with program A under the microscope all print lines were seen to overlap, i.e., the print lines of underlying layers could not be observed. Gaps were observed between printed lines in the top layer of samples printed with program B, and print lines of underlying could be observed.

Post Print Processing of Aerosol Jet Printed Collagen Type I and II

All samples printed with program A performed as expected for the post-print processing with no signs of dissolution, and clear signs of enhanced structural integrity when handled. However, samples printed with program B appeared thinner, by eye, than those of program A, and some samples appeared to have performed better than others with some samples showing signs of dissolution. However, sample group B still showed signs of structural integrity when handled.

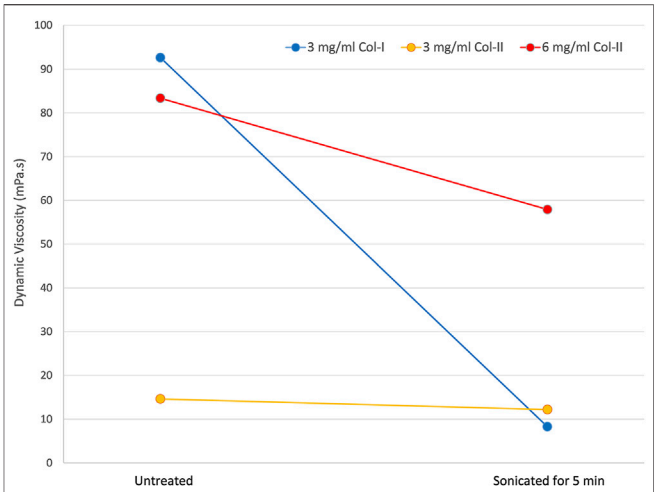

FIGURE 3 | The dynamic viscosity of untreated collagen solutions and the same solutions after a 5-minute treatment with ultrasonic atomization in an aerosol jet printer.

Viscosity

During the treatment with the ultrasonic atomizer all samples generated aerosol soon after initiation of the ultrasound. However, the 3 mg/ml solutions of both collagen type I and type II reached a sufficient rate of aerosol generation for printing almost immediately, whereas the 6 mg/ml collagen type II solution only reached sufficient aerosol generation after around 3 min of the treatment, and the amount of aerosol generated remained low relative to the other solutions. The viscosity of all three solutions dropped as a result of the ultrasonic aerosolization as seen in **Figure 3**. The most viscous solution, 3 mg/ml collagen type I exhibited the greatest change in viscosity. 6 mg/ml collagen type II also exhibiting a large drop in viscosity whereas 3 mg/ml collagen type II measured a relatively small decrease in viscosity.

Circular Dichroism

Typical collagen CD spectra with minima at 198 nm and maxima at 221 nm were measured for all samples, as seen in **Figure 4**. However, in some cases the sample treatment caused a drop in the intensity of these peaks. Collagen type I was shown to be vulnerable to denaturation as a result of exposure to ultrasonic radiation with a drop in the peak intensities resulting change in Rpn from an untreated control of 0.16, to 0.12 after 2 h of ultrasonic radiation. However, there was no significant red-shift of the crossover point and no clear shift of the 198 and 221 nm peaks. Ultrasonic atomization of collagen type I lead to clearer signs of denaturation with a drop in Rpn from 0.16 to 0.08 after 2 h of atomization, and a gradual red-shift in the cross-over point from 213.6 to 214.9 nm.

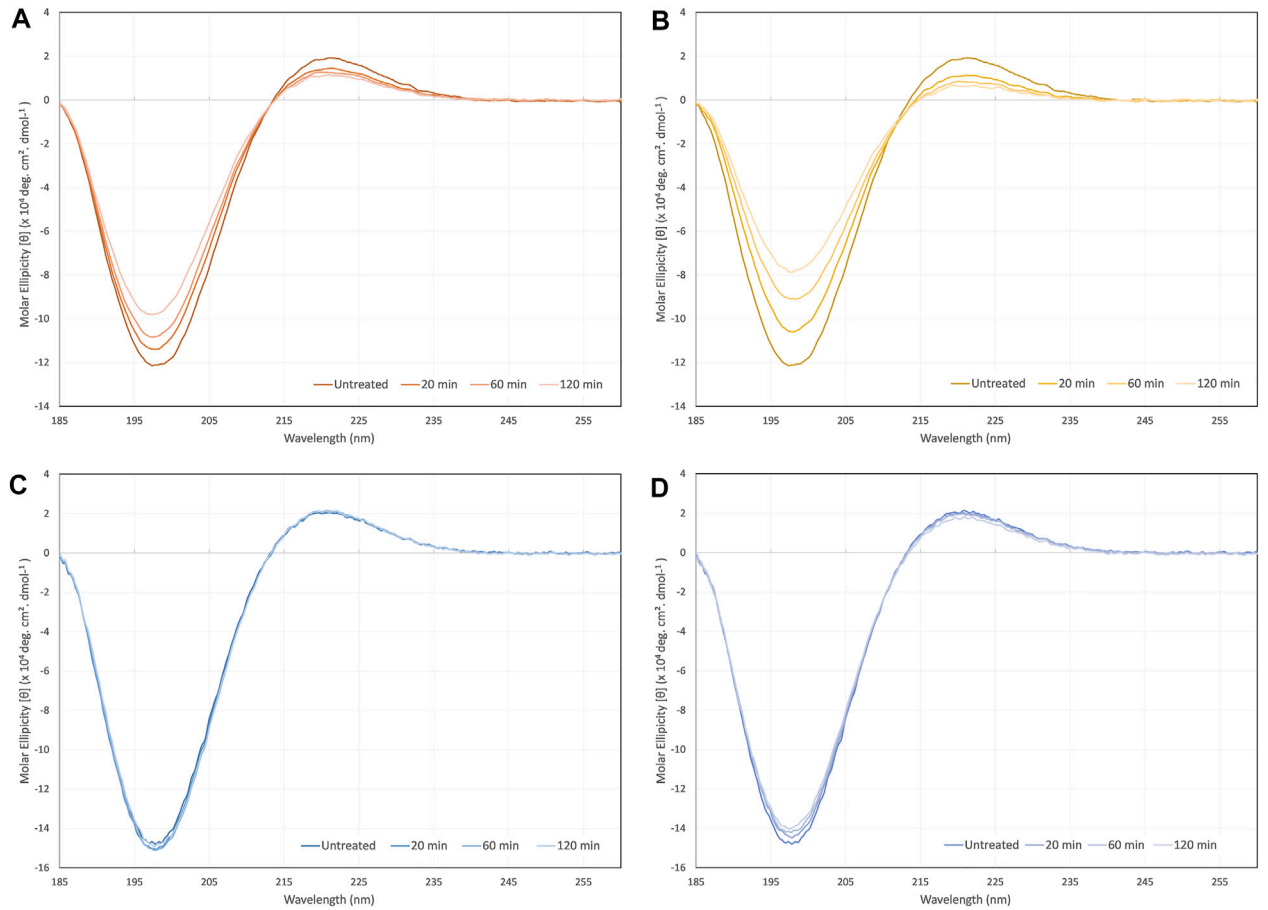

FIGURE 4 | CD spectra of **(A)**collagen type I sonicated non-atomized, **(B)** collagen type I ultrasonically atomized, **(C)** collagen type II sonicated non-atomized, and **(D)** collagen type II ultrasonically atomized.

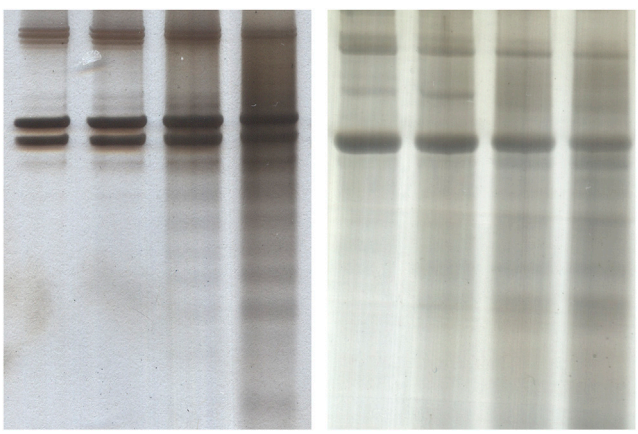

FIGURE 5 | Silver stained SDS-PAGE gels for detecting degradation of collagen of collagen type I **(A)** and collagen type II **(B)** from exposure to ultrasonic atomization. In each case the lanes are in order of (left to right) 0, 20, 60, and 120 min of exposure.

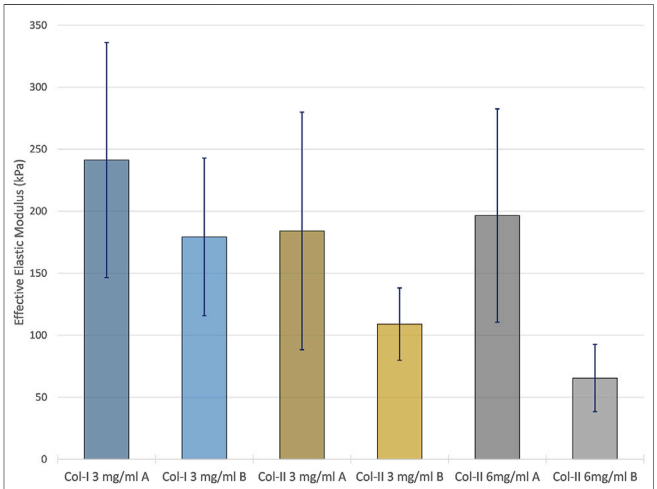

FIGURE 6 | The average effective elastic modulus of each of the sample group measured by nanoindentation using a Hertzian model. Error bars represent the standard deviation of each sample group.

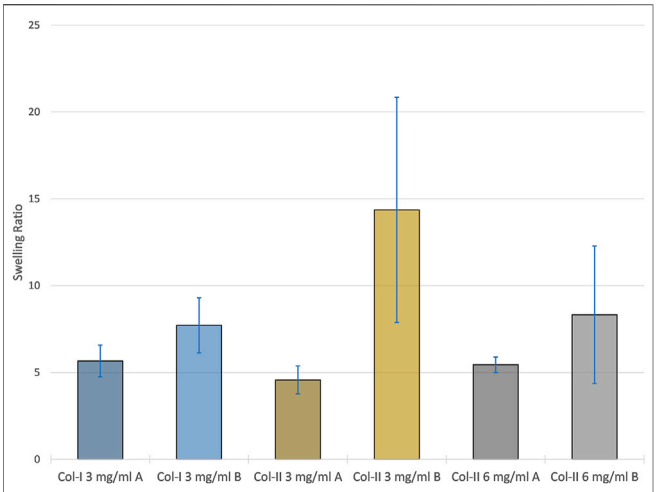

FIGURE 7 | The average swelling ratio of each samples group with error bars representing the standard deviation within each group.

Collagen type II showed far less signs of denaturation due to ultrasonic exposure and atomization. The spectra from samples that were exposed to ultrasonic radiation alone were virtually superimposed on each other and resulted in no significant changes in Rpn. Ultrasonic atomization did lead to gradual decreases in the peak intensities at each time point. The Rpn decreased from an untreated control value of 0.14 to 0.13 after 2 h of ultrasonic atomization. There was no significant shift in the crossover point.

SDS-PAGE

SDS-PAGE revealed that both collagen type I and type II were gradually degraded by ultrasonic atomization as seen in **Figure 5**. The degraded chains did not appear to show any preferential molecular weight, instead a distribution of what could be confused with non-specific staining spread over the lane. The α and β bands became slightly less intense in both cases after 120 min, and the distribution of degraded α and β chains became increasingly intense in the 60- and 120-min treatment lanes.

Nanoindentation

As seen in the nanoindentation results in **Figure 6**, collagen type I printed with program A resulted in the highest average effective elastic modulus, 241.3 ± 94.3 kPa (±SD), while the 6 mg/ml collagen type II samples printed with program B resulted in the lowest average effective elastic modulus with 65.4 ± 27.1 kPa (±SD). The print program and the collagen type were found to be statistically significant factors in relation to the mechanical properties ($p < 0.05$). Collagen type I samples were stiffer than those made with collagen type II, and samples printed with program A were stiffer than those printed with program B.

Swelling Ratio

Samples printed with program B had on average had a higher and more variable swelling ratio as seen in **Figure 7**. The program was found to be the only statistically significant factor in relation to the swelling ratio ($p < 0.05$).

SEM

Distinct layers could be resolved in all samples as seen in **Figure 8**. Whilst in program A samples these layers continued throughout the samples, in samples printed with program B the layers were not always continuous across the section. Most of the samples possessed a very smooth surface topography, however some samples printed with program B had dimples that appeared to continue through several layers.

DISCUSSION

This is the first research article on aerosol jet printing of collagen type I and/or collagen type II, and can be considered a proof-of-concept study. We have previously reported on aerosol jet printing of recombinant human collagen type III (RHCIII) and highlighted some of the challenges involved, particularly the regarding the neutralisation and crosslinking of AJP collagen (Gibney et al., 2021). Aerosol jet printing of collagen type I and type II has proven to be very similar. Print program A was similar to a program used in to print RHCIII, however here it was printed with higher atomizer flow and higher print velocity in an effort to improve the print time. Print program B was developed to increase the surface area of samples and investigate porous prints, but this was also an effort to improve the print time. By increasing the distance between print lines, the print speed could be increased with a lower risk of what we refer to as "*pooling*". Pooling is where two or more print lines coalesce leading to the formation of pools which impair print accuracy and can interfere with proceeding layers since they dry slower. Pooling is more likely to occur at corners since the amount of material printed in a given area increases at corners. However, it is likely that some of the significant differences observed between program A and program B samples here, are the result of a less than optimal neutralization process for the program B samples, so this should be kept in mind when considering these differences. It was apparent upon removal of the neutralization buffer that the program B samples had some signs of dissolution. They also appeared far thinner than program A samples which could be due to dissociation of some collagen during incubation in the neutralizing buffer or could be an effect of the printing pattern. It appears likely that the neutralization buffer requires refinement for samples with increased porosity like the program B samples. A higher ethanol concentration in the neutralization buffer could further slow the absorption of the buffer and prevent dissociation of the molecular collagen from the printed material.

The drop in viscosity of the collagen solutions from exposure to ultrasound has been previously reported (albeit for a much lower frequency of ultrasound, 20 kHz) (Giraud-Guille et al., 1994, 2000). The viscosity measurements were performed twice 2 days apart without any change, so the drop does not seem to be transient at least on that time scale. The drop in viscosity is thought to be the result of an initial break up of supramolecular aggregates remaining in solution, followed by a gradual

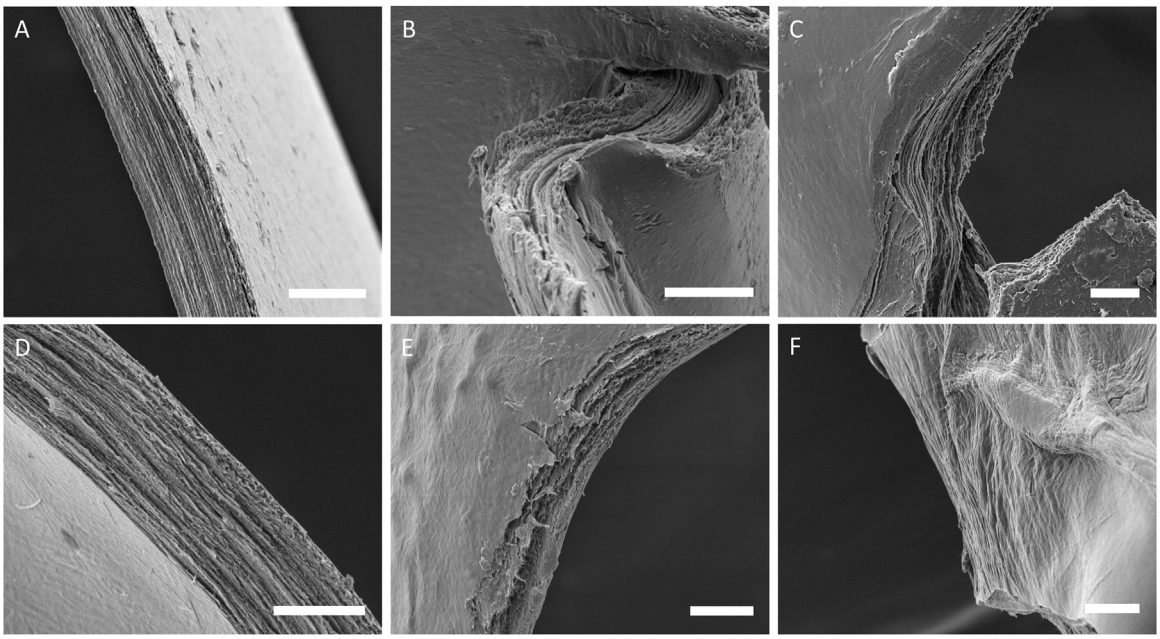

FIGURE 8 | SEM images of cross-sections from sample groups, **(A)** col-I 3 mg/ml A, **(B)** col-II 3 mg/ml A, **(C)** col-II 6 mg/ml A, **(D)** col-I 3 mg/ml B, **(E)** col-II 3 mg/ml B, and **(F)** col-II 6 mg/ml B.

degradation of the collagen as seen in the SDS-PAGE. The shear stress of atomization may also exacerbate this effect of the ultrasound, particularly for collagen type I given the increased unfolding observed for atomized samples versus the non-atomized samples in the CD measurements. The viscosity of the 6 mg/ml collagen type II was considerably higher than the other samples after the atomization treatment, and as noted, there was less atomization occurring for this solution compared to the others. However, the viscosity of the 6 mg/ml would be expected to continue to drop as the atomization time increases. A 6 mg/ml collagen type II solution that was atomized for 1 hour has been measured to have a dynamic viscosity of 7 mPa s. Another explanation for the increased viscosity drop observed for collagen type I solutions compared to collagen type II solutions would be the increased vulnerability of the collagen type I to degradation and unfolding via observed in CD and SDS-PAGE.

It is not clear whether the differences observed between collagen type I and II CD spectra in response to ultrasonic exposure and ultrasonic atomization hold any implications beyond this particular application. The shear forces involved in ultrasonic atomization are likely to be the denaturing factor since ultrasound alone had a less of an impact on the spectra with increasing treatment. There are a number of caveats that must be considered before directly comparing the performance of the two collagen types. The fact that the collagens tested were from different species and from single batches (extractions), thereby makes the findings potentially subject to special variations and batch-to-batch variations. These results were also for monomeric collagen in solution; hence it is difficult to translate any of the findings to assembled collagen fibrils in the ECM. However, even considering these caveats, the fact that ultrasound had no clear impact on collagen type II CD spectra and did on collagen type I spectra is interesting, and at the very least indicates that collagen type II would be more suitable for aerosol jet printing in general. Nevertheless, this does not rule out collagen type I's suitability for aerosol jet printing, since a large proportion of the collagen must remain in a triple helix conformation for the average signal to still retain the collagen triple helix minimum and maximum peaks.

All aerosol jet printed collagen samples possessed remarkable stiffness for bioprinted collagen constructs that have not been covalently crosslinked. The only significant difference between the sample groups, regarding stiffness, was the print program. However, as stated earlier, the differences observed between the samples printed with the program A or B may have more to do with the neutralization of the construct that any intrinsic properties imparted by the print program. Any significant re-solubilization like that seen in some program B samples would disrupt the layered structure of the printing and thereby change the constructs mechanical behaviour. The average effective elastic moduli of the program A samples were 241.3 ± 94.3 kPa, 185.1 ± 95.8 kPa, and 196.6 ± 86.0 kPa (all ±SD) for 3 mg/ml collagen type I samples, and 3 mg/ml and 6 mg/ml collagen type II samples respectively. The highest reported mechanical characterization results for printed collagen found were compressive moduli of around 110 kPa for glutaraldehyde-crosslinked bovine collagen type I, 47.2 ± 14.2 kPa for EDC-crosslinked porcine-hide collagen, and 21.5 ± 1.4 kPa for porcine-tendon collagen type I without any modification (Lode et al., 2016; Lee et al., 2019b; Osidak et al., 2019). The elastic moduli of the aerosol jet printed collagen constructs printed with program A obtained by nanoindentation were all significantly higher. Furthermore, in

separate work where EDC and NHS were added to the neutralizing buffer (40 μg/ml EDC, 24 μg/ml NHS) to crosslink aerosol jet printed 6 mg/ml collagen type II (program A, 576 layers), nanoindentation revealed an average effective elastic modulus of 2.1 ± 0.4 MPa (see supplementary material). These results were compared to results reported on the nanoindentation of dense collagenous tissues. Using a similar Optics11 nanoindenter human ear, septal, and alar cartilage were found to have effective elastic moduli of 1.14 ± 0.71, 2.65 ± 1.78, and 1.26 ± 0.51 MPa respectively (Bos et al., 2018). Similarly, the stroma of human donor corneas were measured to have an average effective elastic modulus of around 75 kPa (Shavkuta et al., 2018). This places aerosol jet printed collagen within reach of replicating the mechanical properties of dense collagenous tissues. Chemical crosslinking could be used to enhance the stiffness of the constructs for closer replication of the stiffest cartilage, whereas different print programs and a deeper understanding of the post-print neutralization could be employed for a closer replication of the weaker collagenous tissues.

For swelling ratio, the only significant difference between sample groups regarding swelling ratio was the print program. Samples printed with program A had a more consistent swelling ratio between and within sample groups whereas program B samples varied a lot between and within sample groups. This could be taken as further evidence of re-solubilization as this would allow collagen to dissociate creating regions within samples with lower density and a higher capacity to absorb water. Evidence of continuous layers traversing entire samples was observed in all program A samples in SEM. However, program B samples possessed regions that appeared amorphous or had very faint signs of layering which were interpreted as signs of re-solubilization. Some program B samples also possessed a strange topography with potholes or dimples which was also interpreted as signs of re-solubilization probably starting at a region where multiple layers were accessible at the surface, like a pore. Nevertheless, the observation of distinct layers in most samples is promising for many applications. We have previously estimated similar layers of RHCIII to be ~330 nm thick, this would likely increase for the 6 mg/ml collagen type II printing since thickness is usually related to the in concentration in aerosol jet printing. Alternating layers of different material could be used to induce certain behaviours in cells, and layers of conductive material could be printed within a collagen construct for electro-stimulation.

It has been shown in this work that aerosol jet printing can be used to generate stiff collagen constructs with hundreds of layers that are suitable for tissue engineering. While some collagen type I was shown to be denatured by the aerosol jet printing process, the effect was gradual. Hence the denaturation would be mitigated somewhat by the addition of fresh collagen to vial with every hour of printing, as is practice during sample production. Collagen type II was shown to be particularly useful for aerosol jet printing due to its lower viscosity, which allowed a greater concentration range to be printed, and its relative invulnerability to the stresses of the AJP process. While the resolution of this printing process limited scale of the constructs, this was achieved using an aerosol jet printer intended for printing small electrical components with just a few layers. The scalability of this method could potentially be improved by designing an aerosol jet printer with the intention to print biomaterials for biofabrication and perhaps combining this with other bioprinting methods. Moreover, the combination of AJP's capability to print high resolution structures with conductive inks and it's demonstrated capability to print collagen will likely be advantageous to the field of electrically stimulated cell culture where inkjet printers have been used to print far more dilute collagen solutions with far fewer layers over conductive material (Weng et al., 2012). The field of bioprinting can only be enhanced with the addition of alternative printing methods and materials, like aerosol jet printing and collagen type II.

DATA AVAILABILITY STATEMENT

The raw data supporting the conclusions of this article will be made available by the authors, without undue reservation.

AUTHOR CONTRIBUTIONS

RG conceived the research topic, the rationale and the plan of the manuscript. EF was the supervisor of the research topic and she obtained funding for this research. All authors contributed to the text and editing of the manuscript.

FUNDING

This research was funded by Research Foundation Flanders (FWO grant number G083117N) and the Flanders Innovation and Entrepreneurship (VLAIO grant number HBC.2017.0067).

ACKNOWLEDGMENTS

The authors would like to acknowledge the contribution of all members of REMODEL research group led by the PI, Dimitrios Zeugolis, in Curam research facility at the National University of Ireland, Galway. Specifically, Eugenia Pugliese, João Coentro, Hector Capella-Monsonís, Meletios-Nikolaos Doulgkeroglou, Ignacio Sallent, and Mehmet Gürdal for their expertise and guidance in the characterization and extraction of bovine Achille's tendon-derived collagen type I and porcine articular cartilage-derived collagen type II. The authors would also like to acknowledge Prof. Tatjana Vogt and Nada Savić for expertise and guidance in CD spectroscopy, and Olivier Degryse for his help in SEM observation.

SUPPLEMENTARY MATERIAL

The Supplementary Material for this article can be found online at: https://www.frontiersin.org/articles/10.3389/fbioe.2021.786945/full#supplementary-material

REFERENCES

Adzhubei, A. A., Sternberg, M. J. E., and Makarov, A. A. (2013). Polyproline-II helix in Proteins: Structure and Function. *J. Mol. Biol.* 425, 2100–2132. doi:10.1016/j.jmb.2013.03.018

Bax, D. V., Davidenko, N., Hamaia, S. W., Farndale, R. W., Best, S. M., and Cameron, R. E. (2019). Impact of UV- and Carbodiimide-Based Crosslinking on the Integrin-Binding Properties of Collagen-Based Materials. *Acta Biomater.* 100, 280–291. doi:10.1016/j.actbio.2019.09.046

Bos, E. J., Pluemeekers, M., Helder, M., Kuzmin, N., van der Laan, K., Groot, M.-L., et al. (2018). Structural and Mechanical Comparison of Human Ear, Alar, and Septal Cartilage. *Plast. Reconstr. Surg. - Glob. Open* 6, e1610–9. doi:10.1097/GOX.0000000000001610

Bosnakovski, D., Mizuno, M., Kim, G., Takagi, S., Okumura, M., and Fujinaga, T. (2006). Chondrogenic Differentiation of Bovine Bone Marrow Mesenchymal Stem Cells (MSCs) in Different Hydrogels: Influence of Collagen Type II Extracellular Matrix on MSC Chondrogenesis. *Biotechnol. Bioeng.* 93, 1152–1163. doi:10.1002/bit10.1002/bit.20828

Bzdek, B. R., Reid, J. P., and Cotterell, M. I. (2020). Open Questions on the Physical Properties of Aerosols. *Commun. Chem.* 3, 105. doi:10.1038/s42004-020-00342-9

Cai, F., Chang, Y.-H., Wang, K., Zhang, C., Wang, B., and Papapolymerou, J. (2016). Low-Loss 3-D Multilayer Transmission Lines and Interconnects Fabricated by Additive Manufacturing Technologies. *IEEE Trans. Microwave Theor. Techn.* 64, 3208–3216. doi:10.1109/TMTT.2016.2601907

Chavan, D., Van De Watering, T. C., Gruca, G., Rector, J. H., Heeck, K., Slaman, M., et al. (2012). Ferrule-top Nanoindenter: An Optomechanical Fiber Sensor for Nanoindentation. *Rev. Scientific Instr.* 83, 115110. doi:10.1063/1.4766959

De Silva, M. N., Paulsen, J., Renn, M. J., and Odde, D. J. (2006). Two-Step Cell Patterning on Planar and Complex Curved Surfaces by Precision Spraying of Polymers. *Biotechnol. Bioeng.* 93, 919–927. doi:10.1002/bit10.1002/bit.20787

Delgado, L. M., Shologu, N., Fuller, K., and Zeugolis, D. I. (2017). Acetic Acid and Pepsin Result in High Yield, High Purity and Low Macrophage Response Collagen for Biomedical Applications. *Biomed. Mater.* 12, 065009. doi:10.1088/1748-605X/aa838d

Diamantides, N., Wang, L., Pruiksma, T., Siemiatkoski, J., Dugopolski, C., Shortkroff, S., et al. (2017). Correlating Rheological Properties and Printability of Collagen Bioinks: The Effects of Riboflavin Photocrosslinking and pH. *Biofabrication* 9, 034102. doi:10.1088/1758-5090/aa780f

Dobre, O., Oliva, M. A. G., Ciccone, G., Trujillo, S., Rodrigo-Navarro, A., Venters, D. C., et al. (2021). A Hydrogel Platform that Incorporates Laminin Isoforms for Efficient Presentation of Growth Factors - Neural Growth and Osteogenesis. *Adv. Funct. Mater.* 31, 2010225. doi:10.1002/adfm.202010225

Drzewiecki, K. E., Malavade, J. N., Ahmed, I., Lowe, C. J., and Shreiber, D. I. (2017). A Thermoreversible, Photocrosslinkable Collagen Bio-Ink for Free-form Fabrication of Scaffolds for Regenerative Medicine. *Technology* 05, 185–195. doi:10.1142/s2339547817500091

Emig, R., Knodt, W., Krussig, M. J., Zgierski-Johnston, C. M., Gorka, O., Groß, O., et al. (2021). Piezo1 Channels Contribute to the Regulation of Human Atrial Fibroblast Mechanical Properties and Matrix Stiffness Sensing. *Cells* 10, 663. doi:10.3390/cells10030663

Feng, Y., Melacini, G., Goodman, M., and Goodman, M. (1997). Collagen-based Structures Containing the Peptoid Residue N-Isobutylglycine (Nleu): Synthesis and Biophysical Studies of Gly-Nleu-Pro Sequences by Circular Dichroism and Optical Rotation. *Biochemistry* 36, 8716–8724. doi:10.1021/bi962980z

Feng, Y., Melacini, G., Taulane, J. P., and Goodman, M. (1996). Acetyl-terminated and Template-Assembled Collagen-Based Polypeptides Composed of Gly-Pro-Hyp Sequences. 2. Synthesis and Conformational Analysis by Circular Dichroism, Ultraviolet Absorbance, and Optical Rotation. *J. Am. Chem. Soc.* 118, 10351–10358. doi:10.1021/ja961260c

Fidler, A. L., Boudko, S. P., Rokas, A., and Hudson, B. G. (2018). The Triple helix of Collagens - an Ancient Protein Structure that Enabled Animal Multicellularity and Tissue Evolution. *J. Cel Sci.* 131, jcs203950. doi:10.1242/jcs.203950

Freudenberg, U., Behrens, S. H., Welzel, P. B., Müller, M., Grimmer, M., Salchert, K., et al. (2007). Electrostatic Interactions Modulate the Conformation of Collagen I. *Biophysical J.* 92, 2108–2119. doi:10.1529/biophysj.106.094284

Freyria, A., Ph, D., Ronzie, M., Ph, D., Cortial, D., Ph, D., et al. (2009). Comparative Phenotypic Analysis of Articular Chondrocytes Cultured within Type I or Type II Collagen Scaffolds. *Tissue Eng. Part. A.* 15, 1233. doi:10.1089/ten.tea.2008.0114

Gibney, R., Patterson, J., and Ferraris, E. (2021). High-Resolution Bioprinting of Recombinant Human Collagen Type III. *Polymers (Basel)* 13, 2973. doi:10.3390/polym13172973

Giobbe, G. G., Crowley, C., Luni, C., Campinoti, S., Khedr, M., Kretzschmar, K., et al. (2019). Extracellular Matrix Hydrogel Derived from Decellularized Tissues Enables Endodermal Organoid Culture. *Nat. Commun.* 10, 5658. doi:10.1038/s41467-019-13605-4

Giraud-Guille, M.-M., Besseau, L., Chopin, C., Durand, P., and Herbage, D. (2000). Structural Aspects of Fish Skin Collagen Which Forms Ordered Arrays via Liquid Crystalline States. *Biomaterials* 21, 899–906. doi:10.1016/S0142-9612(99)00244-6

Giraud-Guille, M.-M., Besseau, L., Herbage, D., and Gounon, P. (1994). Optimization of Collagen Liquid Crystalline Assemblies: Influence of Sonic Fragmentation. *J. Struct. Biol.* 113, 99–106. doi:10.1006/jsbi.1994.1035

Giraud-Guille, M.-M. (1989). Liquid Crystalline Phases of Sonicated Type I Collagen. *Biol. Cel* 67, 97–101. doi:10.1111/j.1768-322x.1989.tb03014.x

Gobeaux, F., Mosser, G., Anglo, A., Panine, P., Davidson, P., Giraud-Guille, M.-M., et al. (2008). Fibrillogenesis in Dense Collagen Solutions: A Physicochemical Study. *J. Mol. Biol.* 376, 1509–1522. doi:10.1016/j.jmb.2007.12.047

Greenfield, N. J. (2007). Using Circular Dichroism Spectra to Estimate Protein Secondary Structure. *Nat. Protoc.* 1, 2876–2890. doi:10.1038/nprot.2006.202

Grunwald, I., Groth, E., Wirth, I., Schumacher, J., Maiwald, M., Zoellmer, V., et al. (2010). Surface Biofunctionalization and Production of Miniaturized Sensor Structures Using Aerosol Printing Technologies. *Biofabrication* 2, 014106. doi:10.1088/1758-5082/2/1/014106

Gudapati, H., and Ozbolat, I. T. (2020). The Role of Concentration on Drop Formation and Breakup of Collagen, Fibrinogen, and Thrombin Solutions during Inkjet Bioprinting. *Langmuir* 36, 15373–15385. doi:10.1021/acs.langmuir.0c02926

Karsdal, M. A. (2016). "Introduction," in *Biochemistry of Collagens, Laminins and Elastin: Structure, Function and Biomarkers*. Elsevier Inc., xix, xxxiv. doi:10.1016/B978-0-12-809847-9.02001-8

Lee, A., Hudson, A. R., Shiwarski, D. J., Tashman, J. W., Hinton, T. J., Yerneni, S., et al. (2019a). 3D Bioprinting of Collagen to Rebuild Components of the Human Heart. *Science* 365, 482–487. doi:10.1126/science.aav9051

Lee, A., Hudson, A. R., Shiwarski, D. J., Tashman, J. W., Hinton, T. J., Yerneni, S., et al. (2019b). 3D Bioprinting of Collagen to Rebuild Components of the Human Heart. *Science* 365, 482–487. doi:10.1126/science.aav9051

Lee, J. M., Suen, S. K. Q., Ng, W. L., Ma, W. C., and Yeong, W. Y. (2021). Bioprinting of Collagen: Considerations, Potentials, and Applications. *Macromol. Biosci.* 21, 2000280. doi:10.1002/mabi.202000280

Lee, W., Debasitis, J. C., Lee, V. K., Lee, J.-H., Fischer, K., Edminster, K., et al. (2009). Multi-layered Culture of Human Skin Fibroblasts and Keratinocytes through Three-Dimensional Freeform Fabrication. *Biomaterials* 30, 1587–1595. doi:10.1016/j.biomaterials.2008.12.009

Leonard, D. W., and Meek, K. M. (1997). Refractive Indices of the Collagen Fibrils and Extrafibrillar Material of the Corneal Stroma. *Biophysical J.* 72, 1382–1387. doi:10.1016/S0006-3495(97)78784-8

Li, Y., Asadi, A., Monroe, M. R., and Douglas, E. P. (2009). pH Effects on Collagen Fibrillogenesis *In Vitro*: Electrostatic Interactions and Phosphate Binding. *Mater. Sci. Eng. C* 29, 1643–1649. doi:10.1016/j.msec.2009.01.001

Lode, A., Meyer, M., Brüggemeier, S., Paul, B., Baltzer, H., Schröpfer, M., et al. (2016). Additive Manufacturing of Collagen Scaffolds by Three-Dimensional Plotting of Highly Viscous Dispersions. *Biofabrication* 8, 015015. doi:10.1088/1758-5090/8/1/015015

Mattei, G., and Breel, E. J. (2017). Measuring Micro-mechanical Properties of (Bio) materials by Nanoindentation. *Opt. B.V. [White Pap.*, 1–6.

Mattei, G., Cacopardo, L., and Ahluwalia, A. (2020). Engineering Gels with Time-Evolving Viscoelasticity. *Materials* 13, 438. doi:10.3390/ma13020438

Mikulowska, A., Metz, C. N., Bucala, R., and Holmdahl, R. (1997). Macrophage Migration Inhibitory Factor Is Involved in the Pathogenesis of Collagen Type II-Induced Arthritis in Mice. *J. Immunol.* 158, 5514–5517. Available at: http://www.ncbi.nlm.nih.gov/pubmed/9164975.

Morgan, K., Clague, R. B., Shaw, M. J., Holt, P. J., Wallace, J. E., and Holt, P. J. (1980). Native Type II Collagen-Induced Arthritis in the Rat. I. Incidence and Humoral Response to Collagen. *Ann. Rheum. Dis.* 39, 285–290. doi:10.1136/ard.39.3.285

Mosser, G., Anglo, A., Helary, C., Bouligand, Y., and Giraud-Guille, M.-M. (2006). Dense Tissue-like Collagen Matrices Formed in Cell-free Conditions. *Matrix Biol.* 25, 3–13. doi:10.1016/j.matbio.2005.09.002

Murphy, S. V., Skardal, A., and Atala, A. (2013). Evaluation of Hydrogels for Bio-Printing Applications. *J. Biomed. Mater. Res.* 101A, 272–284. doi:10.1002/jbm.a.34326

Nagler-Anderson, C., Bober, L. A., Robinson, M. E., Siskind, G. W., and Thorbecke, G. J. (1986). Suppression of Type II Collagen-Induced Arthritis by Intragastric Administration of Soluble Type II Collagen. *Proc. Natl. Acad. Sci.* 83, 7443–7446. doi:10.1073/pnas.83.19.7443

Ng, W. L., Lee, J. M., Zhou, M., Chen, Y.-W., Lee, K.-X. A., Yeong, W. Y., et al. (2020). Vat Polymerization-Based Bioprinting-Process, Materials, Applications and Regulatory Challenges. *Biofabrication* 12, 022001. doi:10.1088/1758-5090/ab6034

Nishihara, T., and Doty, P. (1958). The Sonic Fragmentation of Collagen Macromolecules. *Proc. Natl. Acad. Sci.* 44, 411–417. doi:10.1073/pnas.44.5.411

Osidak, E. O., Karalkin, P. A., Osidak, M. S., Parfenov, V. A., Sivogrivov, D. E., Pereira, F. D. A. S., et al. (2019). Viscoll Collagen Solution as a Novel Bioink for Direct 3D Bioprinting. *J. Mater. Sci. Mater. Med.* 30, 31. doi:10.1007/s10856-019-6233-y

Ozbolat, I. T., and Hospodiuk, M. (2016). Current Advances and Future Perspectives in Extrusion-Based Bioprinting. *Biomaterials* 76, 321–343. doi:10.1016/j.biomaterials.2015.10.076

Park, J. Y., Choi, J.-C., Shim, J.-H., Lee, J.-S., Park, H., Kim, S. W., et al. (2014). A Comparative Study on Collagen Type I and Hyaluronic Acid Dependent Cell Behavior for Osteochondral Tissue Bioprinting. *Biofabrication* 6, 035004. doi:10.1088/1758-5082/6/3/035004

Ragetly, G., Griffon, D. J., and Chung, Y. S. (2010). The Effect of Type II Collagen Coating of Chitosan Fibrous Scaffolds on Mesenchymal Stem Cell Adhesion and Chondrogenesis. *Acta Biomater.* 6, 3988–3997. doi:10.1016/j.actbio.2010.05.016

Raub, C. B., Suresh, V., Krasieva, T., Lyubovitsky, J., Mih, J. D., Putnam, A. J., et al. (2007). Noninvasive Assessment of Collagen Gel Microstructure and Mechanics Using Multiphoton Microscopy. *Biophysical J.* 92, 2212–2222. doi:10.1529/BIOPHYSJ.106.097998

Rutgers, M., Saris, D. B., Vonk, L. A., Van Rijen, M. H., Akrum, V., Langeveld, D., et al. (2013). Effect of Collagen Type I or Type II on Chondrogenesis by Cultured Human Articular Chondrocytes. *Tissue Eng. A* 19, 59–65. doi:10.1089/ten.tea.2011.0416

Sander, E. A., and Barocas, V. H. (2008). Biomimetic Collagen Tissues: Collagenous Tissue Engineering and Other Applications. *Collagen*. New York, NY: Springer LLC, 475–496. doi:10.1007/978-0-387-73906-9_1

Sarreal, R. R., and Bhatti, P. (2020). Characterization and Miniaturization of Silver-Nanoparticle Microcoil via Aerosol Jet Printing Techniques for Micromagnetic Cochlear Stimulation. *Sensors* 20, 6087. doi:10.3390/s20216087

Saunders, R. E., and Derby, B. (2014). Inkjet Printing Biomaterials for Tissue Engineering: Bioprinting. *Int. Mater. Rev.* 59, 430–448. doi:10.1179/1743280414Y.0000000040

Seiti, M., Ginestra, P., Ferraro, R. M., Ceretti, E., and Ferraris, E. (2020). Nebulized Jet-Based Printing of Bio-Electrical Scaffolds for Neural Tissue Engineering: a Feasibility Study. *Biofabrication* 12, 025024. doi:10.1088/1758-5090/ab71e0

Shavkuta, B. S., Gerasimov, M. Y., Minaev, N. V., Kuznetsova, D. S., Dudenkova, V. V., Mushkova, I. A., et al. (2018). Highly Effective 525 Nm Femtosecond Laser Crosslinking of Collagen and Strengthening of a Human Donor Cornea. *Laser Phys. Lett.* 15, 015602. doi:10.1088/1612-202X/aa963b

Sophia Fox, A. J., Bedi, A., and Rodeo, S. A. (2009). The Basic Science of Articular Cartilage: Structure, Composition, and Function. *Sports Health* 1, 461–468. doi:10.1177/1941738109350438

Sorushanova, A., Skoufos, I., Tzora, A., Mullen, A. M., and Zeugolis, D. I. (2021). The Influence of Animal Species, Gender and Tissue on the Structural, Biophysical, Biochemical and Biological Properties of Collagen Sponges. *J. Mater. Sci. Mater. Med.* 32, 12. doi:10.1007/s10856-020-06485-4

van Luyn, M. J. A., van Wachem, P. B., Damink, L. H. H. O., Dijkstra, P. J., Feijen, J., and Nieuwenhuis, P. (1992). Secondary Cytotoxicity of Cross-Linked Dermal Sheep Collagens during Repeated Exposure to Human Fibroblasts. *Biomaterials* 13, 1017–1024. doi:10.1016/0142-9612(92)90153-F

Wallace, B. (2019). The Role of Circular Dichroism Spectroscopy in the Era of Integrative Structural Biology. *Curr. Opin. Struct. Biol.* 58, 191–196. doi:10.1016/j.sbi.2019.04.001

Weng, B., Liu, X., Shepherd, R., and Wallace, G. G. (2012). Inkjet Printed Polypyrrole/collagen Scaffold: A Combination of Spatial Control and Electrical Stimulation of PC12 Cells. *Synth. Met.* 162, 1375–1380. doi:10.1016/j.synthmet.2012.05.022

Williams, N. X., Watson, N., Joh, D. Y., Chilkoti, A., and Franklin, A. D. (2019). Aerosol Jet Printing of Biological Inks by Ultrasonic Delivery. *Biofabrication* 12, 025004. doi:10.1016/j.procbio.2006.09.00710.1088/1758-5090/ab5cf5

Xiao, Y., Kalaitzidou, K., Yao, D., Yeo, W. H., and Harris, T. A. L. (2020). Challenges and Advances in Aerosol Jet Printing of Regenerated Silk Fibroin Solutions. *Adv. Mater. Inter.* 7, 1902005. doi:10.1002/admi.201902005

Xie, J., Bao, M., Bruekers, S. M. C., and Huck, W. T. S. (2017). Collagen Gels with Different Fibrillar Microarchitectures Elicit Different Cellular Responses. *ACS Appl. Mater. Inter.* 9, 19630–19637. doi:10.1021/acsami.7b03883

Xie, S.-A., Zhang, T., Wang, J., Zhao, F., Zhang, Y.-P., Yao, W.-J., et al. (2018). Matrix Stiffness Determines the Phenotype of Vascular Smooth Muscle Cell *In Vitro* and *In Vivo*: Role of DNA Methyltransferase 1. *Biomaterials* 155, 203–216. doi:10.1016/j.biomaterials.2017.11.033

Yan, X., Bain, R. M., and Cooks, R. G. (2016). Organic Reactions in Microdroplets: Reaction Acceleration Revealed by Mass Spectrometry. *Angew. Chem. Int. Ed.* 55, 12960–12972. doi:10.1002/anie.201602270

Ye, D., Chang, C., and Zhang, L. (2019). High-strength and Tough Cellulose Hydrogels Chemically Dual Cross-Linked by Using Low- and High-Molecular-Weight Cross-Linkers. *Biomacromolecules* 20, 1989–1995. doi:10.1021/acs.biomac.9b00204

Yoon, H., Lee, J.-S., Yim, H., Kim, G., and Chun, W. (2016). Development of Cell-Laden 3D Scaffolds for Efficient Engineered Skin Substitutes by Collagen Gelation. *RSC Adv.* 6, 21439–21447. doi:10.1039/c5ra19532b

Yue, L., Wang, S., Wulf, V., and Willner, I. (2019). Stiffness-switchable DNA-Based Constitutional Dynamic Network Hydrogels for Self-Healing and Matrix-Guided Controlled Chemical Processes. *Nat. Commun.* 10, 1–10. doi:10.1038/s41467-019-12697-2

Zeugolis, D. I., Paul, R. G., and Attenburrow, G. (2008). Extruded Collagen-Polyethylene Glycol Fibers for Tissue Engineering Applications. *J. Biomed. Mater. Res.* 85B, 343–352. doi:10.1002/jbm.b.30952

Conflict of Interest: The authors declare that the research was conducted in the absence of any commercial or financial relationships that could be construed as a potential conflict of interest.

Publisher's Note: All claims expressed in this article are solely those of the authors and do not necessarily represent those of their affiliated organizations, or those of the publisher, the editors and the reviewers. Any product that may be evaluated in this article, or claim that may be made by its manufacturer, is not guaranteed or endorsed by the publisher.

frontiers in Bioengineering and Biotechnology

ORIGINAL RESEARCH
published: 05 November 2021
doi: 10.3389/fbioe.2021.766399

TEMPO-Oxidized Cellulose Nanofiber-Alginate Hydrogel as a Bioink for Human Meniscus Tissue Engineering

*Xiaoyi Lan[1,2], Zhiyao Ma[2], Alexander R. A. Szojka[2], Melanie Kunze[2], Aillette Mulet-Sierra[2], Margaret J. Vyhlidal[1], Yaman Boluk[1] and Adetola B. Adesida[2]**

[1]Department of Civil and Environmental Engineering, University of Alberta, Edmonton, AB, Canada, [2]Divisions of Orthopaedic Surgery and Surgical Research, Laboratory of Stem Cell Biology and Orthopaedic Tissue Engineering, Department of Surgery, University of Alberta, Edmonton, AB, Canada

Objective: The avascular inner regions of the knee menisci cannot self-heal. As a prospective treatment, functional replacements can be generated by cell-based 3D bioprinting with an appropriate cell source and biomaterial. To that end, human meniscus fibrochondrocytes (hMFC) from surgical castoffs of partial meniscectomies as well as cellulose nanofiber-alginate based hydrogels have emerged as a promising cell source and biomaterial combination. The objectives of the study were to first find the optimal formulations of TEMPO (2,2,6,6-tetramethylpiperidine-1-oxyl)-oxidized cellulose nanofiber/alginate (TCNF/ALG) precursors for bioprinting, and then to use them to investigate redifferentiation and synthesis of functional inner meniscus-like extracellular matrix (ECM) components by expanded hMFCs.

Methods: The rheological properties including shear viscosity, thixotropic behavior recovery, and loss tangent of selected TCNF/ALG precursors were measured to find the optimum formulations for 3D bioprinting. hMFCs were mixed with TCNF/ALG precursors with suitable formulations and 3D bioprinted into cylindrical disc constructs and crosslinked with $CaCl_2$ after printing. The bioprinted constructs then underwent 6 weeks of *in vitro* chondrogenesis in hypoxia prior to analysis with biomechanical, biochemical, molecular, and histological assays. hMFCs mixed with a collagen I gel were used as a control.

Results: The TCNF/ALG and collagen-based constructs had similar compression moduli. The expression of *COL2A1* was significantly higher in TCNF/ALG. The TCNF/ALG constructs showed more of an inner meniscus-like phenotype while the collagen I-based construct was consistent with a more outer meniscus-like phenotype. The expression of *COL10A1* and *MMP13* were lower in the TCNF/ALG constructs. In addition, the immunofluorescence of human type I and II collagens were evident in the TCNF/ALG, while the bovine type I collagen constructs lacked type II collagen deposition but did contain newly synthesized human type I collagen.

Keywords: tissue engineering, meniscus, 3D bioprinting, cellulose nanofiber, hypoxia

OPEN ACCESS

Edited by:
Derek H. Rosenzweig, McGill University, Canada

Reviewed by:
Vahid Serpooshan, Emory University, United States
Goutam Thakur, Manipal Institute of Technology, India

****Correspondence:***
Adetola B. Adesida
adesida@ualberta.ca

Specialty section:
This article was submitted to Biomaterials, a section of the journal Frontiers in Bioengineering and Biotechnology

Received: *29 August 2021*
Accepted: *13 October 2021*
Published: *05 November 2021*

Citation:
Lan X, Ma Z, Szojka ARA, Kunze M, Mulet-Sierra A, Vyhlidal MJ, Boluk Y and Adesida AB (2021) TEMPO-Oxidized Cellulose Nanofiber-Alginate Hydrogel as a Bioink for Human Meniscus Tissue Engineering. Front. Bioeng. Biotechnol. 9:766399. doi: 10.3389/fbioe.2021.766399

INTRODUCTION

The menisci are a pair of C-shaped fibrocartilages that withstand compressive and tensile forces (Fithian et al., 1990; Leslie et al., 2000; Liang et al., 2018). They are essential for mechanical load distribution and transmission, lubrication, and stability of the knee joint (Makris et al., 2011; Liang et al., 2018). The biomechanical properties are attributed to the presence of functional extracellular matrix (ECM) (Fithian et al., 1990; Leslie et al., 2000; Adesida et al., 2007; Liang et al., 2018). The menisci exhibit regional and zonal variations in their ECM and cellular compositions, reparative capacities, and vascularity with age (Arnoczky and Warren, 1982; Nakata et al., 2001; Chevrier et al., 2009; Sanchez-Adams and Athanasiou, 2009). Type I collagen (collagen I) is found throughout the entire meniscus; type II collagen (collagen II) and aggrecan are usually only found in the inner regions of the meniscus (King, 1936; Nakata et al., 2001; Szojka et al., 2021). The outer region of the meniscus contains collagen I fibre bundles that aligned in the circumferential direction, exhibiting a fibrous connective tissue (ligament and tendon-like) phenotype and a peripheral blood supply (1/3 or less in adults) that provides some healing capacity (King, 1936; Nakata et al., 2001; Szojka et al., 2021). The cell population in the outer meniscus is predominantly fibroblast-like. In contrast, the middle and inner regions (2/3 or more) of the meniscus have a fibrocartilage phenotype that is avascular and non-healing (King, 1936; Nakata et al., 2001; Szojka et al., 2021). The cell population for the inner region of the meniscus are human meniscus fibrochondrocytes (hMFC), which are a mix of fibroblast and chondrocyte-like cells (King, 1936; Nakata et al., 2001; Szojka et al., 2021).

Due to the limited healing capacities of meniscus, patients with meniscus defects or injuries often undergo partial or total meniscectomy, which is known to cause biomechanical changes to joint function with a risk for early knee osteoarthritis development (Fairbank, 1948; Cox et al., 1975; Paradowski et al., 2016). Cell-based meniscus tissue engineering is a promising technology to circumvent this challenge by creating meniscus tissue replacements (Ibarra et al., 2000). By using 3D bioprinting with a "bioink" composed of a biomaterial and cells, can create patient-specific tissues for reconstructive surgery (Murphy and Atala, 2014; Di Bella et al., 2015; Daly et al., 2017). In fact, 3D bioprinting can spatially control the placement of cells, biomaterial, and growth factors in a construct. Therefore, it has the potential to accurately mimic the structure and morphology of tissues and organs (Murphy and Atala, 2014; Mandrycky et al., 2016). Natural hydrogel precursors are attractive for bioinks because of their favourable biocompatible properties and high-water content like human ECM (Markstedt et al., 2015; Skardal et al., 2015; Ávila et al., 2016). To be suitable for printing, the rheological behaviour of the bioink is critical (Paxton et al., 2017; Cooke and Rosenzweig, 2021). The bioink must have shear thinning properties, which allows extrusion through small orifices with a decrease in shear to maintain cell viability. The bioink also needs a high zero-shear viscosity to retain its shape during and after printing (Paxton et al., 2017; Cooke and Rosenzweig, 2021). Beyond rheological properties, the bioink needs to be crosslinkable to retain 3D structures and provide appropriate mechanical properties to the bioprinted constructs (Markstedt et al., 2015; Paxton et al., 2017). Alginate has been proven as a promising crosslinkable material for 3D bioprinting (Markstedt et al., 2015; Müller et al., 2017; Nguyen et al., 2017; Gatenholm et al., 2018; Göhl et al., 2018; Hiller et al., 2018; Wu et al., 2018; Yang et al., 2018; Heggset et al., 2019; Jessop et al., 2019; Ojansivu et al., 2019; Erkoc et al., 2020; Schwarz et al., 2020). It can form a stable hydrogel in the presence of divalent cations such as Ca^{2+} and Ba^{2+} due to the ionic interaction between the cation and the carboxyl functional group by forming "egg-box"-calcium linked junctions (Li et al., 2007a). Alginate is usually mixed with other biomaterials to achieve higher printing resolution (Markstedt et al., 2015; Müller et al., 2017; Nguyen et al., 2017; Heggset et al., 2019; Jessop et al., 2019; Erkoc et al., 2020).

Cellulose, the most abundant renewable biopolymer found in nature, is a linear polysaccharide composed of β (1→4) linked D-glucose units (Dufresne, 2013; Abitbol et al., 2016; Abdul Rashid et al., 2018). The term *nanocellulose* refers to processed cellulose extract with one dimension in the nanometer range (Dufresne, 2013; Abitbol et al., 2016; Gatenholm et al., 2018). Depending on the sources and the preparation method, nanocellulose materials can be categorized into three main groups: bacteria cellulose (BC), cellulose nanofiber (CNF), and cellulose nanocrystal (CNC) (Wang et al., 2020b). The most common nanocellulose used in 3D bioprinting applications is CNF (Wang et al., 2020b). CNFs exhibit shear-thinning behaviour and a high zero shear viscosity, making them useful as a viscous contributor for the bioink. CNFs can be extracted from raw materials by a combination of chemical (e.g., acid hydrolysis, enzymatic reaction, TEMPO oxidation) and mechanical treatments (e.g., high-pressure homogenization and grinding) (Wang et al., 2020b). TEMPO-oxidized CNFs (TCNFs) exhibit a high concentration of carboxyl groups and the new TEMPO-induced carboxyl groups in TCNFs are able to support alginate in the construction of crosslinked network, which enhances the scaffold mechanical strength, porosity, water absorption, and structural integrity (Lin et al., 2012).

This study incorporates hMFCs with TEMPO-oxidized CNF and alginate (TCNF/ALG) precursors to create tissue-engineered meniscus constructs. First, we evaluated the printability and the rheology properties of various formulations of TCNF/ALG precursors as potential bioinks. Then, we evaluated the biological functionality of 3D bioprinted meniscus-like tissue constructs using the optimal formulations, followed by 6 weeks of *in vitro* chondrogenic culture in low oxygen tension (i.e., hypoxia of 3% O_2). Collagen I, the major component of the meniscus fibrocartilage's ECM, served as a reference biomaterial. Hypoxia was used since it has been proven as a stimulus for the maturation of meniscus fibrochondrocytes (Herrera Millar et al., 2021). Our previous research has found that hypoxia and TGF-β3 synergistically mediated the inner meniscus-like tissue matrix formation (Szojka et al., 2019). The schematic diagram of the experimental design is shown in **Figure 1**.

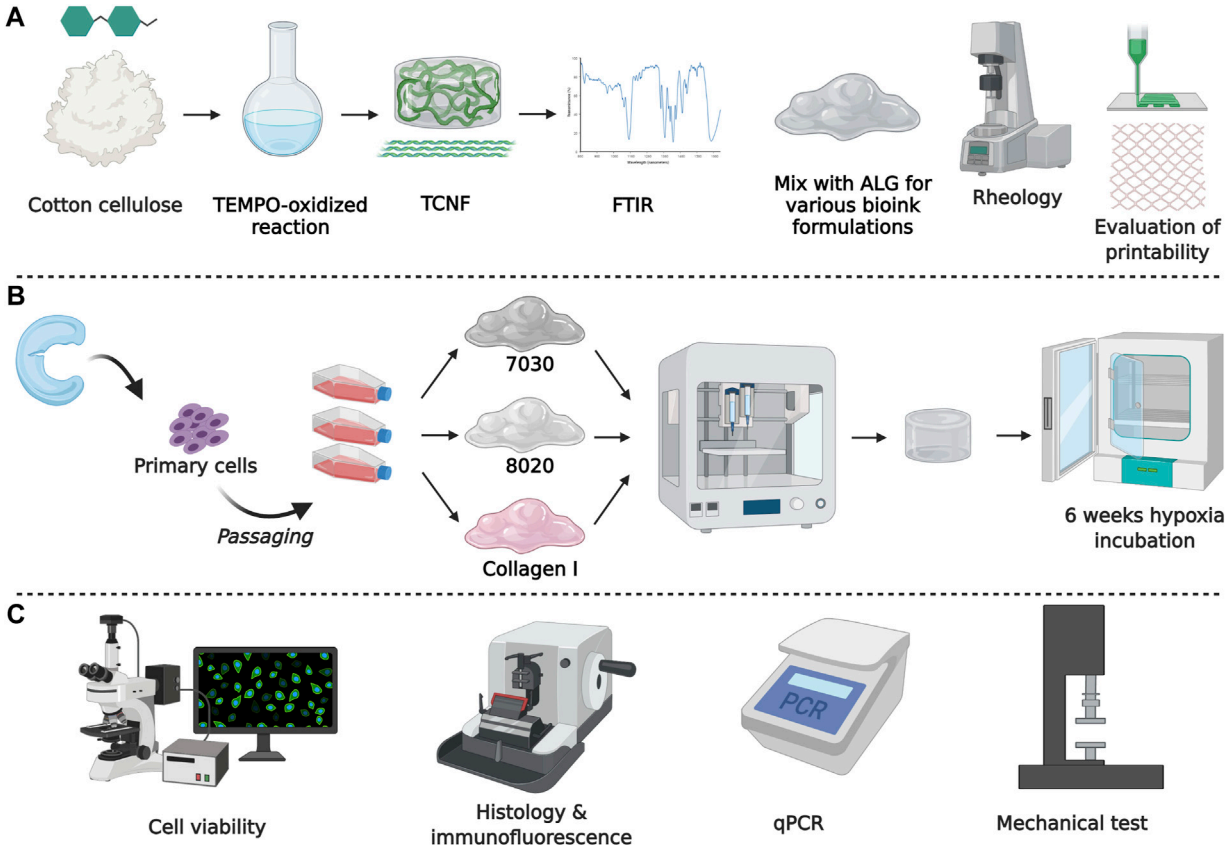

FIGURE 1 | Schematic diagram of the experimental design. **(A)** Biomaterial formation and characterization, **(B)** engineered tissue formation, and **(C)** evaluation of engineered tissues.

MATERIALS AND METHODS

TCNF Synthesis and Preparation of TCNF/ALG Precursors

Native cellulose (10 g, Whatman No. 1 filter paper) was cut into small pieces and immersed in deionized water (DI) water to make 1 L of 1% w/w cellulose pulp slurry. In addition, 0.189 g of TEMPO (Sigma Aldrich, Canada), 1.178 g NaBr (Sigma Aldrich, Canada), and 50 ml of 1.8 M NaClO (Sigma Aldrich, Canada) were added into the cellulose slurry under continuous stirring until dissolved. The pH of the reactants in the flask was maintained at pH = 10.5 by adding 0.5 M NaOH until the pH of the reactant were stable at 10 (Shinoda et al., 2012). The TEMPO-oxidized cellulose was then washed with DI water for 15 times until the conductivity for supernatant was constant (~12.5 μs/cm). The TEMPO-oxidized cellulose nanofiber (TCNF) was prepared by blending the TEMPO-oxidized cellulose for 7 min. The carboxylate content for the TCNF was 0.84 mmol/g. The TCNF was centrifuged and adjusted to 3.5% w/v solid content. Freeze-dried cellulose pulp slurry (pure cellulose) and TCNF were characterized by Fourier Transform Infrared spectroscopy (FTIR).

Sodium alginate (ALG, Alfa Aesar, J61887, United States) was prepared into a 3.5% w/v solution. The concentrated TCNF and the ALG solution were sterilized by autoclave. The TCNF and ALG are mixed into various printing formulations (**Table 1**) with a final solid content of 3.5% w/v.

Rheological Characterization of TCNF/ALG Precursors as Potential Bioink Materials

The rheological properties of all the TCNF/ALG precursors were characterized using a rotatory rheometer (AR-G2, TA Instrument, United States) with a 25 mm parallel-plate geometry. The steady-state flow sweep was characterized under the shear rate from 0.001 to 1,000 s^{-1} at room temperature. The oscillatory frequency sweep was measured under 1% strain (within the linear viscoelastic region) and 1–100 rad/s frequency. The thixotropy tests were done by first fixing the shear rate at 1 s^{-1} for 100 s, followed by a sudden increase in the shear rate to 1,000 s^{-1}, and then a sudden drop in the shear rate to the initial state (1 s^{-1}). The rheology data was analyzed using TRIOS software (TA Instruments, United States).

Assessment of Printing Fidelity Before and After Crosslinking

To assess the printability of the TCNF/ALG precursors, 20 mm × 20 mm × 3 mm blocks with a 30% infill were bioprinted using an

TABLE 1 | TCNF/ALG precursor formulations.

Precursors	Composition	Formulation (% w/v)	Solid content (% w/v)
0100	100% of ALG	ALG: 3.5	3.5
2080	20% TCNF	TCNF: 0.7	3.5
	80% ALG	ALG: 2.8	
5050	50% TCNF	TCNF: 1.75	3.5
	50% ALG	ALG: 1.75	
6040	60% TCNF	TCNF: 2.1	3.5
	40% ALG	ALG: 1.4	
7030	70% TCNF	TCNF: 2.45	3.5
	30% ALG	ALG: 1.05	
8020	80% TCNF	TCNF: 2.8	3.5
	20% ALG	ALG: 0.7	
9010	90% TCNF	TCNF: 3.15	3.5
	10% ALG	ALG: 0.35	

extrusion-based bioprinter (INKREDIBLE+, CELLINK, Sweden). The geometry and printing parameters of the printed constructs were predefined in commercial design software (Slic3r, United States). The needle inner diameter was 0.413 cm (22G). The printing speed was 10 mm/s with each layer height of 0.5 mm (6 layers in total). After bioprinting, a 100 mM $CaCl_2$ solution was added over the bioprinted TCNF/ALG constructs for 3 min followed by a phosphate buffered saline (PBS) rinse. After crosslinking, the precursors with the best printing fidelity were used for further biological functionality evaluation. A commercially available bovine collagen I gel with similar solid content to the TCNF/ALG precursors was used as a control (3.5% w/v, Advanced Biomatrix, United States). The collagen I gel was printed at room temperature and spontaneously polymerized at 37°C. The fidelity parameter (side length of the square blocks (L) before and after the crosslinking, filament diameter) were quantified using ImageJ (Fiji, United States). The contractility from the crosslinking process was calculated as:

$$\text{contractility} = \left(L_{\text{before crosslinking}} - L_{\text{after crosslinking}}\right)/L_{\text{before crosslinking}}$$

Isolation of Human Meniscus Fibrochondrocytes

Meniscus specimens from three (3) male donors were collected from partial meniscectomy surgeries with the approval of the University of Alberta's Health Research Ethics Board - Biomedical Panel (Study ID: Pro00018778). Human meniscus fibrochondrocytes (hMFCs) were isolated enzymatically using collagenase digestion as previously described (Liang et al., 2017). The primary hMFCs were plated at a density of 10^4 cells/cm^2 and expanded to passage 2 (P2) in monolayer culture in high glucose Dulbecco's Modified Eagle Medium (DMEM, Sigma Aldrich, Canada) supplemented with 10 v/v (%) fetal bovine serum (FBS), 1 ng/ml of TGF-β1, and 5 ng/ml of FGF-2 at 37°C in normoxia (~20% O_2) conditions (Liang et al., 2017). Donor information is shown in **Table 2**. The cumulative population doublings of the hMFCs at the end of P2 was 7.0 ± 0.2 (mean ± standard deviation).

3D Bioprinting of TCNF/ALG and Collagen Bioinks

hMFCs at P2 were resuspended in a standard serum-free chondrogenic medium containing 10 ng/ml TGF-β3 (Liang et al., 2017). The cell suspension was mixed with 7030, 8020 precursors (7030, 8020 bioinks), and collagen I gel (COL bioink) to a cell density of 10^7 cells/mL.

To investigate the fibrocartilage formation of the bioprinted constructs after *in vitro* chondrogenic culture, hMFC-laden TCNF/ALG bioinks and COL bioink were bioprinted into cylindrical shapes (7 mm diameter, 3.5 mm height) with an infill rate of 70%. Then bioprinted constructs were crosslinked as before. At the same time, the hMFC-laden COL bioinks were kept in a 37°C incubator for 30 min and then placed in a serum-free chondrogenic medium containing 10 ng/ml TGF-β3 (2 ml/construct, twice per week) for 6 weeks under hypoxic conditions (3% O_2).

Viability in Bioprinted Constructs

hMFCs viability was assessed using Syto 13/Propidium iodide (PI) staining. Syto 13 (S7575, ThermoFisher, United States) is a green live-cell fluorescent nucleic acid stain, and PI (P3566, ThermoFisher) is a red dead-cell fluorescent nuclear and chromosome counterstain. The Syto 13 and PI concentrations in PBS were 6.25 and 15.0 μM, respectively.

Bioprinted constructs of TCNF/ALG (8020, 7030 bioinks) and COL bioinks after 1-day culture were incubated in Syto 13 and PI solution at room temperature for 30 min in the dark. The cell viabilities were viewed under a Nikon confocal laser scanning microscope (Leica TCS SP5). Fluorescence was quantified using Python.

Structural Integrity and Microstructural Evaluation of Bioprinted Constructs

Scanning electron microscopey (SEM., Zeiss Sigma 300 VP-FESEM) was used to observe the TCNF fibre diameter and the ECM formation of the bioprinted constructs after 6 weeks of *in vitro* culture. Each construct was fixed in sodium cacodylate trihydrate buffer containing 2% v/v glutaraldehyde and 2.5% v/v paraformaldehyde overnight.

TABLE 2 | Meniscus donor information.

Donor	Sex	Age	Medical history	Anatomical site	Cumulative population doubling
1	Male	30	ACL reconstruction	Right knee medial	7.0
2	Male	27	Healthy	Left knee medial	7.3
3	Male	16	ACL tear	Right knee lateral	6.8

The samples were then cut in half and washed twice with deionized water to wash away the fixation solution. The samples were further treated with osmium tetroxide and tannic acid before SEM observation. All the reagents were purchased from Electron Microscopy Sciences (Pennsylvania, United States).

Histological and Immunofluorescent Evaluation of Matrix Formation

Bioprinted constructs for three experiment groups (8020, 7030, COL) from the same donor were fixed in 10% (v/v) neutral buffered formalin, dehydrated through a series of alcohol washes, and then embedded in paraffin. The embedded samples were cut into 5 μm sections cross-sectionally.

For histological assessments, the sections were deparaffinized by the xylene substitute, then rehydrated and stained with Safranin-O/Fast Green. Collagens I, II, and X as well as aggrecan were examined by immunofluorescence. In brief, sections were prepared as above. Collagens I and II were counterstained in one slide. Collagen X and aggrecan were stained separately in two slides. The primary antibodies for collagens I and II were rabbit anti-human collagen I (CL50111AP-1, Cedarlane, Canada) and mouse anti-human collagen II (II-II6B3, Develop-mental Studies Hybridoma Bank [DSHB], United States). The primary antibody for type X collagen (collagen X) was rabbit anti-human collagen X (rabbit polyclonal to collagen X, ab58632, Abcam, United States), and the primary antibody for aggrecan was a rabbit anti-human aggrecan (recombinant monoclonal to aggrecan, MA5-32695, ThermoFisher, United States).

After incubation with primary antibodies, the slides were incubated with secondary antibodies for 45 min. The secondary antibodies used for collagens I and II are goat anti-rabbit IgG Alexa Fluor 594 (ab150080, Abcam, United States) and goat anti-mouse IgG Alexa Fluor 488 (ab150117, Abcam, United States). The secondary antibodies used for collagen X and aggrecan were goat anti-rabbit IgG Alexa Fluor 594 (ab150080, Abcam, United States). In addition, all the slides were also stained with 4′,6-diamidino-2′- phenylindole (DAPI, Thermo Fisher Scientific) for 20 min at room temperature to examine the nuclei of hMFCs in each sample. A Nikon Eclipse Ti-S microscope coupled to a DS-U3/Fi2 Color CCD camera with 100x and 200x total magnification was used to capture the histological and immunofluorescent images.

Gene Expression Analysis

Quantitative real-time polymerase chain reaction (qRT-PCR) was used to analyze expression of genes that are chondrogenic and fibrochondrogenic specific (*ACAN, COL1A2, COL2A1, SOX9*) and chondrocyte hypertrophy-related (*COL10A1, MMP13, ALPL, RUNX2*). The analysis was conducted after 6 weeks (42 days) of *in vitro* chondrogenic culture. Total RNA was extracted using TRIzol (Life Technologies, United States). The complementary DNA (cDNA) was synthesized from 100 ng of total RNA using GoScript, Reverse Transcriptase kit (Promega, United States) and 1 μg of oligo (dT) primer. Primer sequences for qPCR were designed using Primer Express 3.0.1 (Thermo Fisher Scientific). Transcript levels for the interested genes were normalized to the housekeeping genes: *β-actin*, *B2M*, and *YWHAZ* using the delta CT method ($2^{-\Delta CT}$). Primer sequences are shown in **Table 3**.

Biomechanical Characterization by Stress Relaxation Tests

The mechanical properties of bioprinted constructs were assessed using a stepwise stress relaxation test using a Biodynamic 5,210 system (TA Instruments, United States). For each experimental group, constructs from $n = 3$ donors were tested. The constructs were preconditioned by 15 cycles of sine wave dynamic compressive loading with an amplitude of 5% tissue height at a frequency of 1 Hz. The following stress relaxation test consisted of 4 incremental strain steps. In each step, the constructs were subjected to a 10% strain ramp at the rate of 50% strain/s and followed by 20 min relaxation under constant strain. All tested constructs reached equilibrium in the given relaxation period. Forces were recorded as a function of time, and stress was calculated by normalizing force to construct cross-section area. The peak modulus was calculated by dividing the maximum stress increment immediately after the compression increment by 10%, the strain increment.

Statistical Analysis

GraphPad Prism 8 was used to perform statistical analysis. The paired two-sample *t*-test was used to analyze the significance level between each sample group (8020 vs. COL, 7030 vs. COL, 7030 vs. 8020) in cell viability and in gene expression after taking the replicate means within donors. Two-way ANOVA was used to determine the statistical differences in stress relaxation tests for various bioinks at different strains with Tukey's test for multiple comparisons. The results were presented as mean ± standard deviation (SD).

RESULTS

Rheology and Printing Fidelity of TCNF/ALG Precursors

Figure 2 presents the FTIR spectra of unmodified pure cellulose and TCNF. After TEMPO-oxidation, the characteristic

TABLE 3 | Primer sequences for quantitative real-time polymerase chain reaction.

Gene	Forward primer (5′)	Reverse primer (3′)
B-actin	AAGCCACCCCACTTCTCTCTAA	AATGCTATCACCTCCCCTGTGT
B2M	TGCTGTCTCCATGTTTGATGTATCT	TCTCTGCTCCCCACCTCTAAGT
YWHAZ	TCTGTCTTGTCACCAACCATTCTT	TCATGCGGCCTTTTTCCA
ACAN	AGGGCGAGTGGAATGATGTT	GGTGGCTGTGCCCTTTTTAC
COL1A2	GCTACCCAACTTGCCTTCATG	GCAGTGGTAGGTGATGTTCTGAGA
COL2A1	CTGCAAAATAAAATCTCGGTGTTCT	GGGCATTTGACTCACACCAGT
SOX9	CTTTGGTTTGTGTTCGTGTTTTG	AGAGAAAGAAAAAGGGAAAGGTAAGTTT
COL10A1	GAAGTTATAATTTACACTGAGGGTTTCAAA	GAGGCACAGCTTAAAAGTTTTAAACA
RUNX2	GGAGTGGACGAGGCAAGAGTTT	AGCTTCTGTCTGTGCCTTCTGG
VCAN	TGCTAAAGGCTGCGAATGG	AAAAAGGAATGCAGCAAAGAAGA
MMP13	AAAAAGGAATGCAGCAAAGAAGA	CGGAGACTGGTAATGGCATCA
ALPL	GCTGTAAGGACATCGCCTACCA	CCTGGCTTTCTCGTCACTCTCA

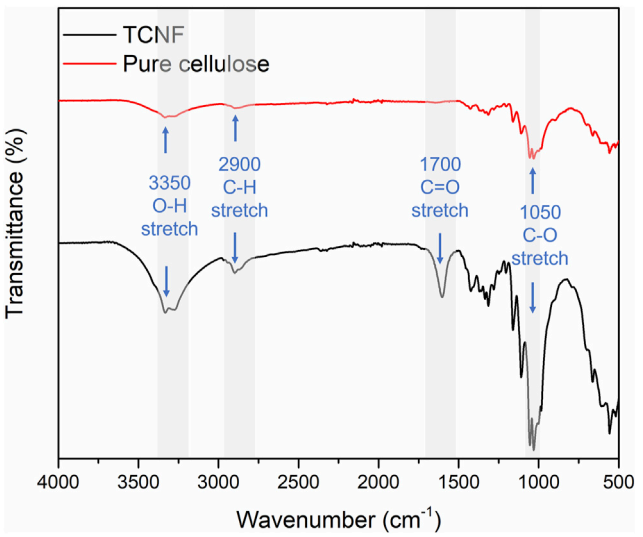

FIGURE 2 | Fourier transform infrared spectroscopy of the pure cotton cellulose and TCNF.

absorption band of carboxyl group (C==O) stretching appeared around 1,650 cm^{-1}, which is assigned to the formation of COO groups after the oxidation and release of nanofibers (El Bakkari et al., 2019). The enhancement of the -OH stretching group around 340 cm^{-1}, C-H at around 2,900 cm^{-1}, and C-O-C at around 1,050 cm^{-1} were also observed in TCNF, which indicated more -OH, C-O-C group are exposed.

The rheology data of the TCNF/ALG precursors were measured to pre-estimate the printability as potential bioink materials. The viscosity vs. shear rate (steady-state flow sweep) of all the TCNF/ALG precursors is shown in **Figure 3A**. All TCNF/ALG precursors exhibited shear-thinning behaviour, in which the viscosity decreased as the shear rate increased. The Power Law model was also used to fit the viscosity vs shear rate curve (0.01–1,000 s^{-1}) to describe the shear-shinning behaviour. The printing pressure of each TCNF/ALG precursors are shown in **Table 4**. The viscosity and shear rate relationship can be described in the equation of the $\eta = K\dot{\gamma}^{n-1}$, where η is viscosity, $\dot{\gamma}$ is the shear rate, K and n are the empirical curves fitting parameters, known as the flow consistency index and flow behaviour index (Middleman, 1977). The fitted power-law parameters (K and n) are shown in **Table 4**. For shear thinning fluid, n always less than 1. The lower the n, the better the shear-thinning behaviour responding to the increase of shear rate. TCNF, 8020, 9010 exhibited and the best shear thinning behaviour, and 5050 exhibited the worst shear-thinning behaviour.

The recovery and thixotropic properties were determined by applying a steady shear rate of 1 s^{-1} for 100 s suddenly increasing the shear rate to 1,000 s^{-1} for 100 s, and then reducing it to 1 s^{-1} for 100 s. **Figure 3B** depicts the thixotropic behaviour of the prepared hydrogels. The viscosity of the all the TCNF/ALG precursors rapidly dropped with an applied shear (printing stage) and recovered quickly after the shear force was removed (post-printing stage). However, all the samples were thixotropic and decreased in viscosity after recovery. The average viscosities of the TCNF/ALG precursors under the three shear rate stages are recorded in **Supplementary Table S1**. The recovery rates (initial/final viscosity) are shown in **Table 4**.

The frequency sweep tests were performed within the linear viscoelastic deformation region. Loss tangent (tan δ), the ratio of loss moduli (G″), and storage moduli (G″) for TCNF/ALG precursors as a function of frequency are shown in **Figure 3C**. The loss tangent (tan δ) determines if a material is solid-like or liquid-like. All the TCNF/ALG precursors showed a solid-like behaviour (G'>G″, tan δ< 1). The pure TCNF, 8020, and 9010 showed the most solid-like behaviour followed by 6040, 7030, 2080, and pure ALG and 5050 showed the least solid-like behaviour.

The TCNF/ALG precursors were then bioprinted into mesh shapes and crosslinked using 100 mM of $CaCl_2$ solution. The bioprinted constructs before and after crosslinking are shown in **Figure 4A**. The printing pressure, filament diameter, and contractility after crosslinking are shown in **Table 4**. Apparent size and shape contractions are observed in the TCNF/ALG precursors with low or no TCNF content (0100, 2080, 5050, 6040). On the other hand, the 7030, 8020, and 9010 showed the lowest contractility (≤10%) and best printing fidelity (finest filament diameter). Due to the relatively low alginate content, the 9010 was too soft to retain its shape during transfer or

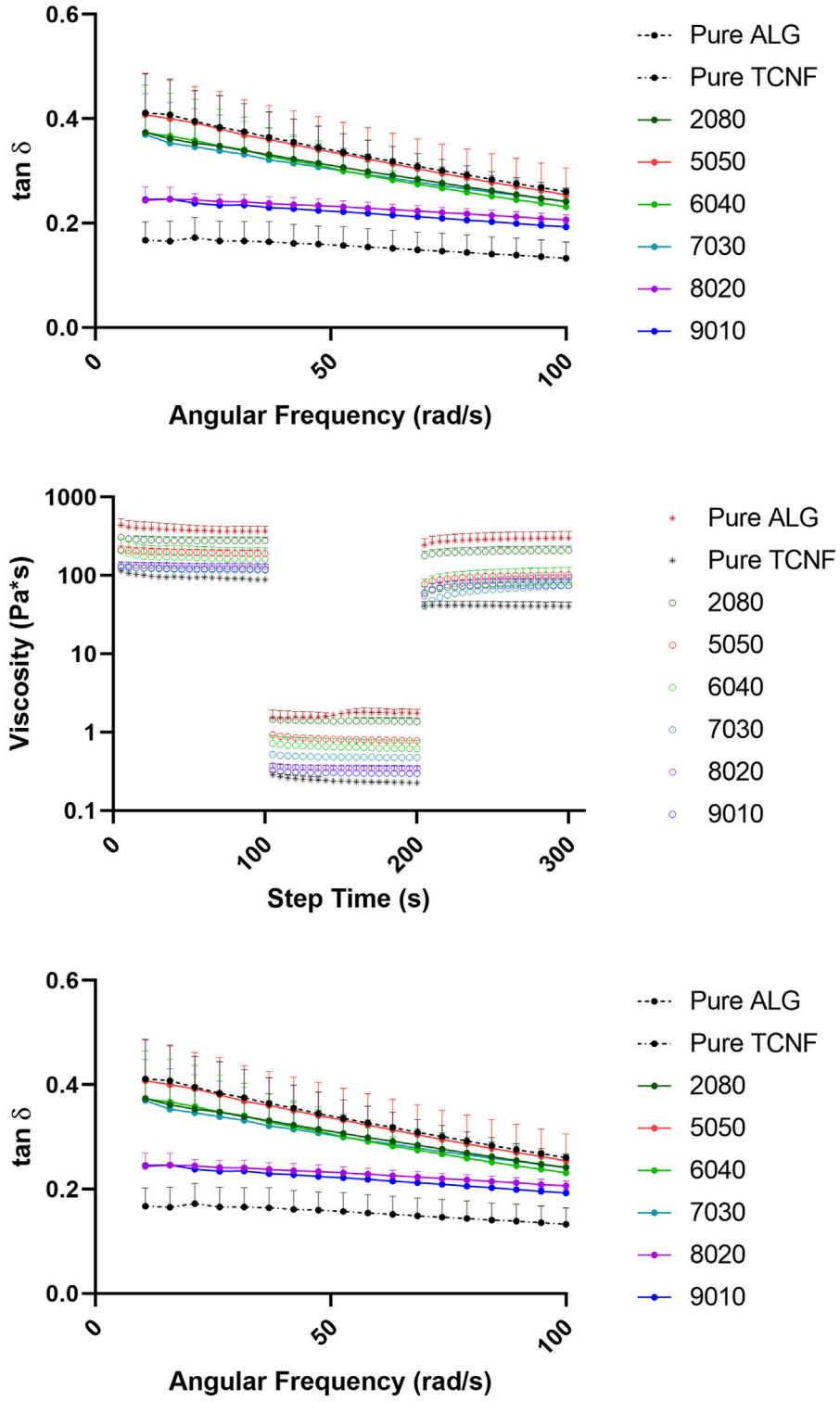

FIGURE 3 | The rheology behaviors of the TCNF/ALG precursors. **(A)** The steady state flow sweeps, strain rate from 0.001 to 1,000 s^{-1}. **(B)** Three-step recovery and thixotropic behavior, low shear rate at 1 s^{-1} for 100 s for initial and final step, high shear rate at 1,000 s^{-1} for 100 s for middle step. **(C)** Loss tangent of the TCNF/ALG precursors from 1 to 100 rad/s. The formulations are described in **Table 1**.

TABLE 4 | Fitted Power-Law parameters, thixotropy recovery rate, printing pressure, filament diameter, and contractility after crosslinking.

	ALG	2080	5050	6040	7030	8020	9010	TNCF
K	432.90	503.13	232.78	194.70	237.04	137.63	155.43	156.43
n	0.24	0.23	0.25	0.19	0.18	0.13	0.14	0.16
Recovery (%)	81.6 ± 5.6	75.2 ± 2.0	53.4 ± 1.6	50.2 ± 13.0	63.7 ± 4.6	71.8 ± 4.1	62.1 ± 2.1	45.1 ± 3.6
Pressure (kPa)	200	155	125	75	75	55	55	—
Filament Diameter	—	—	0.88 ± 0.02	1.04 ± 0.08	0.79 ± 0.02	0.72 ± 0.00	0.76 ± 0.02	—
Contraction (%)	29.5%	28.8%	15.3%	10.2%	9.5%	4.3%	1.0%	—

**The filaments of the mesh printed by pure ALG and 2080 bioink material fused together and their diameter could not be measured.*

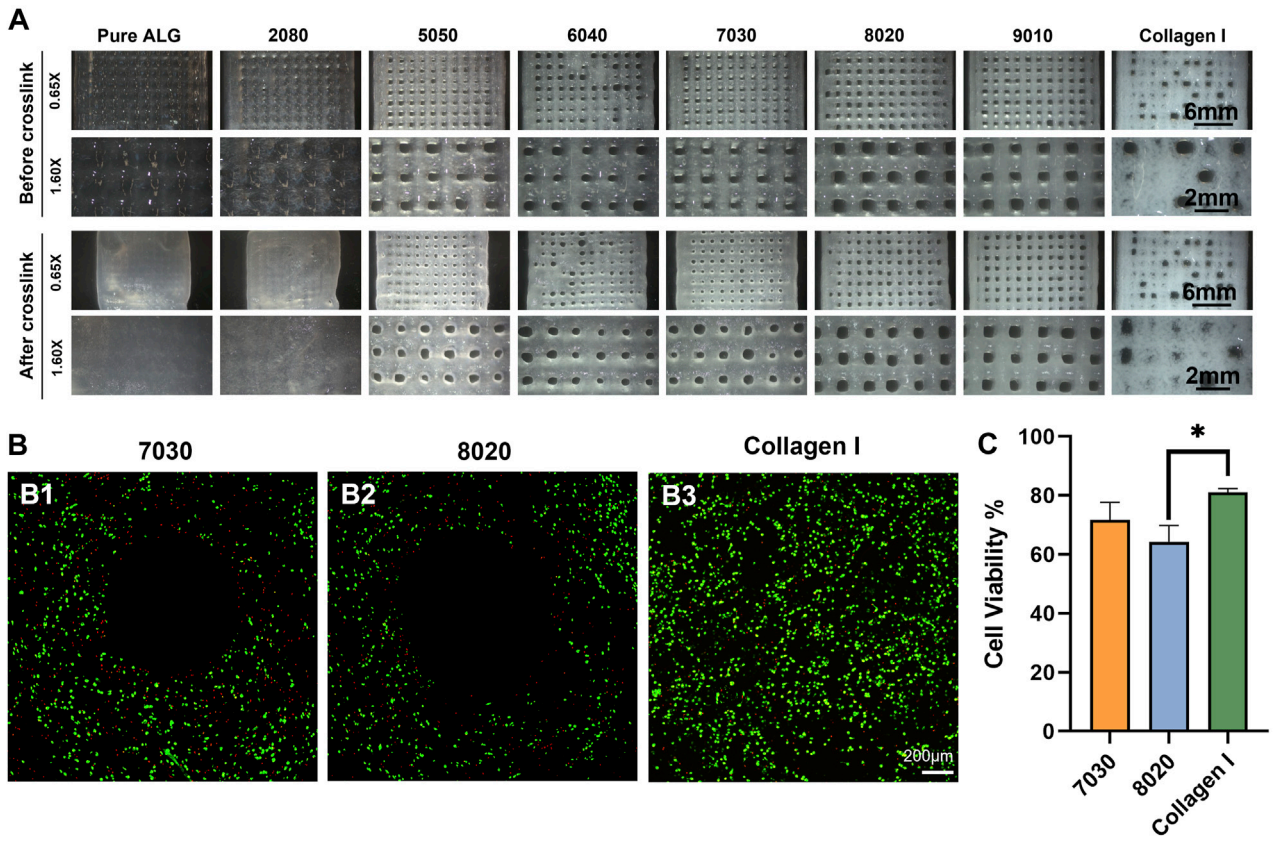

FIGURE 4 | (A) Printed mesh structures using different formulations of TCNF/ALG precursors. **(B)** Live/dead images of the **(B1)** 7030, **(B2)** 8020, and **(B3)** COL bioinks. Live cells appear green and dead cells red. **(C)** Quantitative cell viability of the Live/Dead assay images.

movement of the construct. Therefore, the 7030 and 8020 formulations were selected as bioinks to mix with hMFCs for further biochemical and biomechanical evaluations.

The LIVE/DEAD assay images after bioprinting using a 22 G needle are shown in **Figure 4B**. No statistically significant difference was observed between 7030 and 8020 bioinks (**Figure 4C**). The collagen I bioink showed a significantly higher cell viability compared to the 8020 bioink (**Figure 4C**).

Histological and Biochemical Assessments

It is commonly understood that Safranin-O would only stain when sulfated GAG is present within the sample. Interestingly, we discovered that cellulose nanofibers (TCNF) could also be stained by Safranin-O despite lacking sulfated GAG, as shown in **Supplementary Figure S1** in supplemental materials. Previous studies which used CNFs as biomaterials for cartilage tissue engineering did not report and discuss this phenomenon (Nguyen et al., 2017). Through comparing against cell-free CNF samples, it was still possible to distinguish the Safranin-O positive matrix throughout the histological sections of two TCNF/ALG bioink (**Figures 3A,B**). In contrast, the bioprinted COL bioink did not show any positive safranin-O positive matrix deposition throughout the section (**Figures 5E,F**).

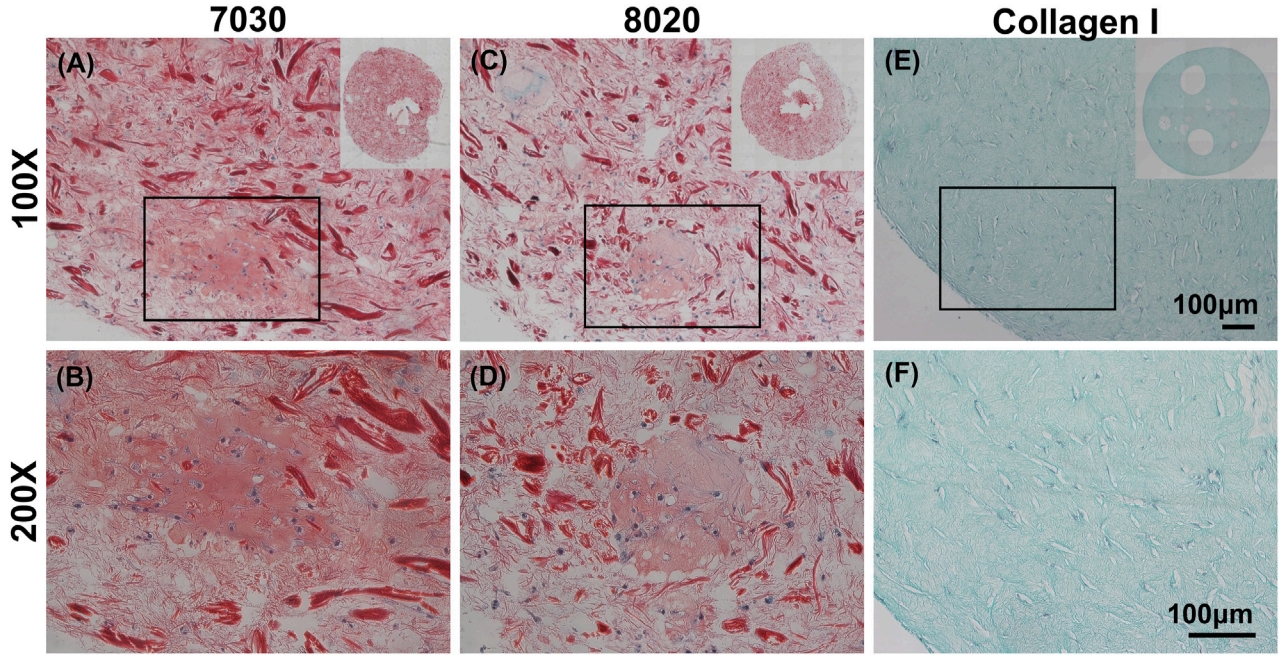

FIGURE 5 | Safranin-O staining (red, stained negatively charged proteoglycans and the TCNF) with Fast Green counterstain (green, stained proteins) and cells stained with hematoxylin of **(A,B)** 7030, **(C,D)** 8020, and **(E,F)** COL I bioinks. Scale bar is 100 μm.

Positive aggrecan immunofluorescent staining was shown in both TCNF/ALG bioinks (**Figures 6A,B**) but not in the COL bioink (**Figure 6C**), which was consistent with the Safranin-O staining results. The immunofluorescence staining also showed a universal presence of collagen I in two TCNF bioinks (**Figures 6D,E**) and the COL bioink (**Figure 6F**). The COL bioink showed more densely packed collagen I compared to the two TCNF/ALG bioinks. However, collagen II was present in the two TCNF/ALG bioinks (**Figures 6D,E**) and not in the COL bioink (**Figure 6F**). The collagen II matrix was most concentrated at the outer edges of the constructs. There was no detectable collagen X immunofluorescence in any constructs (**Figures 6G–I**). The SEM images of the 7030 and 8020 bioinks after 6 weeks of *in vitro* chondrogenic culture are depicted in **Figure 7**. Newly synthesized ECM was observed on the surface of the bioprinted constructs for both 7030 and 8020 bioinks. The TCNF material was visible under the ECM.

The mRNA expression of fibrocartilage-related (*ACAN*, *COL1A2*, *COL2A1*, *SOX9,* and *VCAN*) and bone-related (*COL10A1, MMP13, ALPL,* and *RUNX2*) genes are shown in **Figure 8**. For all these genes, no significant differences were observed between the 7030 and 8020 bioinks. The fibrous markers *COL1A2* and *VCAN* in the COL bioink were higher than in 7030 bioinks with near statistical significance (i.e., p = 0.086 and p = 0.077, respectively). The cartilaginous marker *COL2A1* in the COL bioink was significantly lower compared to the 7030 bioink. No statistically significant difference was observed among the three bioinks in gene expression of *ACAN* and *SOX9*. No significant difference was noted in *ALPL*, and *RUNX2* among the three groups for these bone formation-related genes. On the other hand, there was an upregulation of *MMP13* in the COL bioink compared to 7030 and 8020 with near statistical significance (i.e., p = 0.066 and p = 0.076, respectively). The expression of *COL10A1* in the COL bioink for each donor increased but with no detectable significant difference.

After the strain-controlled unconfined compression test, the peak modulus (instantaneous modulus) was calculated using the force change between the peak and equilibrium forces at each relaxation period. The calculated values were normalized by the cross-sectional area of the 3D bio-printed tissues. The stepwise stress-relaxation as a function of time of one donor (0–10%, 10–20%, 20–30%, and 30–40% strain for each force jump) and the peak modulus as a function of the cumulative strain is shown in **Figures 9A,B**. No significant interaction was observed between material type and strain in the two-way ANOVA. Therefore, only the main effects of each factor, i.e., strain and bioink material, were tested. Strain was the only significant main effect for the compressive modulus, with the significant differences between each strain level, except for 30% vs. 40%.

DISCUSSION

The newly appeared carboxyl group (C=O) indicated the successful oxidation of the cellulose using TEMPO. The exposure of O-H and C-O-C groups may be due to the mechanical processing of the cellulose. The smaller size of the cellulose fibres allowed for exposure of more surface groups.

In the steady-state flow sweep test (**Figure 3A**), all TCNF/ALG precursors exhibited a shear-thinning behaviour, which may be attributed to the loss of chain entanglement as well as the

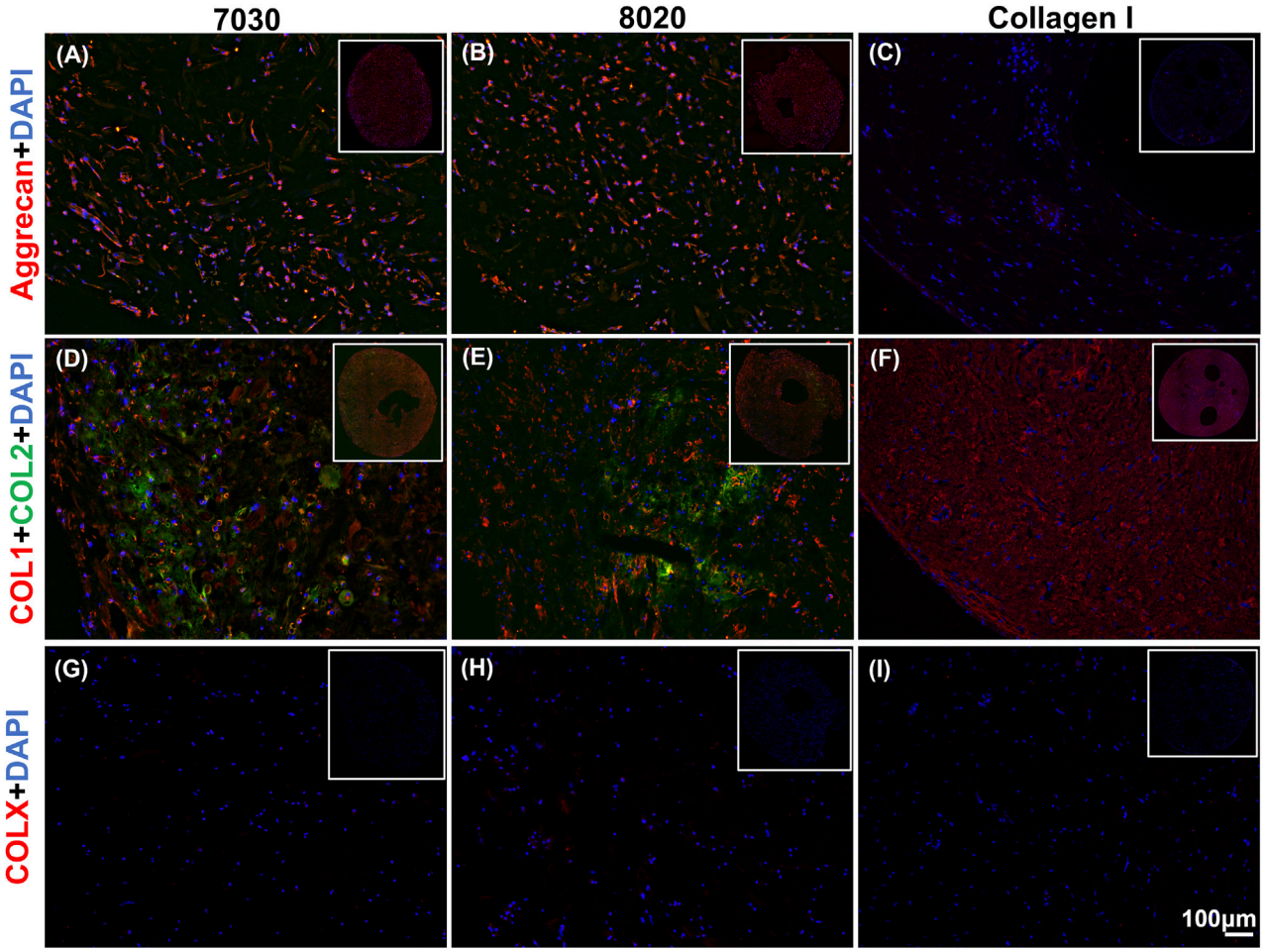

FIGURE 6 | Immunofluorescent staining of **(A–C)** of aggrecan (red), **(D–F)** collagens I and II (red and green, respectively), and **(G–I)** collagen X. The staining of nuclei is blue. Scale bar is 100 μm.

alignment of polymeric chains/fibre under steady-state shear. As the shear rate increases, the entanglement of the hydrogel networks is weakened and the entrapped liquid that resists the flow is released, and therefore induce decreased viscosity. Better shear-thinning behaviour is desired for the 3D bioprinting process, since under fixed printing speed and needle size lower bioink viscosities in the printing needle will result in lower shear stress experienced by cells, resulting in better cell viability. The formulation of the TCNF/ALG precursors has a strong effect on the shear-thinning behaviour. For alginate rich TCNF/ALG precursors (TCNF content between 0 and 50%), increasing the TCNF content did not show a significant change in the shear thinning behavior of the fluid. In contrast, for TCNF-rich TCNF/ALG precursors (TCNF content between 50 and 100%), a higher TCNF content led to better shear-thinning behaviour. Under fixed printing speed, the required printing pressure decreased dramatically as the TCNF content increased due to the enhanced shear-thinning effect (**Table 4**).

The thixotropic property is an important parameter to predict printing fidelity. Abouzeid et al. (2018) found that the higher the recovery rate (initial/finial viscosity) of the bioinks, the better the printing fidelities. They found the printed scaffolds had the best printing fidelity with the most uniform widths and stable shapes at 66% recovery rate, which is the highest recovery rate among the investigated bioink formulations (Abouzeid et al., 2018). However, our results only partially agreed with their findings. The pure ALG (81.6%), 2080 (75.2%), 8020 (71.8%), 7030 (63.7%), and 9010 (62.1%) showed a relatively high recovery rate (recovery >60%). Only 7030, 8020, and 9010 exhibited uniform width and clear edges throughout the printed shape. The filaments printed by pure alginate precursors, which has the highest recovery rate, collapsed and fused with neighbouring filaments. These results show that some other rheology parameters can affect printability as well. Gao et al. (2018) stated that the loss tangent is an important parameter for predicting structural integrity and extrusion uniformity. For pure alginate precursors, the tan δ is 0.41 in the low-frequency range (10 rad/s), which is in the relatively high loss tangent range stated by Gao et al. (2018). The high loss tangent represents lower structural integrity (the collapse and fusion of the bioprinted

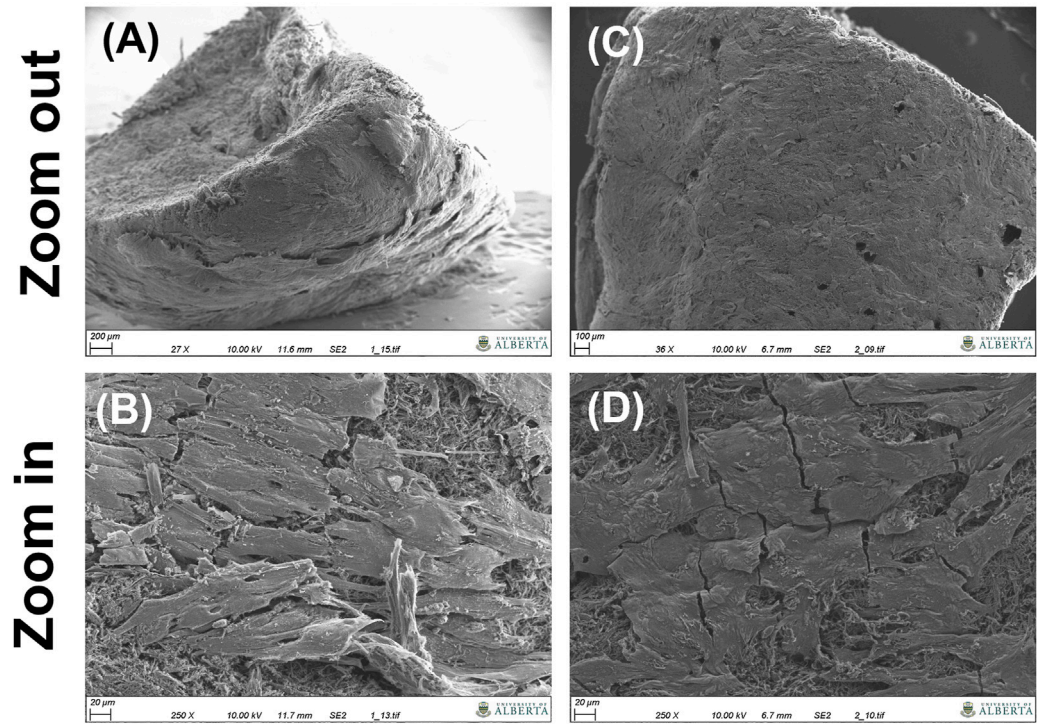

FIGURE 7 | SEM images of the bioprinted constructs after 6 weeks of *in vitro* culture, **(A,B)** the cross-section of the 7030 bioink **(C,D)** surface of the 7030 bioink.

structure), but better extrusion uniformity. The high tan δ explains the reason why pure alginate exhibits poor printing fidelity even it has a high thixotropic recovery rate. This statement is further validated in the bioprinting of collagen I gel. In our previous study, the collagen I gel showed more liquid-like behaviour, requiring it to be printed in a support bath (Lan et al., 2021). In this study, we directly printed the collagen I gel without the supporting bath to compare the printability with TCNF/ALG precursors. We found that the printed collagen I filaments tend to spread out after bioprinting, which resulted in poor printing fidelity.

It is also important for the bioink to retain its original shape during the crosslinking stage. We found that the alginate-rich TCNF/ALG precursors (0100, 2080, 5050, 6040) all exhibited high contractility after printing (≥10%). The contraction of the bioprinted constructs may contribute to the stability of the swelled alginate polymer chains in water after crosslinking. The alginate polymers are first dispersed and swelled in water. By adding the Ca^{2+} ions to alginate, the Ca^{2+} cations are coordinately bound to the COO^{-} group in the alginate polymer chain and arranged into an "egg-box" model (Braccini and Pérez, 2001; Li et al., 2007a). The 7030, 8020, and 9010 showed the best printing fidelity and lowest contractility after bioprinting. Due to the low alginate content of 9010, changing in shape is observed during transporting the bioprinted construct using 9010 (the distortion of the printed shape); therefore, only 7020 and 8020 were mixed with hMFCs (7030, 8020 bioinks) to generate tissue-engineered fibrocartilages.

A LIVE/DEAD assay was performed to investigate the biocompatibility of the bioprinted constructs. The COL bioink showed higher cell viability and higher cell numbers compared to the TCNF/ALG bioinks. It is speculated that the higher cell viability with the COL bioink is due to the relatively lower printing pressure, the presence of cell adhesive motifs in the protein-based hydrogel, and that the hMFCs' natural host material is collagen I.

After 6 weeks of culture, hMFC-deposited ECM was observed in both 7030 and 8020 bioinks under SEM (**Figure 7**). A dense layer of ECM covered the cellulose nanofibers. The histology and immunofluorescence results further confirmed the ECM formation in the 7030 and 8020 bioinks. The staining results suggest that the hMFC-laden TCNF/ALG bioinks (7030, 8020) support development of a more inner meniscus fibrocartilage-like phenotype (presence of sGAG, collagen I and II), while the (bovine) COL bioink supports a more outer meniscus phenotype of no Safranin-O positive ECM with the presence of newly-synthesized human collagen I. Neither the cellulose nanofibers nor the alginate present a natural cell binding site. The lack of a cell-binding site forces the monolayer-expanded hMFCs into a round shape known to promote a chondrogenic phenotype (Daly et al., 2016). In contrast, collagen I presents natural cell-

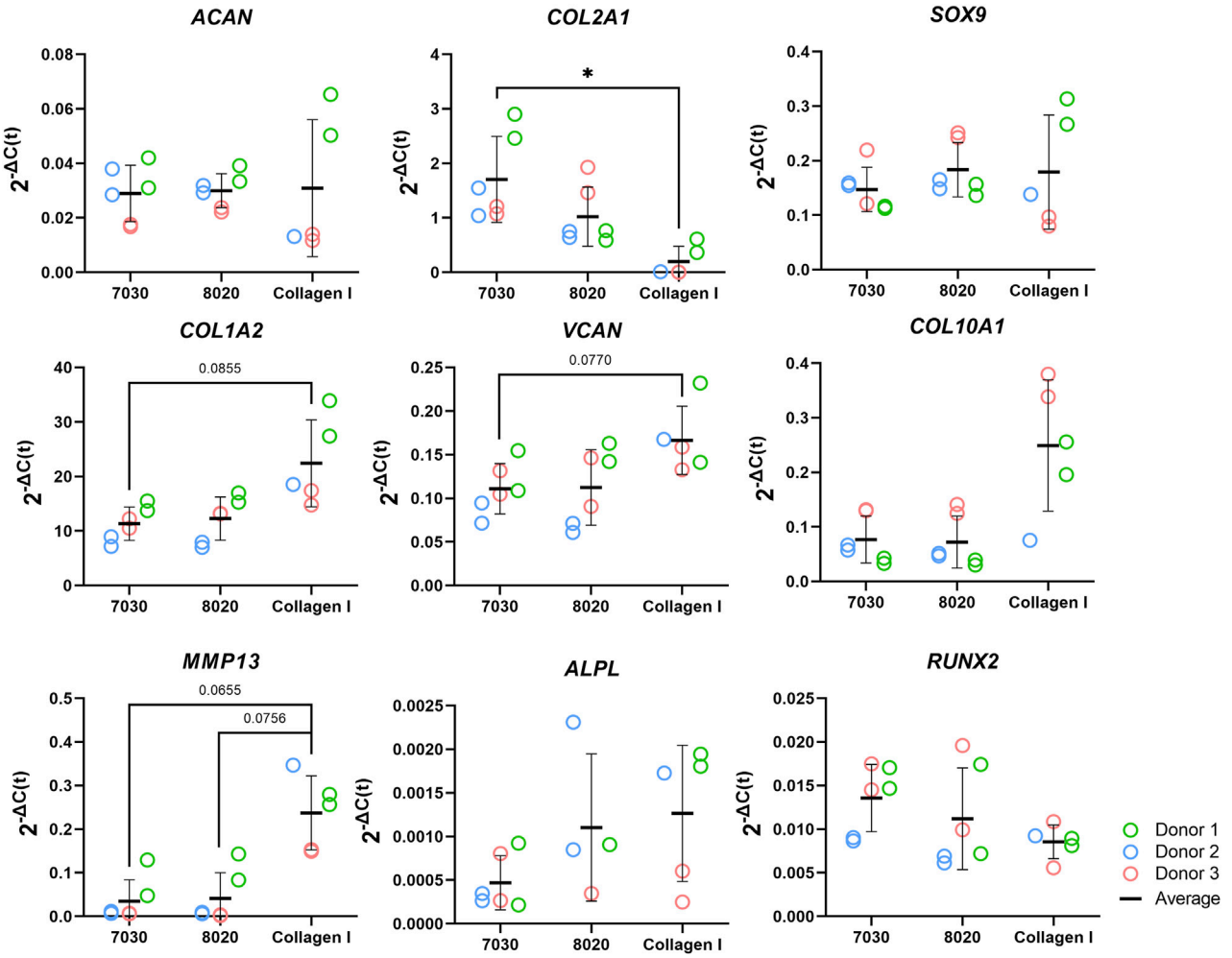

FIGURE 8 | Fibrocartilage related gene expression of bioprinted constructs after 6 weeks of *in vitro* chondrogenic culture (n = 3). * represents $p < 0.05$.

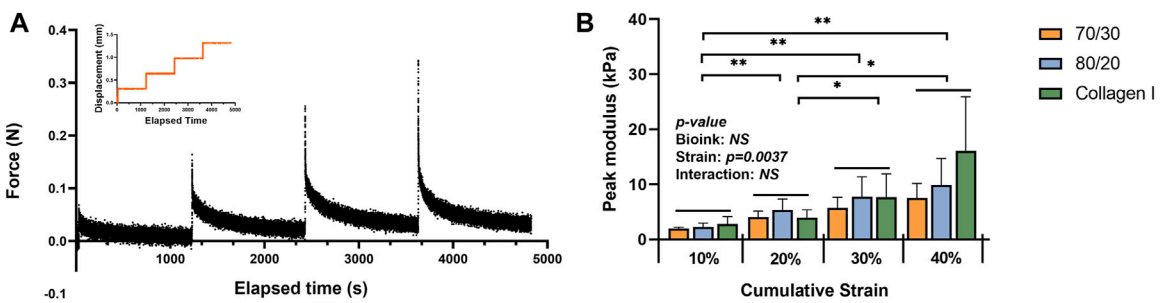

FIGURE 9 | Mechanical properties of the bioprinted constructs: **(A)** an example of data acquisition of the strain-controlled unconfined compression test **(B)** the peak modulus as a function of the cumulative strain (n = 3). * represents $p < 0.05$.

binding motifs through its interaction with the integrins that provide focal adhesion points to the hMFCs (Wang et al., 2020a). The focal adhesions can support cell spreading, which may facilitate the development of more outer meniscus-like phenotypes. The fibrocartilage matrix phenotypes at the mRNA level also agree with the histological and immunofluorescence findings (**Figure 8**).

Our observations agree with Daly et al. (2016)'s finding that alginate and agarose bioinks (bioinks without cell-binding sites) support the development of hyaline-like cartilage tissue, while

GelMA and PEGDA bioinks (bioinks with a native binding site) better support the development of fibrocartilage-like tissue. As shown in **Figure 8**, the lack of cell-binding sites in the TCNF/ALG bioinks correlated with reduced expression of *COL10A1* and *MMP13* (indicators of hypertrophic chondrocytes during endochondral ossification). The upregulation of these two genes is more likely to occur when integrin-binding (α2 integrin) between hMFCs and collagen I is present. The α2 integrin is a subunit of the most known collagen I receptor (α2β1). The interaction between this α2 integrin subunit and collagen I facilitates osteoblastic differentiation, an important event in the expression of the osteogenic phenotype (Mizuno et al., 2000; Bosnakovski et al., 2006).

Although proteoglycans mainly contribute to a tissue's compressive strength, the bioprinted TCNF/ALG bioink constructs did not show a higher compressive modulus compared to the COL bioink-based constructs. The average compressive modulus at the 30–40% strain step was higher than in the two TCNF/ALG bioinks, but no significant difference was observed. Hence, the engineered matrix composition does not fully correspond to the mechanical properties of the engineered tissue. One plausible explanation is that the crosslinking of the COL bioink constructs was augmented via endogenous lysyl oxidase expression, which can be induced by hypoxic culture (Makris et al., 2013). The cations that crosslink alginate chains may also be released into the culture media and washed away during the media changes, which may diminish the mechanical properties of the TCNF/ALG constructs.

One limitation of the present study is the low number of human meniscus donors used, leaving uncertainty regarding donor-to-donor differences. Another limitation is the lack of an *in vivo* study of the bioprinted constructs. The *in vivo* stability of the deposited ECM within the constructs in regard to *in vivo* calcification, bone formation, vascularization, and the retention of the Safranin-O positive ECM after implantation merits future investigation.

DATA AVAILABILITY STATEMENT

The original contributions presented in the study are included in the article/**Supplementary Materials**, and further inquiries can be directed to the corresponding author.

ETHICS STATEMENT

Meniscus specimens from three (3) male donors were collected from partial meniscectomy surgeries with the approval of the University of Alberta's Health Research Ethics Board–Biomedical Panel (Study ID: Pro00018778).

AUTHOR CONTRIBUTIONS

XL designed and conducted the experiments and was responsible for data acquisition, analysis, and initial manuscript writing. ZM assisted with the data analysis, immunofluorescence staining, and manuscript writing. AS helped with mechanical testing and manuscript editing. MK performed qRT-PCR and gene expression data analysis. AM-S assisted with cell isolation and culture. MV helped with histology and cDNA preparation. YB and AA conceived the study, supervised the study, and were responsible for writing and the final review of the manuscript. All authors read and approved the final manuscript.

FUNDING

Financial support was provided by Canadian Institutes for Health Research (No. CIHR MOP 125921) to AA, Edmonton Civic Employees Charitable Assistance Fund (No. RES0041788) to XL, YB and AA, Natural Sciences and Engineering Research Council of Canada-Discovery Grant Program (NSERC RGPIN 06431 to YB; NSERC-RGPIN-2018-06290 to AA), Canadian Foundation for Innovation (CFI 33786) to AA, University Hospital of Alberta Foundation (UHF; RES0028185; RES0045921 AA) and Alberta Cancer Foundation-Mickleborough Interfacial Biosciences Research Program (ACFMIBRP 27128 to AA).

ACKNOWLEDGMENTS

We acknowledge the staff in the Scanning Electron Microscope Laboratory in the Department Earth & Atmospheric Sciences, University of Alberta for taking the SEM images. We acknowledge the help of the Cell Imaging Center in the Faculty of Medicine & Dentistry, University of Alberta for the use of the confocal microscope. The schematic diagram is created with BioRender.com.

SUPPLEMENTARY MATERIAL

The Supplementary Material for this article can be found online at: https://www.frontiersin.org/articles/10.3389/fbioe.2021.766399/full#supplementary-material

REFERENCES

Abdul Rashid, E. S., Muhd Julkapli, N., and Yehye, W. A. (2018). Nanocellulose Reinforced as green Agent in Polymer Matrix Composites Applications. *Polym. Adv. Technol.* 29, 1531–1546. doi:10.1002/pat.4264

Abitbol, T., Rivkin, A., Cao, Y., Nevo, Y., Abraham, E., Ben-Shalom, T., et al. (2016). Nanocellulose, a Tiny Fiber with Huge Applications. *Curr. Opin. Biotechnol.* 39, 76–88. doi:10.1016/j.copbio.2016.01.002

Abouzeid, R. E., Khiari, R., Beneventi, D., and Dufresne, A. (2018). Biomimetic Mineralization of Three-Dimensional Printed alginate/TEMPO-Oxidized Cellulose Nanofibril Scaffolds for Bone Tissue Engineering. *Biomacromolecules* 19, 4442–4452. doi:10.1021/acs.biomac.8b01325

Adesida, A. B., Grady, L. M., Khan, W. S., Millward-Sadler, S. J., Salter, D. M., and Hardingham, T. E. (2007). Human Meniscus Cells Express Hypoxia Inducible Factor-1alpha and Increased SOX9 in Response to Low Oxygen Tension in Cell Aggregate Culture. *Arthritis Res. Ther.* 9, R69–9. doi:10.1186/ar2267

Arnoczky, S. P., and Warren, R. F. (1982). Microvasculature of the Human Meniscus. *Am. J. Sports Med.* 10, 90–95. doi:10.1177/036354658201000205

Bakkari, M. E., Bindiganavile, V., Goncalves, J., and Boluk, Y. (2019). Preparation of Cellulose Nanofibers by TEMPO-Oxidation of Bleached Chemi-Thermomechanical Pulp for Cement Applications. *Carbohydr. Polym.* 203, 238–245. doi:10.1016/j.carbpol.2018.09.036

Bosnakovski, D., Mizuno, M., Kim, G., Takagi, S., Okumura, M., and Fujinaga, T. (2006). Chondrogenic Differentiation of Bovine Bone Marrow Mesenchymal Stem Cells (MSCs) in Different Hydrogels: Influence of Collagen Type II Extracellular Matrix on MSC Chondrogenesis. *Biotechnol. Bioeng.* 93, 1152–1163. doi:10.1002/bit.20828

Braccini, I., and Pérez, S. (2001). Molecular Basis of Ca2+-Induced Gelation in Alginates and Pectins: the Egg-Box Model Revisited. *Biomacromolecules* 2, 1089–1096. doi:10.1021/bm010008g

Chevrier, A., Nelea, M., Hurtig, M. B., Hoemann, C. D., and Buschmann, M. D. (2009). Meniscus Structure in Human, Sheep, and Rabbit for Animal Models of Meniscus Repair. *J. Orthop. Res.* 27, 1197–1203. doi:10.1002/jor.20869

Cooke, M. E., and Rosenzweig, D. H. (2021). The Rheology of Direct and Suspended Extrusion Bioprinting. *APL Bioeng.* 5, 011502. doi:10.1063/5.0031475

Cox, J. S., Nye, C. E., Schaefer, W. W., and Woodstein, I. J. (1975). The Degenerative Effects of Partial and Total Resection of the Medial Meniscus in Dogs? Knees. *Clin. orthopaedics Relat. Res.* 109, 178–183. doi:10.1097/00003086-197506000-00026

Daly, A. C., Critchley, S. E., Rencsok, E. M., and Kelly, D. J. (2016). A Comparison of Different Bioinks for 3D Bioprinting of Fibrocartilage and Hyaline Cartilage. *Biofabrication* 8, 045002. doi:10.1088/1758-5090/8/4/045002

Daly, A. C., Freeman, F. E., Gonzalez-Fernandez, T., Critchley, S. E., Nulty, J., and Kelly, D. J. (2017). 3D Bioprinting for Cartilage and Osteochondral Tissue Engineering. *Adv. Healthc. Mater.* 6, 1700298. doi:10.1002/adhm.201700298

Di Bella, C., Fosang, A., Donati, D. M., Wallace, G. G., and Choong, P. F. M. (2015). 3D Bioprinting of Cartilage for Orthopedic Surgeons: reading between the Lines. *Front. Surg.* 2, 39. doi:10.3389/fsurg.2015.00039

Dufresne, A. (2013). Nanocellulose: a New Ageless Bionanomaterial. *Mater. Today* 16, 220–227. doi:10.1016/j.mattod.2013.06.004

Erkoc, P., Uvak, I., Nazeer, M. A., Batool, S. R., Odeh, Y. N., Akdogan, O., et al. (2020). 3D Printing of Cytocompatible Gelatin-Cellulose-Alginate Blend Hydrogels. *Macromol. Biosci.* 20, 2000106. doi:10.1002/mabi.202000106

Fairbank, T. J. (1948). Knee Joint Changes after Meniscectomy. *The J. bone Jt. Surg. Br. volume* 30-B, 664–670. doi:10.1302/0301-620x.30b4.664

Fithian, D. C., Kelly, M. A., and Mow, V. C. (1990). Material Properties and Structure-Function Relationships in the Menisci. *Clin. orthopaedics Relat. Res.* 252, 19–31. doi:10.1097/00003086-199003000-00004

Gao, T., Gillispie, G. J., Copus, J. S., Pr, A. K., Seol, Y.-J., Atala, A., et al. (2018). Optimization of Gelatin-Alginate Composite Bioink Printability Using Rheological Parameters: a Systematic Approach. *Biofabrication* 10, 034106. doi:10.1088/1758-5090/aacdc7

Gatenholm, P., Martinez, H., Karabulut, E., Amoroso, M., Kölby, L., Markstedt, K., et al. (2018). Development of Nanocellulose-Based Bioinks for 3d Bioprinting of Soft Tissue. *3D Printing and Biofabrication*, 331–352. doi:10.1007/978-3-319-45444-3_14

Göhl, J., Markstedt, K., Mark, A., Håkansson, K., Gatenholm, P., and Edelvik, F. (2018). Simulations of 3D Bioprinting: Predicting Bioprintability of Nanofibrillar Inks. *Biofabrication* 10, 034105. doi:10.1088/1758-5090/aac872

Heggset, E. B., Strand, B. L., Sundby, K. W., Simon, S., Chinga-Carrasco, G., and Syverud, K. (2019). Viscoelastic Properties of Nanocellulose Based Inks for 3D Printing and Mechanical Properties of CNF/alginate Biocomposite Gels. *Cellulose* 26, 581–595. doi:10.1007/s10570-018-2142-3

Herrera Millar, V. R., Mangiavini, L., Polito, U., Canciani, B., Nguyen, V. T., Cirillo, F., et al. (2021). Hypoxia as a Stimulus for the Maturation of Meniscal Cells: Highway to Novel Tissue Engineering Strategies. *Ijms* 22, 6905. doi:10.3390/ijms22136905

Hiller, T., Berg, J., Elomaa, L., Röhrs, V., Ullah, I., Schaar, K., et al. (2018). Generation of a 3D Liver Model Comprising Human Extracellular Matrix in an Alginate/gelatin-Based Bioink by Extrusion Bioprinting for Infection and Transduction Studies. *Ijms* 19, 3129. doi:10.3390/ijms19103129

Ibarra, C., Koski, J. A., and Warren, R. F. (2000). Tissue Engineering Meniscus. *Orthop. Clin. North America* 31, 411–418. doi:10.1016/s0030-5898(05)70160-7

Jessop, Z. M., Al-Sabah, A., Gao, N., Kyle, S., Thomas, B., Badiei, N., et al. (2019). Printability of Pulp Derived crystal, Fibril and Blend Nanocellulose-Alginate Bioinks for Extrusion 3D Bioprinting. *Biofabrication* 11, 045006. doi:10.1088/1758-5090/ab0631

King, D. (1936). The Healing of Semilunar Cartilages. *JBJS* 18, 333–342. doi:10.2307/3045635

Lan, X., Liang, Y., Erkut, E. J. N., Kunze, M., Mulet-Sierra, A., Gong, T., et al. (2021). Bioprinting of Human Nasoseptal Chondrocytes-Laden Collagen Hydrogel for Cartilage Tissue Engineering. *FASEB J.* 35, e21191. doi:10.1096/fj.202002081R

Leslie, B. W., Gardner, D. L., Mcgeough, J. A., and Moran, R. S. (2000). Anisotropic Response of the Human Knee Joint Meniscus to Unconfined Compression. *Proc. Inst. Mech. Eng. H* 214, 631–635. doi:10.1243/0954411001535651

Li, L., Fang, Y., Vreeker, R., Appelqvist, I., and Mendes, E. (2007a). Reexamining the Egg-Box Model in Calcium−Alginate Gels with X-ray Diffraction. *Biomacromolecules* 8, 464–468. doi:10.1021/bm060550a

Li, L., Fang, Y., Vreeker, R., Appelqvist, I., and Mendes, E. (2007b). Reexamining the Egg-Box Model in Calcium−Alginate Gels with X-ray Diffraction. *Biomacromolecules* 8, 464–468. doi:10.1021/bm060550a

Liang, Y., Idrees, E., Andrews, S. H. J., Labib, K., Szojka, A., Kunze, M., et al. (2017). Plasticity of Human Meniscus Fibrochondrocytes: A Study on Effects of Mitotic Divisions and Oxygen Tension. *Sci. Rep.* 7, 12148. doi:10.1038/s41598-017-12096-x

Liang, Y., Idrees, E., Szojka, A. R. A., Andrews, S. H. J., Kunze, M., Mulet-Sierra, A., et al. (2018). Chondrogenic Differentiation of Synovial Fluid Mesenchymal Stem Cells on Human Meniscus-Derived Decellularized Matrix Requires Exogenous Growth Factors. *Acta Biomater.* 80, 131–143. doi:10.1016/j.actbio.2018.09.038

Lin, N., Bruzzese, C., and Dufresne, A. (2012). TEMPO-oxidized Nanocellulose Participating as Crosslinking Aid for Alginate-Based Sponges. *ACS Appl. Mater. Inter.* 4, 4948–4959. doi:10.1021/am301325r

Makris, E. A., Hadidi, P., and Athanasiou, K. A. (2011). The Knee Meniscus: Structure-Function, Pathophysiology, Current Repair Techniques, and Prospects for Regeneration. *Biomaterials* 32, 7411–7431. doi:10.1016/j.biomaterials.2011.06.037

Makris, E. A., Hu, J. C., and Athanasiou, K. A. (2013). Hypoxia-induced Collagen Crosslinking as a Mechanism for Enhancing Mechanical Properties of Engineered Articular Cartilage. *Osteoarthritis and Cartilage* 21, 634–641. doi:10.1016/j.joca.2013.01.007

Mandrycky, C., Wang, Z., Kim, K., and Kim, D.-H. (2016). 3D Bioprinting for Engineering Complex Tissues. *Biotechnol. Adv.* 34, 422–434. doi:10.1016/j.biotechadv.2015.12.011

Markstedt, K., Mantas, A., Tournier, I., Martínez Ávila, H., Hägg, D., and Gatenholm, P. (2015). 3D Bioprinting Human Chondrocytes with Nanocellulose-Alginate Bioink for Cartilage Tissue Engineering Applications. *Biomacromolecules* 16, 1489–1496. doi:10.1021/acs.biomac.5b00188

Martínez Ávila, H., Schwarz, S., Rotter, N., and Gatenholm, P. (2016). 3D Bioprinting of Human Chondrocyte-Laden Nanocellulose Hydrogels for Patient-specific Auricular Cartilage Regeneration. *Bioprinting* 1-2, 22–35. doi:10.1016/j.bprint.2016.08.003

Middleman, S. (1977). *Fundamentals of Polymer Processing*. College: McGraw-Hill.

Mizuno, M., Fujisawa, R., and Kuboki, Y. (2000). Type I Collagen-Induced Osteoblastic Differentiation of Bone-Marrow Cells Mediated by Collagen-?2?1 Integrin Interaction. *J. Cel. Physiol.* 184, 207–213. doi:10.1002/1097-4652(200008)184:2<207::aid-jcp8>3.0.co;2-u

Müller, M., Öztürk, E., Arlov, Ø., Gatenholm, P., and Zenobi-Wong, M. (2017). Alginate Sulfate-Nanocellulose Bioinks for Cartilage Bioprinting Applications. *Ann. Biomed. Eng.* 45, 210–223. doi:10.1007/s10439-016-1704-5

Murphy, S. V., and Atala, A. (2014). 3D Bioprinting of Tissues and Organs. *Nat. Biotechnol.* 32, 773–785. doi:10.1038/nbt.2958

Nakata, K., Shino, K., Hamada, M., Mae, T., Miyama, T., Shinjo, H., et al. (2001). Human Meniscus Cell. *Clin. Orthopaedics Relat. Res.* 391, S208–S218. doi:10.1097/00003086-200110001-00020

Nguyen, D., Hägg, D. A., Forsman, A., Ekholm, J., Nimkingratana, P., Brantsing, C., et al. (2017). Cartilage Tissue Engineering by the 3D Bioprinting of iPS Cells in a Nanocellulose/alginate Bioink. *Sci. Rep.* 7, 658. doi:10.1038/s41598-017-00690-y

Ojansivu, M., Rashad, A., Ahlinder, A., Massera, J., Mishra, A., Syverud, K., et al. (2019). Wood-based Nanocellulose and Bioactive Glass Modified Gelatin-Alginate Bioinks for 3D Bioprinting of Bone Cells. *Biofabrication* 11, 035010. doi:10.1088/1758-5090/ab0692

Paradowski, P. T., Lohmander, L. S., and Englund, M. (2016). Osteoarthritis of the Knee after Meniscal Resection: Long Term Radiographic Evaluation of Disease Progression. *Osteoarthritis and cartilage* 24, 794–800. doi:10.1016/j.joca.2015.12.002

Paxton, N., Smolan, W., Böck, T., Melchels, F., Groll, J., and Jungst, T. (2017). Proposal to Assess Printability of Bioinks for Extrusion-Based Bioprinting and Evaluation of Rheological Properties Governing Bioprintability. *Biofabrication* 9, 044107. doi:10.1088/1758-5090/aa8dd8

Sanchez-Adams, J., and Athanasiou, K. A. (2009). The Knee Meniscus: a Complex Tissue of Diverse Cells. *Cel. Mol. Bioeng.* 2, 332–340. doi:10.1007/s12195-009-0066-6

Schwarz, S., Kuth, S., Distler, T., Gögele, C., Stölzel, K., Detsch, R., et al. (2020). 3D Printing and Characterization of Human Nasoseptal Chondrocytes Laden Dual Crosslinked Oxidized Alginate-Gelatin Hydrogels for Cartilage Repair Approaches. *Mater. Sci. Eng. C* 116, 111189. doi:10.1016/j.msec.2020.111189

Shinoda, R., Saito, T., Okita, Y., and Isogai, A. (2012). Relationship between Length and Degree of Polymerization of TEMPO-Oxidized Cellulose Nanofibrils. *Biomacromolecules* 13, 842–849. doi:10.1021/bm2017542

Skardal, A., Devarasetty, M., Kang, H.-W., Mead, I., Bishop, C., Shupe, T., et al. (2015). A Hydrogel Bioink Toolkit for Mimicking Native Tissue Biochemical and Mechanical Properties in Bioprinted Tissue Constructs. *Acta Biomater.* 25, 24–34. doi:10.1016/j.actbio.2015.07.030

Szojka, A. R. A., Lyons, B. D., Moore, C. N., Liang, Y., Kunze, M., Idrees, E., et al. (2019). Hypoxia and TGF-B3 Synergistically Mediate Inner Meniscus-like Matrix Formation by Fibrochondrocytes. *Tissue Eng. A* 25, 446–456. doi:10.1089/ten.tea.2018.0211

Szojka, A. R. A., Moore, C. N., Liang, Y., Andrews, S. H. J., Kunze, M., Mulet-Sierra, A., et al. (2021). Engineered Human Meniscus' Matrix-Forming Phenotype Is Unaffected by Low Strain Dynamic Compression under Hypoxic Conditions. *PloS one* 16, e0248292. doi:10.1371/journal.pone.0248292

Wang, J., Roberts, S., Kuiper, J. H., Zhang, W., Garcia, J., Cui, Z., et al. (2020a). Characterization of Regional Meniscal Cell and Chondrocyte Phenotypes and Chondrogenic Differentiation with Histological Analysis in Osteoarthritic Donor-Matched Tissues. *Sci. Rep.* 10, 1–14. doi:10.1038/s41598-020-78757-6

Wang, X., Wang, Q., and Xu, C. (2020b). Nanocellulose-Based Inks for 3D Bioprinting: Key Aspects in Research Development and Challenging Perspectives in Applications-A Mini Review. *Bioengineering* 7, 40. doi:10.3390/bioengineering7020040

Wu, Y., Lin, Z. Y., Wenger, A. C., Tam, K. C., and Tang, X. (2018). 3D Bioprinting of Liver-Mimetic Construct with Alginate/cellulose Nanocrystal Hybrid Bioink. *Bioprinting* 9, 1–6. doi:10.1016/j.bprint.2017.12.001

Yang, X., Lu, Z., Wu, H., Li, W., Zheng, L., and Zhao, J. (2018). Collagen-alginate as Bioink for Three-Dimensional (3D) Cell Printing Based Cartilage Tissue Engineering. *Mater. Sci. Eng. C* 83, 195–201. doi:10.1016/j.msec.2017.09.002

Conflict of Interest: The authors declare that the research was conducted in the absence of any commercial or financial relationships that could be construed as a potential conflict of interest.

Publisher's Note: All claims expressed in this article are solely those of the authors and do not necessarily represent those of their affiliated organizations, or those of the publisher, the editors, and the reviewers. Any product that may be evaluated in this article, or claim that may be made by its manufacturer, is not guaranteed or endorsed by the publisher.

frontiers in Bioengineering and Biotechnology

ORIGINAL RESEARCH
published: 16 November 2021
doi: 10.3389/fbioe.2021.749221

Polydopamine Coating-Mediated Immobilization of BMP-2 on Polyethylene Terephthalate-Based Artificial Ligaments for Enhanced Bioactivity

Zhanrong Kang[1†], Dejian Li[1†], Chaoqin Shu[2,3†], Jianhang Du[1], Bin Yu[4], Zhi Qian[1], Zeyuan Zhong[1], Xu Zhang[1], Baoqing Yu[5], Qikai Huang[1], Jianming Huang[1], Yufang Zhu[2], Chengqing Yi[1] and Huifeng Ding[1,4]**

[1]Department of Orthopaedics, Shanghai Pudong Hospital, Fudan University Pudong Medical Center, Shanghai, China, [2]State Key Laboratory of High-Performance Ceramics and Superfine Microstructure, Shanghai Institute of Ceramics, Chinese Academy of Sciences, Shanghai, China, [3]School of Materials Science and Engineering, University of Shanghai for Science and Technology, Shanghai, China, [4]Department of Pain and Rehabilitation, Shanghai Public Health Clinical Center, Shanghai Medical School, Fudan University, Shanghai, China, [5]Shanghai Pudong New Area People's Hospital, Shanghai, China

OPEN ACCESS

Edited by:
Farnaz Ghorbani,
University of Erlangen Nuremberg, Germany

Reviewed by:
Hessam Rezaei,
Islamic Azad University, Iran
Junchao Wei,
Nanchang University, China
Kai Zheng,
University of Erlangen Nuremberg, Germany

***Correspondence:**
Chengqing Yi
ycq3000@126.com
Huifeng Ding
dinghf0118@163.com

†These authors have contributed equally to this work and share first authorship

Specialty section:
This article was submitted to Biomaterials, a section of the journal Frontiers in Bioengineering and Biotechnology

Received: 29 July 2021
Accepted: 04 October 2021
Published: 16 November 2021

Citation:
Kang Z, Li D, Shu C, Du J, Yu B, Qian Z, Zhong Z, Zhang X, Yu B, Huang Q, Huang J, Zhu Y, Yi C and Ding H (2021) Polydopamine Coating-Mediated Immobilization of BMP-2 on Polyethylene Terephthalate-Based Artificial Ligaments for Enhanced Bioactivity. Front. Bioeng. Biotechnol. 9:749221. doi: 10.3389/fbioe.2021.749221

Background/objectives: Polyethylene terephthalate (PET)-based artificial ligaments are one of the most commonly used grafts in anterior cruciate ligament (ACL) reconstruction surgery. However, the lack of favorable hydrophilicity and cell attachment for PET highly impeded its widespread application in clinical practice. Studies found that surface modification on PET materials could enhance the biocompatibility and bioactivity of PET ligaments. In this study, we immobilized bone morphogenetic protein-2 (BMP-2) on the surface of PET ligaments mediated by polydopamine (PDA) coating and investigated the bioactivation and graft-to-bone healing effect of the modified grafts *in vivo* and *in vitro*.

Methods: In this study, we prepared the PDA coating and subsequent BMP-2-immobilized PET artificial ligaments. Scanning electron microscopy (SEM) was used to analyze the morphological changes of the modified grafts. In addition, the surface wettability properties of the modified ligaments, amount of immobilized BMP 2, and the release of BMP-2 during a dynamic period up to 28 days were tested. Then, the attachment and proliferation of rat bone mesenchymal stem cells (rBMSCs) on grafts were examined by SEM and Cell Counting Kit-8 (CCK-8) assay, respectively. Alkaline phosphatase (ALP) assay, RT-PCR, and Alizarin Red S staining were performed to test the osteoinduction property. For *in vivo* experiments, an extra-articular graft-to-bone healing model in rabbits was established. At 8 weeks after surgery, biomechanical tests, micro-CT, and histological staining were performed on harvested samples.

Results: A surface morphological analysis verified the success of the PDA coating. The wettability of the PET artificial ligaments was improved, and more than 80% of BMP-2 stably remained on the graft surface for 28 days. The modified grafts could significantly enhance the proliferation, attachment, as well as expression of ALP and osteogenic-

related genes, which demonstrated the favorable bioactivity of the grafts immobilized with BMP-2 *in vitro*. Moreover, the grafts immobilized with BMP-2 at a concentration of $138.4 \pm 10.6\ ng/cm^2$ could highly improve the biomechanical properties, bone regeneration, and healing between grafts and host bone after the implantation into the rabbits compared with the PDA-PET group or the PET group.

Conclusion: The immobilization of BMP-2 mediated by polydopamine coating on PET artificial ligament surface could enhance the compatibility and bioactivity of the scaffolds and the graft-to-bone healing *in vivo*.

Keywords: artificial ligament, bioactivity, bone morphogenic proteins, graft-to-bone healing, polyethylene terephthalate, surface modification

INTRODUCTION

Anterior cruciate ligament (ACL) injury, which may result in knee instability, secondary cartilage damage, and osteoarthritis (Shelbourne and Gray, 2000; Lohmander et al., 2007; Lidén et al., 2008), is a common injury among young adults and athletes (Zantop et al., 2008; Sofu et al., 2015). Currently, the gold-standard treatment for ACL rupture is ACL reconstruction surgery (Mascarenhas and MacDonald, 2008). Autograft tendon, allograft tendon, or artificial ligaments are available grafts for ACL reconstruction. Compared with allografts or autografts, artificial ligaments can not only meet the demand of stability and flexibility of knee joints, such as tension, flexion, and torsion (Huang et al., 2012; McDonald et al., 2021), but also overcome the drawbacks of donor site morbidity and reduce the incidence of disease transmission (Vaishya et al., 2015; Jia et al., 2017). A ligament advanced reinforcement system (LARS) artificial ligaments made by polyethylene terephthalate (PET) gained popularity in recent decades (Ahldén et al., 2009; Ichiba and Kishimoto, 2009; Karaoglu et al., 2009; Wang et al., 2015). A long-term follow-up on patients who have undergone ACL reconstruction with LARS ligaments reported satisfactory results in 84.6% cases and concluded that LARS ligaments were a safe and suitable option for ACL reconstruction (Parchi et al., 2018). However, the PET ligaments showed low cell affinity, which made it difficult for cell adhesion and led to inadequate interaction with host bone. Therefore, surface modification was introduced to improve the bioactivity of PET ligaments.

Studies have shown that surface modifications using chitosan, hydroxyapatite, graphene (Gustafsson et al., 2012; Vaquette et al., 2013; Li and Chen, 2015), VEGF (Lv et al., 2015), as well as laser could enhance the adhesion, proliferation, and osteogenesis differentiation of cells. Nevertheless, certain drawbacks, including difficult storage as well as uncontrolled delivery of growth factors, potential adverse effects *in vivo*, and laser modification (Li et al., 2017) may even impair the mechanical properties of artificial ligaments itself, hampering the application of these methods. Bone morphogenetic protein-2 (BMP-2), one of the transforming growth factors (TGFs), plays an important role in the initial stage of bone formation (Yao et al., 2020) and tissue regeneration (Poon et al., 2016). BMP-2 could promote the proliferation and osteogenic differentiation of bone mesenchymal stem cells (BMSCs) (Bayat et al., 2017; Yao et al., 2020) and stimulate the maturation of pre-osteoblast, consequently enhancing the secretion of bone-associated protein and mineralization (Zhang et al., 2017), and it is involved in bone metabolism as well (Rawadi et al., 2003; Chen et al., 2004; Cao and Chen, 2005). BMP-2 incorporated scaffolds that showed an excellent ability of osteoinduction and bone formation (Luginbuehl et al., 2004). Enhanced osteogenic differentiation and bone regeneration were observed in BMP-2-incorporated porous collagen scaffolds (Zhang et al., 2012). BMP-2-incorporated HAp-coated artificial ligament showed enhanced osseointegration and osteogenesis in bone tunnel (Jin et al., 2016). However, the conjugation between HAp and BMP-2 was intermediated by the electrostatic interaction (La et al., 2010), which may not sustain a long and stable release period of BMP-2. BMP-2 polypeptide has a short half-life and is easily inactivated *in vivo* alone (Wu et al., 2019), which may pose a negative impact on the effect of BMP-2 incorporation. Effective improvements are needed for BMP-2-immobilized surface modification.

Dopamine (DA), an adhesive protein that is derived from mussels, can be readily polymerized to form polydopamine (PDA)ad-layers by imine formation or Michael addition on the surface of various materials, such as polymers and bioceramics (Lee et al., 2009; Lynge et al., 2011; Wang and Stewart, 2013). Studies have proven that the PDA layer can intermediate the binding of bioactive molecules, such as protein, peptides, and DNA onto the scaffold surface (Lee et al., 2009; Zhou et al., 2010; Ren et al., 2011; Mrowczynski et al., 2013). The quinone/semiquinone formed by the catechol group on the PDA layer results in irreversible covalent conjugation between biomolecules and the surface of organic substitutes using similar Michael addition and Schiff formation reactions (Lee et al., 2007). Yao et al. (2020) found that bone cell differentiation and bone regeneration were enhanced in 3D-printed polylactic acid scaffolds with PDA modification and BMP-2 immobilization. PELA electrospun fibers immobilized with BMP-2 mediated by PDA showed better induction of differentiation into cartilage and bone in an acetabulum defect porcine model compared to the autotendon or PDA-coated PELA electrospun fibers groups (Wu et al., 2020). Previously, we have

successfully incorporated mesoporous bioactive glass onto PET ligaments *via* PDA, and improved biocompatibility and bioactivity of PET ligaments were observed (Yu et al., 2017).

In this study, we aimed to immobilize BMP-2 onto PET ligaments mediated by PDA coating. Then, the influence of modified grafts on the attachment, proliferation, and osteogenic differentiation was tested by rat bone mesenchymal stem cells (rBMSCs). A graft-to-bone healing model was also established in rabbits to evaluate the efficacy of the modified PET ligaments.

MATERIAL AND METHODS

Preparation of PET Sheet Immobilized With BMP-2 Mediated by Polydopamine

PET sheets removed from a LARS ligament were immersed in 75% alcohol solution for 4 h to remove dirt. Subsequently, the sheet was washed with deionized water for three times and dried at 37°C for 24 h. The prepared sheets then were cut into discs with a 1-cm diameter for the following experiments.

Sheets with a 1-cm diameter were immersed in dopamine hydrochloride (Sigma-Aldrich, St. Louis, MO, United States) solution (2 mg/ml, 10 mM Tris-HCL buffer, and pH 8.5) and stirred at 160 rpm in an incubator for 6 h. Samples were thoroughly rinsed with ultrapure water and dried at 37°C overnight. The obtained scaffolds were named as PDA-PET. Polydopamine-coated PET sheets were immersed in BMP-2 (R&D Systems, Minneapolis, MN, United States) solution (250 and 500 ng/ml, 10 mM Tris-HCl buffer, and pH 8.5) and incubated at 37°C overnight. Finally, the prepared scaffolds were washed with ultrapure water and then dried in a drying oven at 37°C for 24 h. The obtained sheets were named as 250B-PDA-PET and 500B-PDA-PET respectively. The pure PET sheets were considered as control.

Characterization of the Grafts

Scanning Electron Microscopy and Fourier-Transform Infrared Spectroscopy

The surface morphologies of all obtained scaffolds were examined by field-emission scanning electron microscope (FE-SEM) (Nova NanoSEM 450, FEI, United States) at a 20-kV accelerating voltage. The samples were vacuum coated with gold by sputtering prior to observation with SEM. The spectra of all grafts were tested using a Fourier transform infrared spectrometer (ATR-FTIR, Nicolet 6700, United States).

Hydrophilicity Properties

Static contact angle measurements were performed by a contact angle meter equipped with a high-resolution CCD camera (FM40Mk2 EasyDrop, Germany) to investigate the surface hydrophilicity of the PET, PDA-PET, 250B-PDA-PET, and 500B-PDA-PET grafts. Each sample was measured at three different locations ($n = 6$). A water drop of 3 μl in volume was placed on the surface of each graft. In that moment, images of droplets on the ligaments were captured using a side-view microscope connected to a camera (Nikon, United States). The contact angle was calculated by applying a spherical approximation using ImageJ 1.48 software.

Quantification of Immobilized BMP-2

Enzyme-linked immunosorbent assay (ELISA) was employed to measure the immobilized amount and long-term release kinetics of BMP-2. The PET sheets were treated with 500 μl of BMP-2 solution and incubated overnight at 37°C. After overnight incubation, supernatant was harvested for the measurement of remaining BMP-2 by an ELISA kit. Meanwhile, the amount of BMP-2 in the original solution (which are not treated with PET sheets) was determined using ELISA, and a difference in the values of the original solutions and the supernatant solutions was used to calculate the amount of immobilized BMP-2 on PET sheets. To investigate the long-term release of BMP-2, the sheets were immersed in 1 ml phosphate-buffered saline (PBS) and incubated at 37°C. At each predetermined time interval (1, 3, 5, 7, 14, 21, and 28 days), the supernatant was harvested and replaced with fresh PBS for continuous incubation until 28 days. The release of BMP-2 in all samples was quantified by an ELISA kit (R&D Systems, Minneapolis, MN, United States), and the results were then expressed according to previous studies (Cho et al., 2014).

In Vitro Experiments

Cell Culture

Bone mesenchymal stem cells derived from Sprague–Dawley rats (rBMSCs) were used to examine the cytocompatibility and bioactivity of the modified PET sheets in this study. rBMSCs were cultured at 37°C in a humidified incubator with 5% CO_2 in MEM alpha medium (α-MEM) (HyClone, United States) containing 10% fetal bovine serum (Gibco, United States) and 100 U/ml penicillin–streptomycin (Sigma), and the medium was replaced every other day. The passage four to five (P4 to P5) rBMSCs was used for the following tests.

Cell Proliferation and Attachment

All grafts were sterilized by ethylene oxide gas before experiment. Thereafter, the scaffolds were transferred into a non-treated 24-well plate. rBMSCs in the logarithmic phase were seeded onto each sheet at a density of 1×10^4 cell.

Cell proliferation was assessed at 1, 3, and 7 days using the Cell Counting Kit-8 (CCK-8, Dojindo, Japan) in this study. At each predetermined time point, the culture medium was removed and the samples were washed with PBS thrice; 360 μl α-MEM medium and 40 μl CCK-8 solution were added into each well. Samples were fully incubated for 4 h at 37°C, and 100 μl of supernatant for each sample was transferred into a non-treated 96-well plate, and absorbance at 450 nm was measured using a microplate reader (TECAN Infinite 200 PRO, Switzerland). We observed cell morphology and adhesion on scaffolds after 5 days of culturing *via* scanning electron microscopy (SEM, FEI Quanta 450). After a scheduled interval, samples were gently rinsed with PBS, fixed in 2.5% glutaral solution at 4°C overnight, washed thrice with ddH_2O, dehydrated in ethanol series (30%, 50%, 70%, 90%, 95%, and 100%; 10 min each, twice), and dried at room temperature. The specimens were gold coated for examination.

Alkaline Phosphatase Assay

Alkaline phosphatase (ALP) activity was determined using an ALP assay kit (Cat. No. P0321, Beyotime). Briefly, rBMSCs were seeded on each sheet at a density of $1 \times 10^5$and then treated with an osteogenic induction medium (10 mM β-glycerophosphate, 50 μM ascorbic acid-2-phosphate, and 100 nM dexamethasone in complete medium) for 7 or 14 days. Samples were washed three times with PBS and dissolved *via* RIPA lysis buffer. Afterwards, the harvested solution was centrifuged at 12,500×*g* for 5 min. Finally, supernatant was collected for ALP activity assay according to the manufacturer's instructions. ALP activity was normalized to the total protein content.

Osteogenesis-Related Gene Expression Analysis

The expression level of osteogenic genes in rBMSCs was examined by RT-PCR. Cells seeded on the sheets were incubated in osteoinductive medium for 7 or 14 days, and total RNA was extracted from the rBMSCs using an RNA extraction kit (Cat. No. AG21017 Accurate Biology, China). Thereafter, the harvested total RNA was reverse-transcribed into complementary DNA (cDNA) using Evo M-MLV RT Kit with gDNA Clean for qPCR II (Cat. No. AG11711, Accurate Biology, China). Osteoblast differentiation-related genes, osteopontin (OPN), runt-related transcription factor 2 (Runx 2), osteocalcin (OCN), and ALP were tested in this study. Gene amplification was performed in the real-time PCR instrument (ABI 7300) using Pro Taq HS Premix Probe qPCR Kit (Cat. No. AG11704, Accurate Biology, China). Glyceraldehyde 3-phosphate dehydrogenase (GAPDH) was regarded as the internal reference gene. Each sample was assayed in triplicate.

Alizarin Red S Staining and Quantitative Analysis of Mineralized Bone Nodules

After incubation in osteogenic induction medium for 21 days, rBMSCs were rinsed in PBS thrice and fixed in 4% paraformaldehyde for 10 min. Then, 0.5% Alizarin Red S (pH 4.3, Sigma) was reacted with each sample at room temperature for 30 min and washed with ddH_2O until water was clean. Then, mineralized nodule was observed under a microscope. The amount of mineralized nodule was quantified as well. The stained samples were treated with 10% (*w*/*v*) cetylpyridinium chloride for 1 h at RT, and the absorbance at 572 nm was measured with a microplate reader (TECAN Infinite 200 PRO, Switzerland).

Animal Experiments

Graft Implantation Into Rabbits

All animal experimental procedures were approved by the Laboratory Animal Welfare and Ethics Committee at our institution. Fifteen mature male New Zealand rabbits (male, 10 weeks old, 2.7 ± 0.3 kg) were randomly assigned to three different groups, named as the PET group, PDA-PET group, and 500B-PDA-PET group. An extra-articular graft-to-bone healing procedure was operated on each rabbit bilaterally. The rabbits were anesthetized with 3% (*w*/*v*) pentobarbital (30 mg/kg) *via* an intraperitoneal injection. Grafts, with a length of 2.0 cm and a diameter of 2.0 mm, were implanted into tunnels drilled by a 2-mm-diameter Kirschner wire through the condyle of the femur. Postoperatively, penicillin (50 KU/kg) were administered through continuous injections for 3 days. The rabbits were sacrificed at 12 weeks after operation for the following tests.

Mechanical Tests

Five freshly harvested femurs were prepared for mechanical tests. A No. 5 WilSuture Poly suture, which is extended out of the drilling tunnel entrance, was used to suture the implanted graft. The sample was mounted onto a special jig, and it was made sure that the tension on each graft was in accordance with the pullout test axis. The load-to-failure test was conducted with a Material Testing System (Instron, United States) at an elongation rate of 2 mm/min. The tensile load was recorded to calculate the ultimate failure load (N).

Micro-Computer Tomography Examination

The harvested femur condyles were fixed in 4% paraformaldehyde for 2 weeks. The samples were scanned by micro-CT (SkyScan 1176, Kontich, Belgium) at 18-μm resolution. Along the longitudinal axis of the femur bone tunnel, a $2 \times 10\ mm^2$ cylindrical region of interest (ROI) was reconstructed from the middle part of the tunnel for each sample. Three-dimensional images were obtained using the 3-D Creator software, and data were analyzed by VGStudio MAX (Volume Graphics, Germany) software. Microstructural parameters such as the bone volume/total volume (BV/TV, %) and bone surface/bone volume (BS/BV, 1/mm) were determined.

Histological Analysis

The femur specimens were fixed in 4% paraformaldehyde for 48 h, decalcified in 5% nitric acid for 2 weeks, and dehydrated in gradient ethanol. Subsequently, the dehydrated specimens were embedded in paraffin for sectioning and staining. Sections were perpendicular to the longitudinal axis of the bone tunnel with a thickness of 5 μm. The slices were stained with hematoxylin and eosin (HE) staining reagent for evaluation. The stained slices were scanned by a histology digital scanning system (NanoZoomer S210, Hamamatsu), and pictures were obtained *via* NDP.view 2 software. Finally, the evaluation of the graft-to-bone healing was conducted with staining images.

Statistical Analysis

The results were expressed as the mean ± standard deviation (SD). Data were analyzed using SPSS 20.0 and GraphPad Prism 10 software. One-way ANOVA and Student's *t*-tests were used to determine the level of significance, and p value less than 0.05 was considered as statistically significant.

RESULTS

Characterizations

We examined the morphology of PET, PDA-PET, 250B-PDA-PET, and 500B-PDA-PET samples *via* SEM. As is shown in **Figure 1**, the pure PET (**Figure 1 A1, A2**) fiber has a smooth surface without any attachment. A layer with fine coarse particles

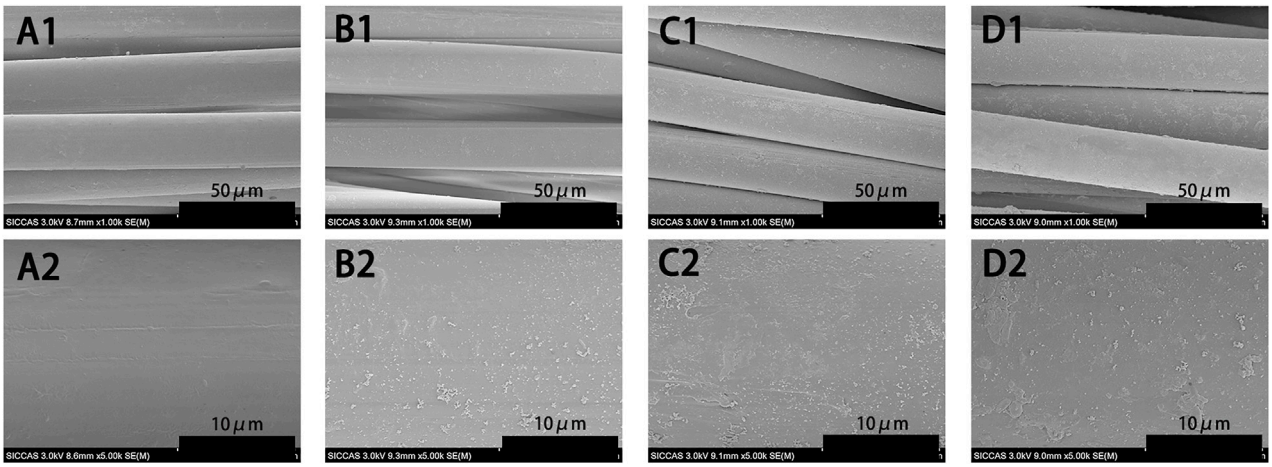

FIGURE 1 | SEM images of pure PET **(A1, A2)**, PDA-PET **(B1, B2)**, 250B-PDA-PET **(C1, C2)**, and 500B-PDA-PET **(D1, D2)**. SEM, scanning electron microscopy; PET, polyethylene terephthalate; PDA, polydopamine

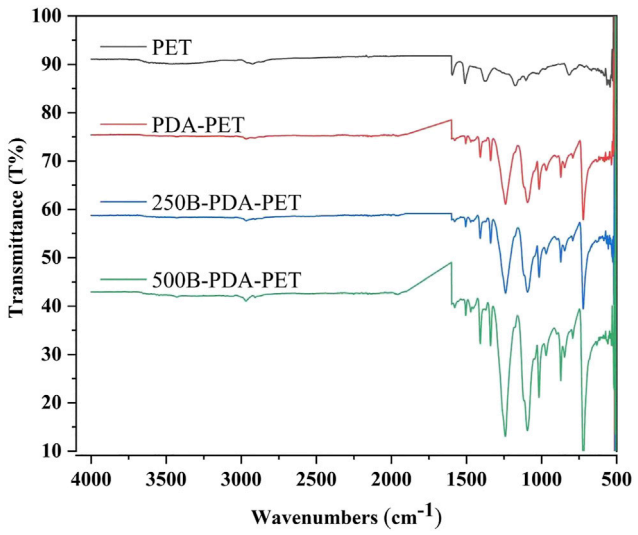

FIGURE 2 | Fourier-transform infrared spectroscopy (FTIR) of PET, PDA-PET, 250B-PDA-PET, and 500B-PDA-PET.

was observed on the surface of the PDA-PET group (**Figure 1 B1, B2**). The 250B-PDA-PET (**Figure 1 C1, C2**) and 500B-PDA-PET (**Figure 1 D1, D2**) also showed a coating with fewer particles than that on the PET group, and the layer modified by BMP-2 seemed thicker than the PDA layer in some areas. For the PDA-PET scaffold, the peaks at 1,506 cm^{-1} (the indole structure of PDA) and 1,281 cm^{-1} (the stretching vibration of catechol hydroxyl) prove the successful coating of PDA. The element component of BMP-2 was identical to that of PDA; therefore, the characteristic absorption peaks in 250B/500B-PDA-PET grafts are similar to those in the PDA-PET group (**Figure 2**, FTIR results).

The water contact angle was also examined to investigate changes in hydrophilicity on the scaffold surface (**Figure 3**). The PET grafts exhibited a static water contact angle of 90.9° ± 5.0° after a measurement time period of 10 s. In the PDA coating or BMP-2-immobilized groups, the water drop penetrated into the surface so fast that a static water contact angle cannot be measured, which demonstrated a better wettability compared to the PET group.

Quantification and Release of Immobilized BMP-2

The amount of immobilized BMP-2 on PDA-coated grafts was measured indirectly (Lee et al., 2012). We found that the amount of BMP-2 increased as the concentration of BMP-2 treatment solutions increased (**Figure 4A**). The grafts treated with 500 ng/ml of BMP-2 showed more immobilized BMP-2 (138.4 ± 10.6 ng/cm^2) compared with those treated with 250 ng/ml (83.1 ± 9.5 ng/cm^2). We then investigated the dynamic release of BMP-2 on PDA-coated scaffolds for up to 28 days. Only the 500B-PDA-PET group was examined. At the initial 7 days, around 14% of immobilized BMP-2 were released, which is nearly five times the release amount during day 7 to day 28. At the end of the 28-day period, the results showed that more than 80% of the immobilized BMP-2 was retained on the surface of grafts (**Figure 4B**).

Cell Attachment and Proliferation

The morphology of rBMSCs cultured on grafts for 1 and 5 days was evaluated using SEM (**Figure 5**). More rBMSCs were observed on the surface of the BMP-2-immobilized grafts than in other groups. Cells seeded on the PDA-PET, 250B-PDA-PET, as well as the 500B-PDA-PET showed multiple cellular morphologies such as pseudopods and lamellipodia. The proliferation of rBMSCs incubated on the grafts for 1, 3, and 7 days was analyzed using CCK-8 (**Figure 6A**). Optical density (OD) values in the 250B-PDA-PET or 500B-PDA-PET group were significantly different compared with the PET group at 3 and 7 days culturing time points ($p < 0.05$).

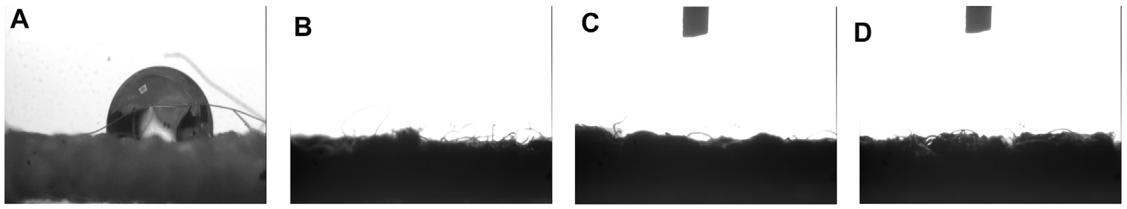

FIGURE 3 | Water contact angle of PET **(A)**, PDA-PET **(B)**, 250B-PDA-PET **(C)**, and 500B-PDA-PET **(D)**.

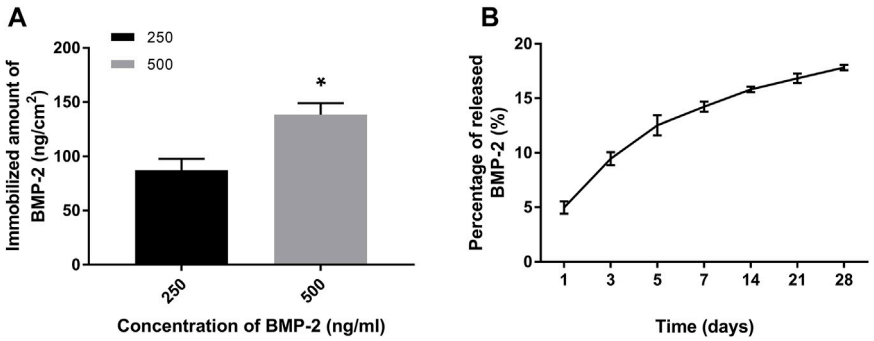

FIGURE 4 | Quantification and release of immobilized BMP-2 on polydopamine-coated PET using ELISA. **(A)** The amount of immobilized BMP-2 on PET fabricated using different BMP-2 concentrations. Asterisk (*) indicates a significant difference compared to the 250 ng/ml immobilized BMP-2 group, $p < 0.05$. **(B)** The dynamic changes of released BMP-2 from the PET during a 28-day period in phosphate-buffered saline (PBS) (37°C).

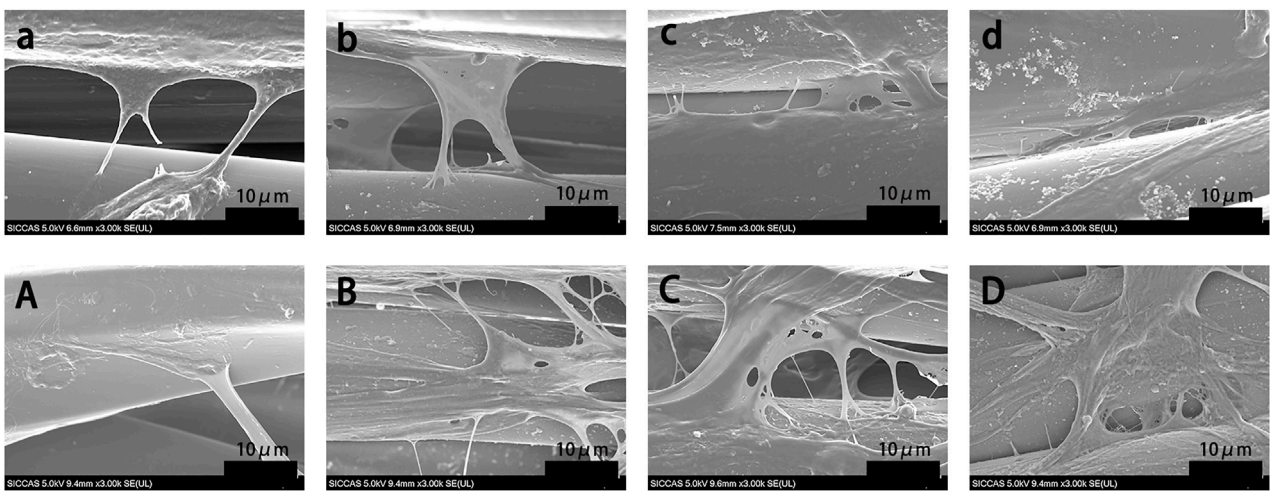

FIGURE 5 | SEM images of rat bone mesenchymal stem cells (rBMSCs) cultured on PET **(a, A)**, PDA-PET **(b, B)**, 250B-PDA-PET **(c, C)**, and 500B-PDA-PET **(d, D)** for 1 day **(a–d)** and 5 days **(A–D)**.

Cell Differentiation *In Vitro*

To investigate the impact of BMP-2-immobilized grafts on the osteogenic differentiation of rBMSCs, we measured ALP activity and the expression levels of osteoblast-specific genes, including OCN, OPN, ALP, and Runx 2, at 7 or 14 days (**Figure 7**). The ALP activity of rBMSCs in the 500B-PDA-PET group was significantly higher than that in other groups at each predetermined time point ($p < 0.05$) (**Figure 6B**). The transcription levels of osteogenesis-related genes, including OPN, OCN, Runx2, and ALP, were analyzed *via* RT-PCR. The results demonstrated that the expression level of these osteogenic markers in the PDA-PET or 250B-PDA-PET or 500B-PDA-PET group was significantly higher than that in the PET group at 14 days

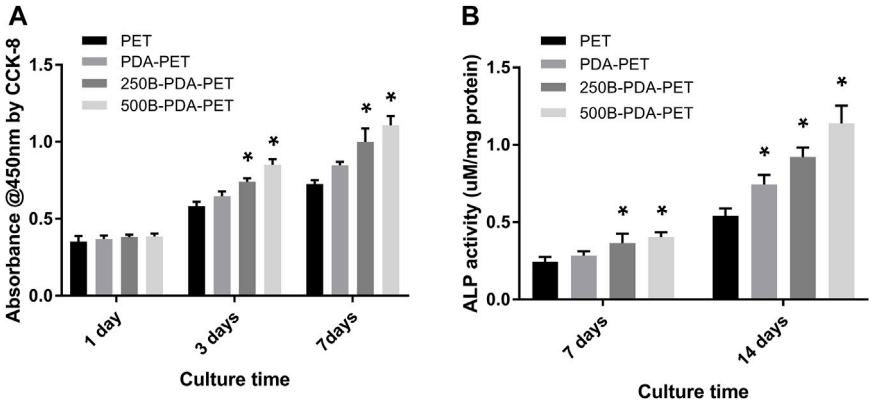

FIGURE 6 | (A) The proliferation of rBMSCs incubated on different groups of grafts at 1, 3, and 7 days using CCK-8. **(B)** Alkaline phosphatase (ALP) activity assay of rBMSCs cultured in an osteogenic induction solution for 7 and 14 days. Asterisk (*) indicates a significant difference compared to the PET group, $p < 0.05$.

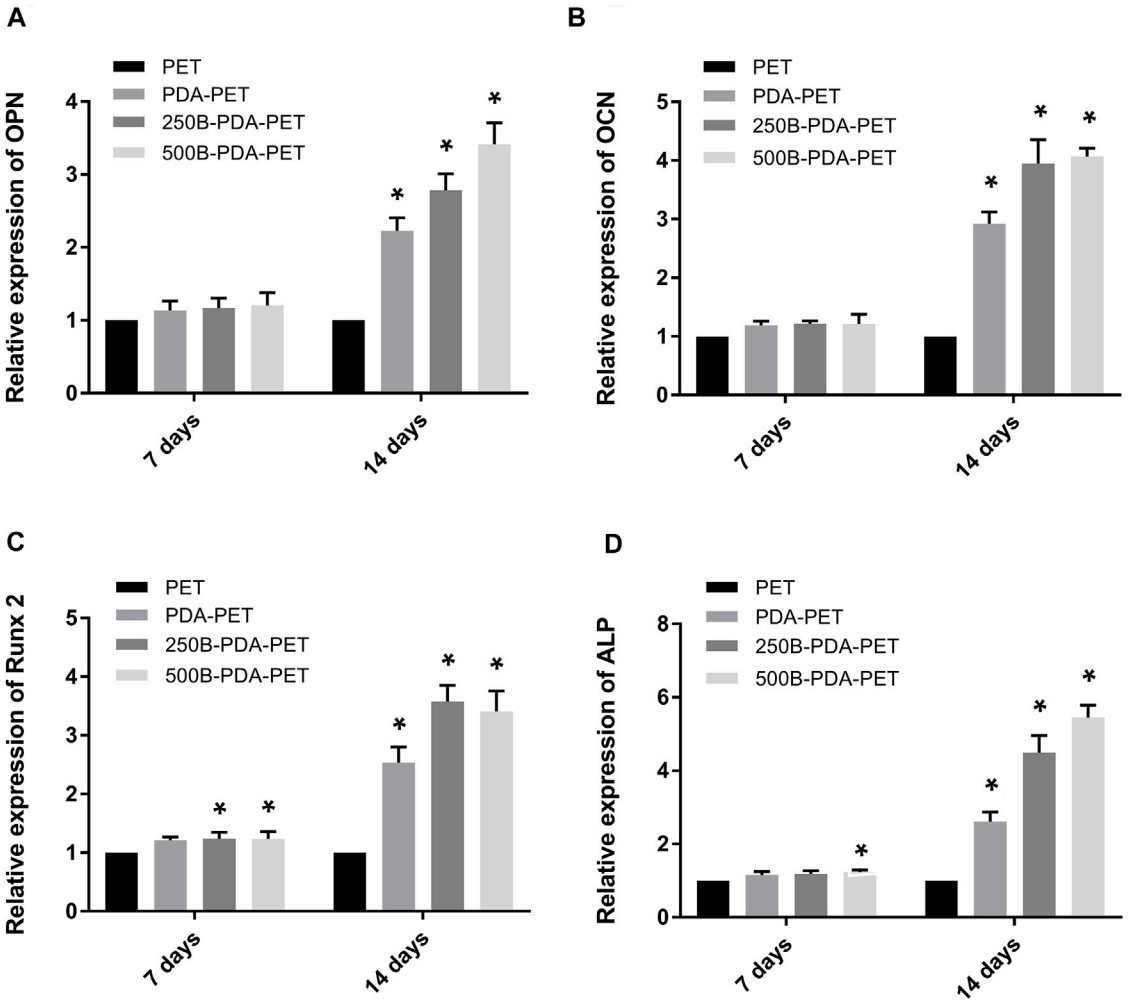

FIGURE 7 | Expression level of **(A)** osteopontin (OPN), **(B)** osteocalcin (OCN), **(C)** runt-related transcription factor 2 (Runx 2), and **(D)** ALP of rBMSCs cultured on different groups of grafts using RT-PCR. Asterisk (*) indicates a significant difference compared to the PET group, $p < 0.05$.

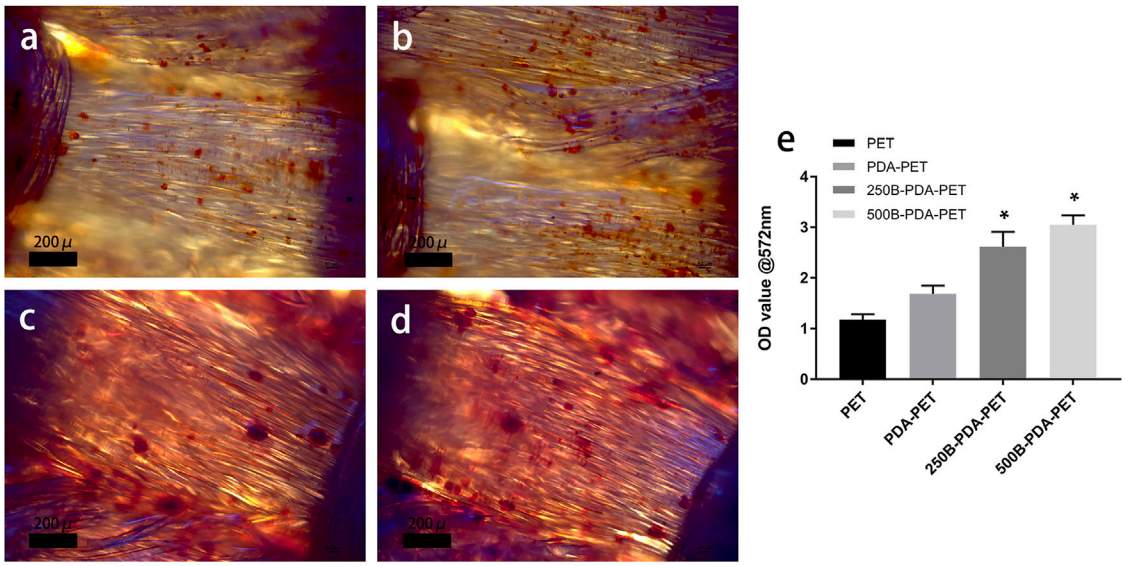

FIGURE 8 | (A) Images of mineralized calcium nodules after 21 days of osteogenic induction using Alizarin Red S staining. **(B)** Quantification of mineralized calcium nodules. Asterisk (*) indicates a significant difference compared to the PET group, $p < 0.05$.

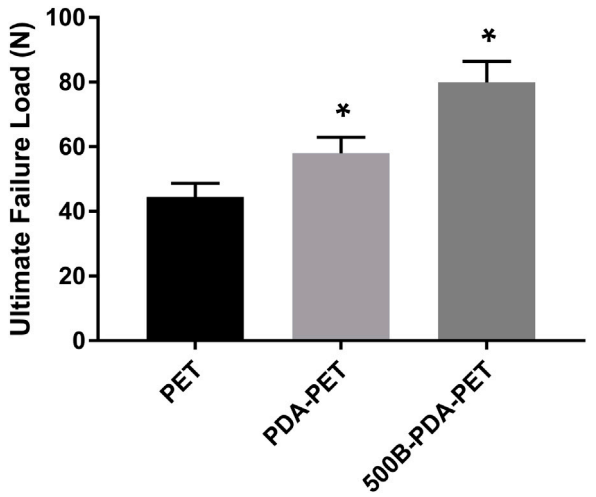

FIGURE 9 | The ultimate failure load of grafts after implantation of 8 weeks. Asterisk (*) indicates a significant difference compared to the PET group, $p < 0.05$.

($p < 0.05$), and the 500B-PDA-PET group showed the highest expression level.

After 21 days of induction, samples were stained using Alizarin Red S, and quantification was performed. As is shown in **Figure 8**, calcium nodule sedimentation was observed on the surface of different grafts. Calcium nodules on the surface of the BMP-2-immobilized group were larger than those on the surface of the PDA-PET or PET group. Quantification of the calcium nodules (**Figure 8B**) showed that there was significantly higher calcification in the 500B-PDA-PET group (OD value 3.91 ± 0.15) than in other groups ($p < 0.05$). These results are consistent with the ALP activity assay.

Mechanical Tests

An extra-articular graft-to-bone healing animal model was used to evaluate the osseointegration of the graft within the host bone. At 8 weeks after implantation, the ultimate failure load of the 500B-PDA-PET group was 79.93 ± 6.49 N and was significantly higher than that of the PET and PDA-PET groups, with an ultimate failure load at 44.25 ± 4.01 N and 58.03 ± 4.91 N, respectively ($p < 0.05$) (**Figure 9**).

Micro-CT for New Bone Formation

The harvested femurs were examined by micro-CT for the evaluation of bone regeneration. Identically sized ROIs around the grafts were reconstructed. Two- and three-dimensional images of reconstruction are presented in **Figure 10**. We found that there was more bone formation around and inside the grafts in the 500B-PDA-PET group than in the other two groups. Microstructural parameter analysis demonstrated that the BV/TV in the 500B-PDA group was significantly higher than those in the PET or PDA-PET group ($p < 0.05$). On the contrary, significant decreases in BS/BV were observed ($p < 0.05$) (**Figure 11**).

Histological Analysis

Histological staining was performed for the evaluation of graft-to-bone healing effect. As the pictures of HE staining show, grafts in the bone tunnel bonded with the host bone by relatively loose fibrous tissue, and almost no visible new bone was formed in the PET group. In the PDA-PET group, the interface between graft and native bone was denser than the PET group, which presented a trend for osteogenic differentiation. In the 500B-PDA-PET

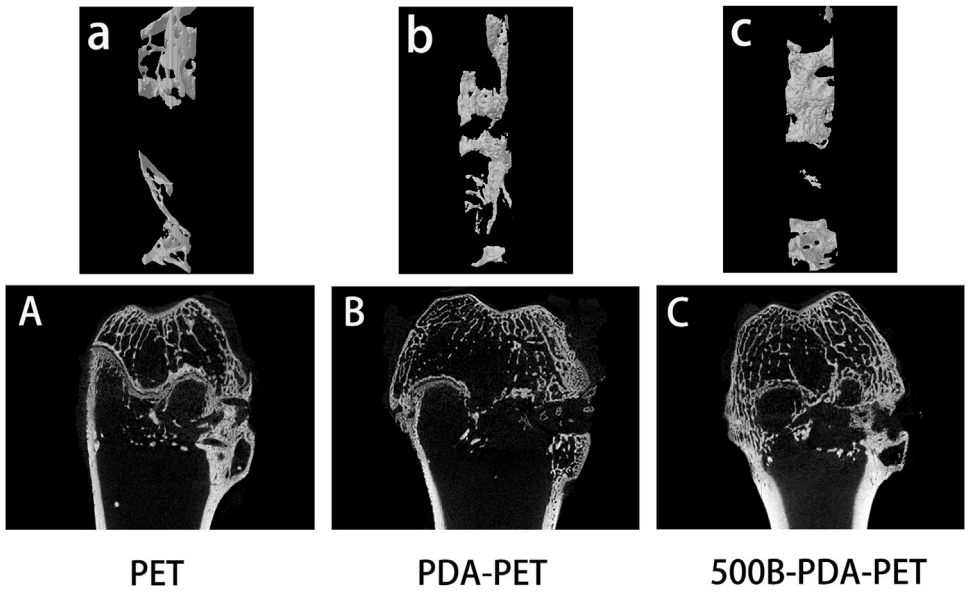

FIGURE 10 | 3D) reconstruction and 2D images of grafts after implantation of 8 weeks.

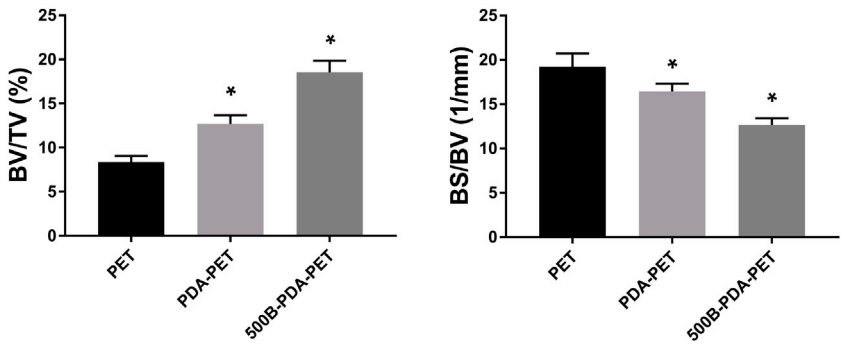

FIGURE 11 | Analysis of new bone formation in bone tunnels after implantation of 8 weeks. BV/TV indicates the bone volume/total volume, and BS/BV indicates the bone surface/bone volume. Asterisk (*) indicates a significant difference compared to the PET group, $p < 0.05$.

group, a tight connection was formed between the scaffolds and host bone with a certain quantity of new bone regeneration. For the PDA-PET group, some new bone formed in the interface, and it seemed to be unmatured (**Figure 12**).

DISCUSSION

The PET ligament is one of the most commonly used artificial grafts in ACL reconstruction, and favorable feedbacks were received for long-term follow-ups. However, the inferior biocompatibility and bioactivity of the PET grafts might result in the enlarged tunnels and failure to reconstruction (Yu et al., 2017). In this study, we successfully ameliorated the surface properties of PET ligaments by the immobilization of BMP-2 *via* PDA coating. Our results proved that the modified PET ligaments could enhance the attachment, proliferation, and osteogenic differentiation of rBMSCs and promote the tight bonding between the grafts and native bone *in vivo*, which was partially attributed to the continuous and stable release of BMP-2.

The characterizations of modified grafts were examined. SEM showed that the surface of PDA-coated grafts as well as BMP-2-immobilized grafts presented a layer with rough particles while the PET grafts presented a smooth surface. In addition, difference of the surface components was observed among groups *via* FTIR. These results combined suggested the successful fabrication of PET grafts with PDA coating and BMP-2 immobilization.

As one of the bone morphogenetic protein families, BMP-2 is widely applied in orthopedic surgeries such as open tibial fractures, articular cartilage damage, non-unions, and lumbar spine fusion (Poon et al., 2016). BMP-2-mediated surface

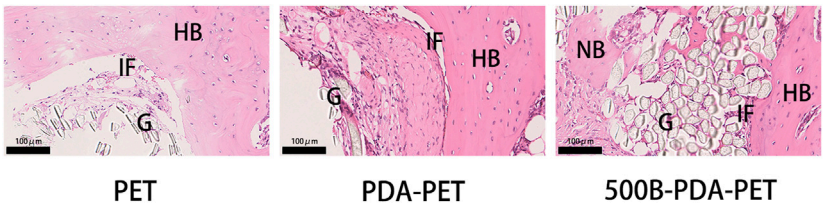

FIGURE 12 | HE) staining of grafts sectioned perpendicularly to the longitudinal axis at 8 weeks. G, graft; HB, host bone; IF, interface; NB, new bone.

modification is beneficial for the successful osseointegration between implants and native bone. Studies showed that BMP-2 was able to promote cell chemotaxis, proliferation, and osteogenic differentiation (Ribeiro et al., 2015) and presented favorable osteoinductive property for bone growth and regeneration (Poon et al., 2016). In light of its excellent bioactivity, BMP-2 has great potential to be developed in the application of surface modification. However, several issues in the immobilization of BMP-2 also trouble the researchers. For example, denaturation and inactivation of BMP-2 easily occur under physiological conditions and when applied alone (Takahashi et al., 2005; Wu et al., 2019). PDA, a polymerized form of dopamine, resulted from the interaction between catechol and amine groups in dopamine in a slightly alkaline solution (Lee et al., 2007). It is an attractive candidate for tissue engineering as articles reported, especially in surface modification. PDA can easily be deposited onto the surface of various grafts to form an ad-layer for bonding with diverse bioactive substances and peptides *via* imine formation or Michael addition (Lee et al., 2009; Ku et al., 2010; Lynge et al., 2011; Chien et al., 2012). The measurement of a water contact angle showed that surface hydrophilicity was greatly ameliorated by PDA coating. However, the water drop penetrated into the coating so fast that a static water contact angle cannot be measured and the difference of static water contact angle between the PET and PDA-PET groups cannot be calculated as well. The enhanced hydrophilicity was beneficial for cell adhesion, thus triggering the intracellular signal pathway and promoting cell proliferation (Kao et al., 2015).

BMP-2 presented a favorable ability to enhance bone healing; however, potential complications also existed, especially off-label use of BMPs (Boden, 2005). The most common complication is extra bone formation, which is called heterotopic ossification (Boraiah et al., 2009). Researchers also found that a high dose (>40 mg) of rhBMP-2 administration is associated with the increased risk of cancer (Dimar et al., 2009). Therefore, we chose the solution at a concentration of 250 and 500 ng/ml, a relatively low dose, to immobilize BMP-2 onto the grafts. Finally, the amounts of BMP-2 immobilized on the graft were 83.1 ± 9.5 ng/cm^2 and 138.4 ± 10.6 ng/cm^2, respectively. During a 28-day dynamic release period, more than 80% of the immobilized BMP-2 was retained. These results are in accordance with previous reports. Cho et al. (2014) found that immobilized BMP-2 on polydopamine-coated PLLA nanofibers showed approximately 90% retention efficiency over 28 days. A hydroxyapatite coating was also used to mediate the immobilization of BMP-2 on a titanium alloy, and a quarter of the immobilized amount of BMP-2 was released during the first 7 days (Cai et al., 2014). Our results showed a stable and continuous delivery of BMP-2 of the modified grafts for a relatively long period, which is favorable for bone regeneration and may avoid dose-related complications *in vivo*. The sustainable release of BMP-2 may lie in the tightly covalent binding between the catechol and quinone groups on PDA and the amino side chains of BMP-2 (Chien and Tsai, 2013).

In cellular experiments, CCK-8 assay showed that OD values in all groups increased with culture time, and the 500B-PDA-PET grafts exhibited a higher OD at 3 and 7 days of culturing than the other groups. More attached cells on the surface of the BMP-2-immobilized group were detected than on the PET group *via* SEM. These results indicated that BMP-2-modified scaffolds could promote the attachment and proliferation of rBMSCs and exhibited better biocompatibility. The ALP activity assay and examination of the transcription levels of osteogenesis-related genes confirmed the improved osteogenic differentiation after PDA coating and BMP-2 immobilization. In addition, the mineralization of the grafts was evaluated *via* Alizarin Red S staining. Larger and more calcium nodules were observed in the 500B-PDA group than in the other three groups, and quantification indicated a significant difference. These results indicated that the immobilization of BMP-2 mediated by PDA coating posed a favorable impact on the differentiation of rBMSCs.

Previous studies detected that a loose granulation fibrous layer was formed between the grafts and host bone (He et al., 2012; Cho et al., 2013; Jiang et al., 2014). And, this might be the main reason for the enlarged bone tunnels, unstable knee joints, or the failure of ACL reconstruction. Our *in vivo* results demonstrated that the ultimate failure load in the 500B-PDA group is significantly higher than that in the PET or PDA-PET group. The micro-CT examination showed a synergic effect of the BMP-2 and PDA on the osseointegration and bone regeneration. BV/TV in the PDA group was significantly higher compared with the PET group, and BV/TV in the 500B-PDA-PET group was significantly higher than that in the PDA-PET group. However, the changes of BS/BV presented an opposite trend. Consistent with the biomechanical tests, the histological staining showed a tight binding between the BMP-2-immobilized grafts and the native bone, indicating an

improved graft-to-bone healing. All these results demonstrated that the BMP-2 and PDA-modified PET artificial ligaments exhibited an enhanced biocompatibility, bioactivity, and osseointegration. However, the specific mechanism cannot be clarified currently, and further investigations need to be performed.

CONCLUSION

In this study, we prepared the PET artificial ligaments immobilized with BMP-2 *via* polydopamine coating. The immobilization of BMP-2 mediated by polydopamine coating on PET artificial ligament surface could enhance the compatibility and bioactivity of the scaffolds and the graft-to-bone healing *in vivo*, which is beneficial for the wide application of PET ligaments.

DATA AVAILABILITY STATEMENT

The raw data supporting the conclusions of this article will be made available by the authors, without undue reservation.

ETHICS STATEMENT

The animal study was reviewed and approved by The Laboratory Animal Welfare and Ethics Committee of Shanghai Pudong Hospital.

AUTHOR CONTRIBUTIONS

ZK, DL, and CS contributed to the whole conduction of the study. JD, BY, and QH performed part of the animal experiments. ZQ, ZZ, QH, and XZ performed the statistical analysis. BY and JH provided guidelines for the conduction of *in vitro* and *in vivo* experiments. ZK wrote the first draft of the manuscript. CY, YZ, and HD contributed to the conception and design of the study. All authors contributed to the article and approved the submitted version.

FUNDING

This study was funded by Academic Leaders Training Program of Pudong Health Committee of Shanghai (Grant No. PWRd2017-03), China; The Talents Training Program of Pudong Hospital affiliated to Fudan University (Project no. PX202001); The Scientific Research Foundation provided by Pudong Hospital affiliated to Fudan University (Project no. YJRCJJ201906); The Outstanding Clinical Discipline Project of Shanghai Pudong (Grant No. PWYgy2018-09), China, the National Science Foundation of China (Grant No. 81972055), Outstanding Leaders Training Program of Pudong Health Committee of Shanghai (Grant No. PWR PWR12021-01), Outstanding Leaders Training Program of Pudong Hospital affiliated to Fudan University (Project No. LJ202102), Talents Training Program of Pudong Hospital affiliated to Fudan University (Project No. YJYJRC202102), Program for Medical Key Department of Shanghai (Grant No. ZK2019C01), the foundation provided by Shanghai Public Health Clinical Center, Shanghai Medical School, Fudan University (KY-GW-2019-18).

REFERENCES

Ahldén, M., Kartus, J., Ejerhed, L., Karlsson, J., and Sernert, N. (2009). Knee Laxity Measurements after Anterior Cruciate Ligament Reconstruction, Using Either Bone-Patellar-Tendon-Bone or Hamstring Tendon Autografts, with Special Emphasis on Comparison over Time. *Knee Surg. Sports Traumatol. Arthrosc.* 17 (9), 1117–1124. doi:10.1007/s00167-009-0846-5

Bayat, M., Shojaei, S., Bahrami, N., Mohamadnia, A., Shojaei, P., and Bahrami, N. (2017). Protein Engineering of Recombinant Human Bone Morphogenetic Protein 2 with Higher Interaction with Ca Phosphate Based Scaffold Used for Osteogenesis. *J. Biomed. Mater. Res.* 105 (10), 2799–2805. doi:10.1002/jbm.a.36143

Boden, S. D. (2005). The ABCs of BMPs. *Orthopaedic Nurs.* 24 (1), 49–52. doi:10.1097/00006416-200501000-00014

Boraiah, S., Paul, O., Hawkes, D., Wickham, M., and Lorich, D. G. (2009). Complications of Recombinant Human BMP-2 for Treating Complex Tibial Plateau Fractures: a Preliminary Report. *Clin. Orthop. Relat. Res.* 467 (12), 3257–3262. doi:10.1007/s11999-009-1039-8

Cai, Y., Wang, X., Poh, C. K., Tan, H. C., Soe, M. T., Zhang, S., et al. (2014). Accelerated Bone Growth *In Vitro* by the Conjugation of BMP2 Peptide with Hydroxyapatite on Titanium alloy. *Colloids Surf. B: Biointerfaces* 116, 681–686. doi:10.1016/j.colsurfb.2013.11.004

Cao, X., and Chen, D. (2005). The BMP Signaling and *In Vivo* Bone Formation. *Gene* 357 (1), 1–8. doi:10.1016/j.gene.2005.06.017

Chen, D., Zhao, M., and Mundy, G. R. (2004). Bone Morphogenetic Proteins. *Growth Factors* 22 (4), 233–241. doi:10.1080/08977190412331279890

Chien, C.-Y., and Tsai, W.-B. (2013). Poly(dopamine)-assisted Immobilization of Arg-Gly-Asp Peptides, Hydroxyapatite, and Bone Morphogenic Protein-2 on Titanium to Improve the Osteogenesis of Bone Marrow Stem Cells. *ACS Appl. Mater. Inter.* 5 (15), 6975–6983. doi:10.1021/am401071f

Chien, H.-W., Kuo, W.-H., Wang, M.-J., Tsai, S.-W., and Tsai, W.-B. (2012). Tunable Micropatterned Substrates Based on Poly(dopamine) Deposition via Microcontact Printing. *Langmuir* 28 (13), 5775–5782. doi:10.1021/la300147p

Cho, H.-j., Madhurakkat Perikamana, S. K., Lee, J.-h., Lee, J., Lee, K.-M., Shin, C. S., et al. (2014). Effective Immobilization of BMP-2 Mediated by Polydopamine Coating on Biodegradable Nanofibers for Enhanced *In Vivo* Bone Formation. *ACS Appl. Mater. Inter.* 6 (14), 11225–11235. doi:10.1021/am501391z

Cho, S., Li, H., Chen, C., Jiang, J., Tao, H., and Chen, S. (2013). Cationised Gelatin and Hyaluronic Acid Coating Enhances Polyethylene Terephthalate Artificial Ligament Graft Osseointegration in Porcine Bone Tunnels. *Int. Orthop. (Sicot)* 37 (3), 507–513. doi:10.1007/s00264-012-1694-3

Dimar, J. R., 2nd, Glassman, S. D., Burkus, J. K., Pryor, P. W., Hardacker, J. W., and Carreon, L. Y. (2009). Clinical and Radiographic Analysis of an Optimized rhBMP-2 Formulation as an Autograft Replacement in Posterolateral Lumbar Spine Arthrodesis. *J. Bone Jt. Surgery Am.* 91 (6), 1377–1386. doi:10.2106/jbjs.h.00200

Gustafsson, Y., Haag, J., Jungebluth, P., Lundin, V., Lim, M. L., Baiguera, S., et al. (2012). Viability and Proliferation of Rat MSCs on Adhesion Protein-Modified PET and PU Scaffolds. *Biomaterials* 33 (32), 8094–8103. doi:10.1016/j.biomaterials.2012.07.060

He, P., Ng, K. S., Toh, S. L., and Goh, J. C. H. (2012). *In Vitro* ligament-bone Interface Regeneration Using a Trilineage Coculture System on a Hybrid Silk Scaffold. *Biomacromolecules* 13 (9), 2692–2703. doi:10.1021/bm300651q

Huang, Z., Bi, L., Zhang, Z., and Han, Y. (2012). Effects of Dimethylolpropionic Acid Modification on the Characteristics of Polyethylene Terephthalate Fibers. *Mol. Med. Rep.* 6 (4), 709–715. doi:10.3892/mmr.2012.1012

Ichiba, A., and Kishimoto, I. (2009). Effects of Articular Cartilage and Meniscus Injuries at the Time of Surgery on Osteoarthritic Changes after Anterior Cruciate Ligament Reconstruction in Patients under 40 Years Old. *Arch. Orthop. Trauma Surg.* 129 (3), 409–415. doi:10.1007/s00402-008-0786-4

Jia, Z.-Y., Zhang, C., Cao, S.-q., Xue, C.-c., Liu, T.-z., Huang, X., et al. (2017). Comparison of Artificial Graft versus Autograft in Anterior Cruciate Ligament Reconstruction: a Meta-Analysis. *BMC Musculoskelet. Disord.* 18 (1), 309. doi:10.1186/s12891-017-1672-4

Jiang, J., Wan, F., Yang, J., Hao, W., Wang, Y., Yao, J., et al. (2014). Enhancement of Osseointegration of Polyethylene Terephthalate Artificial Ligament by Coating of silk fibroin and Depositing of Hydroxyapatite. *Int. J. Nanomed.* 9, 4569–4580. doi:10.2147/ijn.s69137

Jin, S.-K., Lee, J.-H., Hong, J.-H., Park, J.-K., Seo, Y.-K., and Kwon, S.-Y. (2016). Enhancement of Osseointegration of Artificial Ligament by Nano-Hydroxyapatite and Bone Morphogenic Protein-2 into the Rabbit Femur. *Tissue Eng. Regen. Med.* 13 (3), 284–296. doi:10.1007/s13770-016-9051-z

Kao, C.-T., Lin, C.-C., Chen, Y.-W., Yeh, C.-H., Fang, H.-Y., and Shie, M.-Y. (2015). Poly(dopamine) Coating of 3D Printed Poly(lactic Acid) Scaffolds for Bone Tissue Engineering. *Mater. Sci. Eng. C* 56, 165–173. doi:10.1016/j.msec.2015.06.028

Karaoglu, S., Celik, C., and Korkusuz, P. (2009). The Effects of Bone Marrow or Periosteum on Tendon-To-Bone Tunnel Healing in a Rabbit Model. *Knee Surg. Sports Traumatol. Arthrosc.* 17 (2), 170–178. doi:10.1007/s00167-008-0646-3

Ku, S. H., Ryu, J., Hong, S. K., Lee, H., and Park, C. B. (2010). General Functionalization Route for Cell Adhesion on Non-wetting Surfaces. *Biomaterials* 31 (9), 2535–2541. doi:10.1016/j.biomaterials.2009.12.020

La, W.-G., Kang, S.-W., Yang, H. S., Bhang, S. H., Lee, S. H., Park, J.-H., et al. (2010). The Efficacy of Bone Morphogenetic Protein-2 Depends on its Mode of Delivery. *Artif. Organs* 34 (12), 1150–1153. doi:10.1111/j.1525-1594.2009.00988.x

Lee, H., Dellatore, S. M., Miller, W. M., and Messersmith, P. B. (2007). Mussel-inspired Surface Chemistry for Multifunctional Coatings. *Science* 318 (5849), 426–430. doi:10.1126/science.1147241

Lee, H., Rho, J., and Messersmith, P. B. (2009). Facile Conjugation of Biomolecules onto Surfaces via Mussel Adhesive Protein Inspired Coatings. *Adv. Mater.* 21 (4), 431–434. doi:10.1002/adma.200801222

Lee, Y. B., Shin, Y. M., Lee, J.-h., Jun, I., Kang, J. K., Park, J.-C., et al. (2012). Polydopamine-mediated Immobilization of Multiple Bioactive Molecules for the Development of Functional Vascular Graft Materials. *Biomaterials* 33 (33), 8343–8352. doi:10.1016/j.biomaterials.2012.08.011

Li, H., and Chen, S. (2015). Biomedical Coatings on Polyethylene Terephthalate Artificial Ligaments. *J. Biomed. Mater. Res.* 103 (2), 839–845. doi:10.1002/jbm.a.35218

Li, H., Li, J., Jiang, J., Lv, F., Chang, J., Chen, S., et al. (2017). An Osteogenesis/angiogenesis-Stimulation Artificial Ligament for Anterior Cruciate Ligament Reconstruction. *Acta Biomater.* 54, 399–410. doi:10.1016/j.actbio.2017.03.014

Lidén, M., Sernert, N., Rostgård-Christensen, L., Kartus, C., and Ejerhed, L. (2008). Osteoarthritic Changes after Anterior Cruciate Ligament Reconstruction Using Bone-Patellar Tendon-Bone or Hamstring Tendon Autografts: a Retrospective, 7-year Radiographic and Clinical Follow-Up Study. *Arthrosc. J. Arthroscopic Relat. Surg.* 24 (8), 899–908. doi:10.1016/j.arthro.2008.04.066

Lohmander, L. S., Englund, P. M., Dahl, L. L., and Roos, E. M. (2007). The Long-Term Consequence of Anterior Cruciate Ligament and Meniscus Injuries. *Am. J. Sports Med.* 35 (10), 1756–1769. doi:10.1177/0363546507307396

Luginbuehl, V., Meinel, L., Merkle, H. P., and Gander, B. (2004). Localized Delivery of Growth Factors for Bone Repair. *Eur. J. Pharm. Biopharm.* 58 (2), 197–208. doi:10.1016/j.ejpb.2004.03.004

Lv, J., Xiu, P., Tan, J., Jia, Z., Cai, H., and Liu, Z. (2015). Enhanced Angiogenesis and Osteogenesis in Critical Bone Defects by the Controlled Release of BMP-2 and VEGF: Implantation of Electron Beam Melting-Fabricated Porous Ti 6 Al 4 V Scaffolds Incorporating Growth Factor-Doped Fibrin Glue. *Biomed. Mater.* 10 (3), 035013. doi:10.1088/1748-6041/10/3/035013

Lynge, M. E., van der Westen, R., Postma, A., and Städler, B. (2011). Polydopamine-a Nature-Inspired Polymer Coating for Biomedical Science. *Nanoscale* 3 (12), 4916–4928. doi:10.1039/c1nr10969c

Mascarenhas, R., and MacDonald, P. B. (2008). Anterior Cruciate Ligament Reconstruction: a Look at Prosthetics-Ppast, Present and Possible Future. *Mcgill J. Med.* 11 (1), 29–37. doi:10.26443/mjm.v11i1.409

McDonald, L. K., Cosic, F., and Joseph, S. (2021). The Use of the Ligament Augmentation and Reconstruction System for Posterior Cruciate Ligament Reconstruction in Isolated and Multiligament Knee Injuries: A Systematic Review. *Knee* 30, 322–336. doi:10.1016/j.knee.2021.04.008

Mrowczynski, R., Turcu, R., Leostean, C., Scheidt, H. A., and Liebscher, J. (2013). New Versatile Polydopamine Coated Functionalized Magnetic Nanoparticles. *Mater. Chem. Phys.* 138 (1), 295–302. doi:10.1016/j.matchemphys.2012.11.059

Parchi, P. D., Ciapini, G., Paglialunga, C., Giuntoli, M., Picece, C., Chiellini, F., et al. (2018). Anterior Cruciate Ligament Reconstruction with LARS Artificial Ligament-Clinical Results after a Long-Term Follow-Up. *Joints* 6 (2), 75–79. doi:10.1055/s-0038-1653950

Poon, B., Kha, T., Tran, S., and Dass, C. R. (2016). Bone Morphogenetic Protein-2 and Bone Therapy: Successes and Pitfalls. *J. Pharm. Pharmacol.* 68 (2), 139–147. doi:10.1111/jphp.12506

Rawadi, G., Vayssière, B., Dunn, F., Baron, R., and Roman-Roman, S. (2003). BMP-2 Controls Alkaline Phosphatase Expression and Osteoblast Mineralization by a Wnt Autocrine Loop. *J. Bone Miner Res.* 18 (10), 1842–1853. doi:10.1359/jbmr.2003.18.10.1842

Ren, Y., Rivera, J. G., He, L., Kulkarni, H., Lee, D.-K., and Messersmith, P. B. (2011). Facile, High Efficiency Immobilization of Lipase Enzyme on Magnetic Iron Oxide Nanoparticles via a Biomimetic Coating. *BMC Biotechnol.* 11, 63. doi:10.1186/1472-6750-11-63

Ribeiro, F. O., Gómez-Benito, M. J., Folgado, J., Fernandes, P. R., and García-Aznar, J. M. (2015). In Silico Mechano-Chemical Model of Bone Healing for the Regeneration of Critical Defects: The Effect of BMP-2. *PloS one* 10 (6), e0127722. doi:10.1371/journal.pone.0127722

Shelbourne, K. D., and Gray, T. (2000). Results of Anterior Cruciate Ligament Reconstruction Based on Meniscus and Articular Cartilage Status at the Time of Surgery. *Am. J. Sports Med.* 28 (4), 446–452. doi:10.1177/03635465000280040201

Sofu, H., Yildirim, T., Gürsu, S., Issin, A., and Şahin, V. (2015). Short-term Effects of Partial Meniscectomy on the Clinical Results of Anterior Cruciate Ligament Reconstruction. *Knee Surg. Sports Traumatol. Arthrosc.* 23 (1), 184–187. doi:10.1007/s00167-014-2960-2

Takahashi, Y., Yamamoto, M., and Tabata, Y. (2005). Enhanced Osteoinduction by Controlled Release of Bone Morphogenetic Protein-2 from Biodegradable Sponge Composed of Gelatin and β-tricalcium Phosphate. *Biomaterials* 26 (23), 4856–4865. doi:10.1016/j.biomaterials.2005.01.012

Vaishya, R., Agarwal, A. K., Ingole, S., and Vijay, V. (2015). Current Trends in Anterior Cruciate Ligament Reconstruction: A Review. *Cureus* 7 (11), e378. doi:10.7759/cureus.378

Vaquette, C., Viateau, V., Guérard, S., Anagnostou, F., Manassero, M., Castner, D. G., et al. (2013). The Effect of Polystyrene Sodium Sulfonate Grafting on Polyethylene Terephthalate Artificial Ligaments on *In Vitro* Mineralisation and *In Vivo* Bone Tissue Integration. *Biomaterials* 34 (29), 7048–7063. doi:10.1016/j.biomaterials.2013.05.058

Wang, C.-H., Guo, Z.-S., Pang, F., Zhang, L.-Y., Yan, M., Yan, J.-H., et al. (2015). Effects of Graphene Modification on the Bioactivation of Polyethylene-Terephthalate-Based Artificial Ligaments. *ACS Appl. Mater. Inter.* 7 (28), 15263–15276. doi:10.1021/acsami.5b02893

Wang, C. S., and Stewart, R. J. (2013). Multipart Copolyelectrolyte Adhesive of the Sandcastle Worm, Phragmatopoma Californica (Fewkes): Catechol Oxidase Catalyzed Curing through Peptidyl-DOPA. *Biomacromolecules* 14 (5), 1607–1617. doi:10.1021/bm400251k

Wu, J., Zheng, A., Liu, Y., Jiao, D., Zeng, D., Wang, X., et al. (2019). Enhanced Bone Regeneration of the Silk Fibroin Electrospun Scaffolds through the Modification of the Graphene Oxide Functionalized by BMP-2 Peptide. *Int. J. Nanomed.* 14, 733–751. doi:10.2147/ijn.s187664

Wu, R., Gao, G., and Xu, Y. (2020). Electrospun Fibers Immobilized with BMP-2 Mediated by Polydopamine Combined with Autogenous Tendon to Repair Developmental Dysplasia of the Hip in a Porcine Model. *Int. J. Nanomed.* 15, 6563–6577. doi:10.2147/ijn.s259028

Yao, C. H., Lai, Y. H., Chen, Y. W., and Cheng, C. H. (2020). Bone Morphogenetic Protein-2-Activated 3D-Printed Polylactic Acid Scaffolds to Promote Bone Regrowth and Repair. *Macromol Biosci.* 20 (10), e2000161. doi:10.1002/mabi.202000161

Yu, B., Pei, P., Yu, B., Li, D., Zhang, X., Huang, J., et al. (2017). Enhance the Bioactivity and Osseointegration of the Polyethylene-Terephthalate-Based Artificial Ligament via Poly(Dopamine) Coating with Mesoporous Bioactive Glass. *Adv. Eng. Mater.* 19 (5), 1600708. doi:10.1002/adem.201600708

Zantop, T., Wellmann, M., Fu, F. H., and Petersen, W. (2008). Tunnel Positioning of Anteromedial and Posterolateral Bundles in Anatomic Anterior Cruciate Ligament Reconstruction. *Am. J. Sports Med.* 36 (1), 65–72. doi:10.1177/0363546507308361

Zhang, B.-j., He, L., Han, Z.-w., Li, X.-g., Zhi, W., Zheng, W., et al. (2017). Enhanced Osteogenesis of Multilayered Pore-Closed Microsphere-Immobilized Hydroxyapatite Scaffold via Sequential Delivery of Osteogenic Growth Peptide and BMP-2. *J. Mater. Chem. B* 5 (41), 8238–8253. doi:10.1039/c7tb01970j

Zhang, Q., He, Q.-F., Zhang, T.-H., Yu, X.-L., Liu, Q., and Deng, F.-l. (2012). Improvement in the Delivery System of Bone Morphogenetic Protein-2: a New Approach to Promote Bone Formation. *Biomed. Mater.* 7 (4), 045002. doi:10.1088/1748-6041/7/4/045002

Zhou, W.-H., Tang, S.-F., Yao, Q.-H., Chen, F.-R., Yang, H.-H., and Wang, X.-R. (2010). A Quartz crystal Microbalance Sensor Based on Mussel-Inspired Molecularly Imprinted Polymer. *Biosens. Bioelectron.* 26 (2), 585–589. doi:10.1016/j.bios.2010.07.024

Conflict of Interest: The authors declare that the research was conducted in the absence of any commercial or financial relationships that could be construed as a potential conflict of interest.

Publisher's Note: All claims expressed in this article are solely those of the authors and do not necessarily represent those of their affiliated organizations or those of the publisher, the editors, and the reviewers. Any product that may be evaluated in this article, or claim that may be made by its manufacturer, is not guaranteed or endorsed by the publisher.

frontiers in Bioengineering and Biotechnology

ORIGINAL RESEARCH
published: 21 December 2021
doi: 10.3389/fbioe.2021.737074

A Facile Method to Synthesize 3D Pomegranate-like Polydopamine Microspheres

Farnaz Ghorbani[1†‡], *Behafarid Ghalandari*[2‡] *and Chaozong Liu*[3*]

[1]*Department of Orthopedics, Shanghai Pudong Hospital, Fudan University Pudong Medical Center, Shanghai, China,* [2]*State Key Laboratory of Oncogenes and Related Genes, Institute for Personalized Medicine, School of Biomedical Engineering, Shanghai Jiao Tong University, Shanghai, China,* [3]*Institute of Orthopaedic and Musculoskeletal Science, University College London, Royal National Orthopaedic Hospital, London, United Kingdom*

OPEN ACCESS

Edited by:
Hengchong Shi,
Changchun Institute of Applied Chemistry (CAS), China

Reviewed by:
Baolin Guo,
Xi'an Jiaotong University, China
Payam Zarrintaj,
University of Montana, United States
Lulu Han,
Dalian University of Technology, China

***Correspondence:**
Chaozong Liu
chaozong.liu@ucl.ac.uk

†Present address:
Farnaz Ghorbani,
Department of Material Science and Engineering, Institute of Biomaterials, University of Erlangen-Nuremberg, Erlangen, Germany

‡These authors have contributed equally to this work

Specialty section:
This article was submitted to "Biomaterials", a section of the journal Frontiers in Bioengineering and Biotechnology

Received: *06 July 2021*
Accepted: *25 November 2021*
Published: *21 December 2021*

Citation:
Ghorbani F, Ghalandari B and Liu C (2021) A Facile Method to Synthesize 3D Pomegranate-like Polydopamine Microspheres. Front. Bioeng. Biotechnol. 9:737074. doi: 10.3389/fbioe.2021.737074

Nanospheres have found versatile applications in the biomedical field; however, their possible harmful effects on immune and inflammatory systems are also a crucial concern. Inspired by a pomegranate structure, we demonstrated a novel structure for the nanostructured microspheres to overcome the drawbacks of nanospheres without compromising their merits. In this study, 3D pomegranate-like polydopamine microspheres (PDAMS) were synthesized by self-oxidative polymerization of dopamine hydrochloride. Herein, controlling the pH during polymerization led to synthesizing homogeneous agglomerated nano-sized spheres (400–2000 nm) and finally forming tunable and monodisperse micron-sized particles (21 μm) with uniform spherical shape porous microstructure. PDAMS interaction with the potential targets, Bone morphogenetic protein-2 (BMP2), Decorin, and Matrilin-1, was investigated via molecular calculations. Theoretical energy analysis revealed that PDAMS interaction with BMP2, Decorin, and Matrilin-1 is spontaneous, so that a protein layer formation on the PDAMS surface suggests application in bone and cartilage repair. It was also observed that PDAMS presented *in-vitro* degradation within 4 weeks. Here, disappearance of the UV-VIS spectrum peak at 280 nm is accompanied by the degradation of catechol groups. Pomegranate-like PDAMS support the biomimetic formation of hydroxyapatite-like layers, making them appropriate candidates for hard tissue applications. Herein, the appearance of peaks in XRD spectrum at 31.37, 39.57, 45.21, and 50.13° attributed to hydroxyapatite-like layers formation. All these results demonstrated that self-oxidative polymerization under a controllable pH can be a green and straightforward technique for preparing the pomegranate-like PDAMS and providing an innovative basis for further pre-clinical and clinical investigations.

Keywords: biomaterials, biomimetic, nanoparticles, microstructure, protein interaction

INTRODUCTION

Nanospheres are abundantly used in the biomedical area due to their superior properties. However, the toxicity of the nanoparticles, as well as their possible harmful effects on immune and inflammatory systems, severe aggregation, and high inter-particle resistance, are the main concerns in the biomedical application. In order to overcome these limitations, the authors have

developed pomegranate-like spheres inspired by the structure of a pomegranate. *In-vitro* study has demonstrated these biomimetic nanostructured microspheres can overcome the drawbacks of conventional nanoparticles without compromising their merits. Accordingly, such a design can have some benefits as follows: 1) facilitates mass transfer, such as cell nutrients and metabolic waste (Ji et al., 2021); 2) supports adequate swelling with no differences in the final size of microspheres owing to the presence of void space, which can make them suitable structures for the size-dependent applications (Liu et al., 2014); 3) promotes the stability of protein-microsphere interactions (Blekemolen et al., 2018; Luo et al., 2019); 4) provides more anchorage sites and a high level of surface energy to improve cells attachment, facilitate cells migration, proliferation, and differentiation (Zhou et al., 2018); 5) primary agglomerated nanospheres maintain structural integrity and prevent microspheres from crack under the applied stresses (Liu et al., 2014), and 6) improves drug-loading capacity and applies more control on release rate (Ji et al., 2021).

Dopamine, a neurotransmitter, can be spontaneously polymerized to polydopamine (PDA). PDA, a mussel-inspired and melanin-like material, has found expanded application in the biomedical area, including surface modification (Liu et al., 2021), drug delivery (Wang et al., 2021), tissue engineering (bone (Deng et al., 2019), tooth (Hasani-Sadrabadi et al., 2019), nerve (Yan et al., 2020), muscle (Tian et al., 2018), skin (Tang et al., 2019), cartilage (Han et al., 2018), vessel (Zhou et al., 2017)), photothermal therapy (Ruan et al., 2021), microfluidic systems (Kanitthamniyom and Zhang, 2018), and bioimaging (Nurunnabi et al., 2013). Biocompatibility and minimal inflammatory response, high level of hydrophilicity, excellent bioactivity, bio-adhesive properties, anti-bacterial potential, thermal stability, cost-effective and green synthesis technology can be responsible for all-round development (Iqbal et al., 2012; Liu et al., 2013a; Liu et al., 2013b; Gong et al., 2017; Zhao et al., 2019; Steeves and Variola, 2020; De Guzman et al., 2021; Gholami Derami et al., 2021; Park et al., 2021; Sun et al., 2021). According to previous publications, the synthesis of PDA strongly depends on the chemical properties of reaction media; therefore, the concentration, types of alcohol, the ratio of water to alcohol, and pH can affect the polymerization process, as well as the final shape, size, and uniformity of the synthesized structure (Jiang et al., 2014; Ghorbani et al., 2019a). Accordingly, monodisperse 3D pomegranate-like PDA microspheres (PDAMS) were synthesized based on the homogeneous and controlled-agglomeration of PDA nanospheres to compensate for the drawbacks of single nanospheres.

In this work, a green and facile technique was introduced to synthesize the pomegranate-like PDAMS. The resultant PDAMS were subsequently characterized with respect to their morphological property and chemical composition, degradation behavior, and biomineralization potential. In addition, PDAMS interaction with the potential targets, bone morphogenetic protein-2 (BMP2), Decorin, and Matrilin-1, was investigated via molecular calculations, which shows their suitability for hard tissue applications.

MATERIALS AND METHODOLOGY

Nanostructured-PDAMS were synthesized by the oxidative polymerization of dopa-HCl in pH-controlled conditions. Briefly, a solution of isopropanol-DI-water (with a volume ratio of 5:2) was prepared, and the pH was adjusted to 8.5 by adding Tris-buffer (10 mmol/L). Then, dopa-HCl with a concentration of 1.5 mg/ml was added to the prepared solution dropwise. The mixture was stirred at 250 rpm for 3 days at ambient temperature. The pH of the solution was monitored every 5 h and was adjusted to 8.5 by the addition of ammonia solution. Finally, the solution was centrifuged with DI-water, and sediments were lyophilized.

The microstructure of the nanostructured-PDAMS was examined using a field-emission scanning electron microscopy (FE-SEM, MIRA3, TESCAN Co., Czech Republic) at an accelerating voltage of 15 kV after coating a thin layer of gold to reduce charge density. The size distribution was analysed by Image measurement software (KLONK Image Measurement Light, Edition 11.2.0.0). The polymerization was evaluated using Fourier-transforminfrared spectroscopy and proton nuclear magnetic resonance (H-NMR, ECX 400, JEOL Co., United States) spectroscopy. H-NMR spectroscopy was performed through dissolving the microspheres in deuterium oxide (D_2O): DMSO-d_6 (1: 1). The spectra were recorded by a 4 mm MAS probe under an applied frequency of 5,000 Hz at 303 K. *In-vitro* degradation of spheres was evaluated by FE-SEM micrographs and ultraviolet-visible absorption (UV-VIS, Lambd25, Perkin-Elmer Co., United States) spectroscopy. The nanostructured-microspheres were immersed in PBS solution at 37 ± 0.5 °C for 4 weeks before use. At the end of each week, the PBS solution was refreshed. Finally, the samples were washed with DI-water and were lyophilized. The *in-vitro* bioactivity of microspheres was determined by immersion of microspheres in the SBF solution at 37 ± 0.5°C for 4 weeks. The SBF solution was refreshed every 2 days. Finally, the samples were washed with DI-water and were lyophilized. The mineralized microspheres were characterized using FE-SEM micrographs and phase analysis by X-ray diffraction (XRD, PW3710, Philips Co., Netherlands) using Cu-Kα radiation under the operating conditions of 40 kV and 30 mA. XRD patterns compared with JCPDS standards.

Molecular docking calculation using AutoDock Vina (Trott et al., 2009) was performed to evaluate PDAMS binding potential to the critical target proteins of Decorin, Matrilin-1, and BMP2. The 3D structures of BMP2 (PDB ID: 1REW (Keller et al., 2004)), Decorin (PDB ID: 1XCD (Scott et al., 2004)) and Matrilin-1 (PDB ID: 1AQ5 (Dames et al., 1998)) were obtained from the RCSB Protein Data Bank. Docking calculations were carried out with the basic unit size of PDAMS (<2 nm) as the repeated-basic unit, which expanded the computations to acquire the full-length scale. The 3D structure of the repeated-basic unit of PDAMS was modeled with the Hyperchem program, and its geometry was optimized by minimizing the energy using the B3LYP keyword with the 6-31G (d, p) basis set implemented in Gaussian 98 package. The molecular docking simulations were performed according to the classical preparation instruction (Abbasi-Tajarag et al., 2016; Gholamian et al., 2017; Shafaei et al.,

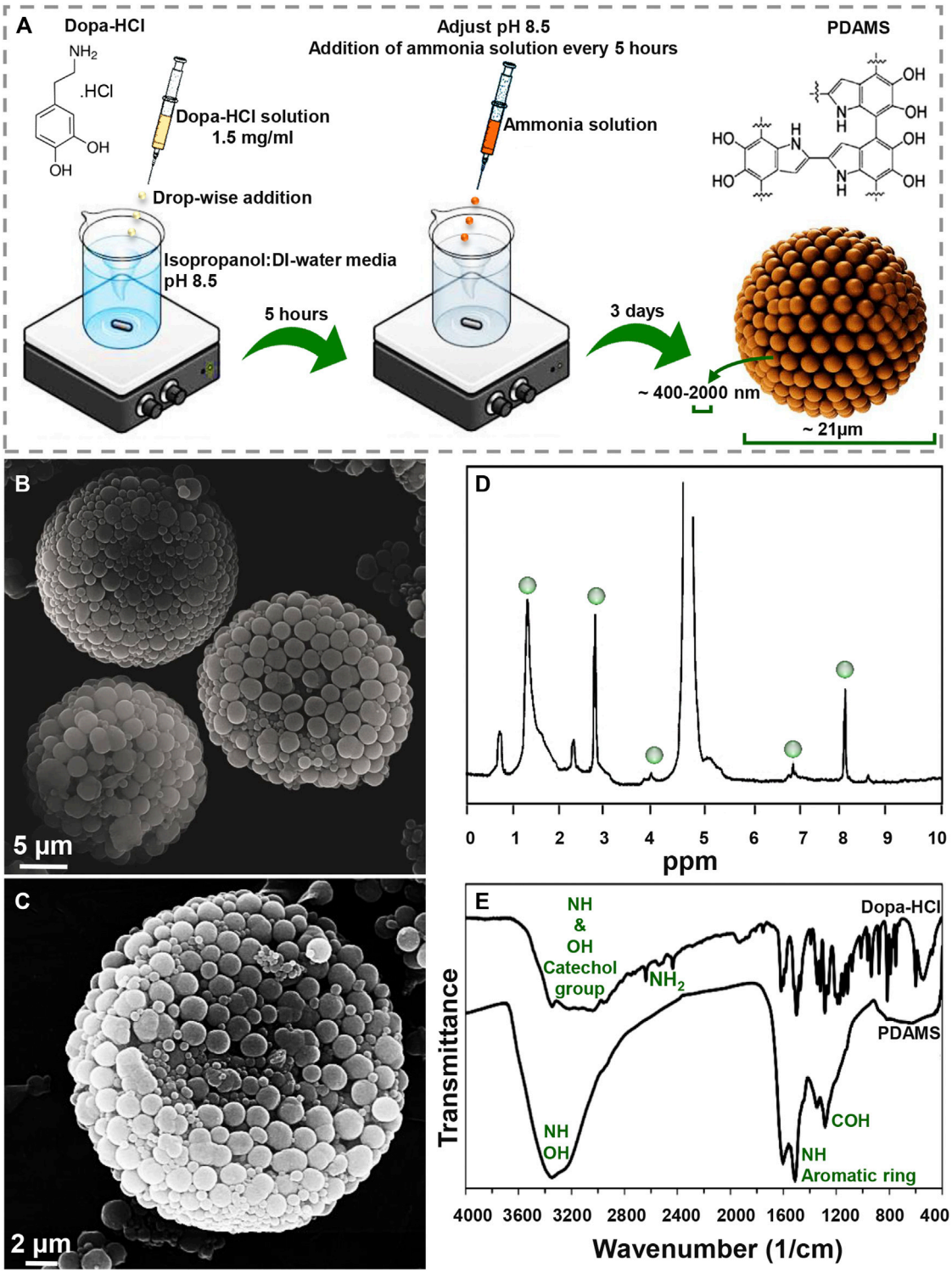

FIGURE 1 | Morphological and chemical observation of pomegranate-like PDAMS **(A)** A schematic of the synthesis process **(B)** FE-SEM micrographs of homogeneous nanostructured PDAMS, which were synthesized by spontaneous oxidation under controlled pH **(C)** FE-SEM micrographs of the inner structure of PDAMS **(D)** H-NMR and **(E)** FTIR of polymerized microspheres.

2017). The VMD package (Morris et al., 2009) and the AutoDock Tools 1.5.4 (Humphrey et al., 1996) were used for input file preparation and data analysis.

RESULTS AND DISCUSSION

Figure 1A presents a schematic of the synthesis procedure of pomegranate-like PDAMS. In this study, the particles were synthesized under self-oxidative polymerization of dopa-HCl in pH 8.5, which was then controlled to be stable within 3 days of synthesis. According to FE-SEM image (**Figure 1B, C**), tunable, spherical, and 3D pomegranate-like architecture PDA particles were prepared with an average size distribution of 21.92 ± 2.07 μm and smooth surface. Homogeneous and uniform agglomeration of primary nano-sized PDA spheres (ranging from 400 nm to 2 μm) led to the formation of the nanostructured-PDAMS with interconnected porous-like structures. This phenomenon may be attributed to controlled-pH, while in a similar study (Ghorbani et al., 2019b) there is no sign of homogeneous agglomeration of PDA nanospheres. Moreover, the void space between the agglomerated nanospheres (ranging from 20–300 nm) led to the formation of a 3D pomegranate-like structure that can facilitate and promote protein-microsphere interactions (Blekemolen et al., 2018; Luo et al., 2019).

The H-NMR spectra of PDAMS (**Figure 1D**) determined the aliphatic protons at 1.4, 2.9, and 4 ppm, which are attributed to (CH_2–C), (CH_2–C/CH_2–N), and (CH_2–N), respectively. The observed peaks at 7 and 8.1 ppm could be assigned to aromatic CH in indole. FTIR spectra (**Figure 1E**) demonstrated aromatic OH stretching vibration at 3,143, 3,065, 3,034, and 2,957 cm^{-1} in dopa-HCl chemical composition. Additionally, intermolecular hydrogen bonds were detected with a broad peak at 3,000–3,400 cm^{-1}. Moreover, disappearance of NH_2 characteristic peaks in PDMS compared with dopa-HCl, which can be observed at 3,210, 2,745, 2,640, and 2,435 cm^{-1}, confirmed the polymerization process. Besides, the vibration of phenolic OH and NH in the catechol groups was proved by the peak that was observed at 3,200–3,500 cm^{-1}. In addition, the presence of the aromatic ring and NH vibration was determined with a sharp peak at 1,605 cm^{-1}. Moreover, both NH and CO vibrations were identified with the absorption peaks at 1,510 and 1,120 cm^{-1}, respectively. The characteristic peaks at 1,345 and 1,284 cm^{-1} were assigned to phenolic OH.

The pH of reaction media has been known as the influencing factor on PDA formation. Generally, the alkali media oxidizes dopa-HCl followed by deprotonation of amine groups under 1,4- Michael addition reaction. Leucodopaminechrome, the product of the reaction, is oxidized and then rearranged to 5,6-dihydroxyindole. The interaction between o-quinone in 5,6-dihydroxyindole structure and catechol groups leads to the formation of PDAMS (Yan et al., 2013; Xiong et al., 2014). Moreover, polymerization of dopa.HCl can lead to pH reduction due to the ring-closing reaction of the monomer and the elimination of hydrogen atoms in the monomer chemical structure (Ju et al., 2011). So, the formation of homogeneous nanostructured PDAMS can be attributed to pH control during the polymerization process. The stability of the pH on higher values can be attributed to the neutralization of acidic monomer, long-lasting, and easy deporatonation of catechol groups, as well as the formation of the nanostructured-microspheres. Also, by keeping the pH in stable alkali values, complete spontaneous oxidation of dopamine will happen at a slower rate. When reactions of dopaminechrome to 5,6-dihydroxyindole and indolequinone are slow, it leads to accumulation reaction products in the media (Salomäki et al., 2018), which accompanies intra/intermolecular cross-linking reactions strong π-π interaction (Ju et al., 2011) that lead to the formation of pomegranate-like PDAMS.

The ratio of isopropanol to water (5:2) was determined in terms of the Hansen solubility parameters theory, as indicated in **Eqs 1, 2** (Jiang et al., 2014). Where D, P, and H are dispersive, polar, and hydrogen bonding solubility parameters, respectively. R_a and **Φ** are the levels of conformity and the volume fraction of each composition, respectively. **Eq. 1** * **2** indicate that the higher degree of uniformity was originated from a high degree of solubility (Lower R_a value).

$$R_a = 1/2\left[4\left(D_{solv}-D_{solu}\right)^2 + \left(P_{solv}-P_{solu}\right)^2 + \left(H_{solv}-H_{solu}\right)^2\right]^{0.5} \quad (1)$$

$$D\left(P,H\right)_{blend} = \Sigma\Phi_{n.comp}D\left(P,H\right)_{n.comp} \quad (2)$$

Degradability of the synthesized structures is an essential factor in the biomedical area that affects the size, shape, and chemical composition of particles (Han et al., 2018). Degradation of PDAMS was illustrated in **Figure 2A, B**. Based on the FE-SEM micrographs (**Figure 2A**), a 4-week immersion of the bioinspired-microspheres in the PBS solution slightly altered the surface, while a low degree of deformation was observed, indicating the stability of PDAMS. According to UV-VIS spectra (**Figure 2B**), the polymerization of dopa-HCl has led to the reduced intensity of the catechol groups peak at 280 nm, which was strongly affected by the pH of reaction media. However, the immersion of PDAMS in the PBS solution is shown to be accompanied by the degradation of catechol groups and disappearance of the related peak at 280 nm. Since catecholamine groups in the chemical composition of PDAMS can facilitate the absorption of the PBS solution and make degradation possible, so degradation of this hydrophilic functional group may reduce the degradation speed. Notably, the size of microspheres was known as an active factor in the degradation process. The microspheres with lower size distribution (less than 300 μm) have a higher tendency to homogeneous degradation (Anderson and Shive, 2012). However, microspheres with a size distribution of more than 10 μm are considered large for the phagocytosis process. Therefore, homogeneous degradation terminates to the reduced size and also facilitates phagocytosis by foreign body giant cells and macrophages (Tabata and Ikada, 2005). Additionally, void space may affect degradation. It is expected that PDAMS provides a higher permeation to fluids and

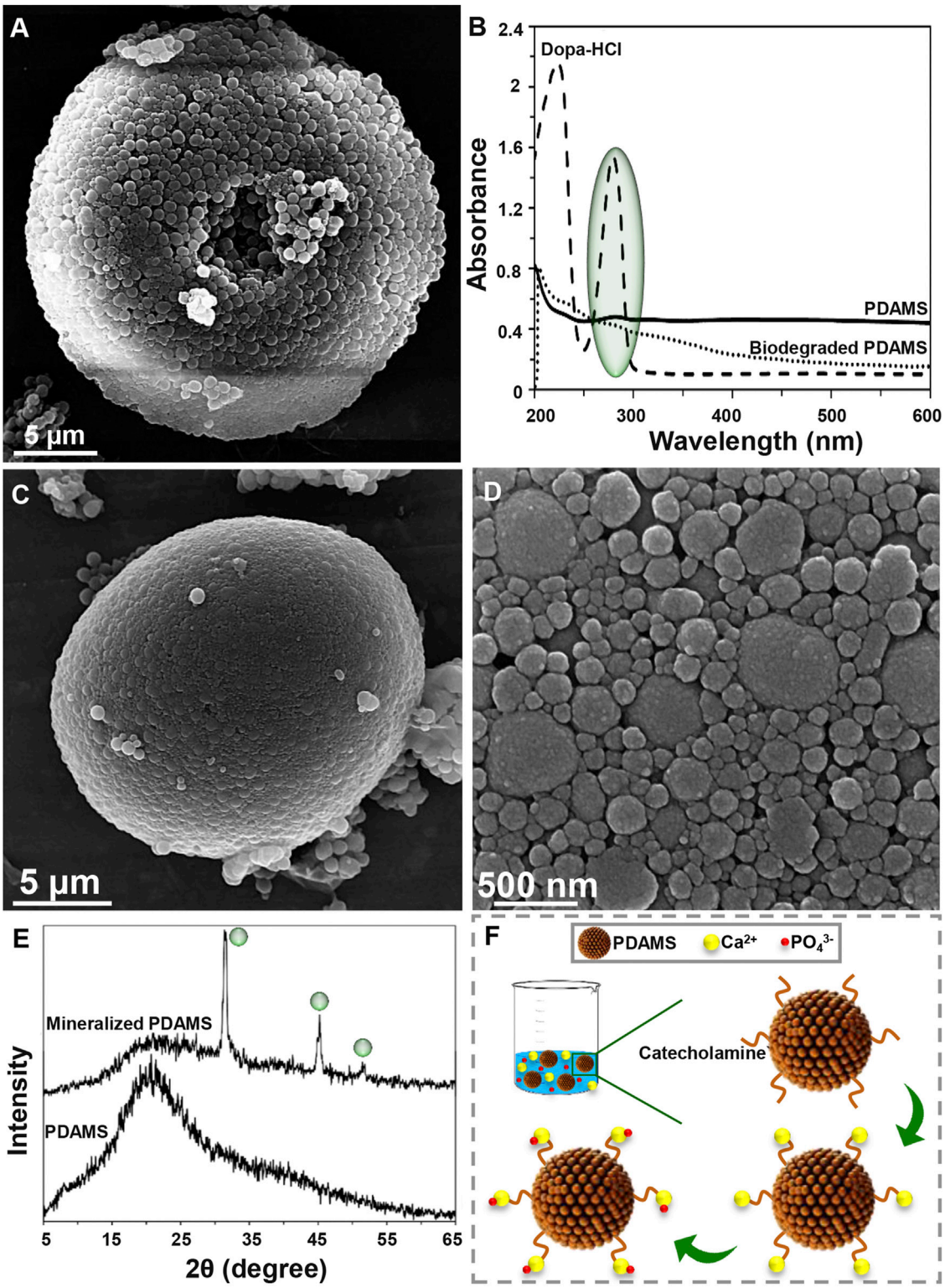

FIGURE 2 | Degradation and bioactivity of pomegranate-like PDAMS **(A)** FE-SEM image and **(B)** UV-VIS spectra of *In-vitro* degraded PDAMS after a 4-weeks immersion in the PBS solution **(C, D)** FE-SEM image and **(E)** XRD spectra of *In-vitro* biomimetic formation of hydroxyapatite-like layers on the PDAMS after a 4-weeks immersion in the SBF solution **(F)** Schematic of biomineralization of hydroxyapatite-like layers on PDAMS.

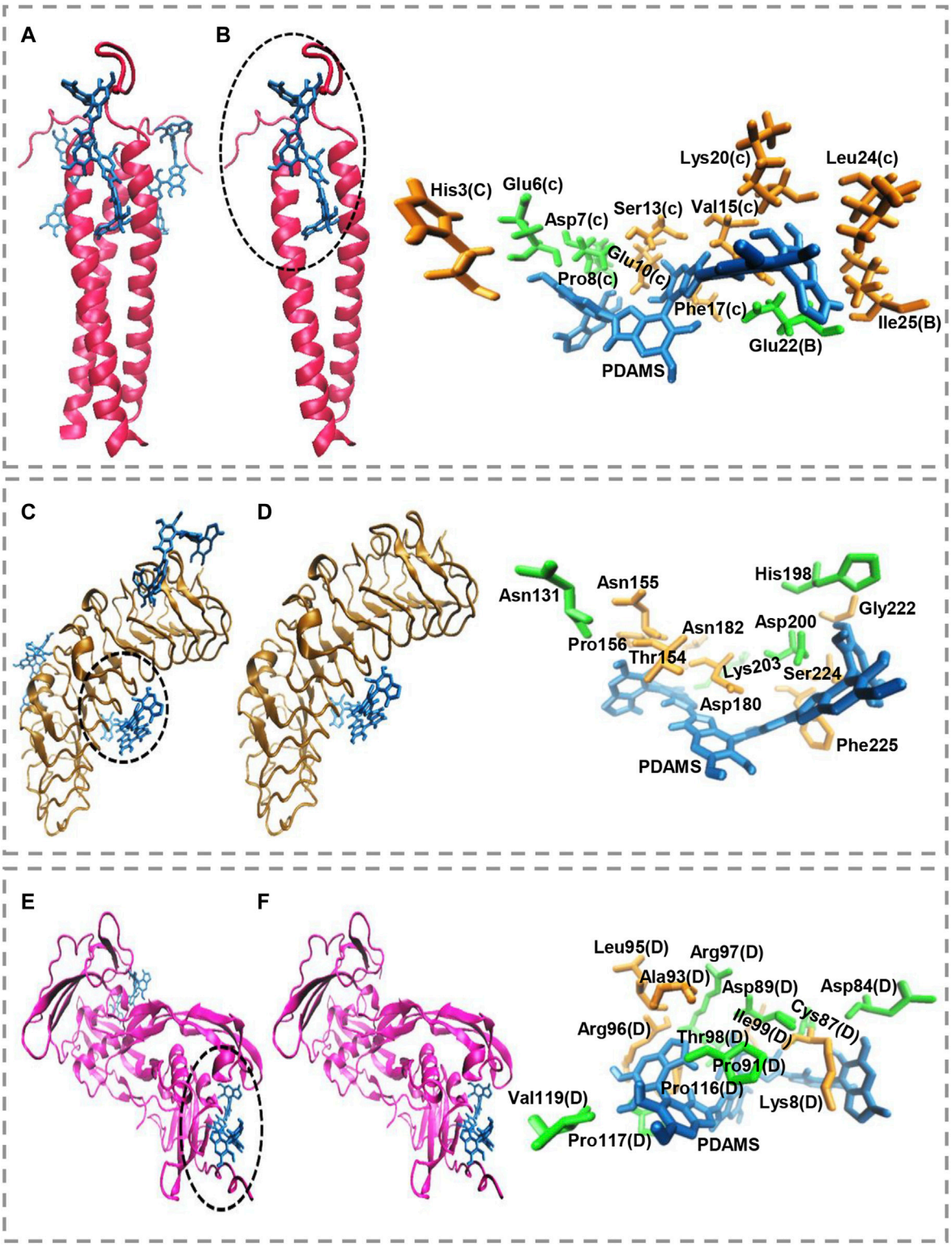

FIGURE 3 | Molecular docking simulation of PDAMS binding to target proteins. The PDAMS is shown as licorice in blue as well as Matrilin-1, Decorin, and BMP2 are shown as cartoon in red, ochre, and magenta, respectively. The main driving forces to form the target proteins-PDAMS complex are Van der Waals interaction and hydrogen bond. Van der Waals interaction and hydrogen bond are shown in orange and green, respectively **(A)** Matrilin-1 interaction with PDAMS **(B)** PDAMS is located between two α-helixes of Matrilin-1 at the head of the coiled-coil. The best mode of PDAMS interaction with Matrilin-1 in the binding site **(C)** Decorin interaction with PDAMS **(D)** The best mode of PDAMS binding to Decorin and the specific interactions in the binding site **(E)** BMP2 interaction with PDAMS **(F)** The best mode of PDAMS interaction with BMP2 and the specific interactions in the binding site.

accelerates degradation than dense structures (Anderson and Shive, 2012).

Potential of particles to support the biomineralization of hydroxyapatite-like layers can make them suitable for hard tissue repair. Also, biomimetic hydroxyapatite has found versatile application due to lack of immune rejection, trauma, and limited supply, among other factors exhibited in other hydroxyapatite sources (Li et al., 2008; Ghorbani et al., 2020). Bioactivity of the nanostructured-PDAMS after immersion of particles in the SBF solution for 4 weeks was shown in **Figure 2C–F**. From the FE-SEM examinations, it was observed that a layer of calcium phosphates with a nanoscale structure has been homogeneously precipitated on the surface of microspheres. The biomimetic mineralization of hydroxyapatite was confirmed by the XRD analysis. According to XRD spectra, the immersion of microspheres in the SBF solution led to the absorption of minerals. The appearance of peaks at 31.37, 39.57, 45.21, and 50.13° attributed to the reflections of (211), (130), (222), and (231) crystalline plates, respectively, which was accompanied with reduction in intensity of the amorphous peak of PDAMS at 2θ angles of approximately 20°. **Figure 2F** presents a schematic of biomineralization. When the microspheres immerse in the SBF solution, PDAMS releases H^+ into the media. Then, negatively surface charge and free catecholamine moieties tend to absorb calcium ions from media and reduce the system's energy. Therefore, the deposited calcium changes the surface charge and provides a suitable site for absorbing phosphate ions and forming the hydroxyapatite layer (Ding et al., 2016). Also, void space in pomegranate-like PDAMS provides a higher surface area to facilitate the absorption and diffusion of body fluids (Liu et al., 2014) to form biomimetic hydroxyapatite.

Molecular docking calculations show the surface of the target proteins structurally adapt to PDAMS's surface (**Figure 3**). In other words, considering the real size of the PDAMS, there is a structural complementary between the surface of the PDAMS and the target proteins. As shown in **Figure 3A**, Matrilin-1 binds to PDAMS from the head of the α-helical coiled-coil. Docking calculations show the PDAMS are located between two α-helixes (**Figure 3B**). The computations indicate the identical behavior of each two α-helixes interaction with PDAMS since Matrilin-1 is a homotrimer. The best mode of PDAMS interaction with Matrilin-1 considering the pose clustering of docking calculations is shown in **Figure 3B**. Docking analysis demonstrates that van der Waals interaction and hydrogen bond are the main driving forces for Matrilin-1 binding to the PDAMS surface.

As shown in **Figure 3C**, PDAMS is located on the surface of the Decorin. Molecular docking calculations demonstrate the entire Decorin surface is prone to interact with the PDAMS. The best pose clustering of docking simulations is considered to show the details of Decorin interaction with PDAMS (**Figure 3D**). Docking analysis reveals the van der Waals interaction and hydrogen bond are the main driving forces for Decorin binding to the PDAMS surface. BMP2 interaction with PDAMS calculated by docking simulation is also shown in **Figure 3E**. Docking calculations illustrate the lateral surfaces of BMP2 interact with PDAMS. The best pose clustering of docking calculations is considered to show the details of BMP2 interaction with PDAMS (**Figure 3F**). Docking analysis indicates the van der Waals interaction and hydrogen bond are the main driving forces for BMP2 binding to the PDAMS surface.

PDAMS's chemical structure and surface property are the main reasons for the predominance of obtained driving forces in the complex formation between PDAMS and target proteins. Also, the theoretical binding energy for all proteins indicates the binding process is spontaneous. The obtained value for PDAMS interaction with Matrilin-1, Decorin, and BMP2 is -39.71 kJ mol^{-1}, -40.96 kJ mol^{-1}, and -45.98 kJ mol^{-1}, respectively. Thus, docking simulations demonstrate PDAMS has a greater affinity to the bone protein than the cartilage protein. Hence, it suggests that more bone protein attaches to the surface of PDAMS. However, altogether, there is desirable structural compatibility between target proteins and PDAMS. Therefore, the structural adaptation will lead to forming a layer of proteins on the PDAMS surface, which theoretically suggested boosting the application of PDAMS in bone and cartilage repair.

CONCLUSION

In this study, a facile method was applied to synthesize 3D pomegranate-like PDAMS. The nanostructured microspheres were synthesized with self-oxidative polymerization of dopa-HCl in alkali media. In this method, the pH was controlled and fixed to 8.5 during the polymerization process that was led to the homogeneous agglomeration of nano-sized spheres and formation of tunable and monodisperse micron-sized particles with uniform spherical shape and porous microstructure. The bioinspired-microspheres showed *in-vitro* degradation within 4 weeks; in addition, these microspheres provide active sites for nucleation of hydroxyapatite-like layers. Molecular docking calculations indicate that target proteins have structural complementary with PDAMS and make complex through a spontaneous process that suggests boosting the application of PDAMS in bone and cartilage repair. This work demonstrated that pomegranate-like PDAMS offer a substrate with initial physicochemical and *in-vitro* properties and facilitate further pre-clinical and clinical investigations for hard tissue repair.

DATA AVAILABILITY STATEMENT

The original contributions presented in the study are included in the article/supplementary material, further inquiries can be directed to the corresponding author.

AUTHOR CONTRIBUTIONS

Ideas and evolution of overarching goals, development and creation of models, conducting an investigation process,

specifically data collection and analysis, presentation of the research work, and preparation of the manuscript have been done by FG and BG. Leadership responsibility for the activity planning and execution, including mentorship external to the core team and acquisition of the financial support for the project leading to this publication have been performed by CL.

FUNDING

This work was financially supported by the Medical Research Council *via* UCL Therapeutic Acceleration Support (TAS) Fund (project no: 564022); and Engineering and Physical Sciences Research Council via DTP CASE Programme (Grant no: EP/T517793/1).

REFERENCES

Abbasi-Tajarag, K., Divsalar, A., Saboury, A. A., Ghalandari, B., and Ghourchian, H. (2016). Destructive Effect of Anticancer Oxali-Palladium on Heme Degradation Through the Generation of Endogenous Hydrogen Peroxide. *J. Biomol. Struct. Dyn.* 34, 2493–2504. doi:10.1080/07391102.2015.1121408

Anderson, J. M., and Shive, M. S. (2012). Biodegradation and Biocompatibility of PLA and PLGA Microspheres. *Adv. Drug Deliv. Rev.* 64, 72–82. doi:10.1016/j.addr.2012.09.004

Blekemolen, M., Tark-Dame, M., and Takken, F. (2018). Visualization and Quantification of Cell-To-Cell Movement of Proteins in Nicotiana Benthamiana. *BIO-PROTOCOL.* 8, e3114. doi:10.21769/BioProtoc.3114

Dames, S. A., Kammerer, R. A., Wiltscheck, R., Engel, J., and Alexandrescu, A. T. (1998). NMR Structure of a Parallel Homotrimeric Coiled Coil. *Nat. Struct. Mol. Biol.* 5, 687–691. doi:10.1038/90444

De Guzman, M. R., Andra, C. K. A., Ang, M. B. M. Y., Dizon, G. V. C., Caparanga, A. R., Huang, S.-H., et al. (2021). Increased Performance and Antifouling of Mixed-Matrix Membranes of Cellulose Acetate With Hydrophilic Nanoparticles of Polydopamine-Sulfobetaine Methacrylate for Oil-Water Separation. *J. Membr. Sci.* 620, 118881. doi:10.1016/j.memsci.2020.118881

Deng, Y., Yang, W.-Z., Shi, D., Wu, M., Xiong, X.-L., Chen, Z.-G., et al. (2019). Bioinspired and Osteopromotive Polydopamine Nanoparticle-Incorporated Fibrous Membranes for Robust Bone Regeneration. *NPG Asia Mater.* 11, 39. doi:10.1038/s41427-019-0139-5

Ding, Y. H., Floren, M., and Tan, W. (2016). Mussel-Inspired Polydopamine for Bio-Surface Functionalization. *Biosurface and Biotribology.* 2, 121–136. doi:10.1016/j.bsbt.2016.11.001

Gholami Derami, H., Gupta, P., Weng, K. C., Seth, A., Gupta, R., Silva, J. R., et al. (2021). Reversible Photothermal Modulation of Electrical Activity of Excitable Cells Using Polydopamine Nanoparticles. *Adv. Mater.* 33, 2008809. doi:10.1002/adma.202008809

Gholamian, A., Divsalar, A., Saiedifar, M., Ghalandari, B., Saboury, A. A., and Koohshekan, B. (2017). Generation of Reactive Oxygen Species via Inhibition of Liver Catalase by Oxalli-Palladium: A Spectroscopic and Docking Study. *Process Biochem.* 52, 165–173. doi:10.1016/j.procbio.2016.10.012

Ghorbani, F., Zamanian, A., and Aidun, A. (2020). Conductive Electrospun Polyurethane-Polyaniline Scaffolds Coated With Poly(vinyl Alcohol)-GPTMS Under Oxygen Plasma Surface Modification. *Mater. Today Commun.* 22, 100752. doi:10.1016/j.mtcomm.2019.100752

Ghorbani, F., Zamanian, A., Behnamghader, A., and Daliri-Joupari, M. (2019a). Bone-Like Hydroxyapatite Mineralization on the Bio-Inspired PDA Nanoparticles Using Microwave Irradiation. *Surf. Inter.* 15, 38–42. doi:10.1016/j.surfin.2019.01.007

Ghorbani, F., Zamanian, A., Behnamghader, A., and Joupari, M. D. (2019b). A Facile Method to Synthesize Mussel-Inspired Polydopamine Nanospheres as an Active Template for *In Situ* Formation of Biomimetic Hydroxyapatite. *Mater. Sci. Eng. C.* 94, 729–739. doi:10.1016/j.msec.2018.10.010

Gong, F., Zhang, J., Ding, L., Yang, Z., and Liu, X. (2017). Mussel-Inspired Coating of Energetic Crystals: A Compact Core-Shell Structure With Highly Enhanced Thermal Stability. *Chem. Eng. J.* 309, 140–150. doi:10.1016/j.cej.2016.10.020

Han, L., Wang, M., Li, P., Gan, D., Yan, L., Xu, J., et al. (2018). Mussel-Inspired Tissue-Adhesive Hydrogel Based on the Polydopamine-Chondroitin Sulfate Complex for Growth-Factor-Free Cartilage Regeneration. *ACS Appl. Mater. Inter.* 10, 28015–28026. doi:10.1021/acsami.8b05314

Hasani-Sadrabadi, M. M., Sarrion, P., Nakatsuka, N., Young, T. D., Taghdiri, N., Ansari, S., et al. (2019). Hierarchically Patterned Polydopamine-Containing Membranes for Periodontal Tissue Engineering. *ACS Nano.* 13, 3830–3838. doi:10.1021/acsnano.8b09623

Humphrey, W., Dalke, A., and Schulten, K. (1996). VMD: Visual Molecular Dynamics. *J. Mol. Graphics.* 14, 33–38. doi:10.1016/0263-7855(96)00018-5

Iqbal, Z., Lai, E. P. C., and Avis, T. J. (2012). Antimicrobial Effect of Polydopamine Coating on *Escherichia coli*. *J. Mater. Chem.* 22, 21608–21613. doi:10.1039/c2jm34825j

Ji, S., Huang, J., Li, T., Luo, X., and Zheng, F. (2021). A Strategy to Synthesize Pomegranate-Inspired Hollow Mesoporous Molecularly Imprinted Nanoparticles by Organic-Organic Self-assembly of Dopamine. *Nano Select.* 2, 328–337. doi:10.1002/nano.202000185

Jiang, X., Wang, Y., and Li, M. (2014). Selecting Water-Alcohol Mixed Solvent for Synthesis of Polydopamine Nano-Spheres Using Solubility Parameter. *Sci. Rep.* 4, 6070. doi:10.1038/srep06070

Ju, K.-Y., Lee, Y., Lee, S., Park, S. B., and Lee, J.-K. (2011). Bioinspired Polymerization of Dopamine to Generate Melanin-Like Nanoparticles Having an Excellent Free-Radical-Scavenging Property. *Biomacromolecules.* 12, 625–632. doi:10.1021/bm101281b

Kanitthamniyom, P., and Zhang, Y. (2018). Application of Polydopamine in Biomedical Microfluidic Devices. *Microfluid Nanofluid.* 22, 24. doi:10.1007/s10404-018-2044-6

Keller, S., Nickel, J., Zhang, J.-L., Sebald, W., and Mueller, T. D. (2004). Molecular Recognition of BMP-2 and BMP Receptor IA. *Nat. Struct. Mol. Biol.* 11, 481–488. doi:10.1038/nsmb756

Li, X., Xie, J., Yuan, X., and Xia, Y. (2008). Coating Electrospun Poly(ε-Caprolactone) Fibers With Gelatin and Calcium Phosphate and Their Use as Biomimetic Scaffolds for Bone Tissue Engineering. *Langmuir.* 24, 14145–14150. doi:10.1021/la802984a

Liu, N., Lu, Z., Zhao, J., Mcdowell, M. T., Lee, H.-W., Zhao, W., et al. (2014). A Pomegranate-Inspired Nanoscale Design for Large-Volume-Change Lithium Battery Anodes. *Nat. Nanotech.* 9, 187–192. doi:10.1038/nnano.2014.6

Liu, X., Cao, J., Li, H., Li, J., Jin, Q., Ren, K., et al. (2013a). Mussel-Inspired Polydopamine: A Biocompatible and Ultrastable Coating for Nanoparticles *In Vivo*. *ACS Nano.* 7, 9384–9395. doi:10.1021/nn404117j

Liu, Y., Ai, K., Liu, J., Deng, M., He, Y., and Lu, L. (2013b). Dopamine-Melanin Colloidal Nanospheres: An Efficient Near-Infrared Photothermal Therapeutic Agent for *In Vivo* Cancer Therapy. *Adv. Mater.* 25, 1353–1359. doi:10.1002/adma.201204683

Liu, Y., Choi, C. K. K., Hong, H., Xiao, Y., Kwok, M. L., Liu, H., et al. (2021). Dopamine Receptor-Mediated Binding and Cellular Uptake of Polydopamine-Coated Nanoparticles. *ACS Nano.* 15, 13871–13890. doi:10.1021/acsnano.1c06081

Luo, R., Yu, Q., Lu, Y., Zhang, M., Peng, T., Yan, H., et al. (2019). 3D Pomegranate-Like TiN@graphene Composites With Electrochemical Reaction Chambers as Sulfur Hosts for Ultralong-Life Lithium-Sulfur Batteries. *Nanoscale Horiz.* 4, 531–539. doi:10.1039/C8NH00343B

Morris, G. M., Huey, R., Lindstrom, W., Sanner, M. F., Belew, R. K., Goodsell, D. S., et al. (2009). AutoDock4 and AutoDockTools4: Automated Docking With Selective Receptor Flexibility. *J. Comput. Chem.* 30, 2785–2791. doi:10.1002/jcc.21256

Nurunnabi, M., Khatun, Z., Nafiujjaman, M., Lee, D.-g., and Lee, Y.-k. (2013). Surface Coating of Graphene Quantum Dots Using Mussel-Inspired Polydopamine for Biomedical Optical Imaging. *ACS Appl. Mater. Inter.* 5, 8246–8253. doi:10.1021/am4023863

Park, J., Lee, S. J., Jung, T. G., Lee, J. H., Kim, W. D., Lee, J. Y., et al. (2021). Surface Modification of a Three-Dimensional Polycaprolactone Scaffold by Polydopamine, Biomineralization, and BMP-2 Immobilization for Potential Bone Tissue Applications. *Colloids Surf. B: Biointerfaces.* 199, 111528. doi:10.1016/j.colsurfb.2020.111528

Ruan, J., Liu, H., Chen, B., Wang, F., Wang, W., Zha, Z., et al. (2021). Interfacially Engineered ZnxMn1-xS@Polydopamine Hollow Nanospheres for Glutathione

Depleting Photothermally Enhanced Chemodynamic Therapy. *ACS Nano.* 15, 11428–11440. doi:10.1021/acsnano.1c01077

Salomäki, M., Marttila, L., Kivelä, H., Ouvinen, T., and Lukkari, J. (2018). Effects of pH and Oxidants on the First Steps of Polydopamine Formation: A Thermodynamic Approach. *J. Phys. Chem. B.* 122, 6314–6327. doi:10.1021/acs.jpcb.8b02304

Scott, P. G., McEwan, P. A., Dodd, C. M., Bergmann, E. M., Bishop, P. N., and Bella, J. (2004). Crystal Structure of the Dimeric Protein Core of Decorin, the Archetypal Small Leucine-Rich Repeat Proteoglycan. *Proc. Natl. Acad. Sci.* 101, 15633–15638. doi:10.1073/pnas.0402976101

Shafaei, Z., Abazari, O., Divsalar, A., Ghalandari, B., Poursoleiman, A., Saboury, A. A., et al. (2017). Effect of a Synthesized Amyl-Glycine1, 10-Phenanthroline Platinum Nitrate on Structure and Stability of Human Blood Carrier Protein, Albumin: Spectroscopic and Modeling Approaches. *J. Fluoresc.* 27, 1829–1838. doi:10.1007/s10895-017-2120-4

Steeves, A. J., and Variola, F. (2020). Elucidating Structure-Function Relationships Governing the Interfacial Response of Human Mesenchymal Stem Cells to Polydopamine Coatings. *J. Mater. Chem. B.* 8, 199–215. doi:10.1039/C9TB02188D

Sun, H., Dong, J., Wang, Y., Shen, S., Shi, Y., Zhang, L., et al. (2021). Polydopamine-Coated Poly(l-Lactide) Nanofibers With Controlled Release of VEGF and BMP-2 as a Regenerative Periosteum. *ACS Biomater. Sci. Eng.* 7, 4883–4897. doi:10.1021/acsbiomaterials.1c00246

Tabata, Y., and Ikada, Y. (2005). Phagocytosis of Polymer Microspheres by Macrophages. *New Polym. Mater.* 94, 107–141. doi:10.1007/BFb0043062

Tang, P., Han, L., Li, P., Jia, Z., Wang, K., Zhang, H., et al. (2019). Mussel-Inspired Electroactive and Antioxidative Scaffolds with Incorporation of Polydopamine-Reduced Graphene Oxide for Enhancing Skin Wound Healing. *ACS Appl. Mater. Inter.* 11, 7703–7714. doi:10.1021/acsami.8b18931

Tian, H., Wang, Z., Chen, Y., Shao, J., Gao, T., and Cai, S. (2018). Polydopamine-Coated Main-Chain Liquid Crystal Elastomer as Optically Driven Artificial Muscle. *ACS Appl. Mater. Inter.* 10, 8307–8316. doi:10.1021/acsami.8b00639

Trott, O., Olson, A. J., and Vina, A. (2009). AutoDock Vina: Improving the Speed and Accuracy of Docking With a New Scoring Function, Efficient Optimization, and Multithreading. *J. Comput. Chem.* 31, NA. doi:10.1002/jcc.21334

Wang, L., Liu, S., Ren, C., Xiang, S., Li, D., Hao, X., et al. (2021). Construction of Hollow Polydopamine Nanoparticle Based Drug Sustainable Release System and its Application in Bone Regeneration. *Int. J. Oral Sci.* 13, 27. doi:10.1038/s41368-021-00132-6

Xiong, S., Wang, Y., Yu, J., Chen, L., Zhu, J., and Hu, Z. (2014). Polydopamine Particles for Next-Generation Multifunctional Biocomposites. *J. Mater. Chem. A.* 2, 7578–7587. doi:10.1039/c4ta00235k

Yan, J., Wu, R., Liao, S., Jiang, M., and Qian, Y. (2020). Applications of Polydopamine-Modified Scaffolds in the Peripheral Nerve Tissue Engineering. *Front. Bioeng. Biotechnol.* 8, 590998. doi:10.3389/fbioe.2020.590998

Yan, J., Yang, L., Lin, M. F., Ma, J., Lu, X., and Lee, P. S. (2013). Polydopamine Spheres as Active Templates for Convenient Synthesis of Various Nanostructures. *Small.* 9, 596–603. doi:10.1002/smll.201201064

Zhao, D., Kim, J. F., Ignacz, G., Pogany, P., Lee, Y. M., and Szekely, G. (2019). Bio-Inspired Robust Membranes Nanoengineered from Interpenetrating Polymer Networks of Polybenzimidazole/Polydopamine. *ACS Nano.* 13, 125–133. doi:10.1021/acsnano.8b04123

Zhou, J., Guo, X., Zheng, Q., Wu, Y., Cui, F., and Wu, B. (2017). Improving Osteogenesis of Three-Dimensional Porous Scaffold Based on Mineralized Recombinant Human-like Collagen via Mussel-Inspired Polydopamine and Effective Immobilization of BMP-2-Derived Peptide. *Colloids Surf. B: Biointerfaces.* 152, 124–132. doi:10.1016/j.colsurfb.2016.12.041

Zhou, J., Zhang, X., Sun, J., Dang, Z., Li, J., Li, X., et al. (2018). The Effects of Surface Topography of Nanostructure Arrays on Cell Adhesion. *Phys. Chem. Chem. Phys.* 20, 22946–22951. doi:10.1039/C8CP03538E

Conflict of Interest: The authors declare that the research was conducted in the absence of any commercial or financial relationships that could be construed as a potential conflict of interest.

Publisher's Note: All claims expressed in this article are solely those of the authors and do not necessarily represent those of their affiliated organizations, or those of the publisher, the editors and the reviewers. Any product that may be evaluated in this article, or claim that may be made by its manufacturer, is not guaranteed or endorsed by the publisher.

frontiers in Bioengineering and Biotechnology

REVIEW
published: 21 December 2021
doi: 10.3389/fbioe.2021.763031

Microbial-Derived Polyhydroxyalkanoate-Based Scaffolds for Bone Tissue Engineering: Biosynthesis, Properties, and Perspectives

Jian Li[1,2†], Xu Zhang[3,4†], Anjaneyulu Udduttula[1†], Zhi Shan Fan[1], Jian Hai Chen[1,2], Antonia RuJia Sun[1] and Peng Zhang[1*]*

[1]Shenzhen Engineering Research Center for Medical Bioactive Materials, Center for Translational Medicine Research and Development, Shenzhen Institutes of Advanced Technology, Chinese Academy of Sciences, Shenzhen, China, [2]University of Chinese Academy of Sciences, Beijing, China, [3]Key Laboratory of Industrial Biocatalysis, Ministry of Education, Tsinghua University, Beijing, China, [4]Department of Chemical Engineering, Tsinghua University, Beijing, China

OPEN ACCESS

Edited by:
Derek H. Rosenzweig,
McGill University, Canada

Reviewed by:
Jing Han,
Institute of Microbiology (CAS), China
Rahul Gawri,
McGill University, Canada

***Correspondence:**
Jian Li
li.jian@siat.ac.cn
Peng Zhang
peng.zhang@siat.ac.cn

[†]These authors have contributed equally to this work

Specialty section:
This article was submitted to Biomaterials, a section of the journal Frontiers in Bioengineering and Biotechnology

Received: 23 August 2021
Accepted: 17 November 2021
Published: 21 December 2021

Citation:
Li J, Zhang X, Udduttula A, Fan ZS, Chen JH, Sun AR and Zhang P (2021) Microbial-Derived Polyhydroxyalkanoate-Based Scaffolds for Bone Tissue Engineering: Biosynthesis, Properties, and Perspectives. Front. Bioeng. Biotechnol. 9:763031. doi: 10.3389/fbioe.2021.763031

Polyhydroxyalkanoates (PHAs) are a class of structurally diverse natural biopolyesters, synthesized by various microbes under unbalanced culture conditions. PHAs as biomedical materials have been fabricated in various forms to apply to tissue engineering for the past years due to their excellent biodegradability, inherent biocompatibility, modifiable mechanical properties, and thermo-processability. However, there remain some bottlenecks in terms of PHA production on a large scale, the purification process, mechanical properties, and biodegradability of PHA, which need to be further resolved. Therefore, scientists are making great efforts *via* synthetic biology and metabolic engineering tools to improve the properties and the product yields of PHA at a lower cost for the development of various PHA-based scaffold fabrication technologies to widen biomedical applications, especially in bone tissue engineering. This review aims to outline the biosynthesis, structures, properties, and the bone tissue engineering applications of PHA scaffolds with different manufacturing technologies. The latest advances will provide an insight into future outlooks in PHA-based scaffolds for bone tissue engineering.

Keywords: polyhydroxyalkanoates, biopolyester, biodegradability, biocompatibility, synthetic biology, 3D rapid prototyping, bone tissue engineering

INTRODUCTION

Bone tissue exhibits the unique ability of constant healing and remodeling during the lifetime of an individual (Stevens, 2008). It not only provides structural support ensuring adequate load-bearing capacity for the protection of the delicate internal organs of the body but acts as a mineral reservoir for the body to regulate the concentration of key electrolytes in the blood. It is generally believed that the bone has the capacity for spontaneous regeneration for relatively small defects; however, large bone defects, caused by traumatic injury, osteonecrosis, or osseous congenital deformities, would require surgical operation for restoration. The reconstruction of large bone defects remains a great challenge for researchers and orthopedic surgeons. Traditional therapeutic approaches of bony

deficits are available, namely, using autografts, allografts, and xenografts (Fillingham and Jacobs, 2016; Raghuram et al., 2019). Autografts represent the current golden standard of bone transplantation, which possess the optimal characteristics of osteoconduction, osteoinduction, and osteointegration (Cypher and Grossman, 1996). However, their use is not without drawbacks such as supply limitation, variable resorption, and risk of donor site infection (Arrington et al., 1996; Nodarian et al., 2010). Furthermore, autografts often have limited ability to accelerate normal morphogenic and cellular events of fracture healing and remodeling (Mastrogiacomo et al., 2005). Alternatively, in some particularly important situations, when there is a large segmental bone defect, structural support is required, or when the capacity of the autograft is insufficient, allografts and xenografts can be used (Baldwin et al., 2019). A variety of problems associated with allografts and xenografts can be pathogen transmission, limited biological and mechanical properties, and rejection by the recipient's body (Gruskin et al., 2012; Shibuya and Jupiter, 2015). To circumvent the deficiencies associated as reported, the most promising approach to solve the defects of bone transplantation is to study tissue engineering and related technologies to promote bone regeneration.

Bone tissue engineering (BTE) generally involves the employment of favorable biocompatible materials, combining with cells and bioactive factors, as engineered scaffolds that provide a specific microenvironment and architecture to support and promote tissue formations *in vivo* (O'Keefe and Mao, 2011; Peric Kacarevic et al., 2020). A great number of materials including natural materials or synthetic polyesters have been investigated as possible tissue-engineered scaffolds for bone and cartilage defect repair in recent decades (Agarwal and Garcia, 2015). Currently, natural biopolymers include chitosan (CS), collagen (Col), silk fibroin (SF), and synthetic polyesters such as poly(lactic-*co*-glycolic) acid (PLGA), poly(lactic acid) (PLA), polyethylene glycol (PEG), and polyurethane (PU), which have been widely used as a scaffold matrix for bone regeneration (Soundarya et al., 2018; Bharadwaz and Jayasuriya, 2020). An ideal scaffold suitable for BTE applications should not only provide initial mechanical strength and support but should also be degraded gradually and replaced by newly formed host tissue.

Polyhydroxyalkanoates (PHAs) are a class of structurally diverse natural polyesters, synthesized by various microbes and accumulated as intracellular storage compounds of carbon and energy in response to unbalanced culture conditions (Steinbuchel and Valentin, 1995; Chen, 2009). Owing to their exceptional biodegradability, inherent biocompatibility, modifiable mechanical properties, and thermo-processability, recently, PHAs as biopolymeric biomaterials have been widely exploited to design *in vivo* implants for potential therapeutic applications, such as cardiac tissue engineering (Shijun et al., 2016; Bagdadi et al., 2018), vascular tissue engineering (S. T. Cheng, Chen, and Chen, 2008; Zonari et al., 2012), nerve conduit tissue engineering (Hinuber et al., 2014; Schaakxs et al., 2017), and drug delivery vehicles (Pramual et al., 2016; Elmowafy et al., 2019). Very importantly, there is no evidence that PHAs or their biodegradation products are carcinogenic *in vitro* or *in vivo* (Peng et al., 2011; Raza et al., 2018a). However, there remain some bottlenecks in terms of PHA production on a large scale, purity, mechanical properties, and biodegradability, which need to be further addressed to make PHAs a realistic biomaterial. Therefore, scientists are making great efforts *via* synthetic biology and metabolic engineering tools to increase the product yields of PHAs at lower cost and develop PHAs with better physiochemical characteristics to widen biomedical application ranges.

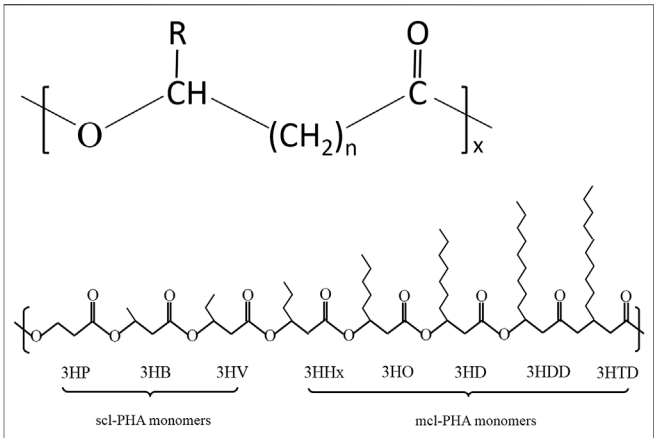

FIGURE 1 | Structure and classification of PHAs. **(A)** General molecular structure of PHAs. n-range of variation from 1 to 4, x--range of variation from 100 to 35,000, R-alkyl group (C_mH_{2m+1}) or functionalized group; **(B)** Schematic diagram of structures of PHA monomers used to synthesize short-chain-length PHA and middle-chain-length PHA.

We have divided this review into three parts. In the first part, we describe the background of PHAs including material properties, function of degradation products, teratogenicity and carcinogenicity of PHAs, and recent progress in synthetic biology and metabolic engineering on PHAs. In the second part, we summarize the manufacturing technologies for scaffold fabrication including conventional technologies and rapid prototyping. Finally, in the third part, an in-depth discussion is conducted with PHAs and PHA-based scaffolds for BTE, following the outlooks of future research emphasis.

THE BACKGROUND OF PHAS

Material Properties of PHAs

PHAs, a similar lipid-like inclusion body, were first discovered in *Bacillus megaterium* and identified as the simplest member of PHAs called poly-3-hydroxybutyrate (PHB) (Lenz and Marchessault, 2005). After that, many different types of PHAs were found and served as storage materials of carbon sources and energy in response to extreme cellular conditions (Choi et al., 2020a). With the developed understanding of PHA biosynthesis, the first commercial production of PHAs was developed by Imperial Chemical Industries (ICI), who prepared PHAs into bioplastics which could replace petroleum-based plastics because

TABLE 1 | Comparative overview of the physical properties of PHAs with conventional petroleum-based polymers.

Polymer		Melting temperature (°C)	Glass transition temperature (°C)	Elastic modulus (GPa)	Elongation to break (%)	Tensile strength (MPa)	References
Composition	**Mol%**						
Homopolymers							
PHB	100	171–180	4–10	3.5–4	0.4–5	11–40	Akaraonye et al. (2010); Ashby et al. (2002); Castilho et al. (2009); Sudesh et al. (2000)
P4HB	100	50–60	−48 to −51	149	1,000	104	Utsunomia et al. (2020); Jiang et al. (2012)
PHO	100	61	-	-	-	6–10	
Copolymers							
P(3HB-*co*-3HV)							
3HB:3HV	91–97: 3–10	162–170	−4 to 2.2	-	-	19–38	Zhang et al. (2009)
	80–90: 10–20	137–156	−1 to 1.7	0.8–1.2	50–100	20–32	Bengtsson et al. (2010); Zakaria et al. (2010)
	70–80: 20–30	138–139	−6 to −0.1	1.37	30	70	Chanprateep et al. (2010); Ciesielski et al. (2015)
P(3HB-*co*-4HB)							
3HB:4HB	95:5	169	−2	1.23	10.7	1.36	Anjum et al. (2016); Chanprateep et al. (2010)
	90:10	159	-	-	-	24	Anjum et al. (2016); Doi et al. (1990)
	84:16	152	−8	-	-	26	Doi et al. (1990)
	76:24	161	−5	0.79	22.2	14	Chanprateep et al. (2008)
	36:64	50	−35	30	-	17	Chanprateep et al. (2008)
	10:90	50	−42	100	-	65	Chanprateep et al. (2008)
P(3HB-*co*-3HA)							
3HB:3HA	98:2	150–167	1	0.95	16	26	Chen et al. (2006)
	94–96: 4–6	133	−8	0.2	680	17	Anjum et al. (2016); Hokamura et al. (2015)
P(3HB-*co*-3HP)	79–87: 13–21	119.8–162.8	−3.1 to −2.1	-	-	-	Yu et al. (2007)
P(3HB-*co*-3HHx)	83–90: 10–17	61–127	−1.2	0.5	113–400	9.4–21	Anjum et al. (2016); Zhang et al. (2009)
Terpolymers							
P(3HB-*co*-3HV-*co*-4HB)							
3HB:3HV:4HB	73:8:19	131	−10.0	0.10	316	12	Kumar et al. (2015)
	63:4:33	–	−14.0	0.10	937	9	
	49:18:33	–	−16.0	0.03	554	2	
	12:12:76	87.3	−21.1	0.14	9	4	Chanprateep and Kulpreecha (2006)
	11: 23–24: 55–56	92–100	−15 to −17	0.4–0.6	3–5	9–10	
	10:40:50	88	−13.7	0.12	300	9	
	4:3:93	55	−51.6	0.13	430	14	
P(3HB-*co*-3HV-*co*-3HHx)							
3HB:3HV:3HHx	75:13:12	101	−1.9	0.07–0.1	740–833	12.8–14.3	Bengtsson et al. (2010); Zhang et al. (2009)
	70:25:5	129	−7.2	–	–	–	
	67:20:13	58–68	−6 to −3.6	–	–	–	
	56:43:1	155	−5.5	–	–	–	
	48:24:28	54	−5.1	–	–	–	
	94:3:3	153–168	2.0	–	–	–	
High-density PE	100	112–132	–	0.4–1.0	12–700	18–33	Anjum et al. (2016); Castilho et al. (2009)
Low-density PE	100	88–100	−36	0.05–0.2	126–600	10–78	Anjum et al. (2016); Watanabe et al. (2009)
PP	100	170–176	−10	0.6–1.7	400–900	27–38	Singh et al. (2015)
Polystyrene	100	110–240	100	3.0–3.1	3–4	50	Capek (2005); Singh et al. (2015)
Polyvinylchloride	100	100–260	82	3.4	20–80	10–60	Singh et al. (2015)
PU	100	195	3400	0.004	-	38	Tian (2020)
Nylon-6,6	100	265	–	2.8	60	83	Anjum et al. (2016); Menezes et al. (2018); Singh et al. (2015)
Polypropylene-terephthalate	-	262	3,400	2.2	7,300	56	Anjum et al. (2016)

of the oil crisis during the 1970s and because they have physical properties similar to those of polypropylene (PP) (Choi et al., 2020b).

To date, more than 150 different PHA monomers have been reported. Depending upon the number of carbon atoms in the PHA monomer, there are three types: short chain length (scl-PHAs), medium chain length (mcl-PHAs), and long chain length (lcl-PHAs) (Li Z. et al., 2016; Lim et al., 2017). **Figure 1** shows the general molecular structure of PHAs with their classification. As a class of polymers, PHAs not only have similarities in their physiochemical characteristics with conventional petroleum-based polymers like PP but also possess unique properties compared with other biopolyesters. A variety of PHAs offers a wide range of performance from hard crystalline to elastic. **Table 1** summarizes the performance comparison of different PHAs with petroleum-derived polymers.

scl-PHAs are stiff and fragile due to their higher degree of crystallinity in the range of 55%–80% (Anjum et al., 2016; Mozejko-Ciesielska and Kiewisz, 2016). As a member of the scl-PHA family, the properties of PHB have been explained thoroughly because of its wide study. Compared with petroleum-based polymers such as PP, PHB has good thermoplastic properties, but its mechanical properties including Young's modulus and tensile strength are poor. Moreover, PHB is optically pure and possesses piezoelectric material properties that contribute to the process of inducing osteogenesis (Philip et al., 2007; Bugnicourt et al., 2014). In contrast, another scl-PHA, poly-4-hydroxybutyrate (P4HB), possesses strong and malleable mechanical properties and has a similar tensile strength to polyethylene (PE). It has extremely elastic properties with elongation at break of approximately 1,000%, compared with PHB, which has an elongation at break of less than 10%. The material properties of P4HB can be changed when combined with other hydroxyl acids (Martin and Williams, 2003). Nevertheless, the high crystallinity, high melting point (T_m), and low glass transition temperature (T_g) make the scl-homopolymers relatively stiff and brittle and limit the range of applications. Therefore, the introduction of different secondary PHA monomers such as 3-hydroxypropionate (3HP) and 3-hydroxyvalerate (3HV) into the copolymers is an alternative strategy, and it greatly increases the flexibility and toughness of the polymer.

mcl-PHAs have properties that are great different from those of scl-PHAs. mcl-PHAs are flexible and behave as semi-crystalline elastomeric materials with low thermal temperature, low tensile strength, and higher elongation at break, for example, poly(3-hydroxyhexanoate-*co*-3-hydroxyoctanoate) (P3HHx3HO) (Rai et al., 2011; Reddy et al., 2003). mcl-PHAs serve as an elastomeric biomaterial under a certain side chain length. With the further increase of the side chain length, they become more sticky or viscous (Hazer and Steinbuchel, 2007). Furthermore, there are also scl–mcl-copolymers composed of scl- and mcl-monomers, for example, PHBHHx, which is suitable for different commercial/biomedical applications because it combines the thermomechanical properties of PE with the physiochemical properties of polyesters. Also, compared with the ductility and process ability of copolymers, those of PHA terpolymers are significantly improved. The PHA terpolymer poly(3-hydroxybutyrate-*co*-3-hydroxyvalerate-*co*-3-hydroxyhexanoate) (PHBVHHx) was synthesized and contained 39 mol% 3HV and 3 mol% 3HHx, whose tensile strength was 12 MPa and elongation at break was 408% while having no melting point. PHAs can be easily soluble in chloroform and other chlorinated solvents.

Biocompatibility and Biodegradability of PHAs

The biocompatibility of the material means that it does not have any adverse effect on a living organism. Good biocompatibility of biomaterials for tissue engineering is a prerequisite for transplantation in humans or animals. Various available PHA materials were tested to demonstrate their biocompatibility both *in vitro* and *in vivo*. It is easy to prove the biocompatibility of PHB and P4HB because their degradable products, 3HB and 4HB, are natural metabolites in the human body. 3HB exists in concentrations of 0.03–0.1 mg/ml in human blood, while 4HB is widely distributed in the brain, lung, heart, liver, muscle, and kidney and excreted as carbon dioxide (Nelson et al., 1981). Moreover, low-molecular-weight PHB complexed with low-density protein and albumin has also been found in blood serum. Cell cycle regulations are important for cell survival. A study by Ahmed et al. (2010) indicated that PHB was good for nerve regeneration, while PHBV was in favor of BTE. Furthermore, another type of PHA known as PHBVHHx has been discovered and tested with the human keratinocyte cell line HaCaT and human umbilical cord Wharton's jelly-derived mesenchymal stem cells (WJ-MSCs) (Ji et al., 2009; Ji et al., 2008). It was found that cell adhesion and proliferation on PHBVHHx membranes were more significant than other tested materials. In addition, the PHBVHHx film also supported the osteogenesis of MSCs (Hu et al., 2009).

Biopolymers as biomaterials should come with the ability to disintegrate themselves into nonhazardous products to prevent inflammatory responses *in vivo*, which is another important aspect of tissue engineering. Hence, information regarding the biodegradation of PHAs is momentous for its exploitation as a biomaterial. The family of PHAs could be decomposed by many enzymes such as lipases and hydrolytic enzymes into their monomers or oligomers. Chenet et al. (2017) found that PHB scaffolds implanted subcutaneously in mice were resorbed 8 weeks after implantation. Simultaneously, osteoid tissue and blood vessel ingrowth into the scaffold was observed. Moreover, through subcutaneous implantation in rabbits, the *in vivo* tissue reaction and biodegradation of PHBHHx, PLA, PHB, PHBHHx, and PEG blends of 1:1 and 1:5 were evaluated. It was shown that the degradation of PLA was the fastest, followed by PHBHHx and finally PHB (Qu et al., 2006). The results show that PHB has the slowest degradation rate because of its higher crystallinity. Thus, the intrinsic biodegradable properties of PHAs make them promising biomaterials in medical applications.

However, biodegradation of PHAs is not only affected by their properties, such as stereoregularity, crystallinity, chemical composition, and surface accessibility to PHA depolymerase,

TABLE 2 | Degradation products of PHAs and their applications.

Degradation products of PHAs	Functions and applications	References
OHB, O3HB4HB, OHBHHx, OmclHA	OHAs in concentrations lower than 20 mg/L did not significantly affect L929 cell viability, while OHAs over 40 mg/L reduced cell viability with more apoptosis, more cell death, delayed cell cycle, and reduced cell proliferation. The cytotoxicity of OHAs decreased with increasing OHA side-chain length	Sun et al. (2007)
OHB, O3HB4HB, OHBHHx	The effect of OHBHHx was the best among all materials tested for gap junction intercellular communication of cells; OHBHHx was especially not harmful to the beta cells and could upregulate extracellular insulin secretion	Yang et al. (2002); Yang et al. (2002)
3-Hydroxybutyrate (3HB)	The cell proliferation and DNA synthesis of cell lines including murine fibroblast L929 cells, human umbilical vein endothelial cells (HUVECs), and rabbit articular cartilages (RACs) were enhanced when treated with concentrations of 3HB ranging from 5 to 100 mg/L. Furthermore, 3HB could obviously inhibit apoptosis and necrosis of L929 cells in high-density cultures	Cheng et al. (2006); Cheng et al. (2005)
3HB	ALP and calcium deposition, which are important biomarkers of mesenchymal stem cell osteogenic differentiation, were significantly intensified in direct proportion to the concentration of 3HB when it was lower than 10 mg/L. Besides, 3HB was an effective bone growth-stimulating agent and able to increase bone mass in mice under a microgravity environment	Cao et al. (2014); Zhao et al. (2007)
3HB	3HB could be utilized as an efficient enzyme-stabilizing and enzyme-protecting additive	O'Connor et al. (2013)
3HB	3HB could inhibit the NLRP3 inflammasome by preventing K+ efflux and reducing ASC oligomerization and speck formation to decrease interleukin IL-1β and IL-18 production in human monocytes	Youm et al. (2015)
3HB	3HB was found to attenuate atherosclerosis in mice by reducing the proportion of M1 macrophage and promote cholesterol efflux through its receptor G-protein-coupled receptor GPR109A	Zhang et al. (2021)
3HB	Increasing 3HB level attenuated NLRP3 inflammasome formation and antagonized proinflammatory cytokine-triggered mitochondrial dysfunction and fibrosis to ameliorate heart failure with preserved ejection fraction (HFpEF) pathogenesis	Deng et al. (2002)
3-Hydroxydecanoic acid (3HD)	Conjugation of anticancer DP18L peptide with 3HD derived from mcl-PHA enhances its anticancer activity; (R)-3-hydroxyalkanoic acids with 9 and 10 carbons were most effective at increasing DP18L activity	Szwej et al. (2015)
3-Hydroxyoctanoic acid (3HO)	The presence of the carboxylic group was found important for antimicrobial activity; 3HO derivatives were inhibitory against a variety of microorganisms but not to mammalian cells	Radivojevic et al. (2016)
3HB methyl ester (3HBME)	3HBME was able to inhibit cell apoptosis under glucose-free condition, rescued activities of mitochondrial respiratory chain complexes that were impaired in Alzheimer's disease patients, and decreased the generation of ROS	Zhang et al. (2013)
3HBME	3HBME could be used as an effective neural protective agent to obviously decrease the apoptosis ratio of mouse glial cells by signaling pathways related to the elevation of cytosolic Ca^{2+} concentration. Mice treated with HBME performed distinctly better in the Morris water maze than either the negative controls or positive controls. It indicated that 3HBME improved learning and memory of mice	Obruca et al. (2016); Xiao et al. (2007)
3HBME	3HBME attenuated the development of osteoporosis in mice under a microgravity environment, helping prevent deterioration of bone microstructure and mechanical property	Cao et al. (2014)

but also by a variety of factors including surface area, physical shape and form, pH, temperature, and moisture (Sudesh et al., 2000; Singh et al., 2019).

Degradation Products of PHAs and Their Biological Functions

The cellular response of PHA degradation products including oligomers (oligo-hydroxyalkanoates, OHAs) and monomers (3-hydroxyalkanoic acids, HAs) is a key factor reflecting the biocompatibility of PHA for tissue engineering applications. The cell viability of mouse fibroblast L929 cells was not significantly affected by oligomer concentration without exceeding 20 mg/L, while the concentration of OHAs exceeds 40 mg/L, resulting in decreased cell viability, increased apoptosis, increased death, and prolonged cell cycle (Sun et al., 2007). 3-Hydroxybutyrate (3HB) is the main degradation product of PHB or its copolymers, namely, a ketone body, which is produced by the breakdown of long-chain fatty acids in the liver. 3HB has a short half-life and good tolerance to humans. Therefore, 3HB as a kind of nutrition or dietary compositions can be administered orally or intravenously to increase the level of ketone body in the blood to treat some diseases (Martin and Williams, 2003). A study showed that cell proliferation and DNA synthesis for several cell types were enhanced when treated with concentrations of 3HB ranging from 5 to 100 mg/L (Cheng et al., 2005). Furthermore, 3HB had an obviously stimulatory effect on cell cycle progression mediated by improving the intracellular Ca^{2+} concentration (Cheng et al., 2006). **Table 2** summarizes the degradation products of PHAs and their applications both *in vitro* and *in vivo*.

The effect of 3HB as an osteopromotive factor on bone formation was demonstrated. The pivotal biomarkers including alkaline phosphatase (ALP) activity and calcium nodule deposition of osteogenesis of murine pre-osteoblast MC3T3-E1 were remarkably intensified, correlating linearly with the concentration of 3HB when it was no more than

10 mg/L. *In vivo*, serum calcium deposition and ALP activity were significantly increased when the 3-month-old ovariectomized rats were treated with 3HB for 12 weeks; osteocalcin was also reduced. Simultaneously, the femur biomechanics was obviously enhanced due to the improved bone mineral density and trabecular bone volume (Zhao et al., 2007). On top of that, the effect of 3HB and its derivative 3-hydroxybutyrate methyl ester (3HBME) on mice was investigated under a simulated microgravity environment (Cao et al., 2014). It was found that bone loss was quickly alleviated when mice were treated with 3HB or 3HBME. This was due to the nuclear factor of activated T-cell cytoplasmic 1 (NFATc1) of pre-osteoclast differentiation being downregulated by 3HB or 3HBME. Decreased transcriptional activity of NFATc1 reduced the number of osteoclasts; thus, the bone tissue absorption was effectively inhibited to ameliorate bone loss in microgravity. Recently, new evidence suggested that 3HB could inhibit the NLRP3 inflammasome rather than undergoing oxidation in the mitochondria to reduce the production of interleukin IL-1β and IL-18 in human monocytes (Youm et al., 2015). Intriguingly, 3HB was also used to decrease the proportion of M1 macrophage and accelerate cholesterol efflux by acting on macrophages through its G-protein-coupled receptor GPR109A to attenuate atherosclerosis in mice (Zhang et al., 2021).

Additionally, the degradation product of polymer P4HB contains P4HB oligomers and 4HB monomers, which can be adopted as drugs to treat some mental diseases such as neurosis, chronic schizophrenia, and Parkinson's disease (Maitre et al., 2016; Utsunomia et al., 2020). So far, there is no evidence that has been reported regarding any cytotoxicity caused by degradation products of PHAs.

Non-teratogenicity and Non-carcinogenicity of PHAs

Many investigations indicated that PHAs have been used as drug delivery vehicles and grafts to support tissue regeneration. However, the possibility of teratogenicity and carcinogenicity induced by PHA matrices is an issue of concern. So far, only little information reports are available with respect to the implication of biodegradable PHAs on the growth of embryos as well as larvae. Li et al. (2016a) carried out a significant experiment to evaluate the influence of PHAs on growth profile of zebrafish larvae. It was found that there were no adverse negative effects of PHA polymers on the growth and development of zebrafish embryos as well as larvae.

Furthermore, Peng et al. (2011) performed interesting research to demonstrate the effect of fast-growing cells on PHA matrices toward tumor progress. The results indicated that no carcinogenic signal was found in least eight passages when the proliferation of rat osteoblasts was cultivated on the films of various PHAs. This observation further demonstrated the normal condition of cells growing and developing on the PHA polymers. This study revealed that common PHAs might be exploited as safe implant materials for supporting cell growth without a sign of vulnerability toward tumor formation.

From the above studies, available PHAs might be utilized as safe implant materials in different medical applications to support cell and tissue growth with very limited negative effects.

Synthetic Biology and Metabolic Engineering Strategies for PHA Production

Although PHAs are potential candidates for biomedical materials, the high cost of manufacturing PHAs is the main constraint that limits its range of applications on an industrial scale. Therefore, enhanced PHA production strategies based on synthetic biology and metabolic engineering are being developed and utilized to lower the production cost of PHAs (**Figure 2**).

Synthetic biology as a tool involving mathematics and systems biology has been utilized to design biological parts and biosystems with new or improved properties, whereas metabolic engineering focuses on the engineering of microbial cell factories for production of fuels and chemicals using DNA-editing approaches (Keasling, 2014; Keasling, 2008; Schwille, 2013). Synthetic biology tools have increasingly been employed to solve scientific and technical challenges in metabolic engineering. In recent years, there have been incremental studies on account of synthetic biology and metabolic engineering technologies to improve the PHA product yields at lower cost and their development in a broad range of microorganisms including *Halomonas bluephagenesis* (Chen et al., 2016; Meng and Chen, 2018; Zheng et al., 2020), *Ralstonia eutropha* (Raberg et al., 2018; Bhatia et al., 2019), *Pseudomonas putida* (Prieto et al., 2016; Weimer et al., 2020), *Aeromonas hydrophila* (Mozejko-Ciesielska et al., 2019), *Haloferax mediterranei* (Lu et al., 2008; Lin et al., 2021), and recombinant *Escherichia coli* (Rahman et al., 2013; Jung et al., 2019).

More recently, Tan et al. (2011) reported a halophilic chassis strain named *Halomonas bluephagenesis* TD01 (*Halomonas bluephagenesis* TD01), which was successfully exploited for PHA production under non-sterile and continuous fermentation conditions for 14 days (Tan et al., 2011). Moreover, in *H. bluephagenesis* TD01, genetic manipulation was implemented by metabolic engineering or synthetic biology to facilitate different PHA fabrication or production. For example, using low-cost glucose as single carbon source to synthesize P34HB with a high ratio of 4HB, the recombinant *H. bluephagenesis* TD01 harboring two interrelated 4HB biosynthesis pathways including four heterologous genes encoding 2-oxoglutarate decarboxylase (ogdA), succinate semialdehyde dehydrogenase (gabD), 4-hydroxybutyrate dehydrogenase (4hbD) and 4-hydroxybutyrate-CoA transferase (orfZ), endogenousgene controlled expression of succinate semialdehyde dehydrogenase (gabD) was knockout, which was competed with 4HB synthesis flux, increasing the molar ratio 4HB from 0.17 to 17.04 mol% (Ye et al., 2018). On the other hand, CRISPR/Cas9 gene-editing system was constructed in *H. bluephagenesis* TD01, resulting in achieving the deletion and insertion of 4.5 kb gene, which only took about 3 weeks in *H. bluephagenesis* TD01 (Qin et al., 2018). Using this gene-editing system, the *prpC* gene,

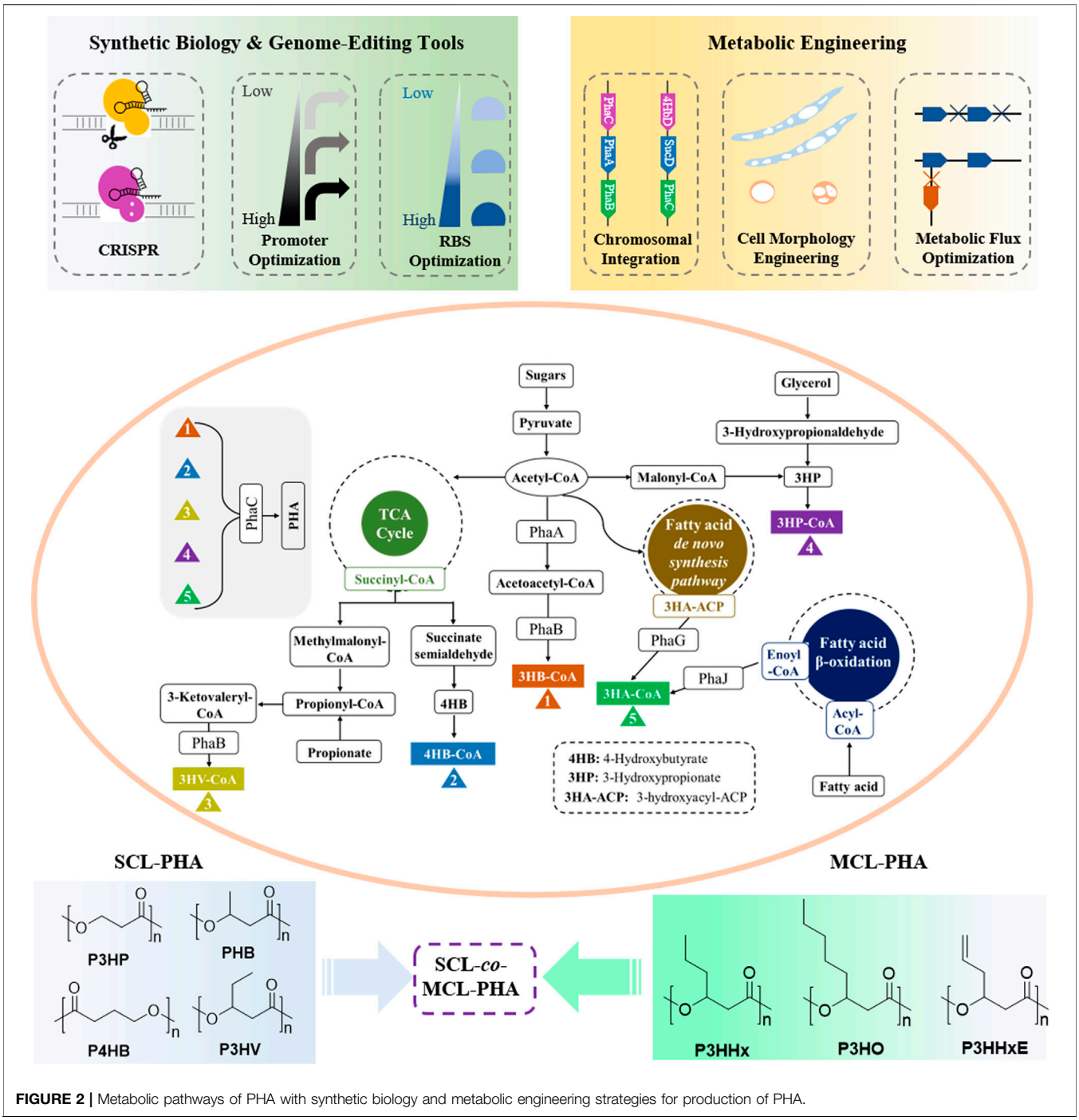

FIGURE 2 | Metabolic pathways of PHA with synthetic biology and metabolic engineering strategies for production of PHA.

encoding 2-methylcitrate synthase, in *H. bluephagenesis* TD01 was deleted for enhanced capacity of the *ΔprpC* mutant to synthesize PHBV with increasing 3HV fraction approximately 16-folds (Qin et al., 2018). The convenient and scaled genome-editing approach vastly quickens up the development of *H. bluephagenesis* TD01 as chassis of the next generation industrial biotechnology (NGIB) (Chen and Jiang, 2018).

Recent years, recent advances in synthetic biology including CRISPR gene-editing system, promoter, and ribosome-binding site (RBS) optimization, and metabolic engineering containing chromosomal integration, cell morphology engineering, and metabolic flux optimization, have been employed to manipulate microorganisms to gain more efficient PHA production at low cost. **Figure 2** shows the major biosynthesis pathways of PHA with possible engineering strategies for production of PHA (Choi et al., 2020b; Zhang et al., 2020). In addition, with the discovery of more novel and effective synthetic techniques, various PHAs with excellent performances including

homopolymers, copolymers, block polymers, and functional polymers will be designed and produced. These will promote PHA materials in the application of regenerative medicine on its way.

MANUFACTURING TECHNOLOGIES FOR SCAFFOLD FABRICATION IN TISSUE ENGINEERING

Currently, various methods have been utilized to fabricate PHA scaffolds. In this section, the conventional techniques to create PHA scaffolds will be discussed including electrospinning, particulate leaching, thermally induced-phase separation (TIPS) and solvent casting methods. In addition, this section discussed the 3D printing technology designed functional PHA scaffold systems.

Conventional Techniques for Scaffold Fabrication

The simple and effective strategies of solvent casting and particulate leaching have been used to fabricate scaffolds. These methods are intended to develop polymeric solutions with uniform salt particles distribution and certain size by dissolution in specific organic solvents. Followed by the formation of 2D films or 3D scaffolds by evaporation of solvents to lead to the reinforcement of slat particles into the matrix system. Further, they were immersed in ddH_2O to remove any unreacted salt by leaching process to generate the extremely porous network. The porosity, shape, and size could be well controlled by the usage of the porogen (Plikk et al., 2009; Hokmabad et al., 2017). The composites of PHBV-β-Ca_2SiO_4 were fabricated using solvent cast and particle leach methods by Wang et al. They studied the porosity and osteogenic properties of composites and confirmed the 87% porosity and good cell attachment, the proliferation of MG-63 cells respectively. Also, they mentioned that usages of organic solvents in this method are a major disadvantage due to their toxic nature to cells, bioactive small molecules and proteins (Wang et al., 2013).

Thermally induced phase separation (TIPS) for the fabrication of scaffolds is commonly used to prepare 3D scaffolds. This method involves quenching of the polymer solution and undergoing a liquid-liquid phase separation including rich and poor phases of polymers. Subsequently, the rich and poor phases of polymers endure the solidification and sublimation process to form a scaffold with well interconnected porous. The mechanical properties, pore morphology and the porosity of the scaffold can be disturbed by the type of polymers/solvents and their concentrations and quenching and phase separation temperatures (Rowlands et al., 2007). Li et al. (2008) reported that maleated PHBHHx scaffolds were fabricated by TIPS. They compared the maleated PHBHHx with pure PHBHHx, the maleated PHBHHx scaffolds showed virtuous behavior in terms of surface energy/charge, hydrophilic and porosity, which encouraged the promising growth of cells.

Electrospinning is an attractive technique to produce fibrous scaffolds with required morphology, porosity and diameter distribution ranging from nano to submicrometer. Nanofibrous scaffolds exhibit superior biological properties than non-nanofibrous due to their high surface-to-volume ratio and well interconnected porous network which are easier for cell communications and therefore they are considered as potential candidates for tissue engineering applications (Xue et al., 2019). PHB and PHBV electrospun scaffolds were fabricated with a diameter of micro and nano size using the electrospinning method (Kundrat et al., 2019; Kaniuk et al., 2020; Kim et al., 2020). The electrospun fibers exhibited controlled surface hydrophobicity to the benefit of cell growth and infiltration (Volova et al., 2014). Interestingly, Wang et al. (2012) developed PHBHHx-based spun scaffolds and examined their biological behavior by exposing them to rat-derived MSCs and proved their differentiation into osteoblasts. Also, they fabricated the randomly oriented and well aligned PHBHHx-based spun fibers scaffolds. The regular alignment of fibers enhanced the proliferation and differentiation of MSCs when compared with randomly oriented fibers networks. It's well-known that the electrospinning technique is highly skilled in reproducing fibrous scaffolds for tissue engineering applications. However, this technique has a major obstacle in controlling the porosity of scaffolds for a wide range of clinical applications.

3D Printing for PHA Scaffold Fabrication

3D printing technique works based on additive manufacturing principles. This technique is highly recommended for fabricating 3D scaffolds with controlled porous internal design, desired shape, and size (Mota et al., 2015). Also, this method could be adopted to incorporate biological agents and small biomolecules into scaffold systems while production of 3D scaffolds. 3D printing involves a layer-by-layer process that includes different types of techniques such as direct ink writing (DIW), fused deposition modeling (FDM) and selective laser sintering (SLS). Among these techniques, the 3D printing method is an adequate technique to generate particular scaffold structures with appropriate microenvironments for better cellular functions including infiltration, cell adhesion, proliferation and differentiation. **Table 3** shows the comparison of traditional and 3D printing techniques used to fabricate scaffolds.

DIW is an extrusion-based 3D printing technique (Li et al., 2019). In the fabrication of PHA scaffolds, the ink is generally prepared by dissolving the PHA particles into an organic solvent to form a homogeneous solution with rheological properties. The ink is extruded through a thin nozzle by a computer controlled robotic deposition system, as well as supporting its own weight during assembly. After printing, the cooling or drying need to be adopted to completely remove the organic solvent from the scaffold.

SLS is a solid freeform fabrication technique, in which various compositions of nanopowders are used to create physical models *via* a selective solidification process. Diermannet al. (2019) investigated the degradation behavior of high molecular weight PHBV scaffolds manufactured by SLS without using predesigned porous architecture. The results indicated that the manufactured

TABLE 3 | Comparative overview of manufacturing technologies for scaffold fabrication.

Techniques	Advantages	Disadvantages	References
Solvent-casting and particle leaching	Easiness and low cost	Use of organic solvents Limited to 2D structure No customization	Goh and Ooi (2008); Ye et al. (2018b)
Freeze-drying	Retained bioactivity Controllable pore size	High time and energy utilization Use of organic solvent	Wu et al. (2010)
Gas foaming	Good mechanical strength High porosity	High heating requirement Poor interconnection of pore structures	Ji et al. (2012)
Sol-gel technique	Formation of a variety of structures	Use of organic solvents Weak mechanical strength	Figueira (2020) Zheng and Boccaccini (2017)
TIPS	Simple controlling process Less affinity of defect formation Various microstructures of scaffolds	Use of organic solvents Time-consuming No control on final geometry	Li et al. (2008); Rowlands et al. (2007)
Emulsification	High surface area-to-volume ratio	Limited design freedom No significant 3D development	Piacentini et al. (2017)
Electrospinning	High surface area-to-volume ratio Controllable porous construction	Use of organic solvents Difficulties to achieve 3D structure	Xue et al. (2019)
DIW	Construct internal channels Retained bioactive molecules	Difficult to remove unbounded powder from curved channels	Li et al. (2019)
FDM	Excellent mechanical strength Good porosity No need of toxic solvents	Generation of fibers with regular size and molten phase of material requirement	Vyavahare et al. (2020)
SLS	Good accuracy Short time process No need of post-process	High-cost running process Release of toxic gases	Mazzoli (2013)
Stereolithography	Fabrication of complex internal structures Retained bioactive molecules	Limited to photopolymers	Melchels et al. (2010)

PHBV scaffolds using SLS also exhibited adequate mechanical properties and satisfactory structural integrity even if immersed in phosphate-buffered saline solution for 6 weeks. Henceforth, they proved that PHBV has good thermal stability and could be a highly cost-effective choice for the fabrication of scaffolds. Duan et al. (2011), developed scaffolds with the combination of PHBV and calcium phosphate (CaP) by SLS for bone regeneration applications. They developed reproducible PHBV-CaP scaffolds by optimization of several factors of the SLS technique such as scan, speed, laser power and thickness of layers. Finally, they proved that SLS has the competency to produce good standard and refined complex architecture with porous structures to meet the tissue engineering criteria.

FDM is a layer-by-layer melt-extrusion approach that consists of heating the biopolymer above its glass transition temperature to form a thick solution and then deposing the extruded material still hot to render the adhesion with the underneath layers which already cooled down and hardened. Despite FDM being considered as the promising 3D printing technique in a wide range of applications, with different polymers, its utilization for PHA biomedical devices is still extremely challenging. Because of the narrow melt processing temperature window of this technique hinders its application in production of 3D PHA porous scaffolds. So far, only four scientific research works have been published, and they evaluated the applicability as preliminary investigations (Kosorn et al., 2017; Wu and Liao, 2017; Ausejo et al., 2018).

In conclusion, 3D rapid prototyping has been used for processing various micro-structures with controllable factors including shape/size and interconnectivity of pores, which was suitable for cell growth and rapid nutrient diffusion. However, the above-mentioned techniques have their pros and cons. Though, the adopted technique could be more focused on fulfilling the necessities of the particular tissues to be regenerated or healed.

PHAS AND PHA-BASED SCAFFOLDS FOR BTE

Blending, Surface or Chemical Modification for Improved Application Properties of PHAs

PHAs including PHB, P4HB, PHBHHx, PHBV and PHO have been investigated materials for tissue regeneration (Ray and Kalia, 2017). However, PHAs are kinds of natural long chain fatty acid molecules with hydrophobic properties and lack of modifiable active groups. These features make them inconvenient for use in various applications, although PHAs show their excellent biodegradability. To enhance their usage, several strategies including blending, surface and chemical modifications have been employed to change their physiochemical characteristics to fulfill the requirements of medical applications. The blending option can be valuable considered for developing new kinds of polymers with enhanced performance, and the disadvantages of the parent polymers can be evitable. Therefore, PHA family members blending with each other or with other polymers can

significantly improve PHA performance by choosing the proper compositions of the blend and preparation conditions, which is beneficial for expanded applications. Yang et al. (2002) systematically studied the blending of PHB with PHBHHx and their biomedical applications. The results uncovered the growth of L929 on the blending films exhibited marked improvement than growth on PHB films, which demonstrated that the blends have better biocompatibility contributed by PHBHHx. The following detailed studies have revealed that the surface of pure PHB film is the existence of many pores and protrusions, which are caused by PHB with a high degree of crystallization and rapid rate of crystallization. This rough morphology surface may be responsible for inhibiting cell adhesion and growth. However, the crystallization behavior of PHB decreased dramatically when PHBHHx was added to PHB. As a result, the films of PHB and PHBHHx blending exhibited the regular and smooth surface, which availed cell adhesion and growth. In another study, the physical properties of PHBHHx such as thermal stability, flexibility, and mechanical strength were improved when PHBHHx was blended with P34HB. The PHBHHx/P34HB blend exhibited the roughest surface and had the highest viability of chondrocytes when the weight ratio of PHBHHx/P34HB is 4:2. The results indicated that this blend could be beneficial to cartilage tissue engineering (Luo et al., 2009).

PLA is a linear biopolymer chemically synthesized from lactic acid that has been utilized as implant material with FDA approval. However, the extensive adoption of PLA at the commercial level has been hindered by the low-impact toughness and low end-use temperature. Hence, to overcome the drawbacks associated with PLA, fillers and impact modifiers are often added into PLA. Hence, blending PLA with PHA was considered as an effective method to change the properties of polymers. Several studies have focused onthe blend of PHA with PLA. Gerard and Budtova (2012) indicated that PLA/PHBV blends served a significant role in improving the thermal stability of PHBV. Even though PLA and PHBV are brittle polymers, blends containing a small amount of PHBV into PLA matrix showed an obvious ductile plastic deformation. Besides, various ratios of PHB and PEG were blended to form films used to test blood compatibility. The results found that PEG played an essential role in delaying clotting time and reducing thrombocyte adherence (Cheng et al., 2003).

In addition to blending, surface modification is another simple and effective approach for expanding the application of PHAs (Xue et al., 2018). Although PHBHHx displays good mechanical properties compared with PHB, it is very difficult to introduce active groups into the polyester carbon chain of PHBHHx, which leads to its applications restricted. However, a study revealed that the hydrophilicity of PHBHHx could be increased by strong alkaline treatment to further avail cell growth. This was due to the presence of more charged hydroxyl and carboxyl groups produced on the surfaces of the PHBHHx after the treatments. Through this kind of modification, the surface area and surface roughness of the material were increased, which is beneficial for cell survival and growth. Furthermore, the surface hydrolyzed PHBHHx films significantly presented fibronectin adsorption and enhanced MC3T3-E1 cell attachment and proliferation compared to unmodified films (Li et al., 2005). The surfaces of PHAs can bind several amphiphilic proteins like PHA granule binding protein (PhaP), PHA synthesis repressor protein (PhaR) and poly-β-hydroxybutyrate depolymerase (PhaZ) through strong hydrophobic interaction. Arginine-glycine-aspartate (RGD) is a tripeptide involved in cell adhesion, and generally regarded as an efficient way to modify biomaterials for guiding cell behavior for tissue regeneration. Previous studies showed PhaP-RGD fusion protein was used to coat the films of PLA, PHBV and PHBHHx, which led to increasing polymer surface hydrophilicity to facilitate cell adhesion, spreading, migration, and proliferation compared with their corresponding uncoated films (Dong et al., 2010). Xie conducted a study (Xie et al., 2013), using a fusion protein abbreviated as PhaP-IKVAV to coat the films of PHBVHHx, PHBHHx and PLA respectively, which distinctly promoted the rat neural stem cells (NSCs) adhesion, proliferation and neural differentiation compared to uncoated materials. Furthermore, it was found that human vascular smooth muscle cells (HVSMCs) cultured on films of PHAs coated with PhaR-KQAGDV oligopeptide, which showed better cell adhesion and growth than controls (Dong et al., 2012).

Additionally, different methods of chemical modifications including chlorination, carboxylation, epoxidation, and grafting have been carried out on PHA modification (Moore et al., 2005; Hazer and Steinbuchel, 2007). Acquired new physiochemistry characteristics like convertible glass transition and melting temperatures, increased hydrophilicity will be endowed into the polymers of PHAs *via* chemical modifications (Arslan et al., 2007; Raza et al., 2018b). Therefore, chemical modification is the simple and controllable way to alter the polymer structure with predictable properties, which are beneficial to further enlarge the space of their applications.

Intrinsic PHAs and PHA Composites-Based Scaffolds for BTE

PHAs have been studied as a suitable substrate for tissue engineering on account of their excellent biodegradability, biocompatibility and thermo-processability. Among kinds of tissue regeneration applications, especially, in BTE, various types of PHAs and PHA composites-based scaffolds have been frequently adopted to support bone tissue growth both *in vitro* and *in vivo*. Rabbit bone morrow-derived mesenchymal stem cells (rBMSCs) were cultured on PHBHHx, PHB, and PLA 3D scaffolds respectively to assess their osteogenesis responses (Wang et al., 2004). It was found that the morphology of the cells altered from spindle fibrous into osteoblast-like cells with round cell shape. More specially, the cells grown on PHBHHx scaffolds presented specific markers of osteogenesis including high alkaline phosphatase activity, strong calcium nodule deposition than that on PHB and PLA scaffolds respectively. This contributed by the suitable roughness of PHBHHx surface better for osteogenic differentiation, implicating that PHBHHx was a promising biomaterial for bone tissue regeneration.

More recently, Chen lab reported that highly open porous microspheres (OPMs) made of PHBVHHx were fabricated by a

modified method of gas-in-oil-in-water double emulsion, namely, PHA OPMs, which possess excellent connections from internal pores to outside surface as injectable carriers for repair complexly shaped tissue defects (Wei et al., 2018). PHA OPMs supported stronger osteogenic differentiation of human bone marrow derived mesenchymal stem cells (hMSCs) *in vitro* compared with traditional PHA microspheres with less porous hollow and PLA OPMs. ALP activity detected on/in PHA OPMs was significantly higher than both PHA HMs and PLA OPMs groups on days 4 and 7 during osteogenic induction. In addition, abundant new bone tissue was observed growing into PHA OPMs than other tested materials in an ectopic bone formation mouse model. PHA OPMs seem to be a potential medical scaffold which are not only beneficial for osteogenic differentiation of hMSCs *in vitro*, but also helps to repair the bone defect *in vivo*. One study on P34HB fiber scaffolds were prepared by electrospinning, which obviously upregulated osteogenic-related genes expression of mouse adipose-derived stem cells such as Runx2, OPN and OCN with induction. This finding indicated that fiber scaffolds of P34HB are potential candidates for BTE (Fu et al., 2014).

However, to further improve the mechanical properties and bioactivity, various PHA composites-based scaffolds including hydroxyapatite (HAp), bioactive glass (BG) and ceramics have been extensively studied for the repairment of bone defects. When HAp was incorporated into PHB to be fabricated scaffolds, not only the compressive elastic modulus and maximum stress of the PHB/HAp scaffolds were improved, but also enhanced osteoblast responses to the scaffolds (Ramier et al., 2014; Ding et al., 2016). PHBHHx composite scaffold with polylactide-grafted hydroxyapatite as compatibilizer has been systematically investigated including superficial roughness and wettability, mechanical strength, as well as *in vitro* bioactivity (Ma et al., 2017). The results demonstrated that the attachment and viability of hMSCs improved when cells seeded on PHBHHx based composite scaffold combined with surface-graft HAp compatibilizer. Moreover, the osteogenesis related genes including COL I, Runx2, OCN and OPN were up-regulated, thus made for osteogenic differentiation, indicating that this kind of scaffold might be a suitable matrix as bone substitutes.

Overall, therefore, PHAs and PHA composites-based scaffolds are potential candidates for BTE.

CONCLUSION AND FUTURE PERSPECTIVE

It is still a major clinical challenge for reconstruction of large bone defects. Autografts, allografts, and xenografts as traditional therapeutic approaches have been restricted because of their disadvantages. In recent decades, a variety of materials including natural materials or synthetic polyesters have been investigated as possible tissue-engineered scaffolds for bone and cartilage defects repaired. PHAs are biopolyesters produced by many microorganisms. Due to the excellent biodegradability, biocompatibility, and adjustable mechanical properties, PHAs allow being exploited as great attractive biopolymeric biomaterials over other polyesters. More importantly, because of its slow degradation rate (6 months–2 years) and high hydrolytic stability *in vivo*, PHAs are more suitable for long-term applications, especially in the area of bone tissue regeneration.

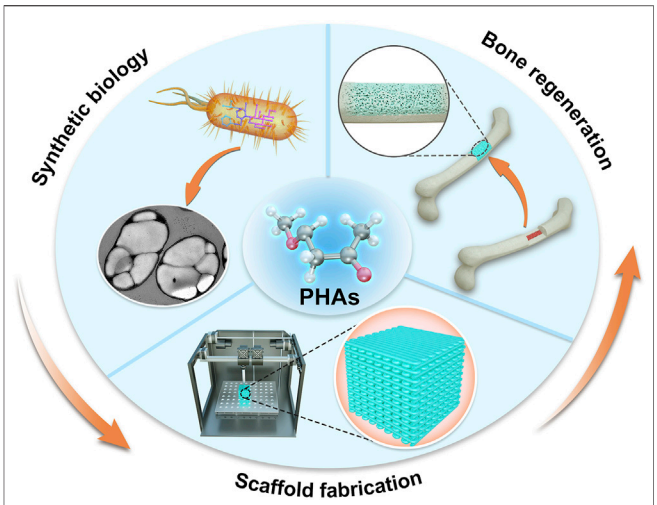

FIGURE 3 | Schematic diagram of the production, fabrication, and applications of PHAs in BTE.

In this review, the effect of degradation products such as 3HB, 4HB were discussed, including the improvement of cell adhesion, proliferation, and treatment of neurodegenerative disorders. However, in practical applications, PHAs still have only a very limited market in both clinical and industrial materials compared with mature conventional petroleum-derived polymers. There are two main reasons: 1) the major drawback is the high production cost of PHAs. 2) Unexploited manufacturing methods for PHA scaffolds and strong hydrophobicity of PHAs. To meet these challenges, two strategies can be adopted: first, constructing a strain chassis of producing diverse PHAs at low cost with high PHA yields, using a simple fermentation process. To achieve this goal, recently, scientists are dying of great efforts to make *halophiles* as a candidate of a super chassis by synthetic biology and metabolic engineering approaches for producing PHAs (Chen X. et al., 2017). For example, Chen and co-workers indicated that diverse properties of PHAs with high cell density and high substrates conversion rate could be produced by *H. bluephagensis* TD01 (Ye H. et al., 2018; Ling et al., 2018). On the other hand, for the sake of driving the application of PHAs, various modified 3D rapid prototyping technologies should be matched with PHA materials. Moreover, physical and chemical modification methods also should be developed to improve their performance for biomedical applications. With the significant alteration of their surface, mechanical properties and regulable rate of degradation, modified PHA polyesters are widely employed for scaffolds to fulfill the requirements of BTE.

Scaffold design requires certain parameters to satisfy the need for tissue regeneration. The recent advances in various methods of PHA scaffolds fabrication were also summarized. Among these scaffold fabrication techniques, 3D rapid prototyping has recently been recommended as an advanced method for fabricating different microstructures to be suitable for cell growth and rapid nutrient diffusion. So far, due to the fewer animal experiments *in vivo* for PHA scaffolds have been investigated, resulting in the limitation of data analysis about immune response of implants to various tissues. Therefore, there is an urge to increase studies on the animal trials of PHAs so that there is more data collected and make them successful biomaterials for bone regeneration. Taken together, developing biomedical applications, especially BTE of PHAs or PHA-based biomaterials not only involves low-cost production, but also needs to consider the fabrication method of PHA scaffolds and the *in vivo* experimental performance before clinical trials (**Figure 3**).

AUTHOR CONTRIBUTIONS

JL and XZ conceived and designed the review; JL, XZ, AU, ZF, and JC studied the literature; JL, XZ, and AU wrote the manuscript; AS and PZ give revision advices to the manuscript.

FUNDING

This research was financially supported by the National Natural Science Foundation of China (92068117, 81871809), Foreign cooperation project of Chinese Academy of Sciences (172644KYSB20190032), Guangdong Basic and Applied Basic Research Fund (2020B1515120052), the development and reform Commission of Shenzhen Municipality (2019, No. 561), Shenzhen International Collaborative Project (GJHZ20200731095009028), and Tsinghua University-INDITEX Sustainable Development Fund (TISD201907).

REFERENCES

Agarwal, R., and García, A. J. (2015). Biomaterial Strategies for Engineering Implants for Enhanced Osseointegration and Bone Repair. *Adv. Drug Deliv. Rev.* 94, 53–62. doi:10.1016/j.addr.2015.03.013

Ahmed, T., Marçal, H., Lawless, M., Wanandy, N. S., Chiu, A., and Foster, L. J. R. (2010). Polyhydroxybutyrate and its Copolymer with Polyhydroxyvalerate as Biomaterials: Influence on Progression of Stem Cell Cycle. *Biomacromolecules* 11 (10), 2707–2715. doi:10.1021/bm1007579

Akaraonye, E., Keshavarz, T., and Roy, I. (2010). Production of Polyhydroxyalkanoates: the Future green Materials of Choice. *J. Chem. Technol. Biotechnol.* 85 (6), 732–743. doi:10.1002/jctb.2392

Anjum, A., Zuber, M., Zia, K. M., Noreen, A., Anjum, M. N., and Tabasum, S. (2016). Microbial Production of Polyhydroxyalkanoates (PHAs) and its Copolymers: A Review of Recent Advancements. *Int. J. Biol. Macromolecules* 89, 161–174. doi:10.1016/j.ijbiomac.2016.04.069

Arrington, E. D., Smith, W. J., Chambers, H. G., Bucknell, A. L., and Davino, N. A. (1996). Complications of Iliac Crest Bone Graft Harvesting. *Clin. Orthopaedics Relat. Res.* 329, 300–309. doi:10.1097/00003086-199608000-00037

Arslan, H., Hazer, B., and Yoon, S. C. (2007). Grafting of Poly(3-Hydroxyalkanoate) and Linoleic Acid onto Chitosan. *J. Appl. Polym. Sci.* 103 (1), 81–89. doi:10.1002/app.24276

Ashby, R., Solaiman, D., and Foglia, T. (2002). The Synthesis of Short- and Medium-Chain-Length Poly(hydroxyalkanoate) Mixtures from Glucose- or Alkanoic Acid-Grown Pseudomonas Oleovorans. *J. Ind. Microbiol. Biotechnol.* 28 (3), 147–153. doi:10.1038/sj/jim/700023110.1038/sj.jim.7000231

Bagdadi, A. V., Safari, M., Dubey, P., Basnett, P., Sofokleous, P., Humphrey, E., et al. (2018). Poly(3-hydroxyoctanoate), a Promising New Material for Cardiac Tissue Engineering. *J. Tissue Eng. Regen. Med.* 12 (1), e495–e512. doi:10.1002/term.2318

Baldwin, P., Li, D. J., Auston, D. A., Mir, H. S., Yoon, R. S., and Koval, K. J. (2019). Autograft, Allograft, and Bone Graft Substitutes: Clinical Evidence and Indications for Use in the Setting of Orthopaedic Trauma Surgery. *J. Orthopaedic Trauma* 33 (4), 203–213. doi:10.1097/Bot.0000000000001420

Bengtsson, S., Pisco, A. R., Johansson, P., Lemos, P. C., and Reis, M. A. M. (2010). Molecular Weight and thermal Properties of Polyhydroxyalkanoates Produced from Fermented Sugar Molasses by Open Mixed Cultures. *J. Biotechnol.* 147 (3-4), 172–179. doi:10.1016/j.jbiotec.2010.03.022

Bertoldo Menezes, D., Reyer, A., and Musso, M. (2018). Investigation of the Brill Transition in Nylon 6,6 by Raman, THz-Raman, and Two-Dimensional Correlation Spectroscopy. *Spectrochimica Acta A: Mol. Biomol. Spectrosc.* 190, 433–441. doi:10.1016/j.saa.2017.09.055

Bharadwaz, A., and Jayasuriya, A. C. (2020). Recent Trends in the Application of Widely Used Natural and Synthetic Polymer Nanocomposites in Bone Tissue Regeneration. *Mater. Sci. Eng. C* 110, 110698. doi:10.1016/j.msec.2020.110698

Bhatia, S. K., Gurav, R., Choi, T.-R., Jung, H.-R., Yang, S.-Y., Song, H.-S., et al. (2019). Poly(3-hydroxybutyrate-co-3-hydroxyhexanoate) Production from Engineered Ralstonia Eutropha Using Synthetic and Anaerobically Digested Food Waste Derived Volatile Fatty Acids. *Int. J. Biol. Macromolecules* 133, 1–10. doi:10.1016/j.ijbiomac.2019.04.083

Bugnicourt, E., Cinelli, P., Lazzeri, A., and Alvarez, V. (2014). Polyhydroxyalkanoate (PHA): Review of Synthesis, Characteristics, Processing and Potential Applications in Packaging. *Express Polym. Lett.* 8 (11), 791–808. doi:10.3144/expresspolymlett.2014.82

Cao, Q., Zhang, J., Liu, H., Wu, Q., Chen, J., and Chen, G.-Q. (2014). The Mechanism of Anti-osteoporosis Effects of 3-hydroxybutyrate and Derivatives under Simulated Microgravity. *Biomaterials* 35 (28), 8273–8283. doi:10.1016/j.biomaterials.2014.06.020

Capek, I. (2005). Nature and Properties of Ionomer Assemblies. II. *Adv. Colloid Interf. Sci.* 118 (1-3), 73–112. doi:10.1016/j.cis.2005.06.005

Castilho, L. R., Mitchell, D. A., and Freire, D. M. G. (2009). Production of Polyhydroxyalkanoates (PHAs) from Waste Materials and By-Products by Submerged and Solid-State Fermentation. *Bioresour. Tech.* 100 (23), 5996–6009. doi:10.1016/j.biortech.2009.03.088

Chanprateep, S., Buasri, K., Muangwong, A., and Utiswannakul, P. (2010). Biosynthesis and Biocompatibility of Biodegradable Poly(3-Hydroxybutyrate-Co-4-Hydroxybutyrate). *Polym. Degrad. Stab.* 95 (10), 2003–2012. doi:10.1016/j.polymdegradstab.2010.07.014

Chanprateep, S., Katakura, Y., Visetkoop, S., Shimizu, H., Kulpreecha, S., and Shioya, S. (2008). Characterization of New Isolated Ralstonia Eutropha Strain A-04 and Kinetic Study of Biodegradable Copolyester Poly(3-Hydroxybutyrate-Co-4-Hydroxybutyrate) Production. *J. Ind. Microbiol. Biotechnol.* 35 (11), 1205–1215. doi:10.1007/s10295-008-0427-5

Chanprateep, S., and Kulpreecha, S. (2006). Production and Characterization of Biodegradable Terpolymer Poly(3-Hydroxybutyrate-Co-3-Hydroxyvalerate-Co-4-Hydroxybutyrate) by Alcaligenes Sp. A-04. *J. Biosci. Bioeng.* 101 (1), 51–56. doi:10.1263/jbb.101.51

Chen, G.-Q. (2009). A Microbial Polyhydroxyalkanoates (PHA) Based Bio- and Materials Industry. *Chem. Soc. Rev.* 38 (8), 2434–2446. doi:10.1039/b812677c

Chen, G.-Q., Jiang, X.-R., and Guo, Y. (2016). Synthetic Biology of Microbes Synthesizing Polyhydroxyalkanoates (PHA). *Synth. Syst. Biotechnol.* 1 (4), 236–242. doi:10.1016/j.synbio.2016.09.006

Chen, G.-Q., and Jiang, X.-R. (2018). Next Generation Industrial Biotechnology Based on Extremophilic Bacteria. *Curr. Opin. Biotechnol.* 50, 94–100. doi:10.1016/j.copbio.2017.11.016

Chen, J.-Y., Song, G., and Chen, G.-Q. (2006). A Lower Specificity PhaC2 Synthase from Pseudomonas Stutzeri Catalyses the Production of Copolyesters

Consisting of Short-Chain-Length and Medium-Chain-Length 3-hydroxyalkanoates. *Antonie Van Leeuwenhoek* 89 (1), 157–167. doi:10.1007/s10482-005-9019-9

Chen, X., Yin, J., Ye, J., Zhang, H., Che, X., Ma, Y., et al. (2017a). Engineering Halomonas Bluephagenesis TD01 for Non-sterile Production of Poly(3-Hydroxybutyrate-Co-4-Hydroxybutyrate). *Bioresour. Tech.* 244, 534–541. doi:10.1016/j.biortech.2017.07.149

Chen, Z., Song, Y., Zhang, J., Liu, W., Cui, J., Li, H., et al. (2017b). Laminated Electrospun nHA/PHB-Composite Scaffolds Mimicking Bone Extracellular Matrix for Bone Tissue Engineering. *Mater. Sci. Eng. C* 72, 341–351. doi:10.1016/j.msec.2016.11.070

Cheng, G., Cai, Z., and Wang, L. (2003). Biocompatibility and Biodegradation of Poly(hydroxybutyrate)/poly(ethylene Glycol) Blend Films. *J. Mater. Sci. Mater. Med.* 14 (12), 1073–1078. doi:10.1023/B:JMSM.0000004004.37103.f4

Cheng, S.-T., Chen, Z.-F., and Chen, G.-Q. (2008). The Expression of Cross-Linked Elastin by Rabbit Blood Vessel Smooth Muscle Cells Cultured in Polyhydroxyalkanoate Scaffolds. *Biomaterials* 29 (31), 4187–4194. doi:10.1016/j.biomaterials.2008.07.022

Cheng, S., Chen, G., Leski, M., Zou, B., Wang, Y., and Wu, Q. (2006). The Effect of D,l-β-Hydroxybutyric Acid on Cell Death and Proliferation in L929 Cells. *Biomaterials* 27 (20), 3758–3765. doi:10.1016/j.biomaterials.2006.02.046

Cheng, S., Wu, Q., Yang, F., Xu, M., Leski, M., and Chen, G.-Q. (2005). Influence of Dl-β-Hydroxybutyric Acid on Cell Proliferation and Calcium Influx. *Biomacromolecules* 6 (2), 593–597. doi:10.1021/bm049465y

Choi, S. Y., Cho, I. J., Lee, Y., Kim, Y. J., Kim, K. J., and Lee, S. Y. (2020a). Microbial Polyhydroxyalkanoates and Nonnatural Polyesters. *Adv. Mater.* 32 (35), 1907138. doi:10.1002/adma.201907138

Choi, S. Y., Rhie, M. N., Kim, H. T., Joo, J. C., Cho, I. J., Son, J., et al. (2020b). Metabolic Engineering for the Synthesis of Polyesters: A 100-year Journey from Polyhydroxyalkanoates to Non-natural Microbial Polyesters. *Metab. Eng.* 58, 47–81. doi:10.1016/j.ymben.2019.05.009

Ciesielski, S., Możejko, J., and Pisutpaisal, N. (2015). Plant Oils as Promising Substrates for Polyhydroxyalkanoates Production. *J. Clean. Prod.* 106, 408–421. doi:10.1016/j.jclepro.2014.09.040

Cypher, T. J., and Grossman, J. P. (1996). Biological Principles of Bone Graft Healing. *J. Foot Ankle Surg.* 35 (5), 413–417. doi:10.1016/s1067-2516(96)80061-5

Deng, Y., Zhao, K., Zhang, X.-f., Hu, P., and Chen, G.-Q. (2002). Study on the Three-Dimensional Proliferation of Rabbit Articular Cartilage-Derived Chondrocytes on Polyhydroxyalkanoate Scaffolds. *Biomaterials* 23 (20), 4049–4056. doi:10.1016/S0142-9612(02)00136-9

Diermann, S. H., Lu, M., Edwards, G., Dargusch, M., and Huang, H. (2019). In Vitrodegradation of a Unique Porous PHBV Scaffold Manufactured Using Selective Laser Sintering. *J. Biomed. Mater. Res.* 107 (1), 154–162. doi:10.1002/jbm.a.36543

Ding, Y., Li, W., Müller, T., Schubert, D. W., Boccaccini, A. R., Yao, Q., et al. (2016). Electrospun Polyhydroxybutyrate/Poly(ε-caprolactone)/58S Sol-Gel Bioactive Glass Hybrid Scaffolds with Highly Improved Osteogenic Potential for Bone Tissue Engineering. *ACS Appl. Mater. Inter.* 8 (27), 17098–17108. doi:10.1021/acsami.6b03997

Doi, Y., Segawa, A., and Kunioka, M. (1990). Biosynthesis and Characterization of Poly(3-Hydroxybutyrate-Co-4-Hydroxybutyrate) in Alcaligenes Eutrophus. *Int. J. Biol. Macromolecules* 12 (2), 106–111. doi:10.1016/0141-8130(90)90061-E

Dong, C.-L., Li, S.-Y., Wang, Y., Dong, Y., Tang, J. Z., Chen, J.-C., et al. (2012). The Cytocompatability of Polyhydroxyalkanoates Coated with a Fusion Protein of PHA Repressor Protein (PhaR) and Lys-Gln-Ala-Gly-Asp-Val (KQAGDV) Polypeptide. *Biomaterials* 33 (9), 2593–2599. doi:10.1016/j.biomaterials.2011.12.020

Dong, Y., Li, P., Chen, C.-b., Wang, Z.-h., Ma, P., and Chen, G.-Q. (2010). The Improvement of Fibroblast Growth on Hydrophobic Biopolyesters by Coating with Polyhydroxyalkanoate Granule Binding Protein PhaP Fused with Cell Adhesion Motif RGD. *Biomaterials* 31 (34), 8921–8930. doi:10.1016/j.biomaterials.2010.08.001

Duan, B., Cheung, W. L., and Wang, M. (2011). Optimized Fabrication of Ca-P/PHBV Nanocomposite Scaffolds via Selective Laser Sintering for Bone Tissue Engineering. *Biofabrication* 3 (1), 015001. doi:10.1088/1758-5082/3/1/015001

Elmowafy, E., Abdal-Hay, A., Skouras, A., Tiboni, M., Casettari, L., and Guarino, V. (2019). Polyhydroxyalkanoate (PHA): Applications in Drug Delivery and Tissue Engineering. *Expert Rev. Med. Devices* 16 (6), 467–482. doi:10.1080/17434440.2019.1615439

Figueira, R. B. (2020). Hybrid Sol-Gel Coatings for Corrosion Mitigation: A Critical Review. *Polymers* 12 (3), 689. doi:10.3390/polym12030689

Fillingham, Y., and Jacobs, J. (2016). Bone Grafts and Their Substitutes. *Bone Jt. J* 98-B (1), 6–9. doi:10.1302/0301-620x.98b1.3635010.1302/0301-620X.98B.36350

Fu, N., Deng, S., Fu, Y., Li, G., Cun, X., Hao, L., et al. (2014). Electrospun P34HB Fibres: a Scaffold for Tissue Engineering. *Cell Prolif.* 47 (5), 465–475. doi:10.1111/cpr.12122

Gerard, T., and Budtova, T. (2012). Morphology and Molten-State Rheology of Polylactide and Polyhydroxyalkanoate Blends. *Eur. Polym. J.* 48 (6), 1110–1117. doi:10.1016/j.eurpolymj.2012.03.015

Goh, Y. Q., and Ooi, C. P. (2008). Fabrication and Characterization of Porous poly(L-Lactide) Scaffolds Using Solid-Liquid Phase Separation. *J. Mater. Sci. Mater. Med.* 19 (6), 2445–2452. doi:10.1007/s10856-008-3366-9

Gonzalez Ausejo, J., Rydz, J., Musioł, M., Sikorska, W., Sobota, M., Włodarczyk, J., et al. (2018). A Comparative Study of Three-Dimensional Printing Directions: The Degradation and Toxicological Profile of a PLA/PHA Blend. *Polym. Degrad. Stab.* 152, 191–207. doi:10.1016/j.polymdegradstab.2018.04.024

Gruskin, E., Doll, B. A., Futrell, F. W., Schmitz, J. P., and Hollinger, J. O. (2012). Demineralized Bone Matrix in Bone Repair: History and Use. *Adv. Drug Deliv. Rev.* 64 (12), 1063–1077. doi:10.1016/j.addr.2012.06.008

Hazer, B., and Steinbüchel, A. (2007). Increased Diversification of Polyhydroxyalkanoates by Modification Reactions for Industrial and Medical Applications. *Appl. Microbiol. Biotechnol.* 74 (1), 1–12. doi:10.1007/s00253-006-0732-8

Hinüber, C., Chwalek, K., Pan-Montojo, F. J., Nitschke, M., Vogel, R., Brünig, H., et al. (2014). Hierarchically Structured Nerve Guidance Channels Based on Poly-3-Hydroxybutyrate Enhance Oriented Axonal Outgrowth. *Acta Biomater.* 10 (5), 2086–2095. doi:10.1016/j.actbio.2013.12.053

Hokamura, A., Wakida, I., Miyahara, Y., Tsuge, T., Shiratsuchi, H., Tanaka, K., et al. (2015). Biosynthesis of Poly(3-Hydroxybutyrate-Co-3-Hydroxyalkanoates) by Recombinant *Escherichia coli* from Glucose. *J. Biosci. Bioeng.* 120 (3), 305–310. doi:10.1016/j.jbiosc.2015.01.022

Hu, Y.-J., Wei, X., Zhao, W., Liu, Y.-S., and Chen, G.-Q. (2009). Biocompatibility of Poly(3-Hydroxybutyrate-Co-3-Hydroxyvalerate-Co-3-Hydroxyhexanoate) with Bone Marrow Mesenchymal Stem Cells. *Acta Biomater.* 5 (4), 1115–1125. doi:10.1016/j.actbio.2008.09.021

Ji, C., Annabi, N., Hosseinkhani, M., Sivaloganathan, S., and Dehghani, F. (2012). Fabrication of Poly-DL-Lactide/polyethylene Glycol Scaffolds Using the Gas Foaming Technique. *Acta Biomater.* 8 (2), 570–578. doi:10.1016/j.actbio.2011.09.028

Ji, G.-Z., Wei, X., and Chen, G.-Q. (2009). Growth of Human Umbilical Cord Wharton's Jelly-Derived Mesenchymal Stem Cells on the Terpolyester Poly(3-Hydroxybutyrate-Co-3-Hydroxyvalerate-Co-3-Hydroxyhexanoate). *J. Biomater. Sci. Polym. Edition* 20 (3), 325–339. doi:10.1163/156856209X412191

Ji, Y., Li, X.-T., and Chen, G.-Q. (2008). Interactions between a Poly(3-Hydroxybutyrate-Co-3-Hydroxyvalerate-Co-3-Hydroxyhexanoate) Terpolyester and Human Keratinocytes. *Biomaterials* 29 (28), 3807–3814. doi:10.1016/j.biomaterials.2008.06.008

Jiang, X., Sun, Z., Marchessault, R. H., Ramsay, J. A., and Ramsay, B. A. (2012). Biosynthesis and Properties of Medium-Chain-Length Polyhydroxyalkanoates with Enriched Content of the Dominant Monomer. *Biomacromolecules* 13 (9), 2926–2932. doi:10.1021/bm3009507

Jung, H.-R., Yang, S.-Y., Moon, Y.-M., Choi, T.-R., Song, H.-S., Bhatia, S., et al. (2019). Construction of Efficient Platform *Escherichia coli* Strains for Polyhydroxyalkanoate Production by Engineering Branched Pathway. *Polymers* 11 (3), 509. doi:10.3390/polym11030509

Kaniuk, Ł., Krysiak, Z. J., Metwally, S., and Stachewicz, U. (2020). Osteoblasts and Fibroblasts Attachment to Poly(3-Hydroxybutyric Acid-Co-3-Hydrovaleric Acid) (PHBV) Film and Electrospun Scaffolds. *Mater. Sci. Eng. C* 110, 110668. doi:10.1016/j.msec.2020.110668

Keasling, J. D. (2008). Synthetic Biology for Synthetic Chemistry. *ACS Chem. Biol.* 3 (1), 64–76. doi:10.1021/cb7002434

Keasling, J. (2014). Synthetic Biology for Synthetic Chemistry. *New Biotechnol.* 31, S9. doi:10.1016/j.nbt.2014.05.1633

Kim, H. S., Chen, J., Wu, L.-P., Wu, J., Xiang, H., Leong, K. W., et al. (2020). Prevention of Excessive Scar Formation Using Nanofibrous Meshes Made of Biodegradable Elastomer Poly(3-Hydroxybutyrate-Co-3-Hydroxyvalerate). *J. Tissue Eng.* 11, 204173142094933. doi:10.1177/2041731420949332

Kosorn, W., Sakulsumbat, M., Uppanan, P., Kaewkong, P., Chantaweroad, S., Jitsaard, J., et al. (2017). PCL/PHBV Blended Three Dimensional Scaffolds Fabricated by Fused Deposition Modeling and Responses of Chondrocytes to the Scaffolds. *J. Biomed. Mater. Res.* 105 (5), 1141–1150. doi:10.1002/jbm.b.33658

Kumar, P., Sharma, R., Ray, S., Mehariya, S., Patel, S. K. S., Lee, J.-K., et al. (2015). Dark Fermentative Bioconversion of Glycerol to Hydrogen by Bacillus Thuringiensis. *Bioresour. Tech.* 182, 383–388. doi:10.1016/j.biortech.2015.01.138

Kundrat, V., Cernekova, N., Kovalcik, A., Enev, V., and Marova, I. (2019). Drug Release Kinetics of Electrospun PHB Meshes. *Materials* 12 (12), 1924. doi:10.3390/ma12121924

Lenz, R. W., and Marchessault, R. H. (2005). Bacterial Polyesters: Biosynthesis, Biodegradable Plastics and Biotechnology. *Biomacromolecules* 6 (1), 1–8. doi:10.1021/bm049700c

Li, J., Yun, H., Gong, Y., Zhao, N., and Zhang, X. (2005). Effects of Surface Modification of Poly (3-Hydroxybutyrate-Co-3-Hydroxyhexanoate) (PHBHHx) on Physicochemical Properties and on Interactions with MC3T3-E1 Cells. *J. Biomed. Mater. Res.* 75a (4), 985–998. doi:10.1002/jbm.a.30504

Li, L., Lin, Q., Tang, M., Duncan, A. J. E., and Ke, C. (2019). Advanced Polymer Designs for Direct-Ink-Write 3D Printing. *Chem. Eur. J.* 25 (46), 10768–10781. doi:10.1002/chem.201900975

Li, X.-T., Sun, J., Chen, S., and Chen, G.-Q. (2008). In Vitroinvestigation of Maleated Poly(3-Hydroxybutyrate-Co-3-Hydroxyhexanoate) for its Biocompatibility to Mouse Fibroblast L929 and Human Microvascular Endothelial Cells. *J. Biomed. Mater. Res.* 87a (3), 832–842. doi:10.1002/jbm.a.31890

Li, X., Li, X., Chen, D., Guo, J.-L., Feng, D.-F., Sun, M.-Z., et al. (2016a). Evaluating the Biological Impact of Polyhydroxyalkanoates (PHAs) on Developmental and Exploratory Profile of Zebrafish Larvae. *RSC Adv.* 6 (43), 37018–37030. doi:10.1039/c6ra04329a

Li, Z., Yang, J., and Loh, X. J. (2016b). Polyhydroxyalkanoates: Opening Doors for a Sustainable Future. *NPG Asia Mater.* 8, e265. doi:10.1038/am.2016.48

Lim, J., You, M., Li, J., and Li, Z. (2017). Emerging Bone Tissue Engineering via Polyhydroxyalkanoate (PHA)-based Scaffolds. *Mater. Sci. Eng. C* 79, 917–929. doi:10.1016/j.msec.2017.05.132

Lin, L., Chen, J., Mitra, R., Gao, Q., Cheng, F., Xu, T., et al. (2021). Optimising PHBV Biopolymer Production in Haloarchaea via CRISPRi-Mediated Redirection of Carbon Flux. *Commun. Biol.* 4 (1), 1007. doi:10.1038/s42003-021-02541-z

Ling, C., Qiao, G.-Q., Shuai, B.-W., Olavarria, K., Yin, J., Xiang, R.-J., et al. (2018). Engineering NADH/NAD+ Ratio in Halomonas Bluephagenesis for Enhanced Production of Polyhydroxyalkanoates (PHA). *Metab. Eng.* 49, 275–286. doi:10.1016/j.ymben.2018.09.007

Lu, Q., Han, J., Zhou, L., Zhou, J., and Xiang, H. (2008). Genetic and Biochemical Characterization of the Poly(3-Hydroxybutyrate- Co -3-Hydroxyvalerate) Synthase in Haloferax Mediterranei. *J. Bacteriol.* 190 (12), 4173–4180. doi:10.1128/JB.00134-08

Luo, L., Wei, X., and Chen, G.-Q. (2009). Physical Properties and Biocompatibility of Poly(3-Hydroxybutyrate-Co-3-Hydroxyhexanoate) Blended with Poly(3-Hydroxybutyrate-Co-4-Hydroxybutyrate). *J. Biomater. Sci. Polym. Edition* 20 (11), 1537–1553. doi:10.1163/092050609x12464345023041

Ma, Z., Zeng, F., Wang, J., Yang, S., and Liu, C. (2017). Enhanced Cell Affinity of PHBHHx Composite Scaffold with Polylactide-Graft-Hydroxyapatite as Compatibilizer. *Mater. Sci. Eng. C* 80, 472–483. doi:10.1016/j.msec.2017.06.003

Maitre, M., Klein, C., and Mensah-Nyagan, A. G. (2016). Mechanisms for the Specific Properties of γ-Hydroxybutyrate in Brain. *Med. Res. Rev.* 36 (3), 363–388. doi:10.1002/med.21382

Martin, D. P., and Williams, S. F. (2003). Medical Applications of Poly-4-Hydroxybutyrate: a strong Flexible Absorbable Biomaterial. *Biochem. Eng. J.* 16 (2), 97–105. doi:10.1016/S1369-703x(03)00040-8

Mastrogiacomo, M., Muraglia, A., Komlev, V., Peyrin, F., Rustichelli, F., Crovace, A., et al. (2005). Tissue Engineering of Bone: Search for a Better Scaffold. *Orthod. Craniofac. Res.* 8 (4), 277–284. doi:10.1111/j.1601-6343.2005.00350.x

Mazzoli, A. (2013). Selective Laser Sintering in Biomedical Engineering. *Med. Biol. Eng. Comput.* 51 (3), 245–256. doi:10.1007/s11517-012-1001-x

Melchels, F. P. W., Feijen, J., and Grijpma, D. W. (2010). A Review on Stereolithography and its Applications in Biomedical Engineering. *Biomaterials* 31 (24), 6121–6130. doi:10.1016/j.biomaterials.2010.04.050

Meng, D.-C., and Chen, G.-Q. (2017). Synthetic Biology of Polyhydroxyalkanoates (PHA). *Synth. Biol. - Metab. Eng.* 162, 147–174. doi:10.1007/10_2017_3

Moore, T., Adhikari, R., and Gunatillake, P. (2005). Chemosynthesis of Bioresorbable Poly(γ-Butyrolactone) by Ring-Opening Polymerisation: a Review. *Biomaterials* 26 (18), 3771–3782. doi:10.1016/j.biomaterials.2004.10.002

Mota, C., Puppi, D., Chiellini, F., and Chiellini, E. (2015). Additive Manufacturing Techniques for the Production of Tissue Engineering Constructs. *J. Tissue Eng. Regen. Med.* 9 (3), 174–190. doi:10.1002/term.1635

Możejko-Ciesielska, J., and Kiewisz, R. (2016). Bacterial Polyhydroxyalkanoates: Still Fabulous? *Microbiol. Res.* 192, 271–282. doi:10.1016/j.micres.2016.07.010

Możejko-Ciesielska, J., Marciniak, P., and Szacherska, K. (2019). Polyhydroxyalkanoates Synthesized by Aeromonas Species: Trends and Challenges. *Polymers* 11 (8), 1328. doi:10.3390/polym11081328

Nelson, T., Kaufman, E., Kline, J., and Sokoloff, L. (1981). The Extraneural Distribution of ?-Hydroxybutyrate. *J. Neurochem.* 37 (5), 1345–1348. doi:10.1111/j.1471-4159.1981.tb04689.x

Nodarian, T., Sariali, E., Khiami, F., Pascal-Mousselard, H., and Catonné, Y. (2010). Iliac Crest Bone Graft Harvesting Complications: A Case of Liver Herniation. *Orthopaedics Traumatol. Surg. Res.* 96 (5), 593–596. doi:10.1016/j.otsr.2010.03.016

O'Connor, S., Szwej, E., Nikodinovic-Runic, J., O'Connor, A., Byrne, A. T., Devocelle, M., et al. (2013). The Anti-cancer Activity of a Cationic Anti-microbial Peptide Derived from Monomers of Polyhydroxyalkanoate. *Biomaterials* 34 (11), 2710–2718. doi:10.1016/j.biomaterials.2012.12.032

O'Keefe, R. J., and Mao, J. (2011). Bone Tissue Engineering and Regeneration: From Discovery to the Clinic-An Overview. *Tissue Eng. B: Rev.* 17 (6), 389–392. doi:10.1089/ten.teb.2011.0475

Obruca, S., Sedlacek, P., Mravec, F., Samek, O., and Marova, I. (2016). Evaluation of 3-hydroxybutyrate as an Enzyme-Protective Agent against Heating and Oxidative Damage and its Potential Role in Stress Response of Poly(3-Hydroxybutyrate) Accumulating Cells. *Appl. Microbiol. Biotechnol.* 100 (3), 1365–1376. doi:10.1007/s00253-015-7162-4

Peng, S.-W., Guo, X.-Y., Shang, G.-G., Li, J., Xu, X.-Y., You, M.-L., et al. (2011). An Assessment of the Risks of Carcinogenicity Associated with Polyhydroxyalkanoates through an Analysis of DNA Aneuploid and Telomerase Activity. *Biomaterials* 32 (10), 2546–2555. doi:10.1016/j.biomaterials.2010.12.051

Perić Kačarević, Ž., Rider, P., Alkildani, S., Retnasingh, S., Pejakić, M., Schnettler, R., et al. (2020). An Introduction to Bone Tissue Engineering. *Int. J. Artif. Organs* 43 (2), 69–86. doi:10.1177/0391398819876286

Philip, S., Keshavarz, T., and Roy, I. (2007). Polyhydroxyalkanoates: Biodegradable Polymers with a Range of Applications. *J. Chem. Technol. Biotechnol.* 82 (3), 233–247. doi:10.1002/jctb.1667

Piacentini, E., Dragosavac, M., and Giorno, L. (2017). Pharmaceutical Particles Design by Membrane Emulsification: Preparation Methods and Applications in Drug Delivery. *Cpd* 23 (2), 302–318. doi:10.2174/1381612823666161117160940

Plikk, P., Målberg, S., and Albertsson, A.-C. (2009). Design of Resorbable Porous Tubular Copolyester Scaffolds for Use in Nerve Regeneration. *Biomacromolecules* 10 (5), 1259–1264. doi:10.1021/bm900093r

Pramual, S., Assavanig, A., Bergkvist, M., Batt, C. A., Sunintaboon, P., Lirdprapamongkol, K., et al. (2016). Development and Characterization of Bio-Derived Polyhydroxyalkanoate Nanoparticles as a Delivery System for Hydrophobic Photodynamic Therapy Agents. *J. Mater. Sci. Mater. Med.* 27 (2), 40. doi:10.1007/s10856-015-5655-4

Preethi Soundarya, S., Haritha Menon, A., Viji Chandran, S., and Selvamurugan, N. (2018). Bone Tissue Engineering: Scaffold Preparation Using Chitosan and Other Biomaterials with Different Design and Fabrication Techniques. *Int. J. Biol. Macromolecules* 119, 1228–1239. doi:10.1016/j.ijbiomac.2018.08.056

Prieto, A., Escapa, I. F., Martínez, V., Dinjaski, N., Herencias, C., de la Peña, F., et al. (2016). A Holistic View of Polyhydroxyalkanoate Metabolism inPseudomonas Putida. *Environ. Microbiol.* 18 (2), 341–357. doi:10.1111/1462-2920.12760

Qin, Q., Ling, C., Zhao, Y., Yang, T., Yin, J., Guo, Y., et al. (2018). CRISPR/Cas9 Editing Genome of Extremophile Halomonas Spp. *Metab. Eng.* 47, 219–229. doi:10.1016/j.ymben.2018.03.018

Qu, X., Wu, Q., Zhang, K., and Chen, G. (2006). *In Vivo* studies of Poly(3-Hydroxybutyrate-Co-3-Hydroxyhexanoate) Based Polymers: Biodegradation and Tissue Reactions. *Biomaterials* 27 (19), 3540–3548. doi:10.1016/j.biomaterials.2006.02.015

Raberg, M., Volodina, E., Lin, K., and Steinbüchel, A. (2018). Ralstonia eutrophaH16 in Progress: Applications beside PHAs and Establishment as Production Platform by Advanced Genetic Tools. *Crit. Rev. Biotechnol.* 38 (4), 494–510. doi:10.1080/07388551.2017.1369933

Radivojevic, J., Skaro, S., Senerovic, L., Vasiljevic, B., Guzik, M., Kenny, S. T., et al. (2016). Polyhydroxyalkanoate-based 3-hydroxyoctanoic Acid and its Derivatives as a Platform of Bioactive Compounds. *Appl. Microbiol. Biotechnol.* 100 (1), 161–172. doi:10.1007/s00253-015-6984-4

Raeisdasteh Hokmabad, V., Davaran, S., Ramazani, A., and Salehi, R. (2017). Design and Fabrication of Porous Biodegradable Scaffolds: a Strategy for Tissue Engineering. *J. Biomater. Sci. Polym. Edition* 28 (16), 1797–1825. doi:10.1080/09205063.2017.1354674

Rai, R., Yunos, D. M., Boccaccini, A. R., Knowles, J. C., Barker, I. A., Howdle, S. M., et al. (2011). Poly-3-hydroxyoctanoate P(3HO), a Medium Chain Length Polyhydroxyalkanoate Homopolymer from *Pseudomonas mendocina*. *Biomacromolecules* 12 (6), 2126–2136. doi:10.1021/bm2001999

Raghuram, A., Singh, A., Chang, D. K., Nunez, M., and Reece, E. M. (2019). Bone Grafts, Bone Substitutes, and Orthobiologics: Applications in Plastic Surgery. *Semin. Plast. Surg.* 33 (3), 190–199. doi:10.1055/s-0039-1693020

Rahman, A., Linton, E., Hatch, A. D., Sims, R. C., and Miller, C. D. (2013). Secretion of Polyhydroxybutyrate in *Escherichia coli* Using a Synthetic Biological Engineering Approach. *J. Biol. Eng.* 7 (1), 24. doi:10.1186/1754-1611-7-24

Ramier, J., Grande, D., Bouderlique, T., Stoilova, O., Manolova, N., Rashkov, I., et al. (2014). From Design of Bio-Based Biocomposite Electrospun Scaffolds to Osteogenic Differentiation of Human Mesenchymal Stromal Cells. *J. Mater. Sci. Mater. Med.* 25 (6), 1563–1575. doi:10.1007/s10856-014-5174-8

Ray, S., and Kalia, V. C. (2017). Biomedical Applications of Polyhydroxyalkanoates. *Indian J. Microbiol.* 57 (3), 261–269. doi:10.1007/s12088-017-0651-7

Raza, Z. A., Abid, S., and Banat, I. M. (2018a). Polyhydroxyalkanoates: Characteristics, Production, Recent Developments and Applications. *Int. Biodeterioration Biodegradation* 126, 45–56. doi:10.1016/j.ibiod.2017.10.001

Raza, Z. A., Riaz, S., and Banat, I. M. (2018b). Polyhydroxyalkanoates: Properties and Chemical Modification Approaches for Their Functionalization. *Biotechnol. Prog.* 34 (1), 29–41. doi:10.1002/btpr.2565

Reddy, C. S. K., Ghai, R., Rashmiand Kalia, V. C. (2003). Polyhydroxyalkanoates: an Overview. *Bioresour. Tech.* 87 (2), 137–146. doi:10.1016/S0960-8524(02)00212-2

Rowlands, A. S., Lim, S. A., Martin, D., and Cooper-White, J. J. (2007). Polyurethane/poly(lactic-co-glycolic) Acid Composite Scaffolds Fabricated by Thermally Induced Phase Separation. *Biomaterials* 28 (12), 2109–2121. doi:10.1016/j.biomaterials.2006.12.032

Schaakxs, D., Kalbermatten, D. F., Pralong, E., Raffoul, W., Wiberg, M., and Kingham, P. J. (2017). Poly-3-hydroxybutyrate Strips Seeded with Regenerative Cells Are Effective Promoters of Peripheral Nerve Repair. *J. Tissue Eng. Regen. Med.* 11 (3), 812–821. doi:10.1002/term.1980

Schwille, P. (2013). Editorial: Chemistry Needed: Synthetic Biology as a New Incentive for Interdisciplinarity. *Angew. Chem. Int. Ed.* 52 (10), 2616–2617. doi:10.1002/anie.201300062

Shibuya, N., and Jupiter, D. C. (2015). Bone Graft Substitute. *Clin. Podiatric Med. Surg.* 32 (1), 21–34. doi:10.1016/j.cpm.2014.09.011

Shijun, X., Junsheng, M., Jianqun, Z., and Ping, B. (2016). *In Vitro* three-dimensional Coculturing Poly3-Hydroxybutyrate-Co-3-Hydroxyhexanoate with Mouse-Induced Pluripotent Stem Cells for Myocardial Patch Application. *J. Biomater. Appl.* 30 (8), 1273–1282. doi:10.1177/0885328215612115

Singh, A. K., Srivastava, J. K., Chandel, A. K., Sharma, L., Mallick, N., and Singh, S. P. (2019). Biomedical Applications of Microbially Engineered Polyhydroxyalkanoates: an Insight into Recent Advances, Bottlenecks, and Solutions. *Appl. Microbiol. Biotechnol.* 103 (5), 2007–2032. doi:10.1007/s00253-018-09604-y

Singh, M., Kumar, P., Ray, S., and Kalia, V. C. (2015). Challenges and Opportunities for Customizing Polyhydroxyalkanoates. *Indian J. Microbiol.* 55 (3), 235–249. doi:10.1007/s12088-015-0528-6

Steinbüchel, A., and Valentin, H. E. (1995). Diversity of Bacterial Polyhydroxyalkanoic Acids. *Fems Microbiol. Lett.* 128 (3), 219–228. doi:10.1016/0378-1097(95)00125-O

Stevens, M. M. (2008). Biomaterials for Bone Tissue Engineering. *Mater. Today* 11 (5), 18–25. doi:10.1016/S1369-7021(08)70086-5

Sudesh, K., Abe, H., and Doi, Y. (2000). Synthesis, Structure and Properties of Polyhydroxyalkanoates: Biological Polyesters. *Prog. Polym. Sci.* 25 (10), 1503–1555. doi:10.1016/S0079-6700(00)00035-6

Sun, J., Dai, Z., Zhao, Y., and Chen, G. (2007). *In Vitro* effect of Oligo-Hydroxyalkanoates on the Growth of Mouse Fibroblast Cell Line L929. *Biomaterials* 28 (27), 3896–3903. doi:10.1016/j.biomaterials.2007.05.011

Szwej, E., Devocelle, M., Kenny, S., Guzik, M., O'Connor, S., Nikodinovic-Runic, J., et al. (2015). The Chain Length of Biologically Produced (R)-3-hydroxyalkanoic Acid Affects Biological Activity and Structure of Anti-cancer Peptides. *J. Biotechnol.* 204, 7–12. doi:10.1016/j.jbiotec.2015.02.036

Tan, D., Xue, Y.-S., Aibaidula, G., and Chen, G.-Q. (2011). Unsterile and Continuous Production of Polyhydroxybutyrate by Halomonas TD01. *Bioresour. Tech.* 102 (17), 8130–8136. doi:10.1016/j.biortech.2011.05.068

Tian, S. (2020). Recent Advances in Functional Polyurethane and its Application in Leather Manufacture: A Review. *Polymers* 12 (9), 1996. doi:10.3390/polym12091996

Utsunomia, C., Ren, Q., and Zinn, M. (2020). Poly(4-Hydroxybutyrate): Current State and Perspectives. *Front. Bioeng. Biotechnol.* 8, 257. doi:10.3389/fbioe.2020.00257

Volova, T., Goncharov, D., Sukovatyi, A., Shabanov, A., Nikolaeva, E., and Shishatskaya, E. (2014). Electrospinning of Polyhydroxyalkanoate Fibrous Scaffolds: Effects on Electrospinning Parameters on Structure and Properties. *J. Biomater. Sci. Polym. Edition* 25 (4), 370–393. doi:10.1080/09205063.2013.862400

Vyavahare, S., Teraiya, S., Panghal, D., and Kumar, S. (2020). Fused Deposition Modelling: a Review. *Rpj* 26 (1), 176–201. doi:10.1108/Rpj-04-2019-0106

Wang, N., Zhou, Z., Xia, L., Dai, Y., and Liu, H. (2013). Fabrication and Characterization of Bioactive β-Ca2SiO4/PHBV Composite Scaffolds. *Mater. Sci. Eng. C* 33 (4), 2294–2301. doi:10.1016/j.msec.2013.01.059

Wang, Y.-W., Wu, Q., and Chen, G.-Q. (2004). Attachment, Proliferation and Differentiation of Osteoblasts on Random Biopolyester Poly(3-Hydroxybutyrate-Co-3-Hydroxyhexanoate) Scaffolds. *Biomaterials* 25 (4), 669–675. doi:10.1016/S0142-9612(03)00561-1

Wang, Y., Gao, R., Wang, P.-P., Jian, J., Jiang, X.-L., Yan, C., et al. (2012). The Differential Effects of Aligned Electrospun PHBHHx Fibers on Adipogenic and Osteogenic Potential of MSCs through the Regulation of PPARγ Signaling. *Biomaterials* 33 (2), 485–493. doi:10.1016/j.biomaterials.2011.09.089

Watanabe, S., Sano, N., Noda, I., and Ozaki, Y. (2009). Surface Melting and Lamella Rearrangement Process in Linear Low Density Polyethylene. *J. Phys. Chem. B* 113 (11), 3385–3394. doi:10.1021/jp809686m

Wei, D.-X., Dao, J.-W., and Chen, G.-Q. (2018). A Micro-Ark for Cells: Highly Open Porous Polyhydroxyalkanoate Microspheres as Injectable Scaffolds for Tissue Regeneration. *Adv. Mater.* 30 (31), 1802273. doi:10.1002/adma.201802273

Weimer, A., Kohlstedt, M., Volke, D. C., Nikel, P. I., and Wittmann, C. (2020). Industrial Biotechnology of Pseudomonas Putida: Advances and Prospects. *Appl. Microbiol. Biotechnol.* 104 (18), 7745–7766. doi:10.1007/s00253-020-10811-9

Wu, C. S., and Liao, H. T. (2017). Interface Design of Environmentally Friendly Carbon Nanotube-Filled Polyester Composites: Fabrication, Characterisation, Functionality and Application. *Express Polym. Lett.* 11 (3), 187–198. doi:10.3144/expresspolymlett.2017.20

Wu, X., Liu, Y., Li, X., Wen, P., Zhang, Y., Long, Y., et al. (2010). Preparation of Aligned Porous Gelatin Scaffolds by Unidirectional Freeze-Drying Method. *Acta Biomater.* 6 (3), 1167–1177. doi:10.1016/j.actbio.2009.08.041

Xiao, X.-Q., Zhao, Y., and Chen, G.-Q. (2007). The Effect of 3-hydroxybutyrate and its Derivatives on the Growth of Glial Cells. *Biomaterials* 28 (25), 3608–3616. doi:10.1016/j.biomaterials.2007.04.046

Xie, H., Li, J., Li, L., Dong, Y., Chen, G.-Q., and Chen, K. C. (2013). Enhanced Proliferation and Differentiation of Neural Stem Cells Grown on PHA Films Coated with Recombinant Fusion Proteins. *Acta Biomater.* 9 (8), 7845–7854. doi:10.1016/j.actbio.2013.04.038

Xue, J., Wu, T., Dai, Y., and Xia, Y. (2019). Electrospinning and Electrospun Nanofibers: Methods, Materials, and Applications. *Chem. Rev.* 119 (8), 5298–5415. doi:10.1021/acs.chemrev.8b00593

Xue, Q., Liu, X.-B., Lao, Y.-H., Wu, L.-P., Wang, D., Zuo, Z.-Q., et al. (2018). Anti-infective Biomaterials with Surface-Decorated Tachyplesin I. *Biomaterials* 178, 351–362. doi:10.1016/j.biomaterials.2018.05.008

Yang, X., Zhao, K., and Chen, G.-Q. (2002). Effect of Surface Treatment on the Biocompatibility of Microbial Polyhydroxyalkanoates. *Biomaterials* 23 (5), 1391–1397. doi:10.1016/S0142-9612(01)00260-5

Ye, H., Zhang, K., Kai, D., Li, Z., and Loh, X. J. (2018a). Polyester Elastomers for Soft Tissue Engineering. *Chem. Soc. Rev.* 47 (12), 4545–4580. doi:10.1039/c8cs00161h

Ye, J., Hu, D., Che, X., Jiang, X., Li, T., Chen, J., et al. (2018b). Engineering of Halomonas Bluephagenesis for Low Cost Production of Poly(3-Hydroxybutyrate-Co-4-Hydroxybutyrate) from Glucose. *Metab. Eng.* 47, 143–152. doi:10.1016/j.ymben.2018.03.013

Youm, Y.-H., Nguyen, K. Y., Grant, R. W., Goldberg, E. L., Bodogai, M., Kim, D., et al. (2015). The Ketone Metabolite β-hydroxybutyrate Blocks NLRP3 Inflammasome-Mediated Inflammatory Disease. *Nat. Med.* 21 (3), 263–269. doi:10.1038/nm.3804

Yu, F., Dong, T., Zhu, B., Tajima, K., Yazawa, K., and Inoue, Y. (2007). Mechanical Properties of Comonomer-Compositionally Fractionated Poly[(3-Hydroxybutyrate)-Co-(3-Mercaptopropionate)] with Low 3-mercaptopropionate Unit Content. *Macromol. Biosci.* 7 (6), 810–819. doi:10.1002/mabi.200600295

Zakaria, M. R., Ariffin, H., Mohd Johar, N. A., Abd-Aziz, S., Nishida, H., Shirai, Y., et al. (2010). Biosynthesis and Characterization of Poly(3-Hydroxybutyrate-Co-3-Hydroxyvalerate) Copolymer from Wild-type Comamonas Sp. EB172. *Polym. Degrad. Stab.* 95 (8), 1382–1386. doi:10.1016/j.polymdegradstab.2010.01.020

Zhang, H.-F., Ma, L., Wang, Z.-H., and Chen, G.-Q. (2009). Biosynthesis and Characterization of 3-hydroxyalkanoate Terpolyesters with Adjustable Properties byAeromonas Hydrophila. *Biotechnol. Bioeng.* 104 (3), 582–589. doi:10.1002/bit.22409

Zhang, J., Cao, Q., Li, S., Lu, X., Zhao, Y., Guan, J.-S., et al. (2013). 3-Hydroxybutyrate Methyl Ester as a Potential Drug against Alzheimer's Disease via Mitochondria protection Mechanism. *Biomaterials* 34 (30), 7552–7562. doi:10.1016/j.biomaterials.2013.06.043

Zhang, S. J., Li, Z. H., Zhang, Y. D., Chen, J., Li, Y., Wu, F. Q., et al. (2021). Ketone Body 3-Hydroxybutyrate Ameliorates Atherosclerosis via Receptor Gpr109a-Mediated Calcium Influx. *Adv. Sci.* 8 (9), 2003410. doi:10.1002/advs.202003410

Zhang, X., Lin, Y., Wu, Q., Wang, Y., and Chen, G.-Q. (2020). Synthetic Biology and Genome-Editing Tools for Improving PHA Metabolic Engineering. *Trends Biotechnol.* 38 (7), 689–700. doi:10.1016/j.tibtech.2019.10.006

Zhao, Y., Zou, B., Shi, Z., Wu, Q., and Chen, G.-Q. (2007). The Effect of 3-hydroxybutyrate on the *In Vitro* Differentiation of Murine Osteoblast MC3T3-E1 and *In Vivo* Bone Formation in Ovariectomized Rats. *Biomaterials* 28 (20), 3063–3073. doi:10.1016/j.biomaterials.2007.03.003

Zheng, K., and Boccaccini, A. R. (2017). Sol-gel Processing of Bioactive Glass Nanoparticles: A Review. *Adv. Colloid Interf. Sci.* 249, 363–373. doi:10.1016/j.cis.2017.03.008

Zheng, Y., Chen, J.-C., Ma, Y.-M., and Chen, G.-Q. (2020). Engineering Biosynthesis of Polyhydroxyalkanoates (PHA) for Diversity and Cost Reduction. *Metab. Eng.* 58, 82–93. doi:10.1016/j.ymben.2019.07.004

Zonari, A., Novikoff, S., Electo, N. R. P., Breyner, N. M., Gomes, D. A., Martins, A., et al. (2012). Endothelial Differentiation of Human Stem Cells Seeded onto Electrospun Polyhydroxybutyrate/polyhydroxybutyrate-Co-Hydroxyvalerate Fiber Mesh. *PLoS One* 7 (4), e35422. doi:10.1371/journal.pone.0035422

Conflict of Interest: The authors declare that the research was conducted in the absence of any commercial or financial relationships that could be construed as a potential conflict of interest.

Publisher's Note: All claims expressed in this article are solely those of the authors and do not necessarily represent those of their affiliated organizations, or those of the publisher, the editors and the reviewers. Any product that may be evaluated in this article, or claim that may be made by its manufacturer, is not guaranteed or endorsed by the publisher.

GLOSSARY

PHAs Polyhydroxyalkanoates

PHB Poly-3-hydroxybutyrate

P4HB Poly-4-hydroxybutyrate

P3HO Poly-3-hydroxyoctanoate

P3HP Poly-3-hydroxyproiponate

scl Short chain length

mcl Medium chain length

T_m Melting point temperature

T_g Glass transition temperature

3HB 3-hydroxybutyrate

4HB 4-hydroxybutyrate

3HP 3-hydroxypropionate

3HV 3-hydroxyvalerate

3HHx 3-hydroxyhexanoate

3HO 3-hydroxyoctanoate

3HD 3-hydroxydecanoate

3HDD 3-hydroxydodecanoate

3HTD 3-hydroxytetradecanoate

scl-*co*-mcl-PHA (short-*co*-medium)-chain length-PHA

CRISPR Clustered regularly interspaced short palindromic repeats

RBS Ribosome-binding site

PhaC PHAsynthase

PhaA β-ketothiolase: PhaB: Acetoacetyl-CoA reductase

4HbD 4-hydroxybutyrate dehydrogenase

SucD Succinate semialdehyde dehydrogenase

PhaG 3-hydroxyacyl-ACP:CoA transacylase

PhaJ enoyl-CoA hydratase

3HB-CoA 3-hydroxybutyrate-CoA

4HB-CoA 4-hydroxybutyrate-CoA

3HV-CoA 3-hydroxyvaleryl-CoA

3HP-CoA 3-hydroxyproiponate-CoA

3HA-CoA 3-hydroxyacyl-CoA

P34HB Poly (3-hydroxybutyrate-*co*-4- hydroxybutyrate)

PHBHHx Poly (3-hydroxybutyrate-*co*-3-hydroxyhexanoate)

PHBV Poly (3-hydroxybutyrate-*co*-3-hydroxyvalerate)

P3HHx3HO Poly(3-hydroxyhexanoate-*co*-3-hydroxyoctanoate)

PHBVHHx Poly(3-hydroxybutyrate-*co*-3-hydroxyvalerate-*co*-3-hydroxyhexanoate)

OHB Oligo(3-hydroxybutyrate)

O3HB4HB Oligo(3-hydroxybutyrate-*co*-4-hydroxybutyrate)

OHBHHx Oligo(3-hydroxybutyrate-*co*-3-hydroxyhexanoate)

OmclHA Medium-chain-length oligo(3-hydroxyalkanoate)

PP Polypropylene

PE Polyethylene

PEG Poly(ethylene glycol)

frontiers in Bioengineering and Biotechnology

REVIEW
published: 12 January 2022
doi: 10.3389/fbioe.2021.787538

Cartilage Tissue Engineering Approaches Need to Assess Fibrocartilage When Hydrogel Constructs Are Mechanically Loaded

Hamed Alizadeh Sardroud[1]*, *Tasker Wanlin*[2], *Xiongbiao Chen*[1,3] and *B. Frank Eames*[1,2]

[1]Division of Biomedical Engineering, College of Engineering, University of Saskatchewan, Saskatoon, SK, Canada, [2]Department of Anatomy, Physiology, and Pharmacology, University of Saskatchewan, Saskatoon, SK, Canada, [3]Department of Mechanical Engineering, College of Engineering, University of Saskatchewan, Saskatoon, SK, Canada

Chondrocytes that are impregnated within hydrogel constructs sense applied mechanical force and can respond by expressing collagens, which are deposited into the extracellular matrix (ECM). The intention of most cartilage tissue engineering is to form hyaline cartilage, but if mechanical stimulation pushes the ratio of collagen type I (Col1) to collagen type II (Col2) in the ECM too high, then fibrocartilage can form instead. With a focus on Col1 and Col2 expression, the first part of this article reviews the latest studies on hyaline cartilage regeneration within hydrogel constructs that are subjected to compression forces (one of the major types of the forces within joints) *in vitro*. Since the mechanical loading conditions involving compression and other forces in joints are difficult to reproduce *in vitro*, implantation of hydrogel constructs *in vivo* is also reviewed, again with a focus on Col1 and Col2 production within the newly formed cartilage. Furthermore, mechanotransduction pathways that may be related to the expression of Col1 and Col2 within chondrocytes are reviewed and examined. Also, two recently-emerged, novel approaches of load-shielding and synchrotron radiation (SR)–based imaging techniques are discussed and highlighted for future applications to the regeneration of hyaline cartilage. Going forward, all cartilage tissue engineering experiments should assess thoroughly whether fibrocartilage or hyaline cartilage is formed.

Keywords: cartilage tissue engineering, mechanical compression, *in vitro*, *in vivo*, Col1, Col2, hyaline, fibrocartilage

OPEN ACCESS

Edited by:
Farnaz Ghorbani,
University of Erlangen Nuremberg, Germany

Reviewed by:
Emeline Groult,
UMS3760 Institut de Biologie et Chimie des Protéines (IBCP), France
Megan Elin Cooke,
McGill University, Canada
Hemanth Gudapati,
Duke University, United States

***Correspondence:**
Hamed Alizadeh Sardroud
hamed.alizadeh@usask.ca

Specialty section:
This article was submitted to Biomaterials, a section of the journal Frontiers in Bioengineering and Biotechnology

Received: *30 September 2021*
Accepted: *10 December 2021*
Published: *12 January 2022*

Citation:
Alizadeh Sardroud H, Wanlin T, Chen X and Eames BF (2022) Cartilage Tissue Engineering Approaches Need to Assess Fibrocartilage When Hydrogel Constructs Are Mechanically Loaded. Front. Bioeng. Biotechnol. 9:787538. doi: 10.3389/fbioe.2021.787538

INTRODUCTION

In osteoarthritis (OA), articular cartilage at the end of bones, such as in the knee or elbow joint, degrades by various injuries or normal wear and tear caused by aging. In addition, cartilage damage can affect the mobility of injured young patients (Buckwalter and Mankin, 1998). Articular cartilage is hyaline cartilage, an avascular tissue that contains chondrocytes within a dense extracellular matrix (ECM) mainly composed of proteoglycans and collagen type II (Col2) (Landinez et al., 2009; Becerra et al., 2010). Since hyaline cartilage does not have self-healing potential, various clinical strategies, such as partial or total joint replacement, microfracture, and chondrocyte implantation, have been developed and employed to treat damaged articular cartilage. However, these treatments do not result in ever-lasting outcomes, and patients typically need

secondary surgeries. Relevant to this review article, another challenge of these treatments is that they can lead to formation of fibrocartilage, which has inferior mechanical properties to hyaline cartilage in carrying out the function of articular cartilage (Li K et al., 2017).

To provide a more permanent solution to articular cartilage damage, cartilage tissue engineering (CTE) is an interdisciplinary approach that combines knowledge of engineering and cell biology. In this regard, various synthetic and natural biomaterials with proper biocompatibilities have been used to fabricate hydrogel, polyester-based solid, and/or hybrid constructs (Little et al., 2011; Olubamiji et al., 2016a; Olubamiji et al., 2016b; You et al., 2016; You et al., 2017; Armiento et al., 2018; You et al., 2018; Sadeghianmaryan et al., 2020). Hydrogels have received much interest as scaffolds for CTE studies because similar to native cartilage, cells can be impregnated within hydrated polymer networks to maintain chondrocyte morphology and phenotype (Vega et al., 2017).

A major limitation, however, is that hydrogels do not have adequate mechanical strength to withstand applied forces after *in vivo* implantation, and this force application can change the type of cartilage formed. Applied forces are transmitted to the impregnated cells, which respond by expressing such proteins as Col1 and Col2 (Bian et al., 2010; Nebelung et al., 2012). The presence of Col1 is a big problem for articular cartilage regeneration because hyaline cartilage has little to no Col1, whereas Col1 is a marker of fibrocartilage (Ham, 1965). Bioreactors have been utilized *in vitro* to simulate the joint's compressive forces *in vivo*. To various levels of success, mechanical stimulation of hydrogels promoted some biological activities of chondrocytes, including non-specific measures of collagen secretion (Schulz and Bader, 2007; Natenstedt et al., 2015). However, a critical aspect of such studies is to see what type of collagens was produced in response to compression forces *in vitro*. If the ratio of Col1: Col2 is relatively high, then the experiment produced a more fibrocartilage-like tissue, which has inferior biological and mechanical properties to hyaline cartilage when seeking to regenerate articular cartilage.

Whether implanted hydrogels work for hyaline cartilage regeneration *in vivo*, where various physiological and mechanical factors are involved, needs to be investigated before going to clinical applications (Chu et al., 2010). To be fair, the *in vivo* mechanical environment of joints is extremely complex, making it extremely difficult to simulate using a bioreactor. The implantation of hydrogel constructs within the joints of various animal models needs to be investigated to see whether the resulting tissue formed is the desired hyaline cartilage or fibrocartilage. Again, the ratio of Col1:Col2 produced in these experiments is critical, so we begin by reviewing how current *in vitro* and *in vivo* studies have analyzed specific collagen expression in determining whether hydrogel-loaded constructs produce hyaline cartilage or fibrocartilage.

In almost every experimental study to date, the implanted constructs need to be extracted by invasive and destructive techniques after euthanizing the animals in order to evaluate the type of cartilage formed. Different visualizing tools can also be utilized to assess tissue regeneration and construct degradation without the need to sacrifice the animals (Izadifar et al., 2016b; Ning et al., 2021). By using the novel imaging techniques covered in this review, the number of required animals for preclinical experiments would be reduced, and these methods can be adapted for future clinical applications.

Cells respond to applied mechanical forces by varying biochemical signals that can affect gene expression within the cells (Knobloch et al., 2008). Some CTE studies illustrated that compressive force applied to mono-layer chondrocytes or 3D chondrocyte-impregnated hydrogels activate cellular signaling pathways (Allen et al., 2012; Bougault et al., 2012; Sanz-Ramos et al., 2012). Several signaling mechanisms are involved in mechanical stimulation of chondrocytes, and their influence on gene expression will be also reviewed in this article.

As an overview for this article, mechanical compressive loading can play a crucial role in the regeneration of new hyaline cartilage within hydrogel constructs by stimulating cells to express collagen genes and depositing these collagens to the ECM. The cartilage in joints is abundant in Col2, but deposition of Col1 from the impregnated cells can lead to a fibrocartilage-like tissue with inferior mechanical and biological properties compared to native articular cartilage. Thus, the generation of Col1 and Col2 in mechanically loaded, chondrocyte-impregnated hydrogels is the focus of this article.

Hyaline vs. Fibrocartilage: Cellular, Molecular, and Mechanical Differences

Hyaline cartilage is a shiny, white, translucent, and flexible cartilage and can be found in the articular surfaces of movable joints such as knee and elbow. Other than joints, hyaline cartilage is also present in the rib tips, nose, larynx, and the rings of the trachea (Parsons, 1998). Cell types do differ between hyaline cartilage and fibrocartilage, but they are two types of chondrocytes: one is called a hyaline matrix–rich chondrocyte, and the other is a cell-rich fibrous chondrocyte (Benjamin and Ralphs, 1991). Articular cartilage has a very low cell density (5% of cartilage mass), and hyaline matrix–rich chondrocytes are surrounded by the cartilage ECM either as single cells or as clusters of cells (Anderson et al., 1964). In total, 30% of the hyaline cartilage ECM by weight is a solid component that is rich in ground substance including mostly glycosaminoglycans (GAGs) and Col2 fibers. Sulfation of GAGs in the ECM attracts water, which makes up 70% of the ECM of hyaline cartilage by weight and gives articular cartilage its tremendous compressive resistant strength (Brown and Eames, 2016). Articular cartilage has four different zones, including a superficial zone, a middle or transitional zone, a deep zone, and a calcified zone. Contents of the GAGs and collagens vary from the superficial zone to the calcified zone. The collagen content decreases from the top to the bottom of the articular cartilage, whereas the GAGs increase in this direction. Apart from the very thin superficial zone, the other zones are types of hyaline cartilage. The mechanical properties of articular cartilage also vary according to the zonal organization of the ECM molecules, and the compressive modulus increases from the superficial zone

TABLE 1 | Summary of characteristics of hyaline and fibrocartilage.

	Hyaline	Fibrocartilage
Location	Joints, rib tips, nose, larynx, and the rings of the trachea	Intervertebral discs of the spine, tendons, and ligaments and jaw
Appearance	Shiny, white, and translucent	White, dense, and opaque
Cell type	Hyaline matrix–rich chondrocytes	Cell-rich fibrous chondrocytes and fibroblasts
Cell organization	Round single or cluster of cells in lacunae	Single and small groups of cells in lacunae, round or aligned in rows
ECM	GAGs and Col2	GAGs, Col1, and Col2

to the calcified zone of the articular cartilage (Schinagl et al., 1997).

Fibrocartilage is a white, dense, opaque, and flexible cartilage located in the intervertebral discs of the spine, tendons, ligaments, and jaw (Benjamin and Ralphs, 2004). Cell density within fibrocartilage is higher than that in hyaline cartilage, and the two major types of cells in fibrocartilage are chondrocytes and fibroblasts. Single or very small groups of fibroblasts and cell-rich fibrous chondrocytes are in lacunae, and their shape can be round, but most fibrocartilage lacunae are axially aligned with the collagen fibers (Benjamin and Evans, 1990). In contrast to hyaline cartilage, fibrocartilage has abundant Col1 in addition to Col2. Fibrocartilage contains denser and spatially organized collagen fibers than hyaline cartilage, so fibrocartilage is the strongest type of cartilage in the body (Poole et al., 1982; Kheir and Shaw, 2009). Critically for current clinical problems in articular cartilage regeneration, fibrocartilage also has very low levels of GAGs, which means that it lacks the compressive resistant force needed at surfaces of articulating joints (Armiento et al., 2019).

Table 1 shows the differences between hyaline cartilage and fibrocartilage. The main difference between them is the high level of Col1 in fibrocartilage, whereas Col1 is very low or absent in hyaline cartilage. Also, the different ECM features of hyaline and fibrocartilage give them different mechanical features from each other. Hyaline cartilage has high compressive and low tensile properties, whereas fibrocartilage has low compressive and high tensile properties.

In Vitro Bioreactors Can Mimic *In Vivo* Compression Forces

Mechanical forces at an appropriate magnitude in a physiological range are essential for the maintenance of hyaline cartilage to prevent its degeneration. These forces stimulate chondrocytes for the biosynthesis of cartilaginous molecules needed for the integrity and maintenance of cartilage. However, over-loading can result in cartilage damage and degenerative joint diseases (Musumeci, 2016). Native cartilage in joints endures different mechanical forces without getting damaged, and hence fabricated cartilage constructs must withstand similar mechanical forces meanwhile generating and maintaining hyaline cartilage.

In this regard, biodynamic machines have been utilized as *in vitro* bioreactors to culture cell-impregnated hydrogels in order to understand how cells might respond to the physiological or superphysiological loadings that they might encounter if they were implanted *in vivo*. However, many types of force exist in joints, and simulating all those forces in a single bioreactor is not feasible (Wimmer et al., 2004; Grad et al., 2011). Hence, most of the custom-made or commercial bioreactors have been developed to apply a single type of force, such as compression (Kisiday et al., 2004; El-Ayoubi et al., 2011), tension (Lee J. K et al., 2017; Wu S et al., 2017), or shear (Marlovits et al., 2003; Gemmiti and Guldberg 2009). Multi-force bioreactors also have been developed to include two types of force, such as compression and linear shear stress, in a bioreactor chamber (Marlovits et al., 2003; Waldman et al., 2007). Compressive loading is one of the major mechanical forces applied on articular cartilage (Martel-Pelletier et al., 2008), and accordingly, most *in vitro* studies investigated the responses of cells to compressive forces (Hunter et al., 2002; Bryant et al., 2008; Pelaez et al., 2009; Wang et al., 2009).

Hydrogels are a popular type of constructs for CTE applications and have been used extensively for *in vitro* mechanical compressions and *in vivo* implantations (Bryant et al., 2008). These constructs are soft polymeric networks with low mechanical properties. Hydrogels will never mimic cartilage ECM because at most a hydrogel has a few 100 kPa compression modulus that is 0.03–1% of native cartilage having a compression modulus of 0.08–320 MPa increasing from the superficial to the calcified zone (Schinagl et al., 1997; Yang and Temenoff, 2009; Karimi et al., 2015). The effects of mechanical compression on chondrocytes impregnated within hydrogels both *in vitro* and *in vivo* will be discussed in the following sections.

Static Compression Suppressed Cartilage Regeneration

Application of a compression force can be in a static force regime by which a constant compressive strain is subjected to the engineered constructs for a continuous and limited time. Compressive strain is the deformation of the constructs in one spatial dimension due to the applied compressive force. Various studies applied static compression loadings on cartilage explants and engineered cartilage constructs. However, this type of force regime did not show satisfactory results of cartilage growth and even inhibited the secretion of cartilage ECM (Jones et al., 1982; Gray et al., 1988; Mouw et al., 2007). For example, bovine cartilage explants were compressed for 24 h, and as a result, transcription levels for *Col2a1* and *aggrecan* were down-regulated compared to those of unloaded samples (Fitzgerald et al., 2004). Chondrocytes seeded on non-woven polyglycolic acid (PGA) composites and subjected to 50% static compression for 24 h resulted in 35 and 57% reduction in total protein and sulfated GAG secretion,

respectively (Davisson et al., 2002). Static compression of agarose gels did not change the biosynthesis of cartilage over short periods of loading but did reduce cartilage production after longer durations of compression (Buschmann et al., 1995). 25 and 50% static compression of chondrocytes cultured in Col1 hydrogels inhibited both *Col1a2* and *Col2a1* expressions after 24 h (Hunter et al., 2002). ECM pore sizes of cells might be reduced due to static compression when they are impregnated in hydrogels. Consequently, nutrient transportation into cells is reduced, suppressing the expression of cartilage ECM (Freeman et al., 1994; Guilak et al., 1995). Such widely reported inhibitory effects of static compression on chondrocytes led most researchers to switch to dynamic compression force applications.

Dynamic Compression Showed Limited Positive Effects on Cartilage Regeneration

In the natural environment of a joint, articular cartilage is subjected to dynamic forces during walking, running, and jumping motions (Chen C et al., 2013). Therefore, recent studies subjected hydrogel constructs to dynamic forces in order to observe the response of chondrocytes (Sauerland et al., 2003; Martel-Pelletier et al., 2008; Ryan et al., 2009).

Two major parameters within dynamic compression systems are the magnitude of compressive strain and the duration of loading. Human joints undergo cartilage deformations during physiological movements. Various techniques have estimated the applied physiological strains, when human joints move, to be in a range of 3–20% cartilage thickness deformation (Armstrong et al., 1979; Macirowski et al., 1994; Eckstein et al., 1999; Eckstein et al., 2000). Consequently, CTE *in vitro* compression studies worked in this strain range, mostly using 10% strain as a simulated physiological strain (Mauck et al., 2000; Mauck et al., 2003; Lima et al., 2007).

The GAG content was commonly analyzed in samples subjected to physiological compression strains, but unfortunately, specifying the levels of Col1 and Col2 production, which would be required to analyze fibrocartilage formation, were neglected in most studies (Mauck et al., 2000; Shelton et al., 2003; Kisiday et al., 2004). For example, chondrocyte-impregnated agarose hydrogels were subjected to 3% dynamic strain with different frequencies ranging from 0.001 to 1.0 Hz for different loading durations. Higher DNA and GAG accumulation were reported at 23 days (a relatively late timepoint) in the dynamically loaded samples (Buschmann et al., 1995). Assessment of hydroxyproline to indicate total collagen content was performed on chondrocytes seeded in agarose, fibrin, or peptide hydrogels that were loaded with different strains (2.5–14%) (Mauck et al., 2000; Mauck et al., 2003; Hunter et al., 2004; Kisiday et al., 2004). For example, chondrocyte-impregnated agarose gel discs were dynamically loaded using a custom-designed bioreactor at a frequency of 1 Hz and 10% strain for 4 weeks. Both GAG and hydroxyproline contents were greater for the loaded samples than unloaded controls at day 21 (Mauck et al., 2000). Initial cell density in these experiments also positively influenced both mechanical properties and cartilage tissue growth within the 10% strain-loaded hydrogels. The dynamic force regime had 1 Hz frequency and was applied 2 h per day and 5 days per week. Enhancement in GAG and collagen content (~150%) and mechanical properties (~2 fold) were observed with 10×10^6 cells/ml. Mechanical properties were improved compared to the unloaded group, especially when using a higher cell density, but GAG and collagen contents were the same for loaded and unloaded samples (Mauck et al., 2003). The total collagen content could be indirectly quantified through hydroxyproline content; however, this assessment does not reveal how much Col1 vs. Col2 was produced in the loaded constructs.

In contrast, a few studies assayed Col1 and Col2 specifically within loaded constructs in the range of physiological strain (~10%). *Col2a1* promoter activity was decreased when chondrocyte-impregnated agarose hydrogels were subjected to 10% strain dynamic loading at 1 Hz frequency for a relatively short experimental time of 3 h (Mauck et al., 2007). Chondrocytes impregnated in photopolymerized methacrylated hyaluronic acid (HA) constructs were subjected to 10% strain dynamic loading with a frequency of 1 Hz for 1 and 5 days (Chung et al., 2008). Compared to the unloaded group, loaded samples upregulated both *Col1a1* and *Col2a1* gene expression and had an increased *Col2a1/Col1a1* ratio. However, these samples were loaded for relatively short time periods compared to the *in vivo* situation, which subjects constructs to loading for many years, if not decades.

Long-term loading better reflects *in vivo* conditions, but most studies on chondrocyte-impregnated hydrogels loaded for a relatively long time only reported Col2 production, disregarding assessments for Col1. This is a huge gap in current CTE compression studies. However, data are still useful on how cells in a hydrogel environment respond to loading by producing Col2, but whether these data reflect hyaline cartilage or fibrocartilage formation is an unanswered question. For example, stronger Col2 staining was seen in agarose constructs that underwent long-term loading (Kelly et al., 2008; Ng et al., 2009). Brighter staining of GAGs, Col2, and aggrecan was observed in alginate hydrogels impregnated with osteoarthritic chondrocytes that were dynamically compressed with 15% strain at 1 Hz over 2 weeks, than that in unloaded samples (Jeon et al., 2012). However, other studies showed decreased Col2 production. For example, Col2 deposition was reduced in both juvenile and adult chondrocyte-impregnated poly (ethylene glycol) (PEG) hydrogels that were subjected to long-term (14 days) dynamic compressive loading at 1 Hz and 10% strain (Farnsworth et al., 2013). Unfortunately, there was no assessment for Col1 deposition in this study.

In a bad omen for hydrogel-only CTE approaches, several studies showed that long-term dynamic loading of hydrogel constructs stimulated chondrocytes to produce fibrocartilage-like tissue, such as a reduction in Col2 or increase in Col1 production. Long-term dynamic loading of PEG hydrogels with 15% strain compression at 1 Hz frequency upregulated *Col1a2* gene expression, relative to the unloaded group, but these expression levels returned to that seen in the unloaded group at a later timepoint. On the other hand, *Col2a1* expression did not change in the loaded group in this study over 7 days of compression (Bryant et al., 2008). Higher accumulation of Col2 was observed in Col1 hydrogels loaded with 10% strain at 0.3 Hz

TABLE 2 | Summary of information for various *in vitro* compression strategies.

	Static	Dynamic	
Type of force	Constant force application.	Alternative force application.	
Strain range	Wide range of strains up to 50%.	3-20 % strain.	
Normally used frequency	No frequency	1 Hz	
Duration pattern	Continual and for a single period.	Consecutive periods: 1. Short-term loading: time scales of hours to days. 2. Long-term loading: time scale of weeks.	
Faults	❖ General faults: • Does not simulate mechanically dynamic conditions of a joint.	❖ General faults: • Many studies analyzed GAGs and/or total collagen. • Studies analyzed only Col2, neglecting Col1. ❖ Short-term loadings' fault: • Not simulating long periods of loadings in the joint.	❖ Long-term loadings' fault: • Only few studies assessed Col1 vs Col2.
Key findings	Down-regulates the biosynthesis of cartilaginous molecules.	Short-term loading: • Not satisfactory results in terms of Col1, Col2, and Col1/Col2.	Long-term loading: • Upregulation of Col2. • Upregulation of Col1. • High levels of Col1/Col2.

than that in the unloaded samples after 28 days of loading (Nebelung et al., 2012). However, no significant difference in the *Col2a1*/*Col1a1* ratio was found between loaded and unloaded samples, and this ratio was less than one for the loaded constructs. A Col2/Col1 ratio less than one indicated the formation of a fibrocartilage-like tissue under this applied physiological strain.

For *in vitro* studies that loaded hydrogel constructs, the lack of assessing both Col1 and Col2 is very problematic. However, the general outcome could be that short-term loading is useful for upregulation of Col2, although these experiments do not simulate long-term force application experienced in articular cartilage *in vivo*. When both Col1 and Col2 were analyzed, current long-term *in vitro* loading studies of chondrocyte-impregnated hydrogel constructs suggested that fibrocartilage was forming instead of hyaline cartilage. Specifically, long-term loading of hydrogels did not result in higher Col2 and/or lower level of Col1 production. **Table 2** summarizes key findings and characteristics of different *in vitro* compression experiments on chondrocyte-impregnated hydrogel constructs.

Implantation Studies Can Elucidate Function of Hydrogels in *In Vivo*

Animal Models for Articular Cartilage Regeneration

Examining the *in vivo* function of fabricated hydrogels within animal models is essential before moving forward to clinical applications because these experiments test the performance of CTE constructs in a preclinical setting. Implantation of constructs into joints is much better than other sites, such as subcutaneous implantations to mimic the force environment of future clinical applications; however, studies investigating the formation of cartilage in subcutaneously implanted hydrogels are a useful first step for observing the function of chondrocyte-impregnated constructs *in vivo*. Performing an *in vivo* CTE study requires consideration of several different parameters, such as the size and weight of the animal, joint size, cartilage thickness, load distribution within the joint, costs, convenience of the operation, and animal handling (Malda et al., 2013; Moran et al., 2016). Animals used for implantation of hydrogel CTE constructs generally fall into two categories, small and large models, and multiple types of animals from each group will be discussed below.

Rodents such as mice and rats are cost-effective small animal models that are also easy to breed and house. However, cartilage implantation in joints of these animals has been rarely carried out because the very small joint size makes it difficult to perform an operation (Gelse et al., 2003; Kuroda et al., 2006). Mice and rats also have very thin cartilage with thin layers of chondrocytes, so the outcomes of implantation might not predict human applications. Nevertheless, mouse models have been used for subcutaneous and intramuscular implantation of hydrogel constructs for 6–8 weeks. These implantation sites might be useful for testing the biodegradation of the hydrogels as well as cartilage matrix formations *in vivo*, although they do not provide mechanical conditions existing in joints that might

influence these parameters (Haisch et al., 2000a; AMIEL et al., 2001).

Rabbits have been used extensively for research in the CTE field and implantation of tissue-engineered constructs (Chu et al., 2010). Similar to mice and rats, rabbits are also affordable and easy to breed and house. The joint size of rabbits is larger than that of other small animals, which makes the surgery procedures easier (International, 2005). Rabbits have relatively thicker cartilage (0.3–0.44 mm) than mice and rats (~0.3 mm), although it is still much thinner than human cartilage (~2.35 mm) (Räsänen and Messner, 1996; Frisbie et al., 2006; Vos et al., 2012). Rabbit cartilage showed great endogenous repair in articular defects compared to that of other animals and humans (Hunziker, 1999). The very low self-healing of human cartilage is related to low cell densities (1,800 cells/mm^3), whereas higher cellularity of the rabbits (7,500 cells/mm^3) contributes to more endogenous cartilage repair (Moran et al., 2016).

The sheep is a commonly used large animal model that has similar joint anatomy to the human joint. These animals are easily accessible, cost-effective, and also easy to handle and house. However, they have thinner cartilage (0.4–0.5 mm) than the human cartilage, thus created defects reaching to the subchondral bone region in most studies (Lu et al., 2000; Frisbie et al., 2006). Despite the mentioned disadvantages, sheep can be an appropriate large animal model for assessment of hydrogels in mechanically loaded conditions.

Goats are popular large animal models for cartilage implantation (Brehm et al., 2006; Lind et al., 2008; Marmotti et al., 2013). Their large joint size allows creating large defects in articular cartilage that are unable of spontaneous healing (Jackson et al., 2001; Ahern et al., 2009). The cartilage thickness is around 1.1 mm in goats, greater than that in sheep, but it is still lower than human cartilage thickness (Jackson et al., 2001). Although defects of 12 mm diameter can be created in goats, commonly created defects are smaller than the natural defects in humans. Generally, goats are proper large animal models for the assessment of implants in small cartilage defects (Ahern et al., 2009).

A good example of a large and robust animal model is the horse, and this animal is similar to the human in terms of different aspects of the joint characteristics. Their joint is very big with similar anatomy to the human joint, and they have a thick cartilage region (1.75 mm) (Frisbie et al., 2006; Moran et al., 2016). Cartilage and osteochondral defects with various thickness and diameter can be created in horses because of their great cartilage size. However, their large weight of 400–600 kg causes rigorous loading forces on cartilage (Ahern et al., 2009; Chu et al., 2010). High mechanical forces on the joint, large and expensive facilities for housing and breeding, and specialized personnel and equipment are important factors to be considered for carrying out cartilage surgeries on horses (Ribitsch et al., 2020).

Pig models offer several advantages for cartilage surgeries. Mature pigs have a wide range of weight up to 250 kg, and they mimic human joints in terms of size, mechanical loading, and cartilage thickness (1.5–2 mm), which allows the creation of chondral and osteochondral defects with various sizes. However, their housing and performing operations on them are very costly. Besides, specialized facilities and surgeons are required to perform the surgeries and afterward housing. Nevertheless, if a group of experts could overcome the costs and needs for pig surgery, this animal is an appropriate model for cartilage repair studies (Frisbie et al., 2006; Chu et al., 2010; Meng et al., 2020). On the other hand, many studies have performed surgeries on mini-pigs weighing 40–70 kg to overcome issues with larger pigs, although lower loading forces are on the joints of mini-pigs due to their lighter weight (Christensen et al., 2015).

Selection of an appropriate animal model is crucial to relate the results of an implantation study to clinical settings. In this regard, small animal models, such as rats and rabbits, seem to be good candidates because they are cost-effective in purchasing and housing. The results cannot be correlated to clinical applications because of the various disadvantages mentioned previously. However, they can be used for early stages of assessments such as biodegradation and biocompatibility of the tissue-engineered hydrogels as well as the formation of cartilage ECM *in vivo*. On the other hand, large animals, such as pigs and horses, are more appropriate models for pretesting implants before clinical trials because of the high similarity of their joints to human joints in size, cartilage thickness, joint mechanics, and magnitude of applied forces on cartilage. Summary of this section is illustrated in **Figure 1** with the advantages and limitations related to small and large animal models.

Small Animal Models Are Useful for Initial *In Vivo* Experiments

Different types of hydrogels such as agarose (Armiento et al., 2018), fibrin (Westreich et al., 2004), alginate (Paige et al., 1996; Eslaminejad et al., 2007; Liao et al., 2017), HA (Park et al., 2019), composite hydrogels (Li T et al., 2019) such as chitosan and chondroitin sulfate (CS) (Li C et al., 2019) and also novel biomaterials such as sericin methacryloyl (Qi et al., 2018) have been implanted subcutaneously in mouse and rabbit models. Despite the absence of joint mechanical conditions, subcutaneous investigations are important and appreciated in terms of evaluating hydrogel constructs under a physiological *in vivo* condition.

Most of the subcutaneous implantation studies only assessed cartilage formation by histology and gross observations (Chen et al., 2017). For example, polymerized alginate was used as an injectable gel for cartilage formation, and chondrocyte-impregnated alginate hydrogels were injected subcutaneously into a nude mouse (Paige et al., 1996). Gross and histology observations showed the formation of cartilage-like tissues at 8 and 12 weeks post implantation, but neither the deposition of aggrecan nor collagen molecules were analyzed. Formation of cartilage ECM histology was also reported by implantation of a fibrin hydrogel in rabbit and mouse models (Sims et al., 1998; Westreich et al., 2004). Cartilage formation was reported in 85% of fibrin samples injected into subcutaneous sites of rabbits, and the newly formed tissue appeared like cartilage, from the gross and histological aspects (Westreich et al., 2004). Although these studies reported the formation of cartilage ECM in implanted hydrogels, the assessments were not sufficient, and further

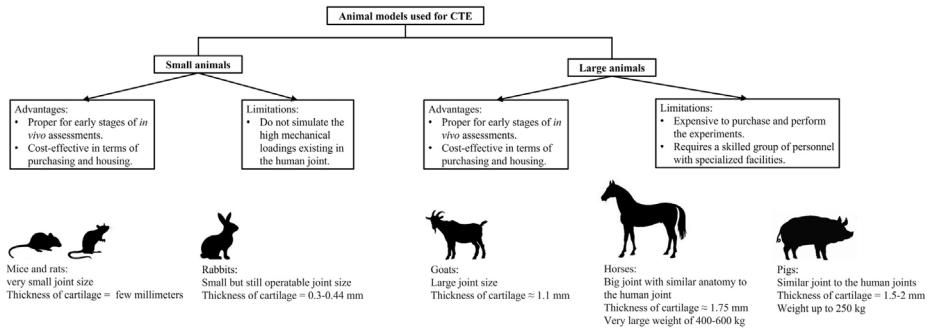

FIGURE 1 | Summary of information for advantages and limitations of small and large animal models used in CTE. Specific characteristics for several animal models are also presented in the figure (images for this part were generated from https://www.istockphoto.com).

analyses must be carried out to determine the type of cartilage formed.

Some studies assessed Col2 deposition within implanted hydrogels (Choi et al., 2007; Yun and Moon, 2008; Öztürk et al., 2020), although few of them performed assessments for production of both Col1 and Col2. For instance, chondrocyte-impregnated recombinant collagen hydrogels supported neocartilage formation by deposition of Col2, although Col1 was also present in the implanted constructs (Pulkkinen et al., 2010). Gelatin methacrylate (GelMA) and glycidyl methacrylate-modified GelMA (GelMAGMA) hydrogels showed the presence of Col2 and slight deposition of Col1 in the dorsa of mice 6 weeks after implantation (Li X et al., 2017).

Subcutaneous implantation is an easier surgery than joint surgeries, but the mechanical environment in the joint is worth performing surgeries and observing the functions of cells in response to forces. After completion of any *in vivo* joint experiment, animals are euthanized, joint samples are extracted, and then sections are generated from OCT or paraffin-embedded explants for further histological and immunohistochemical assessments. Many joint implantation studies focused on evaluating the formation of glycosaminoglycans and collagen fibers by histology assessments (Fragonas et al., 2000; Holland et al., 2005; Kim et al., 2013). Alginate is a popular biomaterial that has been extensively used for cartilage regeneration (Wong et al., 2001; Balakrishnan and Banerjee, 2011). As an example, autologous nasal chondrocytes were impregnated in alginate hydrogels and implanted into rabbit joints. Repaired hyaline cartilage–like tissue was reported in osteochondral defects of the trochlear groove based on histological staining (Chen et al., 2018). Self-settling cellulose-based hydrogels that were impregnated with nasal chondrocytes showed no signs of inflammation 6 weeks after implantation into rabbit knees, and cartilage matrix formed, based on histology and Col2 immunohistochemistry (Vinatier et al., 2009). In a recent study, a novel injectable alginate hydrogel containing porous polymeric microspheres with calcium gluconate as a cross-linker showed evidence of cartilage repair after implantation into the patellar groove of rabbit knees (Liao et al., 2017). Specifically, GAGs and Col2 were highly expressed, and the repaired cartilage appeared to integrate with host cartilage. However, Col1 production was not assessed to determine whether the new cartilage is hyaline cartilage or fibrocartilage.

Necessary assessments of Col1 production must be performed by some sort of immunological analysis in order to assess hyaline cartilage vs. fibrocartilage (Zhao et al., 2015), and only a few studies so far have done so. Chondrocyte-impregnated recombinant collagen hydrogels were implanted into osteochondral defects in the femoral trochlea of rabbits (Pulkkinen et al., 2013). The deeper parts of the defects contained Col2 after 6 months, while Col1 was mostly present in the superficial regions. In a recent study, two types of fibrin gels were implanted into rabbit joints with either redifferentiated or dedifferentiated chondrocytes, and both Col1 and Col2 depositions were tested in the implants. After 6 weeks of implantation, the outcome was more of a fibrocartilage-like tissue for both types of constructs, although deposition of Col2 was still higher than that of Col1. The ratio of Col2/Col1 was reported as 2.8 and 2.1 for dedifferentiated and redifferentiated constructs, respectively (Bianchi et al., 2019). According to these studies, Col2 formation has been generally reported to be high in the implanted defects, but the formation of Col1 was still observed within the defects. Despite this general outcome, a couple of studies reported low Col1 production. For example, Col1 synthesis was not seen in chondrocyte-impregnated collagen type II hydrogels 24 weeks after implantation in rabbit joints (Funayama et al., 2008).

Large Animal Studies Lack Col1 vs. Col2 Assessment for Implanted Hydrogels

Implantation in large animal models can provide a better sight of how the fabricated hydrogels regenerate cartilage in a mechanically analogous environment to human joints. Joints of large animals exhibit multiple mechanical forces, such as compression, sheer, and tension, that are similar to human joints in terms of magnitude and type. Simulating all mechanical forces existing in the joint *in vitro* is not feasible;

hence, it is essential to perform hydrogel implantation in the joints of large animals. However, not many published studies performed hydrogel implantations in large animals, which could be due to technical and economic difficulties related to the surgeries. Studies that implanted the hydrogel in large animals allowed them to walk freely with force loading on all joints. Various assessments have been used to analyze the extracted joint samples, and some have only performed histology analyses. Also, various biomaterials have been used for implantation in different animal models. Therefore, this section will review different hydrogels based on the types of biomaterial used (Liu et al., 2002; Sanz-Ramos et al., 2014).

Fibrin has been a commonly used biomaterial for impregnating chondrocytes and cartilage regeneration within large animal defects, including horses, goats, and pigs (Hendrickson et al., 1994; Van Susante et al., 1999; Peretti et al., 2006). For example, xenografted rabbit chondrocytes were impregnated in fibrin glue and implanted in adult goats. Xenografted defects showed initially better cartilage regeneration, but after 1 year, both grafted and control defects were similar and filled with fibrocartilaginous tissue. After 3 weeks of implantation, 17% of total collagen in the grafted constructs was Col2, and while this number was enhanced to 75% after 1 year, Col1 was not analyzed (Van Susante et al., 1999). In another study, an osteochondral defect in a goat model was treated with a double-phase construct comprised chondrocyte-impregnated fibrin glue upon a hydroxyapatite cylinder (van Susante et al., 1998). Repaired tissue was reported as fibrocartilage based on histology. Nevertheless, several animal studies have reported immunological responses from the host animals to exogenous fibrin implants (Kawabe and Yoshinao, 1991; Haisch et al., 2000b).

Alginate has been also used in several *in vivo* implantation studies for CTE applications (Wong et al., 2001; Balakrishnan and Banerjee, 2011; Farokhi et al., 2020). Chondrocytes and stem cells from different sources that have been cultured within the 3D matrix of alginate hydrogels have synthesized components of cartilage matrix. Despite these findings, few studies implanted alginate hydrogel constructs into the joints of large animal models (Hauselmann et al., 1996; Diduch et al., 2000; Mierisch et al., 2003; Almqvist et al., 2009). Osteochondral defects of sheep joints treated with chondrocyte-impregnated alginate spheres showed no histological sign of cartilage formation 21 days after implantation, containing fibrous tissue with fibroblast-like spindle cells and no safranin O staining (Heiligenstein et al., 2011). Alginate–gelatin composite hydrogels containing periosteal cells and chondrocytes implanted in sheep joints showed higher levels of Col2 and perhaps lower levels of Col1, than the untreated defects (Schagemann et al., 2009). However, Col1 intensity was very close to Col2 in the implanted groups, much higher than that in normal hyaline cartilage, indicating that the newly formed cartilage was likely fibrocartilage.

Collagen has been also used for different tissue engineering applications, including CTE, despite being expensive and having low availability and mechanical properties (Galois et al., 2006). Chondrocyte-impregnated collagen hydrogels were implanted in trochlear defects of a canine model, and fibrous and fibrocartilage tissues were formed within the defects (Nehrer et al., 1998). Regeneration of cartilage was improved by cell-impregnated collagen hydrogels in sheep knees, but the conclusions were only based on histology and quantifications with the Mankin score without any assessments for Col1 and Col2 (Sanz-Ramos et al., 2014). Chondrocytes and bone marrow stromal cells (BMSCs) seeded onto bi-layered collagen matrices formed a lower layer of Col1 and Col3 as a somewhat mechanically stable base, and the upper layer consisted of Col2 (Dorotka et al., 2005). The outcome was greater repair and hyaline-like cartilage regeneration for the seeded implants with a microfracture treatment, based on histology, and Col1 and Col2 staining. Chronologically predifferentiated mesenchymal stem cells (MSCs) impregnated within Col1 hydrogels and implanted in sheep showed better cartilage repair for the predifferentiated MSCs than for chondrocytes in terms of histology and Col2 staining (Marquass et al., 2011). Col1 staining was pretty high in all experimental hydrogel groups, although the article related that to immunoreaction with the Col1 hydrogel itself.

CS, a polysaccharide biomaterial that is a major component of cartilage ECM, has shown beneficial effects for cartilage formation both *in vitro* and *in vivo* (Ronca et al., 1998; Li et al., 2004; Chen W. C et al., 2013). However, similar to all hydrogels, pure CS exhibits low strength as a scaffold and degrades very fast, making *in vivo* application very challenging (Chang et al., 2010). Using CS as a bioadhesive for defects created in goat femoral condyles, cell-free poly (ethylene glycol) diacrylate (PEGDA) hydrogels were injected into the defects with marrow stimulation (Wang et al., 2007). The results showed that safranin O staining was quantitively higher for the hydrogel-treated defects than that for the untreated defects.

Chitosan is a natural polysaccharide and partially de-acetylated derivative of chitin that has structural similarity to the native GAGs present in the cartilage (Suh and Matthew, 2000). Chondrocyte-impregnated chitosan hydrogels implanted in sheep knees showed formation of hyaline-like cartilage after 24 weeks, according to histology and Col2 immunohistochemistry (Hao et al., 2010). Interestingly, the cell density of implanted hydrogels was very high (4×10^7), although it was not discussed as an effective parameter on cartilage formation. In another study, chitosan–glycerol phosphate (GP) was implanted in horse joints to apply high mechanical forces on the hydrogel (Martins et al., 2014). While the hydrogel was biocompatible after 180 days, and cells synthesized Col2 and proteoglycans, Col1 was not assessed.

Several studies used various natural and synthetic materials to fabricate composite constructs to enhance biological properties of the constructs (Filová et al., 2007; Filova et al., 2008). For example, a composite hydrogel of fibrin and HA with autologous chondrocytes was implanted in the knees of miniature pigs, and results were dependent on the initial cell densities, with a lower cell density showing better histological parameters (Rampichová et al., 2010). Immunohistochemistry of Col2 yielded positive staining at the borders of the defects, whereas the center of the defects was characterized by fibrocartilaginous tissue based on the histology scores and low

Col2 staining. Injecting a cell-impregnated hydrogel into a porous scaffold has been a useful method for the fabrication of hybrid composites with enhanced mechanical properties (Filová et al., 2007). For example, chondrocytes impregnated into the fibrin hydrogel or an MPEG-PLGA scaffold/chondrocyte/fibrin composite were compared with an untreated defect or an untreated defect with a microfracture intervention (Lind et al., 2008). The composite construct had the best cartilage repair, based on the macroscopic appearance and histology scores only, without any assessments for Col1 and Col2. As reviewed in this section, very few studies investigated Col1 vs. Col2 production within implanted hydrogels, and they mostly focused on just histology and analysis of Col2. Only one study reported hyaline cartilage formation based on Col1 and Col2 staining (Dorotka et al., 2005), whereas two studies showed high levels of Col1 staining within the implanted hydrogel constructs (Schagemann et al., 2009; Marquass et al., 2011).

Biomedical Imaging as Future Tools for Analyzing Implanted Constructs

Post-surgery assessments for hyaline cartilage regeneration are destructive and invasive and require a high number of animals, which makes *in vivo* operations expensive and complicated (Lind et al., 2008; Heiligenstein et al., 2011; Izadifar et al., 2014; Kundu et al., 2015). Alternative methods have been utilized to visualize implanted constructs in a non-destructive and 3D manner, including confocal microscopy, Raman spectroscopy, optical coherence tomography, positron emission tomography, and single-photon emission computed tomography (Huzaira et al., 2001; Müller and Zumbusch, 2007; Ahearne et al., 2008; Nam et al., 2015). However, these techniques have limitations at increasing tissue depth and volume (Appel et al., 2013; Nam et al., 2015).

Micro-computed tomography (micro-CT) is a helpful tool that can visualize implanted constructs and recognize structural details of the constructs as well as surrounding tissues (Izadifar et al., 2016b; Duan et al., 2021; Ning et al., 2021). However, investigation of hydrogel constructs and soft tissues, such as skin, muscle, and cartilage, is relatively challenging with conventional desktop micro-CT because of its poor contrast with low attenuation coefficients from hydrogels and soft tissues (Muehleman et al., 2002; van Lenthe et al., 2007; Zhu et al., 2011). Further improvements, such as utilizing high-atomic-number element probes or other contrast agents, are required to enhance the quality of the images generated from desktop micro-CT scanning (Mizutani and Suzuki, 2012; Pauwels et al., 2013). For this reason, micro-CT has been mostly used to evaluate implanted hard scaffolds in bone to visualize the formation of new bone in the implants (Hedberg et al., 2005; von Doernberg et al., 2006; Renghini et al., 2009).

Micro-CT can visualize formation of calcified cartilage, which is a mineralized tissue of articular cartilage unlike most cartilage that is unmineralized. In one study, cartilage-derived matrix (CDM) scaffolds alone and as a composite scaffold with a calcium phosphate (CaP) base were implanted into osteochondral defects of horse joints, and micro-CT analysis visualized newly formed calcified cartilage and the CaP component of the composite as well as their integration with surrounding native bone (Bolaños et al., 2017). Formation of mineralized tissue was also distinguished using micro-CT in hybrid 3D-printed PCL/fibrin constructs that were implanted in rabbit joints (Shao et al., 2006). Although the degree of bone regeneration could be quantified from the micro-CT data, visualization of cartilage regeneration was not possible. Magnetic resonance imaging (MRI) has been also utilized to characterize regeneration of cartilage after implantation of tissue-engineered constructs. Ramaswamy et al. used MRI to analyze the implanted photopolymerizable poly [ethylene glycol] diacrylate (PEODA) hydrogel within the rabbit chondral defects (Ramaswamy et al., 2008). MRI neither allowed to visualize the amount of the tissue filling within the defects nor could determine whether the implanted hydrogels were maintained within the defects. Transverse relaxation time (T_2) was measured in this study, and other similar studies, as a parameter to investigate the regrowth of cartilage (Watrin-Pinzano et al., 2004; Keinan-Adamsky et al., 2006; Ramaswamy et al., 2008). Ramaswamy and coworkers found that there was a negative and linear relationship between the MRI T_2 parameter and the percentage of tissue filling (Ramaswamy et al., 2008). However, a major drawback with MRI scanning is low resolution of the generated images and distinguishing the implanted hydrogel constructs from the surrounding cartilage might be challenging with MRI.

Synchrotron-radiation (SR)–based imaging technique is a novel tool that offers coherent collimated X-rays comprised a high flux of photons that are originated from a storage ring or other type of specialized particle accelerators. Synchrotron X-ray beams with high-energy photons can diffuse through the dense structures such as bone and not only visualize the bony structure but also whatever is being implanted inside the tissue. Fusion of the micro-CT technique and novel SR-based techniques such as phase-contrast imaging (PCI) and diffraction enhanced imaging (DEI) have enabled the imaging of structures such as hydrogels and cartilage that have low absorption coefficients and attenuation contrasts. Micro-CT–SR-based PCI utilizes refraction effects besides the conventional absorption effects to create a phase shift as the X-ray beam propagates through the materials with different X-ray refractive indexes. The phase shift can be observed at edges of the structures, and as a result, the contrast can be enhanced anywhere that the difference in X-ray absorption is weak (Parsons et al., 2008; Elfarnawany et al., 2017). PC X-ray refraction can be more than one thousand times sensitive than the conventional micro-CT absorption contrast (Zhang and Luo, 2011; Appel et al., 2013). Different imaging techniques including SR-radiography, PCI, and DEI were compared at the same energy for imaging of the scaffolds fabricated from poly (lactide) (PLLA) and chitosan under *in situ* conditions of rat muscle tissues. The scaffolds and tissues were not visible with conventional laboratory–based radiography, and PCI could faintly show them. However, DEI images visualized the tissues very clearly, and the scaffolds were distinguished because X-ray scatter could be rejected in DEI (Zhu et al., 2011). 2D and 3D images of printed PCL scaffolds

implanted in pig joints *in situ* were also visualized using the DEI technique. Microstructures of the scaffolds were visible, and size of the strands and pores were measurable (Izadifar et al., 2014). 3D-printed hybrid PCL/alginate constructs were imaged in the subcutaneous region of a murine model, and PCI could visualize regeneration of cartilage ECM as well as hydrogel strands *in vitro*. Moreover, degradation of the biomaterials and integration with the host tissues could be evaluated (Olubamiji et al., 2017). However, hydrogel strands are faintly visualized using these techniques, and thus their 3D volume-rendering is challenging.

SR-based imaging as well as MRI techniques have shown a promising ability to visualize low-density structures, and SR-based imaging has been also utilized for *in vivo* experiments too (Bayat et al., 2005; Wang et al., 2020). However, their resolution still needs to be improved to get images with distinguishable components in a 2D and 3D manner. Also, current SR-imaging tools cannot distinguish between different cartilage tissues such as hyaline and fibrocartilage. This ambitious idea requires developments in future research to upgrade the tools and techniques of SR-imaging that would help to scan the animals *in vivo* and find out the type and amount of newly formed cartilages without need for euthanasia of the animals.

How Mechanotransduction Pathways Regulate Chondrocytes Biochemical Activities

Mechanical loading is sensed by mechanoreceptors on the surface of chondrocytes and transduced for intracellular responses wherein different signaling pathways are initiated, altering gene expression and synthesis of cartilaginous molecules. The process of converting mechanical cues to biochemical reactions is called mechanotransduction. Understanding the underlying mechanism of mechanotransduction is helpful to avoid activation of pathways that would lead to expression of undesired molecules, importantly Col1 for CTE.

Various studies have reported undesirable Col2/Col1 ratios in the ECM of chondrocytes that were subjected to mechanical loadings. Therefore, it is important to understand signaling mechanisms within chondrocytes that increase the expression of Col1 or decrease Col2 expression. Then, a design could be justified to deactivate pathways favoring Col1 expression or activate pathways that stimulate Col2 expression. In this regard, some CTE studies evaluated the effect of mechanical forces on Col1 and Col2 expression but did not include research into how mechanotransduction signaling pathways worked when the tissue-engineered constructs were loaded (Mauck et al., 2000; Wang et al., 2009). However, osteoarthritis research has identified several pathways which are mechanically stimulated in chondrocytes and affect the composition of cartilage ECM, and they will be discussed in the following paragraphs.

TGF-β Signaling

In chondrocytes, transforming growth factor-β (TGF-β) signaling is commonly activated by mechanical stimulation and is highly dependent on the composition of surrounding matrix (Zhao et al., 2020), and this has been shown in mechanically loaded cartilage hydrogels (Allen et al., 2012; Bougault et al., 2012). In addition to TGF-β, the pericellular matrix (PCM) enables participation in mechanotransduction by growth factors such as fibroblast growth factor -2 (FGF-2) and bone morphogenetic protein (BMP). This is accomplished through binding of these growth factors to PCM proteins such as heparan sulfate-perlecan (HS-perlecan) followed by release of these growth factors when the PCM deforms due to mechanical stress (Vincent et al., 2007; Tang et al., 2018; Zhao et al., 2020). Two studies of TGF-β signaling in chondrocytes showed that TGF-β signaling upregulates SOX9, an important activator of Col2 expression, and downregulates RUNX2, an important activator of Col1 expression (Chen et al., 2012; Fang et al., 2016). Neither of these studies used mechanical stress to induce TGF-β activity, but the upregulation of a Col2 activator and downregulation of a Col1 activator provide strong evidence that TGF-β signaling can favor hyaline cartilage formation.

TGF-β uses canonical signaling to activate SMAD that both stimulate SOX9 activity and inhibit RUNX2 activity (Chen et al., 2012; Fang et al., 2016). Accumulation of SMAD proteins in the nucleus can lead to induction of HtrA1, a serine protease that breaks down structural proteins in the PCM (Xu et al., 2014), reducing their ability to impact binding of growth factors with their cell surface receptors. Without the PCM acting as a barrier, the tyrosine kinase receptor DDR2 is then able to bind to Col2 in the ECM, which may oppose hyaline cartilage formation. DDR2 can also increase IL-1β, an inflammatory molecule, which may hinder hyaline cartilage formation. In addition, DDR2 is capable of activating RUNX2, an important inducer of Col1, in differentiating osteoblasts and maturing chondrocytes (Hirose et al., 2020). The stimulation of DDR2 as a result of TGF-β signaling, likely caused by elevated mechanical stress, may increase the levels of MMP-13 and RUNX2, therefore breaking down collagen while increasing the synthesis of Col1 and thus opposing the formation of hyaline cartilage. This would be an opposite response to normal TGF-β signaling, which favors hyaline cartilage formation, warranting further research.

In addition, YAP and TAZ are two mechanosensitive proteins that help SMADs accumulate in the nucleus, potentially contributing to the increase in TGF-β signaling (Varelas et al., 2010; Xu et al., 2014); however, this has yet to be observed in chondrocytes. YAP and TAZ might be more active when high levels of mechanical stress prevent their inhibition by Hippo (Zhao et al., 2020). This would mean that the increase in TGF-β signaling is dependent on the level of mechanical stress the cell is subjected to. Taken together, the effects of TGF-β signaling are much more complex than simply favoring the formation of hyaline cartilage and that overactivity is associated with osteoarthritis and cartilage degradation (Bottini et al., 2019).

αV Integrin Signaling

Integrins are a large family of transmembrane receptors and are known for their interactions with extracellular proteins. Numerous integrins transduce mechanical stress and are essential for cartilage health (Yanoshita et al., 2018). Two of these integrins, αVβ3 and αVβ5, are of particular interest due to their effects on inflammatory molecules in response to high levels

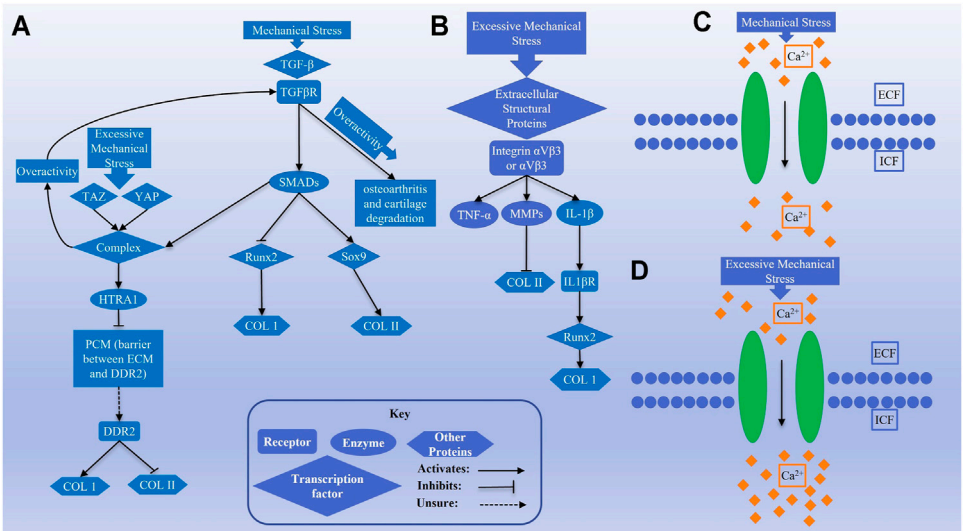

FIGURE 2 | Schematics **(A)** and **(B)** show transforming growth factor-β (TGF-β) and αV integrin signaling pathways, respectively, activated by mechanical stimulation. Schematics **(C)** and **(D)** represent the activity of calcium channels by normal and excessive mechanical stress in chondrocytes.

of mechanical stress. Activation of integrins αVβ3 and αVβ5 upregulated MMP-3 and MMP-13, which break down collagen as well as the inflammatory markers IL-1β and TNF-α (Guan et al., 2015). IL-1β has a role in osteoarthritis progression and has also been shown to cause cartilage degradation via induction of ADAMTS-4 and MMP-13 (Lee H. P et al., 2017). This finding is particularly interesting as the study applied slow-stress relaxation to chondrocytes in a 3D alginate hydrogel, meaning this molecular mechanism has been directly studied in the context of CTE and may be affected by the viscoelastic properties of cartilage tissue (Lee H. P et al., 2017). IL-1β not only has a role in osteoarthritis progression and cartilage degradation but also may contribute to fibrocartilage formation because it can induce Col1 expression through induction of the long noncoding RNA *lncRNA-SAMD14-4* (Du et al., 2020).

Calcium Signaling

One of the most essential mechanisms by which cells respond to mechanical stress is through changes in intracellular calcium concentrations, mediated by various mechanically activated channels (Zhao et al., 2020). Transient receptor potential cation channel subfamily V member 4 (TRPV4) is a calcium channel that responds to moderate levels of stress, becoming activated at approximately 3–8% cyclic tensile strain (CTS). Activation of this channel in chondrocytes by mechanical strain caused a moderate level of calcium influx (O'Conor et al., 2014). TRPV4 function can upregulate Col2 and GAG expression, while downregulating the expression of catabolic proteins, such as nitric oxide synthase 2 (NOS2) and a disintegrin and metalloproteinase with thrombospondin motifs 5 (ADAMTS-5), the latter of which functions similarly to matrix metalloproteinases (MMPs) (Wei et al., 2018). This effect on gene expression by TRPV4 favors the formation of hyaline cartilage. The role of TRPV4 in hyaline cartilage maintenance is further supported by the fact that its dysfunction is associated with osteoarthritic characteristics (Agarwal et al., 2021). PIEZO is another calcium channel that responds to mechanical stress but displays properties that differ greatly from those of TRPV4. PIEZO channels respond to excessive mechanical stress, becoming activated at 13% CTS or greater and causing greater calcium influx than TRPV4 channels (O'Conor et al., 2014). Large calcium influx has the potential to become toxic and cause apoptosis and cartilage degeneration (Zhao et al., 2020). This difference between TRPV4 and PIEZO draws parallels to the difference between moderate and overactive TGF-β signaling, where some signaling seems beneficial to the formation of hyaline cartilage but detrimental when it is overactive. A study of TRPV5 in chondrocytes performed by Wei, et al. provided some insight into what mechanisms TRPV5 and PIEZO may exert their effects through (Loeser, 2014). Calcium influx through TRPV5 activates CAMKII, which then subsequently activates AKT, ERK, JNK, and p38 (Loeser, 2014), providing further evidence that calcium signaling through mechanically activated channels such as TRPV4 and PIEZO may affect Col1 and Col2 expression as the TGF-β and αV integrin signaling mechanisms do. Discussed signaling pathways are schematically shown in **Figure 2** to illustrate how these pathways are acting in response to mechanical forces.

Although previous osteoarthritis literature provided preliminary evidence of which pathways may be involved in the expression of collagen, future studies of cell signaling in CTE should use 3D culture to determine whether the signaling mechanisms of interest are involved in mechanotransduction and analyze the effects of the pathways on Col1 and Col2 expression. This would provide the field of CTE with potential solutions to the problem of fibrocartilage formation in mechanically stimulated, chondrocyte-impregnated hydrogels.

Such solutions could include drugs targeting receptors on the chondrocyte surface, transgenic approaches to silence certain genes, and alternate designs which shield chondrocytes from the applied forces, thereby preventing the overactivity of cellular processes such as calcium, integrin, and TGF-β signaling pathways. Finally, the viscoelastic effects of the stress relaxation rate on cell signaling should be investigated due to the aforementioned ability of the stress relaxation rate to affect IL-1β mechanotransduction. Hydrogel constructs can be designed to have certain viscoelastic properties (Lee et al., 2020), potentially offering another avenue to produce ideal engineered hyaline cartilage.

3D-Bioprinted Hybrid Constructs Can Shield Cells From Applied Forces

Hydrogels are soft hydrated networks, and studies have shown that Col1 production and formation of a fibrocartilage-like tissue is the outcome when chondrocyte-impregnated hydrogels are compressed *in vitro* or implanted in a mechanical environment. Thus, mechanical forces are detrimental for chondrocytes in terms of hyaline cartilage formation. Besides, hydrogels generally have low mechanical properties to withstand high compressive forces after implantation in joint defects.

A hybrid construct composed of a cell-impregnated hydrogel loaded within a solid scaffold that is fabricated from a synthetic polymer is an alternative to enhance the mechanical properties of the constructs and reduce the magnitude of applied force on chondrocytes within the hydrogels. Various types of hybrid constructs have been developed and tested *in vitro* for articular cartilage regeneration; however, few of them studied the effects of loading forces on the production of Col1 vs. Col2 (Lee et al., 2005; Grad et al., 2006; Li et al., 2010). Polyurethane scaffolds filled with chondrocyte-impregnated fibrinogen hydrogels were compressed with a joint-kinematic–mimicking regime that was a combination of various compression movements. The gene expression data showed a significant decrease in *Col1a2* expression in the loaded samples compared to unloaded samples. However, Col1 was still present as a thick layer at the upper regions of the loaded samples, whereas it was observed as a thin layer on the upper surface when the constructs did not experience any loading (Wu Y et al., 2017). In another study, an increase in *Col1a2* gene expression happened in loaded fibrin–polyurethane constructs, compared to that in unloaded constructs. Levels of GAGs and *Col2a1* expression in the loaded samples were similar to those in control constructs (Lee et al., 2005). Composite constructs do not prevent production of Col1 from cells when the constructs are subjected to mechanical forces. The reason is that the applied force on a hybrid hydrogel-loaded construct is not shielded from the hydrogel and impregnated chondrocytes, but it is yet shared between the hydrogel and scaffold portions of the construct. Therefore, the cells still sense a high magnitude of the applied forces. Hence, the architecture of a hybrid construct is crucial to provide a load-shielding structure instead of a load-sharing one.

Novel methods of scaffold fabrications can help to shield the applied force using new tools, such as 3D-bioprinters, which can fabricate hybrid constructs in a layer-by-layer manner with alternating strands of hydrogel and a synthetic polymer. 3D-bioprinted hybrid alginate–PCL constructs were fabricated with embryonic chondrocytes impregnated within the alginate strands (Izadifar et al., 2016a). These constructs supported cartilage differentiation of the impregnated cells both *in vitro* and *in vivo* (Izadifar et al., 2016a; Olubamiji et al., 2017). In a 3D-bioprinted hybrid construct, the size of the alginate and PCL strands can be adjusted to have smaller alginate strands than PCL and that helps cells in the alginate strands to be shielded from applied forces. The structure of a 3D-bioprinted hybrid construct is depicted in **Figure 3** a1-a3, demonstrating how the smaller alginate strands can be protected against the applied forces by the larger PCL strands. Any force-shielding effect only applies to the range of strains when PCL strands do not deform so much that they are the same size as the alginate strands. However, in a 3D-bioprinted hydrogel-only construct, the force is applied on the cell-impregnated hydrogel strands without any shielding effect (**Figure 3** b1-b3), thus the cells sensing the total applied force. **Figure 3** c1-c3 also represents a hybrid hydrogel-loaded scaffold in which the pores of the scaffold are filled with a cell-impregnated hydrogel. This load-sharing design does not help shield cells because when a force is applied, the force is simultaneously transmitted to the hydrogel and synthetic scaffold because there is not any space separating the hydrogel material from the synthetic scaffold.

CONCLUSION AND FUTURE PERSPECTIVES

Mechanical forces, such as compression loading, can be sensed by chondrocytes within hydrogel constructs, thus affecting the cells' fates and cartilage regeneration. A major problem in current studies of chondrocyte-impregnated hydrogel constructs that were subjected to compressive force is that the formation of fibrocartilage was not analyzed, but Col1 expression and fibrocartilage-like tissue often can result from such mechanical loading.

Over the past decades, studies employing bioreactors to simulate compression forces in joints illustrated that static compression had limited effects on cartilage regeneration, which has urged researchers to switch to dynamic compression studies. Many *in vitro* dynamic compression experiments did not do specific assessments for Col1 and Col2 together to distinguish the type of newly formed cartilage. However, multiple studies reported upregulation in *Col2a1* gene expression or Col2 deposition in ECM, which would be a good sign for hyaline cartilage formation as long as Col1 expression was not too high also. Loading studies that did assess Col1 production were not in favor of hyaline cartilage regeneration since they showed upregulation of Col1 in response to the loading forces. These results confirmed that high magnitudes of compression forces promoted cells within hydrogels to produce more Col1 thus forming a fibrocartilage-like tissue. *In vivo* implantation of hydrogel constructs also generally reported Col2 production in hydrogel-treated defects

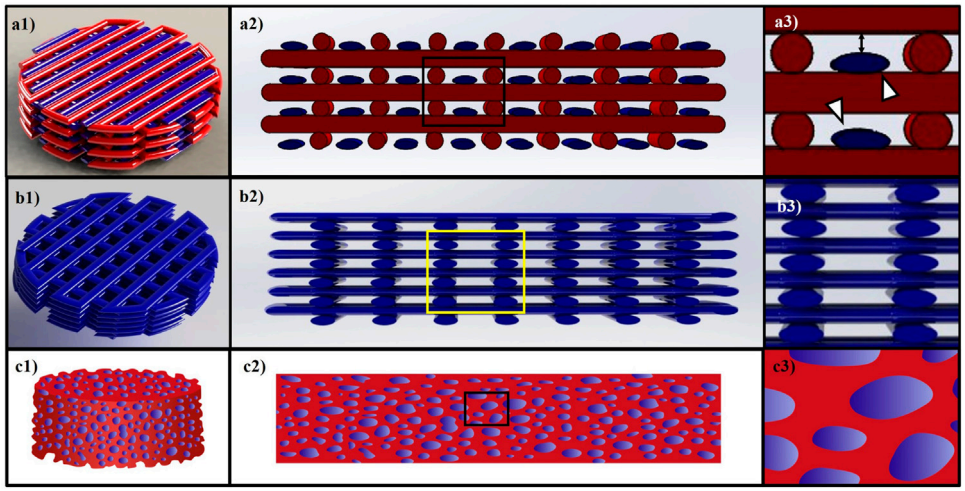

FIGURE 3 | (A1–A3) shows a model of a 3D-bioprinted hybrid alginate/PCL construct. Red and blue colors represent synthetic and cell-impregnated hydrogel strands, respectively. White arrows in **(A3)** point to the smaller hydrogel strands that are shielded by the PCL strands when loading is applied. **(B1–B3)** represents a 3D-bioprinted hydrogel construct, and the cells are impregnated within hydrogel strands without any shielding. **(C1–C3)** is a schematic for a hybrid hydrogel-loaded scaffold that cells are within the hydrogel part, and the applied load is shared between the hydrogel and synthetic part of the construct.

of animals. A few of these studies assessed Col1 within the treated defects and reported a high level of Col1 and formation of a fibrocartilage-like tissue.

In conclusion, chondrocyte-impregnated hydrogels subjected to mechanical compression *in vitro* or implanted *in vivo* in joints appear to form a Col1-positive fibrocartilage-like tissue. A possible solution could be to fabricate a chondrocyte-impregnated construct that shields cells from applied forces to avoid Col1 production. 3D-bioprinting and hybrid constructs are appropriate for this purpose, and their application for CTE was demonstrated in recent studies (Izadifar et al., 2016a). *In vitro* compression experiments should investigate the effects of load-shielding in 3D-bioprinted hybrid constructs, looking to exclude Col1 production. Additionally, *in vivo* implantation of hybrid constructs will also help to investigate cartilage formation in response to the various mechanical forces existing in joints.

Cell signaling studies suggest that various signaling pathways may be involved in the expression of collagens within chondrocytes that are activated by normal or excessive mechanical force. More studies of cell signaling pathways in the field of CTE should be performed with fabricated constructs to determine whether the signaling mechanisms of interest are involved in mechanotransduction and to analyze the effects of those pathways on Col1 and Col2 expression. In order to prevent Col1 deposition from mechanically loaded chondrocytes, *in vitro* loading experiments on hydrogels should reveal how to block pathways that direct Col1 expression within the loaded constructs, resulting in more hyaline-like cartilage formation. In *in vivo* studies, SR-based imaging techniques have shown the ability to visualize materials with low attenuation coefficients, such as hydrogels and soft tissues–like cartilage. Also, SR-based imaging tools should be developed not only for enabling quantitative analysis of implanted constructs and newly formed cartilage but also to distinguish between hyaline cartilage and fibrocartilage within a treated defect. Longitudinal SR-based imaging strategies of *in vivo* animal models have begun, so their application to humans is only a matter of time.

AUTHOR CONTRIBUTIONS

HA, BE, and XC conceived the idea of this review article; TW provided the mechanotransduction section; HA drafted the whole article; and BE and XC provided critical revision of the article.

FUNDING

This study was supported by the University of Saskatchewan Devolved Graduate Scholarship, the University of Saskatchewan CoMBRIDGE grant, and the Natural Sciences and Engineering Research Council of Canada (NSERC) (RGPIN 06396-2019).

ACKNOWLEDGMENTS

The authors thank Amir Hossein Ravanbod for his help in **Figure 3** of the article.

REFERENCES

Agarwal, P., Lee, H.-p., Smeriglio, P., Grandi, F., Goodman, S., Chaudhuri, O., et al. (2021). A Dysfunctional TRPV4–Gsk3β Pathway Prevents Osteoarthritic Chondrocytes from Sensing Changes in Extracellular Matrix Viscoelasticity. *Nat. Biomed. Eng.* 5, 1472–1484. doi:10.1038/s41551-021-00691-3

Ahearne, M., Bagnaninchi, P. O., Yang, Y., and El Haj, A. J. (2008). Online Monitoring of Collagen Fibre Alignment in Tissue-Engineered Tendon by PSOCT. *J. Tissue Eng. Regen. Med.* 2 (8), 521–524. doi:10.1002/term.124

Ahern, B. J., Parvizi, J., Boston, R., and Schaer, T. P. (2009). Preclinical Animal Models in Single Site Cartilage Defect Testing: a Systematic Review. *Osteoarthritis and cartilage* 17 (6), 705–713. doi:10.1016/j.joca.2008.11.008

Allen, J. L., Cooke, M. E., and Alliston, T. (2012). ECM Stiffness Primes the TGFβ Pathway to Promote Chondrocyte Differentiation. *MBoC* 23 (18), 3731–3742. doi:10.1091/mbc.e12-03-0172

Almqvist, K. F., Dhollander, A. A. M., Verdonk, P. C. M., Forsyth, R., Verdonk, R., and Verbruggen, G. (2009). Treatment of Cartilage Defects in the Knee Using Alginate Beads Containing Human Mature Allogenic Chondrocytes. *Am. J. Sports Med.* 37 (10), 1920–1929. doi:10.1177/0363546509335463

Amiel, G. E., Yoo, J. J., Kim, B.-S., and Atala, A. (2001). Tissue Engineered Stents Created from Chondrocytes. *J. Urol.* 165 (6 Part 1), 2091–2095. doi:10.1097/00005392-200106000-00076

Anderson, C. E., Ludowieg, J., Harper, H. A., and Engleman, E. P. (1964). The Composition of the Organic Component of Human Articular Cartilage. *J. Bone Jt. Surg.* 46 (6), 1176–1183. doi:10.2106/00004623-196446060-00002

Appel, A. A., Anastasio, M. A., Larson, J. C., and Brey, E. M. (2013). Imaging Challenges in Biomaterials and Tissue Engineering. *Biomaterials* 34 (28), 6615–6630. doi:10.1016/j.biomaterials.2013.05.033

Armiento, A. R., Alini, M., and Stoddart, M. J. (2019). Articular Fibrocartilage - Why Does Hyaline Cartilage Fail to Repair? *Adv. Drug Deliv. Rev.* 146, 289–305. doi:10.1016/j.addr.2018.12.015

Armiento, A. R., Stoddart, M. J., Alini, M., and Eglin, D. (2018). Biomaterials for Articular Cartilage Tissue Engineering: Learning from Biology. *Acta Biomater.* 65, 1–20. doi:10.1016/j.actbio.2017.11.021

Armstrong, C. G., Bahrani, A. S., and Gardner, D. L. (1979). *In Vitro* measurement of Articular Cartilage Deformations in the Intact Human Hip Joint under Load. *J. Bone Jt. Surg.* 61 (5), 744–755. doi:10.2106/00004623-197961050-00016

Balakrishnan, B., and Banerjee, R. (2011). Biopolymer-based Hydrogels for Cartilage Tissue Engineering. *Chem. Rev.* 111 (8), 4453–4474. doi:10.1021/cr100123h

Bayat, S., Apostol, L., Boller, E., Brochard, T., and Peyrin, F. (2005). *In Vivo* imaging of Bone Micro-architecture in Mice with 3D Synchrotron Radiation Micro-tomography. *Nucl. Instr. Methods Phys. Res. Section A: Acc. Spectrometers, Detectors Associated Equipment* 548 (1-2), 247–252. doi:10.1016/j.nima.2005.03.097

Becerra, J., Andrades, J. A., Guerado, E., Zamora-Navas, P., López-Puertas, J. M., and Reddi, A. H. (2010). Articular Cartilage: Structure and Regeneration. *Tissue Eng. B: Rev.* 16 (6), 617–627. doi:10.1089/ten.teb.2010.0191

Benjamin, M., and Evans, E. J. (1990). Fibrocartilage. *J. Anat.* 171, 1–15.

Benjamin, M., and Ralphs, J. R. (1991). Extracellular Matrix of Connective Tissues in the Heads of Teleosts. *J. Anat.* 179, 137–148.

Benjamin, M., and Ralphs, J. R. (2004). Biology of Fibrocartilage Cells. *Int. Rev. Cytol.* 233, 1–45. doi:10.1016/s0074-7696(04)33001-9

Bian, L., Fong, J. V., Lima, E. G., Stoker, A. M., Ateshian, G. A., Cook, J. L., et al. (2010). Dynamic Mechanical Loading Enhances Functional Properties of Tissue-Engineered Cartilage Using Mature Canine Chondrocytes. *Tissue Eng. A* 16 (5), 1781–1790. doi:10.1089/ten.tea.2009.0482

Bianchi, V. J., Lee, A., Anderson, J., Parreno, J., Theodoropoulos, J., Backstein, D., et al. (2019). Redifferentiated Chondrocytes in Fibrin Gel for the Repair of Articular Cartilage Lesions. *Am. J. Sports Med.* 47 (10), 2348–2359. doi:10.1177/0363546519857571

Bolaños, R. V., Cokelaere, S., McDermott, J. E., Benders, K., Gbureck, U., Plomp, S., et al. (2017). The Use of a Cartilage Decellularized Matrix Scaffold for the Repair of Osteochondral Defects: the Importance of Long-Term Studies in a Large Animal Model. *Osteoarthritis and cartilage* 25 (3), 413–420. doi:10.1016/j.joca.2016.08.005

Bottini, A., Wu, D. J., Ai, R., Le Roux, M., Bartok, B., Bombardieri, M., et al. (2019). PTPN14 Phosphatase and YAP Promote TGFβ Signalling in Rheumatoid Synoviocytes. *Ann. Rheum. Dis.* 78 (5), 600–609. doi:10.1136/annrheumdis-2018-213799

Bougault, C., Aubert-Foucher, E., Paumier, A., Perrier-Groult, E., Huot, L., Hot, D., et al. (2012). Dynamic Compression of Chondrocyte-Agarose Constructs Reveals New Candidate Mechanosensitive Genes. *PloS one* 7 (5), e36964. doi:10.1371/journal.pone.0036964

Brehm, W., Aklin, B., Yamashita, T., Rieser, F., Trüb, T., Jakob, R. P., et al. (2006). Repair of Superficial Osteochondral Defects with an Autologous Scaffold-free Cartilage Construct in a Caprine Model: Implantation Method and Short-Term Results. *Osteoarthritis and cartilage* 14 (12), 1214–1226. doi:10.1016/j.joca.2006.05.002

Brown, D. S., and Eames, B. F. (2016). Emerging Tools to Study Proteoglycan Function during Skeletal Development. *Methods Cel. Biol.* 134, 485–530. doi:10.1016/bs.mcb.2016.03.001

Bryant, S. J., Nicodemus, G. D., and Villanueva, I. (2008). Designing 3D Photopolymer Hydrogels to Regulate Biomechanical Cues and Tissue Growth for Cartilage Tissue Engineering. *Pharm. Res.* 25 (10), 2379–2386. doi:10.1007/s11095-008-9619-y

Buckwalter, J. A., and Mankin, H. J. (1998). Articular Cartilage: Degeneration and Osteoarthritis, Repair, Regeneration, and Transplantation. *Instr. Course Lect* 47, 487–504.

Buschmann, M. D., Gluzband, Y. A., Grodzinsky, A. J., and Hunziker, E. B. (1995). Mechanical Compression Modulates Matrix Biosynthesis in Chondrocyte/agarose Culture. *J. Cel. Sci.* 108 (4), 1497–1508. doi:10.1242/jcs.108.4.1497

Chang, K.-Y., Hung, L.-H., Chu, I.-M., Ko, C.-S., and Lee, Y.-D. (2010). The Application of Type II Collagen and Chondroitin Sulfate Grafted PCL Porous Scaffold in Cartilage Tissue Engineering. *J. Biomed. Mater. Res.* 92A (2), 712–723. doi:10.1002/jbm.a.32198

Chen, C. G., Thuillier, D., Chin, E. N., and Alliston, T. (2012). Chondrocyte-intrinsic Smad3 Represses Runx2-Inducible Matrix Metalloproteinase 13 Expression to Maintain Articular Cartilage and Prevent Osteoarthritis. *Arthritis Rheum.* 64 (10), 3278–3289. doi:10.1002/art.34566

Chen, C., Tambe, D. T., Deng, L., and Yang, L. (2013). Biomechanical Properties and Mechanobiology of the Articular Chondrocyte. *Am. J. Physiology-Cell Physiol.* 305 (12), C1202–C1208. doi:10.1152/ajpcell.00242.2013

Chen, F., Ni, Y., Liu, B., Zhou, T., Yu, C., Su, Y., et al. (2017). Self-crosslinking and Injectable Hyaluronic acid/RGD-Functionalized Pectin Hydrogel for Cartilage Tissue Engineering. *Carbohydr. Polym.* 166, 31–44. doi:10.1016/j.carbpol.2017.02.059

Chen, W.-C., Wei, Y.-H., Chu, I.-M., and Yao, C.-L. (2013). Effect of Chondroitin Sulphate C on Thein Vitroandin Vivochondrogenesis of Mesenchymal Stem Cells in Crosslinked Type II Collagen Scaffolds. *J. Tissue Eng. Regen. Med.* 7 (8), 665–672. doi:10.1002/term.1463

Chen, W., Li, C., Peng, M., Xie, B., Zhang, L., and Tang, X. (2018). Autologous Nasal Chondrocytes Delivered by Injectable Hydrogel for *In Vivo* Articular Cartilage Regeneration. *Cell Tissue Bank* 19 (1), 35–46. doi:10.1007/s10561-017-9649-y

Choi, S. J., Na, K., Kim, S., Woo, D. G., Sun, B. K., Chung, H. M., et al. (2007). Combination of Ascorbate and Growth Factor (TGF β-3) in Thermo-reversible Hydrogel Constructs Embedded with Rabbit Chondrocytes for Neocartilage Formation. *J. Biomed. Mater. Res.* 83A (4), 897–905. doi:10.1002/jbm.a.31403

Christensen, B. B., Foldager, C. B., Olesen, M. L., Vingtoft, L., Rölfing, J. H., Ringgaard, S., et al. (2015). Experimental Articular Cartilage Repair in the Göttingen Minipig: the Influence of Multiple Defects Per Knee. *J. Exp. Orthop.* 2 (1), 13–11. doi:10.1186/s40634-015-0031-3

Chu, C. R., Szczodry, M., and Bruno, S. (2010). Animal Models for Cartilage Regeneration and Repair. *Tissue Eng. Part B: Rev.* 16 (1), 105–115. doi:10.1089/ten.teb.2009.0452

Chung, C., Erickson, I. E., Mauck, R. L., and Burdick, J. A. (2008). Differential Behavior of Auricular and Articular Chondrocytes in Hyaluronic Acid Hydrogels. *Tissue Eng. Part A* 14 (7), 1121–1131. doi:10.1089/ten.tea.2007.0291

Davisson, T., Kunig, S., Chen, A., Sah, R., and Ratcliffe, A. (2002). Static and Dynamic Compression Modulate Matrix Metabolism in Tissue Engineered Cartilage. *J. Orthop. Res.* 20 (4), 842–848. doi:10.1016/s0736-0266(01)00160-7

Diduch, D. R., Jordan, L. C. M., Mierisch, C. M., and Balian, G. (2000). Marrow Stromal Cells Embedded in Alginate for Repair of Osteochondral Defects. *Arthrosc. J. Arthroscopic Relat. Surg.* 16 (6), 571–577. doi:10.1053/jars.2000.4827

Dorotka, R., Windberger, U., Macfelda, K., Bindreiter, U., Toma, C., and Nehrer, S. (2005). Repair of Articular Cartilage Defects Treated by Microfracture and a Three-Dimensional Collagen Matrix. *Biomaterials* 26 (17), 3617–3629. doi:10.1016/j.biomaterials.2004.09.034

Du, G., Li, L., Zhang, X., Liu, J., Hao, J., Zhu, J., et al. (2020). Roles of TRPV4 and Piezo Channels in Stretch-Evoked Ca2+ Response in Chondrocytes. *Exp. Biol. Med. (Maywood)* 245 (3), 180–189. doi:10.1177/1535370219892601

Duan, X., Li, N., Chen, X., and Zhu, N. (2021). Characterization of Tissue Scaffolds Using Synchrotron Radiation Microcomputed Tomography Imaging. *Tissue Eng. Part. C Methods* 27, 573–588. doi:10.1089/ten.tec.2021.0155

Eckstein, F., Lemberger, B., Stammberger, T., Englmeier, K. H., and Reiser, M. (2000). Patellar Cartilage Deformation *In Vivo* after Static versus Dynamic Loading. *J. Biomech.* 33 (7), 819–825. doi:10.1016/s0021-9290(00)00034-8

Eckstein, F., Tieschky, M., Faber, S., Englmeier, K.-H., and Reiser, M. (1999). Functional Analysis of Articular Cartilage Deformation, Recovery, and Fluid Flow Following Dynamic Exercise *In Vivo*. *Anat. Embryol.* 200 (4), 419–424. doi:10.1007/s004290050291

El-Ayoubi, R., DeGrandpré, C., DiRaddo, R., Yousefi, A.-M., and Lavigne, P. (2011). Design and Dynamic Culture of 3D-Scaffolds for Cartilage Tissue Engineering. *J. Biomater. Appl.* 25 (5), 429–444. doi:10.1177/0885328209355332

Elfarnawany, M., Alam, S. R., Rohani, S. A., Zhu, N., Agrawal, S. K., and Ladak, H. M. (2017). Micro-CT versus Synchrotron Radiation Phase Contrast Imaging of Human Cochlea. *J. Microsc.* 265 (3), 349–357. doi:10.1111/jmi.12507

Eslaminejad, M., Taghiyar, L., Kiani, S., and Piryaee, A. (2007). Subcutaneous Transplantation of Marrow–Derived Murine Mesenchymal Stem Cells Cultivated in Alginate and Their Chondrogenesis. *Scientific J. Iran Blood Transfus Organ.* 4 (2), 105–114.

Fang, J., Xu, L., Li, Y., and Zhao, Z. (2016). Roles of TGF-Beta 1 Signaling in the Development of Osteoarthritis. *Histol. Histopathol* 31 (11), 1161–1167. doi:10.14670/HH-11-779

Farnsworth, N. L., Antunez, L. R., and Bryant, S. J. (2013). Dynamic Compressive Loading Differentially Regulates Chondrocyte Anabolic and Catabolic Activity with Age. *Biotechnol. Bioeng.* 110 (7), 2046–2057. doi:10.1002/bit.24860

Farokhi, M., Jonidi Shariatzadeh, F., Solouk, A., and Mirzadeh, H. (2020). Alginate Based Scaffolds for Cartilage Tissue Engineering: a Review. *Int. J. Polymeric Mater. Polymeric Biomater.* 69 (4), 230–247. doi:10.1080/00914037.2018.1562924

Filová, E., Jelínek, F., Handl, M., Lytvynets, A., Rampichová, M., Varga, F., et al. (2008). Novel Composite Hyaluronan/type I Collagen/fibrin Scaffold Enhances Repair of Osteochondral Defect in Rabbit Knee. *J. Biomed. Mater. Res.* 87B (2), 415–424. doi:10.1002/jbm.b.31119

Filová, E., Rampichová, M., Handl, M., Lytvynets, A., Halouzka, R., Usvald, D., et al. (2007). Composite Hyaluronate-type I Collagen-Fibrin Scaffold in the Therapy of Osteochondral Defects in Miniature Pigs. *Physiol. Res.* 56, S5–S16. doi:10.33549/physiolres.931296

Fitzgerald, J. B., Jin, M., Dean, D., Wood, D. J., Zheng, M. H., and Grodzinsky, A. J. (2004). Mechanical Compression of Cartilage Explants Induces Multiple Time-dependent Gene Expression Patterns and Involves Intracellular Calcium and Cyclic AMP. *J. Biol. Chem.* 279 (19), 19502–19511. doi:10.1074/jbc.m400437200

Fragonas, E., Valente, M., Pozzi-Mucelli, M., Toffanin, R., Rizzo, R., Silvestri, F., et al. (2000). Articular Cartilage Repair in Rabbits by Using Suspensions of Allogenic Chondrocytes in Alginate. *Biomaterials* 21 (8), 795–801. doi:10.1016/s0142-9612(99)00241-0

Francis Suh, J.-K., and Matthew, H. W. T. (2000). Application of Chitosan-Based Polysaccharide Biomaterials in Cartilage Tissue Engineering: a Review. *Biomaterials* 21 (24), 2589–2598. doi:10.1016/s0142-9612(00)00126-5

Freeman, P. M., Natarajan, R. N., Kimura, J. H., and Andriacchi, T. P. (1994). Chondrocyte Cells Respond Mechanically to Compressive Loads. *J. Orthop. Res.* 12 (3), 311–320. doi:10.1002/jor.1100120303

Frisbie, D. D., Cross, M. W., and McIlwraith, C. W. (2006). A Comparative Study of Articular Cartilage Thickness in the Stifle of Animal Species Used in Human Pre-clinical Studies Compared to Articular Cartilage Thickness in the Human Knee. *Vet. Comp. Orthop. Traumatol.* 19 (03), 142–146. doi:10.1055/s-0038-1632990

Funayama, A., Niki, Y., Matsumoto, H., Maeno, S., Yatabe, T., Morioka, H., et al. (2008). Repair of Full-Thickness Articular Cartilage Defects Using Injectable Type II Collagen Gel Embedded with Cultured Chondrocytes in a Rabbit Model. *J. orthopaedic Sci.* 13 (3), 225–232. doi:10.1007/s00776-008-1220-z

Galois, L., Hutasse, S., Cortial, D., Rousseau, C. F., Grossin, L., Ronziere, M.-C., et al. (2006). Bovine Chondrocyte Behaviour in Three-Dimensional Type I Collagen Gel in Terms of Gel Contraction, Proliferation and Gene Expression. *Biomaterials* 27 (1), 79–90. doi:10.1016/j.biomaterials.2005.05.098

Gelse, K., von der Mark, K., Aigner, T., Park, J., and Schneider, H. (2003). Articular Cartilage Repair by Gene Therapy Using Growth Factor-Producing Mesenchymal Cells. *Arthritis Rheum.* 48 (2), 430–441. doi:10.1002/art.10759

Gemmiti, C. V., and Guldberg, R. E. (2009). Shear Stress Magnitude and Duration Modulates Matrix Composition and Tensile Mechanical Properties in Engineered Cartilaginous Tissue. *Biotechnol. Bioeng.* 104 (4), 809–820. doi:10.1002/bit.22440

Grad, S., Eglin, D., Alini, M., and Stoddart, M. J. (2011). Physical Stimulation of Chondrogenic Cells *In Vitro*: a Review. *Clin. Orthopaedics Relat. Research®* 469 (10), 2764–2772. doi:10.1007/s11999-011-1819-9

Grad, S., Gogolewski, S., Alini, M., and Wimmer, M. A. (2006). Effects of Simple and Complex Motion Patterns on Gene Expression of Chondrocytes Seeded in 3D Scaffolds. *Tissue Eng.* 12 (11), 3171–3179. doi:10.1089/ten.2006.12.3171

Gray, M. L., Pizzanelli, A. M., Grodzinsky, A. J., and Lee, R. C. (1988). Mechanical and Physicochemical Determinants of the Chondrocyte Biosynthetic Response. *J. Orthop. Res.* 6 (6), 777–792. doi:10.1002/jor.1100060602

Guan, P. P., Guo, J. W., Yu, X., Wang, Y., Wang, T., Konstantopoulos, K., et al. (2015). The Role of Cyclooxygenase-2, Interleukin-1β and Fibroblast Growth Factor-2 in the Activation of Matrix Metalloproteinase-1 in Sheared-Chondrocytes and Articular Cartilage. *Sci. Rep.* 5 (1), 10412–10414. doi:10.1038/srep10412

Guilak, F., Ratcliffe, A., and Mow, V. C. (1995). Chondrocyte Deformation and Local Tissue Strain in Articular Cartilage: a Confocal Microscopy Study. *J. Orthop. Res.* 13 (3), 410–421. doi:10.1002/jor.1100130315

Haisch, A., Gröger, A., Radke, C., Ebmeyer, J., Sudhoff, H., Grasnick, G., et al. (2000). Macroencapsulation of Human Cartilage Implants: Pilot Study with Polyelectrolyte Complex Membrane Encapsulation. *Biomaterials* 21 (15), 1561–1566. doi:10.1016/s0142-9612(00)00038-7

Haisch, A., Loch, A., David, J., Pruss, A., Hansen, R., and Sittinger, M. (2000). Preparation of a Pure Autologous Biodegradable Fibrin Matrix for Tissue Engineering. *Med. Biol. Eng. Comput.* 38 (6), 686–689. doi:10.1007/bf02344876

Ham, A. W. (1965). *Histology*. J. B. Lippincott.

Hao, T., Wen, N., Cao, J.-K., Wang, H.-B., Lü, S.-H., Liu, T., et al. (2010). The Support of Matrix Accumulation and the Promotion of Sheep Articular Cartilage Defects Repair *In Vivo* by Chitosan Hydrogels. *Osteoarthritis and cartilage* 18 (2), 257–265. doi:10.1016/j.joca.2009.08.007

Hauselmann, H. J., Masuda, K., Hunziker, E. B., Neidhart, M., Mok, S. S., Michel, B. A., et al. (1996). Adult Human Chondrocytes Cultured in Alginate Form a Matrix Similar to Native Human Articular Cartilage. *Am. J. Physiology-Cell Physiol.* 271 (3), C742–C752. doi:10.1152/ajpcell.1996.271.3.c742

Hedberg, E. L., Kroese-Deutman, H. C., Shih, C. K., Lemoine, J. J., Liebschner, M. A., Miller, M. J., et al. (2005). Methods: a Comparative Analysis of Radiography, Microcomputed Tomography, and Histology for Bone Tissue Engineering. *Tissue Eng.* 11 (9-10), 1356–1367. doi:10.1089/ten.2005.11.1356

Heiligenstein, S., Cucchiarini, M., Laschke, M. W., Bohle, R. M., Kohn, D., Menger, M. D., et al. (2011). In VitroandIn VivoCharacterization of Nonbiomedical- and Biomedical-Grade Alginates for Articular Chondrocyte Transplantation. *Tissue Eng. C: Methods* 17 (8), 829–842. doi:10.1089/ten.tec.2010.0681

Hendrickson, D. A., Nixon, A. J., Grande, D. A., Todhunter, R. J., Minor, R. M., Erb, H., et al. (1994). Chondrocyte-fibrin Matrix Transplants for Resurfacing Extensive Articular Cartilage Defects. *J. Orthop. Res.* 12 (4), 485–497. doi:10.1002/jor.1100120405

Hirose, N., Okamoto, Y., Yanoshita, M., Asakawa, Y., Sumi, C., Takano, M., et al. (2020). Protective Effects of Cilengitide on Inflammation in Chondrocytes under Excessive Mechanical Stress. *Cell Biol Int* 44 (4), 966–974. doi:10.1002/cbin.11293

Holland, T. A., Bodde, E. W. H., Baggett, L. S., Tabata, Y., Mikos, A. G., and Jansen, J. A. (2005). Osteochondral Repair in the Rabbit Model Utilizing Bilayered, Degradable Oligo(poly(ethylene Glycol) Fumarate) Hydrogel Scaffolds. *J. Biomed. Mater. Res.* 75A (1), 156–167. doi:10.1002/jbm.a.30379

Hunter, C. J., Imler, S. M., Malaviya, P., Nerem, R. M., and Levenston, M. E. (2002). Mechanical Compression Alters Gene Expression and Extracellular Matrix Synthesis by Chondrocytes Cultured in Collagen I Gels. *Biomaterials* 23 (4), 1249–1259. doi:10.1016/s0142-9612(01)00245-9

Hunter, C. J., Mouw, J. K., and Levenston, M. E. (2004). Dynamic Compression of Chondrocyte-Seeded Fibrin Gels: Effects on Matrix Accumulation and Mechanical Stiffness. *Osteoarthritis and cartilage* 12 (2), 117–130. doi:10.1016/j.joca.2003.08.009

Hunziker, E. B. (1999). Biologic Repair of Articular Cartilage. *Clin. Orthopaedics Relat. Res.* 367, S135–S146. doi:10.1097/00003086-199910001-00015

Huzaira, M., Rius, F., Rajadhyaksha, M., Anderson, R. R., and González, S. (2001). Topographic Variations in normal Skin, as Viewed by *In Vivo* Reflectance Confocal Microscopy. *J. Invest. Dermatol.* 116 (6), 846–852. doi:10.1046/j.0022-202x.2001.01337.x

International, A. (2005). *Standard Guide for* in Vivo *Assessment of Implantable Devices Intended to Repair or Regenerate Articular Cartilage*. Conshohocken, PA: ASTM International.

Izadifar, Z., Chang, T., Kulyk, W., Chen, X., and Eames, B. F. (2016). Analyzing Biological Performance of 3D-Printed, Cell-Impregnated Hybrid Constructs for Cartilage Tissue Engineering. *Tissue Eng. Part C: Methods* 22 (3), 173–188. doi:10.1089/ten.tec.2015.0307

Izadifar, Z., Chapman, L. D., and Chen, X. (2014). Computed Tomography Diffraction-Enhanced Imaging forIn SituVisualization of Tissue Scaffolds Implanted in Cartilage. *Tissue Eng. Part C: Methods* 20 (2), 140–148. doi:10.1089/ten.tec.2013.0138

Izadifar, Z., Honaramooz, A., Wiebe, S., Belev, G., Chen, X., and Chapman, D. (2016). Low-dose Phase-Based X-ray Imaging Techniques for *In Situ* Soft Tissue Engineering Assessments. *Biomaterials* 82, 151–167. doi:10.1016/j.biomaterials.2015.11.044

Jackson, D. W., Lalor, P. A., Aberman, H. M., and Simon, T. M. (2001). Spontaneous Repair of Full-Thickness Defects of Articular Cartilage in a Goat Model. *The J. Bone Jt. Surgery-American* 83 (1), 53–64. doi:10.2106/00004623-200101000-00008

Jeon, J. E., Schrobback, K., Hutmacher, D. W., and Klein, T. J. (2012). Dynamic Compression Improves Biosynthesis of Human Zonal Chondrocytes from Osteoarthritis Patients. *Osteoarthritis and Cartilage* 20 (8), 906–915. doi:10.1016/j.joca.2012.04.019

Jones, I. L., Klämfeldt, A., and Sandström, T. (1982). The Effect of Continuous Mechanical Pressure upon the Turnover of Articular Cartilage Proteoglycans *In Vitro*. *Clin. Orthop. Relat. Res.* (165), 283–289.

Karimi, T., Barati, D., Karaman, O., Moeinzadeh, S., and Jabbari, E. (2015). A Developmentally Inspired Combined Mechanical and Biochemical Signaling Approach on Zonal Lineage Commitment of Mesenchymal Stem Cells in Articular Cartilage Regeneration. *Integr. Biol.* 7 (1), 112–127. doi:10.1039/c4ib00197d

Kawabe, N., and Yoshinao, M. (1991). The Repair of Full-Thickness Articular Cartilage Defects. Immune Responses to Reparative Tissue Formed by Allogeneic Growth Plate Chondrocyte Implants. *Clin. Orthop. Relat. Res.* (268), 279–293.

Keinan-Adamsky, K., Shinar, H., and Navon, G. (2006). Multinuclear NMR and MRI Studies of the Maturation of Pig Articular Cartilage. *Magn. Reson. Med.* 55 (3), 532–540.

Kelly, T.-A. N., Fisher, M. B., Oswald, E. S., Tai, T., Mauck, R. L., Ateshian, G. A., et al. (2008). Low-serum media and Dynamic Deformational Loading in Tissue Engineering of Articular Cartilage. *Ann. Biomed. Eng.* 36 (5), 769–779. doi:10.1007/s10439-008-9476-1

Kheir, E., and Shaw, D. (2009). Hyaline Articular Cartilage. *Orthopaedics and Trauma* 23 (6), 450–455. doi:10.1016/j.mporth.2009.01.003

Kim, K., Lam, J., Lu, S., Spicer, P. P., Lueckgen, A., Tabata, Y., et al. (2013). Osteochondral Tissue Regeneration Using a Bilayered Composite Hydrogel with Modulating Dual Growth Factor Release Kinetics in a Rabbit Model. *J. Controlled Release* 168 (2), 166–178. doi:10.1016/j.jconrel.2013.03.013

Kisiday, J. D., Jin, M., DiMicco, M. A., Kurz, B., and Grodzinsky, A. J. (2004). Effects of Dynamic Compressive Loading on Chondrocyte Biosynthesis in Self-Assembling Peptide Scaffolds. *J. Biomech.* 37 (5), 595–604. doi:10.1016/j.jbiomech.2003.10.005

Knobloch, T. J., Madhavan, S., Nam, J., Agarwal, S., Jr, and Agarwal, S. (2008). Regulation of Chondrocytic Gene Expression by Biomechanical signalsCritical Reviews™ in Eukaryotic Gene Expression. *Crit. Rev. Eukaryot. Gene Expr.* 18 (2), 139–150. doi:10.1615/critreveukargeneexpr.v18.i2.30

Kundu, J., Shim, J.-H., Jang, J., Kim, S.-W., and Cho, D.-W. (2015). An Additive Manufacturing-Based PCL-Alginate-Chondrocyte Bioprinted Scaffold for Cartilage Tissue Engineering. *J. Tissue Eng. Regen. Med.* 9 (11), 1286–1297. doi:10.1002/term.1682

Kuroda, R., Usas, A., Kubo, S., Corsi, K., Peng, H., Rose, T., et al. (2006). Cartilage Repair Using Bone Morphogenetic Protein 4 and Muscle-Derived Stem Cells. *Arthritis Rheum.* 54 (2), 433–442. doi:10.1002/art.21632

Landinez, N., Garzón-Alvarado, D., and Acosta, J. V. (2009). Phenomenology Work Setting for Articular Cartilage Damage. *Rev. Cubana Ortop Traumatol.* 23, 1–28.

Lee, C. R., Grad, S., Gorna, K., Gogolewski, S., Goessl, A., and Alini, M. (2005). Fibrin-polyurethane Composites for Articular Cartilage Tissue Engineering: a Preliminary Analysis. *Tissue Eng.* 11 (9-10), 1562–1573. doi:10.1089/ten.2005.11.1562

Lee, H.-p., Gu, L., Mooney, D. J., Levenston, M. E., and Chaudhuri, O. (2017). Mechanical Confinement Regulates Cartilage Matrix Formation by Chondrocytes. *Nat. Mater* 16 (12), 1243–1251. doi:10.1038/nmat4993

Lee, H. J., Seo, Y., Kim, H. S., Lee, J. W., and Lee, K. Y. (2020). Regulation of the Viscoelastic Properties of Hyaluronate-Alginate Hybrid Hydrogel as an Injectable for Chondrocyte Delivery. *ACS omega* 5 (25), 15567–15575. doi:10.1021/acsomega.0c01763

Lee, J. K., Huwe, L. W., Paschos, N., Aryaei, A., Gegg, C. A., Hu, J. C., et al. (2017). Tension Stimulation Drives Tissue Formation in Scaffold-free Systems. *Nat. Mater* 16 (8), 864–873. doi:10.1038/nmat4917

Li, C., Wang, K., Zhou, X., Li, T., Xu, Y., Qiang, L., et al. (2019). Controllable Fabrication of Hydroxybutyl Chitosan/oxidized Chondroitin Sulfate Hydrogels by 3D Bioprinting Technique for Cartilage Tissue Engineering. *Biomed. Mater.* 14 (2), 025006. doi:10.1088/1748-605x/aaf8ed

Li, K., Zhang, C., Qiu, L., Gao, L., and Zhang, X. (2017). Advances in Application of Mechanical Stimuli in Bioreactors for Cartilage Tissue Engineering. *Tissue Eng. Part B: Rev.* 23 (4), 399–411. doi:10.1089/ten.teb.2016.0427

Li, Q., Williams, C. G., Sun, D. D. N., Wang, J., Leong, K., and Elisseeff, J. H. (2004). Photocrosslinkable Polysaccharides Based on Chondroitin Sulfate. *J. Biomed. Mater. Res.* 68A (1), 28–33. doi:10.1002/jbm.a.20007

Li, T., Song, X., Weng, C., Wang, X., Gu, L., Gong, X., et al. (2019). Silk Fibroin/carboxymethyl Chitosan Hydrogel with Tunable Biomechanical Properties Has Application Potential as Cartilage Scaffold. *Int. J. Biol. macromolecules* 137, 382–391. doi:10.1016/j.ijbiomac.2019.06.245

Li X, X., Zhang, J., Kawazoe, N., and Chen, G. (2017). Fabrication of Highly Crosslinked Gelatin Hydrogel and its Influence on Chondrocyte Proliferation and Phenotype. *Polymers (Basel)* 9 (8), 309. doi:10.3390/polym9080309

Li, Z., Yao, S.-J., Alini, M., and Stoddart, M. J. (2010). Chondrogenesis of Human Bone Marrow Mesenchymal Stem Cells in Fibrin-Polyurethane Composites Is Modulated by Frequency and Amplitude of Dynamic Compression and Shear Stress. *Tissue Eng. Part A* 16 (2), 575–584. doi:10.1089/ten.tea.2009.0262

Liao, J., Wang, B., Huang, Y., Qu, Y., Peng, J., and Qian, Z. (2017). Injectable Alginate Hydrogel Cross-Linked by Calcium Gluconate-Loaded Porous Microspheres for Cartilage Tissue Engineering. *ACS omega* 2 (2), 443–454. doi:10.1021/acsomega.6b00495

Lima, E. G., Bian, L., Ng, K. W., Mauck, R. L., Byers, B. A., Tuan, R. S., et al. (2007). The Beneficial Effect of Delayed Compressive Loading on Tissue-Engineered Cartilage Constructs Cultured with TGF-B3. *Osteoarthritis and Cartilage* 15 (9), 1025–1033. doi:10.1016/j.joca.2007.03.008

Lind, M., Larsen, A., Clausen, C., Osther, K., and Everland, H. (2008). Cartilage Repair with Chondrocytes in Fibrin Hydrogel and MPEG Polylactide Scaffold: an *In Vivo* Study in Goats. *Knee Surg. Sports Traumatol. Arthr* 16 (7), 690–698. doi:10.1007/s00167-008-0522-1

Little, C. J., Bawolin, N. K., and Chen, X. (2011). Mechanical Properties of Natural Cartilage and Tissue-Engineered Constructs. *Tissue Eng. Part B: Rev.* 17 (4), 213–227. doi:10.1089/ten.teb.2010.0572

Liu, Y., Chen, F., Liu, W., Cui, L., Shang, Q., Xia, W., et al. (2002). Repairing Large Porcine Full-Thickness Defects of Articular Cartilage Using Autologous Chondrocyte-Engineered Cartilage. *Tissue Eng.* 8 (4), 709–721. doi:10.1089/107632702760240616

Loeser, R. F. (2014). Integrins and Chondrocyte-Matrix Interactions in Articular Cartilage. *Matrix Biol.* 39, 11–16. doi:10.1016/j.matbio.2014.08.007

Lu, Y., Hayashi, K., Hecht, P., Fanton, G. S., Thabit, G., III, Cooley, A. J., et al. (2000). The Effect of Monopolar Radiofrequency Energy on Partial-Thickness Defects of Articular Cartilage. *Arthrosc. J. Arthroscopic Relat. Surg.* 16 (5), 527–536. doi:10.1053/jars.2000.7690

Macirowski, T., Tepic, S., and Mann, R. W. (1994). Cartilage Stresses in the Human Hip Joint. *J. Biomech. Eng.* 116, 10–18. doi:10.1115/1.2895693

Malda, J., de Grauw, J. C., Benders, K. E. M., Kik, M. J. L., van de Lest, C. H. A., Creemers, L. B., et al. (2013). Of Mice, Men and Elephants: the Relation between Articular Cartilage Thickness and Body Mass. *PloS one* 8 (2), e57683. doi:10.1371/journal.pone.0057683

Marlovits, S., Tichy, B., Truppe, M., Gruber, D., and Schlegel, W. (2003). Collagen Expression in Tissue Engineered Cartilage of Aged Human Articular Chondrocytes in a Rotating Bioreactor. *Int. J. Artif. Organs* 26 (4), 319–330. doi:10.1177/039139880302600407

Marmotti, A., Bruzzone, M., Bonasia, D. E., Castoldi, F., Von Degerfeld, M. M., Bignardi, C., et al. (2013). Autologous Cartilage Fragments in a Composite Scaffold for One Stage Osteochondral Repair in a Goat Model. *Eur. Cel Mater* 26, 15–31. doi:10.22203/ecm.v026a02

Marquass, B., Schulz, R., Hepp, P., Zscharnack, M., Aigner, T., Schmidt, S., et al. (2011). Matrix-Associated Implantation of Predifferentiated Mesenchymal Stem Cells versus Articular Chondrocytes. *Am. J. Sports Med.* 39 (7), 1401–1412. doi:10.1177/0363546511398646

Martel-Pelletier, J., Boileau, C., Pelletier, J.-P., and Roughley, P. J. (2008). Cartilage in normal and Osteoarthritis Conditions. *Best Pract. Res. Clin. Rheumatol.* 22 (2), 351–384. doi:10.1016/j.berh.2008.02.001

Martins, E. A., Michelacci, Y. M., Baccarin, R. Y., Cogliati, B., and Silva, L. C. (2014). Evaluation of Chitosan-GP Hydrogel Biocompatibility in Osteochondral Defects: an Experimental Approach. *BMC Vet. Res.* 10 (1), 197–199. doi:10.1186/s12917-014-0197-4

Mauck, R. L., Byers, B. A., Yuan, X., and Tuan, R. S. (2007). Regulation of Cartilaginous ECM Gene Transcription by Chondrocytes and MSCs in 3D Culture in Response to Dynamic Loading. *Biomech. Model. Mechanobiol* 6 (1), 113–125. doi:10.1007/s10237-006-0042-1

Mauck, R. L., Soltz, M. A., Wang, C. C. B., Wong, D. D., Chao, P.-H. G., Valhmu, W. B., et al. (2000). Functional Tissue Engineering of Articular Cartilage through Dynamic Loading of Chondrocyte-Seeded Agarose Gels. *J. biomechanical Eng.* 122 (3), 252–260. doi:10.1115/1.429656

Mauck, R. L., Wang, C. C.-B., Oswald, E. S., Ateshian, G. A., and Hung, C. T. (2003). The Role of Cell Seeding Density and Nutrient Supply for Articular Cartilage Tissue Engineering with Deformational Loading. *Osteoarthritis and cartilage* 11 (12), 879–890. doi:10.1016/j.joca.2003.08.006

Meng, X., Ziadlou, R., Grad, S., Alini, M., Wen, C., Lai, Y., et al. (2020). Animal Models of Osteochondral Defect for Testing Biomaterials. *Biochem. Res. Int.* 2020, 9659412. doi:10.1155/2020/9659412

Mierisch, C. M., Wilson, H. A., Turner, M. A., Milbrandt, T. A., Berthoux, L., Hammarskjöld, M.-L., et al. (2003). Chondrocyte Transplantation into Articular Cartilage Defects with Use of Calcium Alginate. *J. Bone Jt. Surgery-American* 85 (9), 1757–1767. doi:10.2106/00004623-200309000-00015

Mizutani, R., and Suzuki, Y. (2012). X-ray Microtomography in Biology. *Micron* 43 (2-3), 104–115. doi:10.1016/j.micron.2011.10.002

Moran, C. J., Ramesh, A., Brama, P. A. J., O'Byrne, J. M., O'Brien, F. J., and Levingstone, T. J. (2016). The Benefits and Limitations of Animal Models for Translational Research in Cartilage Repair. *J. Exp. Ortop* 3 (1), 1–12. doi:10.1186/s40634-015-0037-x

Mouw, J. K., Imler, S. M., and Levenston, M. E. (2007). Ion-channel Regulation of Chondrocyte Matrix Synthesis in 3D Culture under Static and Dynamic Compression. *Biomech. Model. Mechanobiol* 6 (1-2), 33–41. doi:10.1007/s10237-006-0034-1

Muehleman, C., Zhong, Z., Williams, J., Kuettner, K., Aurich, M., Han, B., et al. (2002). Diffraction Enhanced X-ray Imaging of the Articular Cartilage of Experimental Animals. *Osteoarthritis and Cartilage* 10, 163–171.

Müller, M., and Zumbusch, A. (2007). Coherent Anti-stokes Raman Scattering Microscopy. *ChemPhysChem* 8 (15), 2156–2170.

Musumeci, G. (2016). The Effect of Mechanical Loading on Articular Cartilage. *J. Funct. Morphol. Kinesiol.* 1, 154–161. doi:10.3390/jfmk1020154

Nam, S. Y., Ricles, L. M., Suggs, L. J., and Emelianov, S. Y. (2015). Imaging Strategies for Tissue Engineering Applications. *Tissue Eng. Part B: Rev.* 21 (1), 88–102. doi:10.1089/ten.teb.2014.0180

Natenstedt, J., Kok, A. C., Dankelman, J., and Tuijthof, G. J. (2015). What Quantitative Mechanical Loading Stimulates *In Vitro* Cultivation Best? *J. Exp. Orthop.* 2 (1), 15. doi:10.1186/s40634-015-0029-x

Nebelung, S., Gavenis, K., Lüring, C., Zhou, B., Mueller-Rath, R., Stoffel, M., et al. (2012). Simultaneous Anabolic and Catabolic Responses of Human Chondrocytes Seeded in Collagen Hydrogels to Long-Term Continuous Dynamic Compression. *Ann. Anat. - Anatomischer Anzeiger* 194 (4), 351–358. doi:10.1016/j.aanat.2011.12.008

Nehrer, S., Breinan, H., Ramappa, A., Hsu, H., Minas, T., Shortkroff, S., et al. (1998). Chondrocyte-seeded Collagen Matrices Implanted in a Chondral Defect in a Canine Model. *Biomaterials* 19 (24), 2313–2328. doi:10.1016/s0142-9612(98)00143-4

Ng, K. W., Mauck, R. L., Wang, C. C.-B., Kelly, T.-A. N., Ho, M. M.-Y., Chen, F. H., et al. (2009). Duty Cycle of Deformational Loading Influences the Growth of Engineered Articular Cartilage. *Cel. Mol. Bioeng.* 2 (3), 386–394. doi:10.1007/s12195-009-0070-x

Ning, L., Zhu, N., Smith, A., Rajaram, A., Hou, H., Srinivasan, S., et al. (2021). Noninvasive Three-Dimensional *In Situ* and *In Vivo* Characterization of Bioprinted Hydrogel Scaffolds Using the X-ray Propagation-Based Imaging Technique. *ACS Appl. Mater. Inter.* 13, 25611–25623. doi:10.1021/acsami.1c02297

O'Conor, C. J., Leddy, H. A., Benefield, H. C., Liedtke, W. B., and Guilak, F. (2014). TRPV4-mediated Mechanotransduction Regulates the Metabolic Response of Chondrocytes to Dynamic Loading. *Proc. Natl. Acad. Sci.* 111 (4), 1316–1321. doi:10.1073/pnas.1319569111

Olubamiji, A. D., Izadifar, Z., Si, J. L., Cooper, D. M. L., Eames, B. F., and Chen, D. X. (2016). Modulating Mechanical Behaviour of 3D-Printed Cartilage-Mimetic PCL Scaffolds: Influence of Molecular Weight and Pore Geometry. *Biofabrication* 8 (2), 025020. doi:10.1088/1758-5090/8/2/025020

Olubamiji, A. D., Izadifar, Z., Zhu, N., Chang, T., Chen, X., and Eames, B. F. (2016). Using Synchrotron Radiation Inline Phase-Contrast Imaging Computed Tomography to Visualize Three-Dimensional Printed Hybrid Constructs for Cartilage Tissue Engineering. *J. Synchrotron Radiat.* 23 (3), 802–812. doi:10.1107/s1600577516002344

Olubamiji, A. D., Zhu, N., Chang, T., Nwankwo, C. K., Izadifar, Z., Honaramooz, A., et al. (2017). Traditional Invasive and Synchrotron-Based Noninvasive Assessments of Three-Dimensional-Printed Hybrid Cartilage Constructs *In Situ*. *Tissue Eng. Part C: Methods* 23 (3), 156–168. doi:10.1089/ten.tec.2016.0368

Öztürk, E., Stauber, T., Levinson, C., Cavalli, E., Arlov, Ø., and Zenobi-Wong, M. (2020). Tyrosinase-crosslinked, Tissue Adhesive and Biomimetic Alginate Sulfate Hydrogels for Cartilage Repair. *Biomed. Mater.* 15 (4), 045019. doi:10.1088/1748-605X/ab8318

Paige, K. T., Cima, L. G., Yaremchuk, M. J., Schloo, B. L., Vacanti, J. P., and Vacanti, C. A. (1996). De Novo cartilage Generation Using Calcium Alginate-Chondrocyte Constructs. *Plast. Reconstr. Surg.* 97 (1), 168–178. doi:10.1097/00006534-199601000-00027

Park, S. H., Seo, J. Y., Park, J. Y., Ji, Y. B., Kim, K., Choi, H. S., et al. (2019). An Injectable, Click-Crosslinked, Cytomodulin-Modified Hyaluronic Acid Hydrogel for Cartilage Tissue Engineering. *NPG Asia Mater.* 11 (1), 1–16. doi:10.1038/s41427-019-0130-1

Parsons, D. W., Morgan, K., Donnelley, M., Fouras, A., Crosbie, J., Williams, I., et al. (2008). High-resolution Visualization of Airspace Structures in Intact Mice via Synchrotron Phase-Contrast X-ray Imaging (PCXI). *J. Anat.* 213 (2), 217–227. doi:10.1111/j.1469-7580.2008.00950.x

Parsons, J. R. (1998). *Cartilage: Handbook of Biomaterial Properties*. Springer, 40–47. doi:10.1007/978-1-4615-5801-9_4

Pauwels, E., Van Loo, D., Cornillie, P., Brabant, L., and Van Hoorebeke, L. (2013). An Exploratory Study of Contrast Agents for Soft Tissue Visualization by Means of High Resolution X-ray Computed Tomography Imaging. *J. Microsc.* 250 (1), 21–31. doi:10.1111/jmi.12013

Pelaez, D., Charles Huang, C.-Y., and Cheung, H. S. (2009). Cyclic Compression Maintains Viability and Induces Chondrogenesis of Human Mesenchymal Stem Cells in Fibrin Gel Scaffolds. *Stem Cell Dev.* 18 (1), 93–102. doi:10.1089/scd.2008.0030

Peretti, G. M., Xu, J.-W., Bonassar, L. J., Kirchhoff, C. H., Yaremchuk, M. J., and Randolph, M. A. (2006). Review of Injectable Cartilage Engineering Using Fibrin Gel in Mice and Swine Models. *Tissue Eng.* 12 (5), 1151–1168. doi:10.1089/ten.2006.12.1151

Poole, A. R., Pidoux, I., Reiner, A., and Rosenberg, L. (1982). An Immunoelectron Microscope Study of the Organization of Proteoglycan Monomer, Link Protein, and Collagen in the Matrix of Articular Cartilage. *J. Cel. Biol.* 93 (3), 921–937. doi:10.1083/jcb.93.3.921

Pulkkinen, H. J., Tiitu, V., Valonen, P., Jurvelin, J. S., Lammi, M. J., and Kiviranta, I. (2010). Engineering of Cartilage in Recombinant Human Type II Collagen Gel in Nude Mouse Model *In Vivo*. *Osteoarthritis and cartilage* 18 (8), 1077–1087. doi:10.1016/j.joca.2010.05.004

Pulkkinen, H. J., Tiitu, V., Valonen, P., Jurvelin, J. S., Rieppo, L., Töyräs, J., et al. (2013). Repair of Osteochondral Defects with Recombinant Human Type II Collagen Gel and Autologous Chondrocytes in Rabbit. *Osteoarthritis and cartilage* 21 (3), 481–490. doi:10.1016/j.joca.2012.12.004

Qi, C., Liu, J., Jin, Y., Xu, L., Wang, G., Wang, Z., et al. (2018). Photo-crosslinkable, Injectable Sericin Hydrogel as 3D Biomimetic Extracellular Matrix for Minimally Invasive Repairing Cartilage. *Biomaterials* 163, 89–104. doi:10.1016/j.biomaterials.2018.02.016

Ramaswamy, S., Gurkan, I., Sharma, B., Cascio, B., Fishbein, K. W., and Spencer, R. G. (2008). Assessment of Tissue Repair in Full Thickness Chondral Defects in the Rabbit Using Magnetic Resonance Imaging Transverse Relaxation Measurements. *J. Biomed. Mater. Res.* 86B (2), 375–380. doi:10.1002/jbm.b.31030

Rampichová, M., Filová, E., Varga, F., Lytvynets, A., Prosecká, E., Kolácná, L., et al. (2010). Fibrin/hyaluronic Acid Composite Hydrogels as Appropriate Scaffolds for *In Vivo* Artificial Cartilage Implantation. *ASAIO J.* 56 (6), 563–568.

Räsänen, T., and Messner, K. (1996). Regional Variations of Indentation Stiffness and Thickness of normal Rabbit Knee Articular Cartilage. *J. Biomed. Mater. Res.* 31 (4), 519–524.

Renghini, C., Komlev, V., Fiori, F., Verné, E., Baino, F., and Vitale-Brovarone, C. (2009). Micro-CT Studies on 3-D Bioactive Glass-Ceramic Scaffolds for Bone Regeneration. *Acta Biomater.* 5 (4), 1328–1337. doi:10.1016/j.actbio.2008.10.017

Ribitsch, I., Baptista, P. M., Lange-Consiglio, A., Melotti, L., Patruno, M., Jenner, F., et al. (2020). Large Animal Models in Regenerative Medicine and Tissue Engineering: To Do or Not to Do. *Front. Bioeng. Biotechnol.* 8, 972. doi:10.3389/fbioe.2020.00972

Ronca, F., Palmieri, L., Panicucci, P., and Ronca, G. (1998). Anti-inflammatory Activity of Chondroitin Sulfate. *Osteoarthritis and Cartilage* 6, 14–21. doi:10.1016/s1063-4584(98)80006-x

Ryan, J. A., Eisner, E. A., DuRaine, G., You, Z., and Hari Reddi, A. (2009). Mechanical Compression of Articular Cartilage Induces Chondrocyte Proliferation and Inhibits Proteoglycan Synthesis by Activation of the ERK Pathway: Implications for Tissue Engineering and Regenerative Medicine. *J. Tissue Eng. Regen. Med.* 3 (2), 107–116. doi:10.1002/term.146

Sadeghianmaryan, A., Naghieh, S., Alizadeh Sardroud, H., Yazdanpanah, Z., Afzal Soltani, Y., Sernaglia, J., et al. (2020). Extrusion-based Printing of Chitosan Scaffolds and Their *In Vitro* Characterization for Cartilage Tissue Engineering. *Int. J. Biol. Macromolecules* 164, 3179–3192. doi:10.1016/j.ijbiomac.2020.08.180

Sanz-Ramos, P., Duart, J., Rodríguez-Goñi, M. V., Vicente-Pascual, M., Dotor, J., Mora, G., et al. (2014). Improved Chondrogenic Capacity of Collagen Hydrogel-Expanded Chondrocytes. *J. Bone Jt. Surg.* 96 (13), 1109–1117. doi:10.2106/jbjs.m.00271

Sanz-Ramos, P., Mora, G., Ripalda, P., Vicente-Pascual, M., and Izal-Azcárate, Í. (2012). Identification of Signalling Pathways Triggered by Changes in the Mechanical Environment in Rat Chondrocytes. *Osteoarthritis and cartilage* 20 (8), 931–939. doi:10.1016/j.joca.2012.04.022

Sauerland, K., Raiss, R. X., and Steinmeyer, J. (2003). Proteoglycan Metabolism and Viability of Articular Cartilage Explants as Modulated by the Frequency of Intermittent Loading. *Osteoarthritis and cartilage* 11 (5), 343–350. doi:10.1016/s1063-4584(03)00007-4

Schagemann, J. C., Erggelet, C., Chung, H.-W., Lahm, A., Kurz, H., and Mrosek, E. H. (2009). Cell-laden and Cell-free Biopolymer Hydrogel for the Treatment of Osteochondral Defects in a Sheep Model. *Tissue Eng. Part A* 15 (1), 75–82. doi:10.1089/ten.tea.2008.0087

Schinagl, R. M., Gurskis, D., Chen, A. C., and Sah, R. L. (1997). Depth-dependent Confined Compression Modulus of Full-Thickness Bovine Articular Cartilage. *J. Orthop. Res.* 15 (4), 499–506. doi:10.1002/jor.1100150404

Schulz, R. M., and Bader, A. (2007). Cartilage Tissue Engineering and Bioreactor Systems for the Cultivation and Stimulation of Chondrocytes. *Eur. Biophys. J.* 36 (4), 539–568. doi:10.1007/s00249-007-0139-1

Shao, X. X., Hutmacher, D. W., Ho, S. T., Goh, J. C. H., and Lee, E. H. (2006). Evaluation of a Hybrid Scaffold/cell Construct in Repair of High-Load-Bearing Osteochondral Defects in Rabbits. *Biomaterials* 27 (7), 1071–1080. doi:10.1016/j.biomaterials.2005.07.040

Shelton, J. C., Bader, D. L., and Lee, D. A. (2003). Mechanical Conditioning Influences the Metabolic Response of Cell-Seeded Constructs. *Cells Tissues Organs* 175 (3), 140–150. doi:10.1159/000074630

Sims, D. C., Butler, P. E. M., Cao, Y. L., Casanova, R., Randolph, M. A., Black, A., et al. (1998). Tissue Engineered Neocartilage Using Plasma Derived Polymer Substrates and Chondrocytes. *Plast. Reconstr. Surg.* 101 (6), 1580–1585. doi:10.1097/00006534-199805000-00022

Tang, X., Muhammad, H., McLean, C., Miotla-Zarebska, J., Fleming, J., Didangelos, A., et al. (2018). Connective Tissue Growth Factor Contributes to Joint Homeostasis and Osteoarthritis Severity by Controlling the Matrix Sequestration and Activation of Latent TGFβ. *Ann. Rheum. Dis.* 77 (9), 1372–1380. doi:10.1136/annrheumdis-2018-212964

Van Susante, J. L. C., Buma, P., Schuman, L., Homminga, G. N., van den Berg, W. B., and Veth, R. P. H. (1999). Resurfacing Potential of Heterologous Chondrocytes Suspended in Fibrin Glue in Large Full-Thickness Defects of Femoral Articular Cartilage: an Experimental Study in the Goat. *Biomaterials* 20 (13), 1167–1175. doi:10.1016/s0142-9612(97)00190-7

Vanlenthe, G., Hagenmuller, H., Bohner, M., Hollister, S., Meinel, L., and Muller, R. (2007). Nondestructive Micro-computed Tomography for Biological Imaging and Quantification of Scaffold-Bone Interaction *In Vivo*. *Biomaterials* 28 (15), 2479–2490. doi:10.1016/j.biomaterials.2007.01.017

Vansusante, J., Buma, P., Homminga, G., Vandenberg, W., and Veth, R. (1998). Chondrocyte-seeded Hydroxyapatite for Repair of Large Articular Cartilage Defects. A Pilot Study in the Goat. *Biomaterials* 19 (24), 2367–2374. doi:10.1016/s0142-9612(98)00158-6

Varelas, X., Samavarchi-Tehrani, P., Narimatsu, M., Weiss, A., Cockburn, K., Larsen, B. G., et al. (2010). The Crumbs Complex Couples Cell Density Sensing to Hippo-dependent Control of the TGF-β-SMAD Pathway. *Developmental Cel.* 19 (6), 831–844. doi:10.1016/j.devcel.2010.11.012

Vega, S., Kwon, M. Y., and Burdick, M. J. (2017). Recent Advances in Hydrogels for Cartilage Tissue Engineering. *eCM* 33, 59–75. doi:10.22203/ecm.v033a05

Vinatier, C., Gauthier, O., Fatimi, A., Merceron, C., Masson, M., Moreau, A., et al. (2009). An Injectable Cellulose-Based Hydrogel for the Transfer of Autologous Nasal Chondrocytes in Articular Cartilage Defects. *Biotechnol. Bioeng.* 102 (4), 1259–1267. doi:10.1002/bit.22137

Vincent, T. L., McLean, C. J., Full, L. E., Peston, D., and Saklatvala, J. (2007). FGF-2 Is Bound to Perlecan in the Pericellular Matrix of Articular Cartilage, where it Acts as a Chondrocyte Mechanotransducer. *Osteoarthritis and cartilage* 15 (7), 752–763. doi:10.1016/j.joca.2007.01.021

von Doernberg, M.-C., von Rechenberg, B., Bohner, M., Grünenfelder, S., van Lenthe, G. H., Müller, R., et al. (2006). *In Vivo* behavior of Calcium Phosphate Scaffolds with Four Different Pore Sizes. *Biomaterials* 27 (30), 5186–5198. doi:10.1016/j.biomaterials.2006.05.051

Vos, T., Flaxman, A. D., Naghavi, M., Lozano, R., Michaud, C., Ezzati, M., et al. (2012). Years Lived with Disability (YLDs) for 1160 Sequelae of 289 Diseases and Injuries 1990-2010: a Systematic Analysis for the Global Burden of Disease Study 2010. *Lancet* 380 (9859), 2163–2196. doi:10.1016/S0140-6736(12)61729-2

Waldman, S., Couto, D. C., Couto, D., Pilliar, M. R., and Kandel, R. (2007). Multi-axial Mechanical Stimulation of Tissue Engineered Cartilage: Review. *eCM* 13 (613), 66–75. doi:10.22203/ecm.v013a07

Wang, D.-A., Varghese, S., Sharma, B., Strehin, I., Fermanian, S., Gorham, J., et al. (2007). Multifunctional Chondroitin Sulphate for Cartilage Tissue-Biomaterial Integration. *Nat. Mater* 6 (5), 385–392. doi:10.1038/nmat1890

Wang, F., Zhou, P., Li, K., Mamtilahun, M., Tang, Y., Du, G., et al. (2020). Sensitive Imaging of Intact Microvessels *In Vivo* with Synchrotron Radiation. *IUCrJ* 7 (5), 793–802. doi:10.1107/S2052252520008234

Wang, P.-Y., Chow, H.-H., Lai, J.-Y., Liu, H.-L., and Tsai, W.-B. (2009). Dynamic Compression Modulates Chondrocyte Proliferation and Matrix Biosynthesis in Chitosan/gelatin Scaffolds. *J. Biomed. Mater. Res.* 91B (1), 143–152. doi:10.1002/jbm.b.31384

Watrin-Pinzano, A., Ruaud, J. P., Cheli, Y., Gonord, P., Grossin, L., Bettembourg-Brault, I., et al. (2004). Evaluation of Cartilage Repair Tissue after Biomaterial Implantation in Rat Patella by Using T2 Mapping. *MAGMA* 17 (3), 219–228. doi:10.1007/s10334-004-0071-7

Wei, Y., Jin, Z., Zhang, H., Piao, S., Lu, J., and Bai, L. (2018). The Transient Receptor Potential Channel, Vanilloid 5, Induces Chondrocyte Apoptosis via Ca2+ CaMKII-dependent MAPK and Akt/mTOR Pathways in a Rat Osteoarthritis Model. *Cell Physiol Biochem* 51 (5), 2309–2323. doi:10.1159/000495874

Westreich, R., Kaufman, M., Gannon, P., and Lawson, W. (2004). Validating the Subcutaneous Model of Injectable Autologous Cartilage Using a Fibrin Glue Scaffold. *Laryngoscope* 114 (12), 2154–2160. doi:10.1097/10.mlg.0000149449.37640.0d

Wimmer, M. A., Grad, S., Kaup, T., Hänni, M., Schneider, E., Gogolewski, S., et al. (2004). Tribology Approach to the Engineering and Study of Articular Cartilage. *Tissue Eng.* 10 (9-10), 1436–1445. doi:10.1089/ten.2004.10.1436

Wong, M., Siegrist, M., Wang, X., and Hunziker, E. (2001). Development of Mechanically Stable Alginate/chondrocyte Constructs: Effects of Guluronic Acid Content and Matrix Synthesis. *J. Orthop. Res.* 19 (3), 493–499. doi:10.1016/s0736-0266(00)90023-8

Wu, S., Wang, Y., Streubel, P. N., and Duan, B. (2017). Living Nanofiber Yarn-Based Woven Biotextiles for Tendon Tissue Engineering Using Cell Tri-culture and Mechanical Stimulation. *Acta Biomater.* 62, 102–115. doi:10.1016/j.actbio.2017.08.043

Wu, Y., Stoddart, M. J., Wuertz-Kozak, K., Grad, S., Alini, M., and Ferguson, S. J. (2017). Hyaluronan Supplementation as a Mechanical Regulator of Cartilage Tissue Development under Joint-Kinematic-Mimicking Loading. *J. R. Soc. Interf.* 14 (133), 20170255. doi:10.1098/rsif.2017.0255

Xu, L., Golshirazian, I., Asbury, B. J., and Li, Y. (2014). Induction of High Temperature Requirement A1, a Serine Protease, by TGF-Beta1 in Articular Chondrocytes of Mouse Models of OA. *Histol. Histopathol* 29, 609–618. doi:10.14670/HH-29.10.609

Yang, P. J., and Temenoff, J. S. (2009). Engineering Orthopedic Tissue Interfaces. *Tissue Eng. Part B: Rev.* 15 (2), 127–141. doi:10.1089/ten.teb.2008.0371

Yanoshita, M., Hirose, N., Okamoto, Y., Sumi, C., Takano, M., Nishiyama, S., et al. (2018). Cyclic Tensile Strain Upregulates Pro-inflammatory Cytokine Expression via FAK-MAPK Signaling in Chondrocytes. *Inflammation* 41 (5), 1621–1630. doi:10.1007/s10753-018-0805-8

You, F., Chen, X., Cooper, D. M. L., Chang, T., and Eames, B. F. (2018). Homogeneous Hydroxyapatite/alginate Composite Hydrogel Promotes Calcified Cartilage Matrix Deposition with Potential for Three-Dimensional Bioprinting. *Biofabrication* 11 (1), 015015. doi:10.1088/1758-5090/aaf44a

You, F., Eames, B. F., and Chen, X. (2017). Application of Extrusion-Based Hydrogel Bioprinting for Cartilage Tissue Engineering. *Ijms* 18 (7), 1597. doi:10.3390/ijms18071597

You, F., Wu, X., Zhu, N., Lei, M., Eames, B. F., and Chen, X. (2016). 3D Printing of Porous Cell-Laden Hydrogel Constructs for Potential Applications in Cartilage Tissue Engineering. *ACS Biomater. Sci. Eng.* 2 (7), 1200–1210. doi:10.1021/acsbiomaterials.6b00258

Yun, K., and Moon, H. T. (2008). Inducing Chondrogenic Differentiation in Injectable Hydrogels Embedded with Rabbit Chondrocytes and Growth Factor for Neocartilage Formation. *J. Biosci. Bioeng.* 105 (2), 122–126. doi:10.1263/jbb.105.122

Zhang, L., and Luo, S. (2011). Micro Soft Tissues Visualization Based on X-Ray Phase-Contrast Imaging. *Tominfoj* 5, 19–25. doi:10.2174/1874431101105010019

Zhao, M., Chen, Z., Liu, K., Wan, Y.-q., Li, X.-d., Luo, X.-w., et al. (2015). Repair of Articular Cartilage Defects in Rabbits through Tissue-Engineered Cartilage Constructed with Chitosan Hydrogel and Chondrocytes. *J. Zhejiang Univ. Sci. B* 16 (11), 914–923. doi:10.1631/jzus.b1500036

Zhao, Z., Li, Y., Wang, M., Zhao, S., Zhao, Z., and Fang, J. (2020). Mechanotransduction Pathways in the Regulation of Cartilage Chondrocyte Homoeostasis. *J. Cel Mol Med* 24 (10), 5408–5419. doi:10.1111/jcmm.15204

Zhu, N., Chapman, D., Cooper, D., Schreyer, D. J., and Chen, X. (2011). X-ray Diffraction Enhanced Imaging as a Novel Method to Visualize Low-Density Scaffolds in Soft Tissue Engineering. *Tissue Eng. Part C: Methods* 17 (11), 1071–1080. doi:10.1089/ten.tec.2011.0102

Conflict of Interest: The authors declare that the research was conducted in the absence of any commercial or financial relationships that could be construed as a potential conflict of interest.

Publisher's Note: All claims expressed in this article are solely those of the authors and do not necessarily represent those of their affiliated organizations, or those of the publisher, the editors, and the reviewers. Any product that may be evaluated in this article, or claim that may be made by its manufacturer, is not guaranteed or endorsed by the publisher.

Advantages of publishing in Frontiers

OPEN ACCESS
Articles are free to read for greatest visibility and readership

FAST PUBLICATION
Around 90 days from submission to decision

HIGH QUALITY PEER-REVIEW
Rigorous, collaborative, and constructive peer-review

TRANSPARENT PEER-REVIEW
Editors and reviewers acknowledged by name on published articles

Frontiers
Avenue du Tribunal-Fédéral 34
1005 Lausanne | Switzerland

Visit us: www.frontiersin.org
Contact us: frontiersin.org/about/contact

REPRODUCIBILITY OF RESEARCH
Support open data and methods to enhance research reproducibility

DIGITAL PUBLISHING
Articles designed for optimal readership across devices

FOLLOW US
@frontiersin

IMPACT METRICS
Advanced article metrics track visibility across digital media

EXTENSIVE PROMOTION
Marketing and promotion of impactful research

LOOP RESEARCH NETWORK
Our network increases your article's readership